A study of glial associated changes in the complexity of primary cortical neurons

Thesis submitted to the University of Dublin, Trinity College

for the degree of Doctor of Philosophy

By

Kate O'Reilly

2021

Supervised by

Prof. Andrew Harkin

School of Pharmacy and Pharmaceutical Sciences
&
Trinity College Institute of Neuroscience,
Trinity College,
Dublin

Declaration

I declare that this thesis is submitted for the degree of Doctor of Philosophy at the University of Dublin, Trinity College and has not been submitted as an exercise for a degree at this or any other university and that it is entirely my own work.

I agree to deposit this thesis in the University's open-access institutional repository or allow the library to do so on my behalf, subject to Irish copyright legislation and Trinity College Library conditions of use and acknowledgement.

I do not consent to the examiner retaining a copy of the thesis beyond the examining period, should they so wish.

Signed

_____

Kate O'Reilly

Acknowledgements

First and foremost, I would like to thank my wonderful supervisor Prof. Andrew Harkin for giving me the opportunity to carry out my PhD research and for warmly welcoming me into his lab. Your unwavering support and guidance over the last three years has meant a great deal to me and I thank you for all I have learnt during my time in TCIN.

I would also like to thank the school of Pharmacy and staff of TCIN for all their assistance over the years. I am indebted to Prof. Mani Ramaswami and Dr. Joern Huelsmeier for kindly allowing me to use their fluorescent microscope and for their technical help with it.

I owe a special thanks to Dr Emmanuel Hermans at the Université catholique de Louvain for his assistance setting up my first radiological assay. I had the pleasure of visiting his lab and learning from his experience.

I extend my heartfelt thanks to Dr. Jennifer David, who was so incredibly patient and helpful with me when I started. I thank her for introducing me to cell culture and for her work setting up the seahorse and Golgi-Cox staining experiments.

This PhD would not have been as enjoyable without the company of my colleagues who experienced the same rollercoaster of experimental disasters and victories. I feel extremely fortunate to have spent the last three years in such wonderful company. Thank you to Jenny, Eoin, Teresa, Valentina and Claire. To Sarah who was with me from start to finish. I would have been lost without your friendship. From bringing cells back to life to running half-marathons, you continuously motivated and encouraged me. Thank you for all the laughter, the cinema nights, the trips away and for making the late nights and weekends in the lab a much more lively and pleasant experience.

I am indebted to my amazing friends including Cliodhna and Aoife, for their positivity, and to everyone who very kindly helped with proof-reading this thesis. To Ania, for her friendship and her support, in every aspect of my life. Our weekly runs, evening chats and our shared love for cream pies was a big part of my PhD life. To Anthony, for his valuable proof-reading, and the endless supplies of coffee and hugs. Thank you for always listening, for your words of encouragement, and reassurance.

Finally, I am eternally grateful to my father Tony, my mother Anna, my sister Ciara and my dog Lizzie, for their love and support, their understanding and their patience throughout the course of my PhD and education. This would not have been possible without you.

Summary

Neuroinflammation and disruptions in the integrity of neuronal circuitry are hallmarks of a range of CNS disorders. There is extensive evidence linking pro-inflammatory signalling and glial dysfunction with neuronal atrophy and impairments in synaptic transmission. As neuronal atrophy and loss of synaptic connections precede cell death, a greater understanding of the neurobiological mechanisms and mediators underlying inflammatory-driven glial cell dysfunction would pave the way for the identification of novel drug targets and drug development strategies for neuroinflammatory and degenerative disorders.

An *in vitro* model of glial neuronal interaction composed of rat mature primary cortical neurons, microglia and astrocytes was used in this project. Neuronal complexity was determined by microtubule associated protein 2 (MAP2) immunocytochemistry and subsequently by Sholl analysis. Synapse number was measured by determination of the co-localised expression of the presynaptic protein synaptophysin and the postsynaptic protein postsynaptic density 95 (PSD-95).

Treatment of enriched primary astrocyte cultures with the astrocyte toxin L-alpha-aminoadipic acid (L-AAA, 0.05, 0.5 mM) induced changes in astrocyte morphology, reduced immunoreactivity of the astrocytic marker glial fibrillary acidic protein (GFAP), reduced expression of the astrocytic markers GFAP and S100β and mitochondrial respiration. Treatment of mature primary cortical neurons at days *in vitro* 21 (DIV 21) with conditioned media from L-AAA treated astrocytes reduced neuronal complexity and synapse formation. Administration of L-AAA into the prelimbic cortex of mice increased the number of thin and stubby spines as measured by Golgi-Cox staining.

Stimulation of primary mixed glial and enriched microglial cells with IFNγ (10 ng/mL) induced changes in cell morphology reflecting a reactive state, and increased expression of pro-inflammatory factors including tumor necrosis factor-alpha (TNF-α) and interleukin- alpha (IL-1α). Conditioned media from IFNγ (10 ng/mL) treated glial cells reduced the complexity and co-localised expression of synaptic markers in mature primary cortical neurons. Treatment of enriched

astrocytic cultures with TNF-α (30 ng/mL) and IL-1α (3 ng/mL) induced the expression and release of interleukin-6 (IL-6) and produced a conditioned media which reduced neuronal complexity and synapse formation in primary cortical neurons. Immunoneutralisation of IL-6 blocked these effects demonstrating a role for IL-6 in mediating reactive astrocyte associated neuronal atrophy.

L-AAA attenuated the release of IL-6 from mixed glial cultures induced by IFNγ and partially attenuated reductions in neuronal complexity and synapse formation induced by conditioned media from IFNγ treated mixed glia. L-AAA also attenuated the expression and release of astrocytic IL-6 following treatment with TNF-α (30 ng/mL) and IL-1α (3 ng/mL). Notably, L-AAA provided greater protection against reductions in neuronal complexity and synapse formation induced by conditioned media from TNF-α and IL-1α treated astrocytes.

Previous studies have shown that IFNγ increases the expression of Indoleamine 2, 3-dioxygenase (IDO), decreases the expression of Kynurenine amino transferase II (KAT II) and has no effect on the expression of Kynurenine monooxygenase (KMO) or Tryptophan 2, 3-dioxygenase (TDO) in mixed glia and enriched microglial cultures. This study further demonstratetd that TNF-α (30 ng/mL) and IL-1α (3 ng/mL) induced the expression of kynurenine pathway enzymes KAT II, KMO, IDO and TDO in enriched primary cortical astrocytic cultures indicating pathway induction. Conversely, IL-6 increased the expression of TDO, reduced the expression of KAT II and KMO and had no effect on KYNU or IDO in enriched primary cortical microglial cultures.

Treatment with the IDO inhibitor 1-methyltryptophan (1-MT) protected against reductions in neuronal complexity induced by conditioned media from IFNγ treated mixed glia and conditioned media from IL-6 treated microglia. This indicates a role for the KP in driving atrophy affiliated with IFNγ and IL-6 activation of primary glia. Kynurenic acid (0.03, 0.1 and 0.3 μM) increased neuronal complexity and synapse formation and protected against reductions in neuronal atrophy and synapse loss induced by conditioned media from IFNγ treated mixed glia and by the neurotoxic microglial metabolite quinolinic acid (1 μM).

Results of this thesis highlight the importance of healthy astrocytes, and the implications of astrocytic dysfunction, glial activation and pro-inflammatory signalling on neuronal complexity and synapse formation *in vitro*. In particular, they point to IL-6 signalling and the KP as attractive targets for the development of novel therapeutics aimed at restoring synaptic connections and promoting neuronal remodelling in CNS disorders affiliated with inflammatory-induced, reactive glial-associated neuronal atrophy.

Table of contents

List of Figures

List of Tables

Abbreviations

+TIPs	Microtubule Plus End Tracking Proteins
1-MT	1-Methyltryptophan
2-DG	2-Deoxy-D glucose
3-HAA	3-hydroxyanthranilic acid
3-HAO	3-hydroxyanthranilic acid 3, 4-dioxygenase
3-HK	3-hydroxykynurenine
Abi1	Abl-interactor 1
ACMSD	Aminocarboxymuconate-semialdehyde decarboxylase
AD	Alzheimer's disease
AhR	Aryl hydrocarbon receptor
ALDH1L1	Aldehyde dehydrogenase family 1, member L1
AMO	Anthranilate 3-monooxygenase
AMPA	α-amino-3-hydroxy-5-methyl-4-isoxazolepropionic acid
ANOVA	Analyses of variance
AQP	Aquaporin
AQP4	Aquaporin-4
AraC	Cytosine β-d-arabinofuranoside
ATP	Adenosine triphosphate
BBB	Blood brain barrier
BCA	Bicinchoninic acid
BDNF	Brain derived neurotrophic factor
BSA	Bovine Serum Albumin 96%
C1q	Complement component 1q
Ca^{2+}	Calcium ion
$CaCl_2$	Calcium chloride
CAM	Cell adhesion molecule
CaMKs	Multiple calcium/calmodulin-dependent protein kinases
cAMP	Adenosine 3',5'-cyclic monophosphate
CCK-8	Cell Counting Kit-8
CD64	Fc-gamma receptor 1

cDNA	Complementary DNA
CDs	Cluster of differentiation molecules
CLC	Cardiotrophin-like cytokine
CM	Conditioned media
CNS	Central nervous system
CNTF	Ciliary neurotrophic factor
CRP	C-reactive protein
CSF	Cerebrospinal fluid
CSF1	Colony-stimulating factor 1
Csf-1R	Colony stimulating factor 1 receptor
CTCF	Corrected total cell fluorescence
Cx30	Connexins 30
DAMP	Damage-associated molecular pattern
DAPI	4´,6-Diamidino-2-phenylindole dihydrochloride
dH20	Distilled water
DIV 0	Days *in vitro* 0
DMEM	Dulbecco's modified eagle media
dNTP	Dinucleotide triphosphates
EAAT	Excitatory amino acid transporter
ECAR	Extracellular acidification rate
ECM	Extracellular matrix
eGFP	Enhanced green fluorescent protein
ELISA	Enzyme-linked immunosorbent assays
ERK	Extracellular signal-regulated kinase
EtOH	Ethanol
FAD	Flavin adenine dinucleotide
FAM	Fluorescein amidite
FBS	Fetal bovine serum
FCCP	Carbonyl cyanide-4-tri-(fluoromethoxy)phenylhydrazone
FGF2	Fibroblast growth factor 2
GABA	Gamma aminobutyric acid

GAPDH	Glyceraldehyde-3-phosphate dehydrogenase
G-CSF	Granulocyte-colony stimulating factor
GDNF	Glial cell line-derived neurotrophic factor
GEF	Rac1-specific guanine nucleotide exchange factor
GFAP	Glial fibrillary acidic protein
GFL	GDNF family ligand
GFP	Green fluorescent protein
GLAST	Glutamate-aspartate transporter
GLT-1	Glutamate transporter 1
GLY	Glycine
GM-CSF	Granulocyte macrophage colony-stimulating factor
gp130	Glycoprotein 130
GPR35	G protein-coupled receptor 35
GR	Glucocorticoid receptor
GS	Glutamine synthetase
H_2O_2	Hydrogen peroxide
H_2SO_4	Sulfuric acid
HCl	Hydrochloric Acid
HD	Huntington's disease
HPA	Hypothalamic pituitary
Iba1	Ionised calcium-binding adapter molecule 1
ICAM-1	Intercellular adhesion molecule 1
ICAM-1	Intracellular cell adhesion molecule 1
IDO	Indoleamine 2, 3-dioxygenase
IFN	Interferon
IFNGR	IFNγ receptor complex
IFNγ	Interferon gamma
IL	Interleukin
IL-1α	Interleukin-1-alpha
IL-1β	Interleukin-1-beta
ILβ6	Interleukin 6

IL-6R	IL-6 α-receptor
iNOS	Inducible NO synthase
iPSC	Induced pluripotent stem cells
IRF1	Interferon regulatory factor 1
ISGs	IFNγ-stimulated genes
JAK	Janus kinase
KAT	Kynurenine aminotransferase
KCl	Potassium chloride
KH_2PO_4	Monopotassium phosphate
KMO	Kynurenine monooxygenase
KP	Kynurenine pathway
KYNA	Kynurenic acid
KYNU	Kynureninase
L-AAA	L-alpha-aminoadipic acid
LIF	Leukemia inhibitory factor
LIMK1	LIM domain kinase 1
L-NAME	L-ω-nitroarginine methyl ester
LPS	Lipopolysaccharide
LTD	Long-term depression
LTP	Long-term potentiation
MAP	Microtubule associated protein
MAPK	Mitogen-activated protein kinase
M-CSF	Macrophage colony-stimulating factor
mGluR	Metabotropic glutamate receptors
$MgSO_4$	Magnesium sulfate
MHCs	Major histocompatibility complexes
MPP+	Methyl-4-phenylpyridinium
MTOCs	Microtubule organising centres
mTOR	Mammalian target of rapamycin
NaCl	Sodium chloride
NAD+	Nicotinamide adenine nucleotide

NaOH	Sodium hydroxide
NBM	Neurobasal media
NeuN	Neuronal nuclear protein
NF-κB	Nuclear factor kappa B
NGF-β	Nerve growth factor beta
NK	Natural killer
NLRP3	NOD-, LRR- and pyrin domain-containing protein 3
NMDA	N-methyl-D-aspartate
NMDAR	NMDA receptor
NO	Nitric oxide
NT-3	Neurotrophin-3
NT-4/5	Neurotrophin-4/5
OCR	Oxygen consumption rates
P1-2	Postnatal day 1 -2
PAMP	Pathogen-associated molecular pattern
PBS	Phosphate buffered saline
PCR	Polymerase chain reaction
PD	Parkinson's disease
PFA	Paraformaldehyde
PFC	Prefrontal cortex
PI3K	Phosphoinositide 3-kinase
PKA	Protein kinase A
PPR	Pattern recognition receptor
PSD	Post synaptic density
PSD-95	Post-synaptic density-95
PTX3	Pentraxin-3
QUIN	Quinolinic acid
Rac1	Rac family small GTPase 1
RAGE	Receptor for Advanced Glycation Endproducts
rDNase	Recombinant deoxyribonuclease
RGMA	Repulsive guidance molecule a

RNA	Ribonucleic acid
RNase	Ribonuclease
ROCK	Rho-associated kinase
ROS	Reactive oxygen species
rpm	Rotations per minute
RT-PCR	Real-time Polymerase Chain Reaction
S100β	S100 calcium-binding protein beta
SAM	Sympathoadrenal medullary
SEM	Standard error of the mean
sIL-6R	Soluble form of IL-6R
SOCS	Suppressor of cytokine signalling proteins
SSRI	Selective serotonin reuptake inhibitor
STAT	Signal transducer and activator of transcription
TAE	Tris-acetate-EDTA
TDO	Tryptophan 2, 3-dioxygenase
TGF-β	Transforming growth factor-beta
TIAM1	Rac1 associated GEF 1
TLR	Toll-like receptor
TMEM119	Transmembrane protein 119
TNF-α	Tumour necrosis factor-α
TSP	Thrombospondin
VCAM-1	Vascular cell adhesion protein 1
VEGF	Vascular endothelial growth factor
VGLUT	Vesicular glutamate transporter
α7nAChR	α7 nicotinic acetylcholine receptor
β-PIX	Rho guanine nucleotide exchange factor 7
ΔΔCT	Cycle difference corrected for endogenous control

1 General Introduction

1.1 Organisation of the Central Nervous System

The central nervous system (CNS) has a pivotal role in the human body, as a regulator of homeostasis and a coordinator of sensory, motor and cognitive functions. The CNS, which is localised to the brain and spinal cord is composed principally of two cell types, neurons and glia. Neurons are excitable cells capable of producing large, rapid, electrical signals (action potentials), and represent the functional unit of the CNS. By contrast, glial cells (or *neuroglia*), are electrically non-excitable cells and noted primarily for their roles in providing structural and metabolic support (Germann, 2005).

1.2 Neurons

Neurons consist of a cell body (soma) and two neural processes; an axon (a long slender projection that conducts electrical impulses away from the cell body), and dendrite(s) (tree-like structures that receive messages from other neurons). Chemical messengers called “neurotransmitters” are released by presynaptic neurons at neuronal junctions (or synapses) and travel across the synapse to communicate with postsynaptic neurons. The primary function of dendrites is to receive messages (input) and direct them towards the cell body. Axons, primarily function in the propagation of electrical signals (output) away from the soma to axon terminals which release neurotransmitters. This highly organised assembly of neural pathways facilitates the CNS in carrying out a plethora of complex processes (Kandel, 2012; Kandel & Eric, 2012).

1.2.1 Neurite outgrowth

The fine structural detail and morphology of neurons is integral to their functioning as the fundamental signalling unit of the CNS. This unit plays a critical role in processing of synaptic inputs, generation of action potentials and formation and maintenance of functional neural networks which are imperative to brain function (Kulkarni & Firestein, 2012; Puppo et al, 2018; Yoshihara et al, 2009). Neuronal function is subject to adaptation. In the normal course of development, neural cells respond to changes in the external environment with parallel changes in information processing and neuronal communication (Kolb et

al, 2017). Perturbations in neuronal development have been correlated with disruption and impairment of brain circuitry evident across a range of CNS diseases (Chen et al, 2019; Fogarty, 2018). More specifically, perturbations in neuronal morphology and synaptic transmission have been identified as characteristic pathophysiological events during prodromal stages of neurodegenerative disorders, where pathogenesis has begun, but classical symptoms permitting diagnosis have not yet developed (Bellucci et al, 2017; Chung et al, 2009; Katsuno et al; Katsuno et al, 2018; López-Doménech et al, 2016; Milnerwood et al, 2010). Understanding the process involved in regulating neuronal outgrowth is imperative for the development of clinical interventions aimed at identifying disease salient biomarkers and maintaining the structural and functional plasticity of the brain (Cline, 2001; Kulkarni & Firestein, 2012; Menéndez-González, 2014).

Neurons develop their defined structure, with axons, dendrites and distinct neurites in response to a sequence of polarity events known as neuronal polarisation (Dotti & Banker, 1987; Lestanova et al, 2016; Yogev & Shen, 2017). The three main stages of neuronal polarisation include; (1) an initial spatial orientation cue, such as the detection of an extracellular signal which inform neurons where the axon and dendrite should grow, (2) local amplification and interpretation of the cue which results in activation of intracellular signalling pathways, and (3) rearrangement in the cytoskeleton into two morphologically distinct processes (Namba et al, 2015).

The neuronal cytoskeleton consists of dynamic structures called microtubules which play pivotal roles in cell polarity and guiding axon development and dendrite arborisation (Menon & Gupton, 2016). Microtubules consist of α- and β-tubulin heterodimers organised into polarised linear protofilaments. They emanate from microtubule organising centres (MTOCs) in the spherical, unpolarised cells characterising the beginning of neuronal development (Kuijpers & Hoogenraad, 2011). Polymerisation of α- and β-tubulin dimers precipitates microtubule differentiation and growth of the plus end directed away from the MTOC. Following differentiation, neurons develop multiple processes termed

"neurites" which extend from the cell body and elongate forming thin protrusions (Dent et al, 2011; Sainath & Gallo, 2015). Microtubule motor proteins such as kinesin-1 are thought to play an important role in neuronal outgrowth by promoting microtubule sliding and membrane protrusion (Winding et al, 2016).

Following neurite elongation, one of the multiple processes becomes the axon, while the others will later develop into dendrites (Menon & Gupton, 2016). Stabilisation of microtubules guides transport of motor proteins and organelles required for the formation of axonal segments (Kapitein & Hoogenraad, 2011). A dynamic structure, known as the growth cone evolves at the tip of the growing axon and is responsible for driving axon elongation and branching (Kahn & Baas, 2016). As the growth cone enlarges it probes the extracellular environment for stimuli and directs the growing axon in a particular direction (Lowery & Van Vactor, 2009). Actin filaments then accumulate forming axonal filopodia (or branches) along the axon shaft. Invasion of these actin-rich filopodia with microtubules results in the maturation of collateral branches (*Figure 1.1*).

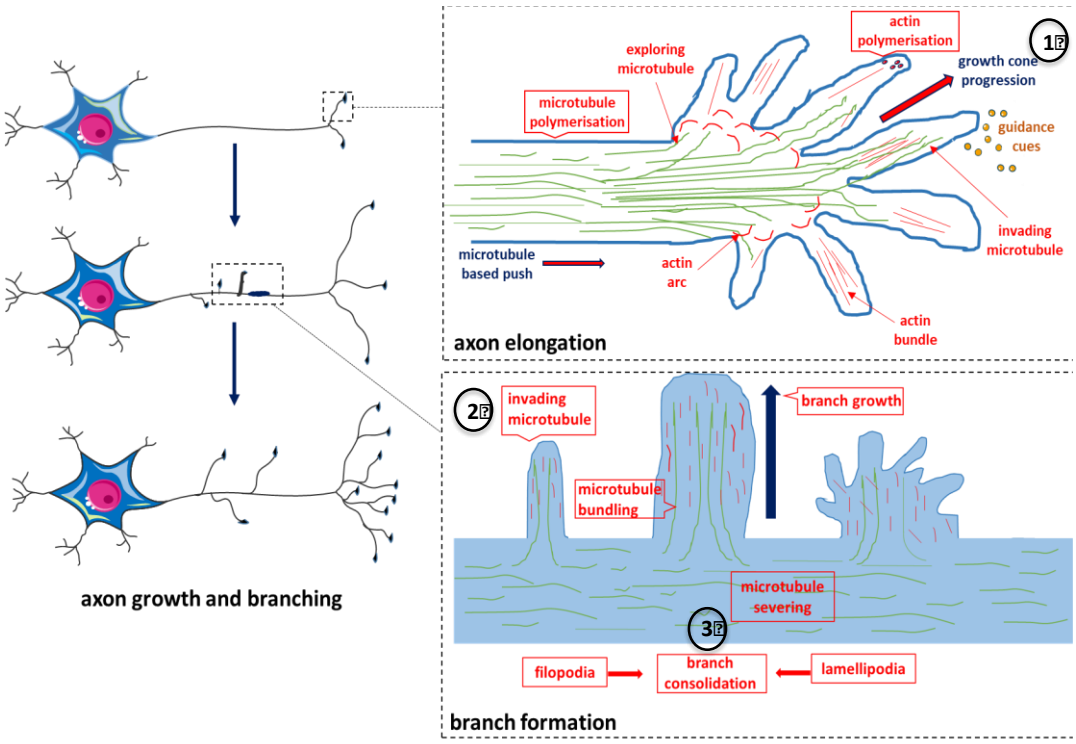

Figure 1.1 Stages of neuronal outgrowth
The neuronal cytoskeleton consists of microtubules which play pivotal roles in cell polarity and guiding axon development and dendrite arborisation. Microtubules

penetrate the central and peripheral domains of the growth cone which undergoes three distinct morphological stages: (1) protrusion, (2) engorgement and (3) consolidation.

Following axon formation, neurites develop into dendrites in a process termed dendritogenesis (Puram & Bonni, 2013). Dendritogenesis is a dynamic developmental process that is regulated by signalling cues and involves extensive cytoskeletal reorganisation (Puram & Bonni, 2013) and progression through the stages of dendritic extension, addition, elongation, retraction and pruning (Emoto, 2012; Jan & Jan, 2010). The dendritic tree of pyramidal neurons differentiates into apical and basal branches which descend from the apex and the base of the soma, respectively (Spruston, 2008). Apical and basal dendrites can be differentiated based on their size, geometry, electrical conduction and their response to neurotrophic factors and other signalling molecules (Arikkath, 2012; McAllister et al, 1995). Spinogenesis, the formation of dendritic spines occurs following dendrite formation and will be discussed in further detail below (see *section 1.2.4*).

Microtubules continue to play critical roles throughout neuronal development in the stabilisation and remodelling of dendrites, transport of motor proteins along the microtubule shaft and regulation of post synaptic density (PSD) proteins and spines (Kapitein & Hoogenraad, 2011; 2015). The continuous remodelling and organisation of microtubules relies on a vast array of microtubule regulating proteins. These include microtubule associated proteins (MAPs), microtubule plus end tracking proteins (+TIPs) and microtubule motor proteins, which modulate microtubule dynamicity, assembly, and stability throughout neuronal development (Lasser et al, 2018).

1.2.2 Microtubule associated protein 2 (MAP2) expression in mature neurons

MAPs are a family of heat stable microtubule-associated proteins found in eukaryotic cells and play important roles in neurite outgrowth and dendrite development within the CNS (Bodakuntla et al, 2019; Kapitein & Hoogenraad, 2015; Lasser et al, 2018). The MAP family share a common microtubule-binding domain and include MAP2, the ubiquitous protein MAP4 and the neuronal

protein tau. Among the MAPs, MAP2 is most abundant in the brain and primarily expressed in neurons (Cassimeris & Spittle, 2001). MAP2 exists in three alternatively spliced, developmentally regulated isoforms. The mature high molecular weight isoforms MAP2a (280 kDa) and MAP2b (270 kDa) are found throughout the life of neurons while the juvenile low molecular weight isoform MAP2c (70 kDa) is found only in immature neurons and some glia cells (Dehmelt & Halpain, 2005). These highly regulated changes in the expression of MAP2 isoforms correlate with the regulation of cytoskeleton dynamics and have been widely regarded as markers of neuronal differentiation (Sanchez et al, 2000; Soltani et al, 2005).

Recent investigations have revealed important functions for MAP2 in neuronal morphogenesis, cytoskeleton dynamics and organelle trafficking in axons and dendrites (Sanchez et al, 2000). In terms of complexity, MAP2 is reported to play a role in the maintenance of cellular architecture, internal organisation and dendrite morphogenesis (Harada et al, 2002; Yamaguchi et al, 2008). More recent research has shown that MAP2 also regulates axonal growth (reviewed by (Gumy et al, 2017) and contributes to the stabilisation of synaptic junctions through association with microtubules (Sanchez et al, 2000).

By contrast, MAP2 dysfunction is a reported characteristic of a multitude of developmental deficits and neurodegenerative disorders (Adlard & Vickers, 2002; Li et al, 2008a; Zhang & Dong, 2012). Research shows that MAP2-dependent neuroplasticity and structural integrity are significantly decreased in the hippocampus and cerebellum during aging, indicating a link between neuronal complexity and age-related pathogenesis (Di Stefano et al, 2001).

1.2.3 Synaptogenesis and synapse formation

One of the most crucial steps in the development of brain circuitry is the formation of synaptic contacts, which are points of connectivity for the transfer of a signal between two neurons (Farhy-Tselnicker & Allen, 2018). This transfer of signal, termed synaptic transmission, involves exocytosis of presynaptic vesicles containing neurotransmitters, transport across the synaptic cleft and

detection of neurotransmitters at receptors on postsynaptic neurons (*Figure 1.2*).

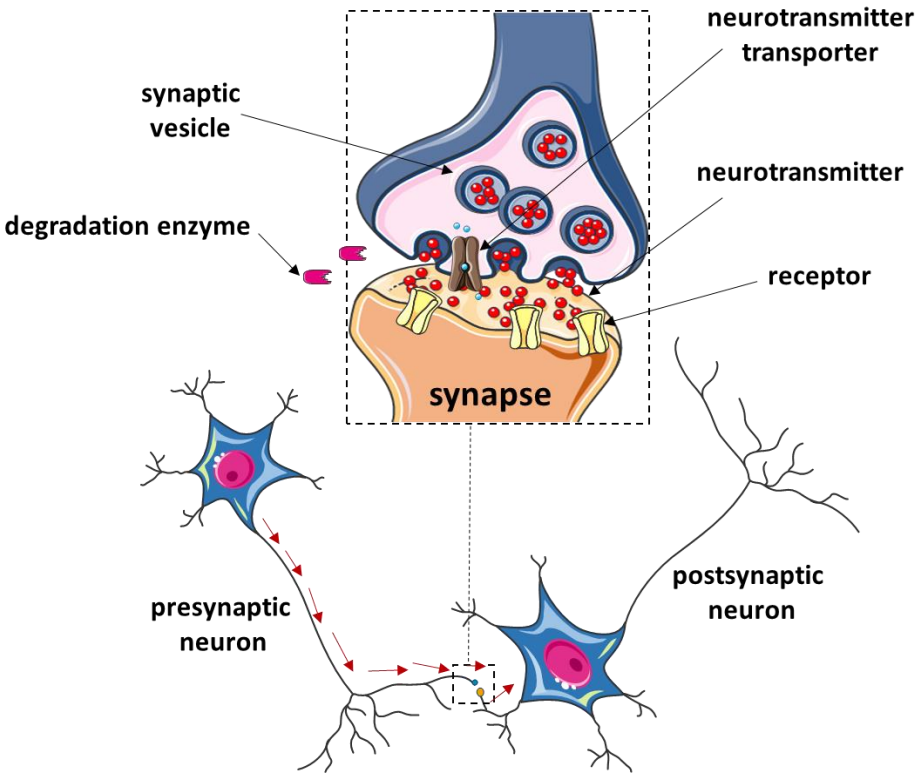

Figure 1.2 Structure of a neuronal synapse
The neuronal synapse is a point of contact for the transmission of signal between two neurons. The presynaptic neuron releases chemical messengers (neurotransmitters) from synaptic vesicles which transition across the synaptic cleft and activate receptors on the corresponding postsynaptic neuron. Activation of receptors on the postsynaptic cell produces a response in distinct signalling pathways.

The development of healthy synapses and precise alignment of pre- and postsynaptic structures at a synaptic junction is essential for ensuring fast and effective synaptic transmission (Biederer et al, 2017). Synaptogenesis is a phenomenon consisting of synapse formation, maturation, stabilisation and potentially elimination. Synapse formation is a multistep process which includes the migration of neurons toward pre-determined locations, axon and dendrite extension and the establishment of precise neuronal connectivity between the presynaptic axon of one neuron and the postsynaptic dendrite of another. Cell adhesion proteins play a critical role in this process by organising scaffolding proteins, stabilising synaptic contacts and initiating downstream cytoskeleton signalling (Bukalo & Dityatev, 2012).

During synaptogenesis, the presynaptic terminal accumulates vesicles, while the postsynaptic side recruits neurotransmitter receptors (Baldwin & Eroglu, 2017). Approximately 3000 synaptic proteins have been identified (Filiou et al, 2010) all of which play important roles in determining the distinct functional role of individual synapses. Synaptophysin has been identified as one of the most abundant pre-synaptic proteins and is employed commonly for identifying and studying pre-synaptic terminals (Micheva et al, 2010) and densities (Glantz et al, 2007). It has also been used as a marker for identifying dysfunctional synaptic connectivity in numerous neuropsychiatric disorders such as schizophrenia where reduced levels of synaptophysin have been reported in the prefrontal cortex (PFC) of subjects (Lewis & Lieberman, 2000). The major component of the post-synaptic specialisation is the scaffolding protein, post-synaptic density-95 (PSD-95). PSD-95 is thought to play an important role in anchoring other synaptic proteins and the glutamatergic N-methyl-D-aspartate (NMDA) receptor at the postsynaptic density (Glantz et al, 2007). Accumulation of synaptic proteins form the pre or post-synaptic 'puncta'- a cluster of synaptic proteins indicating formation of a stable synapse.

In general, excess synapses form during development and obsolete synapses are later eliminated in a process known as 'synaptic pruning' (Petanjek et al, 2011). Excess synapse loss is often considered a pathological hallmark of numerous neurological diseases (Koffie et al, 2011) accentuating the importance of regulating synapse formation and function throughout the lifespan. Astrocytes have been identified as important regulators of synaptic structure and function both by direct contact (Stogsdill et al, 2017) and the secretion of soluble factors (Allen et al, 2012; Farhy-Tselnicker et al, 2017; Hughes et al, 2010) including synaptotrophic extracellular matrix (ECM) proteins and thrombospondins (TSPs) (Chung et al, 2015). Astrocytic process assumes a close structural partnership with both the pre and post-synaptic structures of neuronal synapses. In this context it is possible for neurotransmitters to bind receptors on adjacent astrocyte processes and activate astrocytic signalling pathways which may in turn modulate synaptic behaviour (Papouin et al, 2017; Santello et al, 2012). This functional unit which consists of two neurons and an astrocyte has become well

known as the tripartite synapse (Farhy-Tselnicker & Allen, 2018; Pannasch & Rouach, 2013).

1.2.4 Dendritic spines: formation and function

Spines are membranous protrusions which extend from the main shaft of neuronal dendrites and are specialised to receive excitatory synaptic input and compartmentalise postsynaptic responses (Gulledge et al, 2012; Kasai et al, 2010; Tønnesen & Nägerl, 2016). Understanding spinogenesis, the process of spine formation, is essential for understanding the relationship between synaptogenesis and spinogenesis, and how they contribute to efficient neural circuit wiring and normal brain function.

Three models of spinogenesis have been proposed, namely the Sotelo model, the Miller/Peters model and the filopodial model (García-López et al, 2010). The Sotelo model describes the formation of dendritic spines from dendritic trees according to an autonomous cell program of spinogenesis. The Miller/Peters model describes the formation of dendritic spines from synapses by outgrowth of appendages on dendritic branches, and the filopodial model describes the formation of dendritic spines from a pre-existing filopodium which differentiates in response to neuronal activity.

More recently a “unifying model” for dendritic spine development has been proposed which takes into account neuronal development and plasticity in the formation of dendritic spines (García-López et al, 2010). The unifying model describes three distinct modes of spine differentiation. Mode 1 describes conversion of postsynaptic densities into synapses with development and outgrowth of a presynaptic specialisation opposite them. Mode 2 describes the development of multispines on varicosities on lateral dendritic filopodia following axonal contact. Mode 3 describes the maturation of young dendritic spines following contact with axons. Maturation of spines is thought to encourage interaction with neighbouring axons to form synapses (Shen & Cowan, 2010).

Spines are morphologically classified as thin, mushroom, stubby, filopodia or branched based on their distinct shape and size (Hering & Sheng, 2001; Swanger et al, 2011) (*Figure 1.3*).

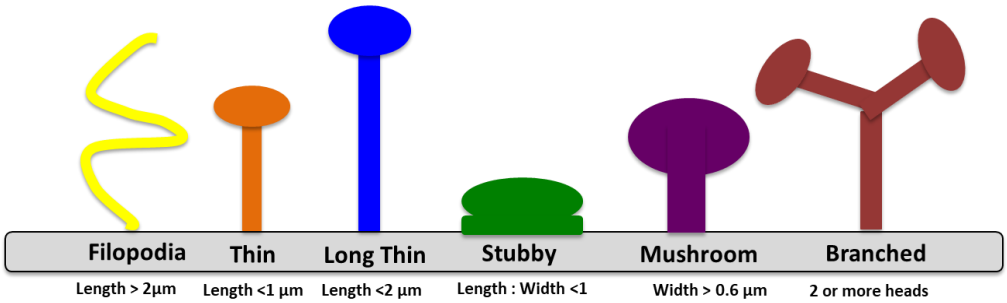

Figure 1.3 Morphological classification of dendritic spines
Dendritic spines are morphologically classified as thin, stubby, mushroom, filopodia or branched based on their shape and size, which may define their roles or functions in neuronal development.

Thin-shaped spines have a thin long neck and small bulbous head; mushroom spines are shorter and have a large mushroom-shaped head. By contrast, stubby spines lack a neck completely. Filopodia spines are longer than 5 µm and do not have a head. They are referred to as the precursors of dendritic spines (Ozcan, 2017). Thin, stubby and filopodia spines are all prevalent during early development (Kanjhan et al, 2016).

Dendritic spines are enriched in actin, and activity-dependent spine growth and remodelling is highly regulated and dependent on signal transduction (Bian et al, 2015; Tønnesen et al, 2014). Spine heads contain glutamatergic NMDA receptors (NMDARs) and there are several lines of evidence to suggest that NMDAR-mediated intracellular signalling regulates spine morphogenesis *(Figure 1.4)*.

Beneath the surface of the spine head membrane is a protein dense thickening known as the PSD (Rochefort & Konnerth, 2012). The PSD contains hundreds of proteins known to play important roles in regulating synaptic plasticity and dendritic spine architecture (Chen et al, 2015; de Bartolomeis et al, 2014). More recent evidence has shown that astrocytic growth factors such as brain derived neurotrophic factor (BDNF) also play a role in spine formation, function and maturation (Bennett & Lagopoulos, 2014; de Pins et al, 2019).

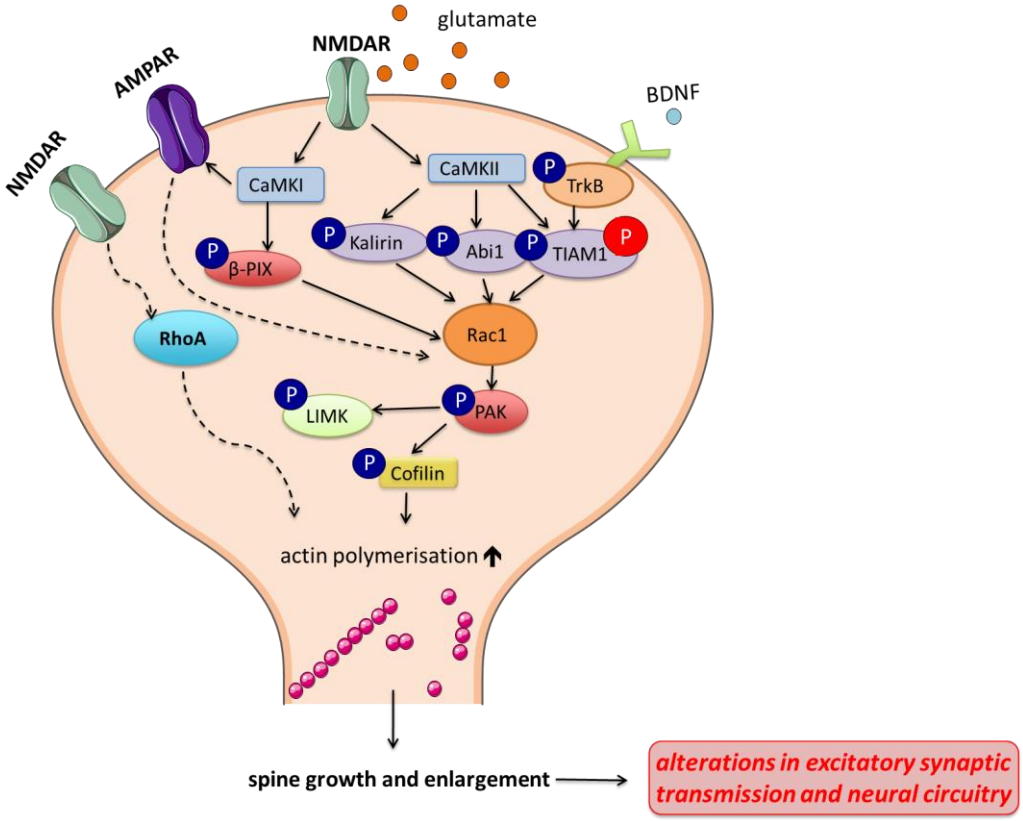

Figure 1.4 Signalling pathways involved in dendritic spine growth and development
Molecular mechanisms by which NMDAR activation regulates spine growth and enlargement include activation of downstream GTPase signalling (Tada & Sheng, 2006). Rac1 and RhoA are members of the family of small GTPases, a class of signalling molecules that transduce extracellular signals to regulate actin assembly in spines (Luo, 2002). Multiple calcium/calmodulin-dependent protein kinases (CaMKs) link the NMDAR to Rac family small GTPase 1 (Rac1) activation. CaMK-mediated phosphorylation of Rac1-specific guanine nucleotide exchange factors (GEFs) such as Kalirin-7, TIAM Rac1 associated GEF 1 (TIAM1) and Rho guanine nucleotide exchange factor 7 (β-PIX), induce Rac1 activity for spine growth and remodelling. CaMKII-mediated phosphorylation of the signalling protein Abl-interactor 1 (Abi1) releases Abi1 resulting in binding and activation of Rac1. Rac1 promotes spine growth through activation of the protein kinase N1 (PAK1) and LIM domain kinase 1 (LIMK1). LIMK1- mediated inhibition of cofilin leads to actin polymerisation. Activation of transforming protein RhoA prevents spine formation and induces spine shortening (Geraldo & Gordon-Weeks, 2009; Tashiro et al, 2000).

The unique morphology of spines engenders them ideal structures to function as postsynaptic compartments for separating synaptic terminals from dendritic shafts and regulating synaptic transmission and plasticity (Harnett et al, 2012; Tønnesen et al, 2014; Yuste, 2013). While the precise functions of spines remain questionable, it is widely agreed that morphological changes in spines provide a reliable index of alterations in excitatory synapses characteristic of behavioural deficits in CNS disorders (Jiang et al, 2013; Penzes et al, 2011; Stuss et al, 2012).

1.2.5 Neuronal atrophy and neurodegeneration

Neuronal atrophy and neuronal loss are poignant hallmarks of neurodegenerative and neuropsychiatric disorders including Alzheimer's disease (AD), Huntington's disease (HD), Parkinson's disease (PD), major depression and schizophrenia (Ahmed et al, 2016; Chen et al, 2014; Krashia et al, 2019; Lieberman et al, 2018; Veijola et al, 2014). Specifically, decreased cortical and limbic brain region volumes, reduced dendritic arborisation, and decreased number of dendritic spines and synaptic connections are well recognised indicators of CNS disorders (Banasr et al, 2011; Duman, 2014). Brain imaging and post-mortem studies of depressed patients illustrate altered brain structure and loss of functioning in brain regions associated with mood and emotion (Czéh & Nagy, 2018; Gigante et al, 2011). Understanding the mechanisms of neuronal growth and survival and the impact of disease at a cellular level is fundamental to the development of novel drug targets and treatment strategies for neurodegenerative and neuropsychiatric disorders where neuronal atrophy is implicated (Banasr et al, 2011; Duman et al, 2012; Malhi & Mann, 2018).

1.3 Glial Cells

Neuroglia are differentiated into four sub-cell types within the CNS (ependymal cells, oligodendrocytes, microglia and astrocytes) and known for their metabolic and structural support. Ependymal cells are epithelial cells that constitute the lining of the four brain ventricles. Oligodendrocytes produce myelin, an insulating sheath of fatty, proteinaceous material that permits rapid and efficient neurotransmission along CNS nerve fibres (Dutta et al, 2018; McDougall et al, 2018). Astrocytes and microglia form the basis of the research in this project and are discussed in more detail below.

1.3.1 Astrocytes

Astrocytes are the most abundant sub glial cell type within the CNS and play crucial roles in maintaining normal brain function including the regulation of brain metabolism and glutamate transmission (Sofroniew & Vinters, 2010a; Zuchero & Barres, 2015). They are non-excitable macroglial cells, distributed

throughout the cerebral matter and were originally described as passive, satellite cells that perform routine housekeeping functions within the CNS. Illumination of their structural complexity, strategic localisation and metabolic capacity, identifies astrocytes as multifunctional regulators of dynamic CNS processes (Lundgaard et al, 2014; Reemst et al, 2016). Recent evidence of astrocyte heterogeneity suggests that different subclasses of astrocytes carry out discrete roles within the CNS, depending on their specific location and interactions with neural elements (Tabata, 2015). Their characteristic non-overlapping organisation, evenly separated processes and strategic co-localisation with neuronal synapses makes them suitably placed as modulators of synaptic activity (Stogsdill et al, 2017) and the secretion of soluble factors (Allen et al, 2012; Farhy-Tselnicker et al, 2017; Hughes et al, 2010). The 'tripartite synapse', comprising two neurons and one astrocyte, accentuates the importance of this unit in modulating synaptic activity and information processing in neural circuits (*Figure 1.5*).

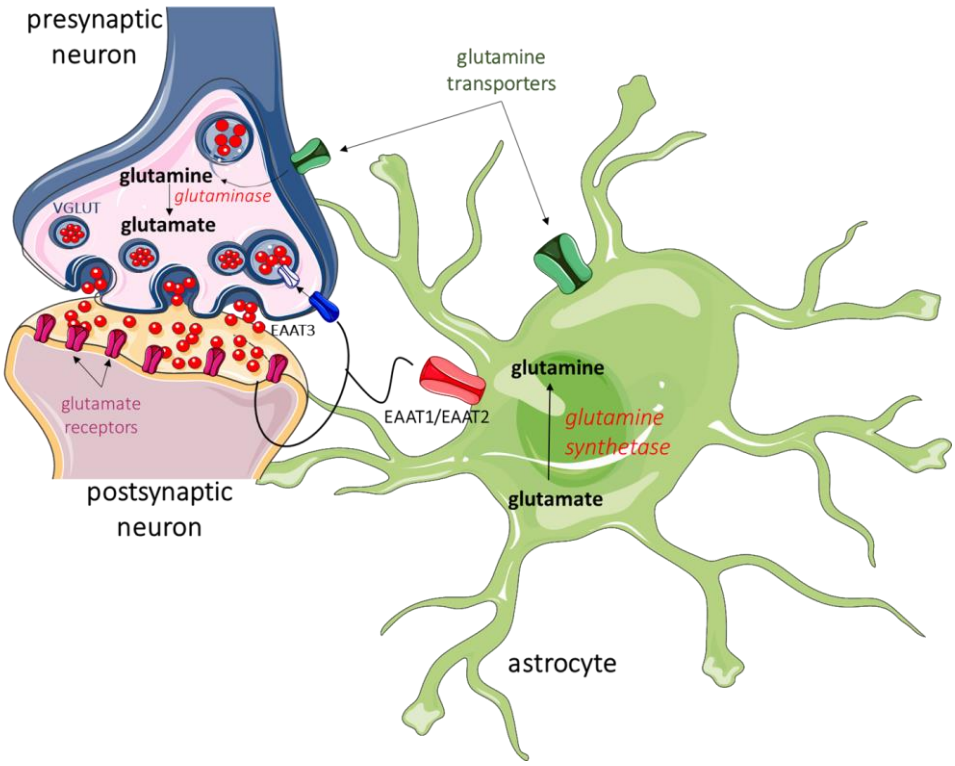

Figure 1.5 The glutamatergic tripartite synapse
The glutamatergic tripartite synapse consists of a presynaptic neuron, postsynaptic neuron and glial cell. Glutamate is released via Ca^{2+} dependant exocytosis and diffuses across the synaptic cleft where it activates glutamate receptors on the postsynaptic neuron. Astrocytes protect against over-excitation by accumulating released glutamate

and facilitating its enzymatic conversion to glutamine by the enzyme glutamine synthase. Glutamine is shuttled back to neurons where its serves as a precursor for glutamate re-synthesis. Glutaminase catalyses the hydrolytic deamidation of glutamine to glutamate and ammonia. Vesicular glutamate transporter; VGLUT. Excitatory amino acid transporter; EAAT.

Astrocytic processes at tripartite synapses express transporters for neurotransmitters such as glutamate, gamma aminobutyric acid (GABA), and glycine, which clear neurotransmitters from the synaptic space, a critical process in transmitter homeostasis (Ishibashi et al, 2019; Schousboe et al, 2014; Sofroniew & Vinters, 2010b).

Astrocytes play several additional and important roles in brain homeostasis including the uptake and conversion of glucose to lactate by anaerobic glycolysis, regulation of synaptic glutamate concentrations, production of glutathione and regulation of cerebral blood flow (*Figure 1.6*).

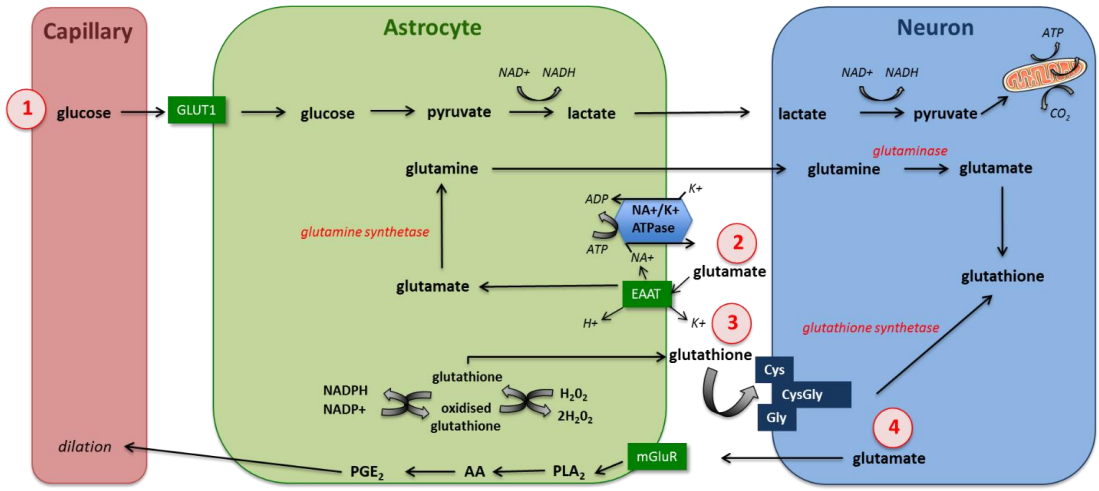

Figure 1.6 Astrocyte function in brain homeostasis
(1) In response to neuronal activity, astrocytes take up glucose from capillaries via the glucose transporter GLUT1. Anaerobic glycolysis converts glucose to lactate intracellularly before shuttling it to neurons, where it is used by mitochondria for energy production. (2) Extracellular glutamate is taken up via the astrocytic EAATs and is converted to glutamine by the enzyme GS. Glutamine is then shuttled back into neurons where it is re-converted into glutamate by the enzyme Glutaminase. (3) Astrocytes provide neurons with the antioxidant glutathione which is cleaved in the extracellular space forming CysGly. Further cleavage of CysGly by neuronal ectopeptidases produces cysteine (Cys) and glycine (Gly) which act as precursors for synthesis of glutathione. (4) Glutamate mediated activation of mGluRs produces calcium transients in astrocytes leading to the activation of cytosolic PLA_2, and the production of AA. AA generates vasodilatory prostaglandins like PGE2 which regulate capillary dilation and cerebral blood flow. Phospholipase A2; PLA_2. Arachidonic acid; AA. prostaglandin E_2; PGE_2.

Astrocytes play a critical role in CNS metabolism including regulation of the astrocyte-neuron lactate shuttle which involves astrocytic shuttling of lactate to neurons where it is utilised by mitochondria for energy production (Belanger et al, 2011; Morita et al, 2019). Enhanced glycogenolysis observed during brain activation, in conjunction with the novel correlation between astrocyte-derived lactate and memory processing further emphasises their salience in cerebral metabolism (Jha & Morrison, 2018; Newman et al, 2011). Given the important role astrocytic metabolism plays in regulating neuronal energy supplies, a reduction or impairment of astrocytic metabolic pathways may have a negative impact on neuronal functioning and development (Rama Rao & Kielian, 2015).

Astrocytes regulate synaptic glutamate concentrations and astrocytic glutamate re-uptake via the family of excitatory amino acid transporter (EAAT) proteins (Benediktsson et al, 2012; Mahmoud et al, 2019). The EAAT family of transporters consists of five Na+ dependent, high-affinity glutamate transporters of which five isoforms have been identified to date: EAAT1, EAAT2, EAAT3, EAAT4, and EAAT5 (Rose et al, 2017; Rose et al, 2018). EAAT1 and EAAT2, in humans are known respectively in murine animals as glutamate-aspartate transporter (GLAST) and glutamate transporter-1 (GLT-1). They are mainly expressed in astrocytes and responsible for the majority (up to 90%) of extracellular glutamate uptake (O'Donovan et al, 2017). EAAT3 is expressed primarily by neuronal cell bodies, EAAT4 is expressed by cerebellar Purkinje cells and EAAT5 is expressed exclusively in the retina (Zhou & Danbolt, 2014).

EAATs employ the Na^+ and K^+ electrochemical gradients to drive uptake of extracellular glutamate. Following uptake astrocytic glutamine synthetase (GS), converts glutamate to glutamine (Dantzer & Walker, 2014) which is then released and taken up by neurons to be recycled for glutamate synthesis (Schousboe et al, 2014). Prior to its release, a family of vesicular glutamate transporters (VGLUTs) transport glutamate into synaptic vesicles for storage (Ormel et al, 2012). This cycling of glutamate, termed the ‘glutamate shunt’ is highly regulated in order to maintain an extracellular concentration below 1 µM (Rose et al, 2017). For example, intracellular astrocytic glutamate down-regulates

the expression of EAAT1 to prevent the synapse becoming depleted of glutamate (Takaki et al, 2012). Inflammation also down-regulates EAATs and can result in failure of astrocytes to remove excess extracellular glutamate (Takaki et al, 2012).

Astrocytes provide neuroprotection via the production of the antioxidant glutathione which plays a critical role in the detox of reactive oxygen species (ROS) such as hydrogen peroxide (H_2O_2). More recently they have become known for the their role in neuroprotection via the secretion of soluble factors which protect neurons against toxic stimuli such as glutamate, corticosterone, methylmercury (Takemoto et al, 2015) and reactive oxygen and nitrogen species (Yates, 2015). These factors can be collected in the form of culture media – termed "conditioned media" (CM).

Astrocytes also play a role in the regulation of cerebral blood flow via the production of vasodilators. They produce vasodilators like prostaglandins in response to intracellular calcium transients or activation of metabotropic glutamate receptors (mGluR) on the astrocyte surface (Attwell et al, 2010; Gordon et al, 2011).

1.3.2 Molecular markers for the immunohistochemical identification of astrocytes markers

1.3.2.1 Glial fibrillary acidic protein (GFAP)

GFAP is a protein involved in the formation of intermediate filaments that is expressed exclusively by protoplasmic and fibrous astrocytes in the CNS (Sukhorukova et al, 2015). It has been well established as the prototypical marker for astrocyte identification both *in vivo* and *in vitro* (Sofroniew & Vinters, 2010a). GFAP exists in different isoforms and splice variants including GFAP α, β, γ, δ, and κ which are expressed heterogeneously under healthy and pathological disease states (Sullivan, 2014). It is reported to play an important role in stabilising astrocyte morphology (Moeton et al, 2016) and motility (Schiweck et al, 2018).

It is now widely accepted that astrocytes respond to CNS insults by altering their morphology including changes in the cytoskeleton. These changes can be studied and quantified by targeting GFAP (Sun & Jakobs, 2012). Alterations in GFAP have been identified in a plethora of neuropsychiatric disorders including chronic stress and depression (Rajkowska & Stockmeier, 2013; Sanacora & Banasr, 2013). Up-regulation of GFAP has become a classical hallmark of reactive astrocytes in primates and rodents (Gallo & Deneen, 2014; Herculano-Houzel, 2014; Hol & Pekny, 2015; Pekny & Pekna, 2014). Post-mortem brain studies in patients of major depressive disorder report a reduction in GFAP expression and reduction in the number of GFAP+ cells in brain regions such as the PFC (Nagy et al, 2015), anterior cingulate cortex (Gittins & Harrison, 2011) and hippocampus (Cobb et al, 2016; Torres-Platas et al, 2016).

While GFAP expression has become a prototypical marker for the identification of astrocytes, it is important to recognise the limitations of this marker (Zhang et al, 2019). GFAP is reported to be associated with only reactive astrocytes (Sofroniew & Vinters, 2010a) and may thus be considered a sensitive and reliable marker only for astrocytes responding to CNS injuries. GFAP immunohistochemistry labels main stem branches but is not necessarily present throughout the entire astrocytic cytoplasm. This can markedly underestimate the extent of astrocyte branching and volume. To add to this, GFAP expression is dynamically regulated by a myriad of inter and intra-cellular signalling molecules and is affected by regional and local variability (Sofroniew & Vinters, 2010a).

The intermediate filament proteins vimentin and nestin (Pekny et al, 2014) in addition to the transporters GLT-1 and GLAST, S100 calcium-binding protein beta (S100β), aquaporin 4 and connexins 30 (Cx30) and Cx4, (Matias et al, 2019) are among other astrocyte markers that have been employed in the study of astrocyte function and morphology. GLT-1, GS and S100β are regarded as a mature astrocyte markers (Jones et al, 2017). One advantage of GS is that it stains a wide array of astrocytes' subtypes in many regions where GFAP is not effective (Anlauf & Derouiche, 2013). However, as most of these markers are primarily distributed at the membrane of astroglial processes, rather than

throughout the cell soma, immunostaining for individual astrocytes has proven difficult when relying on one marker alone (Nagelhus & Ottersen, 2013).

1.3.2.2 S100β

The glycoprotein S100β is an astrocyte-derived calcium binding protein which is highly expressed by astrocytes of the CNS (Zhu et al, 2013). It is a member of the family of S100 proteins, which play important roles in cell differentiation, protein phosphorylation and cytoskeletal assembly (Donato et al, 2013). S100β specifically plays an important role in cytoskeletal and cell cycle regulation (Shimamoto et al, 2014). It has been used to immunohistochemically identify astrocytes and reactive astrocytes (Guerra et al, 2011).

Astrocyte secretion of S100β is modulated by various stimuli (Sorci et al, 2013). The bacterial endotoxin Lipopolysaccharide (LPS) is known to cause neurodegeneration (Batista et al, 2019; Pena-Ortega, 2017) and has been shown to decrease S100β secretion from cultured astrocytes (Guerra et al, 2011). In low nanomolar quantities S100β demonstrates neurotrophic and neuroprotective properties and is reported to promote neuronal survival and neurite outgrowth (Gazzolo & Michetti, 2010). At higher micromolar concentrations, S100β is reported to be neurotoxic and has been linked with neuroinflammation, astrogliosis, microgliosis, and neurite proliferation (Hajduková et al, 2015; Mori et al, 2010). S100β is reported to stimulate microglial migration and interact with the Receptor for Advanced Glycation Endproducts (RAGE), a ubiquitous, transmembrane immunoglobulin-like receptor known to initiate a signalling cascade associated with pathological inflammatory events (Bongarzone et al, 2017; Lasič et al, 2016).

S100β acts as a pro-inflammatory cytokine and a damage-associated molecular pattern (DAMP) factor, a factor which is released in the early stages of injury triggering tissue response to damage (Braun et al, 2017; Chen & Nuñez, 2010). Over expression or elevated levels of S100β have been documented in CNS pathologies such as major depression (Schroeter et al, 2013), AD (Chaves et al, 2010) and stroke (Zhao & Rempe, 2010). As such, there is now sufficient

evidence to reasonably confirm a role for S100β in neural injury and inflammation. S100β is less of an astrocyte-specific marker than GFAP and should not be definitively employed as a marker of astrocyte damage or dysfunction (Sorci et al, 2010). Other markers which are more specific to astrocytes include the aldehyde dehydrogenase family 1, member L1 (ALDH1L1) and aquaporin 4 (AQP4) (Sun et al, 2017; Zhang et al, 2019).

1.3.2.3 Aldehyde dehydrogenase family 1 (ALDH1L1)

ALDH1L1 is a folate enzyme required for the conversion of 10-formyltetrahydrofolate to tetrahydrofolate, a crucial step in several biochemical reactions including *de novo* nucleotide biosynthesis (Boesmans et al, 2014). Research has shown that the ALDH1L1 gene is expressed in radial glia in the midline of the embryonic CNS as well as neuronal precursors (Foo & Dougherty, 2013; Winchenbach et al, 2016). Transcriptional profiling in postnatal brain has shown that this marker is primarily expressed in astrocytes (Koh et al, 2017). Complete labelling of astrocytes can be achieve with ALDH1L1, justifying its use as a novel astrocytic marker (Tien et al, 2012; Yang et al, 2011).

ALDH1L1 is considered a reliable marker for non-reactive astrocytes that express low or undetectable levels of GFAP (Koh et al, 2017). One of the main advantages of ALDH1L1 over GFAP is that it is a highly specific antigenic marker for astrocytes with a broader pattern of astrocyte expression (Molofsky et al, 2013; Yang et al, 2011). Nevertheless, ALDH1L1 transcriptional activity has also been found in neurons in the anterior dorsal thalamus. Thus the selectivity of this marker remains elusive (Foo & Dougherty, 2013).

1.3.2.4 AQP4 an astrocytic protein implicated in neuronal plasticity

The aquaporins (AQPs) are a family of water channels expressed throughout mammalian tissues with AQP1, AQP3, AQP4, AQP5, AQP6, AQP8, AQP9, and AQP12 primarily expressed in the brain (Badaut et al, 2014). AQP4 has been recognised as the main water channel in the neuropil of the CNS and is primarily located on the perivascular endfeet of astrocytes where it mediates water movement between intra- and extracellular compartments (Nagelhus &

Ottersen, 2013). Water influx through astrocyte AQP4 is essential for the clearance of glutamate and potassium from the synaptic cleft (Haj-Yasein et al, 2012). In addition to mediating water movement, APQ4 plays an important role in development and maintenance of the blood brain barrier (BBB) (Ikeshima-Kataoka, 2016), K+ buffering, astrocyte migration and calcium signalling (Haj-Yasein et al, 2012; Nagelhus & Ottersen, 2013).

Studies using AQP4 knockout (AQP4−/−) mice have identified AQP4 as a potential regulator of synaptic plasticity, critical to a variety of higher brain functions including cognition, learning and memory (Scharfman & Binder, 2013; Skucas et al, 2011; Szu & Binder, 2016). AQP4−/− mice demonstrate a combination of impaired long-term potentiation (LTP) and delayed long-term depression (LTD) compared to wild type mice following theta-burst stimulation (Skucas et al, 2011) accentuating the important role of AQP4 in modulating brain plasticity.

Abnormalities in AQP4 expression have been reported in several neurological disorders including AD (Xu et al, 2015), PD (Sun et al, 2016; Thenral & Vanisree, 2012; Zhang et al, 2016), epilepsy (Alvestad et al, 2013; Binder et al, 2012), traumatic brain injury (Liang et al, 2015) and stroke (Liang et al, 2015). Increased expression of AQP4 has been demonstrated in the cerebrum, cerebellum, and peripheral nerves following treatment of marmosets with methylmercury (Yamamoto et al, 2012). These correlations highlight AQP4 as functionally relevant to disease physiology (Hubbard et al, 2018).

1.3.3 Glial support in structural plasticity of neurons

Neural plasticity refers to the ability of the CNS to adapt in response to changes in the environment through modifications in neural networks (Bono et al, 2017; Roelfsema & Holtmaat, 2018; Takesian & Hensch, 2013; von Bernhardi et al, 2017), connectivity (Bailey et al, 2015; Frischknecht et al, 2014; Huganir & Nicoll, 2013) and integrative functions such as learning, memory and cognition (Censor et al, 2010; Hummel et al, 2010; Soltoggio et al, 2018; Zeng et al, 2019).

There is increasing interest in the role glia play in regulating the structural changes and synaptic plasticity of neurons. Glia are thought to promote neurite

outgrowth and guide synapse formation by guiding neurons toward their target (Eroglu & Barres, 2010; Farhy-Tselnicker & Allen, 2018; Papouin et al, 2017; Reemst et al, 2016). Astrocytes, in particular, due to their strategic co-localisation with neurons and end-feet contact with central capillaries, ideally places them as important regulators of neurite outgrowth and synaptogenesis (Clarke & Barres, 2013; Farhy-Tselnicker & Allen, 2018).

There is increasing evidence demonstrating a role for astrocytes in regulating neuronal outgrowth and dendritic morphology (Previtera et al, 2010; Sofroniew & Vinters, 2010a) through the release of neuroactive substances (or gliotransmitters) such as adenosine triphosphate (ATP) (Butt, 2011; Lee et al, 2013a), ECM molecules (Frischknecht et al, 2014; Lam et al, 2019; Myers et al, 2011; Toy & Namgung, 2013) and neurotrophic growth factors (Nowacka & Obuchowicz, 2012; Takemoto et al, 2015). The neurotrophins are a family of proteinaceous growth factors that assume pivotal roles in CNS homeostasis, neuronal outgrowth and neuroprotection (Kowiański et al, 2018; Miyamoto et al, 2015; Weishaupt et al, 2014). Members of the neurotrophin family include BDNF, nerve growth factor β (NGF-β), neurotrophin-3 (NT-3) and neurotrophin-4/5 (NT-4/5)). Neurotrophins are synthesised as precursors (or [1]*pro-neurotrophins*) (Mowla et al, 2001). Glial cell line-derived neurotrophic factor (GDNF) and fibroblast growth factor 2 (FGF2) are members of the GDNF family ligand (GFL) and FGF super family respectively, that also exhibit potent neurotrophic properties (Araújo et al, 2017; Caraci et al, 2012; Noda et al, 2014; Tenenbaum & Humbert-Claude, 2017). Vascular endothelial growth factor (VEGF) is primarily noted for its angiogenic properties, but VEGF-mediated neurotrophism and neuroprotection has also been reported (Lladó et al, 2013).

Since initial discovery of the neurotrophins (Levi-Montalcini, 1987) research has since identified multiple neurotrophin receptors and signalling pathways that regulate downstream antioxidant and anti-apoptotic mechanisms critical to

[1]Neurotrophins are initially synthesised as precursors (or *pro-neurotrophins*). Pro-neurotrophins are cleaved intracellularly by furin or pro-convertases at a highly conserved amino-acid cleavage site releasing the mature protein. This proteolytic cleavage provides a degree of biological regulation as pro-forms preferentially activate the p75 receptor stimulating apoptosis, while mature forms selectively activate Trk receptors inducing cell survival mechanisms.

neuronal survival (Lawn et al, 2015; Uren & Turnley, 2014). Activation of astrocytic β1 / β2 and α1-adreoceptors results in the release of neurotrophic growth factors and increased neurite outgrowth (Kajitani et al, 2012). Activation of the β2-adrenoceptor specifically results in release of GDNF, IL-6 and FGF2 and up-regulation of the neurotrophic signalling pathways phosphoinositide 3-kinase (PI3K), mitogen-activated protein kinase (MAPK) and signal transducer and activator of transcription (STAT3) (Day et al, 2014).

In addition to neuronal outgrowth, glial cells are known to play important roles in the formation and maintenance of neuronal synapses (Chung et al, 2015; Chung et al, 2013; Eroglu & Barres, 2010; Farhy-Tselnicker et al, 2017; Papouin et al, 2017). Traditionally, astrocytes have been associated with synapse formation and reactive microglia have been associated with synapse dysfunction (Lynch et al, 2010). Early research indicates that retinal ganglion cells form fewer synapses in the absence of astrocytes in culture (Pfrieger & Barres, 1997) while conditioned media derived from healthy astrocytes induces synaptogenesis. There is also increasing evidence that astrocytes play a direct role in regulating synaptic transmission via the release of gliotransmitters such as glutamate, purines (ATP and adenosine), GABA, and D-serine which directly alter neuronal excitability (Araque et al, 2014; Diniz et al, 2012b). Methods of inducing astrocyte impairment have proven particularly useful for studying astrocyte-neuronal interactions and the impact of healthy astrocytes on neuronal integrity. The glutamate analogue α-Aminoadipate (L-AAA) has received particular attention as an effective method of selectively inducing astrocytic impairment *in vivo* and *in vitro*. L-AAA reportedly enters astroglial cells via Na+-dependent glutamate transporters and induces a transient dysfunction by inhibiting cellular functions including protein synthesis and metabolic processes (Brown & Kretzschmar, 1998; Lima et al, 2014; Olney et al, 1980; Smiałowska et al, 2013). *In vitro* studies have shown that L-AAA reduces the expression of astrocytic GFAP and GLAST (David et al, 2018) while *in vivo* studies report a prominent depletion of GFAP+ and S100β+ astrocytes up to 48 hours post injection (Khurgel et al, 1996). L-AAA-induced astrocyte dysfunction in rats predisposes to neuronal loss and dendritic atrophy (Lima et al., 2014) indicating the salience of healthy

astrocytes in brain wiring and circuitry. It has been employed experimentally to model astrocytic impairment both *in vivo* and *in vitro* (David et al, 2018; Lee et al, 2013b; Lima et al, 2014; O'Neill et al, 2019) and will be discussed in more detail in Chapter 3.

There is some evidence that microglia may also be critical for synapse maintenance and similar dysfunctions in homeostatic microglial activity may lead to synapse loss. Microglia are an important source of BDNF which may have direct implication on synaptogenesis and synaptic function (Parkhurst et al, 2013). However, in contrast to astrocytes, microglia release microglial-associated factors including inflammatory cytokines and glutamate which are known to induce neuronal atrophy and synapse loss (Doucet et al, 2015). A large number of *in vitro* assays have demonstrated that conditioned media from activated microglia induces synapse loss in primary neuronal cultures following the release of soluble microglial-associated factors including tumour necrosis factor-alpha (TNF-α), nitric oxide (NO), and IL-6 (Azevedo et al, 2013; Wang et al, 2015). More recent data shows that activated microglia release interleukin-1 alpha (IL-1α), TNF-α, and complement component 1q (C1q) which induce the neurotoxic astrocyte phenotype (Liddelow et al, 2017), which may in turn have negative effects on synapse formation and function.

1.3.4 Microglia

Microglia, the brain's primary resident immune cells are multifunctional, phagocytic regulators of cerebral immunity (Lenz & Nelson, 2018). These cells are predominantly found in the grey matter with their highest densities in the hippocampus, substantia nigra and basal ganglia. They account for approximately 5-10% of the adult brain population (Frost & Schafer, 2016). Microglia are derived from early embryonic macrophage-like mesodermal precursor cells during development which migrate to the brain parenchyma where they become resident immune cells (Ginhoux et al, 2013).

During brain development microglia are involved in synaptogenesis, synaptic pruning and axon remodelling (Pont-Lezica et al, 2011; Tremblay & Majewska,

2011). In the adult brain, however, they play a primary role in innate immunity (Lenz & Nelson, 2018), removing neurotoxic debris (Arcuri et al, 2017) and releasing neurotrophic and anti-inflammatory molecules (Loane & Byrnes, 2010b). There is also evidence to support their role in promoting neurogenesis (Yuan et al, 2017).

1.3.4.1 Microglial activation causes microglial-mediated neurotoxicity

Under normal circumstances microglia assume a down-regulated or "resting" state, characterised by a ramified morphology, small soma and fine motile protrusions (Arcuri et al, 2017; Vinet et al, 2012). This resting microglial phenotype is reported to play an important support role in synaptogenesis, neurogenesis and the release of neurotrophic factors (Ferrini & De Koninck, 2013; Sato, 2015). Under these conditions they release minimal cytokines and chemokines (Arcuri et al, 2017). However, they are highly motile and actively scan their environment for disruptions in brain homeostasis using their fine processes which undergo continuous cycles of extension and retraction (Szepesi et al, 2018). Resting microglia express low levels of surface markers such as CD11b, F4/80, Fc-gamma receptor 1 (CD64), and CD115 (Csf-1R) and ionised calcium-binding adapter molecule 1 (Iba1) which are typically present on many other tissue macrophages and/or monocytes (Gautier et al, 2012).

Iba1 is widely recognised as the prototypical immunohistological marker for microglia and is up-regulated following microglial activation (Guttenplan & Liddelow, 2019). An increase in Iba1-immmunoreactivity traditionally parallels with inflammatory induction, hypertrophy and white matter damage in stress responsive regions of the brain (Bachstetter et al, 2013; DiSabato et al, 2016; Tynan et al, 2010). Microglia constitutively express toll-like receptors (TLRs) (Heneka et al, 2015), a class of pattern recognition receptors (PRRs) which facilitate recognition and internalisation of pathogen-associated molecules that are foreign to the host. Examples of pathogen-associated molecules that activate microglia via the TLRs include pathogen-associated molecular patterns (PAMPs) such as endotoxins and endogenous DAMPs such as heat shock proteins (Lamkanfi & Dixit, 2012; Maslanik et al, 2013).

Following exposure to immunological stimuli, microglia undergo a series of morphological and functional changes and assume an activated state characterised by amoeboid morphology, retracted processes and upregulation of major histocompatibility complexes (MHCs) and complement receptors (Segal & Giger, 2016). Increased expression of cell surface markers assist recruitment of chemotactic cells from the periphery and encourage formation of phagocytic microglia (Vergara et al, 2019). Depending on the environmental milieu and stimulus, different microglial activation states (M1, M2a, M2b, M2c) have been proposed (Cherry et al, 2014; Franco & Fernández-Suárez, 2015; Orihuela et al, 2016; Prajeeth et al, 2014; Yuan et al, 2017; Zhou et al, 2017). Microglia activated by LPS, IFNγ or TNF-α assume the pro-inflammatory ‘‘M1’’ (‘‘classically activated’’) phenotype which is known to release a variety of pro-inflammatory cytokines including interleukin-1- β (IL-1β), TNF-α, STAT3, IL-6, IL-12, IL-23 (Boche et al, 2013). Conversely, the anti-inflammatory M2 phenotype is reported to promote tissue remodeling and angiogenesis by releasing the anti-inflammatory cytokines IL-10, IL-4, IL-13, and transforming growth factor- β (TGF-β) (Czeh et al, 2011).

Activated microglia (Kierdorf & Prinz, 2013) play a beneficial role when activated in a controlled manner. In general, rapid and acute activation of microglia in response to CNS injury is considered neuroprotective as it aims to combat the immediate insult and reinstate homeostasis via regulation of trophic and inflammatory mechanisms (Szepesi et al, 2018; Ueno et al, 2013). On the other hand, microglial activation that is augmented or prolonged results in morphological transition to an amoeboid shape with retracted dendritic processes, an enlarged soma and up-regulation of cell surface markers including TLRs, intracellular cell adhesion molecule 1 (ICAM-1), Iba1, cluster of differentiation molecules (CDs) and MHCII (Tian et al, 2012). Microglial activation of this kind has become widely recognised as a hallmark of chronic inflammation preceding neuronal cell death (Bachiller et al, 2018; Carniglia et al, 2017).

1.3.4.2 Microglial activation and neuroimmune cross-talk drives neuroinflammation

Microglial activation is habitually self-limiting, resolving once the invading pathogen has been contained. However, failure for an inflammatory stimulus to subside may result in an unbridled inflammatory response that is detrimental to surrounding cells and tissue (Bachiller et al, 2018; Carniglia et al, 2017; Skaper et al, 2018). The microglial derived inflammatory mediators ROS, NO, TNF-α, and interleukin IL-1β, in particular, are reported to amplify the immune response and contribute to neuronal cell death (Carniglia et al, 2017). Thus, regulation of the inflammatory response entails a delicate balance between activating protective mechanisms and dampening response to factors that may themselves inflict significant tissue pathology.

Reciprocal neuron–microglia communication is mediated by various mechanisms including contact-dependent mechanisms and the release of soluble factors and extracellular vesicles (Posfai et al, 2019). Microglial processes can interact directly with and eliminate synapses in an activity-dependant manner (Tremblay et al, 2010; Tremblay et al, 2011). This refinement in neuronal circuitry is crucial in brain development and primarily mediated by the microglial marker CD11b (Schafer et al, 2012). Microglia also have receptors which recognise and respond to neuron-derived soluble factors such as neurotrophins, neuropeptides, neurotransmitters, anti-inflammatory cytokines and chemokines (Szepesi et al, 2018). CX_3CL1 (known as fractalkine), colony-stimulating factor 1 (CSF1), and TGF-β are among the many soluble factors released by neurons that regulate microglia (Butovsky et al, 2014; Elmore et al, 2014; Kierdorf & Prinz, 2013). CX_3CL1 is one of the most prominent factors constitutively released from neurons that maintains microglia in a quiescent state by binding its receptor CX_3CR1. ATP released with increased neuronal activity also attracts microglial processes that then reduce neuronal activity via contact-mediated mechanisms (Davalos et al, 2005).

Microglia also modulate neuronal function by releasing cytokines, prostaglandins and neurotrophic factors which bind to neuronal receptors facilitating a bi-directional communication. Recent research has identified extracellular vesicles

as an important means of communication between cells in the CNS (Basso & Bonetto, 2016) and activated microglia release distinct populations of extracellular vesicles in response to various stimuli (Yang et al, 2018). Extracellular vesicles containing bioactive compounds such as metabolic enzymes, proteins, and genetic materials (Dickens et al, 2017; Lachenal et al, 2011) influence the behaviour of recipient cells via the transfer of receptors, intracellular proteins or mRNA (Basso & Bonetto, 2016).

While several pathways of communication are involved in neuronal-microglial cross-talk, the NOD-, LRR- and pyrin domain-containing protein 3 (NLRP3) inflammasome is a critical, convergent pathway worth noting. This multiprotein complex is primarily expressed in microglia, macrophages and astrocytes (Walsh et al, 2014a) and is a cytoplasmic PRR that recognises PAMPs and DAMPs induced by infectious agents and disease-related processes (Guo et al, 2015; Schroder & Tschopp, 2010). Activation of the inflammasome requires two independent signals. First, PRR ligands prime immune cells by inducing the transcription and translation of pro-IL-1β. Secondly, a signal such as ATP, triggers the formation of the inflammasome complex. Activation of the NLRP3 inflammasome regulates the activity caspase 1, which cleaves pro-inflammatory cytokines including IL-1β into their mature forms for release.

While microglia are primarily responsible for initiating inflammatory processes, it is true that neuroinflammation is a complex signalling phenomenon involving all CNS cell types and there is growing evidence to support astrocytic engagement in maintaining this process. While microglia are likely to play significant roles in initiating inflammatory response, it is likely that they are further amplified by astrocytes (Glass et al, 2010a).

1.3.4.3 Microglial activation drives the neurotoxic A1 astrocytic phenotype

Neuroinflammation and ischaemia are known to induce two different types of reactive astrocytes; the neurotoxic A1 type and the protective A2 type (Zamanian et al, 2012). During CNS injury astrocytes undergo transformation to the reactive A1 phenotype (Anderson et al, 2014; Liddelow & Barres, 2017) which is known

for its role in disease pathogenesis. Conditioned media derived from activated microglial cultures contains elevated levels of the microglial factors IL-1α, TNF-α, and C1q which work synergistically to induce the expression of this A1 reactive astrocyte phenotype (Yates, 2017). As a result, application of this combination of microglial factors to non-reactive astrocytes has been employed as a novel model to study A1 astrocytes *in vitro* (Liddelow et al, 2017).

A1 astrocytes are known for their loss of traditional astrocytic functions; they have a decreased ability to induce synapse formation and to promote neuronal survival and growth. Gene transcriptome analyses has shown that A1 reactive astrocytes up-regulate many genes including complement cascade genes which are known to be destructive to synapses (Hong et al, 2016). The inability for activated microglia to induce cell death has revealed the important role of A1 reactive astrocytes in mediating microglia-induced neurotoxicity and the salience of glial-cross talk in the pathogenesis of neuroinflammation. *In vitro* application of conditioned media from A1 astrocytes to retinal ganglion cells resulted in a 50% reduction in the number of synapses (Liddelow & Barres, 2017). Studies strongly suggest that A1 neuroinflammatory reactive astrocytes are regulated via NFkB signalling (Lian et al, 2015), which may account for their neurotoxic capacity.

By contrast, A2 astrocytes are induced by ischaemia (Zamanian et al, 2012) and promote neuronal growth and synapse repair. Their role in CNS recovery (Hayakawa et al, 2014) is likely due to the activation of the Janus kinase (JAK)–signal transducer and activator of transcription (STAT) 3 pathway. This pathway regulates multiple cell functions including proliferation, differentiation and growth during brain development (Kanski et al, 2014).

1.3.4.4 Microglial activation and signalling *in vitro*

Exposure of microglia to IFNγ and/or LPS have been traditionally employed as the mainstay methods of modelling microglia activation *in vitro* (Timmerman et al, 2018). TLR4 is the primary receptor for LPS and mediates several pro-inflammatory pathways including the phosphoinositide 3-kinase/protein kinase B

(PI3K/AKT), MAPK and mammalian target of rapamycin (mTOR), ultimately leading to nuclear factor kappa B (NF-κB) activation (Lively & Schlichter). NF-κB activation results in the production of pro-inflammatory cytokines such as TNF-α and IL-1β during neuroinflammation (Zhang et al, 2017b). *In vitro*, LPS has shown to significantly induce the transcriptional activation of pro-inflammatory factors, including inducible NO synthase (iNOS), IL-6 and TNF-α in BV2 microglial cell line (Kumar et al, 2014). LPS activated microglia inhibit neurite outgrowth and induced growth cone collapse of cortical neurons via upregulation of the cell surface repulsive guidance molecule A (RGMa) *in vitro* (Kitayama et al, 2011). LPS-induced microglial activation also induces loss of the presynaptic protein synaptophysin in mouse hippocampal slices, indicating a strong implication for glial associated inflammation in the disruption of synapses (Sheppard et al, 2019).

1.3.4.5 IFNγ mediated microglial activation

IFNγ has also been identified as a potent microglial activator *in vitro* known to induce morphological changes, up-regulation of CD11b and CD68 and the release of pro-inflammatory cytokines; IL-1β, TNF-α, IL-6, and NO (Lively & Schlichter; Papageorgiou et al, 2016). IFNs are a superfamily of cytokine secreted by immune and non-immune cells during pathogenic infection (Chen et al, 2017). They are classified into three distinct subtypes: type I, type II and type III, all of which trigger intracellular signalling cascades via the Jak-STAT pathway (Kim et al, 2015; Seif et al, 2017). Type I IFNs include IFN-α and IFN-β, type II IFNs consists of only IFNγ and type III IFNs comprise of IL-28/29. The term *interferon* is derived from the ability of these cytokines to interfere with viral replication. Type I and type III IFNs play an important role in host defence by increasing the expression of MHC class I on virus-infected cells.

IFNγ plays important roles in early immunological responses including regulation of macrophage activation, neutrophil and monocyte function, and MHC-I and -II expression (Turner et al, 2014). There is also evidence of a role for IFNγ as a cell growth inhibitor which may play an important role in the protection against tumor development (Green et al, 2017). IFNγ is secreted predominately by

activated immune cells such as T cells and natural killer cells (Pallmer & Oxenius, 2016) but may also be secreted by microglia and astrocytes. It produces its effects through interactions with the IFNγ receptor complex (IFNGR) on the surface of target cells (*Figure 1.7*).

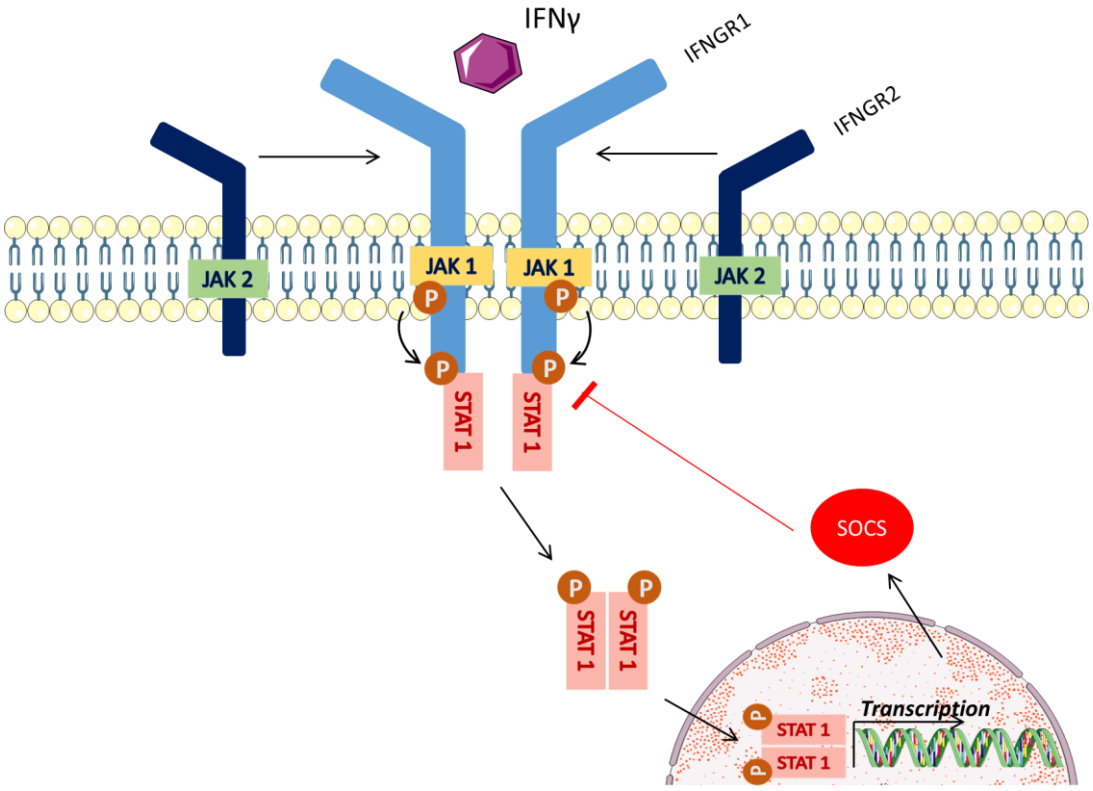

Figure 1.7 Signalling at the IFNγ receptor
IFNγ produces its effects through interactions with the IFNγ receptor complex (IFNGR) on the surface of target cells. Ligand binding to IFNGR1 results in association of IFNGR1 and IFNGR2. Association of the receptor complex signals transphosphorylation of tyrosine kinases JAK1 (associated with IFNGR1) and autophosphorylation of JAK2 (associated with IFNGR2). Activation of the signalling pathway STAT1 includes translocation to the nucleus and transcription of IFNγ related genes. Suppressor of cytokine signalling proteins; SOCS. Signal transducers and activators of transcription; STAT.

The IFNGR is a heterodimeric complex consisting of an alpha subunit IFNGR1 (90 kDa) and a beta subunit IFNGR2 (60 kDa). Ligand binding results in phosphorylation of tyrosine kinases JAK1 (associated with IFNGR1) and JAK2 (associated with IFNGR2). Activated JAKs phosphorylate specific tyrosine residues on the receptor polypeptides, which serve as a docking site for STAT proteins (Larkin et al, 2013; Ottum et al, 2015). Docking of STATs to the receptor via src-homology 2 domains results in JAK mediated phosphorylation,

dissociation of STATs from the receptor and transfer to the nucleus (Stark & Darnell, 2012).

Of the seven STAT family members, STAT1 has been identified as the primary downstream effector of IFNγ. Following JAK mediated phosphorylation, STAT1 homodimerises and translocates to the nucleus, where it initiates transcription of IFNγ-stimulated genes (ISGs). ISGs play important roles in viral clearance, cell cycle control, and inflammatory signalling (Au-Yeung et al, 2013; Majoros et al, 2017). IFNγ increases the expression of MHC class I and II on target cells in a STAT1-dependent manner (Meissl et al, 2017). This pathway is negatively regulated by several mechanisms including the induction of suppressors of cytokine signalling (SOCS) proteins whose genes are induced by STATs and which bind to JAK or cytokine receptors supressing further signalling (Yoshimura et al, 2012). SOCS-1 and SOCS-3 negatively regulate IFNγ signalling via interaction with JAK1/2 (Larkin et al, 2013). Deletion of SOCS leads to IFNγ-dependent chronic inflammation (Alexander & Hilton, 2004; Alexander et al, 1999).

Microglial activation by IFNγ involves increased expression of cell surface molecules and production of pro-inflammatory cytokines which facilitates infiltration of immune cells (Boche et al, 2013; Browne et al, 2013; Dungan et al, 2014). IFNγ serves in the priming of microglia, producing changes in morphology, receptors and cytokine release profile (Perry & Holmes, 2014). It induces hypertrophy with shortening and flattening of cellular processes, up-regulation of MHC-II and CD86, and increased levels of IL-6 and TNF-α (Grau et al, 1997; Kong et al, 2002; Papageorgiou et al, 2016). Activation of the IFNγ signalling pathway plays important role in apoptosis, neuronal atrophy and synapse loss (de Weerd & Nguyen, 2012) and increased levels of IFNγ have been implicated in numerous CNS pathologies (Seifert et al, 2014). Several observations suggest that the signals resulting from the binding of IFNγ to its receptor are dependant on the number of surface receptors transducing the signal. The IFNγ receptor is ubiquitously expressed allowing IFNγ to act upon most cell types and elicit a response in various body tissues (Hu & Ivashkiv, 2009). However, the IFNGR2 chain is often considered the limiting factor because while it is constitutively

expressed, its expression level is tightly regulated by cellular differentiation and activation states (Bach et al, 1997; Schroder et al, 2004). Furthermore, expression levels of the receptor are known to fluctuate under various pathological conditions and have shown to be upregulated in response to various pro-inflammatory cytokines such as IL-1 and TNF-α, resulting in an enhanced ability of cells to respond to lower concentrations of IFNγ. Increased expression of the IFNγ receptor by IL-1β specifically has shown to be dependent on NF-κB transactivation (Shirey et al, 2006).

1.3.5 IL-6 in neuroinflammation and glial homeostasis

IL-6 is one of the primary pro-inflammatory cytokines released from activated glia during inflammation (Boche et al, 2013; Glass et al, 2010b). It is a member of the group of four-helical bundle cytokines which also includes IL-11, IL-31, cardiotrophin-1, ciliary neurotrophic factor (CNTF), cardiotrophin-like cytokine (CLC), granulocyte-colony stimulating factor (G-CSF), leptin, leukemia inhibitory factor (LIF), neuropoietin and oncostatin M (Unver & McAllister, 2018). Transcription of IL-6 involves NF-kB signalling and is effectively induced by the NF-kB-activating factors LPS, IL-1, and TNF-α (Wolf et al, 2014).

Under normal physiological conditions IL-6 levels in the brain are relatively low but increase dramatically during inflammation (Chen et al, 2016b; Giménez-Llort et al, 2012; Zheng et al, 2016). Overproduction of IL-6, in turn, has shown to lead to chronic neuroinflammation and neurodegeneration associated with a multitude of neurological and neuropsychiatric disorders (Chen et al, 2018; Dowlati et al, 2010; Dursun et al, 2015; Rothaug et al, 2016).

IL-6 elicits its effects by binding the IL-6 receptor complex which consists of the IL-6 α-receptor (IL-6R) and the signal-transducing β-subunit glycoprotein 130 (gp130) (Erta et al, 2012) (*Figure 1.8*). Binding of IL-6 to its membrane-bound IL-6R induces classical or “cis” signalling and anti-inflammatory effects (Hoge et al, 2013). In this case, the IL-6/IL-6R complex associates with a second receptor protein, gp130, which dimerises and initiates cellular signalling (Scheller et al, 2014). Suppressor of cytokine signalling 3 (SOCS3) is an important negative regulator of gp130 which is rapidly up-regulated by IL-6 and leads to negative

feedback of gp130 signalling. Classical signalling plays a neuroprotective role in the CNS including neural tissue regeneration and bacterial defence (Rose-John, 2017). Neuroprotective roles of IL-6 include its ability to promote nerve regeneration following inflammatory stimuli, protect against neurotoxic effects of methyl-4-phenylpyridinium (MPP+), and protect against neuronal loss during infection (Chucair-Elliott et al, 2014; Leibinger et al, 2013; Xia et al, 2015).

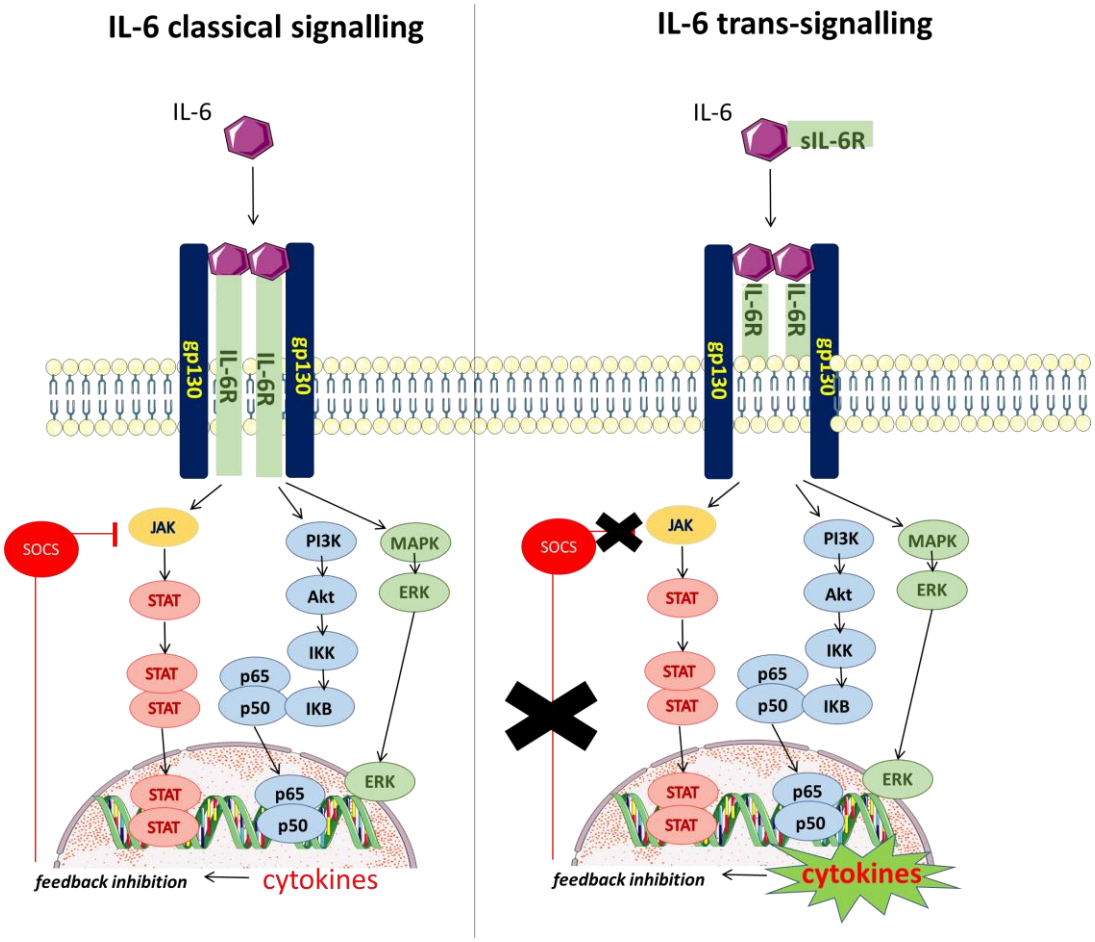

Figure 1.8 IL-6 activates classical or trans-signalling
In cells with a membrane-bound IL-6 receptor (IL-6R) IL-6 binds the receptor leading to IL-6 classical signalling. In cells that express the membrane gp130 but lack the cell-surface IL-6R, IL-6 initiates trans-signalling by binding the soluble IL-6R (sIL-6R) forming a sIL-6R/IL-6 complex. Formation of this complex activates the JAK/STAT3 signalling pathway. Classical IL-6 signalling is important for the acute-phase immunological response and promotes anti-inflammatory activities, whereas trans-signalling promotes pro-inflammatory activities. The pathway is negatively regulated by Suppressor of cytokine signalling proteins (SOCS).

Binding of IL-6 to the soluble form of IL-6R (sIL-6R) is termed trans-signalling. It occurs in cells expressing gp130 resulting in the production of pro-inflammatory cytokines and chronic inflammation (Rose-John, 2012; Wolf et al, 2014). Trans-

signalling is known to play a role in neuronal degeneration (Rothaug et al, 2016) and is regarded as the prevailing mechanism responsible for IL-6 mediated pathology (Baran et al, 2018; Campbell et al, 2014). The basis of trans-signalling is sIL-6R binding to IL-6 in the extra cellular matrix forming the IL-6/sIL-6R complex. This complex has an increased binding affinity to membrane-bound gp130 subunits, resulting in signalling in any cell type that express gp130 (Jones et al, 2005). gp130 is ubiquitously expressed in almost all cell types including astrocytes and neurons and permits trans-signalling following complexation of sIL-6R with IL-6 in these cells where the surface-bound IL-6R is not expressed (Erta et al, 2012).

1.4 The Kynurenine pathway – forging a link between neuroinflammation, neuronal atrophy and degeneration

Pro-inflammatory cytokines including IL-6 induce a specific metabolic pathway known as the Kynurenine pathway (KP) (Kindler et al, 2019; Prendergast et al, 2011). The KP is a tryptophan catabolism pathway that is induced in times of stress and immune activation. Initially tryptophan is converted to kynurenine and subsequently into a range of metabolites with neuro-modulatory properties (*Figure 1.9*).

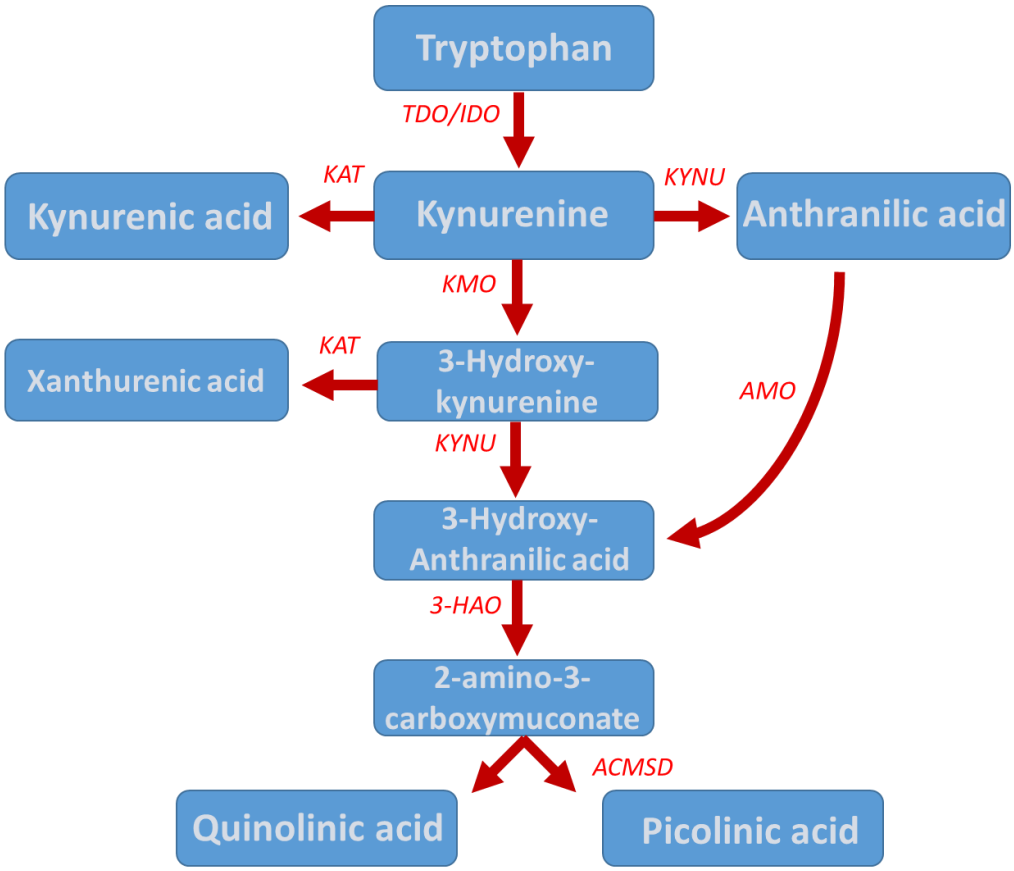

Figure 1.9 The Kynurenine pathway
The initial conversion of tryptophan to kynurenine requires induction of either of the rate limiting enzymes tryptophan 2, 3-dioxygenase (TDO), or indoleamine 2, 3-dioxygenase (IDO). Kynurenine is transaminated into kynurenic acid (KYNA) by kynurenine aminotransferase (KAT), or converted to 3-hydroxykynurenine (3-HK) by kynurenine monooxygenase (KMO). Alternatively, kynurenine may be converted directly to anthranilic acid by kynureninase (KYNU). Anthranilic acid can then be converted directly to 3-hydroxyanthranilic acid (3-HAA) by anthranilate 3-monooxygenase (AMO). 3-HK is then metabolised into 3-HAA by kynureninase (KYNU) or transaminated into xanthurenic acid by KAT. 3-HAA is further metabolised to the unstable intermediate, 2-amino-3-carboxymuconate by 3-hydroxyanthranilic acid 3, 4-dioxygenase (3-HAO). It may then be enzymatically converted to picolinic acid, or non-enzymatically transformed to quinolinic acid by the enzyme aminocarboxymuconate-semialdehyde decarboxylase (ACMSD).

The KP has important physiological roles associated with anti-pathogenic responses (Szalardy et al, 2012). It is important for energy metabolism during the immune response as it drives production of nicotinamide adenine nucleotide (NAD+), an important co-factor for energy production and cell viability (Castellano-Gonzalez et al, 2019; O'Farrell & Harkin, 2017). In recent years the KP has become implicated in several CNS disorders and the regulation of kynurenine metabolism has been intensively investigated (Haroon et al, 2012; Schwarcz et al, 2012a). The pathway has been implicated in a range of neuropsychiatric

disorders and neurodegenerative diseases (Bohar et al, 2015; Karakuła-Juchnowicz et al, 2014; Reus et al, 2015) including AD, PD, multiple sclerosis and stroke (Cuartero et al, 2014; Lim et al, 2010; Maddison & Giorgini, 2015; Tan et al, 2012b). The KP has therefore become an important target for the development of biomarkers and treatments for a range of CNS-related illnesses.

1.4.1 The KP, metabolites and enzymes

Tryptophan is an essential α-amino acid required for protein synthesis and as a precursor for neurological compounds including serotonin and melatonin (Schwarcz et al, 2012a). Tryptophan circulates in the blood, with 70-90% bound to albumin, and is transported in the form of this tryptophan-albumin complex across the BBB where free tryptophan is released into the brain (Höglund et al, 2019). Glial cells take up free tryptophan which is metabolised through the KP resulting in the production of neuroactive metabolites and NAD+ (Schwarcz et al, 2012a; Vecsei et al, 2013).

The initial conversion of tryptophan to kynurenine requires induction of either of the rate limiting enzymes, tryptophan 2, 3-dioxygenase (TDO), or indoleamine 2, 3-dioxygenase (IDO). Under normal physiological conditions kynurenine is derived from peripheral sources. However, during neuroinflammation >98% is produced locally. Kynurenine is converted to kynurenic acid (KYNA) by the kynurenine aminotransferase (KAT) enzymes, of which there are four main subtypes (KATI, KAT II, KAT III, KAT IV). All four subtypes of KAT are involved to varying degrees in the irreversible transamination of kynurenine to KYNA (Agudelo et al, 2014; Zinger et al, 2011). KAT II is primarily responsible for the production of KYNA (75%) in the brain due to the inability of KYNA to cross the BBB (Zinger et al, 2011). It is expressed in both microglia and astrocytes (Guillemin et al, 2007; Guillemin et al, 2001).

Alternatively, kynurenine may be converted to 3-hydroxykynurenine (3-HK) by the flavin adenine dinucleotide dependent monooxygenase enzyme kynurenine monooxygenase (KMO), or to anthranilic acid by kynureninase (KYNU). 3-HK is further metabolised to 3-hydroxyanthranilic acid (3-HAA) by KYNU, or to

xanthurenic acid by KAT. 3-HAA undergoes further conversion to the unstable intermediate, 2-amino-3-carboxymuconate by 3-hydroxyanthranilic acid 3, 4-dioxygenase (3-HAO). This metabolite is further enzymatically converted to picolinic acid, or non-enzymatically transformed to quinolinic acid (QUIN) (Fujigaki et al, 2017; Lugo-Huitrón et al, 2013; Vecsei et al, 2013).

IDO is one of the rate limiting enzymes involved in the initial conversion of tryptophan to kynurenine. It has a broader substrate specificity than TDO. It is expressed extra-hepatically in the intestine, lung, placenta, brain and spleen and in astrocytes, macrophages, microglia and neurons (Lim et al, 2010) in the CNS and periphery (Mándi & Vécsei, 2012). IDO is induced by pro-inflammatory cytokines and inflammatory stimuli such as IFNγ (Mándi & Vécsei, 2012; Wirthgen et al, 2017). IDO may also be indirectly induced by low-grade inflammation and stress-inducible pathways (Kiank et al, 2010).

TDO, is a homotetrameric enzyme primarily expressed in the liver and expressed in lower levels in astrocytes, neurons and endothelial cells (Wu et al, 2013). Its expression is regulated by various mechanisms including the availability of tryptophan (Kim et al, 2013; Myint & Kim, 2014). TDO is induced by corticosteroids and glucagon, however there is also evidence that it may be indirectly induced by immune activation and glucocorticoid receptor activation (Walker et al, 2013). Stress-induced activation of the hypothalamic pituitary adrenal (HPA) axis activates TDO via the release of glucocorticoids from the adrenals and activation of intracellular glucocorticoid receptors (Kim & Jeon, 2018; O'Farrell & Harkin, 2015). Changes in the expression of TDO mRNA in the developing and adult brain suggests that TDO is important to the development of specific brain regions including the hippocampus and cerebellum (Kanai et al., 2010). Thus, it is hypothesised that altered TDO expression may predispose to behavioural changes characteristically associated with neuropsychiatric disorders in adult life (Funakoshi et al, 2011).

1.4.2 KP compartments in the CNS

The KP is known to be differentially compartmentalised within astrocytes and microglia, often termed the "neuroprotective" and "neurotoxic" branches, respectively. Based on this compartmentalisation, KMO and KATs regulate the balance of QUIN:KYNA uptake and metabolism. Following the initial production of KYN from IDO, KP enzymes downstream are differentially expressed resulting in two functionally distinct KP branches (Fujigaki et al, 2017) (*Figure 1.10*).

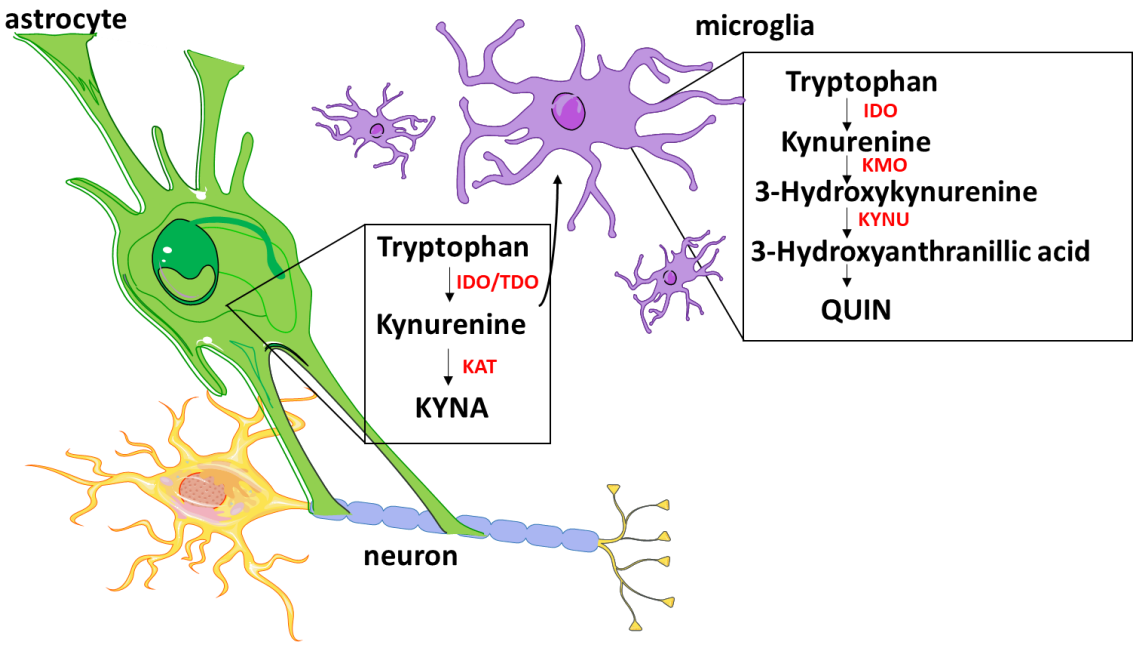

Figure 1.10 Compartmentalisation of the kynurenine pathway
The KP is compartmentalised differentially within astrocytes and microglia in the CNS. Astrocytic uptake and metabolism of tryptophan results in the production of the neuroprotective metabolite KYNA. On the other hand, microglial uptake and metabolism of tryptophan results in the production of the neurotoxic metabolites 3-HK, 3-HAA and QUIN. The excitotoxic metabolite QUIN acts at NMDA-type glutamate receptors and synergises with 3-HK resulting in oxidative stress.

Astrocytes preferentially express KAT which drives the neuroprotective arm (Dostal et al, 2017) and the production of KYNA (Rossi et al, 2019; Schwarcz et al, 2012a). The lack or limited expression of KMO in astrocytes means they are unable to produce the neurotoxic metabolite QUIN (Kindler et al, 2019). Hence, the astrocytic arm is often considered the 'neuroprotective arm'. Microglia, on the other hand preferentially express the enzymes KMO and KYNU (Garrison et al, 2018a; Suzuki et al, 2019) resulting in downstream production of the neurotoxic metabolites 3-HK, 3-HAA, and QUIN (Lugo-Huitron et al, 2013;

Pierozan et al, 2015). Microglia preferentially express KMO, on the outer membrane of mitochondria which is responsible for the generation of neurotoxic KP metabolites (Garrison et al, 2018a; Hutchinson et al, 2017; Parrott et al, 2016; Raison et al, 2010). Thus, the microglial arm is often regarded as the 'neurotoxic arm' of the KP.

Preferentially targeting one arm of the KP may provide a means to counterbalance shifts in pathway activation in neurological disorders (O'Farrell & Harkin, 2015). However, it is important to bear in mind that astrocytes also produce KYN which can be taken up by neighbouring microglia and may indirectly contribute to production of QUIN. Furthermore, as both cells express IDO, inflammatory cytokines have the potential to activate both arms of the pathway (Dostal et al, 2017) and it may be an over-simplification to consider the two branches of the pathway distinct.

1.4.3 Neuroactive effects of kynurenine pathway metabolites and consequences for neuronal viability and plasticity

Imbalance of KP metabolites is reported in a plethora neuropsychiatric disorders such as depression, anxiety and schizophrenia (Lovelace et al, 2016; Parrott et al, 2016; Tan et al, 2012a) as well as neurodegenerative diseases such as AD, PD and HD (Dantzer & Walker, 2014; O'Farrell & Harkin, 2015; Vecsei et al, 2013). Elevated levels of neurotoxic KP metabolites in neurological diseases implies imbalance between the two branches of the KP (Tan et al, 2012a). KP metabolites are reported to act on various neuronal targets modulating neuronal function (Szalardy et al, 2012; Verstraelen et al, 2014a) neuronal transmission, neuronal viability, complexity and plasticity (Ferrante et al., 2013).

1.4.3.1 Kynurenic acid

KYNA is regarded as the primary neuroprotective metabolite of the KP. As KYNA cannot cross the BBB it must be transported first in the form of kynurenine. KYNA acts as an endogenous, competitive antagonist of the NMDAR and a weak antagonist of the α-amino-3-hydroxy-5-methyl-4-isoxazolepropionic acid (AMPA) and kainate receptors (Vécsei et al, 2012). Regulation of KAT activity maintains

KYNA at a physiological concentration between 0.14 and 1.58 µM (Turski et al, 2013). In this range KYNA acts as an antagonist at the glycine recognition and co-agonist sites of the NMDAR complex (Szalardy et al, 2012) as well as a non-competitive inhibitor of the α7 nicotinic acetylcholine receptor (α7nAChR) (Albuquerque & Schwarcz, 2013) suppressing presynaptic glutamate release (Vécsei et al, 2012). At higher concentrations KYNA can also act as an antagonist of the AMPA receptor and glutamate binding sites of the NMDAR which may be important in providing protection against excitotoxicity (Ramos-Chávez et al, 2018; Schwarcz et al, 2012a).

In addition to its effects at glutamate receptors, KYNA has several other targets. It can also bind the G protein-coupled receptor 35 (GPR35) and the aryl hydrocarbon receptor. The exact role of these receptors in the CNS requires further research (Schwarcz et al, 2012a). In addition to its actions at receptors, KYNA is noted for its antioxidant capacity and ability to scavenge free radicals (Lugo-Huitron et al, 2011). Despite its neuroprotective qualities, KYNA may become toxic above physiological concentrations resulting in the disruption of glutamatergic transmission with implications on neuronal functioning and connectivity.

1.4.3.2 3-Hydroxyanthranilic acid and 3-Hydroxykynurenic acid

3-HAA and 3-HK are neurotoxic metabolites that contribute to the generation of free radicals (Bohar et al, 2015; Lovelace et al, 2016), lipid peroxidation and oxidative stress (Parrott & O'Connor, 2015). 3-HAA and 3-HK inhibit various complexes of the electron transport chain (Schuck et al, 2007) resulting in mitochondrial dysfunction (Maes, 2011) and activation of oxidative and nitrosative pathways thought to play a role in neuronal damage and death (Glass et al, 2010a; Maes, 2011; Muller, 2013; Reyes-Ocampo et al, 2015a). The toxicity of 3-HK on neuronal cultures has been attributed to its ability to generate ROS and initiate apoptosis (Zinger et al, 2011). Increased levels of 3-HK have been reported in numerous neuropsychiatric disorders including AD, PD and HD (Bohár et al, 2015).

1.4.3.3 Quinolinic acid

Of the three neurotoxic metabolites QUIN is considered the most important in terms of biological activity. Brain concentrations of QUIN are usually maintained at nanomolar concentrations. However, levels rise drastically during inflammation (Lugo-Huitron et al, 2013) and above 300 nM QUIN is reported to become toxic (Guillemin, 2012).

The toxicity of QUIN is exerted mainly through NMDAR-mediated excitotoxicity. QUIN acts as a weak, competitive agonist of the NMDAR at the NR2A and NR2B subunits (Guillemin, 2012). Due to its higher affinity for the NR2B subunit it is found predominately in the forebrain (Vécsei et al, 2012). QUIN-induced activation of the NMDAR has been shown to produce excitotoxicity associated with neuronal damage in the rat brain (Zinger et al, 2011). QUIN-induced neuronal injury is thought to result from interference with the axonal cytoskeleton (Pierozan et al, 2015) and can be rescued with the NMDAR antagonist MK801 (Pierozan et al, 2010).

In addition to its activity at the NMDAR, QUIN can directly stimulate glutamate release from neurons and inhibit its uptake by astrocytes (Lugo-Huitrón et al, 2013). This impairment of the glutamate-glutamine cycling can lead to increased synaptic glutamate concentrations and excitotoxicity-induced neuronal damage (Pierozan et al, 2012). It is also known to generate ROS through lipid peroxidation resulting in mitochondrial and cell damage (González Esquivel et al, 2017a).

1.4.4 The KP in neuroinflammation

Imbalance of KP metabolites has been demonstrated in neuroinflammatory events including excitotoxicity, oxidative stress (Pérez-De La Cruz et al, 2012) and mitochondrial dysfunction (López-Doménech et al, 2016; Reyes-Ocampo et al, 2015a). Under physiological conditions the KP is tightly regulated. However, immune stimulation and pro-inflammatory mediators including TNF-α, IFNγ, IL-6 and IL-1β are known to induce KP enzymes (Dantzer, 2017; Schwieler et al, 2015; Zunszain et al, 2012).

IFNγ is the most potent inducer of IDO and has been traditionally employed as a microglial activator (Vécsei et al, 2012; Wirthgen et al, 2017). It can induce the neurotoxic enzymes KMO and KYNU and is regarded as the primary stimulus for studying KP activation *in vitro* (Lim et al, 2013; Pallotta et al, 2011). Unbridled production of pro-inflammatory cytokines, abnormally elevated expression of chemokines and infiltration of circulating immune cells are events of chronic neuroinflammation (Glass et al, 2010b) that have been linked with induction of KP enzymes and KP activation. Microglia isolated from KMO-/- mice display a reduced pro-inflammatory response compared to wild-type (Garrison et al, 2018b).

Stress mediated activation of the HPA axis (O'Farrell & Harkin, 2017) and KP enzymes (Gibney et al., 2014) has been extensively investigated. Stress and inflammation are associated with neuronal atrophy, characterised by loss of synaptic connections in key cortical and limbic brain regions implicated in depression (Duman, 2014; Duman et al, 2016; Liu et al, 2017b). Thus, it is plausible that stress-induced activation of the KP may also contribute to alterations in the structural plasticity of neurons and remodelling of synaptic connections.

1.5 Aims and objectives

Previous *in vitro* research has shown that conditioned media drawn from IFNγ treated mixed glia and microglia result in reductions in neurite outgrowth and reduction in the co-localised expression of synaptic proteins. More recent research suggests that reactive astrocytes contribute to glial driven neuronal atrophy and L-AAA-induced astrocyte impairment may be protective in this context. Nevertheless, knowledge of the distinct mechanisms underlying glial mediated changes in neuronal integrity and plasticity under inflammatory conditions is currently limited. The primary aim of this thesis is to investigate selected mechanisms and mediators involved in inflammatory driven, astroglial associated alterations in neuronal integrity, complexity and co-localisation of synaptic proteins *in vitro*.

In order to extend our knowledge of the impact of L-AAA induced astrocyte impairment, this thesis aims to characterise the impact of L-AAA on inflammatory-naïve primary cortical astrocytes; the effects of L-AAA on astrocytic morphology, expression of astrocytic markers and measures of oxygen consumption rate and glycolysis. Following on, this thesis aims to further determine the effects of L-AAA on stimulated reactive astrocytes and the impact of conditioned media drawn from reactive astrocytes treated with L-AAA on the integrity of mature primary cortical neurons.

The second part of this research explores selected mechanisms associated with IFNγ-driven glial activation using enriched cultures of primary cortical microglia and astrocytes. It aims to illustrate a role for reactive astrocytes in mediating inflammatory driven neuronal atrophy and examines the role of a candidate cytokine IL-6, in mediating glial associated changes in neuronal integrity and inflammatory associated neuronal atrophy *in vitro*.

The final section of this thesis aims to assess a potential role for KP induction as a mediator of inflammatory-driven glial-associated deficits in neuronal complexity. Efforts to rescue these effects are made by pharmacologically inhibiting the KP in glial cells. A greater understanding of these mechanisms is of interest in the context of identifying targets and developing novel treatments for inflammatory CNS disorders.

2 Materials and Methods

2.1 Materials

2.1.1 *In vitro* studies

2.1.1.1 Animals

Wistar rats (male/female)	Comparative Medicine, TCD

2.1.1.2 General equipment

Aspirator pump	Integra Biosciences
Autoclave	Sanyo, Ireland
Axio Imager Z1	Carl Zeiss
Biosafety cabinet	ADS Laminaire, France
Centrifuge: Legend RT+	Sorvall, Ireland
Gyro rocker	Stuart, Ireland
Haemocytometer	VWR, Ireland
Laminar flow hood	ADS Laminaire, France
Microscope: CKX41	Olympus, UK
Microscope: Axio Imager Z1	Carl Zeiss, UK
Nanodrop® ND1000 Spectrophotometer	Thermo Fisher Scientific
Needles, hypodermic (25G)	Microlance BD
Peristatic pump	Gilson
pH meter	Mettler-Toledo, Ireland
Plate reader	Biotek
Scale (precision)	Mettler-Toledo, Ireland
SP8 confocal microscope	Leica
StepOnePlus™ Real-Time PCR System	Applied Biosystems
Thermal Cycler (PTC-200 Peltier)	MJ Research, US
Thermo Steri Cycle CO_2 Incubator Hepa Class 100	Bio-Sciences Limited, Ireland
Vortex	Ika, Ireland
Water bath	Grant, Ireland
XF24 Analyser	Seahorse, Biosciences

2.1.1.3 General consumables

6-, 24- and 96-well plates	Sarstedt, Ireland

Biosphere filter tips (10, 20, 100, 200, 1000 µL)	Sarstedt Ltd., Ireland
Cell culture flasks (T-75 cm^2)	Corning, Ireland
Cell scrapers	Sarstedt, Ireland
Cell strainers (40 µm)	BD Falcon VWR, Ireland
Falcon tubes (15 mL, 50 mL)	Sterile Sarstedt, Ireland
Filter units (0.22 µm), single-use (Millex)	Millipore, Ireland
Glass coverslips (13 mm)	VWR, Ireland
Haemocytometer	VWR, Ireland
Laboratory tissue rolls	VWR Int., Ireland
Microscope slides 76 mm x 26 mm	Fisher Scientific, Ireland
Microtubes (0.5 mL, 1.5 ml, 2 mL)	Sarstedt, Ireland
Parafilm	VWR, Ireland
Microscope slides 76 mm x 26 mm	Fisher Scientific, Ireland
Microtubes (0.5 mL, 1.5 mL, 2 mL)	Sarstedt, Ireland
Pasteur pipettes (3.5 mL)	Sarstedt, Ireland 45
Petri dishes (90 mm)	Fisher Scientific, Ireland
Pipettes (manual and automated)	Gilson Inc.
Pipette tips (200 µL, 1000 µL)	Sarstedt, Ireland
Pipettes (5 mL, 10 mL, 25 mL), sterile	Sarstedt, Ireland
Scalpels, disposable, sterile (Swann-Morton)	Fisher Scientific, Ireland
Serological pipette (10, 25 mL)	Sarstedt, Ireland
Syringes (20 mL, 50 mL)	Fisher Scientific, Ireland
Syringe filters (0.2 µm)	Pall Corporation, USA
Transfer pipettes (sterile; 3 mL)	Sarstedt, Ireland
XF24-well cell culture plate	Seahorse, Biosciences

2.1.1.4 General laboratory chemicals

Absolute Ethanol	Hazmat, TCD
β-mercaptoethanol	Sigma Aldrich, Ireland
Biocidal ZFTM	WAK-Chemie, Germany
Calcium chloride ($CaCl_2$)	Sigma Aldrich, UK
Dimethyl sulfoxide	Sigma Aldrich, UK

D-(+)-Glucose Bioextra	Sigma Aldrich, UK
Fluorescein sodium salt	Sigma Aldrich, UK
HEPES	Sigma Aldrich, UK
Magnesium sulfate ($MgSO_4$)	Fisher Scientific Ltd
Methanol	VWR Int., Ireland
Microscint 40	PerkinElmer
Monopotassium phosphate (KH_2PO_4)	Fisher Scientific Ltd
N-Methyl-D-glucamine	Fisher Scientific Ltd
Potassium chloride (KCl)	Fisher Scientific Ltd
Sodium chloride (NaCl)	Sigma Aldrich, Ireland
Sodium hydroxide (NaOH)	Sigma Aldrich, Ireland
Triton X-100	Sigma Aldrich, UK
Trypan Blue (0.4%)	Sigma Aldrich, UK
Trypsin-EDTA solution (0.25%)	Sigma Aldrich, UK
Un-buffered DMEM	Seahorse, Biosciences
Virkon	Antec Int., USA

2.1.1.5 Cell Culture reagents

B-27 Supplement	Gibco, UK
Bovine serum albumin	Sigma Aldrich, Ireland
Donkey serum	Sigma Aldrich, Ireland
Dulbecco's modified Eagle medium: F12	Labtech Int., UK
Dulbecco's phosphate buffered saline (10X)	Sigma Aldrich, UK
Foetal Bovine Serum- heat inactivated	Invitrogen, UK
Fungizone	Invitrogen, UK
Glutamax	Gibco, UK
Granulocyte macrophage colony-stimulating factor	R&D Systems, UK
Horse serum	Sigma Aldrich, Ireland
Macrophage colony-stimulating factor	R&D Systems, UK
Neurobasal A medium	Invitrogen, UK
Normal goat serum	Sigma Aldrich, Ireland

Penicillin-streptomycin	Invitrogen, UK
Poly-D-lysine hydrobromide	Sigma Aldrich, UK
Poly-L-lysine hydrobromide	Sigma Aldrich, UK
Trypan Blue (0.4%)	Sigma Aldrich, UK
Trypsin-EDTA solution (0.25)	Sigma Aldrich, UK
Vectashield mounting medium with DAPI	Vector Laboratories, UK

2.1.1.6 Experimental treatments

3-Hydroxyanthranillic acid	Sigma Aldrich, UK
3-Hydroxykynurenine	Sigma Aldrich, UK
pEGFP-C1 Lifeact-EGFP Plasmid	Addgene, UK
Glutamate	Sigma Aldrich, UK
Glycine	Sigma Aldrich, UK
Interleukin-6	Peprotech, Ireland
Interleukin-6 Neutralising antibody	Biotechne, UK
Interleukin-1 alpha	Peprotech, Ireland
Quinolinic acid	Sigma Aldrich, UK
Kynurenic acid	Sigma Aldrich, UK
L-alpha-aminoadipic Acid (L-AAA)	Sigma Aldrich, Ireland
Recombinant rat Interferon-gamma (IFNγ)	Peprotech, Ireland
Tumor necrosis factor alpha (TNF-α)	Sigma Aldrich, UK

2.1.1.7 Assay Kits

BCA Protein Assay Kit	Fisher Scientific, Ireland
BioRad Protein Assay Dye Reagent	Thermo Scientific Piercef
CCK-8 Assay Kit	Dojindi labs, Japan
Coomassie Plus (Bradford) Protein Assay Kit	Thermo Scientific Pierce
Rat IL-1 alpha DuoSet ELISA kit	R&D Systems, UK
Rat IL-6 DuoSet ELISA kit	R&D Systems, UK
Rat TNF-α ELISA Max Deluxe kit	Biolegend, Ireland

2.1.1.8 Molecular materials and reagents

Aspartic Acid D-[2,3-3H]-, 250µCi (9.25MBq)	Perkin Elmer, UK
Biosphere filter tips (10, 20, 200, 1000 µL)	Sparks Labs, Ireland
Molecular grade ethanol	Sigma Aldrich, UK
High capacity cDNA archive kit	Applied Biosystems, UK
Microamp 96-well reaction plate	Applied Biosystems, UK
Nucleospin* RNA II Isolation kit	Macherney-Nagel, Germany
Nunc-Immuno™ MicroWell™ 96 well	Sigma Aldrich, UK
Optical adhesive covers	Applied Biosystems, UK
Paraformaldehyde	Sigma Aldrich
PCR minitubes	Sarstedt, Ireland
RNase-free microtubes (1.5 mL)	Ambicon Inc., USA
RNase-free water	Macherney-Nagel, Germany
RNaseZap* wipes	Ambicon Inc., USA
TaqMan* Gene Expression Assays	Applied Biosystems, UK
TaqMan* Universal PCR Master Mix	Applied Biosystems, UK

2.1.1.9 Fluorescent immunocytochemistry

Name	Host species	Manufacturer	Catalogue Number	Dilution
B-III tubulin	Mouse	Promega	G7121	1:1000
GFAP	Rabbit	Dako	Z0334	1:500
Iba1/AIF1	Goat	abcam	ab5076	1:1000
PSD-95	Mouse	Thermo Fischer Scientific	MA1-046	1:500
Synaptophysin	Rabbit	Thermo Fischer Scientific	PA1-1043	1:500
MAP2 (2a+2b)	Mouse	Sigma Aldrich	M1406	1:1000
Drebrin A (DAS2)	Rabbit	Immuno-Biological Laboratories	28023	1:150, 1:200

Table 2.1 Primary antibodies used for immunocytochemistry

Name	Host species	Manufacturer	Catalogue Number	Dilution
Alexa Fluor 488 anti-rabbit	Goat	Life technologies	A11008	1:500
Alexa Fluor 488 anti-goat	Rabbit	Invitrogen	A27012	1:500
Alexa Fluor 546 anti-rabbit	Goat	Thermo Fisher Scientific	A11035	1:500
Alexa Fluor 488 anti-chicken	Goat	Thermo Fisher Scientific	A11039	1:500
Alexa Fluor 546 anti-rabbit	Goat	Biosciences	A11010	1:1000
Alexa Fluor 488 anti-mouse	Goat	Thermo Fisher Scientific	A11001	1:1000
Alexa Fluor 546 anti-mouse	Goat	Biosciences	A11003	1:500

Table 2.2 Secondary antibodies used for immunocytochemistry

2.1.2 *In vivo* studies

2.1.2.1 Animals

C57Bl6/J mice (male), 9-14 weeks old	Charles River or Harlan, UK

2.1.2.2 Chemicals and reagents

Bovine Serum Albumin 96% (BSA)	Sigma Aldrich
Corn oil	Mazola
Ethanol (EtOH)	Sigma Aldrich
Elite Vectastain© ABC kit	Vector laboratories, UK
DPX mounting medium	Fisher Scientific, Ireland
Hydrochloric Acid (HCl)	BDH Chemicals
Gelatin	Sigma Aldrich, Ireland
Methanol	Sigma Aldrich
Paraformaldehyde	Sigma Aldrich
Sodium Chloride (NaCL)	BDH Chemicals
Sodium Hydroxide (NaOH)	Sigma Aldrich
Sulfuric acid (H_2SO_4)	Sigma Aldrich
Triton-X	Sigma Aldrich

Tween 20	Sigma Aldrich
Xylene	Sigma Aldrich

2.1.2.3 General consumables

6-well plates	Fisher Scientific
Containers (70 mL)	Sarstedt
Calibrated pipets (microcapillary 1-5 µL)	Sigma Aldrich
Falcon tubes (15 mL, 50 mL), sterile	Sarstedt
Glass coverslips 22 mm x 50 mm	Fisher Scientific
Microscope slides 76 mm x 26 mm	Fisher Scientific
Microtome blades (c35 type)	Lab. Instr. & Supply
Microtubes (0.5 mL, 1.5mL, 2mL)	Sarstedt
PCR tubes (0.2 mL)	Sarstedt
Pipette tips (10 µL, 200, 1000)	Sarstedt
Transfer pipettes (3.5 mL)	Sarstedt
Scalpels, disposable, sterile (Swann-Morton)	Fisher Scientific

2.1.2.4 General equipment

Axio Imager Z1	Carl Zeiss
Axiovert 200M	Zeiss
20x IX81-long focal length Fluorescent microscope	Olympus
Centrifuge: Legend RT+	Sorvall, Ireland
Cryostat	Leica
Vibratome	Leica
Gyro rocker	Stuart
Micropipette puller (P-87)	Sutter Instrument
Microscope CKX41	Olympus
SP8 confocal Microscope	Leica
Needles, hypodermic (25G)	Microlance BD
Peristatic pump	Gilson

PH meter	Mettler-Toledo
Surgical ear bars	Kopf Instruments, Ireland
Stereotactic frame	Kopf instruments, Ireland
Syringes, plastic (1 mL)	B-Braun

2.1.2.5 Animal care

Betadine	
EMLA 5% w/w cream	AstraZeneca
Euthanimal (Pentobarbital)	Alfasan
Tissue adhesive (Surgibond®)	SMI AG

2.1.2.6 Experimental treatments

L-alpha-aminoadipic acid (L-AAA)	Sigma Aldrich, Ireland

2.2 Methods

2.2.1 *In vitro* experiments

2.2.1.1 Aseptic techniques

Aseptic technique was utilised during all cell culture work in order to maintain a sterile environment free from fungal, bacterial and viral infections which could otherwise alter normal cellular function. Aseptic techniques included the use of sterile disposable plastics, and sterilisation of all reusable glassware and plastic by autoclaving at 121°C for 30-60 minutes prior to use. Distilled water (dH_20) was also sterilised by autoclaving. Dissection kit instruments were cleaned with Virkon and sterilised by autoclaving.

All cell culture work was carried out in a laminar flow hood (ADS Laminaire, France). The laminar flow hood prevents contamination from airborne pathogens by filtering air and permitting only a sterile airflow to come into contact with cells. The laminar hood surfaces were wiped down with 70% EtOH before and after use and exposed to ultraviolet light for 15-30 minutes after use. The hood was cleaned regularly with Biocidal ZF and Virkon when not in use. All items transferred into the flow hood were sprayed lightly with 70% EtOH to prevent

transfer of pathogens from the external environment into the culture work area. Disposable latex gloves were worn at all times while working in the culture area. Gloves were sprayed with 70% EtOH before entering the hood and changed regularly during cell culture work. Cells were maintained at 37°C in a 5% CO_2 humidified atmosphere provided by a Thermo Steri Cycle CO_2 Hepa Class 100 Incubator. The incubator and laminar flow hood were cleaned regularly with Biocidal ZF to maintain a sterile environment when not in use.

2.2.1.2 Preparation of culture media

Culture media for primary neuronal cultures: Neurobasal media (NBM) supplemented with 1% (v/v) penicillin-streptomycin, 0.1% (v/v) fungizone and 1% (v/v) glutamax was used to maintain primary neuronal cultures. 5 mL of penicillin-streptomycin, 500 µL of fungizone and 5 mL of glutamax were filter-sterilised using a 0.2 µm syringe filter into a 500 mL bottle of NBM. NBM was aliquoted into 50 mL falcon tubes, sealed with parafilm and refrigerated until further use. Prior to use NBM was supplemented with 1% B-27 producing complete NBM (referred to as complete NBM (cNBM))

Culture media for primary mixed glial cultures: Dulbecco's modified Eagle's medium (DMEM) F12 supplemented with 10% (v/v) heat-inactivated fetal bovine serum (FBS), 1% (v/v) penicillin-streptomycin and 0.1% (v/v) fungizone (referred to as complete DMEM (cDMEM)) was used to maintain primary mixed glial cultures. In short, 50 mL of FBS, 5 mL of penicillin-streptomycin and 500 µL of fungizone were filter-sterilised using a 0.2 µm syringe filter and added to a 500 mL bottle of cDMEM. cDMEM was aliquoted into 50 mL falcon tubes, sealed with parafilm and refrigerated until required for use.

For primary enriched microglial cultures: DMEM was supplemented as described above and granulocyte macrophage colony-stimulating factor (GM-CSF; 10 µg/mL) and macrophage colony-stimulating factor (M-CSF; 5 µg/mL) were added immediately to cDMEM before use to give a final concentration of 10 ng/mL of each.

For primary astrocytic cultures: DMEM F12 was supplemented as described for mixed glial cultures. cDMEM was aliquoted into 50 mL falcon tubes, sealed with parafilm and refrigerated until required for use.

Phosphate buffered saline (PBS): 1X PBS was prepared by diluting 5 mL 10X PBS to 50 mL with dH_2O.

2.2.1.3 Preparation of experimental treatments

Following preparation, stock solutions were filter-sterilised using a 0.2 µm syringe filter, aliquoted and stored at -20/-80^{o}C for future use. Experimental compounds and Kynurenine pathway metabolites were prepared fresh each time. Stock solutions were diluted to working concentrations in the appropriate pre-heated media immediately prior to treatment (*Table 2.3*).

Compound name	**Molecular weight (g/mol)**	**Stock Concentration**	**Solvent**
L-alpha-aminoadipic acid (L-AAA)	161.16	25 mM	cNBM
1-Methyltryptophan (L) (1-MT)	218.25	20 mM	cNBM
3-Hydroxyanthranillic acid (3-HAA)	153.14	1 mM	cNBM
3-Hydroxykynurenine (3-HK)	224.21	1 mM	cNBM
Recombinant rat Interleukin-6 (IL-6)	n/a	0.2 mg/mL	PBS
Recombinant rat Interleukin-1 alpha (IL-1α)	n/a	2 mg/mL	cNBM
IL-6 neutralising antibody	n/a	200 µg/mL	PBS
Glutamate (Glu)	147.13	10 mM	cNBM
Glycine (Gly)	75.07	10 mM	cNBM
Kynurenic acid (KYNA)	189.97	1 mM	cNBM
Quinolinic acid (QUIN)	167.12	4 µM	[2]DMSO
Recombinant rat interferon-gamma (IFNγ)	n/a	100 µg/mL	0.1% [4]BSA in PBS
Recombinant rat tumor necrosis factor (TNF-α)	n/a	60 ng/µL	Sterile dH_20

Table 2.3 Table of compounds, molecular weights and solvents

[1]NBM (Neurobasal media)
[2]DMSO (dimethyl sulfoxide)
[3]TRIM (1-(2-Trifluoromethylphenyl) imidazole)
[4]BSA (bovine serum albumin)

2.2.1.4 Preparation of Poly-D-Lysine coverslips for neurons

Poly-D-lysine was prepared by reconstituting 5 mg with 50 mL sterile dH_2O to obtain a stock concentration of 0.1 mg/mL. This solution was then filter-sterilised using a 0.2 µm syringe filter and frozen at -20°C in 5 mL aliquots until further use. Each Poly-D-lysine aliquot was diluted prior to use by adding 5 mL sterile tissue culture grade water giving a working concentration of 50 µg/mL.

Glass coverslips (13 mm) were placed in the wells of a 24-well plate and sterilised under ultraviolet light for 60 minutes. Coverslips were aseptically coated by placing a drop of Poly-D-lysine solution (75 µL) on the centre of each coverslip which was then left for 45 minutes. The poly-D-lysine was removed by aspiration and stored again at 4°C for reuse up to 3 times. Coverslips were washed twice with sterile tissue culture grade water and left to dry fully for approximately 2 hours. Any remaining droplets were removed with a Pasteur pipette. Once dry, plates were sealed with parafilm and stored in the fridge for up to two weeks or at -80°C for up to two months.

2.2.1.5 Preparation of Poly-L-Lysine coverslips for glia

Poly-L-lysine was prepared by reconstituting 5 mg with 50 mL sterile tissue culture grade water to obtain a stock concentration of 0.1 mg/mL. This solution was then filter-sterilised using a 0.2 µm syringe filter and frozen at -20°C in 5 mL aliquots until further use. Glass coverslips (13 mm) were placed in the wells of a 24-well plate and sterilised under ultraviolet light for 60 minutes. Coverslips were aseptically coated by placing a drop of Poly-L-lysine solution (100 µL) on the centre of each coverslip which was then left for 10-20 minutes. The poly-L-lysine was removed by aspiration and the coverslips were washed thoroughly with sterile tissue culture grade water. Poly-L-lysine was stored again at 4°C for reuse up to 3 times. Plates were left to dry fully for approximately 2 hours. Any remaining droplets were removed with a Pasteur pipette. Once dry, plates were

sealed with parafilm and stored in the fridge for up to two weeks or at -80°C for up to two months.

2.2.1.6 Preparation of primary cortical neuronal cultures

Trypsin-EDTA, B-27, cNBM, cDMEM and plates were pre-warmed in the incubator before starting the dissection. Cultures of primary cortical neurons were prepared as previously described (Day et al, 2014; McNamee et al, 2010a) from postnatal day 1 -2 (P1-2) neonate Wistar rat pups under sterile conditions in a laminar flow hood. Pups were decapitated using a large, sharp scissors. A smaller scissors was then used to cut through the skin and along the midline to reveal the skull. Cutting along the midline ensured no pressure was placed on the brain. A curved forceps was used to carefully remove the brain. The brain was then placed on a sterile petri dish. A straight forceps was used to remove the surrounding meninges and obvious blood vessels. Cortical tissue from both hemispheres was removed from the rest of the brain and placed in a drop of pre-warmed cDMEM to prevent it drying out.

The tissue was then transferred into trypsin-EDTA (5 mL) and incubated for 2 minutes at 37°C. 5 mL cDMEM was then added to deactivate the trypsin. The suspension solution was gently triturated and then centrifuged at 2,000 rpm for 4 minutes at 21°C. The supernatant was removed and the cell pellet was re-suspended in 5 mL cDMEM and gently triturated to give a homogenous suspension. The cell suspension was passed through a cell strainer with a 40 µm filter into a new sterile falcon tube and centrifuged at 2,000 rpm for 4 minutes at 21°C. The supernatant was discarded. The pellet was then re-suspended in 1 mL of pre-warmed cNBM (dilution 1:100) and gently triturated until a homogenous cellular suspension was obtained. The resulting neuronal cell suspension was counted using the trypan blue exclusion method.

2.2.1.7 Neuronal cell counting and plating

The trypan blue method of counting works on the premise that viable cells with intact cellular membranes have the ability to exclude trypan blue dye whereas dead cells do not. Cells were first diluted 1:50 in cNBM and again at 1:2 with

trypan blue producing a total dilution of 1:100. A glass haemocytometer was used to count the cells under a light microscope (Olympus CKX41). Following counting, the cell suspension was diluted with cNBM to give a final concentration of 3 x 10^5 cells/mL. For Sholl analysis and synaptic protein co-localisation experiments, 100 µL of this dilution was gently pipetted on the centre of a poly-D-lysine coated coverslip in 24-well plates. The concentrated cells were then incubated at 37°C for a minimum of 2 hours to allow adherence of neurons before being topped up with 200 µL of warm cNBM. The day of plating was referred to as to as *days in vitro* 0 (DIV 0). Media was replaced with fresh pre-warmed cNBM every 4-6 days. Immature neurons used for Sholl analysis were treated with compounds at DIV 3 and fixed for immunocytochemistry at DIV 4. Mature neurons used for Sholl analysis and synaptic protein co-localisation studies were treated with compounds at DIV 18-21 and fixed for immunocytochemistry.

2.2.1.8 Preparation of mixed glial cultures

Cultures of primary cortical mixed glial cells were prepared as previously described (McNamee et al, 2010a) from P2-3 neonatal Wistar rat pups under sterile conditions in a laminar flow hood. These cultures consisted of approximately 70% astrocytes and 30% microglia (Day et al, 2014). Pups were decapitated and brains were removed as previously described for primary cortical neuronal cultures.

Cortical tissue from both hemispheres was removed from the rest of the brain and placed in a drop of pre-warmed cDMEM to prevent it drying out. The finely chopped cortical tissue was then placed in 6 mL pre-warmed cDMEM and placed in the incubator for 20 minutes at 37°C in a humidified, 5% CO_2 atmosphere. Following this, the tissue was triturated until homogenous, passed through a sterile cell strainer (40 µm) into a new 50 mL falcon tube and centrifuged at 2,000 rpm for 3 minutes at 21°C. The supernatant was removed and the pellet was re-suspended in 1 mL cDMEM. 5 mL DMEM was added to the bottom of each T75 cm^2 flask and the 1 mL cell suspension was added on top. Flasks were placed into an incubator at 37°C and 5% CO_2 for 2 hours to allow adherence of

cells to the bottom of the flask. After 2 hours, flasks were topped up by adding an additional 5 mL cDMEM. The day of plating was referred to as DIV 0. Media was replaced every 4-5 days by removing and discarding old media and pipetting 10 mL fresh, pre-warmed cDMEM down along the sides of the flask to prevent disturbing cells.

Mixed glia were plated when 90% confluent, usually between days 10-14 DIV. Prior to plating, the media was removed from the T75 cm^2 flasks, and 3 mL fresh pre-warmed cDMEM was added. Cells were scraped and the cell suspension was collected and centrifuged at 2,000 rpm for 5 minutes at 21°C. The supernatant was discarded and the pellet was re-suspended in 2.4 mL cDMEM. 100 µL of cell suspension was added to each well and left to incubate for 2 hours to allow adherence. Wells were topped up with 200 µL cDMEM after 2 hours. Mixed glia were left for a minimum of 24 hours before treating.

2.2.1.9 Preparation of enriched primary astrocytic cultures

Primary astrocytic cultures were prepared from primary mixed glial cultures as described above (Day et al, 2014). Once 90% confluent, the mixed glia were separated by placing the T75 cm^2 flasks in an orbital cell shaker at 200 rpm for 2 hours at 37°C to remove microglia from the astrocytic monolayer. Flasks were tapped 10 times on the culture hood surface to encourage the separation of microglial cells. Cells were scraped and the cell suspension was collected and centrifuged at 2,000 rpm for 5 minutes at 21°C. The supernatant was discarded and the pellet was re-suspended in 2.4 mL cDMEM. 100 µL of cell suspension was added to each well and left to incubate for 2 hours to allow adherence. Wells were topped up with 200 µL cDMEM after 2 hours.

2.2.1.10 Preparation of enriched primary microglial cultures

Primary astrocytic cultures were prepared from primary mixed glial cultures as described above (Day et al, 2014). Granulocyte macrophage-colony stimulating factor (GM-CSF, 10 ng/mL) and macrophage-colony stimulating factor (M-CSF, 10 ng/mL) were added to the media to promote microglial proliferation. Both GM-CSF and M-CSF were added every 2-3 days when the media was changed.

Microglia were separated after 14 days as described above. T75 cm^2 flasks were placed on an orbital cell shaker at 200 rpm for 2 hours at 37°C to remove microglia from the astrocytic monolayer. The cell suspension was collected and spun at 2,000 rpm for 5 minutes at 21°C. The supernatant was discarded and the pellet was re-suspended in 2.4 mL cDMEM. 100 µL of cell suspension was added to each well and left to incubate for 2 hours to allow adherence. Wells were topped up with 200 µL cDMEM containing GM-CSF (10 ng/mL) and M-CSF (10 ng/mL) after 2 hours. Microglia were treated approximately 24-48 hours after plating.

2.2.1.11 Analysis of cell viability using the CCK-8 assay

The Cell Counting Kit-8 (CCK-8) assay (Dojindi labs, Kumamoto, Japan) was used to measure neuronal viability in accordance with the manufacturers protocol. Mature neurons were treated for 24 hours. After 24 hours the treatment was removed and replaced with 320 µL fresh media and 10 µL CKK-8 solution per well. The plate was incubated at 37°C for 1 hour and 100 µL sample from each well was then transferred to individual wells of a 96-well plate. The plate was read using a microplate reader at an absorbance of 450 nm.

The CCK-8 assay uses the water-soluble tetrazolium salt WST-8 [2-(2-methoxy-4-nitrophenyl)-3-(4-nitrophenyl)-5-(2,4-disulfophenyl)-2H-tetrazolium, monosodium salt]. WST-8 is reduced by dehydrogenases in cells to give an orange coloured product (formazan), which is soluble in tissue culture medium. The amount of the formazan dye generated by dehydrogenases in cells is directly proportional to the number of living cells. Cell viability can be estimated measuring the absorbance of formazan at 450 nm using a microplate reader (Ishiyama et al, 1997; Ishiyama et al, 1996; Jo et al, 2015).

2.2.1.12 Glial immunocytochemistry

2.2.1.13 Iba1 staining for microglia

For microglia complexity and immunofluorescence studies cells were fixed with 4% paraformaldehyde (PFA) for 30 minutes in a fume hood. Cells were then washed 3 times with PBS. Non-specific binding sites were blocked by applying a

blocking buffer containing 5% horse serum and 2% donkey serum in PBS containing 0.1% Triton-X (PBS-T) for 30 minutes on a rocker. After 30 min, the blocking buffer was removed and 200 µL anti-Iba1 primary antibody [polyclonal goat; ab5076] in blocking buffer (1:1000) was added to each well and left overnight at 4°C. Cells were washed 3 times with PBS (3 x 5-minute washes). They were then stained with 200 µL Alexa Fluor 488 secondary antibody [mouse anti-goat; A27012] diluted in PBS (1:500) and left for 2 hours on a rocker at room temperature in a light-protected environment provided by wrapping in tinfoil. Secondary antibody was removed and cells were washed 3 times with PBS before adding dH_2O to each well. A small drop of Vectashield fluorescent mounting media containing DAPI ((4´,6-Diamidino-2-phenylindole dihydrochloride), which is a counter-stain for DNA, was placed on the microscope slides (1-1.2 mm). Coverslips were lifted from the plate using a forceps and placed inverted onto the drop of mounting medium. Any excess Vectashield was gently removed using tissue paper. Coverslips were left to dry for approximately 2 hours. The edges of the coverslips were then sealed using nail varnish and the slides were allowed to dry in a light-protected environment before storage in the dark at 4°C.

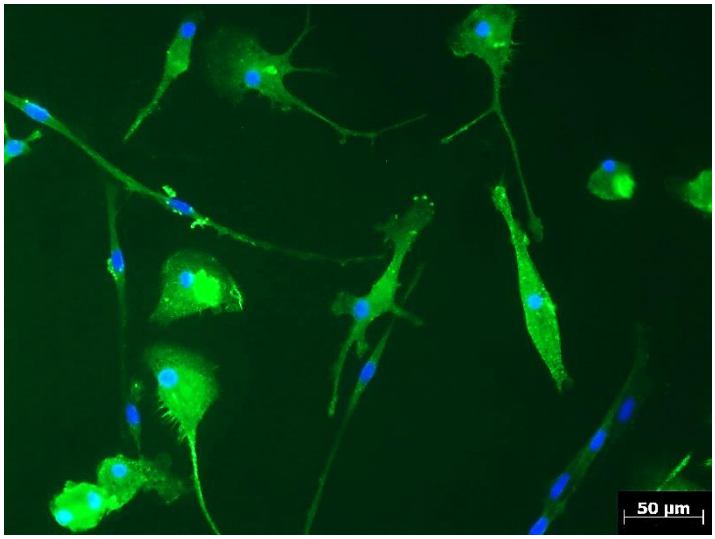

Figure 2.1 Fluorescent image of microglial cultures
Representative cultures of enriched primary microglia cultures stained with anti-Iba1 (green) and DAPI (blue).

2.2.1.14 Astrocyte complexity and GFAP immunofluorescence

Enriched astrocyte cultures were fixed with 4% PFA for 30 minutes in a fume hood. Cells were then washed 3 times with PBS. Non-specific binding sites were

blocked by applying a blocking buffer (5% horse serum and 2% donkey serum in PBS-T) to the wells for 30 minutes, while placing the plate on a rocker. After 30 minutes the blocking buffer was removed and 200 µL anti-GFAP primary antibody [rabbit; Z0334] diluted in blocking buffer (1:500) was added to each well and left overnight at 4°C. Cells were washed 3 times with PBS (3 x 5-minute washes). They were then stained with 200 µL Alexa Fluor 488 secondary antibody [goat anti-rabbit; A11008] diluted in PBS (1:500) and left for 2 hours on a rocker at room temperature in a light-protected environment provided by wrapping in tinfoil. Secondary antibody was removed and cells were washed 3 times with PBS (3 x 5-minute washes). Glass coverslips were then removed and mounted onto glass slides as described above.

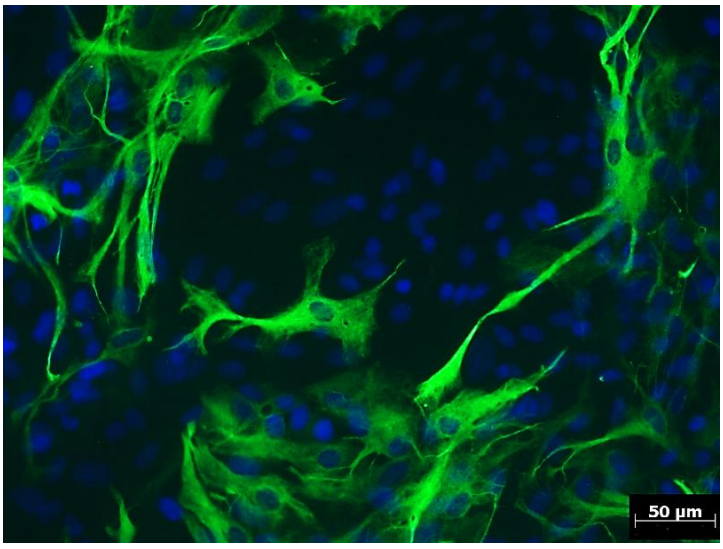

Figure 2.2 Fluorescent image of enriched astrocyte cultures
Representative cultures of enriched primary astrocyte cultures stained with anti-GFAP (green) and DAPI (blue).

2.2.1.15 Determination of the purity of enriched primary cortical glial cultures

Enriched primary astrocytic and microglial cultures were prepared from primary mixed glial cultures as described above (Day et al, 2014). The purity of enriched astrocyte cultures **(A)** was determined by staining for GFAP as described above using an anti-GFAP primary antibody [rabbit; Z0334] diluted in blocking buffer (1:500) and Alexa Fluor 488 secondary antibody [goat anti-rabbit; A11008] diluted in PBS (1:500). Glass coverslips were then removed and mounted onto glass slides as described above. The number of GFAP+ stained cells were quantified using Image J and compared to the total number of cells per well to

determine the average percentage purity of the cultures. The estimated average purity of enriched astrocyte cultures was determined to be 75 %. Similarly, the purity of enriched microglia cultures **(B)** was determined by staining for Iba1 using an anti-Iba1 primary antibody [polyclonal goat; ab5076] diluted in blocking buffer (1:1000) and Alexa Fluor 488 secondary antibody [mouse anti-goat; A27012] diluted in PBS (1:500). Glass coverslips were then removed and mounted onto glass slides as described above. The number of Iba1+ stained cells were quantified using Image J and compared to the total number of cells per well to determine the average percentage purity of the cultures. The estimated average purity of enriched microglial cultures was determined to be 98 %.

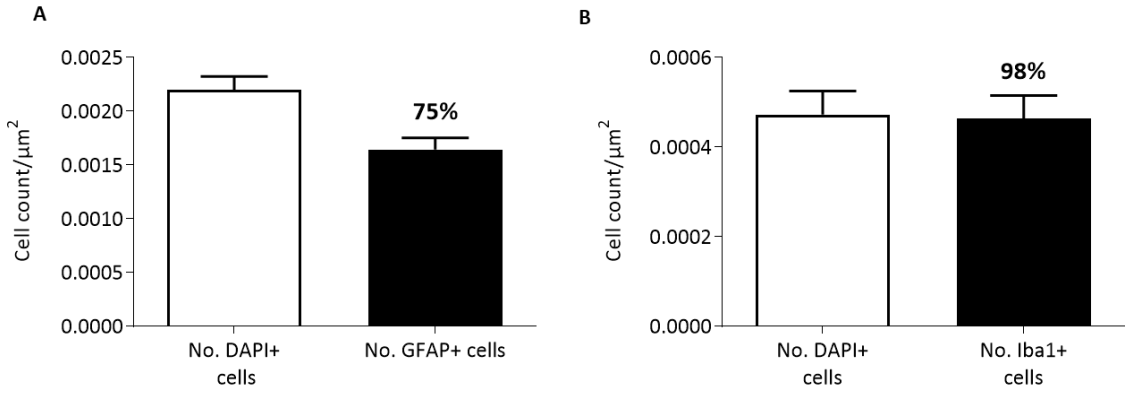

Figure 2.3 Purity of enriched primary cortical glia cultures
To determine the average percentage purity of enriched astrocyte cultures (A), GFAP+ stained cells were quantified and compared to the total number of cells per well (DAPI). To determine the average percentage purity of enriched microglial cultures (B), Iba1+ stained cells were quantified and compared to the total number of cells per well (DAPI).

2.2.1.16 Aquaporin-4 (AQP4) immunocytochemistry in primary cortical enriched astrocyte cultures

Astrocyte cultures were fixed with 4% PFA for 30 minutes in the laminar flow hood. Cells were then washed 3 times with PBS and permeabilised for 10 minutes with PBS-T (PBS +0.01% Triton X-100). Non-specific binding sites were blocked by applying a blocking buffer (10% donkey serum in PBS-T) to the wells and leaving the plate at room temperature for 1 hour. The blocking buffer was removed and cells were washed once in PBS. 200 µL primary antibody containing anti-aquaporin-4 [rabbit; AB3594] and anti-GFAP [chicken; 4674] diluted in PBS-T (1:1000) was applied to each well and left at 4^{o}C overnight. Cells were then

washed 3 times with PBS-T. Cells were then stained with 200 µL secondary antibody containing Alexa Fluor 546 secondary antibody [goat anti-rabbit; A11035] and Alexa Fluor 488 secondary [goat anti-chicken; A11039] diluted in PBS-T (1:500). This was applied to each well and left on a rocker at room temperature in a light-protected environment provided by wrapping in tinfoil for 2 hours. Secondary antibody was removed and cells were washed 3 times with PBS (3 x 5-minute washes). Glass coverslips were then removed and mounted onto glass slides as described above.

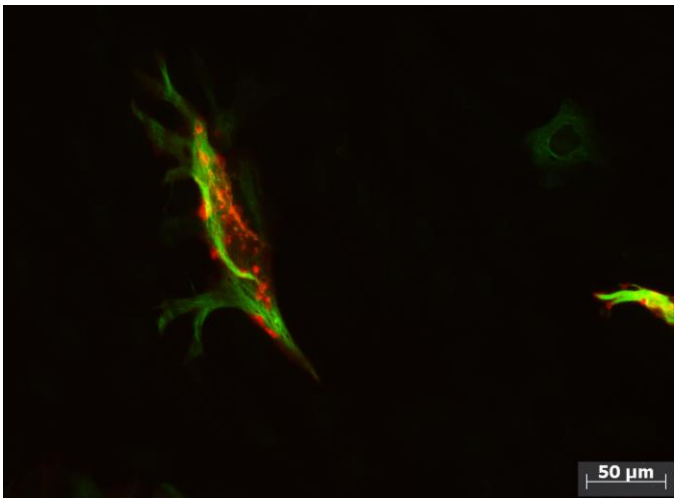

Figure 2.4 Representative image of AQP4 staining
Representative image of astrocyte cultures (DIV 15) stained with anti-AQP4 (red), anti-GFAP (green) and DAPI (blue).

2.2.1.17 Analysis of glia complexity and immunofluorescence

Coverslips were visualised at 20X magnification using an AxioImager Z1 epifluorescent microscope with a Zeiss AxioCam HR camera and AxioVision 4.8.2 software. 7 images were taken per coverslip and 5 cells were analysed per image. A constant exposure was maintained throughout all images. Mean cell area and perimeter were quantified using the particle measurement feature on ImageJ (1.51s, USA). Iba1 and GFAP immunoreactivity were quantified by calculating the corrected total cell fluorescence (CTCF) using the ImageJ integrated density feature. A total of 140 neurons were analysed per treatment group per experiment (n ≥3). The following formula was applied to account for non-fluorescent background regions:

CTCF = [integrated density – (area of selected cell) x mean fluorescence of background]

2.2.2 Immature neuron staining with β-III tubulin for Sholl analysis

Following treatment, media was removed from each well and cells were washed once in PBS. Cells were fixed by adding 300 µL ice-cold methanol to each well and leaving the plates at -20°C for 20 minutes. Methanol was then removed and the coverslips were washed 3 times with PBS. After 3 x 5 minute washes, non-specific interactions were blocked by adding 300 µL blocking buffer (4 % NGS in PBS) to each well and the plate was left on a rocker at room temperature for 2 hours. The blocking buffer was discarded and cells were washed 3 times in PBS. Primary antibody (200 µL) containing anti- β-III tubulin [mouse; G7121] in PBS (1:1000) was added to each well and left overnight at 4°C. The primary antibody was removed and the cells were washed 3 times in PBS. Secondary antibody containing Alexa Fluor 488 [goat anti-mouse; A11001] in PBS (1:2000) was added and left for 2 hours on a rocker at room temperature in a light-protected environment provided by wrapping in tinfoil. Secondary antibody was removed and cells were washed 3 times (3 x 5 minute washes) with PBS. Glass coverslips were then removed and mounted onto glass slides as described above. Coverslips were visualised at 20X magnification using an AxioImager Z1 epifluorescent microscope with a Zeiss AxioCam HR camera and AxioVision 4.8.2 software.

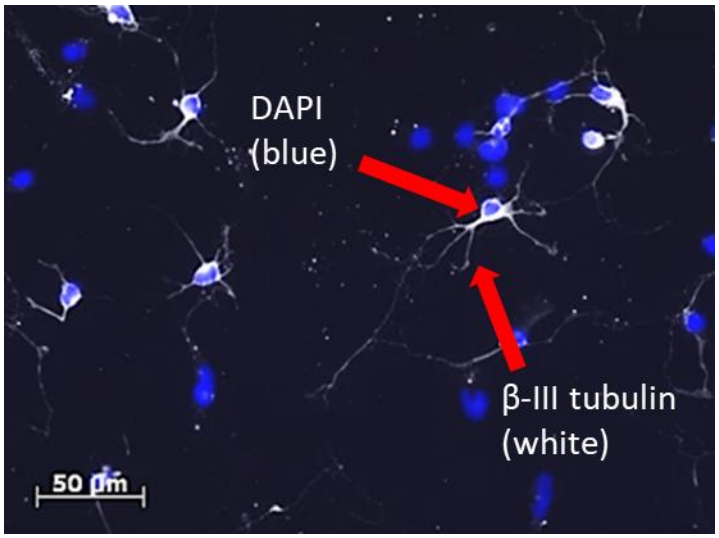

Figure 2.5 Representative image of β-III tubulin staining
Representative cultures of immature (DIV 3) primary cortical neurons stained with anti-β-III tubulin (white) and DAPI (blue) followed by fluorescent microscopy (20X magnification).

Coverslips included in the analysis displayed a healthy neuronal network throughout the entire coverslip. 5-7 individual images were captured from each coverslip and 6 coverslips per experimental condition were typically collected for analysis. Where possible, groups were blinded and cells were selected in the DAPI channel to avoid bias. Sholl analysis is a widely used method for quantifying and graphically representing neurite morphology. The protocol is adapted from Sholl (SHOLL, 1953) and Gutierrez and Davies (Gutierrez & Davies, 2007). This analysis involves placing concentric rings with regular radial increments over the neuron and quantifying the number of neurites intersecting each ring using the following equation: $x_i = x_{i-1} + b_i - t_i$. In this case "xi" is the number of neurites for the "ith" segment, "bi" is the number of branches occurring in the "ith" segment and "ti" the number of terminations in that segment. This equation was programmed into Matlab (R2012b) to allow for a semi-automated procedure. Inter-ring interval was 10 µm and 25 concentric rings were used. The number of neuritic branches, relative neuritic length, number of primary neurites and Sholl profile were measured for each neuron. The Sholl profile maps the number of neuritic branches at each radial distance from the cell soma.

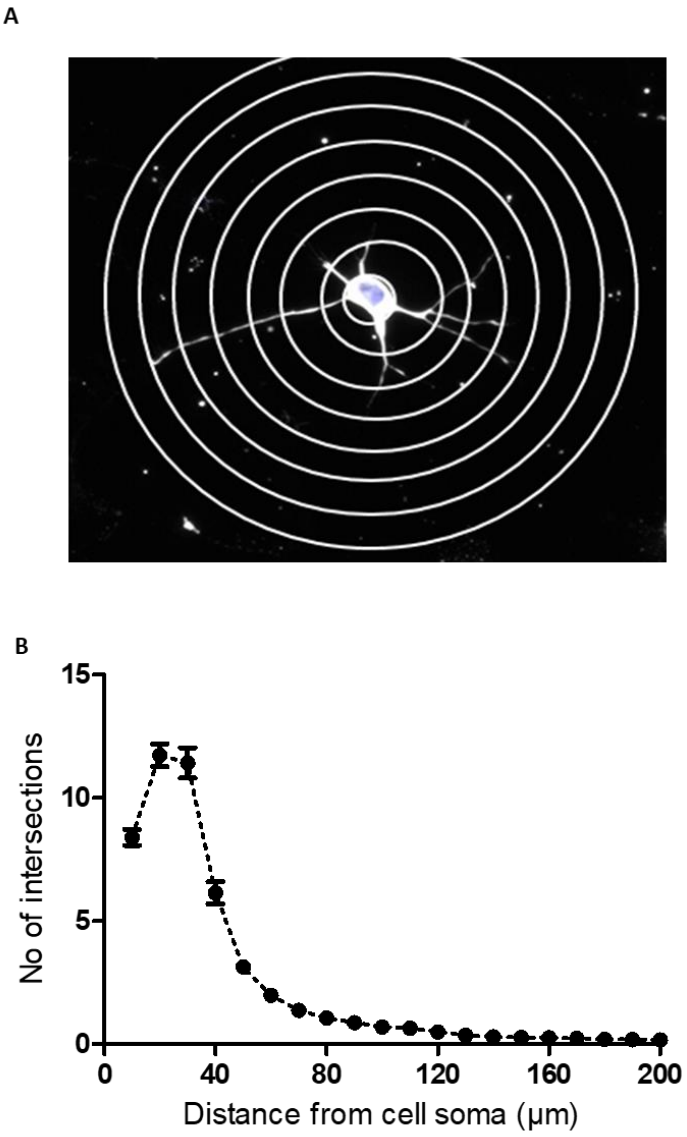

Figure 2.6 Sholl analysis
Representative image of a rat cortical neuron stained with β-III tubulin (white) and DAPI (blue) with overlaying concentric rings (A) and a typical Sholl profile (B).

2.2.3 Mature neuron staining with MAP2 for Sholl analysis

Following treatment, media was removed from each well and the cells were fixed in 4% PFA by adding 400 µL 4% PFA in PBS to each well for 20 minutes at room temperature. PFA was then removed and the coverslips were washed 3 times with PBS. After three washes, non-specific interactions were blocked by adding 300 µL blocking buffer containing 2% NGS, and 2% BSA in PBS-T to each well and the plate was left on a rocker at room temperature for 2 hours. The blocking buffer was discarded and 200 µL primary antibody containing MAP2 [mouse; M1406] in blocking buffer (1:1000) was added to each well and left overnight at 4°C. The primary antibody was removed and cells were washed 3

times in PBS (3 x 5 minute washes). Secondary antibody containing Alexa Fluor 546 [goat anti-mouse; A11003] in PBS-T (1:500) was added and left for 2 hours on a rocker at room temperature in a light-protected environment provided by wrapping in tinfoil. Secondary antibody was removed and cells were washed 3 times with PBS (3 x 5 minute washes). Glass coverslips were then removed and mounted onto glass slides for imaging and Sholl analysis as described above.

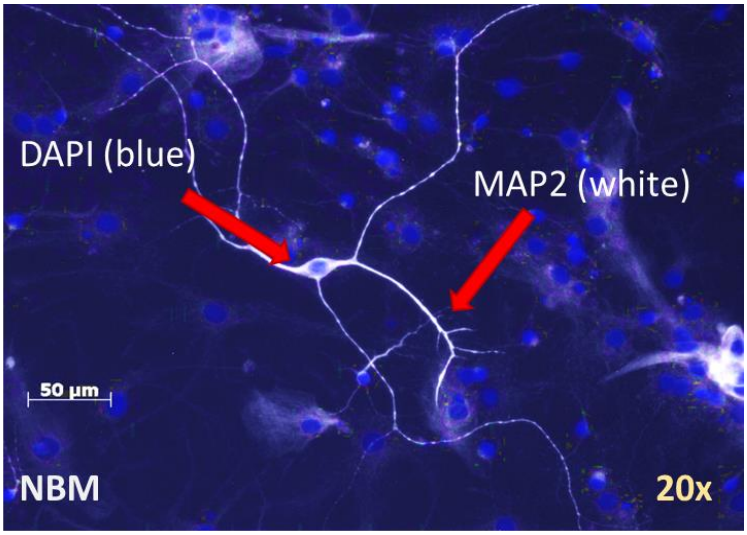

Figure 2.7 Representative image of MAP2 staining
Representative cultures of mature (DIV 21) primary cortical neurons stained with anti-MAP2 (white) and DAPI (blue) followed by fluorescent microscopy (20X magnification).

2.2.4 Analysis of the co-localisation of synaptic markers in mature neurons

The synaptogenesis procedure was adapted from Ippolito and Eroglu (Ippolito & Eroglu, 2010). Mature neurons (DIV 18-21) were treated for 24 hours and fixed in ice-cold methanol as described above. The cells were permeabilised and blocked using a blocking buffer consisting of 50% NGS + 0.2% triton-X in PBS for 30 minutes, on a rocker at room temperature. The blocking buffer was removed and cells were washed with PBS. 200 µL of primary antibody cocktail containing the pre-synaptic marker anti-synaptophysin [rabbit; PA1-1043] and the post-synaptic marker anti-PSD-95 [mouse; MA1-046] diluted in PBS (1:500) was added to each well and left on overnight at 4°C. 200 µL of secondary antibody cocktail containing Alexa Fluor secondary antibody 546 [goat anti-rabbit; A11010] and Alexa Fluor 488 secondary antibody [goat anti-mouse; A11001] diluted in PBS (1:1000) was added to the wells and left for 2 hours on a rocker at room temperature in a light-protected environment provided by wrapping in tinfoil.

Secondary antibody was removed and cells were washed 3 times with PBS (3 x 5 minutes washes). Glass coverslips were then removed and mounted onto glass slides as described above.

Coverslips were visualised at 40X magnification using an AxioImager Z1 epifluorescent microscope with a Zeiss AxioCam HR camera and AxioVision 4.8.2 software. Coverslips included in the analysis displayed a healthy neuronal network. The optimum exposure intensity for both the synaptophysin and PSD-95 channels was determined using a control coverslip and was maintained throughout. 5-7 individual images were captured from each coverslip and 6 coverslips per experimental condition were typically collected for analysis. Where possible, groups were blinded. The analysis was adapted from Ippolito and Eroglu, using the ImageJ analysis programme (Ippolito & Eroglu, 2010). For image analysis, individual images were opened in ImageJ and a region of interest was outlined around the cell of interest. The Puncta Analyser was used to adjust the thresholds of the red channel (synaptophysin) and green channel (PSD-95) so that the intensity corresponded to discrete individual puncta. Minimum puncta size was set at a value of 4 for each experiment. Threshold values were standardised based on control-treated neurons in order to maintain a consistent approach for comparison between groups. For the purpose of this analysis, synapses were defined as “co-localised puncta” resulting from the signal generated with the pre-synaptic synaptophysin and post-synaptic PSD-95. The number of co-localised puncta were quantified using the ImageJ ‘Puncta Analyser’ plugin.

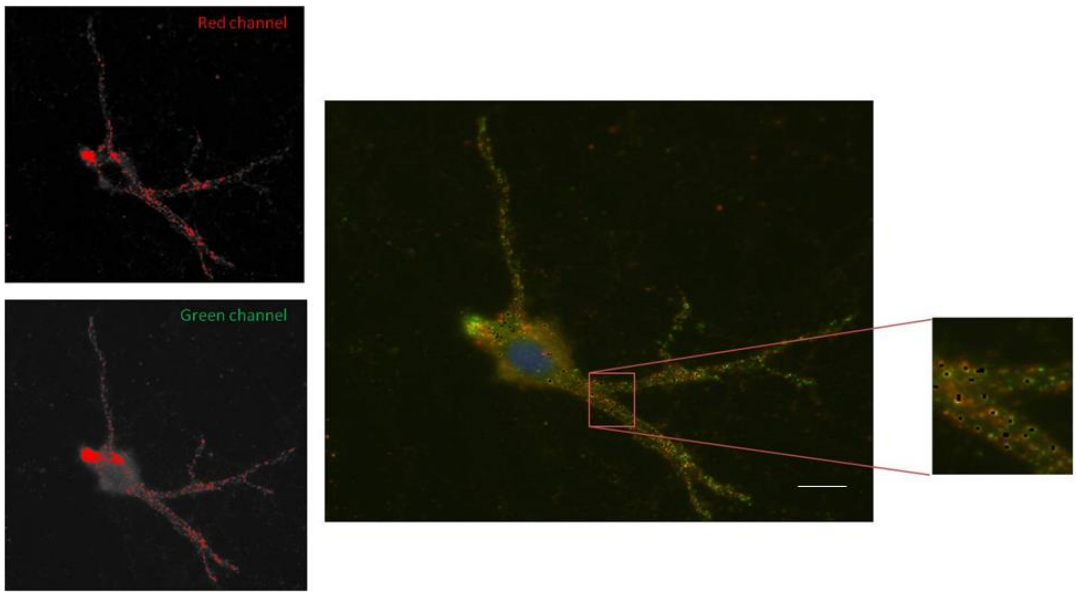

Figure 2.8 Fluorescent image of mature neurons stained with anti-synaptophysin and anti-PSD-95

Neurons stained with the pre-synaptic marker, synaptophysin (red channel image) and the post-synaptic marker, PSD-95 (green channel image). Merged image displays points of co-localisation (black dots).

2.2.5 Quantitative polymerase chain reaction (PCR)

2.2.5.1 Harvesting cells for mRNA analysis

Prior to carrying out ribonucleic acid (RNA) extraction all surfaces were wiped down with RNaseZap® wipes (Ambion, UK) to prevent RNA breakdown or contamination. Following cell culture treatment, media was removed and cells were lysed by adding 350 µL RA1 lysis buffer supplemented with 1% β-mercaptoethanol to each well. Cells were pooled where necessary. Cells were scraped from the base of wells using a 1000 µL filtered pipette tip and the lysate was transferred to a 2 mL RNase-free Eppendorf. Pipette tips were changed between treatment groups in order to prevent cross-contamination. Cell lysates were harvested and stored at -80°C for subsequent RNA extraction.

2.2.5.2 RNA extraction

RNA was extracted from samples using a NucleoSpin® RNA kit (Macherey-Nagel) according to the procedure outlined in the manufacturer's instructions. Cell lysates were added to Nucleospin® filter columns in a collecting tube and filtered using a centrifuge for 1 minute at 11,000 x g. The filter column was discarded and 350 µL of 70% EtOH was added to the filtered lysate and mixed by pipetting

up and down approximately five times to adjust RNA binding conditions. The mixture was then loaded into a NucleoSpin® RNA column and centrifuged for 30 seconds at 11,000 x g in order to let the RNA bind to the silica column. The silica membrane was placed in a new collecting tube (2 mL) and was desalted using 350 µL of Membrane Desalting Buffer (MDB) to allow the recombinant deoxyribonuclease (rDNase) digest more effectively and centrifuged for 1 minute at 13,000 rpm. 95 µL of the rDNase reaction mixture (10 µL reconstituted rDNase and 90 µL Reaction Buffer for rDNase) was added onto the centre of the silica membrane of the NucleoSpin® RNA column and left for 15 minutes at room temperature. Following incubation, the silica membrane was washed several times in order to digest any contaminating DNA. Firstly, the membrane was washed using 200 µL of Buffer RA2 to inactivate the rDNAse and centrifuged for 30 seconds at 11,000 x g. The column was then changed to a new 2 mL collection tube. The membrane was dried by washing two more times using 600 µL RA3 and centrifuging for 30 seconds at 13,000 rpm and then using 250 µL RA3 and centrifuging for 2 minutes at 11,000 x g. The column was then placed into a nuclease-free collection tube and the flow-through discarded. The pure RNA was eluted in 40 µL RNase free water by centrifuging for 1 minute at 11,000 x g into a new RNase-free collection Eppendorf. RNA samples were either equalised or stored at -80°C until required.

2.2.5.3 RNA equalisation

RNA extraction samples prepared above were defrosted slowly on ice if they had been stored at -80°C. They were kept on ice throughout the RNA equalisation procedure. A Nanodrop® ND1000 (Nano Drop Technologies, Thermo Fisher Scientific) was the spectrophotometer used to quantify total RNA concentrations in each sample. 1 µL of RNase-free water was used to blank the Nanodrop. Samples were gently and quickly vortexed (Genie 2, Scientific Industries) prior to reading. Two absorbance readings (ng/mL) were obtained for 1 µL of each RNA sample in duplicate and a final average concentration was recorded. Purity was demonstrated by the A260/280 ratio where a ratio of 2 indicates highly pure RNA. The sensor was cleaned with absorbent paper between sample readings.

The RNA samples were equalised using RNase-free H_2O to the lowest recorded concentration of RNA.

2.2.5.4 Complementary deoxyribonucleic acid (cDNA) synthesis

Complementary DNA (cDNA) was reverse transcribed from equalised RNA using a High Capacity cDNA Reverse Transcription Kit (Biosciences) according to the protocol provided. An equal volume of equalised RNA (10 µL) was mixed with an equal volume (10 µL) of cDNA Mastermix (containing RT Buffer (Reverse Transcriptase), dNTPs, random primers, multiscribe RT and RNase-free H2O). The samples were mixed, briefly centrifuged and placed into a Thermal Cycler (PTC-200 Peltier Thermal Cycler DNA Engine) and set to the "AbCDNA" programme which ran at 25°C for 10 minutes, 37°C for 120 minutes and 85°C for 5 minutes. Upon completion of the programme, the samples were removed and frozen at -20°C until required for polymerase chain reaction (PCR) analysis.

2.2.5.5 Real-time Polymerase Chain Reaction (RT-PCR)

Assessment of target genes was carried out using Taqman® Gene Expression Assays, containing specific target primers and a FAM® dye labelled MGB (minor groove binding) target probe. Glyceraldehyde-3-phosphate dehydrogenase (GAPDH) was used as an endogenous control to normalise gene expression between samples and was quantified using a VIC-labelled probe for rat GAPDH.

4 µL of each cDNA sample was added to an individual well in a PCR plate. Primer mixes were made up using TaqMan® Fast Advanced Master Mix, the primer of interest and GAPDH as the endogenous control. Primers were gently vortexed and 6 µL was added to each well making up a final volume of 10 µL. The plate was sealed with an optically clear plastic cover and centrifuged at 800 rpm, 4^{o} for 30 seconds. The plate was analysed using the quantitative PCR thermocycler (Applied Biosystems) and Step One software. The Comparative CT method and fast run were chosen and the target gene expression was assessed using a TaqMan gene expression assay. Target gene expression was assessed relative to the endogenous control GAPDH. Samples were assayed in one run (40 cycles),

which consists of 2 stages: a Holding stage [50°C for 2 minutes, and 95°C for 20 seconds] and a Cycling stage [95°C for 1 second, and 60°C for 20 seconds].

Target	Taqman Gene Expression Assay ID
TNF-α	Rn00562055_m1
IL-1β	Rn00580432
S100β	Rn04219408
GFAP	Rn00566603
1ba1 (AIF1)	Rn00574125
IL-1α	Rn00566700_m1
IL-6	Rn01410330_m1
Aadat (KAT II)	Rn00567882_m1
IDO1	Rn01482210_m1
KMO	Rn00665313_m1
KYNU	Rn00588108_m1
TDO2	Rn00574499_m1

Table 2.4 List of FAM-labelled MGB target probes used in PCR

2.2.5.6 Analysis of quantitative PCR data

The gene expression of all the quantitative PCR was assessed using the ΔΔCT method (Applied Biosystems RQ software). This method quantifies gene expression of treated samples to a control sample as 'fold change' i.e. the difference in the number of cycles (CT) between sample and control. It involves setting a fluorescence threshold when the PCR reaction is in the exponential phase i.e. when the PCR reaction is optimal or 100% efficient. It is this threshold against which CT is measured to provide a measure of gene expression. Samples demonstrating high fluorescence have low CT readings indicating greater amplification and hence, greater gene expression. When a PCR is 100% efficient a difference of one-cycle indicates a 2-fold difference in copy number, similarly a 5-fold difference indicates a 32-fold difference. Fold change is quantified by

subtracting the CT of the endogenous control (GAPDH) from the CT of the target gene for each sample. This difference denoted as ΔCT indicates differences in cDNA quantity. The ΔCT of the control sample is then subtracted from itself and all the other samples giving the ΔΔCT (cycle difference corrected for endogenous control). The control sample always has a ΔΔCT value of 0. ΔΔCT is converted into a fold difference, which is used to determine related change in expression. qPCR data was exported into an Excel file and fold change values were visualised using GraphPad Prism 6.

2.2.6 Enzyme-linked immunosorbent assays (ELISA)

2.2.6.1 Harvesting cultures for ELISA

Following treatment, cell supernatants were removed and collected in the laminar flow cabinet and stored at -80°C for future protein analysis.

2.2.6.2 ELISA

The sandwich ELISA method was used to determine IL-1α, TNF-α and IL-6 protein concentrations in samples using a Rat IL-1α DuoSet ELISA kit, Rat TNF-α ELISA Max Deluxe kit and a Rat IL-6 DuoSet ELISA kit. Each ELISA was performed as per the manufacturer's guidelines supplied (*Table 2.5*). Briefly, diluted capture antibody (50 µL) was added to each well of a 96-well plate (Nunc-Immuno™) for the appropriate amount of time.

The plate was washed four times with PBS-0.05% Tween (PBS-T) wash buffer and then blocked by adding 150 µL of pre-filtered reagent diluent to each well. The plate was washed four times as above before loading the standards and samples (100 µL) in duplicate. The plate was washed four times as above and 50 µL of diluted detection antibody was added to each well for the required amount of time. The plate was washed as described and 100 µL of diluted streptavidin conjugated to horseradish-peroxidase (strep-HRP) was added to each well. The plate was washed five times and 50 µL of substrate solution containing 3,3',5,5'-tetramethylbenzidine (TMB) was added to each well for 20 minutes in a light protected area at room temperature to allow colour development. The reaction was stopped by adding 50 µL stop solution (2 N H_2SO_4) to each well after colour

change was observed. Absorbance was read immediately at 450 nm using a microplate reader (Synergy HT, BioTek Instruments, USA) and Gen 5 program. Wavelength correction was set to an absorbance of 540 nm to maximise accuracy. Protein concentrations were calculated from the resulting standard curve.

ELISA	TNF-α	IL-1α	IL-6
Capture antibody	Hamster anti-rat, diluted 1:200 in coating buffer, incubated overnight at 2°C - 8°C	Mouse anti-rat IL-1α reconstituted in PBS, incubated overnight at room temperature	Mouse anti-rat IL-6 reconstituted in PBS, incubated overnight at room temperature
Wash buffer	0.05% Tween 20 in PBS, pH 7.2-7.4	0.05% Tween 20 in PBS, pH 7.2-7.4	0.05% Tween 20 in PBS, pH 7.2-7.4
Reagent diluent (blocking buffer)	Assay Diluent A, incubated for 1 hour at room temperature	1% BSA in PBS, pH 7.2-7.4, 0.2 µm filtered, incubated for 1 hour at room temperature	1% BSA in PBS, pH 7.2-7.4, 0.2 µm filtered, incubated for 1 hour at room temperature
Substrate solution	1:1 mixture of Colour Reagent A (H_2O_2) and Colour Reagent B (Tetramethylbenzidine)	1:1 mixture of Colour Reagent A (H_2O_2) and Colour Reagent B (Tetramethylbenzidine)	1:1 mixture of Colour Reagent A (H_2O_2) and Colour Reagent B (Tetramethylbenzidine)
Standards	Recombinant rat TNF-α reconstituted in Assay Diluent to a high standard of 1,000 pg/mL, incubated for 2 hours at room temperature	Recombinant rat IL-1α reconstituted in Reagent Diluent to a high standard of 8,000 pg/mL, incubated for 2 hours at room temperature	Recombinant rat IL-6 reconstituted in Reagent Diluent to a high standard of 4,000 pg/mL, incubated for 2 hours at room temperature
Detection antibody	Biotinylated goat anti-rat TNF-α, diluted in 1:200 in Assay Diluent A, incubated for 1 hour at room temperature	Biotinylated goat anti-rat IL-1α, diluted in Reagent Diluent with 2% heat inactivated NGS, incubated for 2 hours at room temperature	Biotinylated goat anti-rat IL-6, diluted in Reagent Diluent with 2% heat inactivated NGS, incubated for 2 hours at room temperature
HRP-conjugated antibody	Streptavidin conjugated to horseradish-peroxidase 1:1,000 in Assay Diluent A, incubated for 30 minutes at room temperature	Streptavidin conjugated to horseradish-peroxidase diluted 1:40 in reagent diluent, incubated for 20 minutes at room temperature	Streptavidin conjugated to horseradish-peroxidase diluted 1:40 in reagent diluent, incubated for 20 minutes at room temperature
Stop solution	2N H_2SO_4	2 N H_2SO_4	2N H_2SO_4

Table 2.5 Chemicals required for ELISA

2.2.7 Seahorse experiment

The Seahorse extracellular flux (XF) analyzer (Seahorse Bioscience) apparatus was used to measure glycolysis and oxidative phosphorylation (through oxygen consumption) simultaneously in the same cells (Zhang & Zhang, 2019). The extracellular acidification rate (ECAR) of the surrounding media provides an indicator of glycolysis. This is essentially considered a measurement of pH as changes in ECAR predominately result from the excretion of lactic acid per unit time. Oxygen consumption rates (OCR) provides an indicator of basal respiration, ATP-linked respiration, proton leak respiration, maximal respiratory capacity and non-mitochondrial respiration.

2.2.7.1 Astrocyte preparation and treatment

Enriched primary cortical astrocytes (DIV 14) were treated with L-AAA diluted in pre-warmed cDMEM at a concentration of 0.5 mM for 24 hours. A total volume of 500 µL of treatment was applied per well of the XF24-well plates for 24 hours.

2.2.7.2 Measurement of OCR

OCR was assessed using an Extracellular Flux (XF) Analyser (Seahorse Biosciences) which employs optical sensors to measure the OCR in cells attached to the cultured plate (Plitzko & Loesgen, 2018). Real-time measurements of OCR were made by isolating a small volume (about 2 µL) of medium above a monolayer of cells within a microplate.

On the day prior to analysis, the Seahorse apparatus was hydrated by adding 1 mL Seahorse XF Calibrant solution into each well of the plate and leaving it in an incubator (37°C, without CO_2) overnight. On the day of analysis, the treatment was removed and 500 µL of unbuffered sea-horse media supplemented with 10 mM glucose was added slowly to each well. The media was removed again and 600 µL of the same unbuffered media supplemented with glucose was added and left in an incubator (37°C in a 21% O_2) for 1 hour. The inhibitors Oligomycin (2 µM), carbonyl cyanide-4-(trifluoromethoxy)phenylhydrazone (FCCP) (0.5 µM), Rotenone A (0.1 µM)/Antimycin A (4 µM) and 2-Deoxy-D glucose (2-DG) (30 mM)

were diluted in unbuffered sea-horse media and 75 µL was added to the appropriate wells of the seahorse plate.

OCR was measured at 37°C under basal conditions in the presence of oligomycin (2 µM), which shows how much OCR is due to ATP synthesis. Injection of FCCP (0.5 µM) encourages the movement of protons into the mitochondrial matrix independent of the ATP synthase. This helps maintain the membrane potential, increasing the flow of electrons across the electron transport chain to maximum speed. FCCP, thus reveals the maximal respiratory capacity (maximal OCR) of the cells. Injection of Rotenone A (0.1 µM) and antimycin A (4 µM) results in complete inhibition of the electron transport chain, permitting quantification of non-mitochondrial oxygen consumption. Mitochondrial reserve capacity is calculated by subtracting basal respiration from the maximal respiratory capacity.

Oligomycin	Complex V inhibitor (ATP synthase inhibitor)
FCCP	Mitochondrial uncoupler
Rotenone A	Electron Transport Chain Complex I inhibitor
Antimycin A	Electron Transport Chain Complex III inhibitor

Table 2.6 Inhibitors used to measure OCR and ECAR with the (XF) Analyser

2.2.7.3 Measurement of ECAR using Extracellular Flux Analyser

ECAR measurement is based on a measure of acidification (pH). It is derived from the excretion of lactic acid after its conversion from pyruvate in anaerobic glycolysis, and from CO_2 production by the tricarboxylic acid cycle. Plate preparation was carried out on the day before analysis as previously described. On the day of analysis, the treatment was removed and unbuffered media supplemented with glucose was added and left in an incubator (37°C in, 21% O_2) for 1 hour. First, the glycolytic rate was measured 1 hour after glucose was supplied. Glucose is supplied to feed glycolysis and the difference between ECAR before and after glucose addition provides a measure of the glycolytic rate. Oligomycin (2 µM) was injected in order to measure of the maximal glycolytic reserve capacity. Finally, the glycolysis inhibitor 2-DG (30 mM), was injected.

2.2.7.4 Determination of protein quantification

Following the sea-horse experiment, protein quantification was carried out using the Thermo Scientific™ Pierce™ bicinchoninic acid (BCA) Protein Assay. The BCA Assay, is based on the premise that the reduction of Cu^{+2} to Cu^{+1} by protein in an alkaline medium, and combined with BCA permits the highly sensitive and selective colorimetric detection of Cu+1. Chelation of two molecules of BCA with one cuprous ion results in the formation of a purple-coloured reaction product detectable at 562 nm. In this case, astrocytes were re-suspended in 20 µL of lysis buffer and samples and standards were diluted in lysis buffer. Protein quantification of samples was determined from a standard curve of BSA measured at an absorbance of 562 nm.

2.2.8 D-[^{3}H]-aspartate Uptake Measurement

Primary astrocytic cultures were prepared from primary mixed glial cultures as described above (Day et al, 2014). Astrocytes were grown for two weeks in a T75 cm^2 flask in cDMEM, which was replaced every 4-5 days. At 14 DIV microglia were detached from the astrocyte monolayer by shaking off as previously described. Astrocytes were isolated and plated onto a 24-well plate coated with Poly-L-lysine to promote adherence and were matured for one week in cDMEM.

Astrocytes were treated at 21 DIV with L-AAA (0.05 mM, 0.15 mM, 0.5 mM) for 24 hours before D-[^{3}H]-aspartate uptake measurement. After 24 hours the treatment was removed and replaced with fresh media for 2 hours to remove any possible direct interference of the toxin. After 2 hours the plates were transferred to a radiological suite and placed on a rack in a 37°C water bath and left for 10-15 minutes to adjust to temperature. Media was gently aspirated using an aspirator pump. Cells were rinsed three times with 300 µL Krebs NaCl buffer (25 mmol/L HEPES, 4.8 mmol/L KCl, 1.2 mmol/L KH_2PO_4, 1.3 mmol/L $CaCl_2$, 1.2 mmol/L $MgSO_4$, 6 mmol/L glucose and 140 mmol/L NaCl, pH 7.4). 300 µL of D-[^{3}H]-aspartate (50 nmol/L, specific activity of 16.5 Ci/mmol, Perkin Elmer) was added to each well at 15 second intervals to ensure a precise total of 6 minutes uptake per well. After 6 min, the uptake was stopped by rinsing three times with 300 µL ice cold Krebs choline buffer (25 mmol/L HEPES, 4.8 mmol/L KCl, 1.2

mmol/L KH_2PO_4, 1.3 mmol/L CaCl2, 1.2 mmol/L $MgSO_4$, 6 mmol/L glucose and 120 mmol/L choline, pH 7.4). Cells were lysed by adding 500 µL of NaOH 0.1 N per well (Dumont et al, 2014). A 5 µL aliquot from each well was added to 5 mL Microscint in separate scintillation vials in duplicate. Radioactivity was measured using the Microscint 40 scintillation liquid and the TopCount NXT Microplate Scintillation and Luminescence Counter (Perkin Elmer). A fraction of the lysate was used for protein quantification.

2.2.8.1 Bradford protein quantification

Following the uptake assay, protein quantification was carried out using the Bradford method and BioRad Protein Assay Dye Reagent (BioRad). The protein assay is based on the premise that when mixed with a protein solution, the acidic Coomassie-dye reagent changes colour from brown to blue in proportion to the amount of protein present in the sample. Protein quantification is based on comparison to the colour response of a series of known dilutions of BSA. Glutamate uptake rate was expressed as picomole of D-[^{3}H]-aspartate transported per minute and per milligram of protein.

2.2.9 *In vivo* experiments

2.2.9.1 Animals

All animal procedures were carried out in accordance with the European Council Directive 1986 (86/609/EEC) and were approved by the BioResources Ethics Committee of Trinity College Dublin. Male C57BL6/J mice aged 9-14 weeks old (Charles River, UK or Harlan, UK) were kept in a 12 hours/12 hours light/dark cycle (lights on from 8am to 8pm) with access to food and water ad libitum. Mice were singly housed and handled for 5 days prior to surgery.

2.2.9.2 Intracortical administration of L-AAA by stereotactic surgery

For surgery, mice were initially anesthetised by IP injection using avertin (1.25g 2,2,2, tribromoethanol; 2.5 mL tertiary amyl alcohol; 100 mL distilled water) and secured in a stereotactic frame. L-AAA (Sigma Aldrich) (50 µg/µL; 1 µL; 0.2 µL/min) or PBS was administered bilaterally into the pre limbic cortex (PLC; 1.7

mm anteroposterior, –0.4mm dorsolateral and depth –2.5mm from Bregma). A total volume of 1 µL was injected at each site of administration.

Aseptic techniques were employed throughout the surgery to prevent contamination or infection. All surfaces and instruments were disinfected with EtOH 70% prior to carrying out the procedure. Surgical equipment was cleaned between each surgery with EtOH 70%. The head of the animal was also carefully cleaned with Betadine surgical scrub.

2.2.9.3 Perfusion

Mice were sacrificed by intraperitoneal injection with Euthanimal (Pentobarbital) (0.1 mL at 50 mg/mL) 72 hours following surgery. They were then transcardially perfused with saline 0.9% solution for 3 minutes in preparation for Golgi-cox staining (super Golgi Kit, Bioenno Tech, Irvine, CA, USA). In this case the descending thoracic aorta was clamped to increase perfusion flow to the head. An incision was made in the left ventricle of the heart and a cannula was inserted. Once perfusion started, the right atrium of the heart was cut to allow drainage.

2.2.9.4 Golgi-Cox staining and dendritic spine analysis

The superGolgi Kit (Bioenno) was used to label dendritic spines of neurons based on the principle of Golgi-Cox impregnation (Bioenno Tech, Irvine, CA, USA). Following transcardial perfusion, brains were collected, rinsed and incubated for 10 days in Impregnation solution (Solution A). Brains were then transferred into Post-impregnation buffer (Solution B: 30g reagent B in 90 mL dH_2O) for 1 day, renewed and kept at 4°C. Following staining, brains were sliced into coronal sections (150 µm) using a Vibratome and fresh collecting solution (Solution B). Slices were mounted on gelatine subbed slides for image analysis. Slides were then washed in 0.01 M PBS-Triton for 20-30 minutes and then placed in a diluted solution C in a closed staining jar. Slides were then placed in reagent D post-staining buffer for 20 minutes in a dark area and washed with 0.01 M PBS-Triton, 3 times for 5 minutes. The slides were rinsed briefly in distilled water, washed 4 times in absolute alcohol for 5 minutes and washed once with xylene for 5

minutes. A coverslip was placed on top using DPX mounting medium and coded to obscure the experimental group of each animal until the final step of statistical analysis.

2.2.9.5 Image acquisition and dendritic spine analysis

Z-stacks for spine analysis were acquired using an Olympus IX81 inverted live-imaging microscope at a magnification 600x (60x objective). Images of the regions of interest were acquired at a magnification 200x (20x objective) to quantify the number of primary neurites. 5 neurons per mouse were selected based on three main criteria; 1) non-truncated dendrites, 2) dark and uniform staining along all projections and 3) isolated from neighbouring stained neurons. 7 apical and 5 basal dendritic segments 30 µm in length were imaged per neuron. Neuron Studio software was used to remodel the dendrites, to quantify and morphologically classify spines as stubby (no neck), mushroom (head diameter: 4 µm and neck length < 2 µm), or thin (head diameter smaller than the neck length: > 2 µm). Values were calculated by averaging the number of spines divided by the dendritic length.

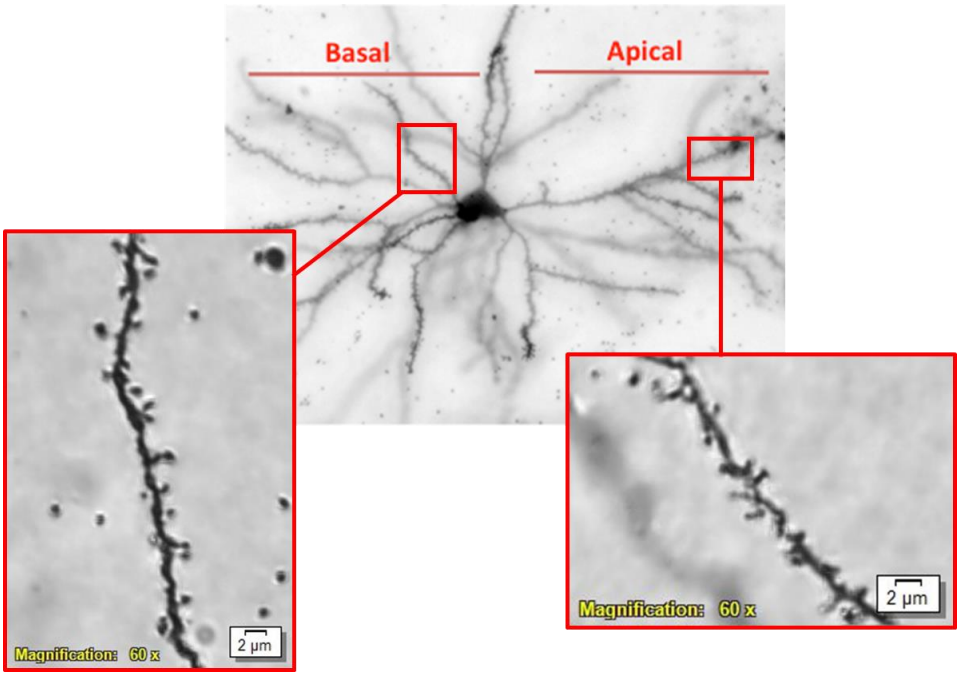

Figure 2.9 Representative image of Golgi-cox stained apical and basal dendritic spines in the PLC

Z-stacks of apical and basal spines in brain slices from the mouse PLC following Golgi-Cox staining. Images were acquired using a live-imaging microscope (60x objective).

2.3 Statistical analysis

All data were analysed using GraphPad Prism 8. Data were tested for normality using the Shapiro-Wilk test before applying parametric analysis. Data are expressed as group means with standard errors (SEM) and Student‘s t tests or analyses of variance (ANOVA) were performed where appropriate. In cases where a statistically significant change was found following one, two or repeated measures ANOVA, *post hoc* comparisons were performed to identify group differences using the Newman-Keuls test. Repeated measures ANOVA was used to analyse Sholl profile data. PCR data was normalised to express results as a fold change of control samples. Data were deemed significant when $P < 0.05$ (*), $P < 0.01$ (**) or $P < 0.001$ (***).

3 The effect of conditioned media from L-AAA exposed astrocytes on complexity and the expression of synaptic proteins in primary rat cortical neurons

3.1 Introduction

Astrocytes play an important regulatory role in a plethora of CNS processes including cerebral metabolism (Barros et al, 2013; Stobart & Anderson, 2013), neuronal outgrowth (Fang et al, 2019; Morel et al, 2017), synapse formation (Farhy-Tselnicker & Allen, 2018; Shen et al, 2016; Stogsdill et al, 2017) and dendrite morphology (Withers et al, 2017; Zhu et al, 2016; Zuchero & Barres, 2015). Astrocytes support and encourage neuronal guidance and development through the provision of ECM molecules (Ferrer-Ferrer & Dityatev, 2018; Lam et al, 2019; Wiese et al, 2012) and the secretion of soluble factors which enhance neurite growth and provide neuroprotection against toxic stimuli (Bylicky et al, 2018; Lu et al, 2015; Previtera et al, 2010; Takemoto et al, 2015). Astrocytic derived neurotrophic factors promote neuronal growth and resilience via activation of the cell survival signalling cascades MAPK and PI3K (Askvig & Watt, 2015; Day et al, 2014; Fujibayashi et al, 2015; Jha et al, 2015; Lui et al, 2012).

Secreted neurotrophic factors can be collected *in vitro* in the form of culture media from astrocytes – termed conditioned media. Conditioned media from healthy astrocytes is trophic and promotes outgrowth of immature primary cortical neurons and increases the co-localisation of synaptic proteins in mature neurons indicative of synapse formation (David et al, 2018). Conditioned media also protects neurons following exposure to neurotoxic and disease salient stimuli such as glutamate (Doucet et al, 2015; Lu et al, 2015), corticosterone (Zhu et al, 2006), methylmercury (Takemoto et al, 2015) and reactive oxygen and nitrogen species (Yates, 2015). Stimulation of astrocytic β2 adrenoceptors, in particular results in the release of neurotrophic growth factors including FGF-2, GDNF, IL-6, BDNF and NGF-β from astrocytes into the surrounding conditioned media (Day et al, 2014).

Given their multifaceted role in promoting neuronal outgrowth and synapse formation it is not surprising that there is increasing evidence linking astrocytic impairment to neuronal atrophy and synaptic dysfunction underlying a variety of neuropsychiatric diseases such as AD, PD (Halliday et al, 2011; Verkhratsky et al,

2010) and schizophrenia (Czéh & Nagy, 2018; Nagy et al, 2015; Rajkowska & Stockmeier, 2013; Sanacora & Banasr, 2013).

3.1.1 Using L-AAA as a tool to induce astrocyte impairment *in vitro*

Alpha aminoadipic acid (AAA) is a glutamate analogue which has been employed experimentally to model astrocytic impairment and investigate the impact of astrocyte impairment on neuronal integrity both *in vivo* and *in vitro* (David et al, 2018; Lee et al, 2013b; Lima et al, 2014; O'Neill et al, 2019).

AAA is a six carbon homologue of glutamate (*Figure 3.1*) and intermediate product of lysine metabolism which occurs naturally in the brain (Hallen et al, 2013). Its selective gliotoxic properties were originally reported during neurotoxicity testing studies when injection of AAA into infant mice produced non-neuronal degeneration (Olney et al, 1971). The L-isomer (L-AAA) exerted extreme gliotoxic damage compared to mild toxicity produced by the D isomer (D-AAA) (Olney et al, 1980). Early studies report changes in the integrity of astrocytes including disruption of the astrocytic network and a prominent reduction in the number of GFAP+ and S100β+ cells following injection of L-AAA into the amygdala of rats (Khurgel et al, 1996). Additional studies report localised degeneration specific to astrocytes following intra striatal injections of L-AAA in rats (Khurgel et al, 1996; Takada & Hattori, 1986), whereby morphological appearance and the density of neurons in the astrocyte-free zone remain unchanged. More recent research has shown that delivery of L-AAA to the medial prefrontal cortex (mPFC) produces astrocyte dysfunction, indicated by a loss of GFAP+ astrocytes in the targeted region and corollary effects on neurons such as dendritic atrophy and a reduction in neuronal nuclear protein (NeuN) immunoreactivity (Lima et al, 2014).

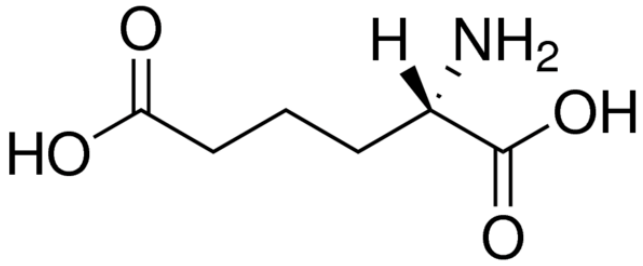

Figure 3.1 Chemical structure of L-alpha-aminoadipic acid (L-AAA)
L-AAA is a glutamate analogue that differs from glutamate by one single methylene group. L-AAA has been shown to exhibit specific astrocytic toxicity including the inhibition of astrocytic enzymes and protein synthesis following uptake through astrocytic glutamate transporters (Pena et al, 2017).

Studies *in vitro* have since reported on the toxic selectivity of the compound towards astrocytes (David et al, 2018). L-AAA is primarily taken up by astrocytes, where it accumulates intracellularly and induces a transient dysfunction characterised by disruption of protein synthesis and metabolic processes (Smiałowska et al, 2013). *In vitro* studies indicate that L-AAA likely exerts its effects via inhibition of glutamine synthetase (GS) (inhibiting the conversion of glutamate to glutamine) and by the inhibition of γ-glutamylcysteine synthetase (inhibiting the synthesis of glutathione) (Brown & Kretzschmar, 1998; McBean, 1994; Voss et al, 2016) (*Figure 3.2*). Inhibition of the production of the endogenous excitatory amino acid receptor antagonist kynurenic acid, has been proposed as an additional method of action of L-AAA based on previous observations where a 2-hour application of L-AAA reduced kynurenic acid production by 60% in neocortical slices from adult cerebral cortex (Voss et al, 2016).

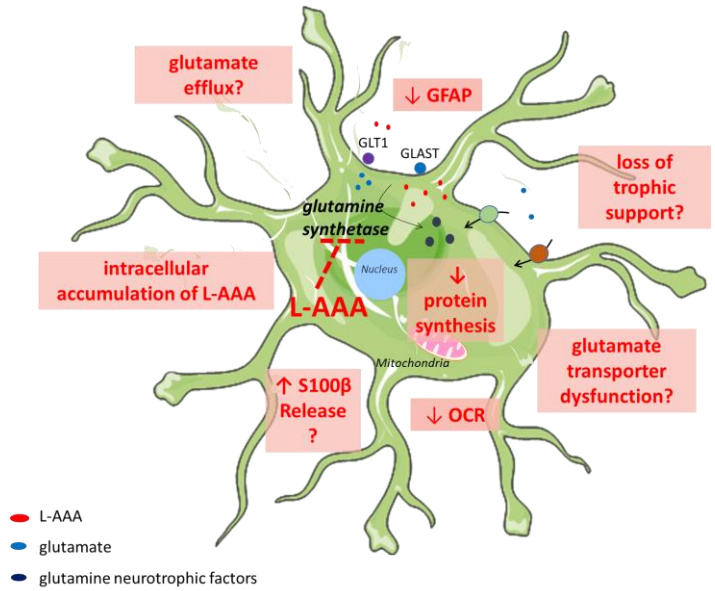

Figure 3.2 Proposed mechanism of action of L-AAA
Studies reporting on the toxic selectivity of L-AAA towards astrocytes suggest that L-AAA likely exerts its effects via (1) inhibition of the activity of astrocytic enzymes glutamine synthetase and γ-glutamylcysteine synthetase resulting in the inhibition of astrocytic conversion of glutamate to glutamine and inhibition of glutathione synthesis, (2) inhibition of protein synthesis and (3) impairment of astrocytic glutamate transporter systems. Glutamate-aspartate transporter; GLAST. Glutamate transporter-1; GLT-1.

In this study, the effects of L-AAA-induced astrocyte dysfunction using primary cortical cultures are assessed *in vitro*. The effects of L-AAA on the immunoreactivity of GFAP and AQP4, morphology of astrocytic cells, the expression of astrocytic markers and measures of astrocytic ATP production, mitochondrial respiration and glycolysis are quantified. Previous work has shown that healthy astrocytes provide support to neurons and increase the complexity of immature neurons and synapse formation of primary mature cortical neurons *in vitro* (David et al, 2018). Following on, the effects of conditioned media obtained from L-AAA treated astrocytes on mature primary cortical neurons, are assessed to examine the impact of astrocyte dysfunction on neurite outgrowth and co-localisation of pre and postsynaptic proteins.

This study adds to our current understanding by further investigating the effect of conditioned media from L-AAA treated astrocytes on complexity and the expression of synaptic markers in mature neurons, which are more representative of the complexity of neurons in the adult brain (Balu & Coyle, 2011; Coyle et al, 2012).

Concentrations of L-AAA were chosen based on prior research which used a similar range of concentrations on astrocytes (Brown & Kretzschmar, 1998; Nishimura et al, 2000). It has been accepted that astrocyte-specific effects predominate in the dose range 0.5–1.0 mM. A ten-fold dose reduction has also been included to account for the increased sensitivity of mature neuronal cultures to external stimuli (Voss et al, 2016; Zhou et al, 2011). Previous viability studies (Alamar blue test) demonstrate that 48-hour treatment with L-AAA (0.5 mM) has no effect on astrocyte or neuronal viability (David et al, 2018). The L-AAA dose used for assessing dendritic spine density in vivo was also chosen based on previous studies investigating astrocyte impairment *in vivo* (Lee et al, 2013b; Lima et al, 2014) and one study indicating that one single dose of L-AAA (50 µg/µL) produces a robust reduction in GFAP immunoreactivity (David et al, 2018).

3.1.2 Markers of L-AAA-induced changes in glial morphology

Astrocytes respond to CNS insults by altering their morphology and GFAP has been employed traditionally as an astrocyte marker to qualify and quantify such changes experimentally (Pekny & Pekna, 2014; Sun & Jakobs, 2012). Up-regulation of GFAP, including increased number and length of GFAP-positive processes has been well established as a classical hallmark of reactive astrocytes in primates and rodents (Gallo & Deneen, 2014; Herculano-Houzel, 2014; Hol & Pekny, 2015; Pekny & Pekna, 2014). However, despite its widespread use, the role of GFAP as a specific astrocyte marker is becoming increasingly questionable (Zhang et al, 2019) and novel data suggests that expression of GFAP is more complicated than originally described (*see section 1.3.1.2*). Data suggests that it may only be associated with reactive astrocytes and is further affected by both regional and local variability (Sofroniew & Vinters, 2010a). Resultantly, it was of interest to investigate the effect of L-AAA on AQP4 as a second marker that is highly expressed in astrocytes. For this experiment primary cortical astrocytes (DIV 14) were treated with L-AAA (0.05, 0.15, 0.5 mM) for 24 hours. Fixation and immunocytochemistry were performed to determine the effect of L-AAA on AQP4 immunoreactivity.

Microglia morphology is also assessed using the immunocytochemical marker Iba1. Iba1 is a 7-kDa actin-binding cytoplasmic protein expressed primarily in microglia (Walker & Lue, 2015). It stains both resting and activated cells and has been employed traditionally to examine morphological features of microglial cells at the light microscopic level (Fernández-Arjona et al, 2017; Torres-Platas et al, 2014; Vinet et al, 2012). As a pan-microglial marker, Iba1 expression is a well-established indicator of microglial motility and migration (Minett et al, 2016). Expression of Iba1 is thought to increase with microglial activation and inflammation, where it is reported to play a key role in phagocytosis and actin-crosslinking involved in membrane ruffling (Hopperton et al, 2018; Minett et al, 2016). Since membrane ruffling is essential for the morphological transition from a quiescent ramified state to an activated amoeboid state, up-regulation of Iba1 expression often coincides with this conversion. Up-regulation of Iba1 is also a well-recognised hallmark of numerous CNS pathologies (Kozlowski & Weimer, 2012).

3.2 Aims

The overall aim of the study outlined in this chapter is to examine the effect of L-AAA-induced astrocyte impairment on neuronal integrity. Moreover, this investigation aims to determine a role for astrocyte dysfunction in mediating changes in neuronal integrity by employing mature cortical neuronal cultures. Subsequently, the effect of conditioned media from L-AAA treated astrocytes (CM L-AAA) on neuronal complexity, including the number of neuritic branches, neurite length, the number of primary neurites, and the Sholl profile were examined. Finally, this study extends to an *in vivo* model by examining the effect of L-AAA on the morphology of dendritic spines and number of primary dendrites in the prelimbic cortex (PLC) of mice.

The specific aims of this study are to investigate the effects of L-AAA (1) on GFAP immunoreactivity and astrocyte morphology, (2) on Iba1 immunoreactivity and microglia morphology, (3) on AQP4 immunoreactivity, (4) on the expression of astrocytic and microglial markers, (5) on astrocytic ATP production, oxygen consumption rates (OCR) and extracellular acidification rates (ECAR), (6) on astrocytic uptake of [^{3}H] aspartate, (7) the effect of conditioned media from L-AAA treated rat primary enriched astrocytic cultures on the complexity and co-localised expression of pre-synaptic synaptophysin and post-synaptic PSD-95 in rat primary cortical neuronal cultures, and (8) the effect of L-AAA on the density of dendritic spines in the PLC of mice.

Previous work carried out to assess the effects of conditioned media from L-AAA treated enriched astrocytic cultures has been with primary cortical immature neurons. The utilisation of a mature neuron model and translation into an *in vivo* mouse model provide a better representation of the impact of astrocytic impairment on neuronal growth and synaptic connectivity in the adult brain. Re-evaluation of the effects of astrocytic impairment on neurite outgrowth and synapse formation corresponds with the increasing body of literature attributing astrocytic dysfunction to neuronal atrophy and synaptic dysconnectivity, which in turn, have become well-recognised hallmarks of the pathophysiology of a number of degenerative and neuropsychiatric disorders.

3.3 Results

3.3.1 Effect of L-AAA on GFAP immunoreactivity and the morphology of enriched astrocyte cultures

To investigate if L-AAA affects GFAP immunoreactivity and astrocyte morphology, enriched primary cortical astrocytes (DIV 14) were treated with L-AAA (0.05, 0.5 mM) for 24 hours. Fixation and immunocytochemistry were performed to determine the effect of L-AAA on GFAP and AQP4 immunoreactivity and astrocyte morphology (mean cell area, perimeter and soma: area ratio). Concentrations of L-AAA were chosen based on prior research which demonstrates that astrocyte-specific effects such as a reduction in protein synthesis predominate in the dose range 0.5–1.0 mM, without effecting astrocyte viability (Brown & Kretzschmar, 1998; Nishimura et al, 2000; Voss et al, 2016).

One-way ANOVA of **GFAP immunoreactivity** showed an effect of L-AAA [$F_{(2, 156)} = 47.11$, $P < 0.001$]. *Post hoc* analysis revealed a dose-dependent decrease in GFAP immunoreactivity following treatment with L-AAA (0.05, 0.5 mM) ($P < 0.001$) compared to control DMEM. [*Figure 3.3 (A)*]. One-way ANOVA of astrocyte **mean cell area** also showed an effect of L-AAA [$F_{(2, 154)} = 131.2$, $P < 0.001$]. *Post hoc* analysis revealed a decrease in the mean cell area of astrocytes following treatment with both concentrations of L-AAA (0.05, 0.5 mM) ($P < 0.001$) compared to control DMEM [*Figure 3.3 (B)*]. Similarly, one-way ANOVA of astrocyte **cell perimeter** showed an effect of L-AAA [$F_{(2, 158)} = 135.2$, $P < 0.001$]. *Post hoc* analysis revealed decreases in the cell perimeter of astrocytes following treatment with both concentrations of L-AAA (0.05, 0.5 mM) ($P < 0.001$) compared to control DMEM [*Figure 3.3 (C)*]. Treatment of primary cortical astrocytes with L-AAA-induced a dose-dependent reduction on the **expression of AQP4** [$F_{(3, 274)} = 22.06$, $P < 0.001$]. *Post hoc* analysis revealed a significant decrease in AQP4 immunoreactivity for astrocytes treated with all three concentrations of L-AAA (0.05, 0.15, 0.5 mM) compared to control DMEM ($P < 0.001$) [*Figure 3.5*].

3.3.2 Effect of L-AAA on Iba1 immunoreactivity and the morphology of enriched microglial cultures

To investigate if L-AAA affects Iba1 immunoreactivity and microglia morphology, enriched primary cortical microglia (DIV 15) were treated with L-AAA (0.05, 0.5 mM) for 24 hours. Fixation and Iba1 immunocytochemistry were performed to determine the effect of L-AAA on Iba1 immunocytochemistry and microglia morphology (mean cell area, perimeter and soma: area ratio).

One-way ANOVA of **Iba1 immunoreactivity** showed no effect of L-AAA [$F_{(2, 148)}$ = 0.320, P = 0.726] [*Figure 3.4 (A)*]. One-way ANOVA of microglial **mean cell area** also showed no effect of L-AAA [$F_{(2, 179)}$ = 0.289, P = 0.749] [*Figure 3.4 (B)*]. Similarly, one-way ANOVA of microglia **cell perimeter** showed no effect of L-AAA [$F_{(2, 179)}$ = 0.584, P = 0.5588] *[Figure 3.4 (C)*].

3.3.3 Effect of L-AAA on the mRNA expression of astrocytic markers GFAP, S100β, IL-1β, and IL-6

To investigate the effects of L-AAA on the mRNA expression of astrocytic markers, cultures of enriched primary cortical astrocytes (DIV 14) were treated with L-AAA (0.05, 0.5 mM) for 24 hours. Cells were harvested for RNA extraction followed by RT-PCR. mRNA expression of the markers GFAP, S100β, IL-1β, and IL-6 were quantified.

Treatment of primary cortical astrocytes with L-AAA had a dose-dependent effect on the mRNA expression of **GFAP** [$F_{(2, 21)}$ = 12.91, P < 0.001]. *Post hoc* analysis revealed no effect of L-AAA (0.05 mM) on GFAP mRNA expression. However, a decrease in GFAP mRNA expression following treatment with L-AAA (0.5 mM) was determined compared to control DMEM (P < 0.001) [*Figure 3.6 (A)*]. Treatment of primary cortical astrocytes with L-AAA also had a dose-related effect on the mRNA expression of **S100β** [$F_{(2, 21)}$ = 6.759, P = 0.005]. *Post hoc* analysis revealed no effect of L-AAA (0.05 mM) on S100β mRNA expression. However, a decrease in S100β mRNA expression following treatment with L-AAA (0.5 mM) was revealed compared to control DMEM (P < 0.01) [*Figure 3.6 (B)*]. Similarly, treatment of primary cortical astrocytes with L-AAA had a dose-related effect on the mRNA expression of **IL-1β** [$F_{(2, 10)}$ = 14.20, P = 0.001]. *Post hoc*

analysis revealed no effect of L-AAA (0.05 mM) on IL-1β mRNA expression. However, a decrease in IL-1β mRNA expression following treatment with L-AAA (0.5 mM) was revealed compared to control DMEM ($P < 0.01$) [*Figure 3.6 (C)*]. Treatment of primary cortical astrocytes with L-AAA had no effect on the mRNA expression of **IL-6** [$F_{(2, 14)} = 0.6567$, $P = 0.534$] [*Figure 3.6 (D)*].

3.3.4 Effect of L-AAA on the mRNA expression on microglial markers TNF-α, IL-1α, and Iba1

To investigate the effects of L-AAA on the mRNA expression of microglial markers, cultures of enriched primary cortical microglia (DIV 15) were treated with L-AAA (0.05, 0.5 mM) for 24 hours. Cells were harvested for RNA extraction followed by RT-PCR. mRNA expression of the markers TNF-α, IL-1α, and Iba1 were quantified. Stimulation of primary cortical microglia with L-AAA had no effect on the mRNA expression of **TNF-α** [$F_{(2, 15)} = 1.425$, $P = 0.271$], **IL-1α** [$F_{(2, 21)} = 2.205$, $P = 0.135$] or **Iba1** [$F_{(2, 21)} = 0.537$, $P = 0.592$] [*Figure 3.7 (A-C)*].

3.3.5 Effects of L-AAA on astrocytic mitochondrial respiration and glycolysis

To investigate the effect of L-AAA on astrocyte metabolism, primary cortical astrocytes (DIV 14) were treated with L-AAA (0.5 mM) for 24 hours and the OCR and ECAR were assessed as an indicator of mitochondrial respiration and glycolysis using the Extracellular Flux Analyzer (Seahorse Biosciences) as previously described.

L-AAA reduced basal mitochondrial respiration [$T_{(8)} = 2.759$, $P = 0.025$], maximal mitochondrial respiration [$T_{(8)} = 5.23$, $P = 0.001$] and ATP-linked mitochondrial respiration [$T_{(8)} = 3.203$, $P = 0.013$], compared to control DMEM (Student's T test) [*Figure 3.8 (A-C)*]. L-AAA had no effect on basal glycolysis [$T_{(8)} = 0.375$, $P = 0.717$], glycolytic reserve [$T_{(8)} = 0.186$, $P = 0.857$], glycolytic capacity [$T_{(8)} = 0.349$, $P = 0.736$], compared to control DMEM (Student's T test) [*Figure 3.8 (D-F)*].

3.3.6 Effects of L-AAA on the uptake of [^{3}H] aspartate in enriched cortical astrocyte cultures

Aspartate uptake was evaluated by developing an uptake assay using D-aspartate, a transportable analogue of L-glutamate, which is not metabolised

and does not interact with glutamate receptors. To investigate the effect of L-AAA on astrocytic uptake of [^{3}H] aspartate primary cortical astrocytes were matured (DIV 21) and treated with L-AAA (0.5, 0.15 and 0.5 mM) or control DMEM for 24 hours. Treatments were removed and fresh media was replaced directly before quantification of the uptake of the radiolabelled glutamate analogue [^{3}H]-D-aspartate (50 nM, Perkin Elmer, USA). Protein quantification was carried out using the Bradford protein quantification assay as previously described. Results showed that treatment of primary cortical astrocytes with L-AAA had no effect on the uptake of [^{3}H] aspartate compared to control DMEM [$F_{(3, 129)} = 1.413$, $P = 0.242$] [*Figure 3.9*].

3.3.7 Effects of direct application of L-AAA and conditioned media from L-AAA treated astrocytes on the complexity of mature neurons

Primary cortical astrocytes (DIV 14) were treated with L-AAA (0.05, 0.5 mM) for 24 hours and the resulting conditioned media was collected and applied to mature primary cortical neurons (DIV 21) for 24 hours. Fixation and immunocytochemistry were performed to determine the effect of conditioned media from L-AAA treated astrocytes on neuronal complexity by Sholl analysis. Mature neurons (DIV 21) were also treated directly with L-AAA (0.05, 0.5 mM) for 24 hours before fixation and immunocytochemistry in order to assess whether L-AAA impacted directly upon neurite complexity.

When examining the effect of conditioned media from L-AAA treated astrocytes, one-way ANOVA of **neuritic branches** showed an effect of treatment [$F_{(4, 496)} = 17.13$, $P < 0.001$]. *Post hoc* analysis revealed an increase in the number of neuritic branches for neurons treated with conditioned media from untreated astrocytes ($P < 0.001$). *Post hoc* analysis revealed reductions in the number of neuritic branches following treatment with all tested concentrations of L-AAA (0.05, 0.15, 0.5 mM) compared to conditioned media from untreated astrocytes ($P < 0.001$) [*Figure 3.10 (A)*]. One-way ANOVA of **neuritic length** showed an effect of treatment [$F_{(4, 584)} = 180.0$, $P < 0.001$]. *Post hoc* analysis revealed an increase in the neuritic length for neurons treated with control conditioned media ($P < 0.001$). *Post hoc* analysis revealed reductions in neuritic length

following treatment with all tested concentrations of L-AAA (0.05, 0.15, 0.5 mM) compared to conditioned media from untreated astrocytes ($P < 0.001$) [*Figure 3.10 (B)*]. One-way ANOVA of the number of **primary neurites** showed no effect of treatment [$F_{(4, 590)} = 3.384$, $P = 0.009$] [*Figure 3.10 (C)*]. Two-way repeated measures ANOVA of the **number of neuritic branches at specific distances from the neuronal cell soma** showed an effect of distance [$F_{(19, 11153)} = 1171$, $P < 0.001$], an effect of treatment [$F_{(4, 587)} = 159.5$, $P < 0.001$] and an effect of interaction [$F_{(76, 11153)} = 28.67$, $P < 0.001$]. Conditioned media from untreated astrocytes increased neuritic branching at all distances between 30-170 µm from the cell soma compared to control NBM. Conditioned media from L-AAA treated astrocytes decreased neuritic branching at all distances between 10-100 µm from the cell soma compared to conditioned media from untreated astrocytes [*Figure 3.10 (D)*].

On the other hand, when examining the effect of the direct application of L-AAA to primary cortical neruons one-way ANOVA of **neuritic branches** showed no effect of direct treatment with L-AAA [$F_{(2, 355)} = 1.004$, $P = 0.368$] [*Figure 3.11 (A)*]. One-way ANOVA of **neuritic length also** showed no effect of direct treatment with L-AAA [$F_{(2, 354)} = 0.155$, $P = 0.857$] [*Figure 3.11 (B)*]. *Simialrly*, one-way ANOVA of the number of **primary neurites** showed no effect of direct treatment with L-AAA [$F_{(2, 353)} = 0.187$, $P = 0.829$] [*Figure 3.11 (C)*]. Two-way repeated measures ANOVA of the **number of neuritic branches at specific distances from the neuronal cell soma** showed an effect of distance [$F_{(19, 6620)} = 637.7$, $P < 0.0001$], showed no effect of treatment [$F_{(2, 6620)} = 1.324$, $P = 0.266$] and no effect of interaction [$F_{(38, 6620)} = 0.983$, $P = 0.500$]. L-AAA slightly decreased neuritic branching at 40-50 µm ($P < 0.01$) from the cell soma compared to control NBM [*Figure 3.11 (D)*].

3.3.8 Effect of direct application of L-AAA and conditioned media from L-AAA treated astrocytes on co-localisation of synaptic proteins in mature primary cortical neurons

Primary cortical astrocytes (DIV 14) were treated with L-AAA (0.05, 0.5 mM) for 24 hours and the resulting conditioned media was collected and applied to mature primary cortical neurons (DIV 21) for 24 hours. Fixation and

immunocytochemistry were performed to determine the effect of conditioned media from L-AAA treated astrocytes on synaptic protein co-localisations. Mature neurons (DIV 21) were also treated directly with L-AAA (0.05, 0.5 mM) for 24 hours before fixation and immunocytochemistry in order to assess whether L-AAA impacted directly upon synaptic protein co-localisations alone.

One-way ANOVA of **synaptophysin puncta** showed an effect of treatment [$F_{(3, 35)} = 20.35$, $P < 0.001$]. *Post hoc* analysis revealed reductions in the number of synaptophysin puncta following treatment with conditioned media from L-AAA (0.05, 0.5 mM) treated astrocytes compared to conditioned media from untreated astrocytes ($P < 0.001$) [*Figure 3.12 (A)*]. One-way ANOVA of **PSD-95 puncta** also showed an effect of treatment [$F_{(3, 35)} = 11.56$, $P < 0.001$]. *Post hoc* analysis revealed reductions in the number of PSD-95 puncta following treatment with conditioned media from L-AAA (0.05 mM) treated astrocytes compared to conditioned media from untreated astrocytes ($P < 0.01$) [*Figure 3.12 (B)*]. One-way ANOVA of **co-localised synaptic puncta** showed an effect of treatment [$F_{(3, 35)} = 17.54$, $P < 0.001$]. *Post hoc* analysis revealed an increase in the number of co-localised synaptic puncta following treatment with conditioned media from untreated astrocytes ($P < 0.01$) compared to NBM. *Post hoc* analysis also revealed reductions in the expression of co-localised synaptic markers following treatment with conditioned media from L-AAA (0.05, 0.5 mM) treated astrocytes compared to conditioned media from untreated astrocytes ($P < 0.001$) [*Figure 3.12 (C)*].

When examining the effect of direct application of L-AAA, one-way ANOVA of **synaptophysin puncta** showed an effect of treatment [$F_{(2, 256)} = 6.116$, $P = 0.003$]. *Post hoc* analysis revealed a decrease in the number of synaptophysin puncta following treatment with L-AAA (0.5 mM) compared to control NBM ($P < 0.01$) [*Figure 3.13 (A)*]. One-way ANOVA of **PSD-95 puncta** also showed an effect of treatment [$F_{(2, 260)} = 4.496$, $P = 0.01$]. *Post hoc* analysis revealed a decrease in the number of PSD-95 puncta following treatment with L-AAA (0.05 mM) compared to control NBM ($P < 0.01$) [*Figure 3.13 (B)*]. Simialrly, one-way ANOVA of **co-localised synaptic puncta** showed an effect of treatment [$F_{(2, 261)} = 5.7$, $P =$

0.004]. *Post hoc* analysis revealed a decrease in the number of co-localised synaptic puncta following treatment with L-AAA (0.05 mM) compared to control NBM ($P < 0.05$), and following treatment with L-AAA (0.01 mM) compared to control NBM ($P < 0.01$) [*Figure 3.13 (C)*].

3.3.9 Effects of L-AAA on neuritic branching and dendritic spine density in the PLC of mice

To assess the effect of L-AAA on dendritic spine density and neuronal complexity, L-AAA (50 µg/µL; 1 µL) or PBS was administered to the PLC of male C57Bl6/J 9-12 weeks old mice (BioResources, Trinity College Dublin). 72 hours following L-AAA administration, animals were euthanised and brains were collected for Golgi-Cox staining. Quantification and morphological classification of spines was carried out using NeuronStudio as described in the Materials and Methods (section *2.2.9.5*).

Results showed that delivery of L-AAA to the PFC increased **dendritic spine density**. Two-way ANOVA of spine density on basal dendrites showed an effect of L-AAA [$F_{(1, 111)} = 13.15$, $P < 0.001$], an effect of spine subtype [$F_{(2, 111)} = 11.31$, $P < 0.001$] and no L-AAA x spine subtype interaction [$F_{(2, 111)} = 0.24$, $P = 0.8$]. *Post hoc* comparisons revealed that L-AAA administration increased the density of thin spines on basal dendrites compared to control PBS ($P < 0.01$) [*Figure 3.14 (A)*]. Two-way ANOVA of spine density on apical dendrites showed an effect of L-AAA [$F_{(1, 114)} = 19.16$, $P < 0.001$], an effect of spine subtype [$F_{(2, 114)} = 8.962$, $P < 0.001$] and no L-AAA x spine subtype interaction effect [$F_{(2, 114)} = 0.297$, $P = 0.743$]. *Post hoc* comparisons revealed that L-AAA administration increased the density of stubby ($P < 0.05$) and thin spines ($P < 0.01$) on apical dendrites compared to control PBS [*Figure 3.14 (B)*]. Delivery of L-AAA to the PFC had no effect on the number of **primary neurites** [[$T_{(38)} = 0.247$, $P = 0.807$], compared to control PBS vehicle [*Figure 3.14 (E)*].

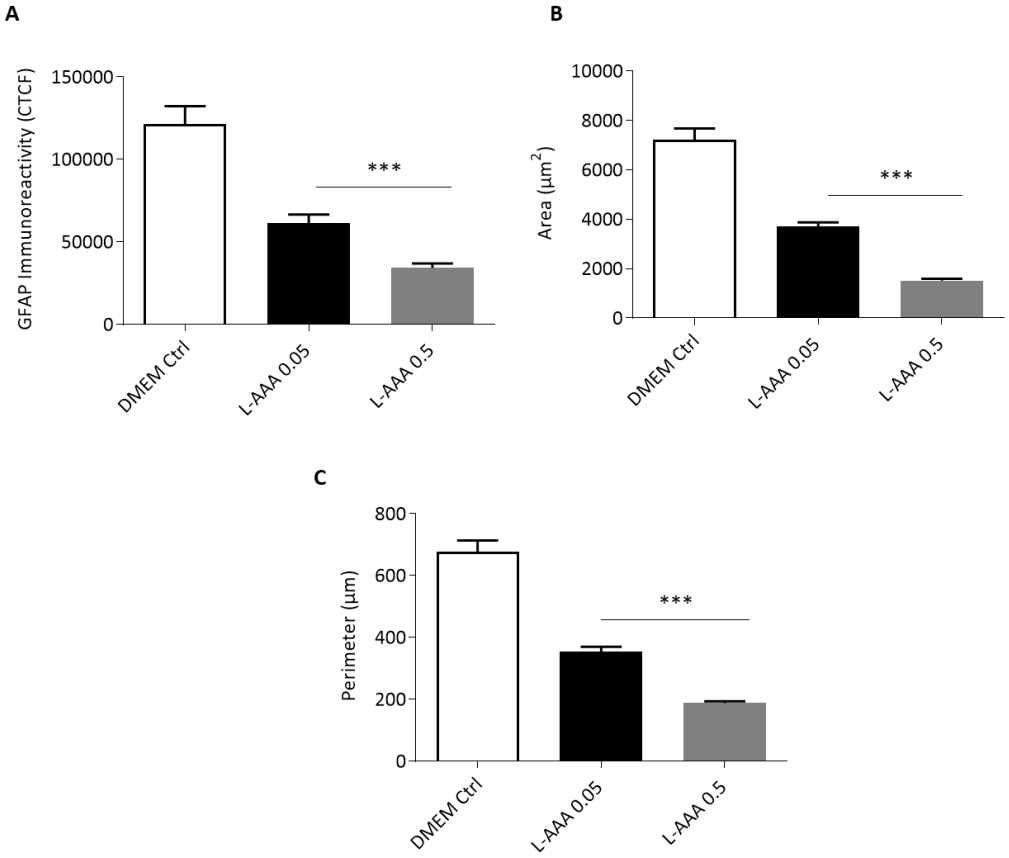

Figure 3.3 L-AAA reduces GFAP immunoreactivity and the mean cell area and perimeter of enriched primary cortical astrocytes.

Enriched primary cortical astrocytes (DIV 14) were treated with L-AAA (0.05, 0.5 mM) for 24 hours before fixation and GFAP immunocytochemistry. Morphological analysis was performed to quantify GFAP immunoreactivity (A), mean cell area (B) and perimeter (C). Data are expressed as mean ± SEM, n=8 coverslips per treatment group from 3 independent experiments. ***P<0.001 vs. control DMEM (Newman-Keuls *post hoc* test).

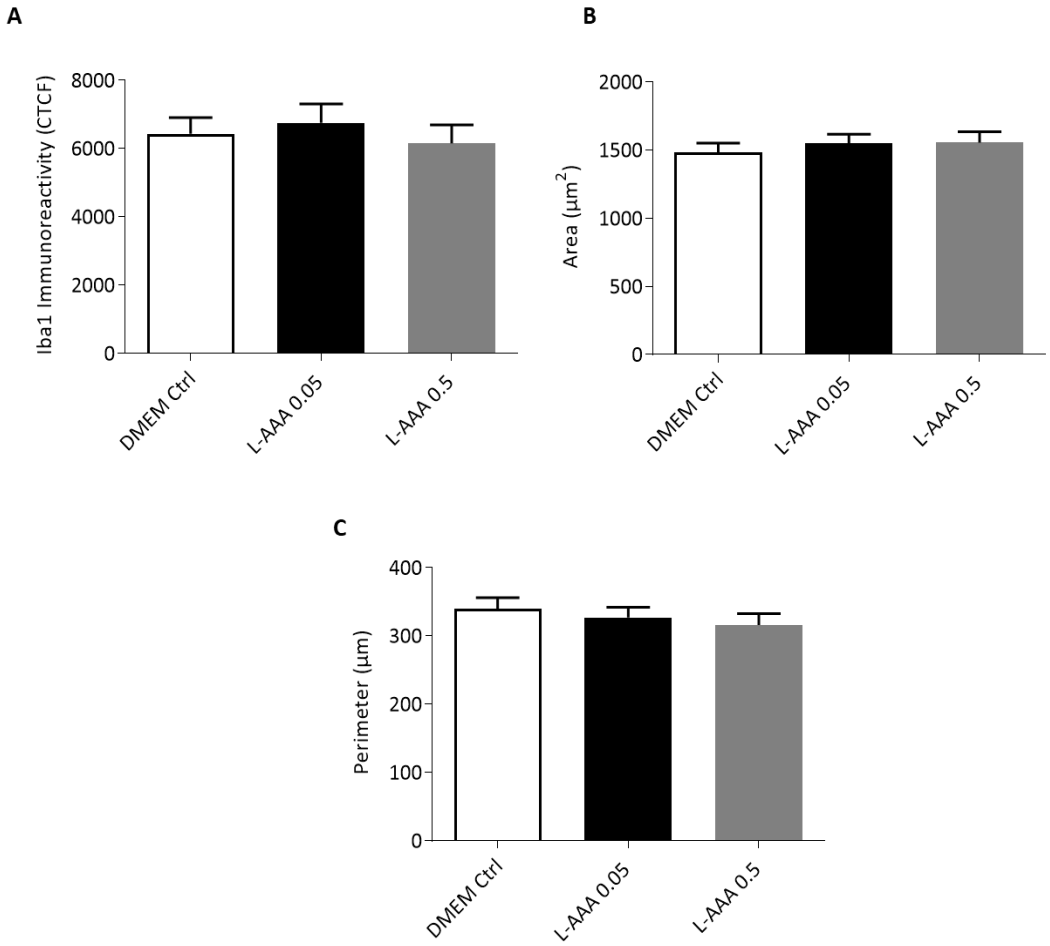

Figure 3.4 L-AAA has no effect on Iba1 immunoreactivity or the morphology of enriched primary cortical microglia.

Enriched microglia (DIV 15) were treated with L-AAA (0.05, 0.5 mM) for 24 hours before fixation and Iba1 immunocytochemistry. Morphological analysis was performed to quantify Iba1 immunoreactivity (A), mean cell area (B) and perimeter (C). Data are expressed as mean ± SEM, n=8 coverslips per treatment group from 3 independent experiments.

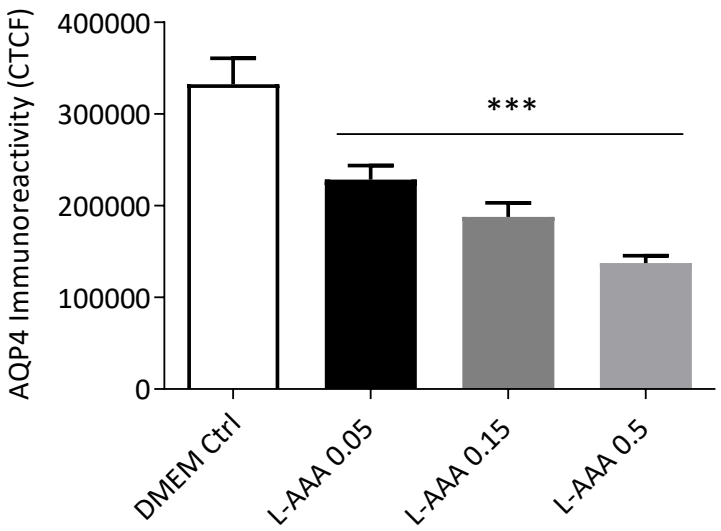

Figure 3.5 L-AAA reduces AQP4 immunoreactivity in enriched primary cortical astrocytes.

Astrocytes (DIV 14) were treated with L-AAA (0.05, 0.15, 0.5 mM) for 24 hours and before fixation and immunocytochemistry for AQP4. Immunoreactivity was quantified by measuring the corrected total cell fluorescence (CTCF). Data are expressed as mean ± SEM, n=6 coverslips per treatment group from 3 independent experiments. ***P<0.001 vs. control DMEM (Newman-Keuls *post hoc* test).

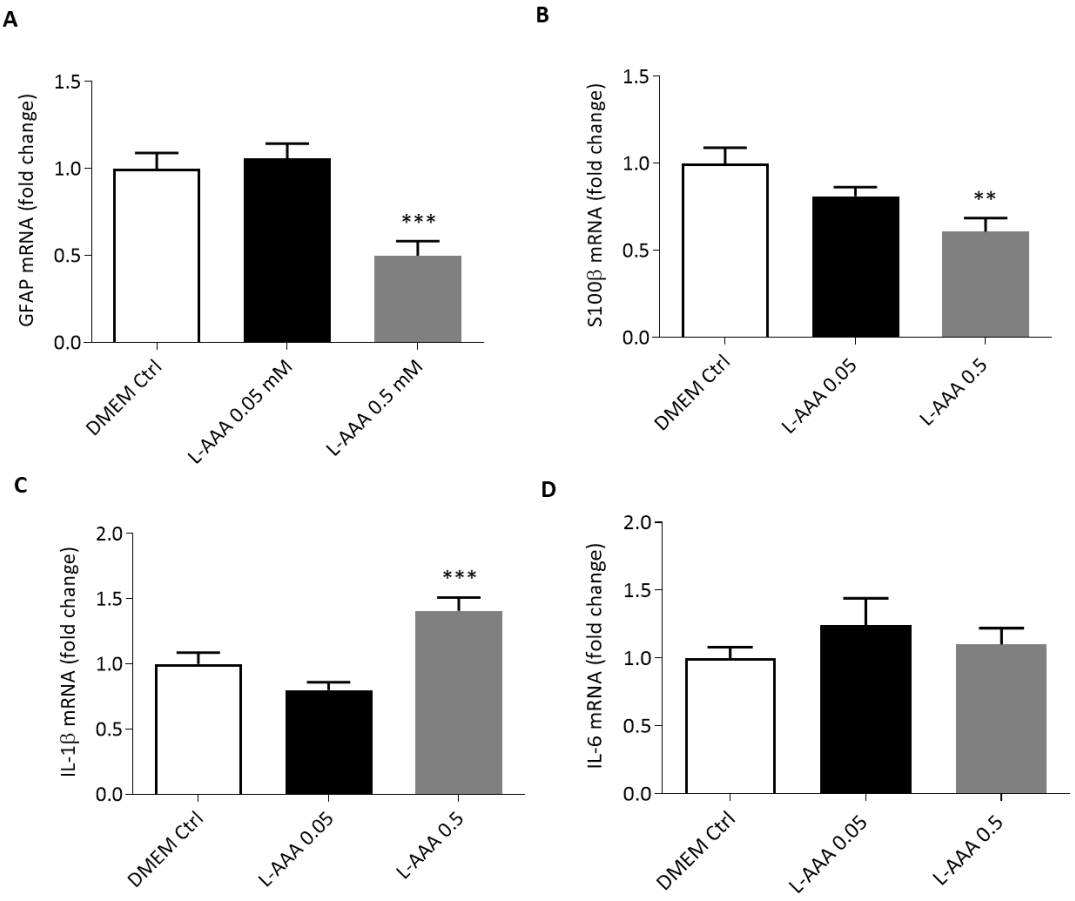

Figure 3.6 L-AAA affects the mRNA expression of markers GFAP, S100β, IL-1β and IL-6 in primary cortical astrocytes.

Enriched astrocytes (DIV 14) were treated with L-AAA (0.05, 0.5 mM) for 24 hours. Cells were harvested for RNA extraction followed by RT-PCR to analyse the expression of GFAP (A), S100β (B), IL-1β (C) and IL-6 (D). Data are expressed as mean ± SEM, n=8 wells per treatment group from 3 independent experiments. ***P<0.001, **P<0.01 vs. control DMEM (Newman-Keuls *post hoc* test).

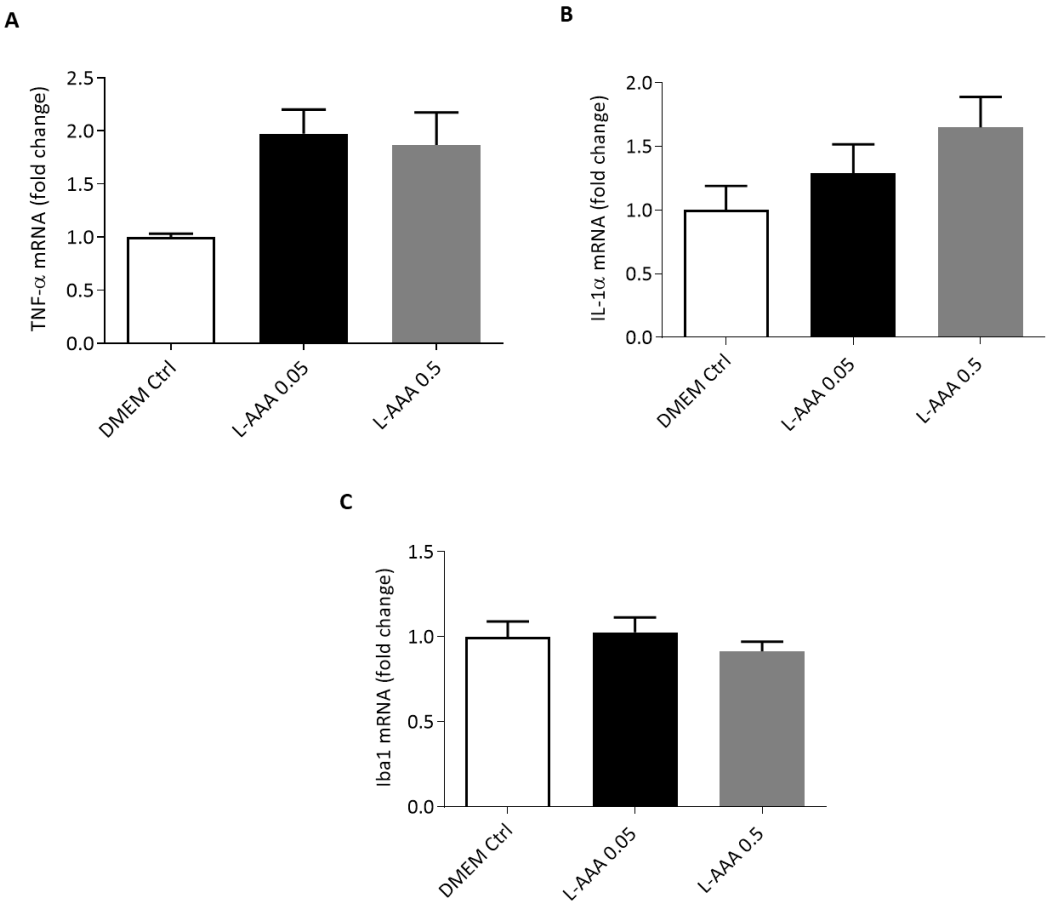

Figure 3.7 L-AAA has no effect on the mRNA expression of TNF-α, IL-1α and Iba1 in primary cortical microglia.

Enriched primary cortical microglia (DIV 15) were treated with L-AAA (0.05, 0.5 mM) for 24 hours. Cells were harvested for RNA extraction followed by RT-PCR to analyse the expression of TNF-α (A), IL-1α (B) and Iba1 (C). Data are expressed as mean ± SEM, n=8 wells per treatment group from 3 independent experiments.

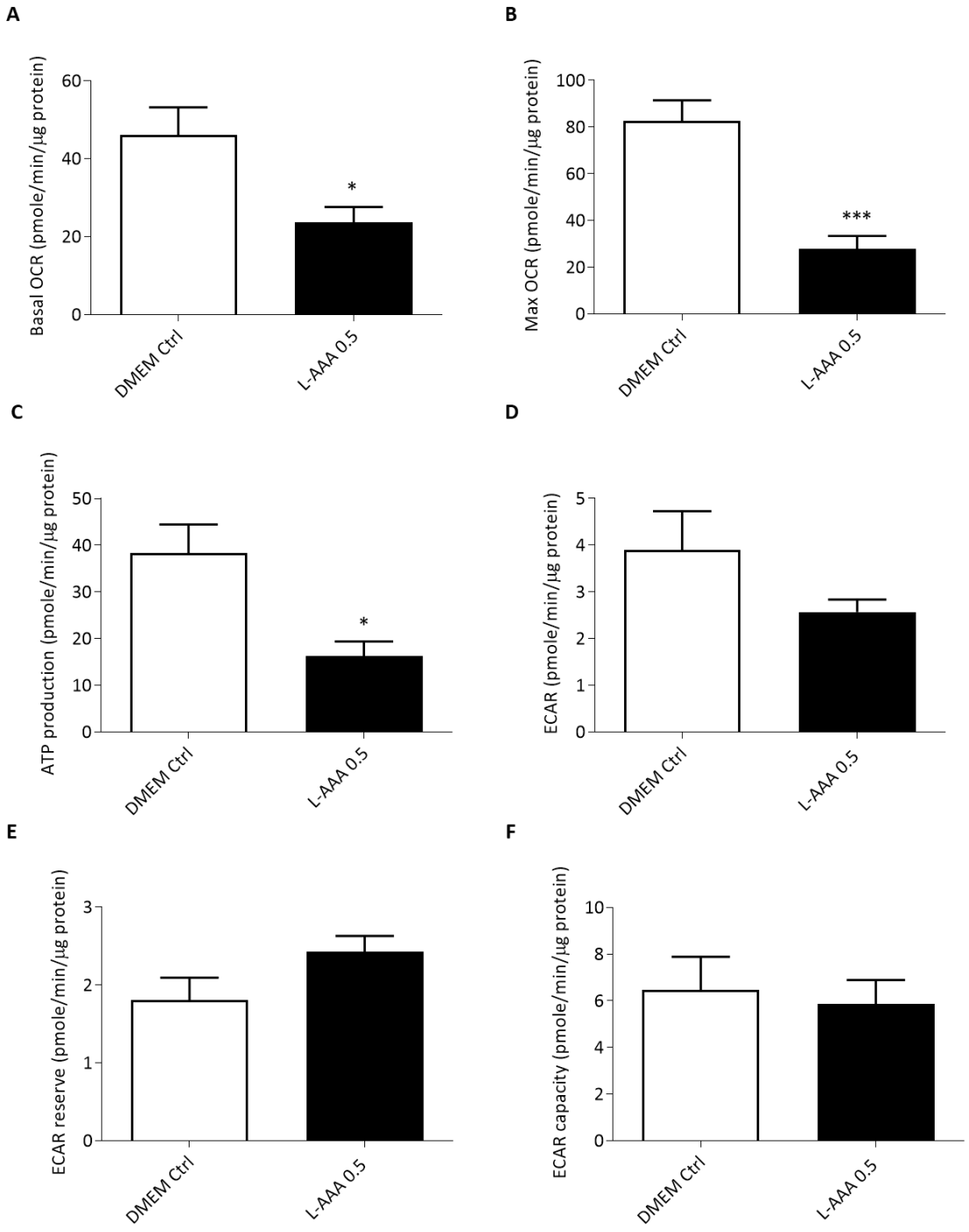

Figure 3.8 L-AAA reduces astrocytic mitochondrial respiration.
Enriched primary cortical astrocytes (DIV 14) were treated for 24 hours with L-AAA (0.5 mM) or control DMEM. The Extracellular Flux Analyzer was used to measure Basal OCR, (A) Max OCR, (B) ATP production (C), ECAR, (D) ECAR reserve (E), and ECAR capacity (F). Data are expressed as mean ± SEM, n=5 coverslips per treatment group from 5 independent experiments. ***P<0.001, *P<0.05 vs. control DMEM (Student's T-test).

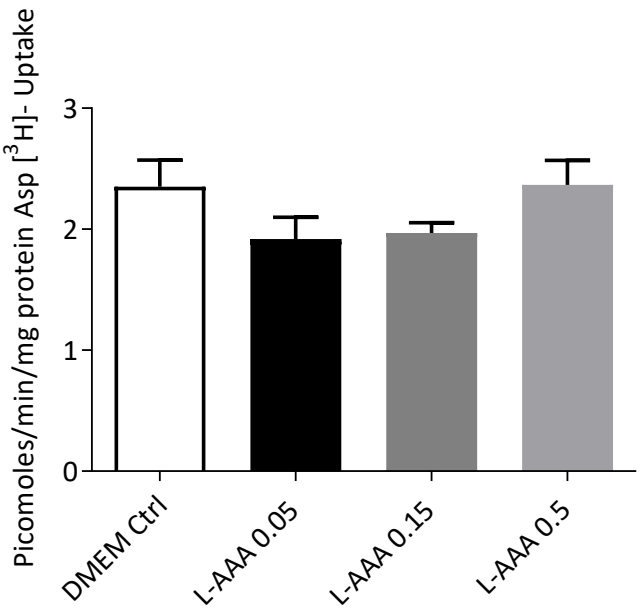

Figure 3.9 L-AAA has no effect on the uptake of [^{3}H] aspartate in mature primary cortical astrocytes.

Astrocytes (DIV 21) were treated directly with L-AAA (0.05, 0.15, 0.5 mM) for 24 hours. Treatments were removed and fresh media was replaced directly before quantification of [^{3}H] aspartate uptake (picomoles) as measured per min/mg astrocytic protein. Data are expressed as mean ± SEM, n=6 wells per treatment group from 3 independent experiments (Newman-Keuls post hoc test).

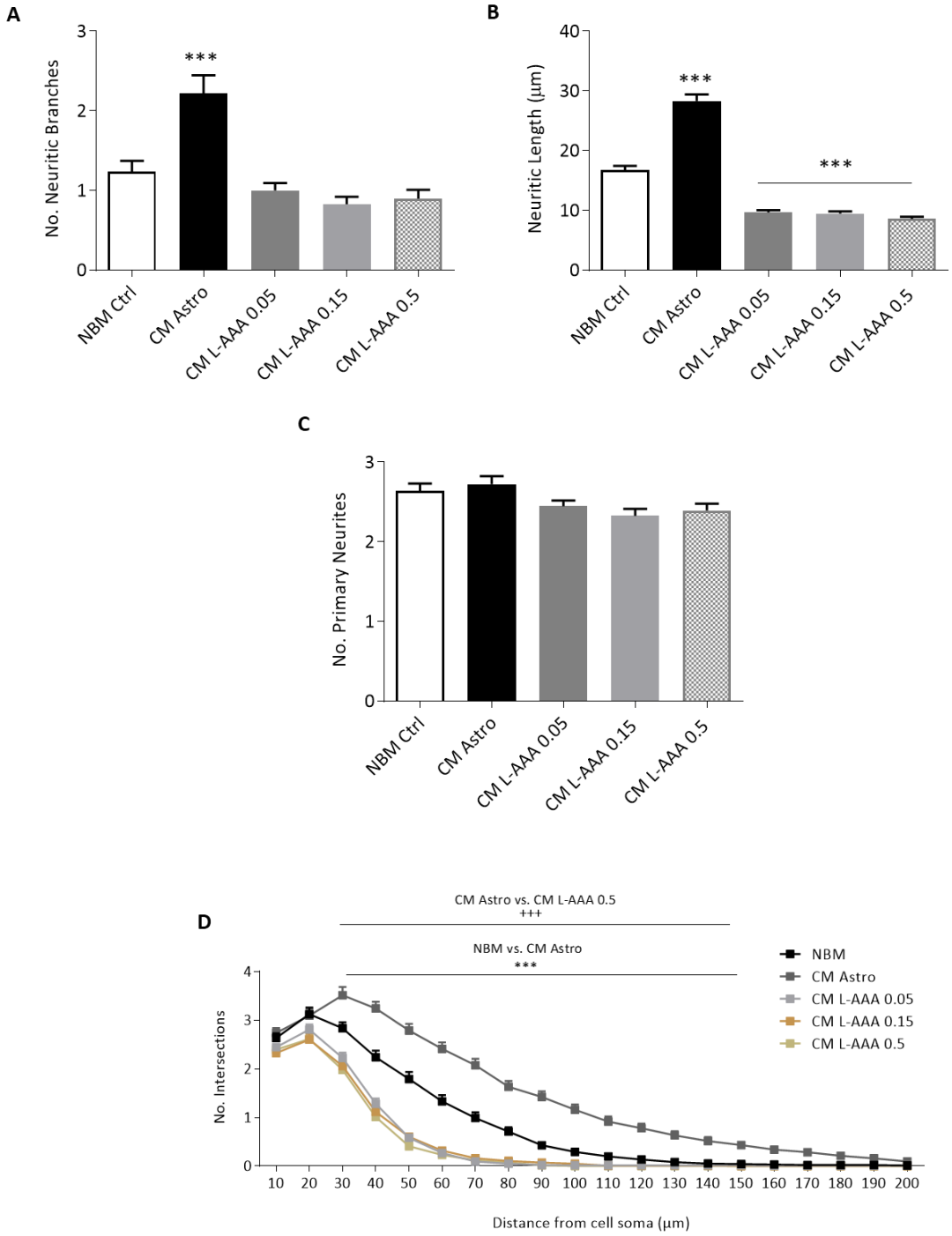

Figure 3.10 Conditioned media from L-AAA treated astrocytes reduces the complexity of mature primary cortical neurons.

Primary cortical astrocytes (DIV 14) were treated with L-AAA (0.05, 0.5 mM) for 24 hours. The resulting conditioned media was collected and applied to mature primary cortical neurons (DIV 21) for 24 hours before fixation and MAP2 immunocytochemistry. Sholl analysis was performed to analyse the number of neuritic branches (A), the neuritic length (B), the number of primary neurites (C), and the Sholl profile (D). Data are expressed as mean ± SEM, n=4 coverslips per treatment group from 4 independent experiments. ***P<0.001 vs. control NBM (Newman-Keuls *post hoc* test).

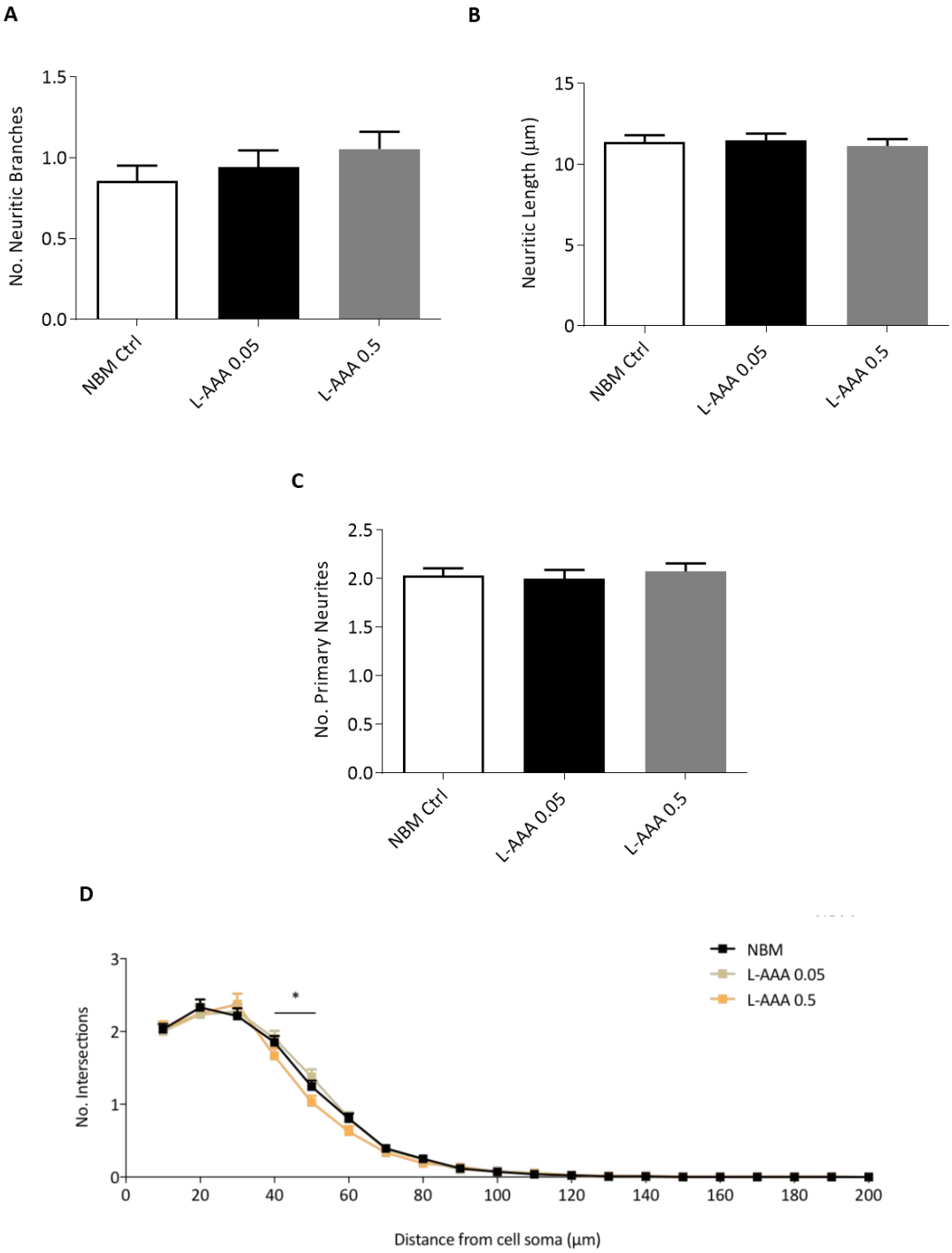

Figure 3.11 Direct application of L-AAA has no effect on the complexity of mature primary cortical neurons.

Mature primary cortical neurons (DIV 21) were treated directly with L-AAA (0.05, 0.5 mM) for 24 hours before fixation and MAP2 immunocytochemistry. Sholl analysis was performed to analyse the number of neuritic branches (A), the neuritic length (B), the number of primary neurites (C), and the Sholl profile (D). Data are expressed as mean ± SEM, n=8 coverslips per treatment group from 3 independent experiments (Newman-Keuls *post hoc* test).

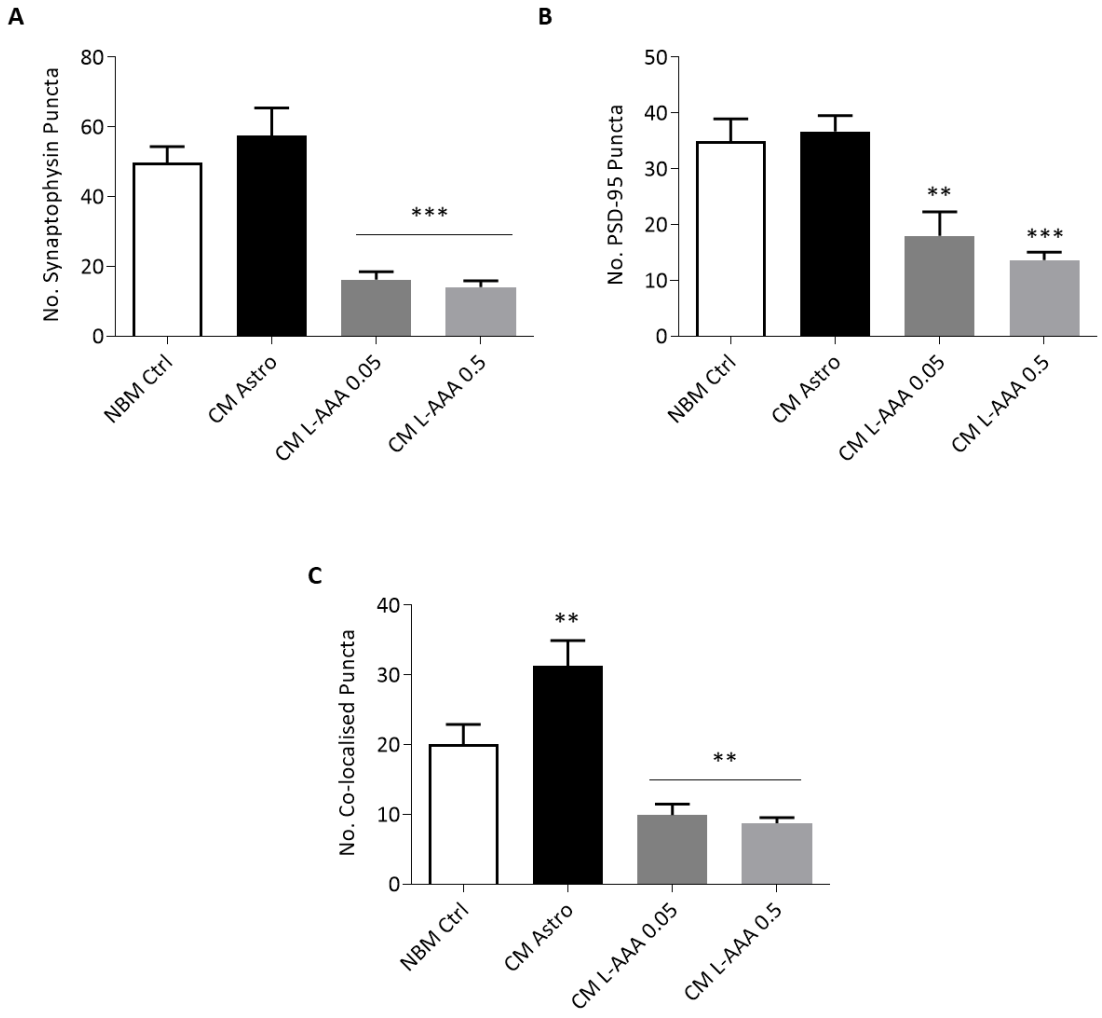

Figure 3.12 Conditioned media from L-AAA treated astrocytes reduces the co-localisation of synaptic proteins in mature primary cortical neurons.
Primary cortical astrocytes (DIV 14) were treated with L-AAA (0.05, 0.5 mM) for 24 hours. The resulting conditioned media was collected and applied to mature primary cortical neurons (DIV 21) for 24 hours before fixation and immunocytochemistry to quantify synaptophysin puncta (A), PSD-95 puncta (B), and co-localised synaptic puncta (C). Data are expressed as mean ± SEM, n=5 coverslips per treatment group from 5 independent experiments. ***P<0.001, **P<0.01, vs. control NBM (Newman-Keuls *post hoc* test).

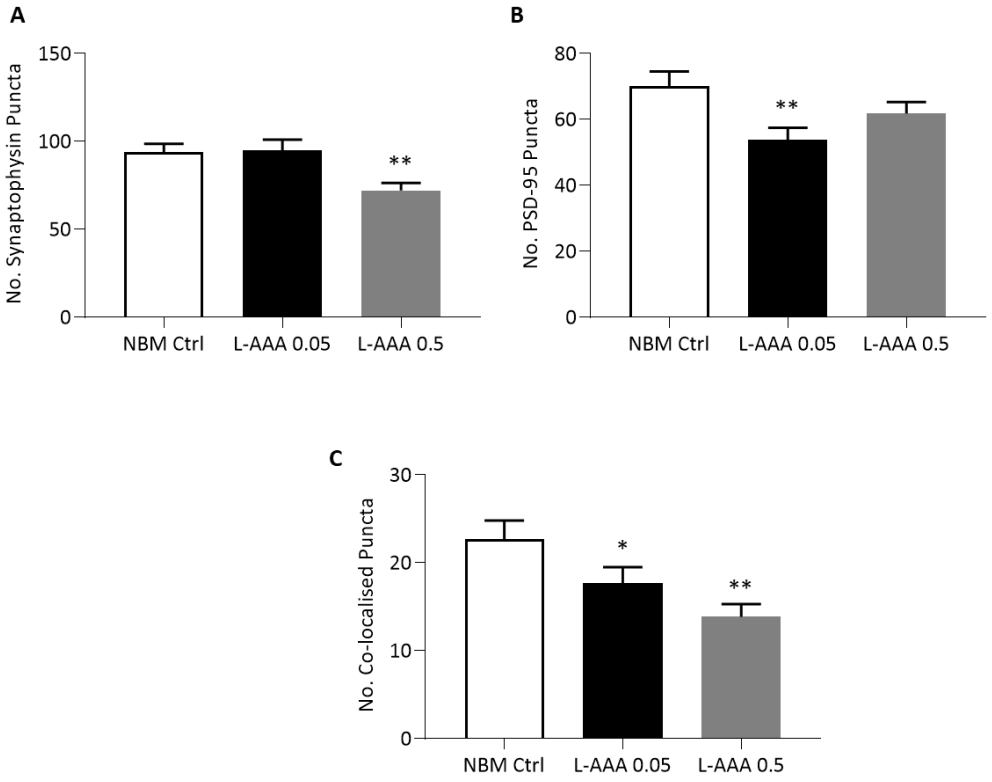

Figure 3.13 L-AAA affects synaptic protein co-localisation in mature primary cortical neurons.

Primary cortical neurons (DIV 21) were treated directly with L-AAA (0.05, 0.5 mM) for 24 hours for 24 hours before fixation and immunocytochemistry to quantify synaptophysin puncta (A), PSD-95 puncta (B), and co-localised synaptic puncta (C). Data are expressed as mean ± SEM, n=8 coverslips per treatment group from 3 independent experiments. **P<0.01, *P<0.05, vs. control NBM (Newman-Keuls *post hoc* test).

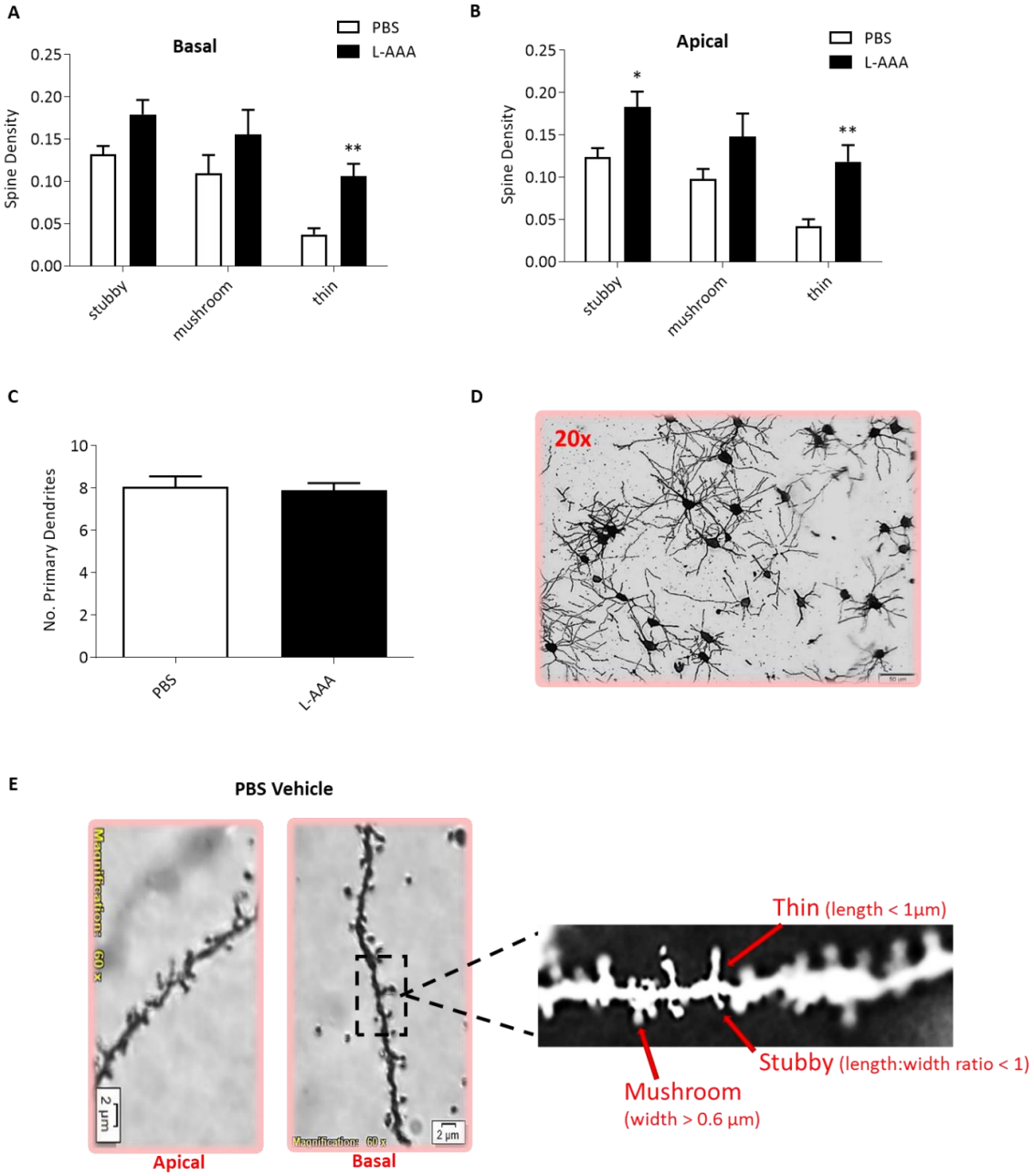

Figure 3.14 L-AAA increases dendritic spine density in the PLC in mice.
L-AAA (50 µg/µL; 1 µL) or PBS was administered to the PLC of male C57Bl6/J mice. 72 hours following L-AAA administration, the animals were euthanised and brains were collected for Golgi-cox staining to analyse spine density (A), apical spine density (B) and the number of primary dendrites (C). Representative images of Golgi-Cox stained primary dendrites (D), and apical and basal spines (E). Data are expressed as mean ± SEM, n=5 neurons per treatment group from 5 independent experiments **P<0.01, *P<0.05, vs. PBS vehicle (Newman-Keuls *post hoc* test).

3.4 Discussion

The results of the present investigation demonstrate that L-AAA induces astrocyte impairment *in vitro* which involves alterations in astrocyte morphology, GFAP immunoreactivity, the expression of astrocytic markers and astrocytic mitochondrial metabolism. By contrast, L-AAA has no effect on microglia morphology, Iba1 immunoreactivity or the mRNA expression of microglial markers.

This study employed an *in vitro* model, consisting of astrocyte derived conditioned media to investigate its effects on neuronal complexity and the expression and co-localisation of synaptic markers in these cells. Previous research has shown that conditioned media drawn from L-AAA treated primary astrocytic cultures reduces the complexity of primary cortical neuronal cultures (DIV 3) *in vitro* (David et al, 2018; O'Toole, 2015). This study extends these findings to mature neurons and demonstrates that conditioned media derived from healthy astrocytes (CM Astro) increases neuronal complexity and synapse number in mature neuronal cultures. It also shows that conditioned media from L-AAA treated astrocytes (CM L-AAA) reduces neurite outgrowth and the co-localised expression of synaptic proteins in mature neurons. Use of the conditioned media transfer model provides further evidence that the neurotrophic and synaptogenic effects observed following transfer of conditioned media from healthy astrocytes are mediated via the secretion of soluble factors into the conditioned media. It is likely that treatment of astrocytes with L-AAA hinders the production or release of neuroprotective and neurotrophic factors.

Results of this study accentuate the salience of healthy astrocytes, and the implications of astrocytic dysfunction, for neuronal development and synapse formation. This study provides further support of the use of L-AAA as a tool to investigate astrocytic dysfunction and provides insights into the role of L-AAA as an astrocyte toxin. Finally, it indicates an important link between astroglial dysfunction and neuronal atrophy.

3.4.1 L-AAA reduces GFAP immunoreactivity but has no effect on Iba1 immunoreactivity

As expected, results of this study demonstrate a concentration-related reduction in GFAP immunoreactivity in enriched primary cortical astrocytes following L-AAA treatment. These results compliment recent *in vivo* studies which show that one single (50 µg/µL; 1 µL) injection of L-AAA into the PLC of mice decreases GFAP immunoreactivity at 72 hours (David et al, 2018). Similar studies have also demonstrated a reduction in GFAP immunoreactivity up to 5 days following the administration of two consecutive daily doses of L-AAA (100 µg/µL, 0.5 µL) in the PLC of rats (Banasr & Duman, 2008; Lee et al, 2013b), and at 2 to 6 days following one single high dose injection of L-AAA (20 µg/µL, 5µL) into the PFC of rats (Lima et al, 2014).

The implications of a reduction in GFAP immunoreactivity are manifold. A reduction in GFAP immunoreactivity in cortical areas has been reported in a plethora of brain disorders including depression (Beauquis et al, 2013; Gittins & Harrison, 2011; Yeh et al, 2011) which sheds translational relevance on the results of this study and the implications of GFAP abnormalities in behavioural deficits associated with affective disorders.

On the other hand, L-AAA had no effect on microglial Iba1 immunoreactivity or morphology *in vitro*, suggesting that it does not affect microglia.

3.4.2 L-AAA reduces the size and perimeter of astrocytes and has no effect on microglial morphology

It has been well recognised that morphological characteristics of astrocytes influence their functions (Şovrea & Boşca, 2013) and comprehensive changes have been observed in astrocyte morphology across a multitude of CNS pathologies (Pekny & Pekna, 2014; Zhou et al, 2019). Astrocytic functions are critically dependent on their spatial relationship with neurons, and normally exhibit a highly ramified morphology in order to optimise this inter-cellular cross talk (Stork et al, 2014). Nevertheless, despite their critical relevance in both normal and disease states, the molecular mechanisms underlying the structural

morphology of astrocytes under distinct conditions are poorly understood (Molofsky et al, 2012).

As expected, results of the present study demonstrate an effect of L-AAA on astrocyte morphology. Treatment with L-AAA produced a dose-dependent reduction in the measure of both mean cell area and perimeter of GFAP+ astrocytes. Findings of this study suggest that L-AAA does not produce the classical reactive astrogliosis 'response in astrocytes (Sofroniew, 2009; Sofroniew & Vinters, 2010b; Zamanian et al, 2012) characterised by up-regulation of GFAP, and an increase in the number, thickness, and length of the cellular processes (Acaz-Fonseca et al, 2019), but instead reduces expression of this marker. The results also concur with reports of a reduction in protein synthesis in cultured rat astrocytes following treatment with L-AAA (Nishimura et al, 2000).

The signalling pathways responsible for these morphological changes remain elusive. GFAP is known to control the Notch signalling pathway in astrocytes, a signalling pathway governing the expression of molecules involved in the regulation of astrocyte morphology. Enhancing Notch signalling through the inhibition of NF-κB and the activation of MAPK is reported to reverse astrocyte hypertrophy resulting in reduced cell size, as observed in this study (Acaz-Fonseca et al, 2019). The gap junction protein connexin (Cx) 30 is another emerging candidate for the regulation of astrocyte morphology. Cx30 is selectively expressed on astrocytes and regulates astrocyte morphology via modulation of the laminin/β1 integrin/Cdc42 polarity pathway (Ghézali et al, 2018; Pannasch et al, 2014). Ultimately, actin remodelling is the primary driving force for morphological plasticity. The Rho family of GTPases such as RhoA, Cdc42, Rac1, and the Rho-associated kinase (ROCK) regulate the actin cytoskeleton through various pathways and thus control cell morphology (Zeug et al, 2018). It is possible that L-AAA induces changes in astrocyte morphology by impacting on any of these mechanisms, however further research is required to elucidate the distinct signalling underlying these changes.

It is possible that a reduction in the morphology of GFAP+ astrocytes produces a loss of GFAP-affiliated functions including a reduction in localised astrocytic

functional proteins. For example, GFAP is molecularly associated with GLAST and hydrogen/sodium exchanger modulating proteins (Sullivan et al, 2007). It is essential in retaining GLAST in the plasma membranes of astrocytes and loss of GFAP yields a reduction in the expression and function of astrocytic GLAST and GLT-1 (Hughes et al, 2004; Li et al, 2008) which are important regulators of synaptic glutamate uptake.

Microglia morphology was also analysed following immunocytochemical staining for Iba1. Results of this study show that L-AAA has no effect on Iba1 expression or microglia morphology suggesting that it does not engender the traditional response associated with microglial activation. This is in line with previous *in vivo* findings which show that L-AAA treatment does not alter the density of Iba1+ microglia or the expression of CD68, two important indicators of microglial reactivity (Brockett et al, 2018; O'Neill et al, 2019).

3.4.3 L-AAA reduces the immunoreactivity of astrocytic AQP4

As expected, results of the present study demonstrate an effect of L-AAA on AQP4 immunoreactivity. Treatment with L-AAA produced a dose-dependent reduction on AQP4 immunoreactivity, similar to that seen with GFAP. These results are akin to previous findings demonstrating plasticity-related changes in GFAP filaments which are accompanied by synergistic alterations in AQP4 expression (Wang & Hatton, 2009). Thus, these results are not surprising considering the previously demonstrated reduction in astrocyte GFAP immunoreactivity, which often parallels with AQP4 expression. Similarly, to GFAP, upregulation of AQP4 is considered a characteristic of reactive astrocytes (Stavale et al, 2013). During inflammation AQP4 facilitates astrocyte migration, AQP4-dependent cytokine release and glial scar formation at sites of brain injury (Li et al, 2011). Simultaneous reductions in AQP4 and GFAP, reportedly provide an indication of astrocyte damage, infiltration by neutrophils, eosinophils and macrophages, disruption of the BBB, and perivascular deposition of activated complement (Papadopoulos & Verkman, 2012).

Resultantly, findings of this study provide confirmation that L-AAA does not produce the classical reactive astrogliosis 'response in astrocytes following CNS injury (Sofroniew, 2009; Sofroniew & Vinters, 2010b; Zamanian et al, 2012) but instead leads to reduced expression of this marker. While further research is required to identify the exact processes underlying L-AAA mediated astrocyte impairment, a reduction in astrocytic AQP4 can thus be regarded as an additional indicator of astrocytic dysfunction in this *in vitro* model of L-AAA-induced astrocyte impairment.

3.4.4 L-AAA affects the mRNA expression of GFAP, S100β, IL-1β and has no effect on IL-6, IL-1α, TNF-α and Iba1

The action of L-AAA was further characterised by assessing its effect on the mRNA expression of a range of astrocytic and microglial markers. As expected, L-AAA produced a robust decrease in GFAP mRNA. These results coincide with the reduction in the morphology of GFAP+ cells and GFAP immunoreactivity.

L-AAA also produced a robust decrease in S100β mRNA expression following 24-hour treatment. This is not surprising since S100β is highly expressed by reactive astrocytes (Mori et al, 2010) and is traditionally associated with increased astrocyte reactivity and inflammatory brain disorder (Brozzi et al, 2009). Increased levels of astrocytic S100β have been observed in the pathophysiology of infectious and inflammatory brain disorders and following exposure of astrocytes to inflammatory stimuli such as TNF-α (Brozzi et al, 2009). Furthermore, increased serum levels of S100β have been positively correlated with the severity of the insult in patients suffering from traumatic brain damage (Steiner et al, 2008). Since high concentrations of S100β have been shown to exert neurotoxic effects and L-AAA reduced the expression of S100β we can infer that L-AAA does not induce a neurotoxic astrocytic phenotype. Analogously to GFAP and AQP4, the reduction of S100β infers that L-AAA-induced astrocyte impairment does not manifest as classical reactive astrogliosis and instead leads to reduced expression of this marker. A reduction in astrocytic S100β mRNA can thus be regarded as an additional indicator of astrocytic dysfunction and characteristic of the *in vitro* model of L-AAA-induced astrocyte impairment.

In contrast to GFAP and S100β, L-AAA produced a robust increase in IL-1β mRNA expression compared to control. This is surprising given that IL-1β is regarded as an important mediator of inflammatory response and one of the first cytokines secreted in response to injury (Zhang et al, 2000). It is rapidly induced in brain tissue following acute brain injury and is thought to contribute to and/or sustain pathophysiological processes. Given that it has been shown to be up-regulated in more classical neurodegenerative diseases, and to this point L-AAA has produced effects opposed to those observed traditionally in inflammatory CNS disorders, it is surprising that L-AAA-induced the up-regulation of this cytokine. However, it is important to recognise that IL-1β is produced as an inactive precursor, termed pro-IL-1β, requiring further activation by 'pathogen associated molecular patterns' (PAMPs) or danger associated molecular pattern (DAMPs) (Lopez-Castejon & Brough, 2011). Thus, while increased mRNA expression of IL-1β can be regarded as an additional indicator of astrocytic dysfunction and characteristic of the *in vitro* model of L-AAA-induced astrocyte impairment, it cannot be inferred that the active cytokine plays a role in the downstream effects of L-AAA-induced astrocyte impairment.

L-AAA had no effect on the mRNA expression of IL-6, a pleiotropic cytokine secreted by astrocytes following exposure to an inflammatory stimulus (Minogue et al, 2012). This provides further indication that L-AAA does not provoke an inflammatory astrocytic phenotype. Conversely, treatment of primary cortical microglia (DIV 14) with L-AAA (0.5 mM) for 24 hours had no effect on the mRNA expression levels of IL-1α, TNF-α and Iba1. These results suggest that L-AAA does not affect prototypical microglial markers and may thus have negligible impact on microglia.

3.4.5 L-AAA reduces astrocytic mitochondrial respiration

All cerebral glycogen is found in astrocytes, indicating the fundamentality of astrocytic glycolysis, glycogenolysis and oxidation to CNS energy metabolism (Barros et al, 2013; Jha & Morrison, 2018; Morita et al, 2019; Newman et al, 2011; Stobart & Anderson, 2013; Yan et al, 2017). Results of this study reveal that L-AAA (0.5 mM) impairs basal and maximal mitochondrial respiration and

adenosine triphosphate (ATP)-linked mitochondrial respiration but has no effect on glycolysis. Specifically, basal OCR, maximal OCR and ATP production were reduced following 24-hour treatment with L-AAA. These results are not surprising given that cellular respiration and mitochondrial function in astrocytes is susceptible to many stimuli (Bambrick et al, 2004).

Astrocytes have high rates of oxidative metabolism and derive a substantial amount of ATP from mitochondrial production. As ATP is essential to many enzymatic reactions the implications of reduced astrocytic mitochondrial respiration are manifold. For example, GS catalyses the ATP-dependent condensation of ammonia and glutamate to form glutamine (Rose et al, 2013). Astrocytic EAATs are energy-dependent and are known to use the Na+ and K+ electrochemical gradients to drive uptake of extracellular glutamate (Cambron et al, 2012; Magistretti & Allaman, 2018; O'Donovan et al, 2017; Stobart & Anderson, 2013). As many astrocytic functions, are energy demanding (Anderson & Swanson, 2000) mitochondrial dysfunction could seriously impair astrocytic neuroprotective function, potentially via the disruption of energy-driven glutamate transport systems and astrocytic glutamate-glutamine cycling.

3.4.6 L-AAA has no effect on the uptake of [^{3}H] aspartate in enriched primary cortical astrocytes

Previous work has shown that L-AAA 0.5 mM reduces the mRNA expression of astrocytic GLAST and GFAP and reduces measures of astrocytic mitochondrial function including basal mitochondrial respiration, maximal mitochondrial respiration and ATP-linked mitochondrial respiration (David et al, 2018). Based on these findings, and considering the astrocytic glutamate/Na^+ co-transporters, which drive glutamate uptake, are dependent on the Na^+ gradient mediated by Na^+, K^+-ATPase, this study sought to investigate if L-AAA also affected astrocytic uptake of [^{3}H] aspartate. For this purpose, a radiological assay was established to quantify the uptake of radiolabelled aspartate following treatment with various concentrations of L-AAA.

Surprisingly, results of this study indicate that L-AAA does not affect the uptake of [^{3}H] aspartate following 24-hour treatment with L-AAA (0.5, 0.15 and 0.5 mM).

Nevertheless, these results are in line with early reports of L-AAA and its putative role as an inhibitor of the intracellular enzymes glutamine synthetase or γ-glutamylcysteine synthetase (Brown & Kretzschmar, 1998; McBean, 1994; Olney et al, 1980). L-AAA may thus exert an effect on astrocytic glutamate-glutamine cycling or glutamine release as opposed to glutamate uptake, although these parameters were not measured in this investigation.

3.4.7 Conditioned media from L-AAA treated astrocytes reduces neuronal complexity

Previous findings show that conditioned media drawn from healthy primary astrocytic cultures increases the complexity of immature (DIV 3) primary cortical neuronal cultures *in vitro* (David et al, 2018), while conditioned media drawn from L-AAA treated astrocytes decreases neuronal complexity. This study adds to current data by further investigating the effect of conditioned media drawn from healthy primary astrocytic cultures and conditioned media from L-AAA treated astrocytes on the complexity of mature primary cortical neuronal cultures.

As expected, conditioned media derived from healthy astrocytes increased the complexity of mature neurons while conditioned media from L-AAA treated astrocytes reduced measures of complexity. These results are not surprising given that astrocytes play crucial roles in promoting neural circuit formation, neurite outgrowth and dendritic branching (Previtera et al, 2010; Sofroniew & Vinters, 2010a; Withers et al, 2017; Zhu et al, 2016; Zuchero & Barres, 2015). They are also in line with long-standing evidence demonstrating that astrocyte dysfunction precedes impairments in neuronal function and viability (Oksanen et al, 2019). Astrocytes are known to regulate neuronal morphology through the provision of ECM molecules, which forms a permissive substrate promoting neuronal guidance and development (Ferrer-Ferrer & Dityatev, 2018; Lam et al, 2019; Previtera et al, 2010). They also release intercellular effector molecules and/or alter gene expression, which directly impact neighbouring neuronal networks and influence axonal and dendritic development and integrity (Toy & Namgung, 2013). In particular, soluble growth factors known as neurotrophic factors, are secreted by astrocytes in the vicinity of neurons which are reported

to provide neuroprotection and enhance neurite growth directly (Bylicky et al, 2018; Takemoto et al, 2015). NGF-β , FGF-2, GDNF, IL-6, and BDNF have all been identified as neurotrophic factors that are released from astrocytes and promote neuronal outgrowth (Farrukh et al, 2018; Martin et al, 2013; Xu et al, 2013).

L-AAA impairs mitochondrial respiration in astrocytes and previous studies have shown that inhibition of astrocyte respiration promotes neurodegeneration in neuron-astrocyte co-cultures (Bolaños & Heales, 2010; Sun et al, 2018). Reduced astrocyte glycogenolysis results in reduced axonal energy supplies which may account for the atrophy observed in this study (Stobart & Anderson, 2013). A reduction in mitochondrial capacity may in fact prevent the conversion of glutamate to glutamine by GS and therefore its supply to neurons. Moreover, astrocytes are reported to shuttle lactate to neurons as a source of pyruvate and it is possible that withdrawal of this support may contribute to the neuronal atrophy observed following astrocyte impairment (Barros et al, 2013; Jha & Morrison, 2018; Magistretti & Allaman, 2018).

Based on the effect of L-AAA on the astrocytic gene expression profile, it appears that L-AAA does not induce a neurotoxic astrocytic phenotype, but instead induces a phenotype with impaired functionality and which produces a conditioned media that is less trophic, rather than specifically neurotoxic. This would also help explain the much greater difference observed between conditioned media from control astrocytes and conditioned media collected from L-AAA treated astrocytes compared to that observed between control NBM and conditioned media from untreated astrocytes. These results also confirm that L-AAA does not directly affect the complexity of mature neuronal cultures inferring that the observed effects are mediated via an astrocytic mechanism.

3.4.8 Conditioned media from L-AAA treated astrocytes reduces synaptic protein co-localisation in mature primary cortical neurons

As expected, results of this study show that conditioned media derived from healthy astrocytes increases the co-localised expression of synaptic markers in mature neurons while conditioned media derived from L-AAA treated astrocytes reduces the expression of synaptic markers. These results as not surprising given

that conditioned media derived from healthy astrocytes increased neuronal complexity while conditioned media derived from L-AAA treated astrocytes reduced it.

In addition to promoting neurite outgrowth, there is compelling evidence that astrocytes are involved in regulating synapse formation and function through various mechanisms both *in vitro and in vivo* (Chung et al, 2015; Clarke & Barres, 2013; Eroglu & Barres, 2010; Papouin et al, 2017). Astrocytes have critical roles in controlling synaptic development, functionality, plasticity and elimination (Allen et al, 2012; Baldwin & Eroglu, 2017; Cheng et al, 2016; Chung et al, 2015; Chung et al, 2013; Diniz et al, 2012a; Lee & Chung, 2019; Papouin et al, 2017; Withers et al, 2017). They release synaptogenic factors which regulate the number and formation of synapses, and other signalling molecules which fine tune the strength of synaptic signals by regulating pre-synaptic vesicle release and post-synaptic receptor composition (Chung et al, 2015). Astrocytic production and release of cell adhesion and extracellular matrix molecules (e.g., neuroligins, glypicans, and laminins) is also required for the formation and function of synapses (Hillen et al, 2018). Astrocyte-secreted factors also play a role in various aspects of long-term potentiation, long-term depression, and synaptic scaling which may also affect the number of functioning synapses (Chung et al, 2015; Kucukdereli et al, 2011).

Conditioned media from healthy astrocytes had a trophic effect in support of previous studies which demonstrated a seven-fold increase in the number of mature, functioning synapses in neuron-astrocyte co-cultures compared to neurons cultured in isolation (Fang et al, 2019). The potential mechanisms underlying astrocyte induced synapse formation and protection of synapses have been extensively reviewed (Cheng et al, 2016; Diniz et al, 2017). It is possible that the release of astrocyte-derived synaptogenic factors into the surrounding conditioned media accounts, at least in part, for this increase in synaptic protein co-localisation (Allen et al, 2012; Chung et al, 2013; Diniz et al, 2012a; Diniz et al, 2012b; Ippolito & Eroglu, 2010; Oksanen et al, 2019; Shen & Cowan, 2010; Wiese et al, 2012).

Conversely, conditioned media from L-AAA treated astrocytes reduced the number of synaptic protein co-localisations when applied to mature primary cortical neuronal cultures. These results are not surprising given the myriad of effects L-AAA induces on astrocyte functioning and given that conditioned media from L-AAA treated astrocytes also reduced neuronal complexity. It is possible that withdrawal of astrocytic support mediated by soluble growth factors also accounts, at least in part, for these observations. L-AAA also directly impacted the co-localisation of synaptic proteins in mature neurons. However, this was to a lesser extent that with conditioned media from L-AAA treated astrocytes. We therefore cannot exclude a direct effect of L-AAA on synaptic markers and consider this a limitation of the astroglial toxin.

3.4.9 L-AAA increases neuritic branching and dendritic spine density in the PLC in mice

It is evident that L-AAA-induced astrocytic impairment has a robust effect on mature neurons *in vitro*. In line with the limitations of employing *in vitro* cultures it is important to acknowledge that they do not accurately represent the complexity of the human adult brain. Therefore, it was of importance to translate these findings into an animal model which would permit similar investigation of the effect of L-AAA mediated astrocyte dysfunction on neuronal integrity.

As expected, there was no difference in the number of primary neurites extending from the cell soma for the different treatment groups. However, administration of L-AAA into the mouse PLC increased immature thin and stubby dendritic spines. No changes were observed in mature mushroom spines. Previous research has shown that acute stress, induced by intermittent tail shocks, increases spine density in the male hippocampus. Our results are akin with these findings as L-AAA resulted in increased spine density compared to vehicle treated controls (Shors, 2002; Shors et al, 2001; Shors et al, 2004). NMDAR antagonism during or following acute stress has previously been shown to prevent stress-induced increase in spine density (Shors et al, 2004). It is thus plausible that L-AAA administration and functional impairment of astrocytes may result in dysfunctional glutamate uptake and increased glutamate availability for

direct activation of NMDARs localised on dendritic spines (Fukazawa et al, 2003). This increase in NMDAR activity may stabilise the actin cytoskeleton and F-actin content of spines (Fukazawa et al, 2003) activating local protein synthesis (Ewald et al, 2008; Huang et al, 2002). Protein synthesis machinery is localised at the base of the spine neck and recruited to activated spines. Activation of the TrkB, Rho GTPase, extracellular signal-regulated kinase (ERK) and protein kinase A (PKA) signalling pathways are known to regulate protein synthesis in dendrites (Yasuda, 2017). Further research is necessary to precisely define the pathways activated by L-AAA-induced astrocyte impairment leading to increased spine density.

As spine formation is dynamic with a high turnover rate, one major limitation of the methodological approach of this investigation is the analysis of spine density at just one point in time. Nevertheless, an increase in dendritic spine density can be regarded as an additional characteristic of astrocytic dysfunction in this *in vivo* model of L-AAA-induced astrocyte impairment.

3.5 Conclusion

Results of the current investigation firstly demonstrate that L-AAA exerts a selective toxicity in astrocytes which involves alterations in astrocyte morphology, GFAP immunoreactivity and mitochondrial respiration and has no effect on microglia morphology, Iba1 immunoreactivity or typical microglial markers. This provides further validation for the use of L-AAA as a tool to induce selective astrocytic ablation both *in vitro* and *in vivo* and demonstrates that withdrawal of astrocytic support profoundly increases the susceptibility of neurons to atrophy and synapse loss (Doucet et al, 2015).

These findings concur with previous reports outlining the neurotrophic and synaptogenic properties of conditioned media derived from healthy astrocytes (Baldwin & Eroglu, 2017; Efremova et al, 2017; Lee & Chung, 2019; Lu et al, 2015; Sofroniew & Vinters, 2010b; Takemoto et al, 2015). However, while knowledge of the supportive role of astrocytes has greatly evolved, these results demonstrate that conditioned media from healthy astrocytes is neurotrophic and synaptogenic and we can infer that the secretion of soluble trophic factors can provide neurotrophic and synaptogenic support. On the other hand, conditioned media derived from L-AAA treated astrocytes reduced measures of neuronal complexity and synaptic protein co-localisation indicating that withdrawal of astrocytic support via L-AAA-induced astrocyte impairment profoundly increases the susceptibility of neurons to atrophy and synapse loss (Doucet et al, 2015). These results highlight the importance of astrocyte-derived conditioned media in synapse formation and development and may implicate L-AAA-induced astrocyte impairment in synapse loss. Furthermore, they imply that glial support is imperative to the formation of neuronal circuitry and a neuron-glial complex may more aptly represent the functional unit of the CNS.

As current data on the role of L-AAA *in vivo* is limited, this study also aimed to extrapolate *in vitro* findings into an *in vivo* mouse model. By examining the effect of L-AAA on the morphology of dendritic spines and number of primary dendrites in the PLC of mice this study provides a valuable contribution and insight to our understanding of the role of L-AAA *in vivo*.

4 Reactive astroglial associated reductions in the complexity of primary cortical neurons; a role for IL-6?

4.1 Introduction

Neuroinflammation is a phenomenon involving a complex biological response to CNS injury (Headland & Norling, 2015) and is a well-recognised characteristic of numerous neurodegenerative and neuropsychiatric disorders (Glass et al, 2010a; Miller & Raison, 2016; Stephenson et al, 2018). Glial activation is a fundamental hallmark of neuroinflammation and is responsible for many of the inflammatory events occurring downstream of the initial CNS infection or insult. Microglial activation, which occurs via the recognition of pathogen-associated molecular patterns (PAMPs) by pattern recognition receptors (PRRs) on their cell surface, is habitually self-limiting. However, chronic or over activation results in excessive production of pro-inflammatory mediators which have deleterious effects on surrounding cells and tissue (Bachiller et al, 2018; Carniglia et al, 2017; Skaper et al, 2018). Elimination of microglia using the colony-stimulating factor 1 receptor (CSF1R) inhibitor has been shown to restore cognitive deficits, attenuate neuronal atrophy and reverse changes in synaptophysin and PSD-95 induced by hippocampal lesions in a mouse model of inducible neuronal loss (Rice et al, 2015). Taken together these findings strongly affiliate inflammatory driven activation of microglia with neuronal atrophy and deficits in behavioural phenotype.

IFNγ is a pro-inflammatory cytokine and potent inducer of microglial activation that is up-regulated in numerous neurological disorders (Frost & Li, 2017). IFNγ is secreted predominately by activated immune cells such as T cells and natural killer cells (Schoenborn & Wilson, 2007). IFNγ assists in mounting an immune response by activating other immune cells and increasing the expression of MHC class I and II on target cells. IFNγ production can be induced in innate-like lymphocytes, by cytokines (primarily IL-12 and IL-18) or following the activation of PRRs during microbial infection or tissue damage. Sustained IFNγ signalling is a characteristic of inflammation seen in autoimmune diseases, such as rheumatoid arthritis, where disease-associated macrophages, which express the IFNγ receptor, show increased sensitisation to inflammatory cytokines in conjunction with increased resistance to glucocorticoids (Hu et al, 2008). The production of IFNγ has also shown to be altered under various conditions associated with

cognitive impairment including chronic stress (Wei et al, 2000), ageing (Wei et al, 2000) and in several neuropsychiatric and neurodevelopmental disorders (Nateghi Rostami et al, 2012).

Previous research has shown that persistent release of IFNγ (aided by TNF-α) is essential for perpetuating glial activation, enhancing the activation of the surrounding glial cells and may contribute to neuronal degeneration *in vivo* (Barcia et al, 2011). While microglia are primarily responsible for initiating inflammatory processes, it is true that neuroinflammation is a complex signalling phenomenon involving all CNS cell types and there is growing evidence to support astrocytic engagement in maintaining the response. Recent research has shown that the combination of microglial factors IL-1α, TNF-α, and C1q are elevated in conditioned media derived from activated microglial cultures and work synergistically to induce the expression of an A1 reactive astrocyte phenotype (Liddelow et al, 2017; Yates, 2017). However, investigation into the effects of reactive astrocytes and conditioned media from reactive astrocytes on neuronal integrity is limited.

4.1.1 TNF-α and IL-1α as mediators of neurotoxic insult

TNF-α is a potent pro-inflammatory signalling molecule that mediates various biological responses by binding to two different receptors on cells, the TNFR1 (p55) and TNFR2 (p75) (Li et al, 2013). TNF-α receptors differ in their expression pattern, downstream signal-transduction cascades, and binding affinity for TNF-α. Resultantly, TNF-α plays a dual role in the CNS and can exert a homeostatic or pathophysiological effect in response to the environment (Montgomery & Bowers, 2012).

In the healthy CNS, TNF-α regulates physiological processes such as synaptic plasticity, learning and memory, and astrocyte-induced synaptic strengthening (He et al, 2012; Lewitus et al, 2014; Santello & Volterra, 2012). Activation of TNFR2 is associated with pro-survival and anti-inflammatory activity (Medler & Wajant, 2019; Probert, 2015) primarily via activation of the PI3K/Akt pathway (Fontaine et al, 2002). On the contrary, activation of TNFR1 is associated with cell

death signalling pathways such as NF-κB, the extracellular signal-regulated kinase (ERK), the c-Jun N-terminal kinase (JNK) and the p38 mitogen-activated protein kinase (p38 MAPK) (Kalliolias & Ivashkiv, 2016; Sabio & Davis, 2014). TNF-α - induced activation of NF-κB is particularly important in inflammation given that NF-κB is a global trans-activator of numerous pro-inflammatory cytokines, chemokines and a critical regulator of leukocyte activation and function (Hayden & Ghosh, 2014; Liu et al, 2017a). Recent research suggests that astrocyte NF-κB activation is exacerbated with increasing levels of microglial activation and NF-κB activation in astrocytes, in turn, regulates proliferation and immune response in microglia (Dokalis & Prinz, 2018; Ouali Alami et al, 2018). This suggests that microglia are the primary source of *de novo* TNF-α production during inflammation, and microglia activation may precede that of astrocytes resulting in cyclical communication between glial cells and signal amplification.

Despite extensive literature reviewing inflammatory-driven release of TNF-α from microglia, the direct effects of TNF-α on astrocyte morphology and function remains largely unexplored. Furthermore, the effects of conditioned media from TNF-α treated astrocytes on neuronal complexity and synapse formation has not yet been investigated. This reveals a gap in knowledge surrounding the implications of activated glia-neuronal cross talk under inflammatory conditions in the CNS. *In vitro* studies were among the first to show that inflammatory cytokines, especially IL-1α and TNF-α cause neuronal death by directly acting on neurons and indirectly via glial production of neurotoxic substances (Thornton et al, 2006; Ye et al, 2013; Yin et al, 2012). However, the precise mechanisms and mediators involved in neuronal damage caused by activated-glial cells remains nebulous.

IL-1α and IL-1β belong to the major family of IL-1 pro-inflammatory cytokines (Weber et al, 2010). IL-1α and IL-1β are first synthesised as precursor proteins that can be enzymatically cleaved. The precursor form of IL-1β is not biologically active and requires cleavage to elicit its inflammatory activity. In comparison, the precursor form of IL-1α is biologically active. IL-1α and IL-1β both play a role in inflammation, particularly through NF-κB–induced transcription of inflammatory

genes and the induction of adhesion molecules and chemokines. IL-1α is constitutively expressed in many cell types in healthy tissues but increases dramatically in response to pro-inflammatory stimuli including mediators of microbial origin with TLR agonistic activities (Rider et al, 2012). It is a key mediator released from necrotic cells to provoke inflammation and its expression is often considered an indicator of disease severity. Leucocyte infiltration is one of the main events perpetuating neuroinflammation and evidence strongly suggests that astrocytes play a key role in regulating leukocyte recruitment and releasing chemoattractant chemokines following IL-1 activation. Despite extensive literature documenting increased microglial expression of IL-1β during inflammation, the effect of microglial activation on IL-1α has been only recently brought into question (Liddelow et al, 2017).

4.1.2 IL-6 as a key astrocyte factor in mediating changes in neuronal integrity

IL-6 is one of the primary cytokines released from activated glia during inflammation (Boche et al, 2013; Glass et al, 2010b) and is reported to play an important role in the physiological homeostasis of neural tissue and the pathogenesis of inflammation (Rothaug et al, 2016). It is a multifunctional cytokine that can be considered pro-inflammatory or anti-inflammatory depending on the amount and conditions in which it is released. Secretion of IL-6 is reported to be one of the multiple ways that astrocytes actively regulate microglia during pro-inflammatory injury and repair, and is therefore an important signalling molecule in the investigation of glial-neuronal cross talk under inflammatory conditions (Hindinger et al, 2012; Kumar et al, 2010).

IL-6 can act on target cells through a receptor complex composed of the full-length IL-6 receptor-α (IL-6Rα) and gp130 or through a soluble IL-6 receptor (Heinrich et al, 2003). Under physiological conditions, IL-6 expression is generally low, however it is strongly up-regulated under pathological conditions such as ischemia and trauma (Suthaus et al, 2012) where it is reportedly involved in axon regeneration (Yang et al, 2012).

Overproduction or accumulation of IL-6 has been linked with neurotoxicity underlying many neuroinflammatory and neurodegenerative disorders (Krstic & Knuesel, 2013). Elevated levels of IL-6 are reported to induce synaptic dysfunction in cultures of rat hippocampal neurons (Walsh et al, 2014b) and is associated with reduced cerebellar volume in transgenic GFAP-IL6 mice (Gyengesi et al, 2019). Overexpression of IL-6 has also been reported to alter cell adhesion and migration (Wei et al, 2011). Thus, while physiological levels of IL-6 are likely to be protective, overexpression of IL-6 may lead to neuroinflammation and loss of neuronal integrity.

4.2 Aims

The overall aim of this chapter is to define characteristics of glial responses to inflammatory stimuli, specifically IFNγ and the combination of TNF-α and IL-1α, including changes in the immunoreactivity and morphology of glial cells. It also aims to investigate the effect of microglia activation on astrocyte reactivity by identifying factors released from activated microglia and applying them directly to astrocytes. The effect of reactive astrocytes on the integrity of mature neurons is also explored by employing conditioned media (CM) studies as a means of modelling inter-cellular crosstalk between neurons and glia. Finally, the study aims to identify factor(s) released by activated astrocytes and examine the impact of these on neuronal complexity and the expression of synaptic markers *in vitro*.

The specific aims of this study are to investigate the effect of (1) IFNγ on the immunoreactivity and morphology of astrocytes and microglia, (2) conditioned media from IFNγ treated glia on the complexity and expression of synaptic markers in mature neurons, (3) TNF-α and IL-1α on GFAP immunoreactivity and the morphology and expression of inflammatory markers in enriched primary cortical astrocytes, (5) conditioned media from TNF-α and IL-1α treated astrocytes on the complexity and expression of synaptic markers in mature neurons, (6) TNF-α and IL-1α on the production of IL-6 in enriched primary cortical astrocytes (7), IL-6 on the complexity and expression of synaptic markers in mature neurons, (8) the neutralisation of IL-6 on reductions in the complexity and expression of synaptic markers in mature neurons induced by conditioned media from TNF-α and IL-1α treated astrocytes.

4.3 Results

4.3.1 Effect of IFNγ on Iba1 immunoreactivity and morphology of enriched primary cortical microglia

To investigate if IFNγ affects Iba1 immunoreactivity and microglial morphology primary cortical microglia (DIV 15) were treated with IFNγ (10 ng/mL) for 24 hours. Fixation and immunocytochemistry for were performed to determine the effect of IFNγ on Iba1 immunoreactivity and microglia morphology (mean cell area, perimeter and soma: area ratio). The concentration of IFNγ (10 ng/mL) was chosen based on prior research which demonstrated that conditioned media from IFNγ (10 ng/mL) treated mixed glia reduced the complexity of immature neurons *in vitro*.

Results of this study showed that treatment of primary cortical microglia with IFNγ reduced **Iba1 immunoreactivity** [$T_{(45)} = 2.801$, $P = 0.008$], **microglia mean cell area** [$T_{(46)} = 3.279$, $P = 0.002$], and **cell perimeter** [$T_{(46)} = 11.50$, $P < 0.001$], and increased the **soma:cell ratio** [$T_{(45)} = 4.777$, $P < 0.001$], compared to control DMEM (Student's T test) [*Figure 4.1 (A-D)*]

4.3.2 Effect of IFNγ on GFAP immunoreactivity and morphology of enriched primary cortical astrocytes

To investigate if IFNγ affects GFAP immunoreactivity and astrocyte morphology primary cortical astrocytes (DIV 14) were treated with IFNγ (10 ng/mL) for 24 hours. Fixation and immunocytochemistry were performed to determine the effect of IFNγ on GFAP immunoreactivity and astrocyte morphology (mean cell area, perimeter and soma: area ratio). Results of this study showed that treatment of primary cortical astrocytes with IFNγ increased **GFAP immunoreactivity** [$T_{(67)} = 8.945$, $P < 0.001$], **astrocyte mean cell area** [$T_{(67)} = 13.53$, $P < 0.001$], and **cell perimeter** [$T_{(69)} = 9.823$, $P < 0.001$], but had no effect on the **soma:cell ratio** [$T_{(66)} = 0.195$, $P = 0.846$], compared to control DMEM (Student's T test) [*Figure 4.2 (A-D)*]

4.3.3 Effect of conditioned media from IFNγ treated astrocytes, microglia and mixed glia on the complexity of mature neurons

To investigate the effect of conditioned media from IFNγ treated glia on mature neurons, primary cortical astrocytes (DIV 14), primary cortical microglia (DIV 15) and primary cortical mixed glia (DIV 14) were treated with IFNγ (10 ng/mL) for 24 hours. The resulting conditioned media was collected and applied to mature primary cortical neurons (DIV 21) for 24 hours. Fixation and MAP2 immunocytochemistry were performed to determine the effect of conditioned media from IFNγ treated glia on neuronal complexity by Sholl analysis. Mature primary cortical neurons (DIV 21) were also treated directly with IFNγ (10 ng/mL) for 24 hours to determine and direct effects of IFNγ on neurite outgrowth.

When examining the effect of conditioned media from IFNγ treated astrocytes, one-way ANOVA of **neuritic branches** showed no effect of conditioned media from IFNγ treated astrocytes [$F_{(2, 421)} = 0.839$, $P = 0.433$] [*Figure 4.3 (A)*]. One-way ANOVA of **neuritic length** showed an effect of conditioned media from IFNγ treated astrocytes [$F_{(2, 423)} = 5.054$, $P = 0.007$]. *Post hoc* analysis revealed an increase in neuritic length following treatment with conditioned media from untreated astrocytes ($P < 0.05$) compared to control NBM, and a decrease in neuritic length following treatment with conditioned media from IFNγ treated astrocytes compared to conditioned media from untreated astrocytes ($P < 0.01$) [*Figure 4.3 (B)*]. One-way ANOVA of the number of **primary neurites** showed no effect of conditioned media from IFNγ treated astrocytes [$F_{(2, 425)} = 0.229$, $P = 0.796$] [*Figure 4.3 (C)*]. Two-way repeated measures ANOVA of the **number of neuritic branches at specific distances from the neuronal cell soma** showed an effect of distance [$F_{(19, 8018)} = 677.8$, $P < 0.001$], an effect of treatment [$F_{(2, 422)} = 6.035$, $P = 0.003$] and an interaction effect [$F_{(38, 8018)} = 1.546$, $P = 0.018$]. Conditioned media from IFNγ treated astrocytes significantly decreased neuritic branching at 50-100 µm from the cell soma compared to conditioned media from untreated astrocytes [*Figure 4.3 (D)*].

When examining the effect of conditioned media from IFNγ treated microglia, one-way ANOVA of **neuritic branches** showed an effect of treatment [$F_{(2, 328)} = 17.92$, < 0.0001]. *Post hoc* analysis revealed a significant decrease in the number

of neuritic branches following treatment with conditioned media from untreated microglia compared to control NBM ($P < 0.001$), and following treatment with conditioned media from IFNγ treated microglia compared to conditioned media from untreated microglia ($P < 0.01$) [*Figure 4.4 (A)*]. One-way ANOVA of **neuritic length** showed an effect of treatment [$F_{(2, 327)} = 18.22$, $P < 0.001$]. *Post hoc* analysis revealed a significant reduction in neuritic length following treatment with conditioned media from untreated microglia and conditioned media from IFNγ treated microglia compared to control NBM ($P < 0.001$) [*Figure 4.4 (B)*]. One-way ANOVA of the number of **primary neurites** showed an effect of treatment [$F_{(2, 332)} = 11.54$, $P < 0.001$]. *Post hoc* analysis revealed a significant reduction in the number of primary neurites following treatment with conditioned media from untreated microglia and following treatment with conditioned media from IFNγ treated microglia compared to control NBM ($P < 0.001$) [*Figure 4.4 (C)*]. Two-way repeated measures ANOVA of the **number of neuritic branches at specific distances from the neuronal cell soma** showed an effect of distance [$F_{(19, 6289)} = 646.3$, $P < 0.001$], an effect of treatment [$F_{(2, 331)} = 11.28$, $P < 0.001$] and an interaction effect [$F_{(38, 6289)} = 5.528$, $P < 0.001$]. Conditioned media from untreated microglia decreased neuritic branching at 10-80 µm from the cell soma compared to control NBM. Conditioned media from IFNγ treated microglia also decreased neuritic branching at 10-80 µm from the cell soma compared to control NBM and at 20-30 µm from the cell soma compared to conditioned media from untreated microglia [*Figure 4.4 (D)*].

When examining the effect of conditioned media from IFNγ treated mixed glia, one-way ANOVA of **neuritic branches** showed an effect of treatment [$F_{(2, 233)} = 7.680$, $P < 0.001$]. *Post hoc* analysis revealed a significant decrease in the number of neuritic branches following treatment with conditioned media from IFNγ treated mixed glia compared to conditioned media from untreated mixed glia ($P < 0.001$) [*Figure 4.5 (A)*]. One-way ANOVA of **neuritic length** showed an effect of treatment [$F_{(2, 230)} = 16.75$, $P < 0.001$]. *Post hoc* analysis revealed a significant increase in neuritic length following treatment with conditioned media from untreated mixed glia compared to NBM control ($P < 0.05$). *Post hoc* analysis also revealed a significant decrease in neuritic length following treatment with

conditioned media from IFNγ treated mixed glia compared to conditioned media from untreated mixed glia ($P < 0.001$) [*Figure 4.5 (B)*]. One-way ANOVA of the number of **primary neurites** showed no effect of treatment [$F_{(2, 233)} = 1.240$, $P = 0.291$] [*Figure 4.5 (C)*]. Two-way repeated measures ANOVA of the **number of neuritic branches at specific distances from the neuronal cell soma** showed an effect of distance [$F_{(19, 4370)} = 324.0$, $P < 0.001$], an effect of treatment [$F_{(2, 230)} = 12.49$, $P < 0.001$] and an interaction effect [$F_{(38, 4370)} = 4.616$, $P < 0.001$]. Conditioned media from untreated mixed glia increased neuritic branching at 30-70, and 110 µm from the cell soma compared to control NBM. Conditioned media from IFNγ treated mixed glia reduced neuritic branching at all distances between 40 and 150 µm from the cell soma and at 170 µm compared to conditioned media from untreated mixed glia [*Figure 4.5 (D)*]

When examining the direct effect of IFNγ on neuronal complexity, results showed that it had no effect on the number of **neuritic branches** [$T_{(188)} = 1.9$, $P = 0.059$], the **neuritic length** [$T_{(1192)} = 0.65$, $P = 0.517$], or the number of **primary neurites** [$T_{(195)} = 0.97$, $P = 0.333$], compared to control NBM (Student's T test) [*Figure 4.6 (A-C)*]. Two-way repeated measures ANOVA of the **number of neuritic branches at specific distances from the neuronal cell soma** showed an effect of distance [$F_{(19, 3860)} = 319.6$, $P < 0.001$], no effect of treatment [$F_{(1, 3860)} = 2.168$, $P = 0.14$] and no interaction effect [$F_{(19, 3860)} = 0.785$, $P = 0.73$] [*Figure 4.6 (D)*].

4.3.4 Effect of conditioned media from IFNγ treated mixed glia on synaptic protein co-localisation in mature primary cortical neurons

To investigate the effect of conditioned media from IFNγ treated mixed glia on synaptic protein co-localisations, primary cortical mixed glia (DIV 14) were treated with IFNγ (10 ng/mL) for 24 hours and the resulting conditioned media was collected and applied to mature (DIV 21) primary cortical neurons for 24 hours. Fixation and immunocytochemistry were performed to determine the effect of conditioned media from IFNγ treated mixed glia on synaptic protein co-localisation.

One-way ANOVA of **synaptophysin puncta** showed an effect of treatment [$F_{(2, 276)} = 23.14$, $P < 0.001$]. *Post hoc* analysis revealed reductions in the number of

synaptophysin puncta following treatment with conditioned media from untreated mixed glia compared to control NBM ($P < 0.01$), and following treatment with conditioned media from IFNγ treated mixed glia compared to conditioned media from untreated mixed glia ($P < 0.001$) [*Figure 4.7 (A)*]. One-way ANOVA of **PSD-95 puncta** showed an effect of treatment [$F_{(2, 289)} = 38.99$, $P < 0.001$]. *Post hoc* analysis revealed an increase in the number of PSD-95 puncta following treatment with conditioned media from untreated mixed glia compared to control NBM ($P < 0.01$), and following treatment with conditioned media from IFNγ treated mixed glia compared to conditioned media from untreated mixed glia ($P < 0.001$) [*Figure 4.7 (B)*]. One-way ANOVA of **co-localised synaptic puncta** showed an effect of treatment [$F_{(2, 272)} = 31.64$, $P < 0.001$]. *Post hoc* analysis revealed an increase in the number of co-localised synaptic puncta following treatment with conditioned media from untreated mixed glia ($P < 0.01$) compared to NBM. *Post hoc* analysis also revealed reductions in the number of co-localised synaptic puncta following treatment with conditioned media from IFNγ treated mixed glia compared to conditioned media from untreated mixed glia [*Figure 4.7 (C)*].

4.3.5 Effect of IFNγ on the mRNA expression of TNF-α, IL-1α, IL-1β and IL-6 in mixed glia

To investigate the effects of IFNγ on the mRNA expression of inflammatory markers in mixed glial, primary cortical mixed glial cultures (DIV 14) were treated with IFNγ (10 ng/mL) for 24 hours. Cells were harvested for RNA extraction followed by RT-PCR. mRNA expression for the inflammatory markers TNF-α, IL-1α, IL-1β, and IL-6 were quantified. To confirm the effect of IFNγ on the mRNA expression of TNF-α, primary cortical mixed glial cultures (DIV 14) were treated with IFNγ (10 ng/mL) for 6 hours and cells were harvested for RNA extraction followed by RT-PCR. Treatment of primary cortical mixed glia with IFNγ for 24 hours reduced the mRNA expression of **TNF-α** [$T_{(14)} = 11.87$, $P < 0.001$], and increased the mRNA expression of **IL-1α** [$T_{(15)} = 9.105$, $P < 0.001$], **IL-1β** [$T_{(11)} = 17.91$, $P < 0.001$] and **IL-6** [$T_{(16)} = 6.286$, $P < 0.001$], compared to control DMEM (Student's T test) [*Figure 4.8 (A-D)*]. Treatment of primary mixed glia with IFNγ

for 6 hours increased the mRNA expression of **TNF-α** [$T_{(16)} = 7.645$, $P < 0.001$] compared to control DMEM (Student's T test) [*Figure 4.8 (E)*].

4.3.6 Effect of IFNγ on the production of TNF-α and IL-1α protein in mixed glia

To investigate the effect of IFNγ on TNF-α and IL-1α protein release from mixed glia, primary cortical mixed glial cultures (DIV 14) were treated with IFNγ (10 ng/mL) for 24 hours. Supernatants were collected for analysis of TNF-α and IL-1α protein release by ELISA. Treatment of primary cortical mixed glia with IFNγ for 24 hours increased the release of **TNF-α** [$T_{(13)} = 37.49$, $P < 0.001$] and **IL-1α** [$T_{(14)} = 6.043$, $P < 0.001$], compared to control DMEM (Student's T test) [*Figure 4.9*].

4.3.7 Effect of IFNγ on the mRNA expression of TNF-α, IL-1α and Iba1 in microglia

To investigate the effects of IFNγ on the mRNA expression of inflammatory markers in microglia, primary cortical microglial cultures (DIV 15) were treated with IFNγ (10 ng/mL) for 24 hours. Cells were harvested for RNA extraction followed by RT-PCR. mRNA expression for the inflammatory markers' TNF-α, IL-1α, and Iba1 were quantified. To confirm the effect of IFNγ on the mRNA expression of TNF-α, primary cortical microglial cultures (DIV 15) were treated with IFNγ (10 ng/mL) for 6 hours and cells were harvested for RNA extraction followed by RT-PCR. Treatment of primary cortical microglia with IFNγ for 24 hours had no effect on the mRNA expression of **TNF-α** [$T_{(10)} = 0.6796$, $P = 0.512$] or **Iba1** [$T_{(14)} = 0.732$, $P = 0.477$], but increased the expression of **IL-1α** [$T_{(10)} = 3.479$, $P = 0.006$] and **IL-6** [$T_{(15)} = 3.729$, $P = 0.002$], compared to control DMEM (Student's T test) [*Figure 4.10 (A-D)*]. Treatment of primary cortical microglia with IFNγ for 6 hours increased the mRNA expression of **TNF-α** [$T_{(13)} = 15.01$, $P < 0.001$] [*Figure 4.10 (E)*].

4.3.8 Effect of IFNγ on the production of TNF-α and IL-1α protein in microglia

To investigate the effect of IFNγ on TNF-α and IL-1α protein release from microglia, primary cortical microglial cultures (DIV 15) were treated with IFNγ (10 ng/mL) for 24 hours. Supernatants were collected for analysis of TNF-α and IL-1α protein release by ELISA. Treatment of primary cortical microglia with IFNγ for 24

hours increased the release of **TNF-α** [$T_{(2)} = 2.499$, $P < 0.001$] and **IL-1α** [$T_{(22)} = 2.288$, $P = 0.003$], compared to control DMEM (Student's T test) [*Figure 4.11*].

4.3.9 Effect of IFNγ on the mRNA expression of GFAP, S100β, IL-1β and IL-6 in astrocytes

To investigate the effects of IFNγ on the mRNA expression of GFAP, S100β, IL-1β and IL-6 in astrocytes, primary cortical astrocyte cultures (DIV 14) were treated with IFNγ (10 ng/mL) for 24 hours. Cells were harvested for RNA extraction followed by RT-PCR. mRNA expression for the markers GFAP, S100β, IL-1β and IL-6 were quantified. Treatment of primary cortical astrocytes with IFNγ for 24 hours reduced the mRNA expression of **GFAP** [$T_{(14)} = 4.384$, $P < 0.001$] and **S100β** [$T_{(14)} = 3.923$, $P = 0.002$], and increased **IL-1β** [$T_{(10)} = 9.518$, $P < 0.001$] and **IL-6** [$T_{(14)} = 8.909$, $P < 0.001$], compared to control DMEM (Student's T test) [*Figure 4.12 (A-D)*].

4.3.10 Effect of TNF-α and IL-1α on GFAP immunoreactivity and morphology of enriched primary cortical astrocytes

To investigate the effects of TNF-α and IL-1α on astrocytic GFAP immunoreactivity and morphology, enriched primary cortical astrocytes (DIV 14) were treated with TNF-α (30 ng/mL) and IL-1α (3 ng/mL) for 24 hours. Fixation and immunocytochemistry were performed to determine the effect of TNF-α and IL-1α on GFAP immunoreactivity and astrocyte morphology (mean cell area, perimeter and soma: area ratio). Concentrations of TNF-α and IL-1α were chosen based on prior research which used a similar range of concentrations on astrocytes (Liddelow et al, 2017).

Treatment of primary cortical astrocytes with TNF-α (30 ng/mL) and IL-1α (3 ng/mL) reduced **GFAP immunoreactivity** [$T_{(90)} = 9.542$, $P < 0.001$], **astrocyte mean cell area** [$T_{(91)} = 13.25$, $P < 0.001$], and **cell perimeter** [$T_{(92)} = 13.32$, $P < 0.001$], but increased the **soma:cell ratio** [$T_{(89)} = 12.20$, $P < 0.001$], compared to control DMEM (Student's T test) [*Figure 4.13 (A-D)*].

4.3.11 Effect of TNF-α and IL-1α on the mRNA expression of GFAP, S100β, IL-1β and IL-6 in primary cortical astrocytes

To investigate the effects of TNF-α and IL-1α on the mRNA expression of the astrocytic markers GFAP, S100β, IL-1β, and IL-6, primary cortical astrocytes (DIV 14) were treated with TNF-α (30 ng/mL) and IL-1α (3 ng/mL) for 24 hours. Cells were harvested for RNA extraction followed by RT-PCR. mRNA expression for the astrocyte markers GFAP, S100β, IL-1β, and IL-6 were quantified.

Treatment of primary cortical astrocytes with TNF-α (30 ng/mL) and IL-1α (3 ng/mL) reduced the mRNA expression of **GFAP** [$T_{(14)} = 8.559$, $P < 0.001$], and **S100β** [$T_{(14)} = 7.452$, $P < 0.001$] and increased **IL-1β** [$T_{(14)} = 2.188$, $P = 0.0461$], and **IL-6** [$T_{(14)} = 3.796$, $P = 0.002$], compared to control DMEM (Student's T test) [*Figure 4.14 (A-D)*].

4.3.12 Effect of conditioned media from TNF-α and IL-1α treated astrocytes on the complexity of mature primary cortical neurons

To investigate the effect of conditioned media from TNF-α and IL-1α treated astrocytes on neuronal complexity, primary cortical astrocytes (DIV 14) were treated with TNF-α (30 ng/mL) and IL-1α (3 ng/mL) for 24 hours. The resulting conditioned media was collected and applied to primary cortical neurons (DIV 21) for 24 hours. Fixation and MAP2 immunocytochemistry were performed to determine the effect of conditioned media from TNF-α and IL-1α treated astrocytes on neuronal complexity by Sholl analysis.

One-way ANOVA of **neuritic branches** showed an effect of treatment [$F_{(2, 194)} = 30.40$, $P < 0.001$]. *Post hoc* analysis revealed an increase in the number of neuritic branches following treatment with conditioned media from untreated astrocytes compared to control NBM ($P < 0.001$), and a decrease in the number of neuritic branches following treatment with conditioned media from TNF-α and IL-1α treated astrocytes compared to conditioned media from untreated astrocytes ($P < 0.001$) [*Figure 4.15 (A)*]. Simialrly, one-way ANOVA of **neuritic length** showed an effect of treatment [$F_{(2, 191)} = 115.9$, $P < 0.001$]. *Post hoc* analysis revealed an increase in neuritic length following treatment with conditioned media from untreated astrocytes compared to control NBM ($P <$

0.001), and a decrease in neuritic length following treatment with conditioned media from TNF-α and IL-1α treated astrocytes compared to conditioned media from untreated astrocytes ($P < 0.001$) [*Figure 4.15 (B)*]. One-way ANOVA of the number of **primary neurites** showed no effect of treatment [$F(2, 194) = 2.013$, $P = 0.136$] [Figure *4.15 (C)*]. Two-way repeated measures ANOVA of the **number of neuritic branches at specific distances from the neuronal cell soma** showed an effect of distance [$F_{(19, 2090)} = 98.36$, $P < 0.001$], an effect of treatment [$F_{(2, 110)} = 51.12$, $P < 0.001$] and an interaction effect [$F_{(38, 2090)} = 8.740$, $P < 0.001$]. Conditioned media from TNF-α and IL-1α treated astrocytes decreased neuritic branching at all distances between 40 and 200 μm from the cell soma compared to conditioned media from untreated astrocytes [*Figure 4.15 (D)*].

4.3.13 Effect of conditioned media from TNF-α and IL-1α treated astrocytes on synaptic protein co-localisation in mature primary cortical neurons

To investigate the effect of conditioned media from TNF-α and IL-1α treated astrocytes on synaptic protein co-localisation in mature neurons, primary cortical astrocytes (DIV 14) were treated with TNF-α (30 ng/mL) and IL-1α (3 ng/mL) for 24 hours. The resulting conditioned media was collected and applied to primary cortical neurons (DIV 21) for 24 hours. Fixation and immunocytochemistry were performed to determine the effect of conditioned media from TNF-α and IL-1α treated astrocytes on synaptic protein co-localisation.

When examining the effect of conditioned media from TNF-α and IL-1α treated astrocytes on synaptic protein co-localisation in mature primary cortical neurons one-way ANOVA of **synaptophysin puncta** showed no effect of treatment [$F_{(2, 158)} = 1.231$, $P = 0.295$] [*Figure 4.16 (A)*]. One-way ANOVA of **PSD-95 puncta** showed no effect of treatment [$F_{(2, 160)} = 2.271$, $P = 0.107$] [*Figure 4.16 (B)*]. One-way ANOVA of **co-localised synaptic puncta** showed an effect of treatment [$F_{(2, 153)} = 3.821$, $P = 0.024$]. *Post hoc* analysis revealed a decrease in the number of co-localised synaptic puncta following treatment with conditioned media from TNF-α and IL-1α treated astrocytes compared to conditioned media from untreated astrocytes ($P < 0.05$) [*Figure 4.16 (C)*].

4.3.14 Effect of TNF-α and IL-1α on the production of IL-6 protein in astrocytes

To investigate the effect of TNF-α and IL-1α on the release of astrocytic IL-6, primary cortical astrocyte cultures (DIV 14) were treated with TNF-α (30 ng/mL) and IL-1α (3 ng/mL) for 24 hours. Supernatants were collected for analysis of IL-6 protein release by ELISA. Treatment of primary cortical astrocytes with TNF-α and IL-1α for 24 hours increased the release of **IL-6** [$T_{(10)} = 79.14$, $P < 0.001$] compared to control DMEM (Student's T test) [*Figure 4.17*].

4.3.15 Concentration-related effect of IL-6 on the complexity of mature neurons

To investigate the effect of IL-6 on neuronal complexity, mature primary cortical neurons (DIV 21) were treated with IL-6 (10, 20, 40, 80, 200 ng/mL) for 24 hours. Fixation and MAP2 immunocytochemistry were performed to determine the concentration-related effect of IL-6 on neuronal complexity by Sholl analysis.

When examining the concentration-related effect of IL-6 on the complexity of mature neurons one-way ANOVA of **neuritic branches** showed an effect of IL-6 [$F_{(5, 472)} = 5.106$, $P < 0.001$]. *Post hoc* analysis revealed a significant reduction in neuritic branching for neurons treated with IL-6 (80 ng/mL) compared to control NBM ($P < 0.001$), and for neurons treated with IL-6 (200 ng/mL) compared to control NBM ($P < 0.01$) [*Figure 4.18 (A)*]. One-way ANOVA of **neuritic length** showed an effect of IL-6 [$F_{(5, 481)} = 10.46$, $P < 0.001$]. *Post hoc* analysis revealed a significant reduction in neuritic length for neurons treated with IL-6 (200 and 80 ng/mL) compared to control NBM ($P < 0.001$) [*Figure 4.18 (B)*]. One-way ANOVA of the number of **primary neurites** showed an effect of IL-6 [$F_{(5, 481)} = 7.468$, $P < 0.001$]. *Post hoc* analysis analysis revealed a significant reduction in the number of primary neurites for neurons treated with IL-6 (200 and 80 ng/mL) compared to control NBM ($P < 0.01$) [*Figure 4.18 (C)*]. Two-way repeated measures ANOVA of the **number of neuritic branches at specific distances from the neuronal cell soma** showed an effect of distance [$F_{(19, 8626)} = 810.9$, $P < 0.001$], an effect of treatment [$F_{(5, 454) = 10.68}$, $P < 0.001$] and an interaction effect [$F_{(95, 8626)} = 3.910$, $P < 0.001$]. *Post hoc* analysis revealed IL-6 (80 ng/mL) reduced neuritic branching at all distances between 10 and 90 µm from the cell soma and IL-6 (200 ng/mL)

reduced neuritic branching at all distances between 10 and 50 µm from the cell soma, compared to control NBM [*Figure 4.*18 *(D)*].

4.3.16 Effect of IL-6 on synaptic protein co-localisation in mature primary cortical neurons

To investigate the effect of IL-6 on synaptic protein co-localisation, primary cortical neurons (DIV 21) were treated with IL-6 (80 ng/mL) for 24 hours. Fixation and immunocytochemistry were performed to determine the effect of IL-6 (80 ng/mL) on synaptic protein co-localisation.

Resuts of this study showed that IL-6 reduced the number of **synaptophysin puncta** [$T_{(238)} = 14.26$, $P < 0.001$], **PSD-95 puncta** [$T_{(241)} = 11.87$, $P < 0.001$], and **the number of co-localised synaptic puncta** [$T_{(243)} = 13.36$, $P < 0.001$], compared to control NBM [*Figure 4.19 (A-C)*].

4.3.17 Effect of IL-6 on the viability of mature primary cortical neurons

To investigate the effect of IL-6 on neuronal viability, primary cortical neurons (DIV 21) were treated with IL-6 (80 ng/mL) for 24 hours. Neuronal viability was assessed using the CCK-8 assay. Results showed that IL-6 had no effect on neuronal viability [$T_{(4)} = 0.1469$, $P = 0.89$] [*Figure 4.20*].

4.3.18 Effect of IL-6 neutralisation on TNF-α and IL-1α-induced release of IL-6 protein from astrocytes

To investigate the effect of IL-6 neutralising antibody on TNF-α and IL-1α-induced release of astrocytic IL-6, primary cortical astrocyte cultures (DIV 14) were treated with TNF-α (30 ng/mL), IL-1α (3 ng/mL) and IL-6 neutralising antibody for 24 hours. Supernatants were collected for analysis of IL-6 protein release by ELISA.

One-way ANOVA of **IL-6** showed an effect of treatment [$F_{(3, 4)} = 213.5$, $P < 0.001$]. *Post hoc* analysis revealed an increase in IL-6 release from astrocytes following treatment with TNF-α and IL-1α compared to control NBM ($P < 0.001$). Co-treatment with IL-6 neutralising antibody prevented this increase bringing levels of IL-6 back to control [*Figure 4.21*].

4.3.19 Effect of IL-6 neutralisation on reductions in neuronal complexity induced by conditioned media from TNF-α and IL-1α treated astrocytes

To investigate the effect of IL-6 neutralisation on reductions in neuronal complexity induced by conditioned media from TNF-α and IL-1α treated astrocytes, primary cortical enriched astrocyte cultures (DIV 14) were treated with TNF-α (30 ng/mL), IL-1α (3 ng/mL) and IL-6 neutralising antibody for 24 hours. The resulting conditioned media was collected and applied to mature primary cortical neurons (DIV 21) for 24 hours. Fixation and MAP2 immunocytochemistry were performed to determine the effect of IL-6 neutralisation on reductions in neuronal complexity induced by conditioned media from TNF-α and IL-1α treated astrocytes.

Conditioned media from TNF-α and IL-1α treated astrocytes reduced the number of **neuritic branches** [$T_{(176)} = 7.038$, $P < 0.001$] compared to control conditioned media. One-way ANOVA showed an effect of treatment [$F_{(2, 242)} = 29.28$, $P < 0.001$]. *Post hoc* analysis revealed an increase in the number of neuritic branches following IL-6 neutralisation compared to conditioned media from TNF-α and IL-1α treated astrocytes alone ($P < 0.001$) [*Figure 4.22 (A)*]. Conditioned media from TNF-α and IL-1α treated astrocytes reduced **neuritic length** [$T_{(178)} = 6.47$, $P < 0.001$] compared to control conditioned media. One-way ANOVA showed an effect of treatment [$F_{(2, 245)} = 25.11$, $P < 0.001$]. *Post hoc* analysis revealed an increase in neuritic length following IL-6 neutralisation compared to conditioned media from TNF-α and IL-1α treated astrocytes alone ($P < 0.001$) [*Figure 4.22 (B)*]. Conditioned media from TNF-α and IL-1α treated astrocytes reduced the number of **primary neurites** [$T_{(179)} = 2.608$, $P = 0.01$] compared to control conditioned media. One-way ANOVA showed an effect of treatment [$F_{(2, 246)} = 9.389$, $P < 0.001$]. *Post hoc* analysis revealed an increase the number of primary neurites following IL-6 neutralisation alone compared to conditioned media from TNF-α and IL-1α treated astrocytes alone [*Figure 4.22 (C)*]. Two-way repeated measures ANOVA of the **number of neuritic branches at specific distances from the neuronal cell soma** showed an effect of distance [$F_{(19, 6600)} = 159.3$, $P < 0.001$], an effect of treatment [$F_{(3, 6600)} = 180.4$, $P < 0.001$] and an interaction effect [$F_{(57, 6600)} = 2.903$, $P < 0.001$]. IL-6 neutralising antibody protected against

reductions induced by conditioned media from TNF-α and IL-1α treated astrocytes at all distances between 10 and 80 μm from the cell [*Figure 4.22 (D)*].

4.3.20 Effect of IL-6 neutralisation on reductions in synaptic protein co-localisation induced by conditioned media from TNF-α and IL-1α treated astrocytes

To investigate the effect of IL-6 neutralisation on reductions in synaptic protein co-localisation induced by conditioned media from TNF-α and IL-1α treated astrocytes, primary cortical astrocyte cultures (DIV 14) were treated with TNF-α (30 ng/mL), IL-1α (3 ng/mL) and IL-6 neutralising antibody for 24 hours. The resulting conditioned media was collected and applied to mature (DIV 21) primary cortical neurons for 24 hours. Fixation and immunocytochemistry were performed to determine the effect of IL-6 neutralisation on reductions in synaptic protein co-localisation induced by conditioned media from TNF-α and IL-1α treated astrocytes.

Results of this study showed that conditioned media from TNF-α and IL-1α treated astrocytes reduced the number of **synaptophysin puncta** [$T_{(129)} = 6.556$, $P < 0.001$] compared to control conditioned media. One-way ANOVA showed an effect of treatment [$F_{(2, 220)} = 19.50$, $P < 0.001$]. *Post hoc* analysis revealed an increase in synaptophysin puncta following IL-6 neutralisation compared to conditioned media from TNF-α and IL-1α treated astrocytes alone ($P < 0.001$) [*Figure 4.23 (A)*]. Conditioned media from TNF-α and IL-1α treated astrocytes reduced the number of **PSD-95 puncta** [$T_{(129)} = 5.693$, $P < 0.001$] compared to control conditioned media. One-way ANOVA showed an effect of treatment [$F_{(2, 218)} = 13.39$, $P < 0.001$]. *Post hoc* analysis revealed an increase in PSD-95 puncta following IL-6 neutralisation compared to conditioned media from TNF-α and IL-1α treated astrocytes alone ($P < 0.001$) [*Figure 4.23 (B)*]. Conditioned media from TNF-α and IL-1α treated astrocytes reduced the number of **co-localised synaptic puncta** [$T_{(129)} = 7.206$, $P < 0.001$] compared to control conditioned media. One-way ANOVA showed an effect of treatment [$F_{(2, 220)} = 28.21$, $P < 0.001$]. *Post hoc* analysis revealed an increase in the number of co-localised synaptic puncta following IL-6 neutralisation compared to conditioned

media from TNF-α and IL-1α treated astrocytes alone ($P < 0.001$) [*Figure 4.23 (C)*].

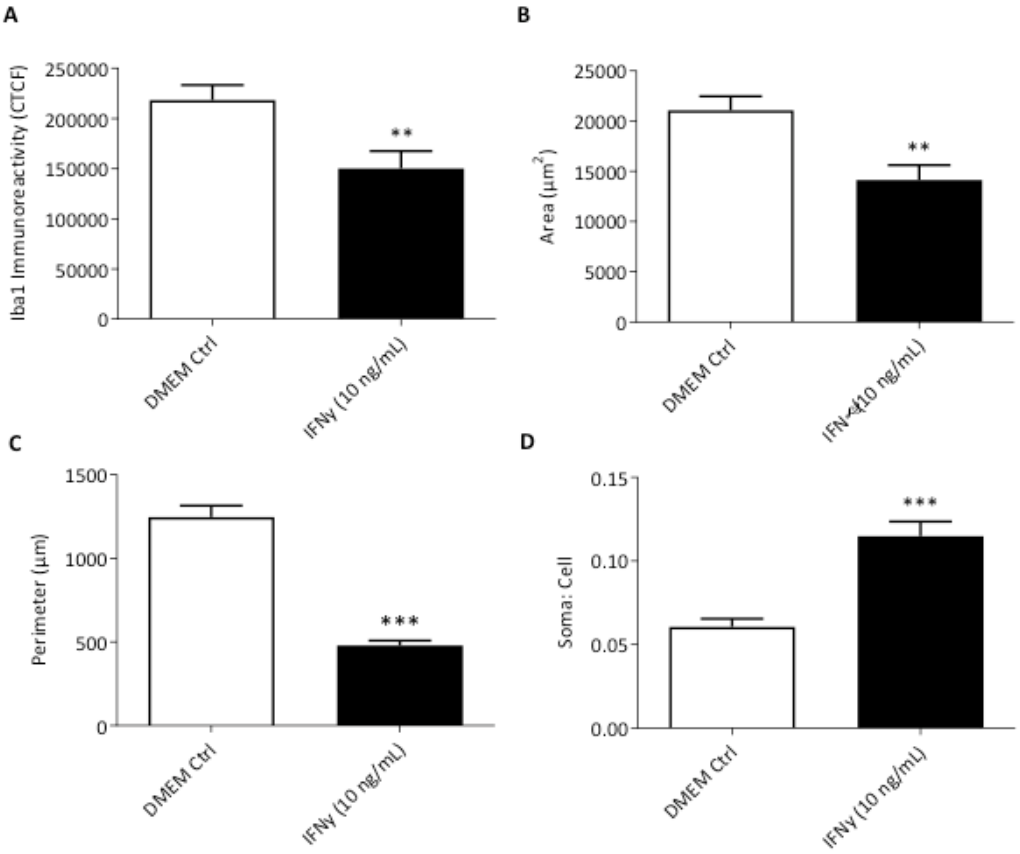

Figure 4.1 IFNγ reduces Iba1 immunoreactivity and the morphology of enriched primary cortical microglia.

Primary cortical microglia (DIV 15) were treated with IFNγ (10 ng/mL) for 24 hours before fixation and Iba1 immunocytochemistry. Morphological analysis was performed to quantify Iba1 immunoreactivity (A), microglia mean cell area (B), mean cell perimeter (C), and the soma:cell ratio (D). Data are expressed as mean ± SEM, n=6-8 coverslips per treatment group from 3 independent experiments. ***P<0.001, **P<0.01 vs. control DMEM (Newman-Keuls *post hoc* test).

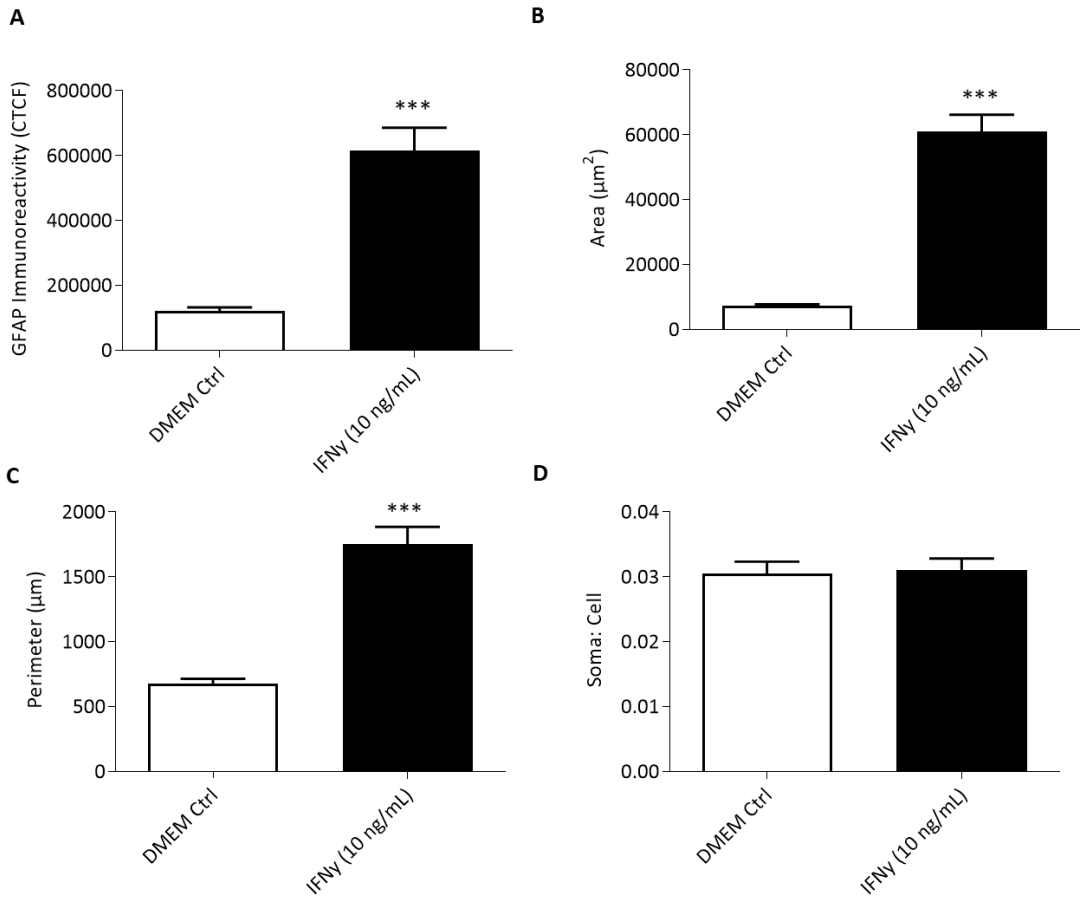

Figure 4.2 IFNγ increases GFAP immunoreactivity and the morphology of enriched primary cortical astrocytes.

Primary cortical astrocytes (DIV 14) were treated with IFNγ (10 ng/mL) for 24 hours before fixation and GFAP immunocytochemistry. Morphological analysis was performed to quantify GFAP immunoreactivity (A), astrocyte mean cell area (B), mean cell perimeter (C) and the soma:cell ratio (D). Data are expressed as mean ± SEM, n=6-8 coverslips per treatment group from 3 independent experiments. ***P<0.001 vs. control DMEM (Newman-Keuls *post hoc* test).

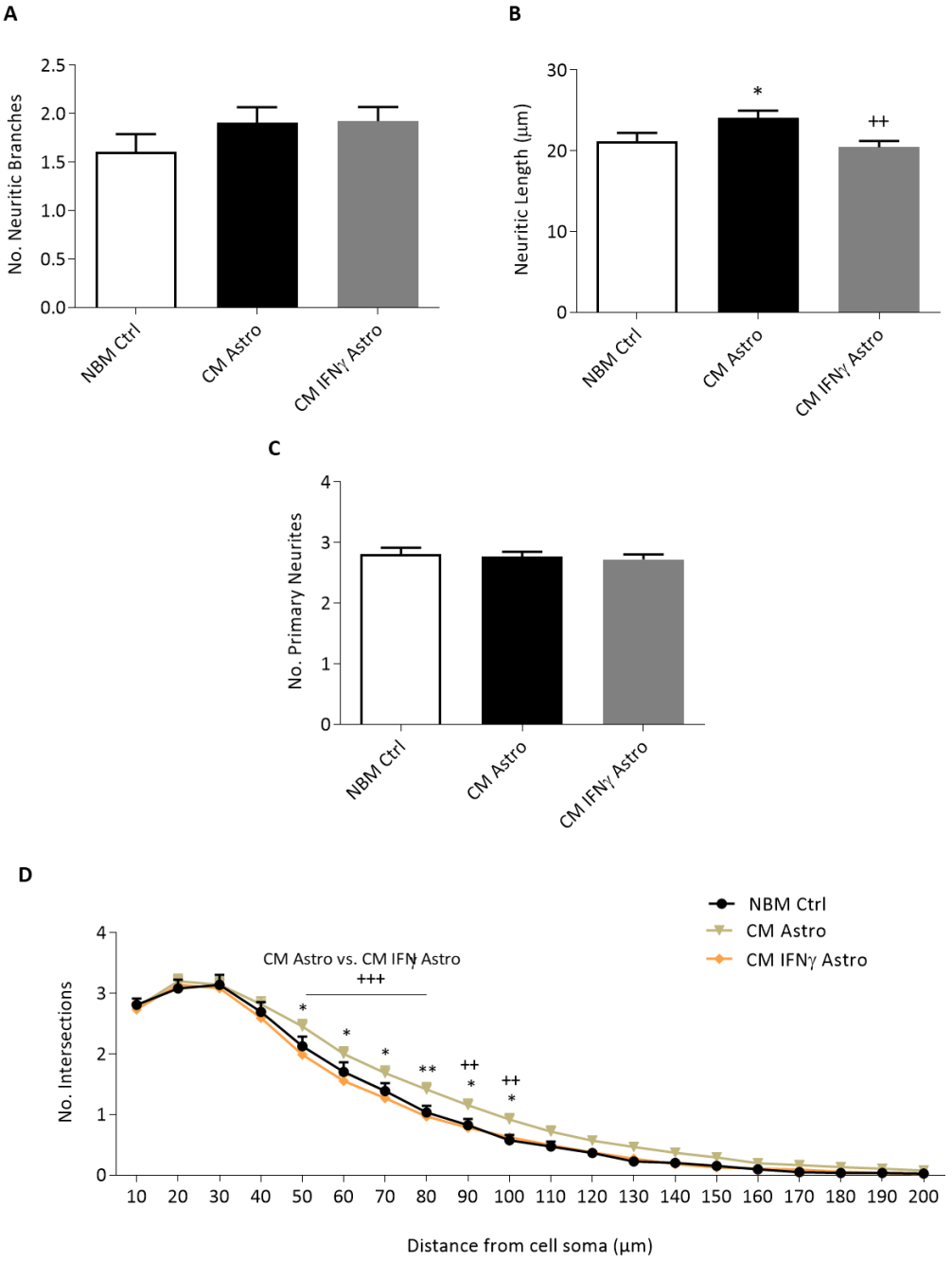

Figure 4.3 Conditioned media from IFNγ treated astrocytes has no effect on the complexity of mature primary cortical neurons.

Primary cortical astrocytes (DIV 14) were treated with IFNγ (10 ng/mL) for 24 hours. The resulting conditioned media was collected and applied to mature primary cortical neurons (DIV 21) for 24 hours before fixation and MAP2 immunocytochemistry. Sholl analysis was performed to analyse the number of neuritic branches (A), the neuritic length (B), the number of primary neurites (C), and the Sholl profile (D). Data are expressed as mean ± SEM, n=8 coverslips per treatment group from 3 independent experiments. **P<0.01, *P<0.05 vs. control NBM, $^{+++}$P<0.001, $^{++}$P<0.01 vs. conditioned media from untreated astrocytes (Newman-Keuls *post hoc* test).

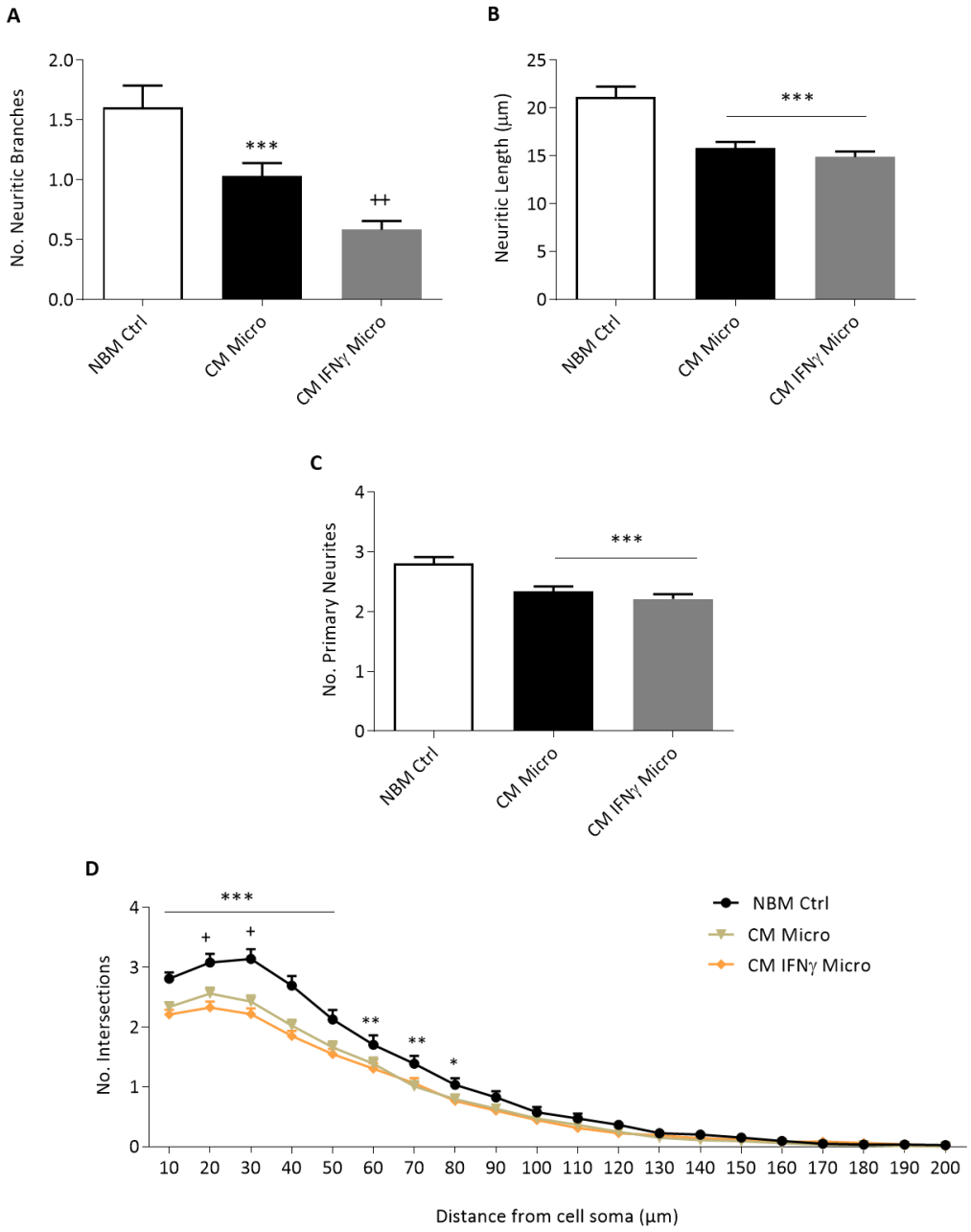

Figure 4.4 Conditioned media from IFNγ treated microglia reduces the complexity of mature primary cortical neurons.

Primary cortical microglia (DIV 15) were treated with IFNγ (10 ng/mL) for 24 hours. The resulting conditioned media was collected and applied to primary cortical neurons (DIV 21) for 24 hours before fixation and MAP2 immunocytochemistry. Sholl analysis was performed to analyse the number of neuritic branches (A), the neuritic length (B), the number of primary neurites (C), and the Sholl profile (D). Data are expressed as mean ± SEM, n=6-8 coverslips per treatment group from 3 independent experiments. ***P<0.001, **P<0.01, *P<0.05 vs. control NBM, $^{+}$P<0.05, $^{++}$P<0.01 vs. CM from untreated microglia (Newman-Keuls *post hoc* test).

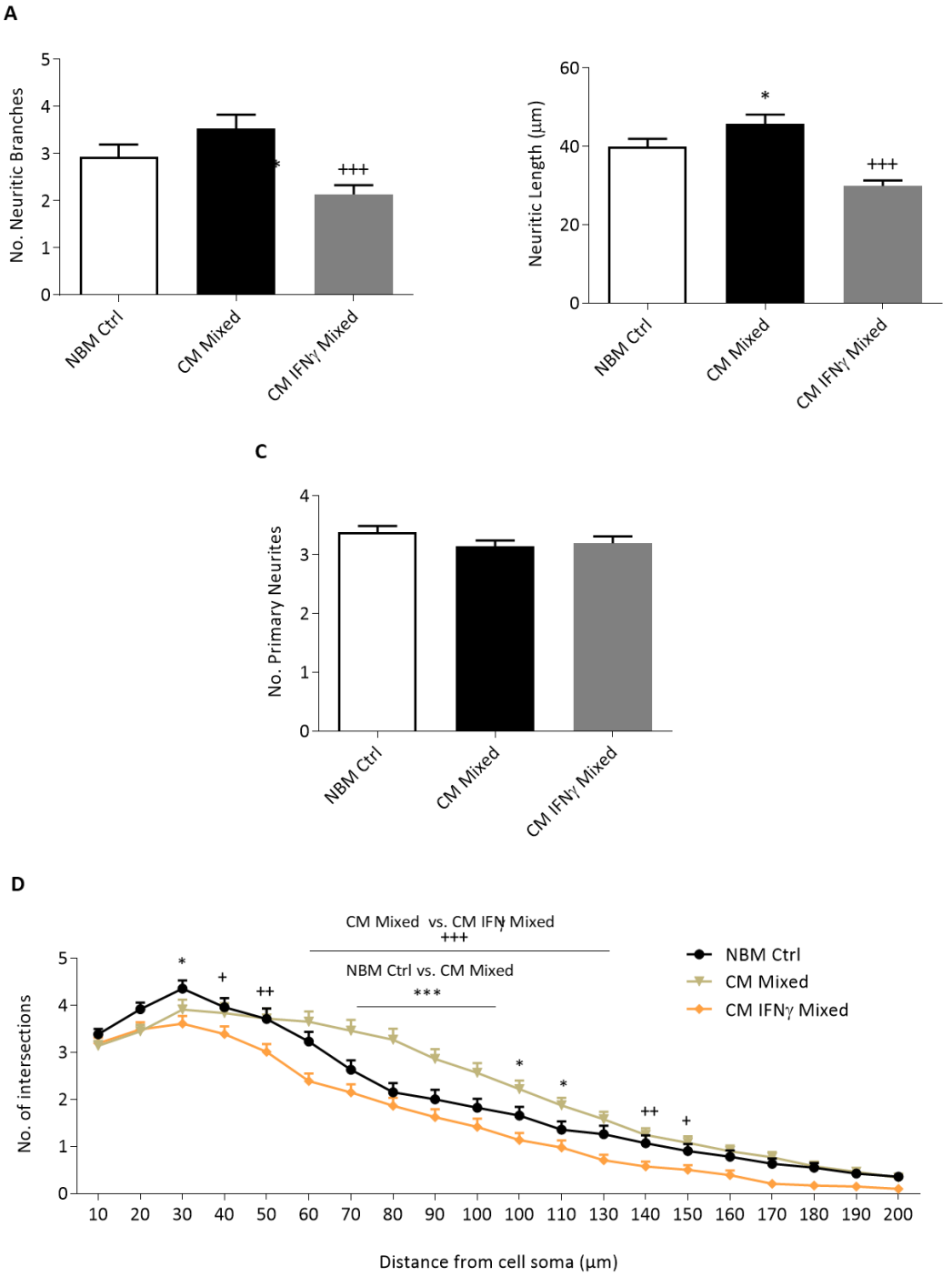

Figure 4.5 Conditioned media from IFNγ treated mixed glia reduces the complexity of mature primary cortical neurons.

Primary cortical astrocytes (DIV 14) were treated with IFNγ (10 ng/mL) for 24 hours. The resulting conditioned media was collected and applied to mature primary cortical neurons (DIV 21) for 24 hours before fixation and MAP2 immunocytochemistry. Sholl analysis was performed to analyse the number of neuritic branches (A), the neuritic length (B), the number of primary neurites (C), and the Sholl profile (D). Data are expressed as mean ± SEM, n=6-8 coverslips per treatment group from 3 independent experiments. ***P<0.001, *P<0.05 vs. control NBM, $^{+}$P<0.05, $^{++}$P<0.01, $^{+++}$P<0.001 vs. CM from untreated mixed glia (Newman-Keuls *post hoc* test).

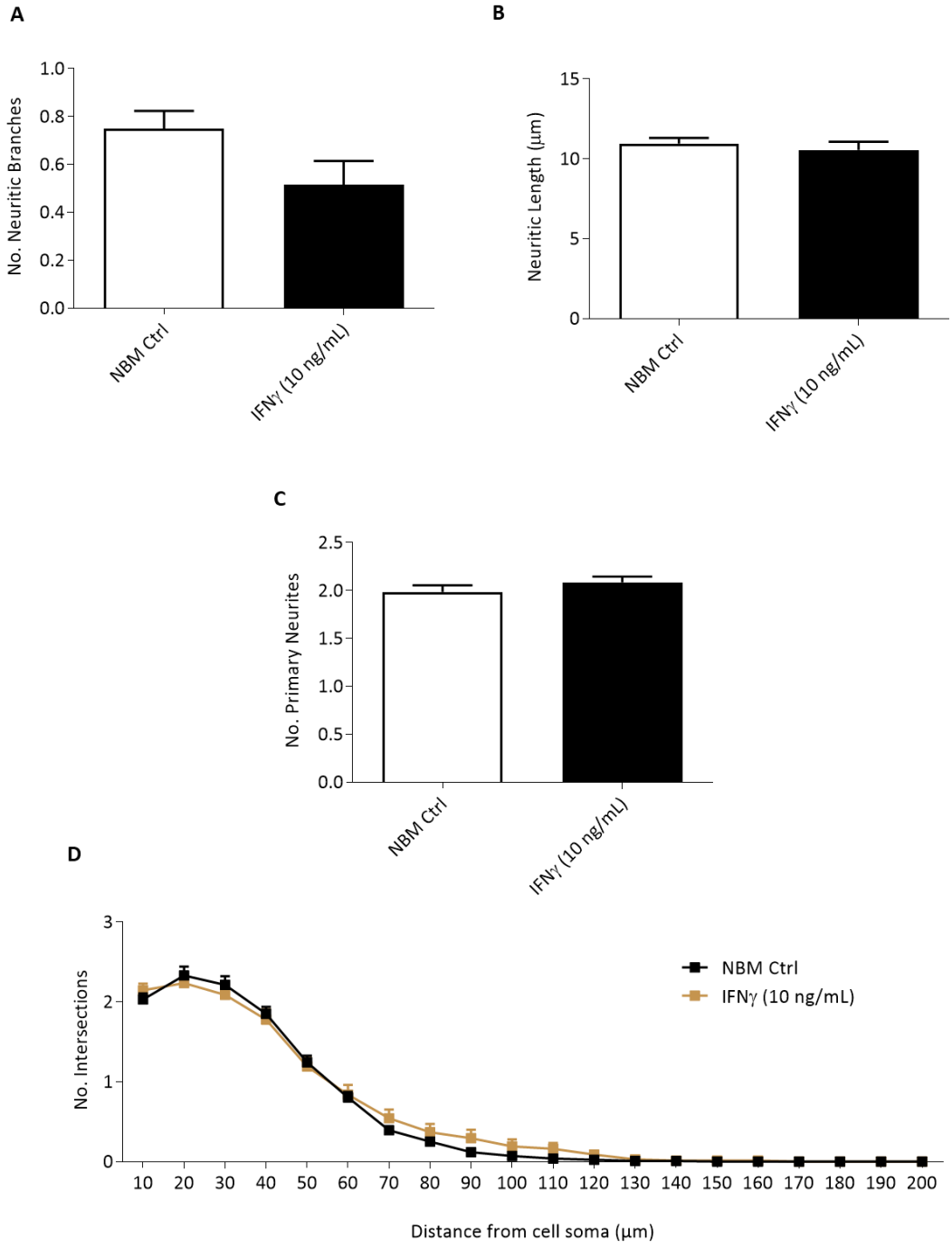

Figure 4.6 Direct treatment of IFNγ has no effect on the complexity of mature primary cortical neurons.

Mature primary cortical neurons (DIV 21) were treated with IFNγ (10 ng/mL) for 24 hours before fixation and MAP2 immunocytochemistry. Sholl analysis was performed to analyse the number of neuritic branches (A), the neuritic length (B), the number of primary neurites (C), and the Sholl profile (D). Data are expressed as mean ± SEM, n=6-8 coverslips per treatment group from 3 independent experiments.

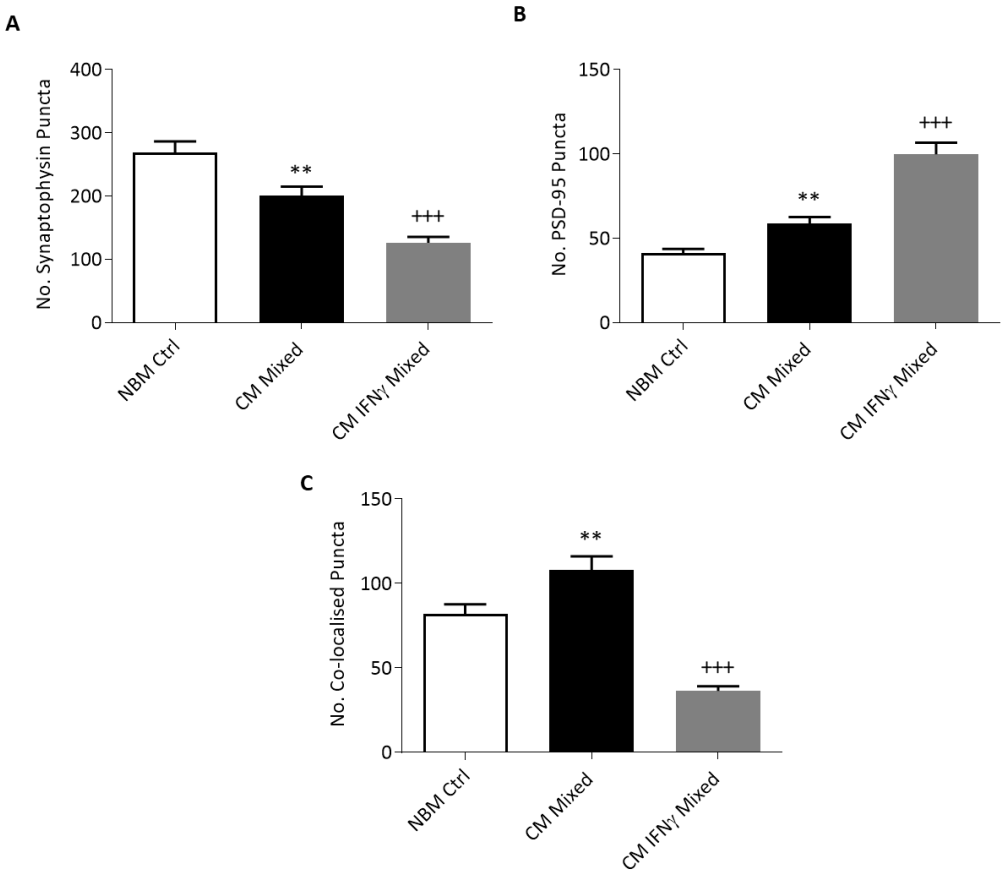

Figure 4.7 Conditioned media from IFNγ treated mixed glia reduces synaptic protein co-localisation in mature primary cortical neurons.

Primary cortical mixed glia (DIV 14) were treated with IFNγ (10 ng/mL) for 24 hours. The resulting conditioned media was collected and applied to mature primary cortical neurons (DIV 21) for 24 hours before fixation and immunocytochemistry to quantify synaptophysin puncta (A), PSD-95 puncta (B), and co-localised synaptic puncta (C). Data are expressed as mean ± SEM, n=6-8 coverslips per treatment group from 4 independent experiments. **P<0.01, vs. control NBM. $^{+++}$P<0.001 vs. CM from untreated mixed glia (Newman-Keuls *post hoc* test)

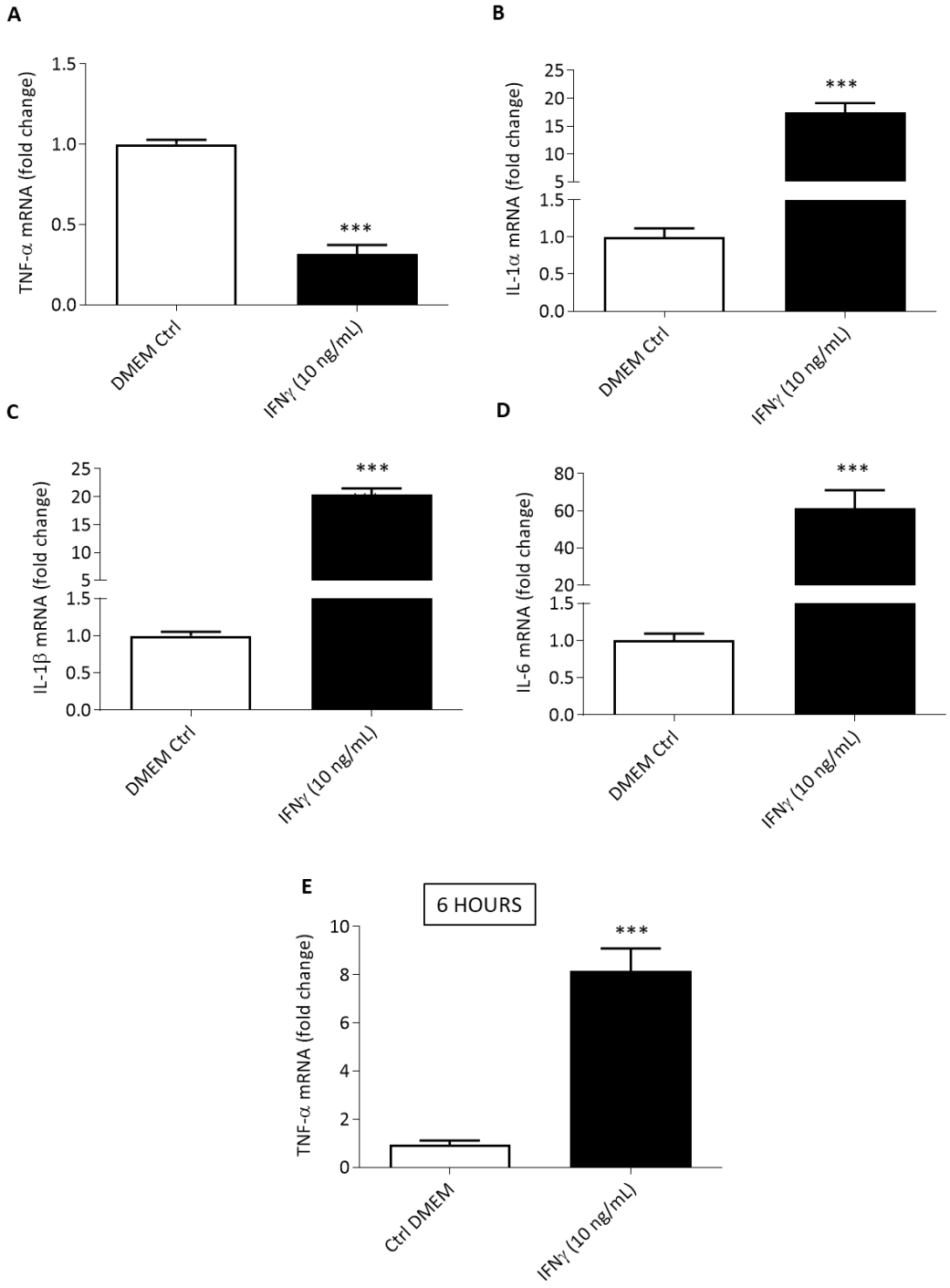

Figure 4.8 Effect of IFNγ on the mRNA expression of TNF-α, IL-1α, IL-1β and IL-6 in primary cortical mixed glia.

Primary mixed glia (DIV 14) were treated with IFNγ (10 ng/mL) for 24 hours. Cells were harvested for RNA extraction followed by RT-PCR for the markers TNF-α (A), IL-1α (B), IL-1β (C) and IL-6 (D). Primary mixed glia (DIV 14) were treated with IFNγ (10 ng/mL) for 6 hours. Cells were harvested for RNA extraction followed by RT-PCR for TNF-α (E). Data are expressed as mean ± SEM, n=8 wells per treatment group from 3 independent experiments. ***P<0.001 vs. control DMEM. (Newman-Keuls *post hoc* test).

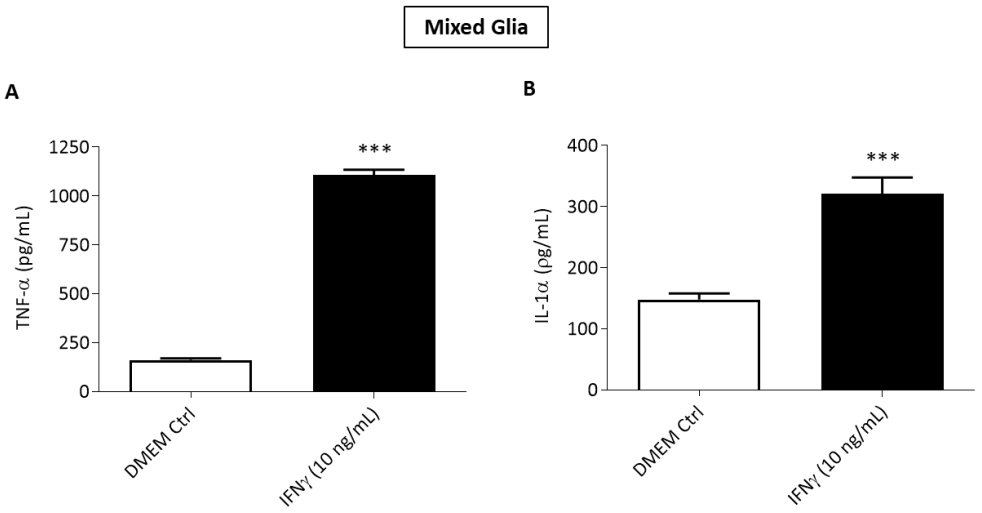

Figure 4.9 IFNγ increases the production of TNF-α and IL-1α protein in primary cortical mixed glia.

Primary cortical mixed glia (DIV 14) were treated with IFNγ (10 ng/mL) for 24 hours. Supernatants were collected for analysis of TNF-α (A) and IL-1α (B) protein release by ELISA. Data are expressed as mean ± SEM, n=8 wells per treatment group from 3 independent experiments. ***P<0.001 vs. control DMEM (Newman-Keuls *post hoc* test).

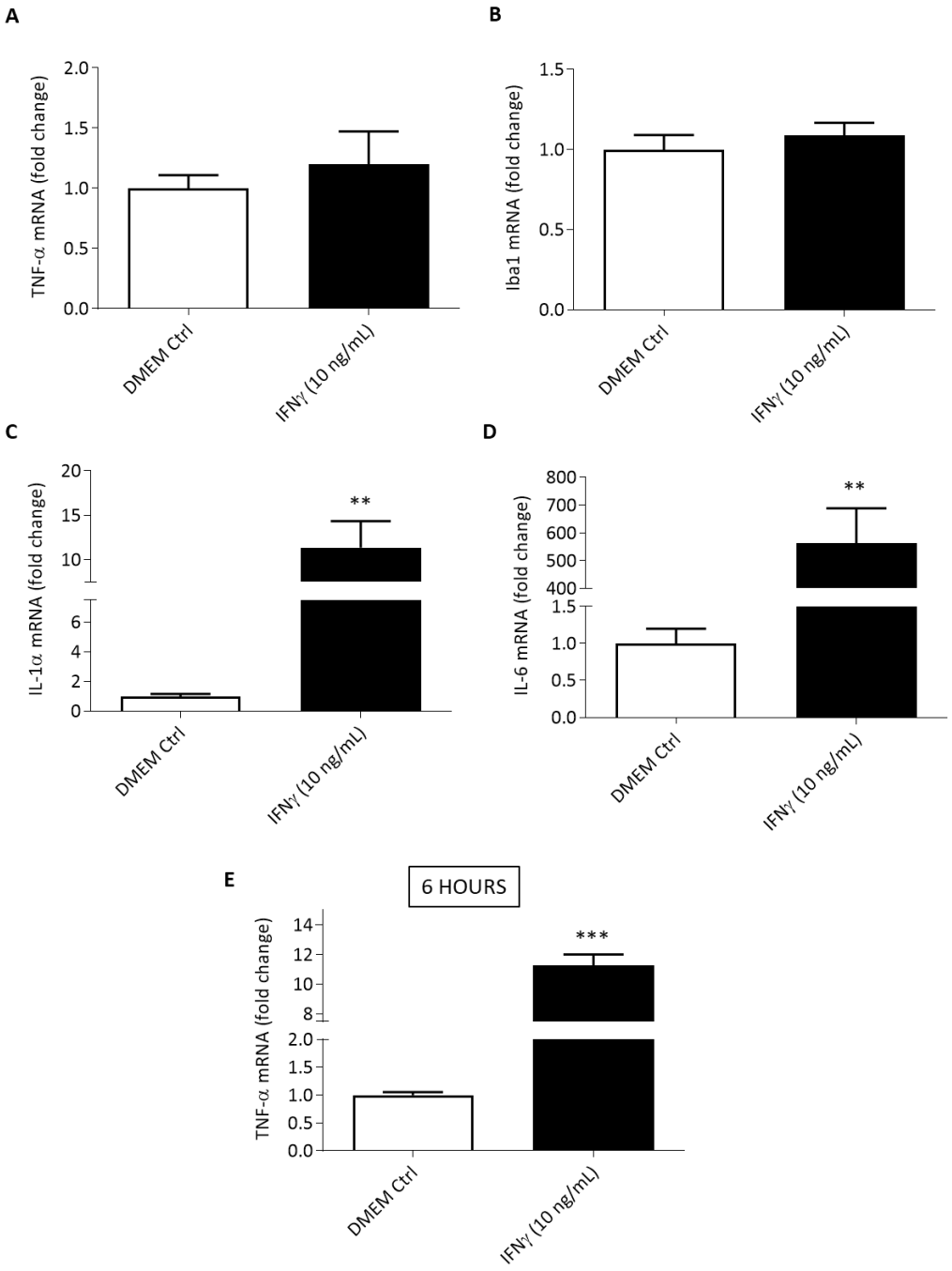

Figure 4.10 Effect of IFNγ on the mRNA expression of TNF-α, IL-1α, IL-6 and Iba1 in microglia.

Primary microglia (DIV 15) were treated with IFNγ (10 ng/mL) for 24 hours. Cells were harvested for RNA extraction followed by RT-PCR for the markers TNF-α (A), Iba1 (B), IL-1α (C), and IL-6 (C). Primary microglia (DIV 15) were treated with IFNγ (10 ng/mL) for 6 hours. Cells were harvested for RNA extraction followed by RT-PCR for TNF-α (D). Data are expressed as mean ± SEM, n=8 wells per treatment group from 3 independent experiments. **P<0.01 vs. control DMEM (Newman-Keuls *post hoc* test).

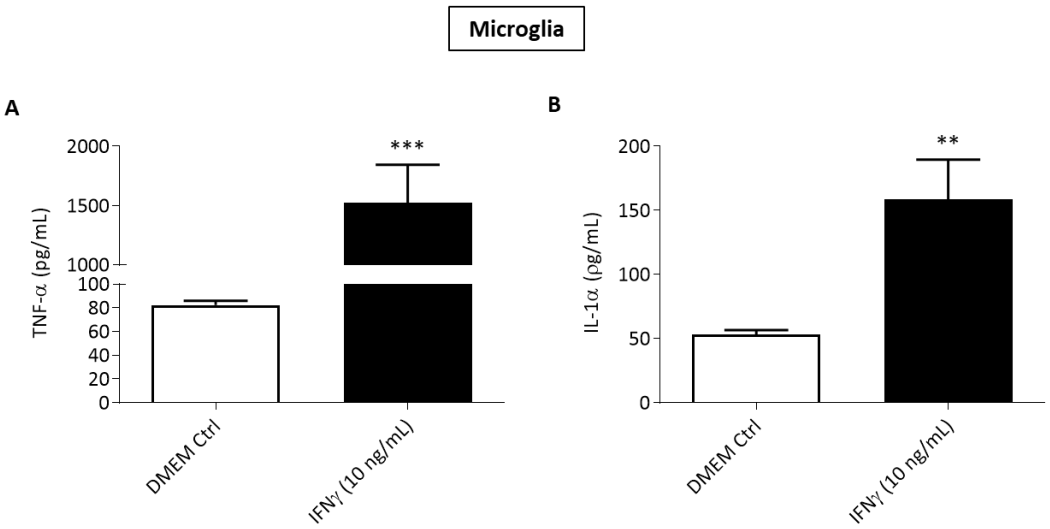

Figure 4.11 IFNγ increases the production of TNF-α and IL-1α in primary cortical microglia.

Primary cortical microglia (DIV 15) were treated with IFNγ (10 ng/mL) for 24 hours. Supernatants were collected for analysis of TNF-α (A) and IL-1α (B) protein release by ELISA. Data are expressed as mean ± SEM, n=8 wells per treatment group from 3 independent experiments. ***P<0.001, **P<0.01 vs. control DMEM (Newman-Keuls *post hoc* test).

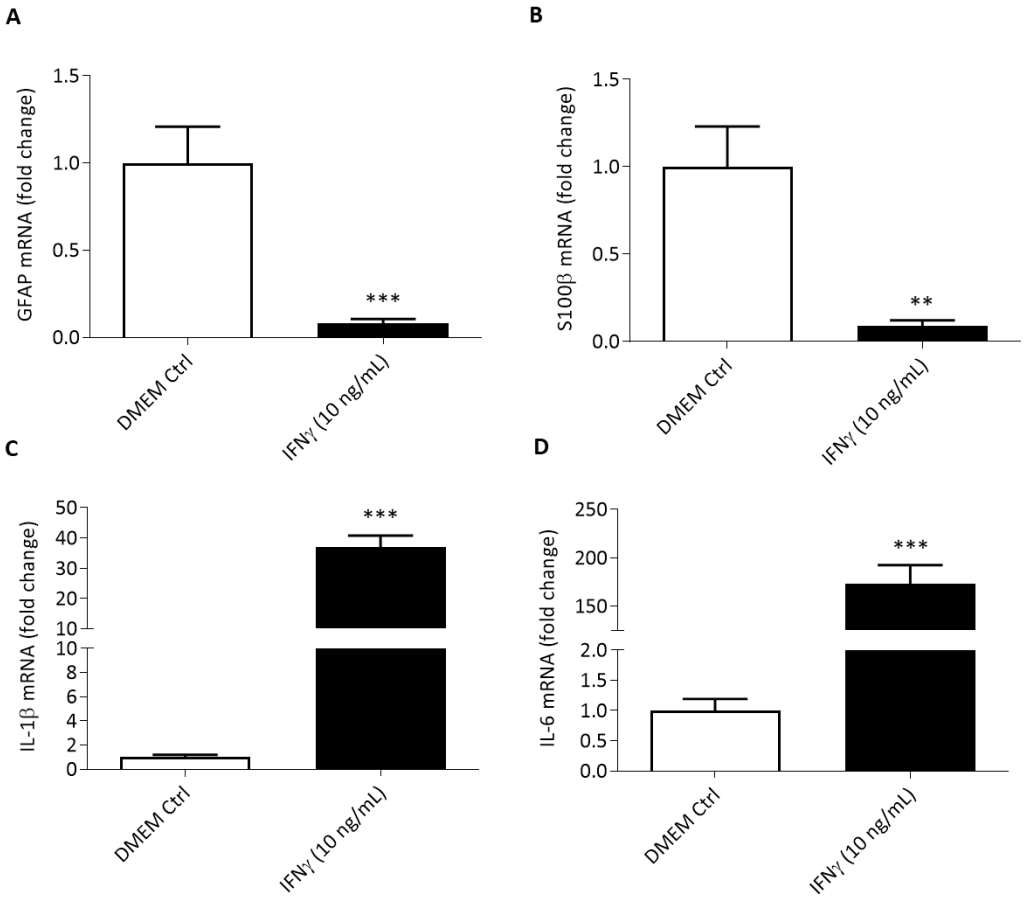

Figure 4.12 Effect of IFNγ on the mRNA expression of GFAP, S100β, IL-1β and IL-6 in primary cortical astrocytes.

Primary astrocytes (DIV 14) were treated with IFNγ (10 ng/mL) for 24 hours. Cells were harvested for RNA extraction followed by RT-PCR to analyse the expression of the markers GFAP (A), S100β (B), IL-1β (C) and IL-6 (D). Data are expressed as mean ± SEM, n=8 wells per treatment group from 3 independent experiments. ***P<0.001, **P<0.01 vs. control DMEM (Newman-Keuls *post hoc* test).

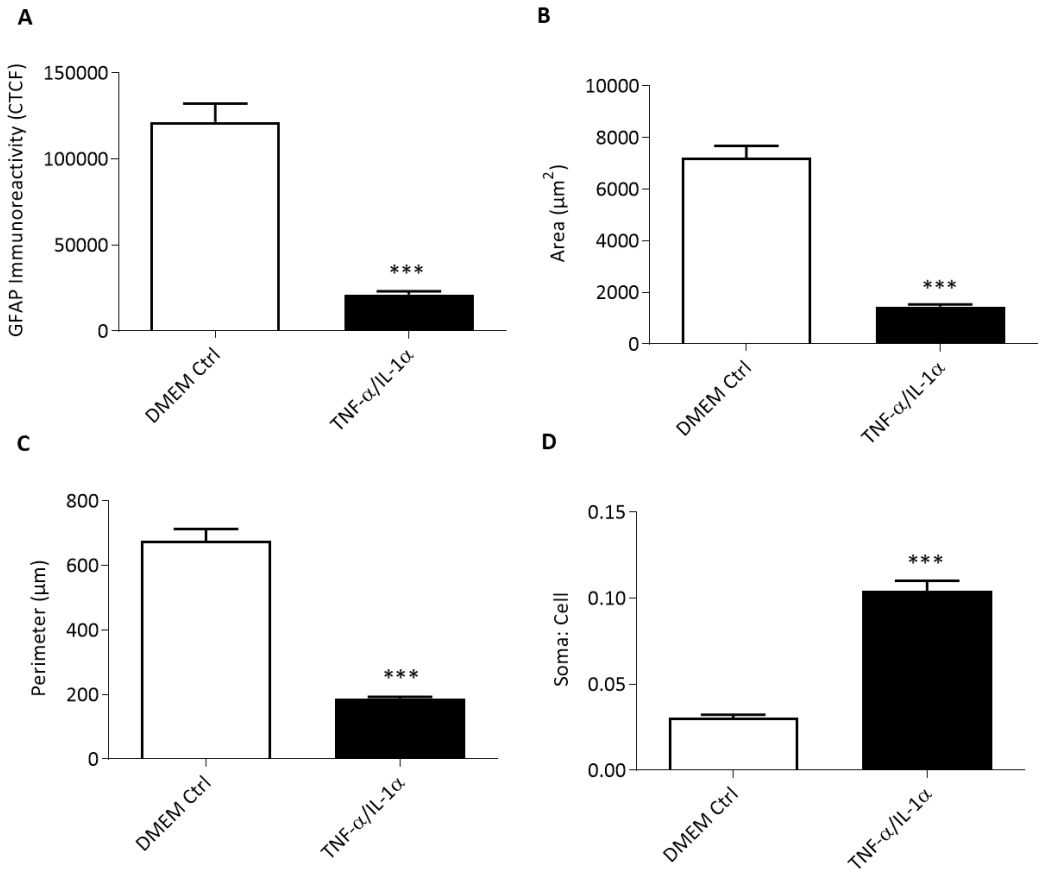

Figure 4.13 TNF-α and IL-1α reduce GFAP immunoreactivity and the morphology of enriched primary cortical astrocytes.

Primary cortical astrocytes (DIV 14) were treated with TNF-α (30 ng/mL) and IL-1α (3 ng/mL) for 24 hours. Morphological analysis was performed to quantify GFAP immunoreactivity (A), astrocyte mean cell area (B), cell perimeter (C), and soma:cell ratio (D). Data are expressed as mean ± SEM, n=8 wells per treatment group from 3 independent experiments. ***P<0.001, vs. control DMEM (Newman-Keuls *post hoc* test).

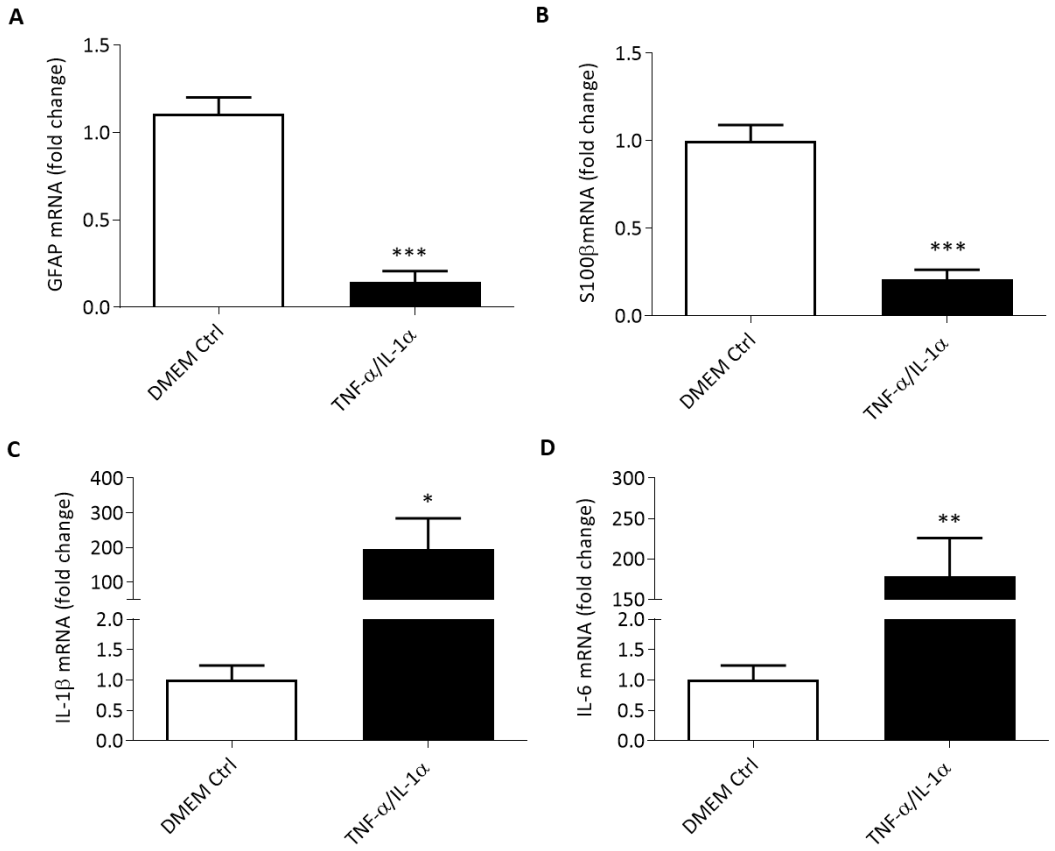

Figure 4.14 Effect of TNF-α and IL-1α on the mRNA expression of GFAP, S100β, IL-1β and IL-6 in primary cortical astrocytes.

Primary cortical astrocytes (DIV 14) were treated with TNF-α (30 ng/mL) and IL-1α (3 ng/mL) for 24 hours. Cells were harvested for RNA extraction followed by RT-PCR for GFAP (A), S100β (B), IL-1β (C) and IL-6 (D). Data are expressed as mean ± SEM, n=8 wells per treatment group from 3 independent experiments. ***P<0.001, **P<0.01, *P<0.05 vs. control DMEM (Newman-Keuls *post hoc* test).

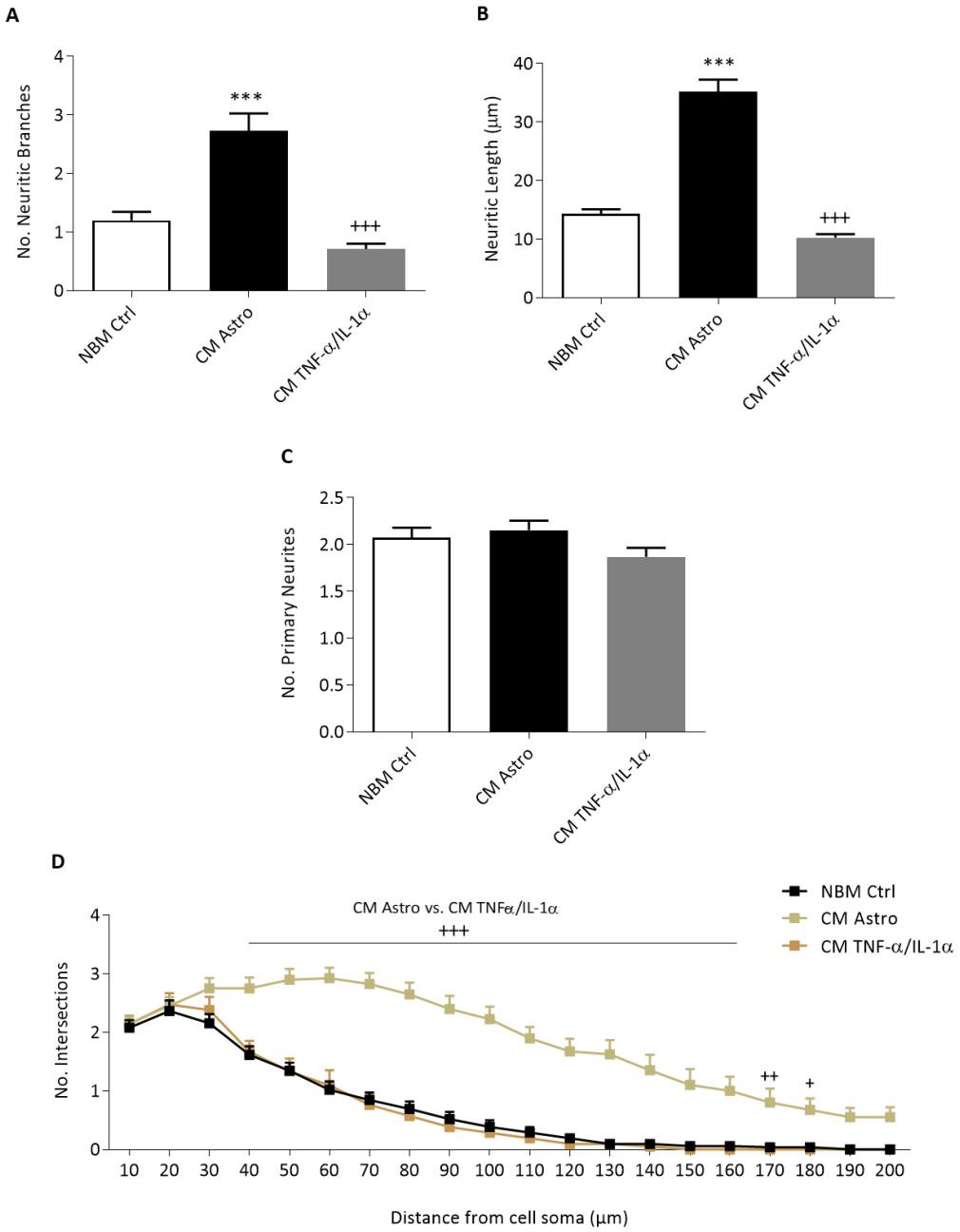

Figure 4.15 Conditioned media from TNF-α and IL-1α treated astrocytes reduces the complexity of mature cortical neurons.

Primary cortical astrocytes (DIV 14) were treated with TNF-α (30 ng/mL) and IL-1α (3 ng/mL) for 24 hours. The resulting conditioned media was collected and applied to mature (DIV 21) primary cortical neurons for 24 hours before fixation and MAP2 immunocytochemistry. Sholl analysis was performed to analyse the number of neuritic branches (A), the neuritic length (B), the number of primary neurites (C), and the Sholl profile (D). Data are expressed as mean ± SEM, n=6-8 coverslips per treatment group from 3 independent experiments. ***P<0.001 vs. control NBM, $^{+++}$P<0.001, $^{++}$P<0.01, $^{+}$P<0.05 vs. CM from TNF-α and IL-1α treated astrocytes (Newman-Keuls *post hoc* test).

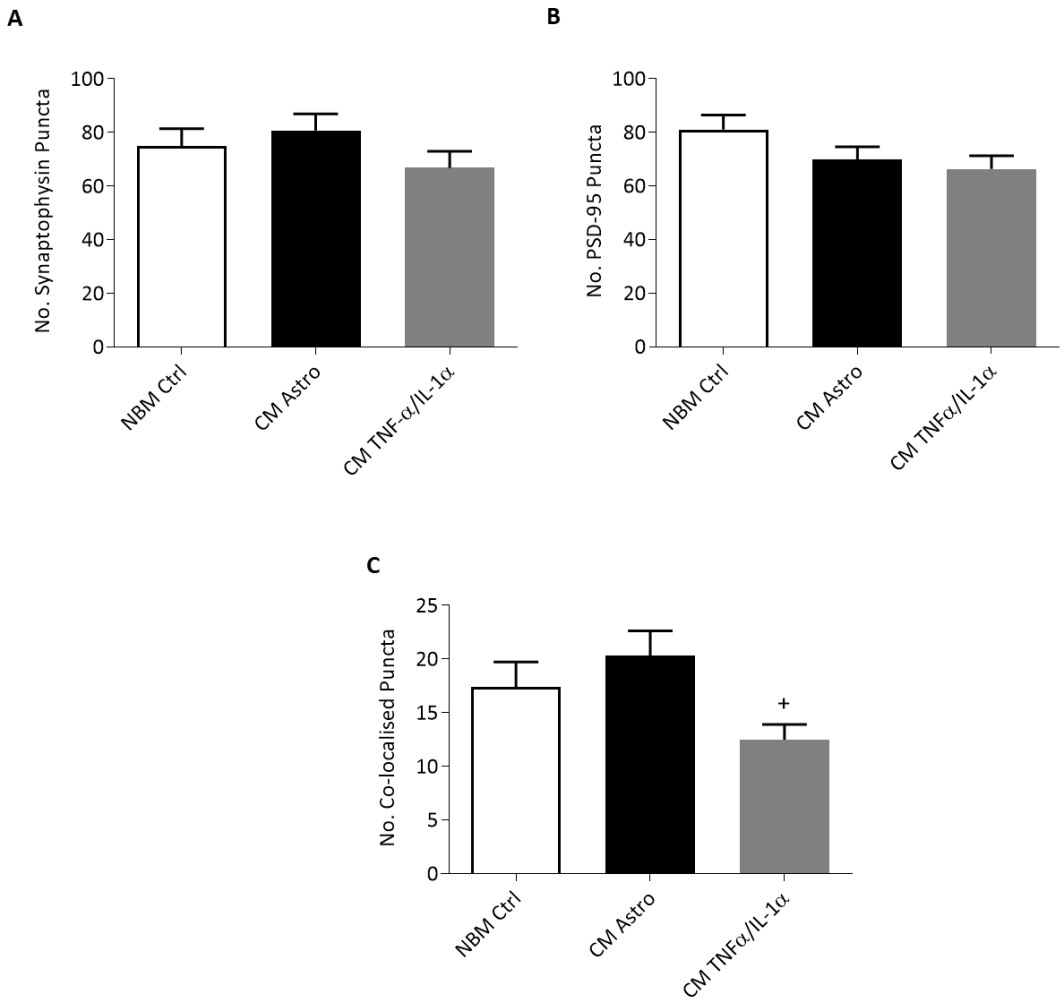

Figure 4.16 Conditioned media from TNF-α and IL-1α treated astrocytes reduces synaptic protein co-localisation in mature primary cortical neurons.

Primary cortical astrocytes (DIV 14) were treated with TNF-α (30 ng/mL) and IL-1α (3 ng/mL) for 24 hours. The resulting conditioned media was collected and applied to mature (DIV 21) primary cortical neurons for 24 hours before fixation and immunocytochemistry to quantify synaptophysin puncta (A), PSD-95 puncta (B), and co-localised synaptic puncta (C). Data are expressed as mean ± SEM, n=6 coverslips per treatment group from 5 independent experiments. $^{+}P<0.05$ vs. CM from TNF-α and IL-1α treated astrocytes (Newman-Keuls *post hoc* test).

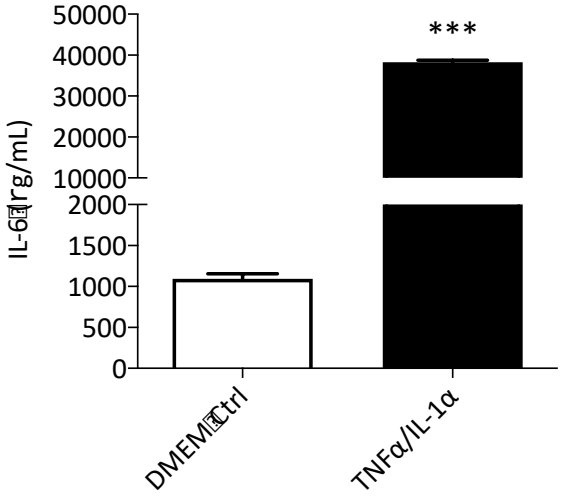

Figure 4.17 TNF-α and IL-1α increases the production of IL-6 protein in primary cortical astrocytes.

Primary cortical astrocytes (DIV 14) were treated with TNF-α (30 ng/mL) and IL-1α (3 ng/mL) for 24 hours. Supernatants were collected for analysis of IL-6 protein release by ELISA. Data are expressed as mean ± SEM, n=8 wells per treatment group from 3 independent experiments. ***P<0.001 vs. control DMEM (Newman-Keuls post hoc test).

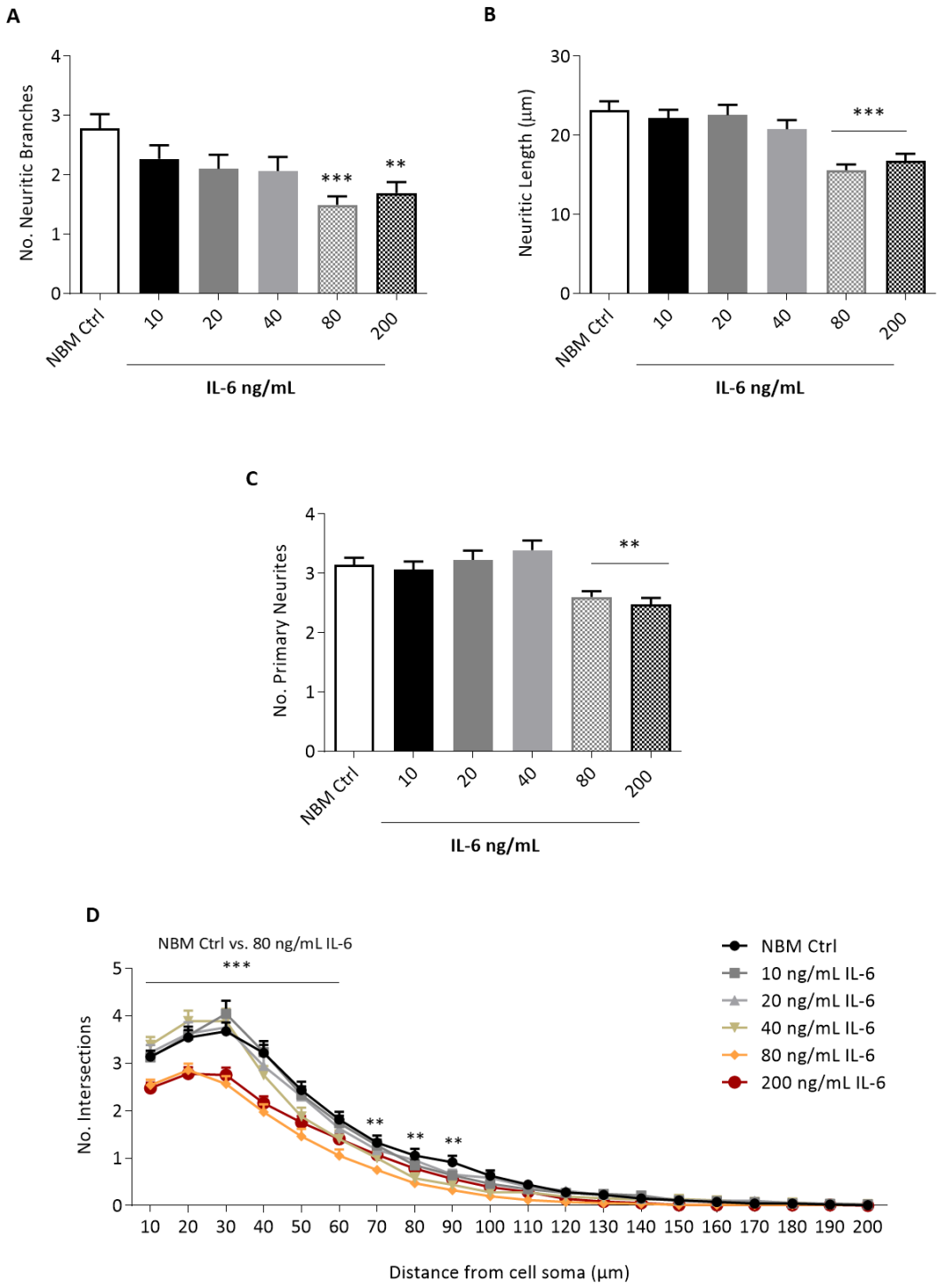

Figure 4.18 Concentration-related effects of IL-6 on the complexity of mature primary cortical neurons.

Primary cortical neurons (DIV 21) were treated with IL-6 (10, 20, 40, 80 and 200 ng/mL) for 24 hours before fixation and MAP2 immunocytochemistry. Sholl analysis was performed to analyse the number of neuritic branches (A), the neuritic length (B), the number of primary neurites (C), and the Sholl profile (D). Data are expressed as mean ± SEM, n=4 coverslips per treatment group from 5 independent experiments. ***P<0.001, **P<0.01, vs. control NBM (Newman-Keuls *post hoc* test).

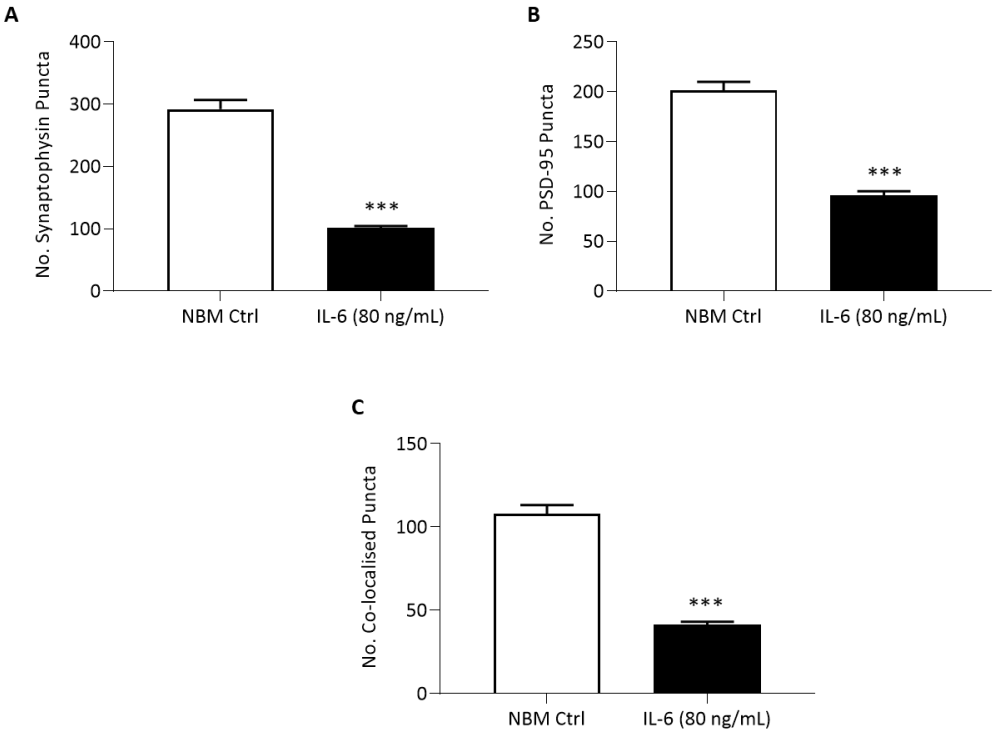

Figure 4.19 IL-6 reduces synaptic protein co-localisation in mature primary cortical neurons.

Mature primary cortical neurons (DIV 21) were treated with IL-6 (80 ng/mL) for 24 hours before fixation and immunocytochemistry to quantify synaptophysin puncta (A), PSD-95 puncta (B), and co-localised synaptic puncta (C). Data are expressed as mean ± SEM, n=6-8 coverslips per treatment group from 3 independent experiments. ***P<0.001 vs. control NBM (Newman-Keuls *post hoc* test).

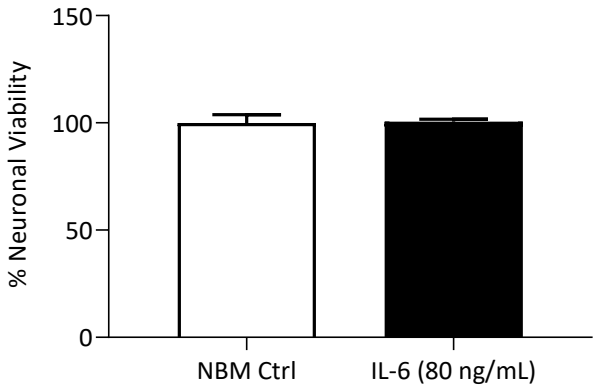

Figure 4.20 IL-6 has no effect on neuronal viability.
Primary cortical neurons (DIV 21) were treated with IL-6 (80 ng/mL) for 24 hours. Neuronal viability was assessed using the CCK assay. Data are expressed as mean ± SEM, n=3 wells per treatment group from 3 independent experiments

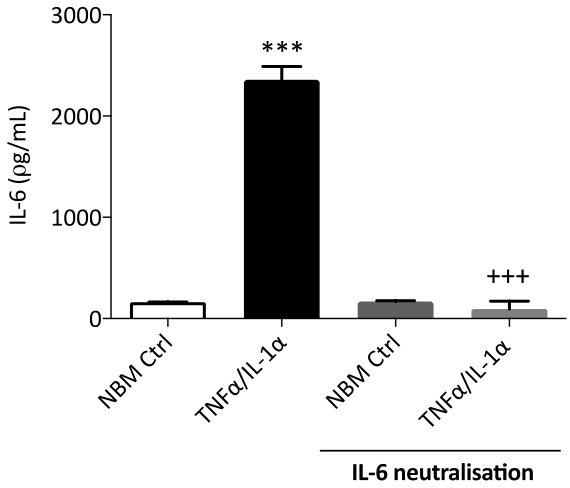

Figure 4.21 IL-6 neutralisation prevents TNF-α and IL-1α-induced release of IL-6 from primary cortical astrocytes.
Primary cortical astrocytes (DIV 14) were treated with [TNF-α (30 ng/mL) and IL-1α (3 ng/mL)] and IL-6 neutralising antibody for 24 hours. Supernatants were collected for analysis of IL-6 protein release by ELISA. Data are expressed as mean ± SEM, n=8 wells per treatment group from 3 independent experiments. ***P<0.001 vs. control DMEM, $^{+++}$P<0.001 vs. TNF-α/IL-1α (Newman-Keuls *post hoc* test).

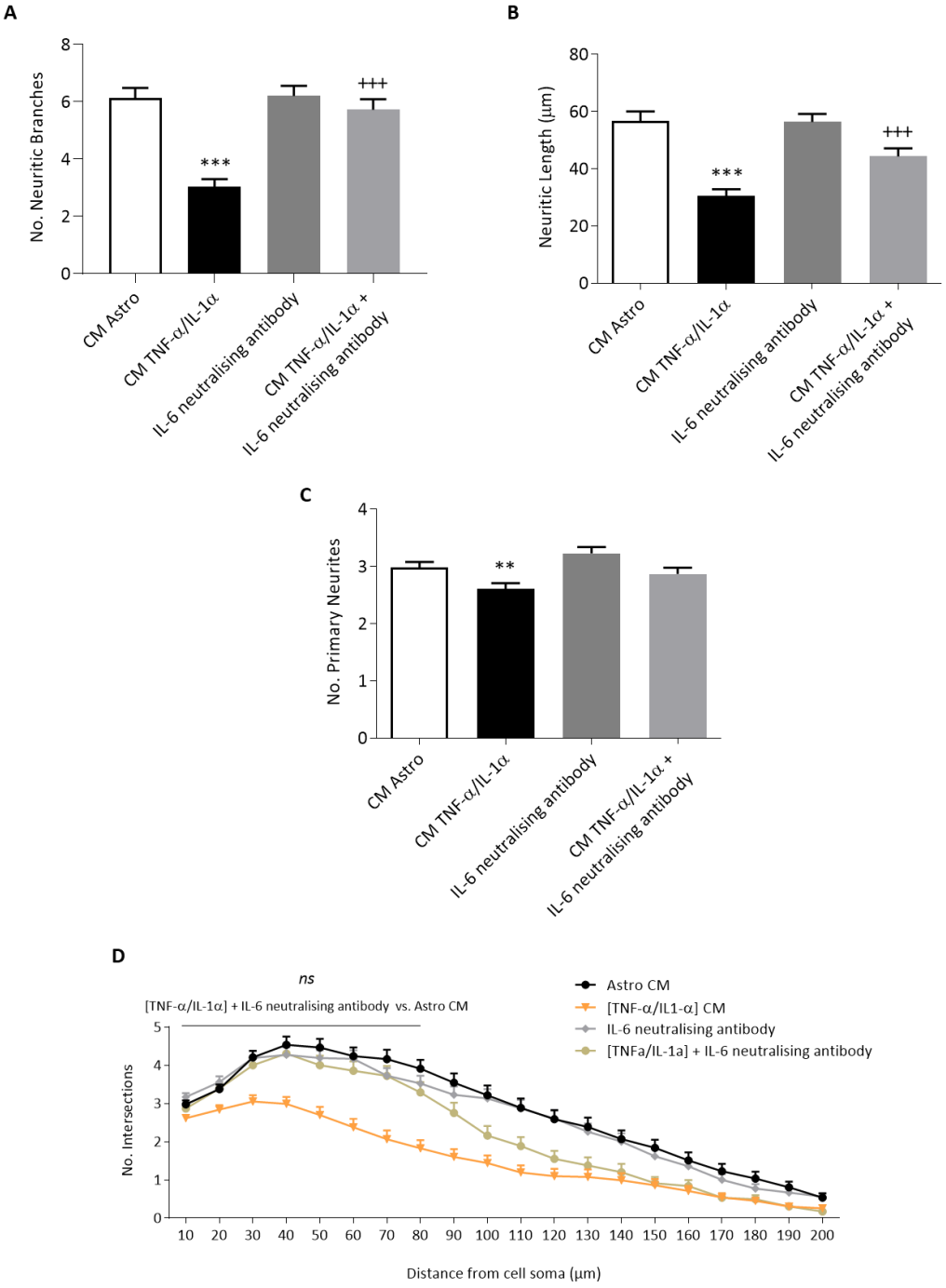

Figure 4.22 Neutralisation of IL-6 attenuates reductions in neuronal complexity induced by conditioned media from TNF-α and IL-1α treated astrocytes.
Primary cortical astrocytes (DIV 14) were treated with [TNF-α (30 ng/mL) and IL-1α (3 ng/mL)] and IL-6 neutralising antibody for 24 hours. The resulting conditioned media was collected and applied to mature (DIV 21) primary cortical neurons for 24 hours before fixation and MAP2 immunocytochemistry. Sholl analysis was performed to analyse the number of neuritic branches (A), the neuritic length (B), the number of primary neurites (C), and the Sholl profile (D). Data are expressed as mean ± SEM, n=6 coverslips per treatment group from 4 independent experiments. ***P<0.001, **P<0.01 vs. control CM Astro, $^{+++}$P<0.001 vs. CM TNF-α/IL-1α (Newman-Keuls *post hoc* test).

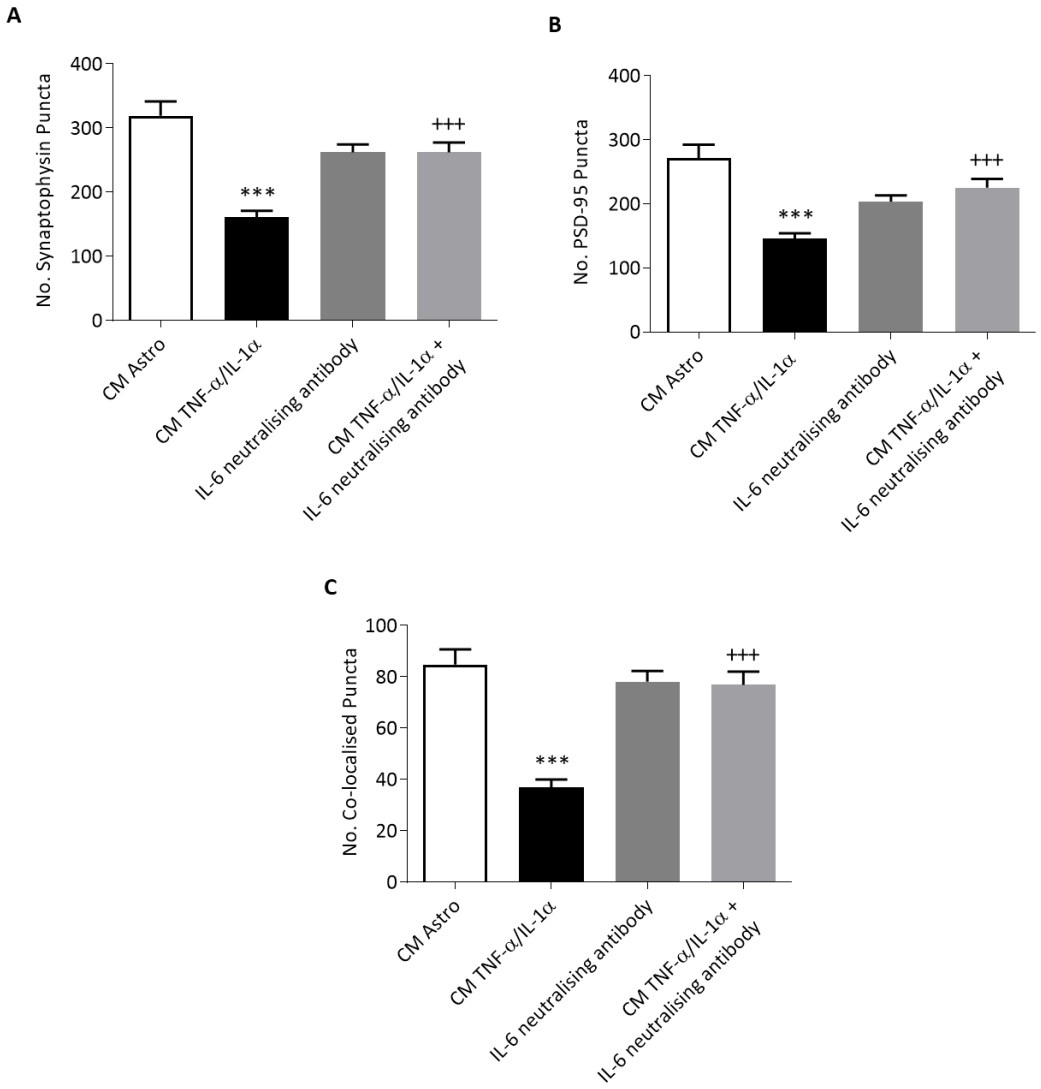

Figure 4.23 Neutralisation of IL-6 attenuates reductions in synaptic protein co-localisation in mature primary cortical neurons induced by conditioned media from TNF-α and IL-1α treated astrocytes.

Primary cortical astrocytes (DIV 14) were treated with [TNF-α (30 ng/mL) and IL-1α (3 ng/mL)], and IL-6 neutralising antibody for 24 hours. The resulting conditioned media was collected and applied to mature (DIV 21) primary cortical neurons for 24 hours before fixation and immunocytochemistry to quantify synaptophysin puncta (A), PSD-95 puncta (B) and co-localised synaptic puncta (C). Data are expressed as mean ± SEM, n=6 coverslips per treatment group from 5 independent experiments. ***P<0.001, vs. CM, $^{+++}$P<0.001 vs. CM TNF-α/IL-1α (Newman-Keuls *post hoc* test).

4.4 Discussion

IFNγ is a well-recognised inducer of inflammation which is up-regulated in numerous neurological disorders (Frost & Li, 2017) and confers advantage over LPS being a strictly pro-inflammatory stimulus (Lively & Schlichter, 2018). IFNγ is one of the most potent inducers of microglial activation *in vitro*, which results in increased expression of microglial cell surface markers and excessive production of pro-inflammatory cytokines which are known to contribute to neuronal atrophy and synapse loss in the CNS (Boche et al, 2013; Browne et al, 2013; Dungan et al, 2014). While microglia are primarily responsible for initiating inflammatory processes, there is growing evidence to support astrocytic engagement in maintaining neuroinflammation. There is increasing evidence for the role of bidirectional interactions and neuronal – activated glial cross talk across a variety of neuroinflammatory conditions (Szepesi et al, 2018; Tian et al, 2012).

Results of this study concur with recent findings demonstrating that the microglial factors TNF-α and IL-1α are elevated in conditioned media derived from activated microglial cultures (Liddelow et al, 2017; Yates, 2017). This study extends these findings to demonstrate that TNF-α and IL-1α induce a reactive astrocytic phenotype which has nocent effects on measures of neuronal integrity *in vitro*. This study also identifies IL-6 as a candidate cytokine which can impact on neuronal complexity and synaptogenesis.

4.4.1 IFNγ has opposing effects on the immunoreactivity and morphology of enriched primary cortical microglia and astrocyte cultures

IFNγ reduced microglia mean cell area, perimeter and Iba1 immunoreactivity but increased the soma: cell ratio. Microglial activation by IFNγ is well characterised and involves increased expression of cell surface molecules and excessive production of pro-inflammatory cytokines such as TNF-α which are known to contribute to neuronal atrophy and synapse loss in the CNS (Boche et al, 2013; Browne et al, 2013; Dungan et al, 2014).

IFNγ reportedly serves in the priming of microglia producing changes in morphology, receptors and cytokine release profile (Perry & Holmes, 2014). The

reduction in mean cell area and perimeter in this study reflects the shortening and flattening of cellular processes characteristic of IFNγ-mediated microglial activation (Colton & Wilcock, 2010; Luo & Chen, 2012). On the other hand, IFNγ increased astrocyte mean cell area, perimeter and GFAP immunoreactivity but had no effect on the soma:cell ratio. As IFNγ is traditionally considered a microglial activator, direct effects of IFNγ on astrocytes remains largely unexplored. Nevertheless, IFNγ has been employed previously to activate astrocytes *in vitro* producing characteristic morphological changes including increased thicknesses of cellular processes and cellular hypertrophy (Pekny & Pekna, 2014). Results of this study concur with these findings as an increase in cell area and perimeter reflect transformation to the reactive, hypertrophic state.

4.4.2 Conditioned media from IFNγ treated glia reduces the complexity and expression of co-localised synaptic markers in mature neurons

Conditioned media from IFNγ treated mixed glia produced a robust decrease in neuritic branching and neuritic length but had no effect on the number of primary neurites. Conditioned media from IFNγ treated microglia also produced a robust decrease in all measures of neuronal complexity including neuritic branching, neuritic length and the number of primary neurites compared to conditioned media from untreated microglia. As expected, conditioned media from IFNγ treated astrocytes decreased neuronal complexity compared to control conditioned media from untreated astrocytes. Conditioned media from IFNγ-treated astrocytes had no effect on neuritic branching or the number of primary neurites but reduced neuritic length.

These results are not surprising given that IFNγ receptors are constitutively expressed on both microglia and astrocytes *in vitro* (Hashioka et al, 2010) and treatment of astrocytes and microglia with IFNγ stimulates production of pro-inflammatory cytokines and chemokines which have an impact on neuronal outgrowth and survival. Results of this study are in line with previous research in the lab as well as a vast body of literature indicting a loss of neuronal complexity during inflammatory conditions. Previous *in vitro* studies have shown that

conditioned media from IFNγ treated mixed glia reduced measures of neuronal complexity, including neuritic length and the number of primary neurites of immature primary cortical neurons (DIV 3) (O'Farrell, 2016a). Results of this study concur with these findings and suggest that conditioned media from IFNγ treated mixed glia produces a more potent effect on the complexity of mature neurons including a greater reduction in neuritic length and number of neuritic branches but has no effect on the number of primary neurites. These results are not surprising given that mature neurons are more susceptible to damage by external stimuli.

Conditioned media from IFNγ treated microglia produced the greatest reduction in neuronal complexity. IFNγ is recognised, in particular for its role in priming microglia under pathological conditions resulting in exaggerated glial activation and responses (Ta et al, 2019). It activates the Janus Kinase/Signal Transducers and Activators of Transcription (JAK/STAT) signalling pathway in microglia resulting in a range of pro-inflammatory pathogenic responses (Yan et al, 2018). IFNγ activation of microglia is known to stimulate the production of pro-inflammatory cytokines including IL-1β, IL-6, TNF-α, and reactive oxygen species which contribute to inflammatory-driven neuronal atrophy (Loane & Byrnes, 2010a; Sundal, 2014). In turn, activated microglia up-regulate the expression of the cell surface repulsive guidance molecule a (RGMa) which is necessary for inhibition of outgrowth and causing growth cone collapse in primary cortical neurons (Kitayama et al, 2011).

Previous *in vitro* studies have shown that IFNγ (10 ng/mL) treatment of microglia induced maximal effects on the mRNA expression and release of the inflammatory cytokine TNF-α, while treatment of astrocytes with IFNγ (100 ng/mL) was required to induce a significant increase in TNF-α mRNA expression. Furthermore, neutralisation of TNF-α protected against reductions in neuronal complexity induced by conditioned media from IFNγ treated mixed glia (O'Neill, 2015). Given that TNF-α is thus largely responsible for the downstream effects of conditioned media from IFNγ treated mixed glia on neuronal outgrowth, use of the lower concentration of IFNγ (10 ng/mL) may account for the greater

reduction in complexity observed with conditioned media from IFNγ treated microglia compared to conditioned media from IFNγ treated astrocytes. Direct treatment of mature neurons with IFNγ had no effect on complexity, confirming that the observed changes are mediated by a glial-associated mechanism or via glial-derived factors.

In terms of synaptic markers, this study shows that conditioned media from mixed glia increases the number of co-localised synaptic puncta and conditioned media from IFNγ treated mixed glia produces a robust decrease in the number of co-localised synaptic puncta. These results are not surprising given that conditioned media from IFNγ treated mixed glia also reduced measures of neuronal complexity and the Sholl profile in mature neuronal cultures. A reduction in neuritic length and branching may itself result in a reduction in the number of synaptic puncta due to fewer sites for connectivity.

Overall these results suggest that conditioned media from IFNγ treated mixed glia reduces neuronal complexity and synapse formation in primary mature cortical neurons accentuating the detrimental impact that IFNγ mediated inflammation may have on neuronal connectivity. Given that conditioned media from IFNγ-treated microglia induced the greatest reduction in complexity suggests that microglial activation may reflect the initial response to inflammation, which drives activation of surrounding glial cells.

While these experiments focused on examining the effect of IFNγ treated glia on neuronal integrity it is important to comment on the varying effect exhibited by conditioned media control treatments. For example, conditioned media from control treated astrocytes had no effect on the number of neuritic branches when examining the effect of IFNγ treated astrocytes on neuronal complexity (*Figure 4.3*) compared to NBM-treated neurons. However, when examining the effect of L-AAA or TNF-α and IL-1α-treated astrocytes on neuronal complexity (*Figures 3.10 and 4.15*), conditioned media from control treated astrocytes significantly increased the number of neuritic branches ($P < 0.005$) compared to NBM-treated neurons. Similarly, a greater increase in neuritic length was observed when examining the effect of L-AAA or TNF-α and IL-1α-treated

astrocytes on neuronal complexity (*Figures 3.10 and 4.15*) compared to the effect of conditioned media from control treated astrocytes observed when examining the effect of IFNγ-treated astrocytes on neuronal complexity (*Figure 4.3*). It is likely that this variability stems from differences in glial-derived contents of the conditioned media. It is also likely that differences in cell numbers across experiments contributed to this variance.

4.4.3 IFNγ induces the mRNA expression of TNF-α, IL-1α, IL-1β and IL-6 in mixed glia

IFNγ reduced the mRNA expression of TNF-α in mixed glia at 24 hours. However, IFNγ increased the mRNA expression of TNF-α in mixed glia when repeated at a 6-hour time point. These results are not surprising given that IFNγ is a potent inducer of TNF-α gene expression in microglia (Mangano et al, 2012; Olmos & Lladó, 2014). Astrocytes are also known to produce TNF-α, however microglia are reputedly the primary source of this cytokine during neuroinflammation (Welser-Alves & Milner, 2013).

IFNγ also increased the mRNA expression of the pro-inflammatory cytokines IL-1α, IL-1β and IL-6, in line with previous data demonstrating release of these cytokines from activated microglia. IL-1α is reportedly increased during inflammation and exacerbated release of IL-1α is involved in disease progression where it is known to produce pathogenic responses and collateral tissue damage (Lukens et al, 2012). IL-1β is also highly expressed within the CNS during neuroinflammatory disease (Ramos et al, 2012). However, as the precursor form of IL-1β is not biologically active and requires enzymatic cleavage to elicit its inflammatory activity it is likely that IL-1β may not directly contribute to any conditioned media-derived effects on neurons. It is plausible that as a regulatory cytokine IL-1β works synergistically to regulate the production of other cytokines such as IL-6 in response to inflammation (Benveniste et al, 1990; Gruol, 2015). IL-6 is a pro-inflammatory cytokine produced by many different cell types in the CNS which is elevated in neuroinflammation (Jensen et al, 2013). Increased production of IL-6 coincides with previous *in vivo* research demonstrating that

glial cells secrete a significant increase in IL-6 at 24 hours following microglial activation (O'Neill et al, 2019).

4.4.4 IFNγ affects the mRNA expression of TNF-α, IL-1α, Il-6 and Iba1 in microglia

These results show that treatment of microglia with IFNγ (10 ng/mL) for 24 hours has no effect on TNF-α, or Iba1 but increases IL-1α and IL-6 mRNA expression. However, IFNγ increased the mRNA expression of TNF-α in microglia when repeated at a 6-hour time point.

These results are expected given the vast body of literature reporting an increase in TNF-α and IL-1α production following microglial activation by inflammatory stimuli (Liddelow et al, 2017; Norden et al, 2016). Previous research has shown that IFNγ increases the mRNA expression and release of TNF-α from microglia after 6 hours but has no effect on the mRNA expression or release of TNF-α from astrocytes (O'Neill, 2015). IFNγ had no effect on Iba1 immunoreactivity which is somewhat surprising given that its expression is reported to increase with microglial activation and inflammation, where it is reported to play a role in membrane ruffling and conversion from a ramified to amoeboid morphology (Hopperton et al, 2018; Minett et al, 2016).

These results also demonstrated an increase in IL-6 mRNA following treatment of microglia with IFNγ. These results are not surprising given that IL-6 is among the traditional pro-inflammatory cytokines putatively release from activated microglia and IL-6 up-regulation is characteristic of the activated microglial phenotype (Czeh et al, 2011). Taken together, these results suggest that microglia may be the primary mediators of IFNγ-induced increase in the mRNA expression of TNF-α in mixed glia.

4.4.5 IFNγ induces the production of TNF-α and IL-1α protein in mixed glia and microglia

IFNγ increased the production and release of TNF-α and IL-1α protein from both mixed glia and microglia. These results are in line with previous findings describing increased levels of TNF-α and IL-1α in the conditioned media from

activated microglia (Liddelow et al, 2017). They are also In line with the theory describing “classically activated’’ microglia. Microglia activated by inflammatory stimuli such as LPS or IFNγ assume a ‘‘classically activated’’ phenotype which is characterised by its role in immune defence and the production of free radicals and the pro-inflammatory cytokines IL-1β, TNF-α, IL-6 (Wang et al, 2015).

Results of this study demonstrate that mixed glia and microglia produce a robust increase in IL-6 protein (1109 ± 25.20 and 1523 ± 320.3 pg/mL, respectively) when treated with IFNγ under the same conditions. Similarly, both mixed glia and microglia produced a robust increase in IL-1α protein (320.9 ± 26.91 and 158.7 ± 30.96 pg/mL, respectively) when treated with IFNγ under the same conditions. Previous studies characterising this mixed cell model reports that system comprises of approximately 70% astrocytes and 30% microglia (Day et al, 2014). These results suggest that microglia, which make up a smaller proportion of mixed glia may be the primary source of inflammatory-driven, *de novo* synthesis of TNF-α and IL-1α. These results coincide with recent data revealing that microglia, not astrocytes, are the major source of inflammatory-driven release TNF-α production (Welser-Alves & Milner, 2013). Previous studies in the lab also demonstrate that immunoneutralisation of TNF-α protects against reductions in neuronal complexity induced by conditioned media from IFNγ stimulated microglia (O'Neill, 2015) identifying TNF-α as a main player in neuronal atrophy associated with IFNγ-mediated microglial activation. There is also evidence to suggest that microglial responses are often rapid, in contrast to the more delayed activation often seen in astrocytes, suggesting that temporally distinct signalling events are required for transition of astrocytes to their reactive phenotype. Taken together these results suggest that TNF-α is one of the primary players in IFNγ-mediated microglia signalling and astrocyte activation likely occurs secondary to microglia activation. On the basis of this, the next section explores the effects of factors released from activated microglia on astrocyte reactivity and astrocyte-neuronal interactions.

4.4.6 IFNγ induces the production of IL-6 protein in mixed glial cultures

Previous studies investigating the effect of LPS-induced microglial activation on astrocyte reactivity show that while IL-1β secretion is also increased in microglial conditioned media (Liddelow et al, 2017), it is unable to induce expression of the astrocytic A1 phenotype. Resultantly, while IFNγ- induced expression of both IL-1β and IL-6, IL-6 was selected as the cytokine of interest for further investigation.

Results of this study show that IFNγ stimulates the release of IL-6 protein from mixed glial cultures. These results are expected given that IL-6 is produced by many different cell types, including astrocytes, microglia, neurons and endothelial cells (Gruol, 2015). *In vitro*, increased expression and release of IL-6 from primary mixed glial cultures has been observed as early as 2 hours following inflammatory stimulus such as LPS (100 ng/ml) (Minogue et al, 2012).

4.4.7 IFNγ affects the mRNA expression of GFAP, S100β, IL-1β and IL-6 in astrocytes

In this study IFNγ reduced the mRNA expression of GFAP and S100β and increased the mRNA expression of IL-1β and IL-6. An increase in GFAP is traditionally linked with increased astrocytic reactivity in response to CNS trauma and is considered a hallmark of neurodegenerative diseases (Hol & Pekny, 2015), while other events such as chronic stress are reported to reduce GFAP mRNA and protein release (Rajkowska & Stockmeier, 2013). A reduction in GFAP is thus considered somewhat surprising given that IFNγ would be expected to increase astrocyte reactivity.

The reduction in S100β is also somewhat surprising given that S100β is reportedly up-regulated during inflammation (Rajkowska and Stockmeier, 2013). Altered levels of S100β are traditionally associated with increased astrocyte reactivity including conversion to the reactive phenotype or astrocyte death which is accompanied by cellular damage and leakage of the marker. Elevated S100β has been correlated with neurodegenerative conditions such as Parkinson's disease, where it is reported to induce neuronal apoptosis (O'Neill et al, 2019).

As expected, IFNγ increased mRNA expression of both IL-1β and IL-6 in line with reports of increased IL-1β and IL-6 in neuroinflammatory conditions (Ramos et al, 2012). These results are also in line with previous *in vivo* research demonstrating that astrocytes secrete a significant increase in IL-6 up to 24 hours following inflammatory stimulus (O'Neill et al, 2019). Increased expression and secretion of IL-6 is observed during various neurodegenerative disorders such as Alzheimer's disease and Parkinson's disease and neuropsychiatric disorders such as major depressive disorder (Hodes et al, 2016) which are characterised by an underlying inflammatory component (Ponath et al, 2018).

4.4.8 TNF-α and IL-1α reduce GFAP immunoreactivity and the morphology of enriched primary cortical astrocytes

Results of this study show that treatment of astrocytes with TNF-α and IL-1α reduces astrocyte mean cell area and perimeter. These results are somewhat surprising considering that TNF-α is among the many factors reported to regulate astrocyte activation (Parpura & Verkhratsky, 2012; Sofroniew & Vinters, 2010b) and reactive astrocytes putatively transform and assume a polygonal shape following treatment with inflammatory mediators (Pekny et al, 2019).

Recent data demonstrates that low concentrations of TNF-α (2 ng/mL) initiates activation of primary rat astrocyte cultures as soon as 2 hours post stimulation with an increase in NF-κB expression and increased cellular production of TNF-α (Wang et al, 2018). The increase in soma:cell ratio may thus reflect astrocyte increased transcriptional activity and induction of NF-κB signalling within the cell (Shih et al, 2015). NF-κB signalling in astrocytes plays a critical role for initiating and maintaining inflammation in the CNS. Therefore, it may be more accurate to describe a reduction in physiological astrocyte activity in response to TNF-α and IL-1α. Overall, the abnormal cellular and nuclear morphology suggests that TNF-α induces astrocyte compromise with a possible increase in transcription of inflammatory signalling mediators.

4.4.9 TNF-α and IL-1α affects the mRNA expression of GFAP, S100β, IL-1β and IL-6 in primary cortical astrocytes

This study shows that TNF-α and IL-1α decreases astrocytic expression of GFAP and S100β and increases IL-1β and IL-6. As expected, this trend is comparable to that observed following treatment of astrocytes with IFNγ. This data coincides with previous *in vivo* research demonstrating that astrocytes secrete a significant increase in pro-inflammatory cytokines including TNF-α and IL-6 at 24 hours following inflammatory-induced activation (Benveniste et al, 1990).

4.4.10 Conditioned media from TNF-α and IL-1α treated astrocytes reduces complexity and synaptic protein co-localisation in mature primary cortical neurons

This study demonstrates that conditioned media from TNF-α and IL-1α treated astrocytes reduces neuronal complexity and synapse formation of mature primary cortical neurons *in vitro*. These results are not surprising given the previously identified changes in astrocyte morphology, gene expression and secretion profile following treatment with TNF-α and IL-1α. Treatment of astrocytes with TNF-α and IL-1α-induced robust effects on astrocyte cell size and shape, including retraction of processes which may also reflect a reduction in potential points of intercellular communication. Furthermore, TNF-α and IL-1α treatment induced astrocyte expression of the pro-inflammatory cytokines, IL-1β and IL-6, both of which can cause direct insult to neurons in elevated concentrations. These results concur with previous studies describing IFNγ and TNF-α-induced activation of astrocytes, leading to increased activation of the NF-κB pathway, production of ROS and NO and further release of IL-1β, IL-6 and TNF-α (Sofroniew, 2014).

Recent data also demonstrates that TNF-α triggers a Ca^{2+} dependent glutamate release from astrocytes that boosts excitatory synaptic activity through a mechanism involving autocrine activation of P2Y1 receptors (Nikolic et al, 2018). Persistent active signalling through this pathway promotes glial glutamate release which drives abnormal synaptic activity identifying an additional link between TNF-α signalling in astrocytes and a reduction in synaptic contacts.

IL-1α signalling in astrocytes involves activation of the IL-1R receptor and downstream signalling events including induction of the transcription factor NF-κB which is a crucial mediator in driving IL-1 mediated induction of adhesion molecules and chemokines (Moynagh, 2005). Given that both TNF-α and IL-1α induce signalling of NF-κB, we cannot preclude a role for NF-κB, in contributing to the observed reductions in neuronal complexity and synapse formation.

4.4.11 TNF-α and IL-1α induce the production of IL-6 protein in primary cortical astrocytes

This study shows that TNF-α and IL-1α increases the release of IL-6 protein from astrocytes indicating that it is contained in the conditioned media of TNF-α and IL-1α treated astrocytes at elevated levels. These results are expected considering that IL-6 is produced by many different cell types, including astrocytes, microglia, neurons and endothelial cells (Gruol, 2015). However, astrocytes are the primary source of IL-6 during neuroinflammation when levels of IL-6 in the brain are elevated and its pathogenic pro-inflammatory effects are observed (Jensen et al, 2013).

4.4.12 IL-6 reduces the complexity and expression of co-localised synaptic markers in mature primary cortical neurons

This study demonstrates that increasing concentrations (80 and 200 ng/mL) of IL-6 reduces all measures of neuronal complexity when applied directly to mature neurons. IL-6 (80 ng/mL) reduced the number of synaptophysin, PSD-95 puncta and co-localised synaptic puncta indicating a negative effect of high concentrations of IL-6 on synapse formation. IL-6 (80 ng/mL) had no effect on cell viability indicating that the atrophic effects of IL-6 observed in this study are not a result of cell death mechanisms.

There is long standing evidence demonstrating a role for IL-6 in the regulation of synaptic transmission (Yang et al, 2012). Combined, these results concur with the large body of literature describing the deleterious role of IL-6 in an inflammatory context. These results parallel with previous studies indicating that IL-6 doses as low as 10 ng/mL reduce inhibitory synaptic transmission in cortical rodent brain slices producing a negative impact of IL-6 on synaptic transmission (Garcia-Oscos

et al, 2012). Indeed, enhanced microglial activation, astrogliosis and overproduction of IL-6 leads to chronic neuroinflammation and neurodegeneration associated with a multitude of neurological and neuropsychiatric disorders (Chen et al, 2018; Dowlati et al, 2010; Dursun et al, 2015; Rothaug et al, 2016).

4.4.13 Immunoneutralisation of IL-6 protects against reductions in neuronal complexity and co-localisation of synaptic proteins in mature primary cortical neurons induced by conditioned media from TNF-α and IL-1α treated astrocytes

This study shows that IL-6 directly reduces neuronal complexity and synapse formation and is produced in elevated quantifies following TNF-α and IL-1α treatment of astrocytes. It was therefore of interest to investigate if neutralisation of IL-6 is protective in the face of TNF-α and IL-1α-induced astrocyte activation.

As expected, IL-6 neutralising antibody blocked the TNF-α and IL-1α-induced reductions in neuronal complexity and synaptic protein co-localisations in mature neurons. These results confirm that the effects of conditioned media from TNF-α and IL-1α treated astrocytes are primarily mediated via IL-6 signalling and highlight IL-6 as an important mediator of neuronal atrophy and synapse loss associated with inflammation.

4.5 Conclusion

Results of this chapter confirm the atrophic and synaptopathic effects of conditioned media from activated glial cells on mature primary cortical neurons. It has been shown that IFNγ and the combination of TNF-α and IL-1α induce changes in glial cell activity including morphology, gene expression and cytokine secretion profiles. This has important implications for the treatment of neuroinflammatory diseases where IFNγ, TNF-α and IL-1α signalling are implicated.

Furthermore, these studies demonstrate that mediators released from activated microglia induce changes in astrocytes which are characteristic of astrocyte transition to a reactive phenotype. Specifically they demonstrate a role for TNF-α and IL-1α in the activation of pro-inflammatory signalling pathways in astrocytes which are associated with neuronal atrophy and synapse loss. IL-6 was also identified as a major mediator of inflammatory driven, glial associated mechanisms of neuronal atrophy and synapse loss following TNF-α and IL-1α-induced astrocyte activation. This highlights the importance of glial-associated interactions in driving impairments in neuronal complexity and synapse loss in IFNγ mediated inflammation and identifies the IL-6 signalling pathway as a therapeutic potential for manipulation in the prevention of inflammatory diseases associated with atrophy and synapse loss.

5 Effect of L-AAA on inflammatory related responses in astrocytes and inflammatory driven, glial associated neuronal atrophy

5.1 Introduction

Astrocytes have become well recognised for their role in enhancing the integrity of neuronal networks, promoting neuronal outgrowth and synapse formation and providing neuroprotection against noxious stimuli (Takemoto et al, 2015). Previous work has demonstrated that conditioned media from healthy astrocytes increases measures of neurite outgrowth and the number of co-localised synaptic puncta in both immature (O'Toole, 2015) and mature primary cortical neuronal cultures. Similar research has shown that conditioned media from healthy astrocytes attenuates glutamate-induced apoptosis in rat spinal cord neurons (Lu et al, 2015) via the release of neurotrophic factors such as BDNF and NGF (Takemoto et al, 2015). Results presented earlier in this thesis showed that conditioned media from L-AAA treated astrocytes reduces measures of neurite outgrowth and the number of co-localised synaptic puncta. These findings indicate that astrocytes have neurotrophic effects and L-AAA-induced astrocyte impairment has a negative impact on neuronal integrity.

Despite the extensive body of literature advocating a neuroprotective role for astrocytes, more recent research suggests that astrocytes can adopt a reactive, neurotoxic phenotype which may drive and sustain microglial activation under inflammatory conditions. Chapter 4 demonstrates that the inflammatory stimuli IFNγ and TNF-α and IL-1α activate glial cells producing a conditioned media which drives neuronal atrophy and synapse loss *in vitro*. In particular, it showed that the inflammatory factors IL-1α and TNF-α are released by activated microglia and induce a reactive astrocyte phenotype with neurotoxic potential. Recent studies also demonstrate a role for reactive astrocytes in sustaining microglial activation as evidenced by an increase in GFAP+ reactive astrogliosis and increased S100β expression following administration of LPS into the nigra of rodents (O'Neill et al, 2019). This chapter extends these findings and explores a novel role for reactive astrocytes in exacerbating inflammatory driven, glial-associated mechanisms of neuronal atrophy and synapse loss *in vitro*.

When tightly regulated neuroinflammation is believed to induce beneficial tissue repair after injury. However, persistent, unbridled inflammatory signalling has

detrimental effects on neuronal integrity as demonstrated in Chapter 4. While inflammatory stimuli may incur direct damage on neurons, inflammatory driven activation of glial cells and glial derived factors, which can be collected in the form of conditioned media, have also shown to drive neuronal atrophy and synapse loss. As such, a great deal of research has explored the potential for novel drug molecules and factors which provide neuroprotection and enhance neurite outgrowth and synapse formation during inflammation.

Previous research shows that cytokines such as interleukin-10 (IL-10) attenuate neuronal apoptosis and promote neurite outgrowth and synapse formation via the JAK1/STAT3 signalling pathway in cultured primary cortical neurons (Chen et al, 2016a). Manipulation of the Rho/ROCK signalling pathway with small-molecules has also been shown to promote neurite outgrowth *in vitro* (Boomkamp et al, 2012). More recently, several natural products have been identified for their neuroprotective qualities. The naturally occurring polyphenolic compound resveratrol reduces neuronal injury following oxygen-glucose deprivation and enhances neurite outgrowth and synaptogenesis by activating Sonic Hedgehog signalling in primary cortical neurons (Tang et al, 2017). Carnosic acid, a phenolic diterpene found in rosemary is also known for its ability to protect neurons from oxidative stress via the keap/Nrf2 transcriptional pathway. Similarly, the natural flavonoid Luteolin, which is found in several types of vegetables, fruits, and medicinal herbs, reportedly induces neurite outgrowth via induction of the MAPK, PKC, and adenosine 3',5'-cyclic monophosphate (cAMP)/PKA signalling pathways (Maruoka et al, 2011).

More recent research provides evidence for astrocytic dysfunction in restricting the development of dopaminergic neuropathology, highlighting reactive astrocytes as key contributors in inflammatory associated neurodegeneration. Intra-nigral injection of LPS induces rapid activation of microglia in the substantia nigra of male Wistar rats within 48 hours and co-administration of L-AAA effectively depletes GFAP+ astrocytes, resulting in a neuroprotective effect (O'Neill et al, 2019). Simultaneous intra-nigral injection of L-AAA in this experimental model of Parkinsonism attenuates the LPS-induced loss of tyrosine

hydroxylase-positive (TH+) dopamine neurons, GFAP+ reactive astrogliosis and increases in nigral S100β expression. A simultaneous reduction in Iba1+ microgliosis, indicates a role for reactive astrocytes in sustaining microglial activation at the interface of dopaminergic neuronal loss in an inflammatory environment.

This novel body of data suggests that astrocytes have varying effects on neuronal plasticity in the presence and absence of inflammatory stimuli. This chapter will extend these findings to investigate the role of astrocytes during inflammatory states and microglial activation using the astrocyte toxin L-AAA. It examines the effect of L-AAA on glial activation, neuronal atrophy and synapse loss driven by conditioned media from inflammatory reactive glia. This includes investigation of the effect of L-AAA on IFNγ and the combination of TNF-α and IL-1α-induced changes in the morphology, immunoreactivity, gene expression profiles and protein release of enriched astrocyte, microglia and mixed glial cultures.

The overall aim of this section will be to examine the effect of L-AAA as a strategy to prevent the release of neurotoxic factors from astrocytes and protect against inflammatory-induced neuronal atrophy and synapse loss associated with reactive microglia-astrocyte cross talk. It is one of the first studies to highlight the role of astrocytes as a perpetuator of pro-inflammatory signalling between glial cells and a contributor to inflammatory driven neuronal atrophy. Previous studies demonstrate a role for activated microglia in driving neuronal loss and selectively killing activated microglia via inhibition of caspase-8 can prevent LPS-induced neuronal death (Fricker et al, 2013). This section explores a novel approach of regulating inflammatory signalling by employing L-AAA-induced astrocyte impairment as a strategy to prevent feedback of pro-inflammatory signalling between reactive glia. In this regard, it may be possible to regulate the propagating, pro-inflammatory cyclical feedback between glia without compromising the immune responsibilities conferred by microglial activation.

With the increasing awareness for the crucial role played by non-neuronal cells in regulating inflammatory responses, research strategies are starting to shift towards the regulation of glial cell activation and glial-associated mechanisms

driving inflammation. Targeting the specific processes and molecules involved in neuroinflammation may provide new therapeutic opportunities for the treatment of inflammatory CNS conditions.

5.2 Aims

The overall aim of the study outlined in this chapter is to examine the effect of L-AAA-induced astrocyte impairment on inflammatory-induced changes in neuronal integrity. Moreover, this investigation aims to determine a role for reactive astrocytes in mediating inflammatory driven neuronal atrophy and synapse loss *in vitro* by employing a model of mature cortical neuronal cultures. Subsequently, the effect of conditioned media from activated and L-AAA treated glia on neuronal complexity, including the number of neuritic branches, neurite length, the number of primary neurites, and the number of branches in relation to varying distances from the cell soma/ body, were examined.

The specific aims of this study are to investigate the effects of L-AAA on (1) IFNγ-induced changes in the mRNA expression of inflammatory markers and their release from mixed glia, (2) IFNγ-induced changes in the mRNA expression of inflammatory markers in enriched microglial and astrocytic cultures, (3) IFNγ-induced changes in the morphology of primary cortical astrocytes, (4) TNF-α and IL-1α-induced changes in the morphology of primary cortical astrocytes, (5) TNF-α and IL-1α-induced changes in the expression and release of inflammatory markers in primary cortical astrocytes, (6) conditioned media from IFNγ treated mixed glia-induced reductions in the complexity of immature and mature neurons and the expression of synaptic markers, (7) conditioned media from TNF-α and IL-1α treated astrocytes-induced reductions in the complexity and expression of synaptic markers in mature primary cortical neurons**.**

Concentrations of L-AAA and IFNγ were chosen based on prior *in vitro* experiments in the lab and concentrations of TNF-α and IL-1α were chosen based on prior research which used a similar range of concentrations when treating astrocytic cultures (Liddelow et al, 2017).

5.3 Results

5.3.1 Effect of L-AAA on IFNγ-induced changes in the mRNA expression of TNF-α, IL-1α, IL-1β and IL-6 in mixed glia

To investigate the effects of L-AAA on IFNγ-induced changes in the mRNA expression of inflammatory markers in mixed glia, primary cortical mixed glial cultures (DIV 14) were co-treated with IFNγ (10 ng/mL) and L-AAA (0.05, 0.5 mM) for 24 hours. Cells were harvested for RNA extraction followed by RT-PCR. mRNA expression for the inflammatory markers TNF-α, IL-1α, IL-1β, IL-6 were quantified. Results of this study showed that IFNγ reduced the expression of **TNF-α** [$T_{(14)} = 4.047$, $P = 0.001$] compared to control DMEM (Student's T test). One-way ANOVA showed no effect of L-AAA on IFNγ-induced reductions in the expression of TNF-α [$F_{(2, 20)} = 2.437$, $P = 0.11$] [*Figure 5.1 (A)*]. IFNγ increased the expression of **IL-1α** [$T_{(16)} = 9.273$, $P < 0.001$] compared to control DMEM (Student's T test). One-way ANOVA showed no effect of L-AAA on IFNγ-induced increase in the expression of IL-1α [$F_{(2, 23)} = 0.432$, $P = 0.65$] [*Figure 5.1 (B)*]. IFNγ also increased the expression of **IL-1β** [$T_{(12)} = 19.39$, $P < 0.001$] compared to control DMEM (Student's T test). One-way ANOVA showed an effect of L-AAA on IFNγ-induced increase in the expression of IL-1β [$F_{(2, 18)} = 8.212$, $P = 0.003$]. *Post hoc* analysis revealed an increase in IL-1β mRNA expression following treatment with [IFNγ + L-AAA 0.05] compared to IFNγ alone ($P < 0.05$) [*Figure 5.1 (C)*].

IFNγ increased the expression of **IL-6** [$T_{(16)} = 6.303$, $P < 0.001$] compared to control DMEM (Student's T test). One-way ANOVA showed an effect of L-AAA on IFNγ-induced increase in the expression of IL-6 [$F_{(2, 23)} = 6.407$, $P = 0.006$]. *Post hoc* analysis revealed a reduction the mRNA expression of IL-6 following treatment with [IFNγ + L-AAA 0.5] compared to IFNγ alone ($P < 0.05$) [*Figure 5.1 (D)*].

5.3.2 Effect of L-AAA on IFNγ-induced release of TNF-α, IL-1α and IL-6 protein from mixed glial cultures

To investigate the effect of L-AAA on IFNγ-induced release of TNF-α, IL-1α and IL-6 protein from mixed glia, primary cortical mixed glial cultures (DIV 14) were co-treated with IFNγ (10 ng/mL) and L-AAA (0.05, 0.5 mM) for 24 hours. Supernatants were collected for analysis of TNF-α, IL-1α and IL-6 protein release

by ELISA. Results of this study showed that IFNγ increased the release of **TNF-α protein** [$T_{(13)} = 29.7$, $P < 0.001$] compared to control DMEM (Student's T test). One-way ANOVA showed an effect of L-AAA on IFNγ-induced increase in the expression of TNF-α [$F_{(2, 21)} = 37.23$, $P < 0.001$]. *Post hoc* analysis revealed an increase in the release of TNF-α protein following treatment with [IFNγ + L-AAA 0.5] compared to IFNγ alone ($P < 0.001$) [*Figure 5.2 (A)*]. IFNγ increased the release of **IL-1α protein** [$T_{(14)} = 6.043$, $P < 0.001$] compared to control DMEM (Student's T test). One-way ANOVA showed an effect of L-AAA on IFNγ-induced increase in the expression of IL-1α [$F_{(2, 20)} = 5.116$, $P = 0.02$]. *Post hoc* analysis revealed a decrease in IL-1α release following treatment with [IFNγ + L-AAA 0.5] compared to IFNγ alone ($P < 0.05$) [*Figure 5.2 (B)*]. IFNγ also increased the release of **IL-6 protein** [$T_{(14)} = 6.232$, $P < 0.001$] compared to control DMEM (Student's T test). One-way ANOVA showed an effect of L-AAA on IFNγ-induced increase in the release of IL-6 [$F_{(2, 21)} = 6.415$, $P = 0.007$]. *Post hoc* analysis revealed a decrease in IL-6 release following treatment with [IFNγ + L-AAA 0.5] compared to IFNγ alone ($P < 0.01$) [*Figure 5.2 (C)*].

5.3.3 Effect of L-AAA and IFNγ on the mRNA expression of TNF-α, IL-1α and Iba1 in microglia

To investigate the effect of L-AAA and IFNγ on the mRNA expression of inflammatory markers in microglia, primary cortical microglial cultures (DIV 15) were co-treated with IFNγ (10 ng/mL) and L-AAA (0.05, 0.5 mM) for 24 hours. Cells were harvested for RNA extraction followed by RT-PCR. mRNA expression for the inflammatory markers TNF-α, IL-1α, and Iba1 were quantified. Results of this study showed that IFNγ had no effect on the mRNA expression of **TNF-α** [$T_{(8)} = 1.321$, $P = 0.22$] (Student's T test). One-way ANOVA showed no effect of L-AAA on the expression of TNF-α [$F_{(2, 20)} = 0.1204$, $P = 0.89$] [*Figure 5.3 (A)*]. IFNγ increased the mRNA expression of **IL-1α** [$T_{(14)} = 2.859$, $P = 0.01$] compared to control DMEM (Student's T test). One-way ANOVA showed no effect of L-AAA on IFNγ-induced increase in the expression of **IL-1α** [$F_{(2, 21)} = 0.119$, $P = 0.89$] [*Figure 5.3 (B)*]. On the other hand IFNγ had no effect on the mRNA expression of **Iba1** [$T_{(14)} = 0.732$, $P = 0.48$] (Student's T test). One-way ANOVA showed no effect of L-AAA on the expression of Iba1 [$F_{(2, 21)} = 0.33$, $P = 0.72$] [*Figure 5.3 (D)*].

5.3.4 Effect of L-AAA on IFNγ-induced changes in the mRNA expression of GFAP, S100β, IL-1β and IL-6 in astrocytes

To investigate the effects of L-AAA on IFNγ-induced changes in the mRNA expression of inflammatory markers in astrocytes, enriched primary cortical astrocyte cultures (DIV 14) were co-treated with IFNγ (10 ng/mL) and L-AAA (0.05, 0.5 mM) for 24 hours. Cells were harvested for RNA extraction followed by RT-PCR. mRNA expression for the inflammatory markers GFAP, S100β, IL-1β and IL-6 in astrocytes were quantified. Results of this study showed that IFNγ reduced the mRNA expression of **GFAP** [$T_{(14)} = 4.384$, $P < 0.01$] compared to control DMEM (Student's T test). One-way ANOVA showed no effect of L-AAA on IFNγ-induced decrease in GFAP [$F_{(2, 21)} = 1.682$, $P = 0.21$] [*Figure 5.4 (A)*]. IFNγ also reduced the mRNA expression of **S100β** [$T_{(14)} = 3.923$, $P = 0.002$] compared to control DMEM (Student's T test). One-way ANOVA showed no effect of L-AAA on IFNγ-induced decrease in S100β [$F_{(2, 21)} = 0.4223$, $P = 0.66$] [*Figure 5.4 (B)*]. On the other hand, IFNγ increased the mRNA expression of **IL-1β** [$T_{(10)} = 9.518$, $P < 0.001$] compared to control DMEM (Student's T test). One-way ANOVA showed no effect of L-AAA on IFNγ induced increase in IL-1β [$F_{(2, 15)} = 0.4182$, $P = 0.67$] [*Figure 5.4 (C)*]. IFNγ increased the mRNA expression of **IL-6** [$T_{(14)} = 8.909$, $P < 0.001$] compared to control DMEM (Student's T test). One-way ANOVA showed no effect of L-AAA on IFNγ-induced increase in IL-6 [$F_{(2, 21)} = 1.731$, $P = 0.2$] [*Figure 5.4 (D)*].

5.3.5 Effect of L-AAA on IFNγ-induced changes in GFAP immunoreactivity and astrocyte morphology

To investigate the effects of L-AAA on IFNγ-induced changes in GFAP immunoreactivity and astrocyte morphology, enriched primary cortical astrocyte cultures (DIV 14) were co-treated with IFNγ (10 ng/mL) and L-AAA (0.05, 0.5 mM) for 24 hours. Fixation and GFAP immunocytochemistry were performed to determine the effect of L-AAA on IFNγ-induced changes in GFAP immunoreactivity and astrocyte morphology (mean cell area, perimeter and soma: area ratio). Results of this study showed that IFNγ increased **GFAP immunoreactivity** [$T_{(67)} = 8.945$, $P < 0.001$] compared to control DMEM (Student's T test). One-way ANOVA showed an effect of L-AAA on IFNγ-induced

increase in GFAP immunoreactivity [$F_{(2, 122)} = 145.0$, $P < 0.001$]. *Post hoc* analysis revealed a decrease in GFAP immunoreactivity following treatment with [IFNγ + L-AAA 0.05] and [IFNγ + L-AAA 0.5] compared to IFNγ alone ($P < 0.001$) [*Figure 5.5 (A)*]. On the other hand, IFNγ decreased astrocyte **mean cell area** [$T_{(88)} = 7.123$, $P < 0.001$] compared to control DMEM (Student's T test). One-way ANOVA showed an effect of L-AAA on IFNγ-induced decrease in mean cell area [$F_{(2, 136)} = 5.525$, $P = 0.005$]. *Post hoc* analysis revealed a decrease in mean cell area following treatment with [IFNγ + L-AAA 0.05] ($P < 0.05$) and [IFNγ + L-AAA 0.5] ($P < 0.01$) compared to IFNγ alone [*Figure 5.5 (B)*]. IFNγ decreased **cell perimeter** [$T_{(88)} = 2.592$, $P = 0.01$] compared to control DMEM (Student's T test). One-way ANOVA showed an effect of L-AAA on IFNγ-induced decrease in cell perimeter [$F_{(2, 134)} = 7.473$, $P < 0.001$]. *Post hoc* analysis revealed a decrease in cell perimeter following treatment with [IFNγ + L-AAA 0.05] and [IFNγ + L-AAA 0.5] compared to IFNγ alone ($P < 0.01$) [*Figure 5.5 (C)*]. IFNγ had no effect on the **soma:cell ratio** [$T_{(66)} = 0.195$, $P = 0.85$] (Student's T test). One-way ANOVA showed no effect of L-AAA treatment [$F_{(2, 40)} = 0.753$, $P = 0.48$] [*Figure 5.5 (D)*].

5.3.6 Effect of L-AAA on TNF-α and IL-1α-induced changes in GFAP immunoreactivity and astrocyte morphology

To investigate the effects of L-AAA on TNF-α and IL-1α-induced changes in GFAP immunoreactivity and astrocyte morphology, enriched primary cortical astrocyte cultures (DIV 14) were co-treated with TNF-α (30 ng/mL), IL-1α (3 ng/mL) and L-AAA (0.05, 0.5 mM) for 24 hours. Fixation and GFAP immunocytochemistry were performed to determine the effect of L-AAA on TNF-α and IL-1α-induced changes in GFAP immunoreactivity and astrocyte morphology (mean cell area, perimeter and soma: area ratio).

Results of this study showed that TNF-α and IL-1α decreased **GFAP immunoreactivity** [$T_{(90)} = 9.54$, $P < 0.001$] compared to control DMEM (Student's T test). One-way ANOVA showed an effect of L-AAA on TNF-α and IL-1α-induced decrease in GFAP immunoreactivity [$F_{(2, 168)} = 61.82$, $P < 0.001$]. *Post hoc* analysis revealed an increase in GFAP immunoreactivity following treatment with [TNF-α/IL-1α + L-AAA 0.05] and [TNF-α/IL-1α + L-AAA 0.5] compared to TNF-α and IL-

1α alone (P < 0.001) [*Figure 5.6 (A)*]. TNF-α and IL-1α decreased astrocyte **mean cell area** [$T_{(91)}$ = 13.25, P < 0.001] compared to control DMEM (Student's T test). One-way ANOVA showed an effect of L-AAA on TNF-α and IL-1α-induced decrease in mean cell area [$F_{(2, 171)}$ = 80.84, P < 0.001]. *Post hoc* analysis revealed an increase in mean cell area following treatment with [TNF-α/IL-1α + L-AAA 0.05] and [TNF-α/IL-1α + L-AAA 0.5] compared to TNF-α and IL-1α alone (P < 0.001) [*Figure 5.6 (B)*]. TNF-α and IL-1α decreased astrocyte **cell perimeter** [$T_{(92)}$ = 13.32, P < 0.001] compared to control DMEM (Student's T test). One-way ANOVA showed an effect of L-AAA on TNF-α and IL-1α-induced decrease in cell perimeter [$F_{(2, 170)}$ = 80.16, P < 0.001]. *Post hoc* analysis revealed an increase in cell perimeter following treatment with [TNF-α/IL-1α + L-AAA 0.05] and [TNF-α/IL-1α + L-AAA 0.5] compared to TNF-α and IL-1α alone (P < 0.001) [*Figure 5.6 (C)*]. TNF-α and IL-1α increased the **soma:cell ratio** [$T_{(89)}$ = 12.20, P < 0.001] compared to control DMEM (Student's T test). One-way ANOVA showed an effect of L-AAA on TNF-α and IL-1α-induced increase in the soma:cell ratio [$F_{(2, 162)}$ = 77.65, P < 0.001]. *Post hoc* analysis revealed an decrease in the soma:cell ratio following treatment with [TNF-α/IL-1α + L-AAA 0.05] and [TNF-α/IL-1α + L-AAA 0.5] compared to TNF-α and IL-1α alone (P < 0.001) [*Figure 5.6 (D)*].

5.3.7 Effect of L-AAA on TNF-α and IL-1α-induced changes in the mRNA expression of GFAP, S100β, IL-1β, IL-6 in astrocytes

To investigate the effects of L-AAA on TNF-α and IL-1α-induced changes in the mRNA expression of astrocytic markers, enriched primary cortical astrocyte cultures (DIV 14) were co-treated with TNF-α (30 ng/mL), IL-1α (3 ng/mL) and L-AAA (0.05, 0.5 mM) for 24 hours. Cells were harvested for RNA extraction followed by RT-PCR. mRNA expression for the astrocyte markers GFAP, S100β, IL-1β, IL-6 were quantified.

TNF-α and IL-1α decreased the mRNA expression of **GFAP** [$T_{(14)}$ = 7.850, P < 0.001] compared to control DMEM (Student's T test). One-way ANOVA showed no effect of L-AAA on TNF-α and IL-1α-induced reductions in GFAP [$F_{(2, 21)}$ = 0.503, P = 0.61] [*Figure 5.7 (A)*]. TNF-α and IL-1α decreased the mRNA expression of **S100β** [$T_{(14)}$ = 7.452, P < 0.001] compared to control DMEM (Student's T test).

One-way ANOVA showed no effect of L-AAA on TNF-α and IL-1α-induced reductions in S100β [$F_{(2, 21)} = 2.613$, $P = 0.10$] [*Figure 5.7 (B)*]. TNF-α and IL-1α increased the mRNA expression of **IL-1β** [$T_{(14)} = 2.188$, $P = 0.05$] compared to control DMEM (Student's T test). One-way ANOVA showed no effect of L-AAA on TNF-α and IL-1α-induced reductions in IL-1β [$F_{(2, 21)} = 0.5210$, $P = 0.60$] [*Figure 5.7 (C)*]. TNF-α and IL-1α increased the mRNA expression of **IL-6** [$T_{(14)} = 3.796$, $P = 0.002$] compared to control DMEM (Student's T test). One-way ANOVA showed an effect of L-AAA on TNF-α and IL-1α-induced increase in IL-6 expression [$F_{(2, 21)} = 4.946$, $P = 0.02$]. *Post hoc* analysis revealed a decrease in IL-6 expression following treatment with [TNF-α/IL-1α + L-AAA 0.5] compared to TNF-α and IL-1α alone ($P < 0.05$) [*Figure 5.7 (D)*].

5.3.8 Effect of L-AAA on TNF-α and IL-1α-induced release of IL-6 protein from astrocytes

To investigate the effect of L-AAA on TNF-α and IL-1α-induced changes the release of astrocytic IL-6, enriched primary cortical astrocyte cultures (DIV 14) were co-treated with TNF-α (30 ng/mL), IL-1α (3 ng/mL) and L-AAA (0.05, 0.5 mM) for 24 hours. Supernatants were collected for analysis of IL-6 protein release by ELISA.

TNF-α and IL-1α increased the release of **IL-6** [$T_{(10)} = 79.14$, $P < 0.001$] compared to control DMEM (Student's T test). One-way ANOVA showed an effect of L-AAA on TNF-α and IL-1α-induced increase in IL-6 release [$F_{(2, 15)} = 111.7$, $P < 0.001$]. *Post hoc* analysis revealed a decrease in IL-6 expression following treatment with [TNF-α/IL-1α + L-AAA 0.5] compared to TNF-α and IL-1α alone ($P < 0.001$) [*Figure 5.8*].

5.3.9 Effect of L-AAA on reductions in the complexity of immature neurons induced by conditioned media from IFNγ treated mixed glia

To investigate the effect of L-AAA on conditioned media from IFNγ treated mixed glia-induced reductions in neuronal complexity, mixed glia cultures (DIV 14) were co-treated with IFNγ (10 ng/mL) and L-AAA (0.05, 0.5 mM) for 24 hours. The resulting conditioned media was collected and applied to immature (DIV 3) neurons for 24 hours. Fixation and β-III tubulin immunocytochemistry were

performed to determine the effect of conditioned media from IFNγ and L-AAA treated mixed glia on neurite outgrowth by Sholl analysis.

Conditioned media from IFNγ treated mixed glia reduced the number of **neuritic branches** [$T_{(189)} = 6.62, P < 0.001$] compared to conditioned media from untreated mixed glia (Student's T test). One-way ANOVA showed an effect of L-AAA on reductions induced by conditioned media from IFNγ treated mixed glia [$F_{(2, 276)} = 4.410, P = 0.01$]. *Post hoc* analysis revealed an increase the number of neuritic branches following treatment with conditioned media from [IFNγ + L-AAA 0.5] treated mixed glia compared to conditioned media from IFNγ treated mixed glia ($P < 0.01$) [*Figure 5.9 (A*)]. Conditioned media from IFNγ treated mixed glia reduced **neuritic length** [$T_{(188)} = 7.486, P < 0.001$] compared to conditioned media from untreated mixed glia (Student's T test). One-way ANOVA showed no effect of L-AAA on reductions induced by conditioned media from IFNγ treated mixed glia [$F_{(2, 274)} = 2.843, P = 0.06$] [*Figure 5.9 (B)*]. Conditioned media from IFNγ treated mixed glia reduced the number of **primary neurites** [$T_{(189)} = 6.268, P < 0.001$] compared to conditioned media from untreated mixed glia (Student's T test). One-way ANOVA showed no effect of L-AAA on reductions induced by conditioned media from IFNγ treated mixed glia [$F_{(2, 275)} = 0.974, P = 0.38$] [*Figure 5.9 (C)*]. Two-way repeated measures ANOVA of the **number of neuritic branches at specific distances from the neuronal cell soma** showed an effect of distance [$F_{(19, 7182)} = 697.5, P < 0.001$], an effect of treatment [$F_{(3, 378)} = 48.65, P < 0.001$] and an interaction effect [$F_{(57, 7182)} = 17.18, P < 0.001$]. *Post hoc* analysis revealed a significant decrease in the Sholl profile at 10-110 µm following treatment with conditioned media from [IFNγ + L-AAA 0.05], and [IFNγ + L-AAA 0.5] treated mixed glia compared to conditioned media from untreated mixed glia. *Post hoc* analysis also revealed a significant increase in the Sholl profile at 10-110 µm following treatment with conditioned media from [IFNγ + L-AAA 0.5] treated mixed glia compared to conditioned media from IFNγ treated mixed glia indicating a protective effect of L-AAA at increasing concentrations ($P < 0.01$) [*Figure 5.9 (D)*].

5.3.10 Effect of L-AAA on reductions in the complexity of mature neurons induced by conditioned media from IFNγ treated mixed glia

To investigate the effect of L-AAA on conditioned media from IFNγ treated mixed glia-induced reductions in neuronal complexity, mixed glia cultures (DIV 14) were co-treated with IFNγ (10 ng/mL) and L-AAA (0.05, 0.5 mM) for 24 hours. The resulting conditioned media was collected and applied to mature (DIV 21) primary cortical neurons for 24 hours. Fixation and MAP2 immunocytochemistry were performed to determine the effect of conditioned media from IFNγ and L-AAA treated mixed glia on neurite outgrowth by Sholl analysis.

Results of this study showed that conditioned media from IFNγ treated mixed glia reduced the number of **neuritic branches** [$T_{(158)} = 3.907, P < 0.001$] compared to conditioned media from untreated mixed glia (Student's T test). One-way ANOVA showed an effect of L-AAA on reductions induced by conditioned media from IFNγ treated mixed glia [$F_{(2, 153)} = 37.26, P < 0.001$]. *Post hoc* analysis revealed a decrease in the number of neuritic branches following treatment with conditioned media from [IFNγ + L-AAA 0.05] and [IFNγ + L-AAA 0.5] treated mixed glia compared to conditioned media from IFNγ treated mixed glia ($P < 0.001$) [*Figure 5.10 (A)*]. Conditioned media from IFNγ treated mixed glia reduced **neuritic length** [$T_{(156)} = 5.781, P < 0.001$] compared to conditioned media from untreated mixed glia (Student's T test). One-way ANOVA showed an effect of L-AAA on reductions induced by conditioned media from IFNγ treated mixed glia [$F_{(2, 152)} = 40.88, P < 0.001$]. *Post hoc* analysis revealed a decrease in neuritic length following treatment with conditioned media from [IFNγ + L-AAA 0.05] and [IFNγ + L-AAA 0.5] treated mixed glia compared to conditioned media from IFNγ treated mixed glia ($P < 0.001$) [*Figure 5.10 (B)*]. Conditioned media from IFNγ treated mixed glia reduced the number of **primary neurites** [$T_{(158)} = 3.907, P < 0.001$] compared to conditioned media from untreated mixed glia (Student's T test). One-way ANOVA showed no effect of L-AAA on reductions induced by conditioned media from IFNγ treated mixed glia [$F_{(2, 153)} = 0.467, P = 0.63$] [*Figure 5.10 (C)*]. Two-way repeated measures ANOVA of the **number of neuritic branches at specific distances from the neuronal cell soma** showed an effect of distance [$F_{(19, 4408)} = 247.3, P < 0.001$], an effect of treatment [$F_{(3, 232)} =$

74.17, P < 0.001] and an interaction effect [$F_{(57, 4408)}$ = 14.10, P < 0.001]. *Post hoc* analysis revealed a significant decrease in the Sholl profile at 10-150 µm following treatment with conditioned media from IFNγ treated mixed glia, conditioned media from [IFNγ + L-AAA 0.05], and conditioned media from [IFNγ + L-AAA 0.5] treated mixed glia compared to control conditioned media. *Post hoc* analysis revealed a lesser decrease in the Sholl profile at 60-70 µm following treatment with conditioned media from [IFNγ + L-AAA 0.5] treated mixed glia compared to conditioned media from IFNγ treated mixed glia, indicating a protective effect of L-AAA at increasing concentrations (P < 0.01) [*Figure 5.10 (D)*].

5.3.11 Effect of L-AAA on reductions in synaptic protein co-localisation in mature primary cortical neurons induced by conditioned media from IFNγ treated mixed glia

To investigate the effect of L-AAA on conditioned media from IFNγ treated mixed glia-induced reductions in the number of synaptic protein co-localisations, mixed glia cultures (DIV 14) were co-treated with IFNγ (10 ng/mL) and L-AAA (0.05, 0.5 mM) for 24 hours. The resulting conditioned media was collected and applied to mature (DIV 21) primary cortical neurons for 24 hours. Fixation and immunocytochemistry were performed to determine the effect of conditioned media from IFNγ and L-AAA treated mixed glia on synaptic protein co-localisation in mature neurons.

Results of this study showed that conditioned media from IFNγ treated mixed glia reduced the number of **synaptophysin puncta** [$T_{(207)}$ = 4.245, P < 0.001] compared to conditioned media from untreated mixed glia (Student's T test). One-way ANOVA showed an effect of L-AAA co-treatment [$F_{(2, 151)}$ = 5.407, P = 0.005]. *Post hoc* analysis revealed a decrease in the number of synaptophysin puncta following treatment with conditioned media from [IFNγ + L-AAA 0.5] treated mixed glia compared to conditioned media from IFNγ treated mixed glia (P < 0.01) [*Figure 5.11 (A)*]. Conditioned media from IFNγ treated mixed glia had no effect on the number of **PSD-95 puncta** [$T_{(189)}$ = 1.160, P = 0.25] compared to conditioned media from untreated mixed glia (Student's T test). One-way ANOVA showed an effect of L-AAA co-treatment [$F_{(2, 283)}$ = 3.602, P = 0.03]. *Post hoc*

analysis revealed an increase in the number of PSD-95 puncta following treatment with conditioned media from [IFNγ + L-AAA 0.05] treated mixed glia compared to conditioned media from IFNγ treated mixed glia ($P < 0.05$) [*Figure 5.11 (B)*]. One-way ANOVA showed an effect on the number of **co-localised synaptic puncta** [$T_{(204)} = 7.443$, $P < 0.001$] compared to conditioned media from untreated mixed glia (Student's T test). One-way ANOVA showed an effect of L-AAA co-treatment [$F_{(2, 287)} = 12.89$, $P < 0.001$]. *Post hoc* analysis revealed an increase in the number of co-localised synaptic puncta following treatment with conditioned media from [IFNγ + L-AAA 0.05] ($P < 0.001$) and [IFNγ + L-AAA 0.05] ($P < 0.01$) treated mixed glia compared to conditioned media from IFNγ treated mixed glia ($P < 0.05$) [*Figure 5.11 (C)*].

5.3.12 Effect of L-AAA on reductions in neuronal complexity induced by conditioned media from TNF-α and IL-1α treated astrocytes

To investigate the effects of L-AAA on reductions in neuronal complexity induced by conditioned media from TNF-α and IL-1α treated astrocytes, enriched primary cortical astrocyte cultures (DIV 14) were treated with TNF-α (30 ng/mL), IL-1α (3 ng/mL) and L-AAA (0.05, 0.5 mM) for 24 hours. The resulting conditioned media was collected and applied to mature (DIV 21) primary cortical neurons for 24 hours. Fixation and MAP2 immunocytochemistry were performed to determine the effect of conditioned media from TNF-α/IL-1α and L-AAA treated astrocytes on neuronal complexity by Sholl analysis.

Results of this study showed that conditioned media from TNF-α and IL-1α treated astrocytes reduced the number of **neuritic branches** [$T_{(126)} = 6.891$, $P < 0.001$] compared to conditioned media from TNF-α and IL-1α treated astrocytes (Student's T test). One-way ANOVA showed an effect of L-AAA on reductions induced by conditioned media from TNF-α and IL-1α treated astrocytes [$F_{(2, 253)} = 3.881$, $P = 0.02$]. *Post hoc* analysis revealed an increase in the number of neuritic branches following treatment with conditioned media from [TNF-α/IL-1α + L-AAA 0.05] and [TNF-α/IL-1α + L-AAA 0.5] treated astrocytes compared to conditioned media from TNF-α and IL-1α treated astrocytes alone ($P < 0.05$) [*Figure 5.12 (A)*]. Conditioned media from TNF-α and IL-1α treated astrocytes reduced **neuritic**

length [$T_{(123)} = 12.66$, $P < 0.001$] compared to conditioned media from untreated astrocytes (Student's T test). One-way ANOVA showed an effect of L-AAA on reductions induced by conditioned media from TNF-α and IL-1α treated astrocytes [$F_{(2, 257)} = 26.46$, $P < 0.001$]. *Post hoc* analysis revealed an increase in neuritic length following treatment with conditioned media from [TNF-α/IL-1α + L-AAA 0.05] ($P < 0.001$) and [TNF-α/IL-1α + L-AAA 0.5] ($P < 0.01$) treated astrocytes compared to conditioned media from TNF-α and IL-1α treated astrocytes alone [*Figure 5.12 (B)*]. Conditioned media from TNF-α and IL-1α treated astrocytes reduced the number of **primary neurites** [$T_{(126)} = 2.010$, $P = 0.05$] compared to control (Student's T test). One-way ANOVA showed an effect of L-AAA on reductions induced by conditioned media from TNF-α and IL-1α treated astrocytes [$F_{(2, 260)} = 8.204$, $P < 0.001$]. *Post hoc* analysis revealed an increase in the number of primary neurites following treatment with conditioned media from [TNF-α/IL-1α + L-AAA 0.5] treated astrocytes compared to conditioned media from TNF-α and IL-1α treated astrocytes alone ($P < 0.01$) [*Figure 5.12 (C)*]. Two-way repeated measures ANOVA of the **number of neuritic branches at specific distances from the neuronal cell soma** showed an effect of distance [$F_{(19, 3480)} = 104.8$, $P < 0.001$], an effect of treatment [$F_{(3, 3480)} = 316.0$, $P < 0.001$] and an interaction effect [$F_{(57, 3480)} = 7.767$, $P < 0.001$]. *Post hoc* analysis revealed a significant decrease in the Sholl profile at 50-140 µm following treatment with conditioned media from TNF-α and IL-1α treated astrocytes compared to conditioned media from untreated astrocytes ($P < 0.001$). However *post hoc* analysis also revealed a significant increase in the Sholl profile at 40-110 µm following treatment with conditioned media from [TNF-α/IL-1α + L-AAA 0.05] treated astrocytes compared to conditioned media from TNF-α and IL-1α treated astrocytes alone, indicating a protective effect for L-AAA [*Figure 5.12 (D)*].

5.3.13 Effect of L-AAA on reductions in synaptic protein co-localisation in mature primary cortical neurons induced by conditioned media from TNF-α and IL-1α treated astrocytes

To investigate the effects of L-AAA on reductions in synaptic protein co-localisation induced by conditioned media from TNF-α and IL-1α treated astrocytes, enriched primary cortical astrocytes cultures (DIV 14) were treated

with TNF-α (30 ng/mL), IL-1α (3 ng/mL) and L-AAA (0.05, 0.5 mM) for 24 hours. The resulting conditioned media was collected and applied to mature (DIV 21) primary cortical neurons for 24 hours. Fixation and immunocytochemistry were performed to determine the effect of conditioned media from TNF-α/IL-1α and L-AAA treated astrocytes on synaptic protein co-localisation.

Results of this study showed conditioned media from TNF-α and IL-1α treated astrocytes had no effect on the number of **synaptophysin puncta** [$T_{(105)} = 1.589$, $P = 0.12$] (Student's T test). One-way ANOVA showed an effect of L-AAA co-treatment [$F_{(2, 152)} = 13.56$, $P < 0.001$]. *Post hoc* analysis revealed an increase in the number of synaptophysin puncta following treatment with conditioned media from [TNF-α/IL-1α + L-AAA 0.5] treated astrocytes compared to conditioned media from TNF-α and IL-1α treated astrocytes alone ($P < 0.001$) [*Figure 5.13 (A)*]. Conditioned media from TNF-α and IL-1α treated astrocytes had no effect on the number of **PSD-95 puncta** [$T_{(107)} = 0.51$, $P = 0.61$] (Student's T test). One-way ANOVA showed no effect of L-AAA co-treatment [$F_{(2, 155)} = 3.424$, $P = 0.04$] [*Figure 5.13 (B)*]. Conditioned media from TNF-α and IL-1α treated astrocytes reduced the number of **co-localised synaptic puncta** [$T_{(103)} = 2.712$, $P = 0.008$], compared to conditioned media from untreated astrocytes (Student's T test). One-way ANOVA showed an effect of L-AAA on reductions induced by conditioned media from TNF-α and IL-1α treated astrocytes [$F_{(2, 154)} = 9.09$, $P < 0.001$]. *Post hoc* analysis revealed an increase in the number of co-localised synaptic puncta following treatment with conditioned media from [TNF-α/IL-1α + L-AAA 0.5] compared to conditioned media from TNF-α and IL-1α treated astrocytes alone ($P < 0.001$) [*Figure 5.13 (C)*].

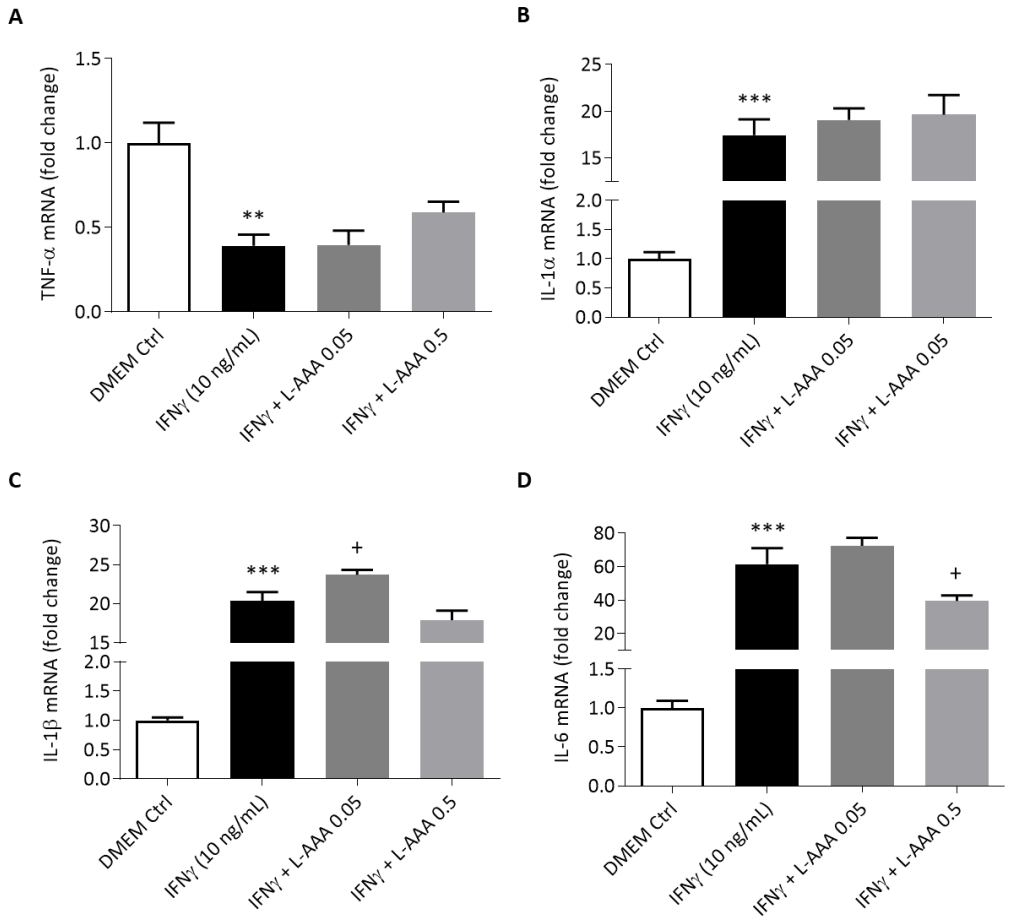

Figure 5.1 Effect of L-AAA on IFNγ-induced changes in the mRNA expression of TNF-α, IL-1α, IL-1β and IL-6 in primary cortical mixed glia.
Primary mixed glia (DIV 14) were treated with IFNγ (10 ng/mL) and L-AAA (0.05, 0.5 mM) for 24 hours. Cells were harvested for RNA extraction followed by RT-PCR to analyse the expression of TNF-α (A), IL-1α (B), IL-1β (C) and IL-6 (D). Data are expressed as mean ± SEM, n=8 wells per treatment group from 4 independent experiments. ***P<0.001, **P<0.01 vs. control DMEM, $^{+}$P<0.05 vs. IFNγ (Newman-Keuls *post hoc* test).

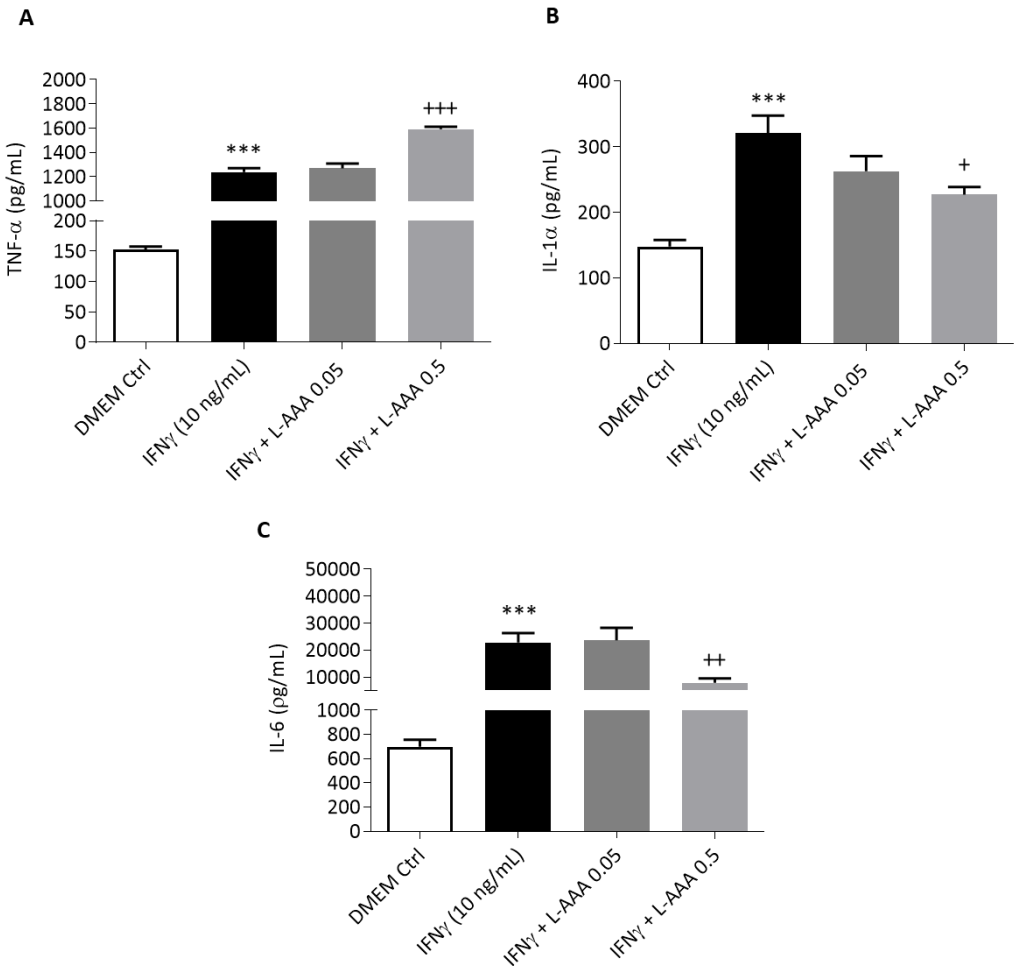

Figure 5.2 L-AAA potentiates IFNγ-induced release of TNF-α and attenuates IFNγ-induced release of IL-1α and IL-6 protein from primary cortical mixed glia.
Primary mixed glia (DIV 14) were treated with IFNγ (10 ng/mL) and L-AAA (0.05, 0.5 mM) for 24 hours. Supernatants were collected for analysis of TNF-α (A), IL-1α (B) and IL-6 (C) protein release by ELISA. Data are expressed as mean ± SEM, n=8 wells per treatment group from 4 independent experiments. ***P<0.001 vs. control DMEM, $^{+++}$P<0.001, $^{++}$P<0.01, $^{+}$P<0.05 vs. IFNγ (Newman-Keuls *post hoc* test).

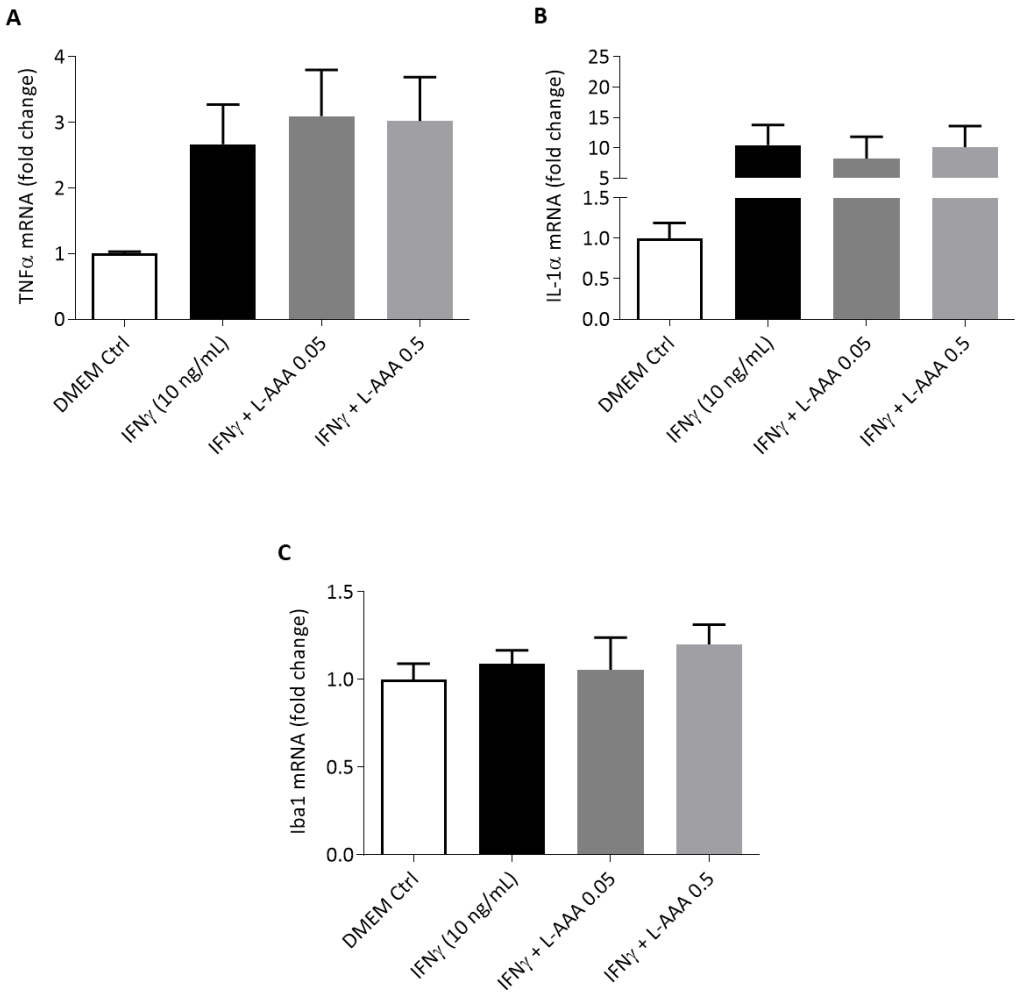

Figure 5.3 Effect of L-AAA and IFNγ on the mRNA expression of TNF-α, IL-1α and Iba1 in primary cortical microglia.

Primary cortical microglia (DIV 15) were treated with IFNγ (10 ng/mL) and L-AAA (0.05, 0.5 mM) for 24 hours. Cells were harvested for RNA extraction followed by RT-PCR to analyse the expression of the markers TNF-α (A), IL-1α (B) and Iba1 (C). Data are expressed as mean ± SEM, n=8 wells per treatment group from 4 independent experiments.

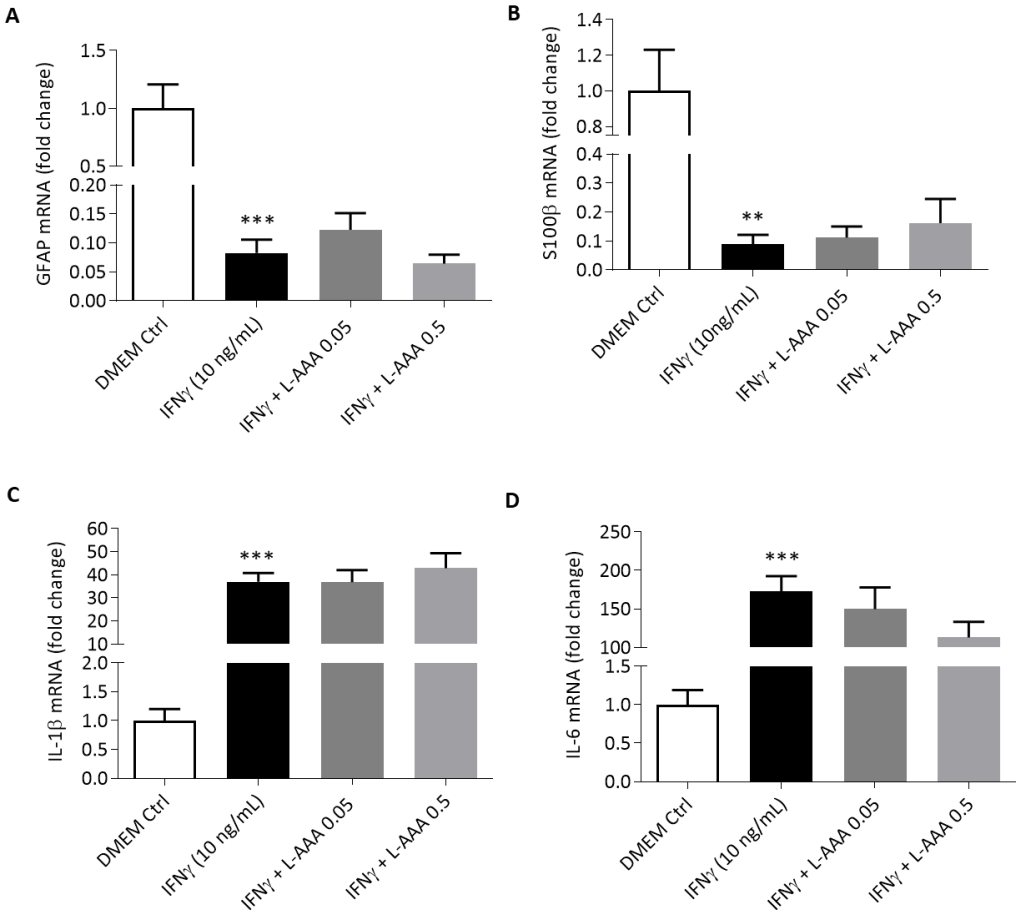

Figure 5.4 Effect of L-AAA on IFNγ-induced changes in the mRNA expression of GFAP, S100β, IL-1β and IL-6 in primary cortical astrocytes.

Primary cortical astrocytes (DIV 14) were treated with IFNγ (10 ng/mL) and L-AAA (0.05, 0.5 mM) for 24 hours. Cells were harvested for RNA extraction followed by RT-PCR to analyse the expression of GFAP (A), S100β (B), IL-1β (C) and IL-6 (D). Data are expressed as mean ± SEM, n=8 wells per treatment group from 4 independent experiments. ***P<0.001, **P<0.01, vs. control DMEM (Newman-Keuls *post hoc* test).

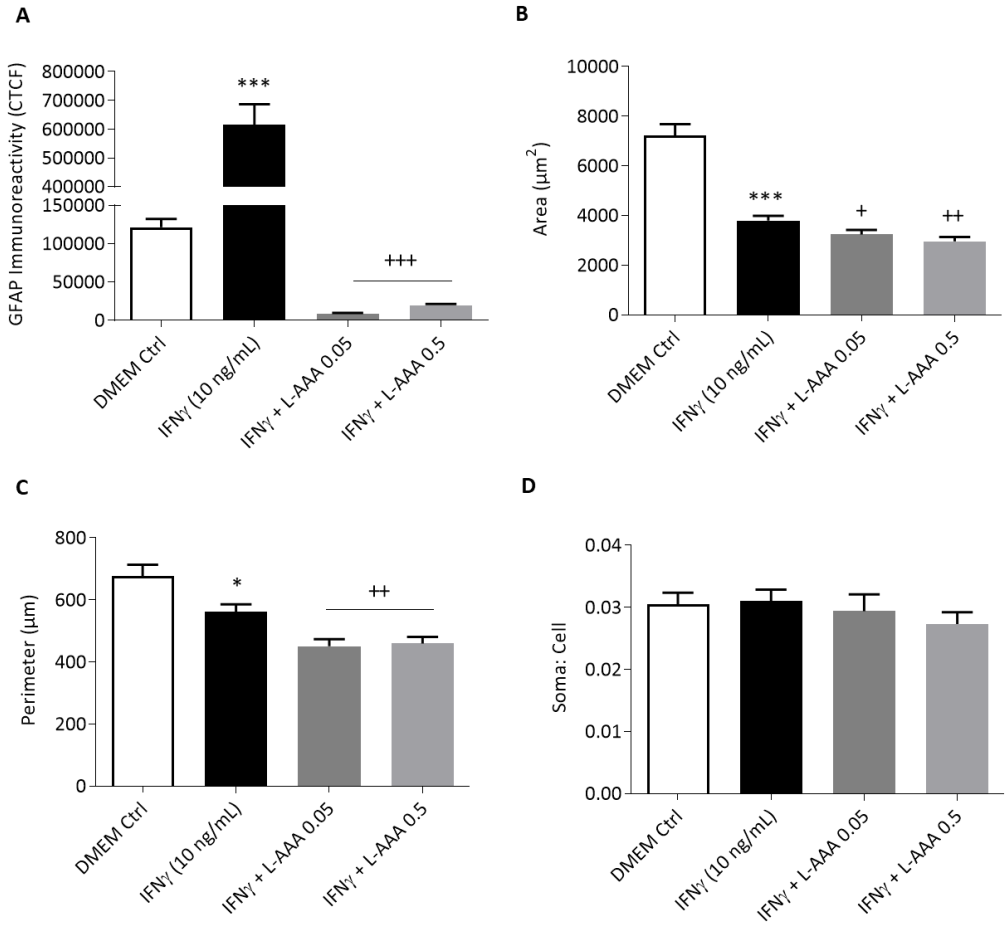

Figure 5.5 Effect of L-AAA on IFNγ-induced changes in GFAP immunoreactivity and astrocyte morphology.

Primary astrocytes (DIV 14) were treated with IFNγ (10 ng/mL) and L-AAA (0.05, 0.5 mM) for 24 hours before fixation and GFAP immunocytochemistry. Morphological analysis was performed to quantify GFAP immunoreactivity (A), mean cell area (B), mean cell perimeter (C) and the soma:cell ratio (D). Data are expressed as mean ± SEM, n=6 coverslips per treatment group from 4 independent experiments. ***P<0.001, *P<0.05 vs. control DMEM, $^{+++}$P<0.001, $^{++}$P<0.01, $^{+}$P<0.05 vs. IFNγ (Newman-Keuls *post hoc* test)

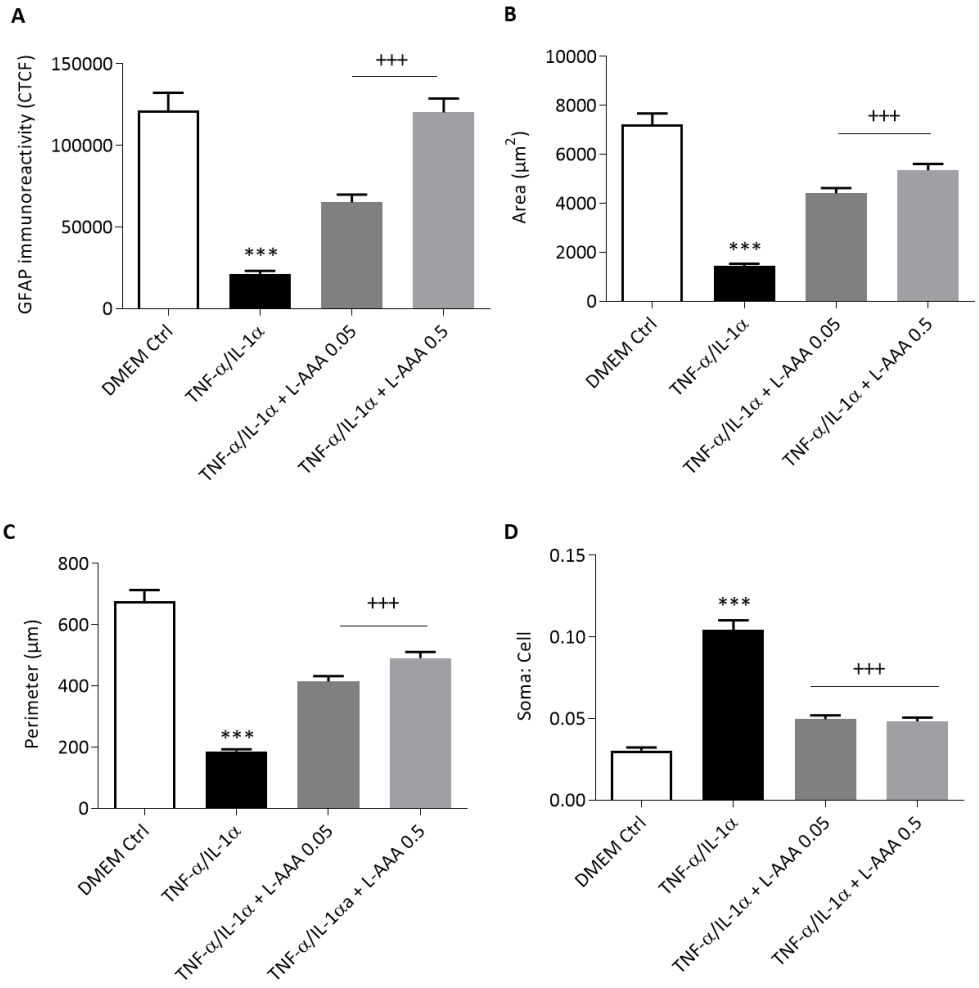

Figure 5.6 L-AAA attenuates TNF-α and IL-1α-induced changes in GFAP immunoreactivity and astrocyte morphology.

Primary cortical astrocytes (DIV 14) were treated with TNF-α (30 ng/mL), IL-1α (3 ng/mL) and L-AAA (0.05, 0.5 mM) for 24 hours before fixation and GFAP immunocytochemistry. Morphological analysis was performed to quantify GFAP immunoreactivity (A), mean cell area (B), mean cell perimeter (C) and the soma:cell ratio (D). Data are expressed as mean ± SEM, n=6 coverslips per treatment group from 4 independent experiments. ***P<0.001 vs. control DMEM, $^{+++}$P<0.001 vs. TNF-α/IL-1α (Newman-Keuls *post hoc* test).

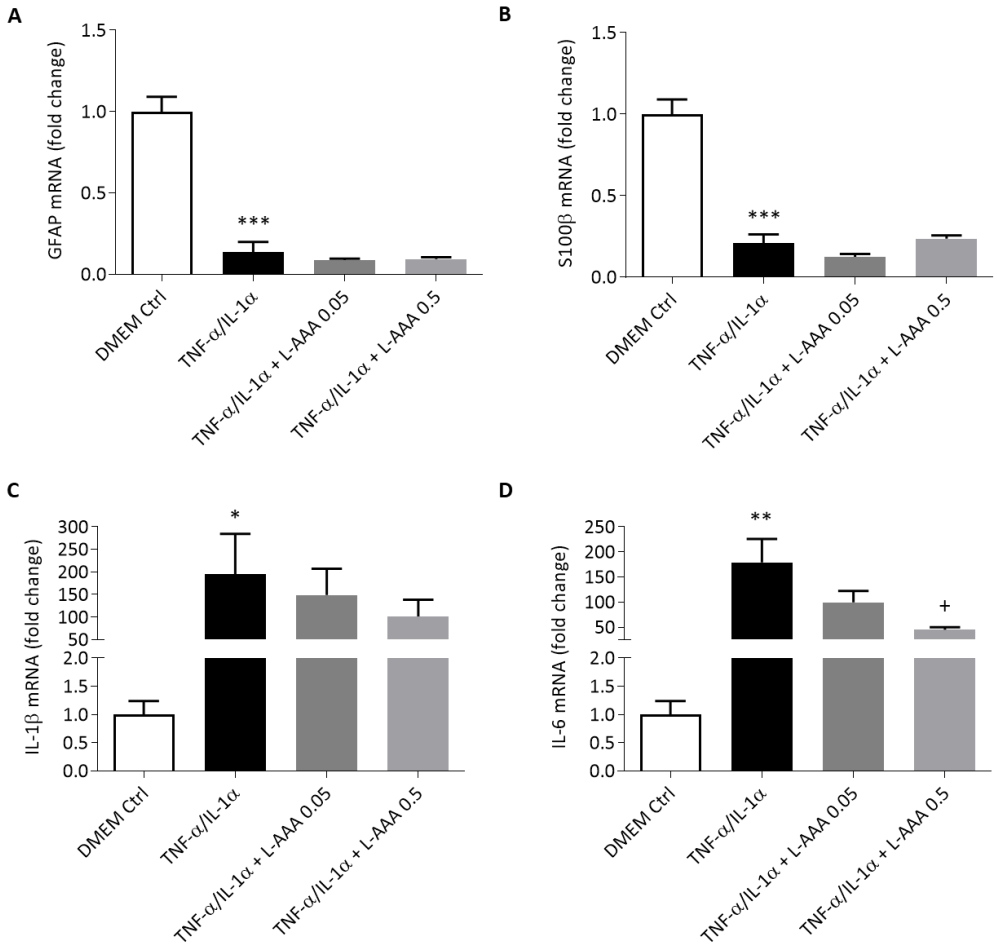

Figure 5.7 L-AAA has no effect on TNF-α and IL-1α-induced changes in the mRNA expression of GFAP, S100β, IL-1β, and IL-6 in primary cortical astrocytes.
Primary cortical astrocytes (DIV 14) were treated with TNF-α (30 ng/mL), IL-1α (3 ng/mL) and L-AAA (0.05, 0.5 mM) for 24 hours. Cells were harvested for RNA extraction followed by RT-PCR to analyse the expression of GFAP (A), S100β (B), IL-1β (C) and IL-6 (D). Data are expressed as mean ± SEM, n=8 wells per treatment group from 4 independent experiments. ***P<0.001, **P<0.01, *P<0.05 vs. control DMEM, $^{+}$P<0.05 vs. TNF-α/IL-1α (Newman-Keuls *post hoc* test).

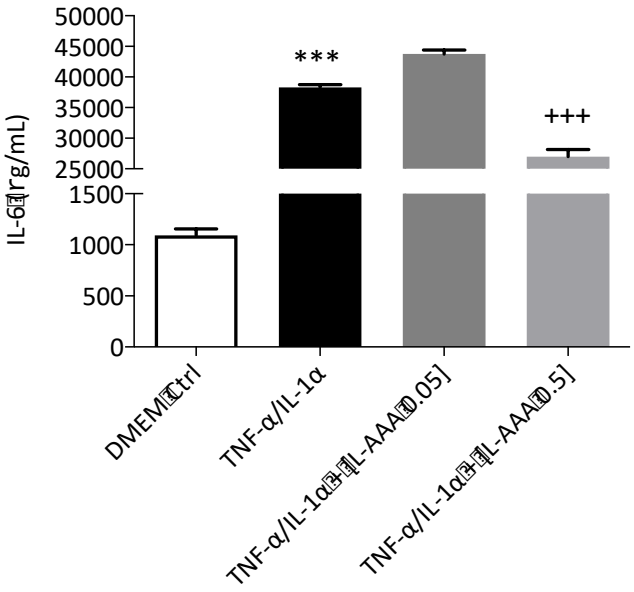

Figure 5.8 L-AAA attenuates TNF-α and IL-1α-induced release of IL-6 protein from primary cortical astrocytes.

Primary cortical astrocytes (DIV 14) were treated with TNF-α (30 ng/mL), IL-1α (3 ng/mL) and L-AAA (0.05, 0.5 mM) for 24 hours. Supernatants were collected for analysis of IL-6 protein release by ELISA. Data are expressed as mean ± SEM, n=8 wells per treatment group from 4 independent experiments. ***P<0.001 vs. control DMEM, $^{+++}$P<0.001 vs. TNF-α/IL-1α (Newman-Keuls *post hoc* test).

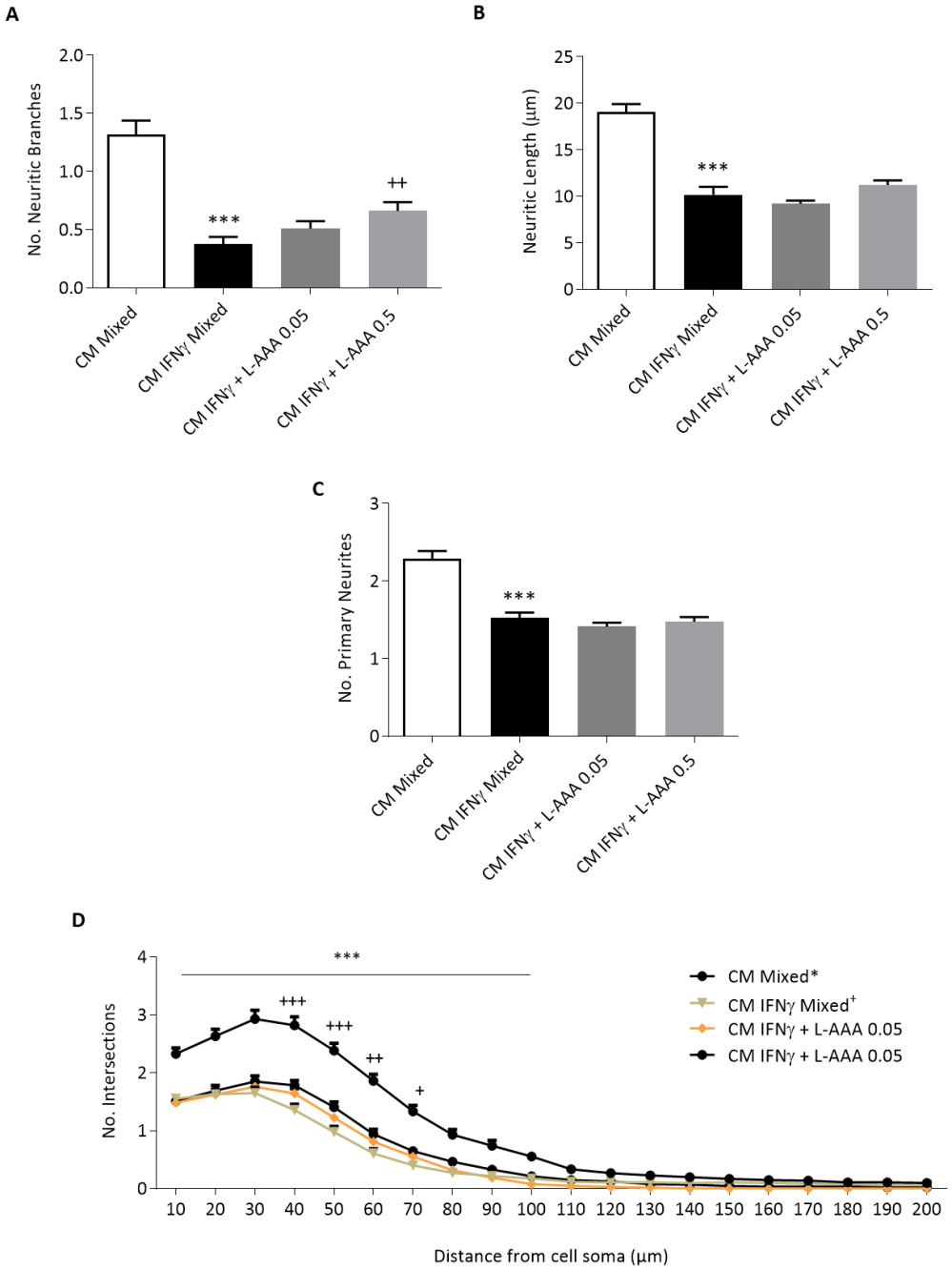

Figure 5.9 L-AAA slightly attenuates reductions in the complexity of immature neurons induced by conditioned media from IFNγ treated mixed glia.

Primary cortical mixed glia (DIV 14) were treated with IFNγ (10 ng/mL) and L-AAA (0.05, 0.5 mM) for 24 hours. The resulting conditioned media was collected and applied to immature (DIV 3) primary cortical neurons for 24 hours before fixation and β-III tubulin immunocytochemistry. Sholl analysis was performed to analyse the number of neuritic branches (A), neuritic length (B), number of primary neurites (C), and the Sholl profile (D). Data are expressed as mean ± SEM, n=5 coverslips per treatment group from 5 independent experiments. ***P<0.001 vs. control conditioned media. $^{+++}$P<0.001, $^{++}$P<0.01, $^{+}$P<0.05 vs. CM IFNγ Mixed (Newman-Keuls *post hoc* test).

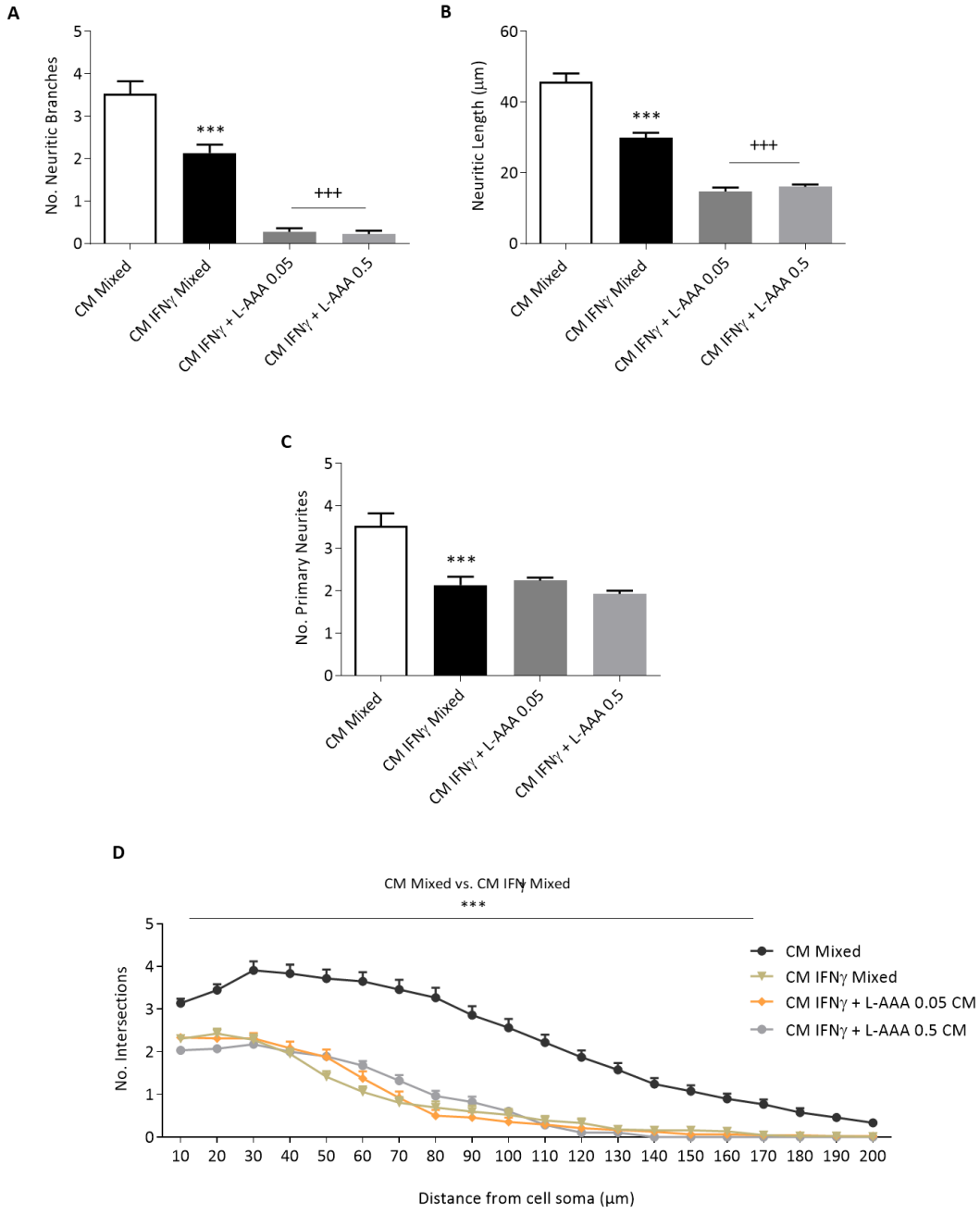

Figure 5.10 L-AAA has no effect on reductions in the complexity of mature neurons induced by conditioned media from IFNγ treated mixed glia.
Primary cortical mixed glia (DIV 14) were treated with IFNγ (10 ng/mL) and L-AAA (0.05, 0.5 mM) for 24 hours. The resulting conditioned media was collected and applied to mature (DIV 21) primary cortical neurons for 24 hours before fixation and MAP2 immunocytochemistry. Sholl analysis was performed to analyse the number of neuritic branches (A), the neuritic length (B), the number of primary neurites (C), and the Sholl profile (D). Data are expressed as mean ± SEM, n=8 coverslips per treatment group from 4 independent experiments. ***P<0.001 vs. CM Mixed, $^{+++}$P<0.001 vs. CM IFNγ Mixed (Newman-Keuls *post hoc* test).

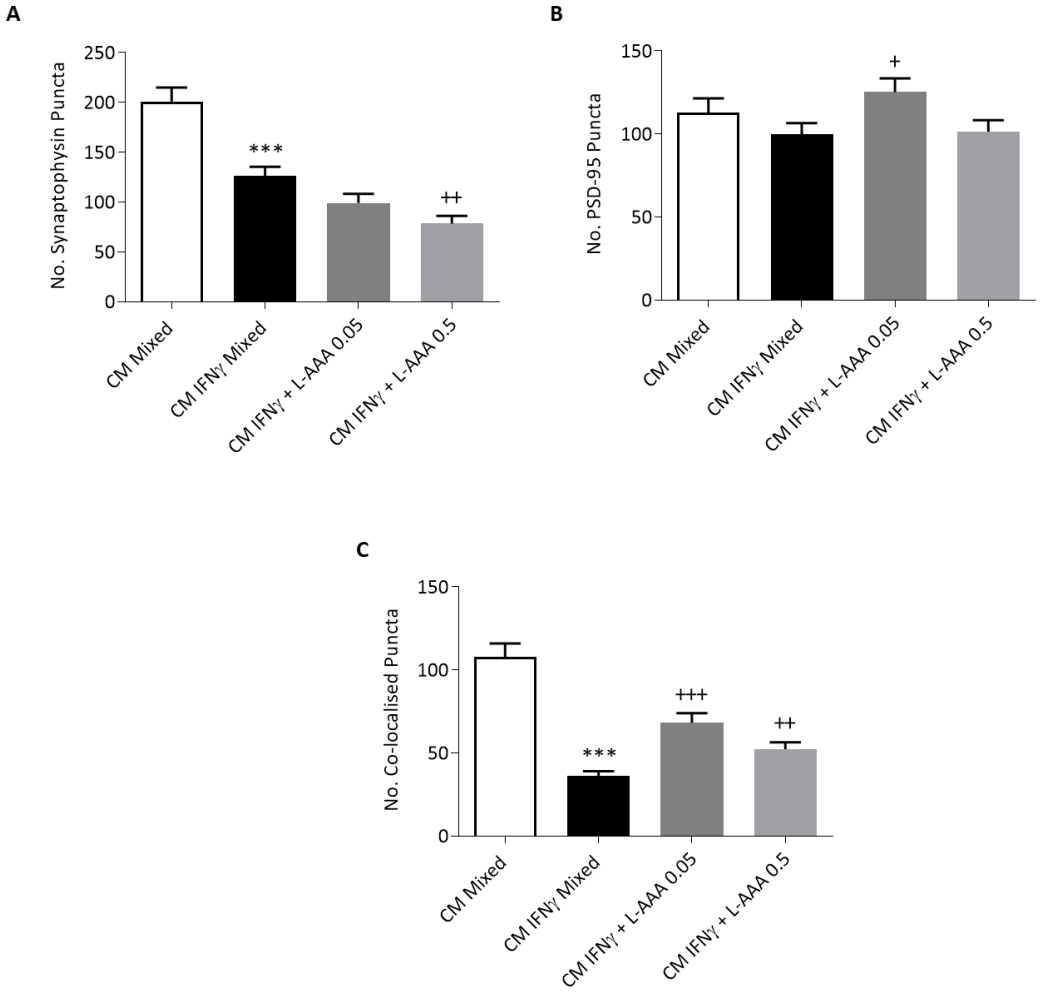

Figure 5.11 Effect of L-AAA on reductions in the co-localisation of synaptic proteins in mature primary cortical neurons induced by conditioned media from IFNγ treated mixed glia.

Primary cortical mixed glia (DIV 14) were treated with IFNγ (10 ng/mL) and L-AAA (0.05, 0.5 mM) for 24 hours. The resulting conditioned media was collected and applied to mature (DIV 21) primary cortical neurons for 24 hours before fixation and immunocytochemistry to quantify the number of synaptophysin puncta (A), PSD-95 puncta (B), and co-localised synaptic puncta (C). Data are expressed as mean ± SEM, n=6 coverslips per treatment group from 4 independent experiments. ***P<0.001, vs. CM Mixed, $^{+++}$P<0.001, $^{++}$P<0.01, $^{+}$P<0.05 vs. CM IFNγ Mixed (Newman-Keuls *post hoc* test).

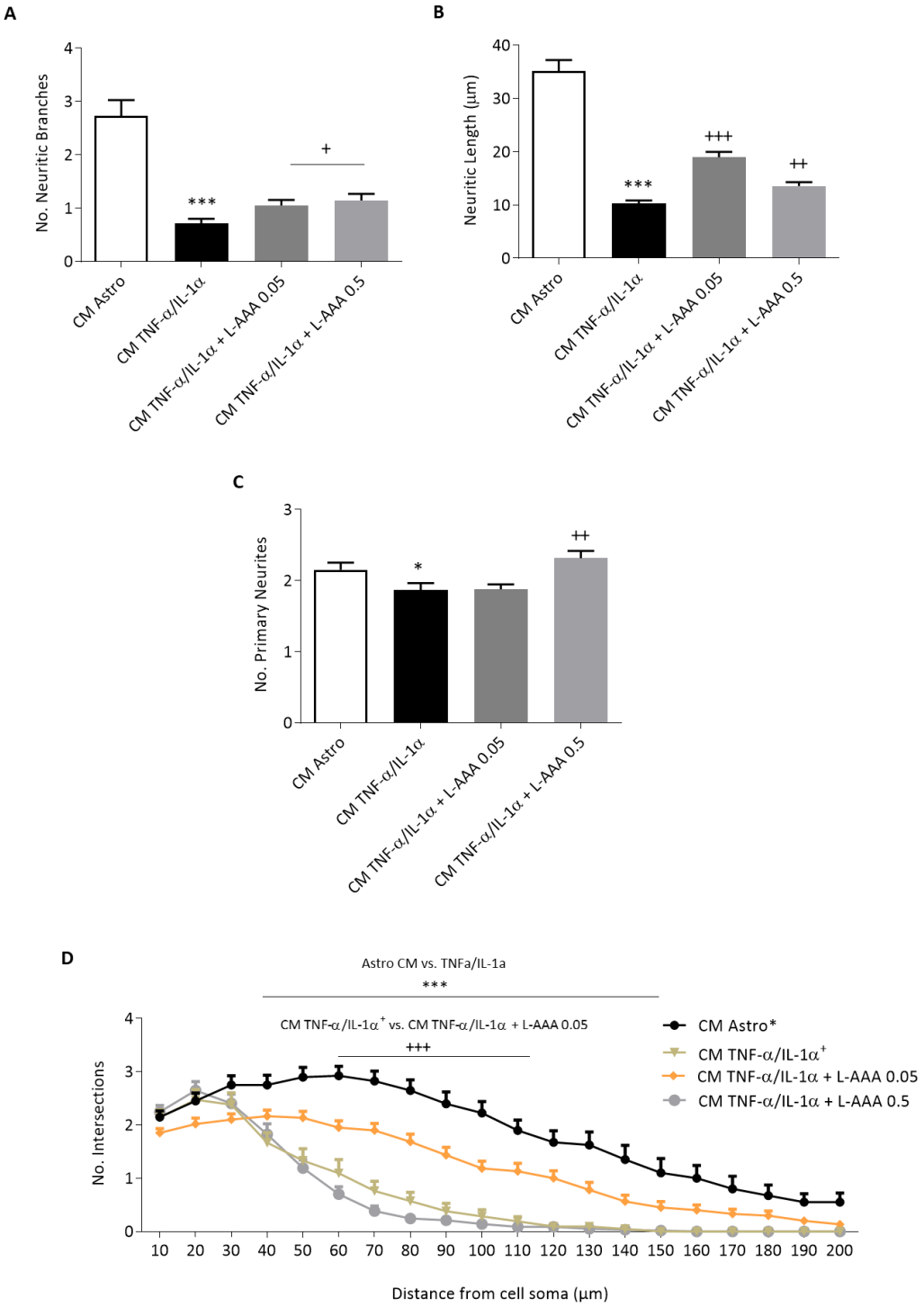

Figure 5.12 L-AAA partially rescues reductions in neuronal complexity induced by conditioned media from TNF-α and IL-1α treated astrocytes.
Primary cortical astrocytes (DIV 14) were treated with TNF-α (30 ng/mL), IL-1α (3 ng/mL) and L-AAA (0.05, 0.5 mM) for 24 hours. The resulting conditioned media was collected and applied to mature (DIV 21) primary cortical neurons for 24 hours before fixation and MAP2 immunocytochemistry. Sholl analysis was performed to analyse the number of neuritic branches (A), the neuritic length (B), the number of primary neurites (C), and the Sholl profile (D). Data are expressed as mean ± SEM, n=6 coverslips per treatment group from 4 independent experiments. ***P<0.001, *P<0.05 vs. CM Astro, $^{+++}$P<0.001, $^{++}$P<0.01, $^{+}$P<0.05 vs. CM TNF-α/IL-1α (Newman-Keuls *post hoc* test).

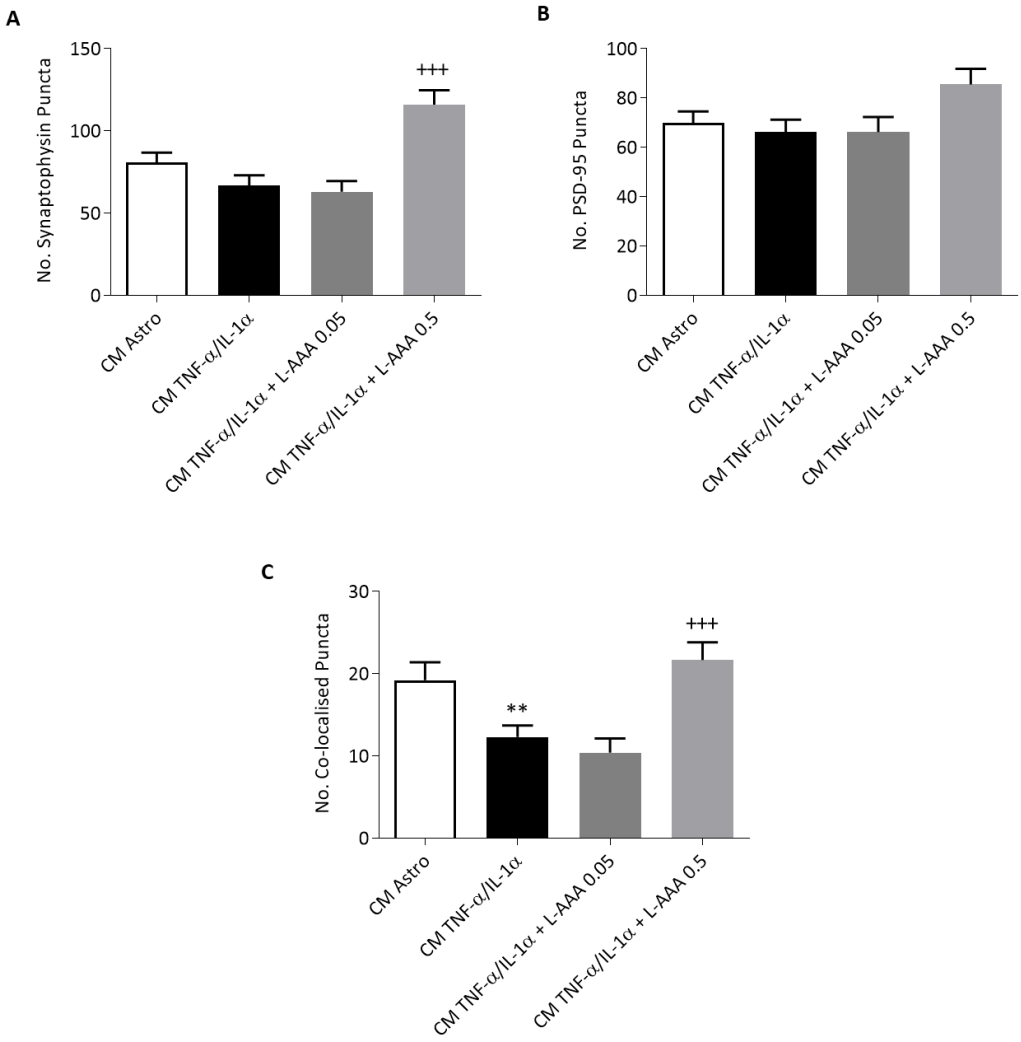

Figure 5.13 L-AAA attenuates reductions in synaptic protein co-localisation in mature primary cortical neurons induced by conditioned media from TNF-α and IL-1α treated astrocytes.

Primary cortical astrocytes (DIV 14) were treated with TNF-α (30 ng/mL), IL-1α (3 ng/mL) and L-AAA (0.05, 0.5 mM) for 24 hours. The resulting conditioned media was collected and applied to mature (DIV 21) primary cortical neurons for 24 hours before fixation and immunocytochemistry to quantify the number of synaptophysin puncta (A), PSD-95 puncta (B), and co-localised synaptic puncta (C). Data are expressed as mean ± SEM, n=6 coverslips per treatment from 4 independent experiments. **P<0.01 vs. CM Astro, $^{+++}$P<0.001 vs CM TNF-α/IL-1α (Newman-Keuls *post hoc* test).

5.4 Discussion

There is intense interest in understanding the cellular and molecular mechanisms that regulate the initiation and progression of CNS inflammation. In particular, there is increasing recognition that microglia and astrocytes play essential roles in propagating and amplifying pro-inflammatory signals. Microglia are the reputed sensors of damage and initiators of multicellular pro-inflammatory signalling. More recently, astrocytes have emerged as cells that elicit potent pro-inflammatory signalling and responses.

As microglia are considered the first responses in inflammation it is not surprising that microglial activation has become recognised as a target to prevent/delay symptoms associated with inflammation. Research suggests that commercially available selective serotonin reuptake inhibitors (SSRIs) suppress microglial responses to inflammatory stimuli. Fluoxetine, sertraline, paroxetine, fluvoxamine and citalopram attenuate LPS-induced microglial production of TNF-α in BV-2 microglia, suggesting that inhibition of microglial activation produces an anti-inflammatory effect (Tynan et al, 2012). More recently, the antibiotic minocycline has been identified as an inhibitor of microglial activation and has been shown to prevent neuropathic pain in animal models of inflammatory bowel disease (Kannampalli et al, 2014) and inflammatory associated pain in chronic prostatitis in mice (Deng et al, 2019). It is also reported to reduce levels of pro-inflammatory cytokines and improves adult neurogenesis in the rat hippocampus (Wadhwa et al, 2017).

Targeting inflammatory-reactive astrocytes is a less common strategy and studies investigating this approach are limited. One previous study investigated a combination of the μ-opioid antagonist naloxone, μ-opioid agonist linalool, and the anti-epileptic agent levetiracetam for its capacity to prevent astrocytes becoming inflammatory-reactive and to restore inflammatory dysregulated cellular changes. The drug combination prevented inflammatory dysregulation of primary cortical astrocytes *in vitro* as demonstrated by an attenuation of LPS-induced alterations in glutamate-evoked Ca^{2+} signalling and reorganisation of actin filaments (Hansson et al, 2016).

The astrocyte toxin L-AAA has also been investigated for its potential to protect against inflammatory-reactive astrocyte responses *in vivo*. The protective effect of L-AAA has been investigated in pain hypersensitivity where it has been employed as a tool to demonstrate that astrocyte activation is a major cause of persistent pain in prostatitis (Deng et al, 2019). Intrathecal injection of L-AAA has shown to effectively alleviate symptoms of mechanical allodynia at 5 weeks after chronic prostatitis/chronic pelvic pain syndrome indicating that spinal astrogliosis is the major cause of persistent mechanical allodynia. This study is among the first to investigate the effects of L-AAA in dysregulating disease salient responses associated with inflammatory-reactive astrocytes. It extends on previous findings by exploring the potential for L-AAA-induced astrocyte impairment as a method of protection against reactive glial associated mechanisms of neuronal atrophy *in vitro*. It also identifies how L-AAA affects the gene expression profile of reactive astrocytes shedding light on the potential mediators involved in inflammatory-driven glial interactions.

5.4.1 Effect of L-AAA and IFNγ on the mRNA expression of inflammatory markers and their release in mixed glia

L-AAA had no effect on IFNγ-induced decrease in TNF-α , or IFNγ-induced increase in IL-1α. Chapter 4 demonstrated that TNF-α and IL-1α are primarily produced from IFNγ activated microglia. These results further suggest that IL-1α and TNF-α are mainly derived from microglia. L-AAA-induced astrocyte impairment would be expected to reduce the expression and release of these proteins in the case of reactive astrocytes contributing to their production.

L-AAA exacerbated IFNγ-induced increase in the expression of IL-1β at the lower concentration. This is somewhat surprising as it suggests synergy of IFNγ and L-AAA in terms of IL-1β expression. As IL-1β is a potent pro-inflammatory cytokine that is primarily produced by microglia and invading monocytes/macrophages (Boato et al, 2011), it also suggests that the source of IL-1β in these cultures is derived principally microglial cells.

L-AAA (0.5 mM) attenuated IFNγ-induced increase in the mRNA expression of IL-6. This is as expected given that IL-6 is released from both activated microglia

and astrocytes (Wang et al, 2015). Chapter 4 demonstrated that activated astrocytes release large amounts of IL-6. It is thus probable that L-AAA reduced the release of IL-6 derived from activated astrocytes but had no effect on the release of IL-6 from activated microglia.

Similarly, L-AAA slightly increased IFNγ-induced increase in TNF-α protein release, however the higher concentration of L-AAA (0.5 mM) attenuated IFNγ-induced increase in IL-1α. This suggests that IFNγ-induced release of TNF-α is primarily mediated by microglia and astrocytes may contribute more to the production of IL-1α. By contrast, the lower concentration of L-AAA (0.05 mM) partially attenuated IFNγ-induced increase in the release of IL-6 protein and the higher concentration of L-AAA (0.5 mM) provided complete protection and reduced levels of IL-6 back to control. This suggests that astrocytes are primarily responsible for IFNγ mediated release of IL-6 from mixed glial cultures.

5.4.2 L-AAA has no effect on IFNγ-induced changes in the mRNA expression of TNF-α, IL-1α and Iba1 in primary cortical microglia

Co-treatment of primary cortical microglia with L-AAA and IFNγ had no effect on the mRNA expression of the inflammatory markers TNF-α, IL-1α or Iba1. These results are as expected given the established role for L-AAA as an astrocyte toxin and provide confirmation that L-AAA does not evoke changes in the expression of traditional, pro-inflammatory microglial markers. Furthermore, they are in line with previous *in vivo* findings demonstrating that L-AAA reduces the number of GFAP+ astrocytes but has no effect on microglial activation, Iba1 immunoreactivity or the number of Iba1+ cells in the substantia nigra of rats following LPS-induced neurotoxicity (O'Neill et al, 2019).

5.4.3 L-AAA has no effect on IFNγ-induced changes the mRNA expression of GFAP, S100β, IL-1β and IL-6 in primary cortical astrocytes

L-AAA had no effect on IFNγ-induced reductions in the mRNA expression of GFAP or S100β. As L-AAA and IFNγ reduced GFAP and S100β expression when applied to astrocytes alone, it is not surprising that they produced a similar decrease when applied in combination. Similarly, L-AAA had no effect on IFNγ-induced increase in the mRNA expression of IL-1β. Again, given that both L-AAA and IFNγ

increased IL-1β alone, it is not surprising that a similar increase was observed following co-treatment with L-AAA and IFNγ. While L-AAA had no effect on IL-6 alone, IFNγ significantly increased its expression and co-treatment with L-AAA had no effect on this increase. This is particularly interesting given that chapter 2 demonstrated an important role from IL-6 in driving neuronal trophy and synapse loss under inflammatory conditions.

5.4.4 Effect of L-AAA on IFNγ-induced changes in GFAP immunoreactivity and astrocyte morphology

L-AAA reversed IFNγ-induced increase in GFAP immunoreactivity and produced a complete reduction of this marker. L-AAA and IFNγ had no effect on the soma:cell ratio. As demonstrated in Chapter 3, higher concentrations of L-AAA reduce GFAP immunoreactivity in enriched astrocyte cultures. It is therefore not surprising that L-AAA protected against IFNγ-induced increases in GFAP immunoreactivity pushing levels lower than control.

L-AAA had no effect on IFNγ-induced reductions in astrocyte mean cell, or cell perimeter. This is not surprising given that L-AAA also reduced the area and perimeter of astrocytes in a concentration-related fashion when applied to astrocytes alone. Co-treatment with L-AAA had no effect on astrocyte morphology indicating that IFNγ-induced changes in astrocyte morphology are not affected by mechanisms of L-AAA-induced astrocyte impairment.

5.4.5 L-AAA attenuates TNF-α and IL-1α-induced changes in GFAP immunoreactivity and astrocyte morphology

Conditioned media from IFNγ treated mixed glia and microglia contains a plethora of pro-inflammatory cytokines, chemokines, and reactive oxidants (Lehnardt, 2010) as well as unknown factors which may both directly damage neurons and directly affect astrocytes. As such, in order to examine the impact of L-AAA-induced astrocyte impairment following inflammatory driven microglia activation, it was of interest to explore the effect of L-AAA on two cytokines which have been identified in the conditioned media of activated microglia. TNF-α and IL-1α have been identified as factors released by activated microglia into the surrounding conditioned media that induce a reactive astrocytic phenotype

(Liddelow et al, 2017). Chapter 4 also demonstrated that these factors are released from IFNγ activated microglia. Thus, as L-AAA, TNF-α and IL-1α act directly on astrocytes it was of interest to next explore this interaction in enriched astrocytic cultures.

L-AAA attenuated reductions in GFAP immunoreactivity, mean cell area and mean cell perimeter induced by TNF-α and IL-1α. L-AAA also attenuated the decrease in the soma:cell ratio induced by TNF-α and IL-1α indicating a protective effect for L-AAA and an attenuation of astrocyte reactivity. These results highlight the potential for reversing changes in astrocyte morphology and reactivity induced by factors released from activated microglia.

5.4.6 L-AAA attenuates TNF-α and IL-1α-induced increase in the mRNA expression and release of IL-6 protein from primary cortical astrocytes

L-AAA had no effect on TNF-α and IL-1α-induced reductions in the mRNA expression of GFAP and S100β. Results from chapter 3 demonstrate that L-AAA reduces GFAP immunoreactivity and the mRNA expression of both GFAP and S100β in primary astrocyte cultures when applied to astrocytes directly. Thus, while initial expectations were that L-AAA may prevent TNF-α and IL-1α-induced changes in the expression of astrocytic markers, it is not surprising that it shifted expression levels towards the same direction that it did both in the presence and absence of inflammatory stimuli. Previous *in vivo* studies concur with these findings as they also demonstrate that L-AAA exerts a prominent depletion of GFAP and S100β *in vivo* (Khurgel et al, 1996). However, these results differ to more recent results observed *in vivo* where the inflammatory stimulus LPS-induced an increase in both GFAP+ reactive astrogliosis and an increase in S100β expression levels (O'Neill et al, 2019), both of which were attenuated by co-injection with L-AAA. Taken together these findings suggest that the effect of activated microglial on astrocyte reactivity varies to some extent *in vivo* and *in vitro*. They also suggest that L-AAA confers a stabilising effect whereby it reverses inflammatory-induced changes in astrocyte morphology and GFAP immunoreactivity *in vitro*.

L-AAA had no effect on TNF-α and IL-1α-induced increase in the mRNA expression of IL-1β, however it did attenuate TNF-α and IL-1α-induced increase in expression of IL-6. Similarly, L-AAA attenuated TNF-α and IL-1α-induced increase in the release of IL-6 protein from astrocytes and in a concentration-related fashion. Chapter 4 demonstrated that elevated levels of IL-6 reduce neuronal complexity and synapse formation. Thus, it is likely that the L-AAA mediated reductions in astrocytic IL-6 under inflammatory conditions may translate into neuroprotective and synaptogenic effects on neurons. Resultantly, the next step sought to investigate if L-AAA, when combined with conditioned media from IFNγ treated mixed glia or conditioned media from TNF-α and IL-1α treated astrocytes can provide neuroprotection against these inflammatory stimuli.

5.4.7 Effect of L-AAA on reductions in neuronal complexity and co-localisation of synaptic proteins induced by conditioned media from IFNγ treated mixed glia

Results of this study show that conditioned media from IFNγ treated mixed glia reduces complexity in immature neuronal cultures and conditioned media from mixed glia co-treated with IFNγ and L-AAA confers no protection. Conditioned media from mixed glia co-treated with IFNγ and L-AAA provided some protection against reductions in the number of neuritic branches induced by conditioned media from IFNγ treated mixed glia alone but had no effect on any other measures of complexity.

Similarly, conditioned media from IFNγ treated mixed glia reduced all measures of neuronal outgrowth in mature neuronal cultures and conditioned media from mixed glia co-treated with IFNγ and L-AAA confers no protection. Conditioned media from mixed glia co-treated with IFNγ and L-AAA had no protective effect on neuronal complexity and actually exacerbated reductions in the number of neuritic branches and neuritic length induced by conditioned media from IFNγ treated mixed glia alone. These results are surprising given that astrocytes make up approximately 70% of these primary mixed glial cultures (McNamee et al, 2010b) and L-AAA would be expected to reduce the levels of pro-inflammatory markers released from reactive astrocytes corollary to astrocytic impairment.

In terms of synaptic protein co-localisations, conditioned media from mixed glia co-treated with IFNγ and L-AAA attenuated reductions in the number of synaptic protein co-localisations induced by conditioned media from IFNγ treated mixed glia alone. This suggests that reactive astrocytes contribute to the reduction in synaptic markers induced by IFNγ signalling in glia.

These results show that IFNγ mediated activation of microglia continues to drive neuronal atrophy and synapse loss in the presence of L-AAA. This suggests that IFNγ-induced inflammatory driven neuronal atrophy and synapse loss is primary mediated via activated microglia. It indicates that there are other factors at play driving inflammatory neuronal atrophy in addition to reactive astrocytes. These results are surprising given that it has been previously shown that inflammatory activated microglia release factors into the conditioned media that drive a reactive astrocyte phenotype and L-AAA has been shown to impair astrocytic function. Chapter 4 identified TNF-α and IL-1α as factors released from activated microglia which induce a reactive, neurotoxic astrocytic phenotype. It may be that as microglia represent the first responders to inflammatory stimuli, astrocytes respond sequentially to the release of microglial associated factors. Thus, as both L-AAA, TNF-α and IL-1α act directly on astrocytes it was of interest to next explore this interaction in enriched astrocytic cultures.

5.4.8 L-AAA attenuates reductions in neuronal complexity and synaptic protein co-localisations in mature neurons induced by conditioned media from TNF-α and IL-1α treated astrocytes

Results of this study show that conditioned media from TNF-α and IL-1α treated astrocytes reduces all measures of neuronal outgrowth and co-treatment of astrocytes with L-AAA attenuating these reductions. Conditioned media from astrocytes co-treated with TNF-α/IL-1α and L-AAA increased the number of neuritic branches, neuritic length, and number of primary neurites compared to conditioned media from TNF-α and IL-1α astrocytes alone. These results suggest that L-AAA-induced astrocyte impairment protects against TNF-α and IL-1α-induced reactive astrocyte associated neuronal atrophy. These results are similar to those found *in vivo* whereby simultaneous intra-nigral injection of L-AAA abrogated LPS-induced loss of tyrosine hydroxylase-positive (TH+) dopamine

neurons in the substantia nigra and degeneration of TH+ dopaminergic nerve terminals in the striatum of rodents (O'Neill et al, 2019). Taken together they suggest that L-AAA-induced astrocyte impairment represents a novel mechanism through which inflammatory driven glial associated neuronal atrophy may be prevented.

In terms of synaptic protein co-localisations, conditioned media from astrocytes co-treated with TNF-α/IL-1α and L-AAA conferred protection against reductions in co-localised synaptic puncta induced by conditioned media from TNF-α and IL-1α treated astrocytes alone. These results are not surprising given that L-AAA also protected against reductions in neuronal complexity induced by conditioned media from TNF-α and IL-1α treated astrocytes alone. Alterations in neuronal complexity often translate to similar changes in synapse formation given that neuronal complexity maps potential points of contact for synapse development.

L-AAA protected against TNF-α and IL-1α-induced changes in astrocyte morphology including a reduction in mean cell area, perimeter and GFAP immunoreactivity, and an increase in the soma:cell ratio. L-AAA also protected against TNF-α and IL-1α-induced expression and release of IL-6. Taken together, L-AAA mediated reversal in changes in astrocytic morphology, immunoreactivity or production of IL-6 may account, at least in part, for the protective effects of L-AAA in the conditioned media studies where co-treatment of astrocytes with L-AAA and TNF-α/IL-1α attenuated the negative effects induced by conditioned media from TNF-α and IL-1α treated astrocytes alone. Chapter 4 demonstrated that elevated levels of IL-6 reduce neuronal complexity and synapse formation *in vitro*. Thus, it is likely that the L-AAA-induced reductions in astrocytic IL-6 account somewhat for the protective effect of L-AAA under TNF-α/IL-1α mediated inflammatory conditions *in vitro*.

5.5 Conclusion

This study provides insight to the effect of L-AAA-induced astrocyte impairment on primary cortical neuronal cultures *in vitro* during various inflammatory stimuli. While it is the first of this type of study to be carried out *in vitro*, these findings concur with previous reports outlining the protective effect of astrocyte impairment in inflammatory driven, glial associated mechanisms of neuronal atrophy *in vivo* (O'Neill et al, 2019). While most research to date focuses on the supportive neurotrophic and synaptogenic properties of astrocytes this is one of the first studies outlining a role for L-AAA-induced astrocyte impairment in the regulation of reactive glial cross talk and associated mechanisms effecting neuronal integrity.

Chapter 4 identified TNF-α and IL-1α as factors released from activated microglia, which induce a reactive, neurotoxic astrocytic phenotype. Thus, as both TNF-α and IL-1α act directly on astrocytes, it was of interest to explore this interaction in enriched astrocytic cultures in more detail in order to tease out a role for L-AAA in response to the release of known factors from activated microglia.

Results of the current investigation firstly demonstrate that L-AAA exerts a selective toxicity in astrocytes under inflammatory conditions which involves alterations in astrocyte morphology, immunoreactivity and gene expression profile of inflammatory markers. They highlight the importance of reactive glial associated mechanisms in driving neuronal atrophy and synapse loss and suggest that disrupting pro-inflammatory cross talk between glia cells may be protective against inflammatory-induced deficits in neuronal circuitry and connectivity. This work provides further validation for the use of L-AAA as a tool to induce selective astrocytic impairment *in vitro* and demonstrates that withdrawal of reactive astrocytic feedback may provide protection in inflammatory conditions associated with reactive astrocyte-microglia cross talk.

6 Kynurenic acid protects against reactive glial-associated reductions in the complexity of primary cortical neurons

6.1 Introduction

The kynurenine pathway (KP) is a tryptophan-metabolising pathway that is highly regulated by the immune system and drives metabolite production in glial compartments (Braidy & Grant, 2017; Glass et al, 2010a; O'Farrell & Harkin, 2015). Induced by stress and inflammatory stimuli, the KP is associated with inflammatory-driven astrocytic and microglial activation. Altered KP activation has been recognised as a hallmark of several neurological disorders that exhibit an underlying neuro-inflammatory phenotype (Glass et al, 2010). In particular, it has been implicated in the pathophysiology of multiple CNS disorders ranging from neuropsychiatric disorders such as depression (Bohar et al, 2015; Karakuła-juchnowicz et al, 2015; Réus et al, 2015b) to neurodegenerative disorders such as AD, PD, multiple sclerosis and stroke (Cuartero et al, 2014; Maddison & Giorgini, 2015; Tan et al, 2012b).

KP metabolites are known to influence neuronal viability, outgrowth and complexity. Direct application of the KP metabolites 3-hydroxyanthranilic acid, 3-hydroxykynurenine and quinolinic acid to primary cortical neurons are reported to reduce neuronal outgrowth, complexity and synapse formation *in vitro* (O'Farrell et al, 2017). Previous work in the lab demonstrates that activation of the KP and its metabolites have significant roles in regulating neuronal atrophy and further proposed that a KP related intervention might be an attractive and effective approach to ameliorating degenerative brain diseases (O'Farrell, 2016b; O'Farrell et al, 2017). Nevertheless, a consolidated picture and understanding of this complex crosstalk between KP metabolites and neurons is currently lacking.

In light of these preliminary findings, this chapter examines the role of inflammatory-driven KP activation on neuronal complexity and synapse formation in mature primary cortical neurons. It also investigates the potential for KP modulation as a strategy to protect against inflammatory-mediated, glial-associated mechanisms of neuronal atrophy and synapse loss characteristic to CNS disorders associated with KP dysfunction (Jones et al, 2015).

Chapter 4 of this thesis demonstrated that TNF-α and IL-1α are released from IFNγ-activated microglia. It also showed that TNF-α and IL-1α-induced an

increase in the expression and release of astrocytic IL-6, which in elevated concentrations causes neuronal atrophy and synapse loss in mature primary cortical neuronal cultures. In addition to IL-6 acting directly on neurons, it is also possible that IL-6 feedbacks and stimulates microglia to release pro-inflammatory cytokines and proteins implicated in cell death signalling pathways (Wang et al, 2015). IL-6 has also been implicated in the activation of the KP.

IL-6 has been shown to activate the KP as evidenced by an increased cell media concentration of KYNA following direct application of IL-6 to cultured human astrocytes (Schwieler et al, 2015). IL-6 has also been shown to increase the expression of the rate limiting KP enzyme IDO both *in vitro* following application of IL-6 to Neuro2a cells and *in vivo* following intra-hippocampal administration of IL-6 to rats (Kim et al, 2012). Furthermore, increased levels of IL-6 in the cerebrospinal fluid (CSF), blood, and post-mortem brains (Bergmans et al, 2019; Gananca et al, 2016), along with elevated plasma levels of L-kynurenine (Sublette et al, 2011) and quinolinic in the CSF (Erhardt et al, 2013), have been reported in suicidal individuals accentuating an important link between neuroinflammation, IL-6 signalling, KP activation and neuropsychiatric disorders.

Chapter 4 and 5 demonstrated that manipulation of glial-derived inflammatory systems provides an approach to attenuating inflammation-associated neuronal atrophy and toxicity. This chapter further extends these findings to examine how targeting the KP may protect against inflammatory-induced neuronal atrophy and synapse loss in mature primary cortical neurons *in vitro*. The potential for the putative neuroprotective metabolite KYNA to protect against these alterations will be explored.

6.1.1 Progression from the BV-2 microglial cell line to primary microglia cultures

Earlier experiments in the lab employed an immortalised murine microglial cell line (BV-2) to investigate a role for the KP in mediating reactive microglial associated reductions in neuronal complexity of immature primary cortical neurons. BV-2 cells are murine microglial cell lines immortalised after infection with a v-raf/vmyc recombinant retrovirus. They express the nuclear v-myc and

the cytoplasmic v-raf oncogene products and the env gp70 antigen on their cell surface. BV-2 cells grow in semi-adherent cultures and express similar characteristics and functionality to that of cultured microglial cells (Bocchini et al, 1992). The use of BV-2 cells aimed to ensure the purity of microglial cells and permitted identification of mediators responsible for BV-2 microglial-induced changes in neuronal viability and complexity.

Previous work in the lab has demonstrated a role for KP activation in microglia-mediated impairment of neurite outgrowth and complexity. Conditioned media from IFNγ-stimulated BV-2 microglia reduced neurite outgrowth and complexity which was prevented by pre-treatment with the IDO inhibitor, 1-methyltryptophan (1-MT) (L), the KMO inhibitor, Ro 61–8048 or the NMDAR antagonist MK801. These findings are in line with previous studies demonstrating that IFNγ-mediated activation of BV-2 microglia induces mRNA expression of the KP enzymes IDO, KMO and KYNU (Chen, Brew, & Guillemin, 2011; Guillemin, Smythe, et al., 2005). These results are also in line with previous research demonstrating the neurotoxic capacity of conditioned media from LPS and IFNγ-activated BV-2 microglia which is likely due to the production and release of microglial factors (Kim et al, 2007).

BV-2 cells respond to LPS in a similar fashion to primary microglia with a 90% overlap in gene expression. However, this response is inferior to that seen with mouse primary microglia (Henn et al, 2009). Furthermore, BV-2 responses to LPS have been found to be inconsistent compared to those of rat primary microglia with respect to inflammatory cytokine release and Iba1 expression (Horvath et al, 2008). Hence, the potential for BV-2 cells to accurately represent primary microglia remains unclear (Butovsky et al, 2014; Henn et al, 2009; Horvath et al, 2008) and BV-2 cells were deemed to be an inadequate model for assessing inflammatory-driven primary microglial responses. This resulted in a move towards the use of primary mixed glial cultures and enriched astrocytic and microglial cultures to investigate the effect of KP activation in glial compartments and resultant effects of glial conditioned media on neuronal integrity.

6.1.2 The Kynurenine pathway – previous findings and existing data

Preliminary experiments have shown that stimulation of mixed glia with the pro-inflammatory cytokine IFNγ induces the expression of IDO and reduces tryptophan concentration in the conditioned media. Transfer of conditioned media from IFNγ-treated BV-2 microglia (O'Farrell et al, 2017) or IFNγ-treated mixed glia (O'Farrell, 2016b) to immature (DIV 3) primary cortical neurons reduces neuronal complexity. This can be reversed by pre-treatment with 1-MT indicating a role for the KP in driving inflammatory-mediated neuronal atrophy (O'Farrell et al, 2017).

Glutamate is an important regulator of dendrite and axon development (Gras et al, 2012a; Gras et al, 2012b) and excess glutamatergic stimulation is a feature of numerous CNS pathologies (Rubio-Casillas & Fernández-Guasti, 2016). Reactive microglia are also known to release glutamate, in addition to neurotoxic KP metabolites, however the ability of KYNA to protect against its effects in mature neurons remains to be investigated. In addition to conditioned media from IFNγ-treated mixed glia, previous studies in the lab have demonstrated that treatment of immature (DIV 3) primary cortical neurons with glutamate (500 µM) and glycine (10 µM) (O'Farrell, 2016a; O'Neill, 2015) or NMDA (100-500 µM) and glycine (10 µM) (O'Toole, 2015) for 24 hours reduces neurite outgrowth (Doucet et al, 2015). Co-treatment of immature (DIV 3) primary cortical neurons with KYNA (0.03, 0.1, 1, 10 µM) protected against glutamate and glycine-induced reductions (O'Farrell, 2016a). This study extends these findings to investigate the effect of glutamate and glycine on the complexity of mature neurons and examine if the putative glutamate antagonist KYNA could protect against glutamate and glycine-induced alterations.

In addition to its effect on complexity, the regulatory role of glutamate in synaptogenesis has also been extensively reviewed [see, (Fedder & Sabo, 2015; Mattson, 2008) for review]. Previous work has identified an important role for glutamate in mediating synapse loss in mature neurons while having no effect on viability (Doucet et al, 2015). Treatment of mature (DIV 18-21) primary cortical neurons with glutamate (50 µM) and glycine (1 µM) reduces the co-localised

expression of synaptic proteins (O'Farrell, 2016a). This study extends these findings to investigate the effect of glutamate and glycine on the co-localisation of synaptic proteins and examine if the putative glutamate antagonist KYNA could protect against glutamate and glycine-induced alterations.

The concentrations of glutamate and glycine employed in this study were selected based on previous findings showing that they have no effect on neuronal viability and based on previous work carried out indicating that the combination of glutamate (500 μM) and glycine (10 μM) reduces outgrowth of immature primary neuronal cultures (Doucet et al, 2015). A 10-fold reduction in concentration was employed in this study to account for the increased sensitivity of mature neurons. Glycine was added as a consequence of it being a co-agonist at the NMDA receptor and given that glutamate-induced neuronal atrophy only occurs in the presence of glycine (Doucet et al, 2015).

In addition to glutamate and glycine there is extensive data illustrating the effect of neuroactive KP metabolites on neuronal transmission, viability, complexity and plasticity (Guillemin, 2012; Lugo-Huitron et al, 2013; Pierozan et al, 2015). Studies *in vitro* have shown that direct application of neurotoxic KP metabolites to immature (DIV 8) primary neurons alters neuronal outgrowth as evidenced by immunostaining for the neuronal markers βIII-tubulin and MAP2 (Pierozan et al, 2015). *In vivo* studies have shown that intra-striatal administration of QUIN induces secretion of TNF-α which plays a central role in neuronal damage through a variety of mechanisms, including the formation of free radicals and enhancement of glutamate-mediated neurotoxicity (Vandresen-Filho et al, 2015).

In contrast to the primary role of QUIN as an NMDAR agonist, 3-hydroxykynurenine (3-HK) and 3-hydroxyanthranilic acid (3-HAA) are accepted to play a primary role as pro-oxidant metabolites (Chiarugi et al, 2001). 3-HK has been shown to induce cell death through apoptosis both *in vivo* and *in vitro* (Okuda et al, 1998). This may be attenuated with various antioxidants, indicating that the generation of ROS is essential to 3-HK toxicity (Okuda et al, 1998). Experiments *in vivo* have shown that the anti-oxidant, N-acetyl-L-cysteine

attenuates 3-HK-induced neurotoxicity in the rat striatum, while MK-801 has no effect. This demonstrates that 3-HK exerts neurotoxicity via the generation of free radicals as opposed to via NMDAR activation (Nakagami et al, 1996). 3-HAA is a highly reactive compound and exhibits similar characteristics to 3-HK (Stone & Darlington, 2002). Both compounds auto-oxidize readily under physiological conditions, producing H_2O_2 and highly reactive hydroxyl radicals (Goldstein et al, 2000). The ability to modify the local redox environment is thought to account, primarily for the toxic and apoptotic effect they have on neurons (Okuda et al, 1998).

More recent research has shown that direct application of 3-HK, 3-HAA and QUIN in combination suppresses outgrowth of immature (DIV 3) primary cortical neurons *in vitro*. Furthermore, pre-treatment with the NMDAR antagonist MK-801 attenuates these reductions indicating an important role for the NMDAR in eliciting the neuroactive effects of these compounds (O'Farrell et al, 2017). Additionally, co-treatment with the putative neuroprotective metabolite KYNA has previously shown to provide concentration-related protection against reductions in neurite outgrowth (DIV 3) induced by glutamate and glycine and the triple metabolite combination of 3-HK, 3-HAA and QUIN (O'Farrell, 2016b).

6.2 Aims

The overall aim of the study outlined in this chapter is to examine the impact of KP activation in reactive primary glia on the integrity of mature primary cortical neurons *in vitro*. Moreover, this investigation aims to determine a role for the KP in driving IL-6 and IFNγ mediated neuronal atrophy and synapse loss in mature primary cortical neurons following stimulation of mixed and primary enriched microglial cultures. Subsequently, the effect of KP metabolites and conditioned media from activated glia on neuronal complexity, including the number of neuritic branches, neurite length, and the number of primary neurites were examined, in addition to the co-localisation of synaptic puncta.

Research investigating changes in neuronal complexity to date have been carried out by Sholl analysis on immature neurons (DIV 3) as it permits visualisation of individual isolated neurons. In order to visualise and study the complexity of mature neurons *in vitro* these studies use an adapted Sholl analysis and MAP2 stained mature neurons (DIV 18-21).

Specific aims of this study are to (1) investigate the effect of TNF-α and IL-1α on the expression of KP enzymes in astrocytes, (2) assess the effects of discrete inflammatory stimuli (IFNγ and IL-6) on KP induction in glial populations, (3) assess the effects of direct application of KP metabolites on the complexity of neurons and the co-localised expression of synaptic markers, (4) determine if KYNA can rescue KP related changes in neuronal atrophy and the co-localised expression of synaptic markers, and (5) determine if pharmacological inhibition of the rate limiting KP enzyme IDO can rescue KP related changes in neuronal atrophy and co-localised synaptic markers.

6.3 Results

6.3.1 Effect of TNF-α and IL-1α on the mRNA expression of kynurenine pathway enzymes in primary cortical astrocytes

To investigate the effect of TNF-α and IL-1α on the mRNA expression of KP enzymes, enriched primary cortical astrocytes (DIV 14) were treated with TNF-α (30 ng/mL) and IL-1α (3 ng/mL) for 24 hours. Cells were harvested for RNA extraction followed by RT-PCR. mRNA expression for the KP enzymes KAT II, TDO2, IDO1, KMO and KYNU were quantified.

Treatment of primary cortical astrocytes with TNF-α and IL-1α reduced the mRNA expression of **KAT II** [$T_{(16)} = 7.358$, $P < 0.001$] and **TDO2** [$T_{(14)} = 6.634$, $P < 0.001$], increased the mRNA expression of **IDO1** [$T_{(15)} = 6.125$, $P < 0.001$] and **KMO** [$T_{(16)} = 5.488$, $P < 0.001$], and had no effect on the mRNA expression of **KYNU** [$T_{(8)} = 0.783$, $P = 0.456$] (Student's T test) [*Figure 6.1 (A-E)*].

6.3.2 Effect of IL-6 on the mRNA expression of kynurenine pathway enzymes in enriched primary cortical microglia

To investigate the effect of IL-6 on the mRNA expression of KP enzymes, primary cortical microglia (DIV 15) were treated with IL-6 (80 ng/mL) for 24 hours. Cells were harvested for RNA extraction followed by RT-PCR. mRNA expression for the KP enzymes KAT II, TDO2, IDO1, KMO and KYNU were quantified.

Results of this study showed that the treatment of primary cortical microglia with IL-6 reduced the mRNA expression of **KAT II** [$T_{(16)} = 2.477$, $P = 0.02$], increased the expression of **TDO2** [$T_{(12)} = 2.563$, $P = 0.02$], had no effect on the mRNA expression of **IDO1** [$T_{(8)} = 0.68$, $P = 0.516$], decreased **KMO** [$T_{(14)} = 3.607$, $P = 0.003$], and had no effect on the mRNA expression of **KYNU** [$T_{(16)} = 1.741$ $P = 0.1009$] (Student's T test) [*Figure 6.2 (A-E)*].

6.3.3 Effect of conditioned media from 1-MT (L) and IFNγ treated mixed glia on the complexity of mature primary cortical neurons

To investigate the effect of conditioned media from 1-MT (L) and IFNγ treated mixed glia on neuronal complexity, mixed glial cultures (DIV 14) were co-treated with 1-MT (L) (0.5 mM) and IFNγ (10 ng/mL) for 24 hours. The resulting

conditioned media was collected and applied to mature primary cortical neurons (DIV 21) for 24 hours. Fixation and MAP2 immunocytochemistry were performed to determine the effect of conditioned media from 1-MT (L) and IFNγ treated mixed glia on neuronal complexity by Sholl analysis.

When examining the effect of conditioned media from 1-MT (L) and IFNγ treated mixed glia on the complexity of mature primary cortical neurons, two-way ANOVA of the number of **neuritic branches** showed an effect of conditioned media from IFNγ treated mixed glia [$F_{(1, 299)} = 16.02$, $P < 0.001$] and an interaction effect [$F_{(1, 299)} = 7.091$, $P = 0.0082$]. *Post hoc* analysis revealed reductions in the number of neuritic branches following treatment with 1-MT (L) ($P < 0.05$), conditioned media from IFNγ treated mixed glia ($P < 0.001$), and conditioned media from IFNγ and 1-MT treated mixed glia ($P < 0.01$) compared to conditioned media from untreated mixed glia. Co-treatment with 1-MT (L) provided some protection as it reduced the number of neuritic branches to a lesser extent than with conditioned media from IFNγ treated mixed glia alone [*Figure 6.3 (A)*]. Two-way ANOVA of **neurite length** showed an effect of conditioned media from IFNγ treated mixed glia [$F_{(1, 304)} = 11.28$, $P < 0.001$] and an interaction effect [$F_{(1, 304)} = 11.91$, $P < 0.001$]. *Post hoc* analysis revealed reductions in neurite length following treatment with conditioned media from IFNγ treated mixed glia ($P < 0.001$) compared to conditioned media from untreated mixed glia. *Post hoc* analysis also revealed an increase in neurite length following treatment with conditioned media from IFNγ and 1-MT (L) treated mixed glia ($P < 0.001$) compared to conditioned media from IFNγ treated mixed glia alone. Co-treatment with 1-MT (L) protected against conditioned media from IFNγ treated mixed glia-induced reductions bringing the length back to control [*Figure 6.3 (B)*]. Two-way ANOVA of the number of **primary neurites** showed no effect of conditioned media from IFNγ treated mixed glia [$F_{(1, 307)} = 2.376$, $P = 0.12$] but showed an interaction effect [$F_{(1, 307)} = 4.197$, $P = 0.04$]. *Post hoc* analysis revealed no difference in the number of primary neurites between treatments [*Figure 6.3 (C)*]. Two-way repeated measures ANOVA of the **number of neuritic branches at specific distances from the neuronal cell soma** showed an effect of distance [$F_{(19, 5814)} = 498.1$, $P < 0.001$], an effect of treatment [$F_{(3, 306)} = 6.670$, $P <$

0.001] and an interaction effect [$F_{(57, 5814)} = 2.870$, $P < 0.001$]. Conditioned media from IFNγ treated mixed glia decreased neuritic branching at 10-90 µm from the cell soma compared to conditioned media from untreated mixed glia. 1-MT (L) protected against these reductions indicating a protective effect for 1-MT (L) [*Figure 6.3 (D)*].

6.3.4 Effect of conditioned media from 1-MT (L) and IL-6 treated microglia on the complexity of mature primary cortical neurons

To investigate the effect of conditioned media from 1-MT (L) and IL-6 treated microglia on neuronal complexity, primary cortical microglial cultures (DIV 15) were co-treated with 1-MT (L) (0.5 mM) and IL-6 (80 ng/mL) for 24 hours. The resulting conditioned media was collected and applied to mature primary cortical neurons (DIV 21) for 24 hours. Fixation and MAP2 immunocytochemistry were performed to determine the effect of conditioned media from 1-MT (L) and IL-6 treated microglia on neuronal complexity by Sholl analysis.

When examining the effect of conditioned media from 1-MT (L) and IL-6 treated microglia on the complexity of mature primary cortical neurons, two-way ANOVA of the number of **neuritic branches** showed an effect of conditioned media from IL-6 treated microglia [$F_{(1, 276)} = 8.193$, $P = 0.005$] and showed an interaction effect [$F_{(1, 276)} = 112.4$, $P < 0.001$]. *Post hoc* analysis revealed reductions in the number of neuritic branches following treatment with conditioned media from IL-6 treated microglia compared to conditioned media from untreated microglia ($P < 0.001$). Co-treatment with 1-MT (L) increased the number of neuritic branches compared to conditioned media from IL-6 treated microglia ($P < 0.001$) bringing it back to control levels [*Figure 6.4 (A)*]. Two-way ANOVA of **neurite length** showed an effect of conditioned media from IL-6 treated microglia [$F_{(1, 278)} = 3.998$, $P = 0.05$] and an interaction effect [$F_{(1, 278)} = 384.9$, $P < 0.001$]. *Post hoc* analysis revealed reductions in neuritic length following treatment with conditioned media from IL-6 treated microglia compared to conditioned media from untreated microglia ($P < 0.001$). Co-treatment with 1-MT (L) increased neuritic length compared to conditioned media from IL-6 treated microglia ($P < 0.001$) bringing it back to control levels [*Figure 6.4 (B)*]. Two-way ANOVA of the number of **primary neurites** showed no effect of conditioned media from IL-6

treated microglia [$F_{(1, 277)} = 0.1459$, $P = 0.70$] but showed an interaction effect [$F_{(1, 277)} = 71.47$, $P < 0.001$]. *Post hoc* analysis revealed reductions in the number of primary neurites following treatment with conditioned media from IL-6 treated microglia compared to conditioned media from untreated microglia ($P < 0.001$). Co-treatment with 1-MT (L) increased the number of primary neurites compared to conditioned media from IL-6 treated microglia ($P < 0.001$) bringing this level back to control [*Figure 6.4 (C)*]. Two-way repeated measures ANOVA of the **number of neuritic branches at specific distances from the neuronal cell soma** showed an effect of distance [$F_{(19, 3629)} = 439.5$, $P < 0.001$], an effect of treatment [$F_{(2, 191)} = 116.1$, $P < 0.001$] and an interaction effect [$F_{(38, 3629)} = 28.94$, $P < 0.001$]. Conditioned media from IL-6 treated microglia decreased neuritic branching at all distances between 10 and 150 µm from the cell soma compared to control NBM and addition of 1-MT protected against these reductions [*Figure 6.4 (D)*].

6.3.5 Effect of kynurenic acid on the complexity of mature primary cortical neurons

To investigate the effect of KYNA on neuronal complexity, mature primary cortical neurons (DIV 21) were treated with KYNA (0.03, 0.1, 1, 10 µM) for 24 hours. Fixation and MAP2 immunocytochemistry were performed to determine the effect of KYNA on neuronal complexity by Sholl analysis. Concentrations of kynurenic acid were chosen based on previous work investigating its effect on primary neurons. Previous findings in the lab demonstrate that that KYNA (0.03 µM) increases neuronal viability, while having no effect on the viability of either immature or mature neurons at any other concentration tested (O'Farrell, 2016b). Additional findings have shown that KYNA has no effect on neuronal viability at concentrations ranging from 0.1-1000 µM (Braidy et al, 2009).

One-way ANOVA of the number of **neuritic branches** showed no effect of KYNA [$F_{(3, 402)} = 2.480$, $P = 0.061$] *[Figure 6.5 (A)*]. One-way ANOVA of **neurite length** showed an effect of KYNA [$F_{(3, 403)} = 13.17$, $P < 0.001$]. *Post hoc* analysis revealed an increase in neurite length following treatment with KYNA (0.1 and 0.3 µM) compared to control NBM ($P < 0.001$) [*Figure 6.5 (B)*]. One-way ANOVA of the number of **primary neurites** showed no effect of KYNA [$F_{(3, 401)} = 1.253$, $P =$

0.290] [*Figure 6.5 (C)*]. Two-way repeated measures ANOVA of the **number of neuritic branches at specific distances from the neuronal cell soma** showed an effect of distance [$F_{(19, 7695)} = 698.1$, $P < 0.001$], an effect of treatment [$F_{(3, 405)} = 11.56$, $P < 0.001$] and an interaction effect [$F_{(57, 7695)} = 4.063$, $P < 0.001$]. KYNA increased neuritic branching at all distances between 40-140 µm from the cell soma compared to control NBM [*Figure 6.5 (D)*].

6.3.6 Effect of kynurenic acid on synaptic protein co-localisation in mature primary cortical neurons

To investigate the effect of KYNA on the co-localisation of synaptic proteins, mature primary cortical neurons (DIV 21) were treated with KYNA (0.03, 0.1, 1, 10 µM) for 24 hours. Fixation and immunocytochemistry were performed to determine the effect of KYNA on synaptic protein co-localisation.

One-way ANOVA of **synaptophysin puncta** showed a concentration-related effect of KYNA [$F_{(3, 565)} = 4.988$, $P = 0.002$]. *Post hoc* analysis revealed an increase in the number of synaptophysin puncta following treatment with KYNA (0.03 and 0.1 µM) compared to control NBM ($P < 0.01$) and following treatment with KYNA (0.3 µM) compared to control NBM ($P < 0.05$) [*Figure 6.6 (A)*]. One-way ANOVA of **PSD-95 puncta** showed a concentration-related effect of KYNA [$F_{(3, 562)} = 11.34$, $P < 0.001$]. *Post hoc* analysis revealed an increase in the number of PSD-95 puncta following treatment with KYNA (0.03 µM and 0.1 µM) compared to control NBM ($P < 0.001$) and following treatment with KYNA 0.3 µM ($P < 0.05$) compared to control NBM [*Figure 6.6 (B)*]. One-way ANOVA of **co-localised synaptic puncta** showed a concentration-related effect of KYNA [$F_{(3, 558)} = 7.356$, $P < 0.001$]. *Post hoc* analysis revealed an increase in the number of co-localised puncta following treatment with KYNA (0.03 and 0.1 µM) compared to control NBM ($P < 0.01$) and following treatment with KYNA (0.3 µM) compared to control NBM ($P < 0.05$) [*Figure 6.6 (C)*].

6.3.7 Effect of kynurenic acid on reductions in the complexity of mature primary cortical neurons induced by conditioned media from IFNγ treated mixed glia

To investigate the effect of KYNA on reductions in neuronal complexity induced by conditioned media from IFNγ-treated mixed glia, mixed glial cultures (DIV 14) were treated with IFNγ (10 ng/mL) for 24 hours. The resulting conditioned media was collected and applied to mature primary cortical neurons (DIV 21) for 24 hours with KYNA (0.03, 0.1, 1, 10 µM). Fixation and MAP2 immunocytochemistry were performed to determine the effect of KYNA on conditioned media from IFNγ treated mixed glia-induced reductions in neuronal complexity by Sholl analysis.

Conditioned media from IFNγ treated mixed glia reduced the number of **neuritic branches** [$T_{(158)} = 3.907$, $P < 0.001$] compared to conditioned media from untreated mixed glia (Student's T test). One-way ANOVA showed an effect of KYNA on reductions induced by conditioned media from IFNγ treated mixed glia [$F_{(3, 284)} = 4.253$, $P = 0.006$]. *Post hoc* analysis revealed an increase in the number of neuritic branches following co-treatment with KYNA 0.3 µM compared to conditioned media from IFNγ treated mixed glia ($P < 0.05$) [*Figure 6.7 (A)*]. Conditioned media from IFNγ treated mixed glia reduced **neurite length** [$T_{(156)} = 5.781$, $P < 0.001$] compared to conditioned media from untreated mixed glia (Student's T test). One-way ANOVA showed an effect of KYNA on reductions induced by conditioned media from IFNγ treated mixed glia [$F_{(3, 280)} = 7.920$, $P < 0.001$]. *Post hoc* analysis revealed an increase in neuritic length following co-treatment with KYNA 0.3 µM compared to conditioned media from IFNγ treated mixed glia alone ($P < 0.001$) [*Figure 6.7 (B)*]. Conditioned media from IFNγ treated mixed glia had no effect on the number of **primary neurites** [$T_{(158)} = 0.337$, $P = 0.74$] (Student's T test). One-way ANOVA showed no effect of KYNA [$F_{(3, 285)} = 0.173$, $P = 0.91$] [*Figure 6.7 (C)*]. Two-way repeated measures ANOVA of the **number of neuritic branches at specific distances from the neuronal cell soma** showed an effect of distance [$F_{(19, 6878)} = 482.4$, $P < 0.001$], an effect of treatment [$F_{(4, 362)} = 10.17$, $P < 0.001$] and an interaction effect [$F_{(76, 6878)} = 3.340$, $P < 0.001$]. *Post hoc* analysis revealed a significant decrease in the Sholl profile at 60-110 µm following treatment with conditioned media from IFNγ treated mixed

glia compared to control conditioned media ($P < 0.001$). *Post hoc* analysis also revealed an increase in the Sholl profile at 60-90 µm and at 100-120 µm ($P < 0.001$) following co-treatment with KYNA 0.3 µM compared to conditioned media from IFNγ treated mixed glia alone [*Figure 6.7 (D)*].

6.3.8 Effect of kynurenic acid on reductions in synaptic protein co-localisation in mature primary cortical neurons induced by conditioned media from IFNγ treated mixed glia

To investigate the effect of KYNA on reductions in the co-localisation of synaptic proteins induced by conditioned media from IFNγ-treated mixed glia, mixed glial cultures (DIV 14) were treated with IFNγ (10 ng/mL) for 24 hours. The resulting conditioned media was collected and applied to mature primary cortical neurons (DIV 21) for 24 hours with KYNA (0.03, 0.1, 1, 10 µM). Fixation and immunocytochemistry were performed to determine the effect of KYNA on conditioned media from IFNγ treated mixed glia-induced reductions in the co-localisation of synaptic proteins.

Conditioned media from IFNγ treated mixed glia reduced the number of **synaptophysin puncta** [$T_{(207)} = 4.245$, $P < 0.001$] compared to conditioned media from untreated mixed glia (Student's T test). One-way ANOVA showed an effect of KYNA on reductions induced by conditioned media from IFNγ treated mixed glia [$F_{(3, 325)} = 47.57$, $P < 0.001$]. *Post hoc* analysis revealed an increase in the number of synaptophysin puncta following co-treatment with KYNA 0.03 µM compared to conditioned media from IFNγ treated mixed glia alone ($P < 0.05$) and following co-treatment with KYNA (0.01 and 0.3 µM) compared to conditioned media from IFNγ treated mixed glia alone ($P < 0.001$) [*Figure 6.8 (A)*]. Conditioned media from IFNγ treated mixed glia increased the number of **PSD-95 puncta** [$T_{(204)} = 5.592$, $P < 0.001$] compared to conditioned media from untreated mixed glia (Student's T test). One-way ANOVA showed an effect of KYNA on the increase in PSD-95 puncta induced by conditioned media from IFNγ treated mixed glia [$F_{(3, 304)} = 19.69$, $P < 0.001$]. *Post hoc* analysis revealed a decrease in the number of PSD-95 puncta following co-treatment with KYNA (0.03, 0.1, 0.3 µM) compared to conditioned media from IFNγ treated mixed glia alone ($P < 0.001$) [*Figure 6.8 (B)*]. Conditioned media from IFNγ treated mixed

glia decreased the number of **co-localised synaptic puncta** [$T_{(204)} = 7.443$, $P < 0.001$] compared to conditioned media from untreated mixed glia (Student's T test). One-way ANOVA showed an effect of KYNA [$F_{(3, 320)} = 45.36$, $P < 0.001$]. *Post hoc* analysis revealed an increase in the number of co-localised puncta following co-treatment with KYNA (0.03 μM) compared to conditioned media from IFNγ treated mixed glia alone ($P < 0.01$), and following co-treatment with KYNA (0.1 and 0.3 μM) compared to conditioned media from IFNγ treated mixed glia alone ($P < 0.01$) [*Figure 6.8 (C)*].

6.3.9 Effect of kynurenic acid on reductions in the complexity of mature primary cortical neurons induced by glutamate and glycine

To investigate the effect of KYNA on glutamate glutamate/glycine-induced reductions in the complexity of mature neurons, primary cortical neuronal cultures were co-treated with KYNA (0.03, 0.1, 1, 10 μM) and glutamate (50 μM)/glycine (1 μM) for 24 hours. Fixation and MAP2 immunocytochemistry were performed to determine the effect of KYNA on glutamate/glycine-induced reductions in neuronal complexity by Sholl analysis.

Results of this study showed that treatment with glutamate and glycine reduced the number of **neuritic branches** [$T_{(138)} = 6.758$, $P < 0.001$] compared to control NBM (Student's T test). One-way ANOVA showed an effect of KYNA on reductions induced by glutamate and glycine [$F_{(3, 205)} = 4.875$, $P = 0.003$]. *Post hoc* analysis revealed an increase in the number of neuritic branches following co-treatment with KYNA 0.1 μM compared to glutamate and glycine ($P < 0.01$) [*Figure 6.9 (A)*]. Treatment with glutamate and glycine reduced **neurite length** [$T_{(140)} = 16.73$, $P < 0.001$] compared to control NBM (Student's T test). One-way ANOVA showed an effect of KYNA on reductions induced by glutamate and glycine [$F_{(3, 214)} = 67.89$, $P < 0.001$]. *Post hoc* analysis revealed an increase in neuritic length following co-treatment with KYNA (0.03, 0.1 and 0.3 μM) compared to glutamate and glycine alone ($P < 0.001$) [*Figure 6.9 (B)*]. Treatment with glutamate and glycine reduced the number of **primary neurites** [$T_{(143)} = 6.788$, $P < 0.001$] (Student's T test). One-way ANOVA showed no effect of KYNA [$F_{(3, 213)} = 1.593$, $P = 0.19$] [*Figure 6.9 (C)*]. Two-way repeated measures ANOVA

of the **number of neuritic branches at specific distances from the neuronal cell soma** showed an effect of distance [$F_{(19, 5358)} = 453.8$, $P < 0.001$], an effect of treatment [$F_{(4, 282)} = 59.17$, $P < 0.001$] and an interaction effect [$F_{(76, 5358)} = 18.19$, $P < 0.001$]. *Post hoc* analysis revealed a decrease in the Sholl profile at 10-120 µm following treatment with glutamate and glycine compared to control NBM ($P < 0.001$). *Post hoc* analysis also revealed an increase in the Sholl profile at 30-100 µm following co-treatment with KYNA 0.3 µM compared to glutamate and glycine alone ($P < 0.001$) [*Figure 6.9 (D)*].

6.3.10 Effect of kynurenic acid on reductions in the co-localisation of synaptic proteins in mature primary cortical neurons induced by glutamate and glycine

To investigate the effect of KYNA on glutamate/glycine-induced reductions in the co-localisation of synaptic proteins, mature (DIV 21) primary cortical neurons were co-treated with KYNA (0.03, 0.1, 1, 10 µM) and glutamate (50 µM)/glycine (1 µM) for 24 hours. Fixation and immunocytochemistry were performed to determine the effect of KYNA on glutamate/glycine-induced reductions in the co-localisation of synaptic proteins. Treatment with glutamate and glycine reduced the number of **synaptophysin puncta** [$T_{(278)} = 4.205$, $P < 0.001$] compared to control NBM (Student's T test). One-way ANOVA showed an effect of KYNA on reductions induced by glutamate and glycine [$F_{(3, 257)} = 4.920$, $P = 0.002$]. *Post hoc* analysis revealed an increase in the number of synaptophysin puncta following co-treatment with KYNA (0.03 µM) compared to glutamate and glycine alone ($P < 0.01$) and following co-treatment with KYNA (0.1 µM) compared to glutamate and glycine alone ($P < 0.05$) [*Figure 6.10 (A)*]. Treatment with glutamate and glycine reduced the number of **PSD-95 puncta** [$T_{(280)} = 2.575$, $P < 0.01$] compared to control NBM (Student's T test). One-way ANOVA showed an effect of KYNA on reductions induced by glutamate and glycine [$F_{(3, 246)} = 5.909$, $P < 0.001$]. *Post hoc* analysis revealed a decrease in the number of PSD-95 puncta following co-treatment with KYNA (0.03 µM) compared to glutamate and glycine ($P < 0.01$), and following co-treatment with KYNA (0.03 and 0.1 µM) compared to glutamate and glycine alone ($P < 0.01$) [*Figure 6.10 (B)*]. Treatment with glutamate and glycine had no effect on the number of **co-localised puncta** [T

$_{(274)}$ = 1.831, P = 0.07] compared to control NBM (Student's T test). One-way ANOVA showed an effect of KYNA on reductions induced by glutamate and glycine [$F_{(3, 254)}$ = 5.869, P < 0.001]. *Post hoc* analysis revealed a concentration-related effect of KYNA on glutamate and glycine reductions. *Post hoc* analysis revealed an increase in the number of co-localised synaptic puncta following treatment with KYNA (0.03 µM) compared to glutamate and glycine (P < 0.001), following treatment with KYNA (0.1 µM) compared to glutamate and glycine (P < 0.01) and following treatment with KYNA (0.3 µM) compared to glutamate and glycine alone (P < 0.001) [*Figure 6.10 (C)*].

6.3.11 Effect of kynurenic acid on reductions in the complexity of mature primary cortical neurons induced by [3-HAA + 3-HK + QUIN]

To investigate the effect of KYNA on [3-HAA + 3-HK + QUIN]-induced reductions in neuronal complexity, mature (DIV 21) primary cortical neurons were co-treated with KYNA (0.03, 0.1, 1, 10 µM) and [3-HAA (0.03 µM) + 3-HK (0.03 µM) + QUIN (0.1 µM)] for 24 hours. Fixation and MAP2 immunocytochemistry were performed to determine the effect of KYNA on [3-HAA + 3-HK + QUIN]-induced reductions in neuronal complexity by Sholl analysis.

Results of this study showed that treatment with [3-HAA + 3-HK + QUIN] reduced the number of **neuritic branches** [$T_{(206)}$ = 7.550, P < 0.001] compared to control NBM (Student's T test). One-way ANOVA showed no effect of KYNA on reductions induced by the triple metabolite combination [$F_{(4, 487)}$ = 1.239, P = 0.29] [*Figure 6.11 (A)*]. Treatment with [3-HAA + 3-HK + QUIN] reduced the **neuritic length** [$T_{(206)}$ = 14.9, P < 0.001] compared to control NBM (Student's T test). One-way ANOVA showed an effect of KYNA on reductions induced by the triple metabolite combination [$F_{(4, 482)}$ = 9.784, P < 0.001]. *Post hoc* analysis revealed an increase in neuritic length following co-treatment with KYNA (0.01 and 0.3 µM) compared to [3-HAA + 3-HK + QUIN] alone (P < 0.001) [*Figure 6.11 (B)*]. Treatment with [3-HAA + 3-HK + QUIN] reduced the **number of primary neurites** [$T_{(205)}$ = 4.494, P < 0.001] compared to control NBM (Student's T test). One-way ANOVA showed no effect of KYNA on reductions induced by the triple metabolite combination [$F_{(4, 485}$) = 0.247, P = 0.91] [*Figure 6.11 (C)*]. Two-

way repeated measures ANOVA of the **number of neuritic branches at specific distances from the neuronal cell soma** showed an effect of distance [$F_{(19, 8170)}$ = 804.7, P < 0.001], an effect of treatment [$F_{(4, 430)}$ = 77.38, P < 0.001] and an interaction effect $F_{(76, 8170)}$ = 6.724, P < 0.001]. *Post hoc* analysis revealed a significant decrease in the Sholl profile at 10-160 µm (P < 0.001) and at 170 µm (P < 0.001) following treatment with the triple metabolite combination compared to control NBM (P < 0.001). *Post hoc* analysis also revealed an increase in the Sholl profile at 40-90 µm following co-treatment with KYNA 0.3 µM compared to [3-HAA + 3-HK + QUIN] alone**,** indicating a protective effect for KYNA at increasing concentrations (P < 0.001) [*Figure 6.11 (D)*].

6.3.12 Effect of kynurenic acid on reductions in synaptic protein co-localisation in mature primary cortical neurons induced by [3-HAA + 3-HK + QUIN]

To investigate the effect of KYNA on [3-HAA + 3-HK + QUIN]-induced reductions synaptic protein co-localisation, mature primary cortical neurons (DIV 21) were co-treated with KYNA (0.03, 0.1, 1, 10 µM) and [3-HAA (0.03 µM) + 3-HK (0.03 µM) + QUIN (0.1 µM)] for 24 hours. Fixation and immunocytochemistry were performed to determine the effect of KYNA on [3-HAA + 3-HK + QUIN]-induced reductions in the co-localisation of synaptic proteins.

Treatment with [3-HAA + 3-HK + QUIN] reduced the number of **synaptophysin puncta** [$T_{(322)}$ = 6.058, P < 0.001] compared to control NBM (Student's T test). One-way ANOVA showed no effect of KYNA on reductions induced by the triple metabolite combination [$F_{(4, 514)}$ = 1.704, P = 0.15] [*Figure 6.12 (A)*]. Treatment with [3-HAA + 3-HK + QUIN] reduced the number of **PSD-95 puncta** [$T_{(331)}$ = 4.189, P < 0.001] compared to control NBM (Student's T test). One-way ANOVA showed no effect of KYNA on reductions induced by the triple metabolite combination [$F_{(4, 514)}$ = 1.072, P = 0.37]. [*Figure 6.12 (B)*]. Treatment with [3-HAA + 3-HK + QUIN] reduced the number of **co-localised puncta** [$T_{(313)}$ = 3.471, P < 0.001] compared to control NBM (Student's T test). One-way ANOVA showed no effect of KYNA on reductions induced by the triple metabolite combination [$F_{(4, 506)}$ = 1.825, P = 0.12] [*Figure 6.12 (C)*].

6.3.13 Effect of kynurenic acid on reductions in the complexity of mature primary cortical neurons induced by QUIN

To investigate the effect of KYNA on QUIN-induced reductions in neuronal complexity, mature (DIV 21) primary cortical neurons were treated with KYNA (0.03, 0.1, 1, 10 µM) and QUIN (0.1 µM) for 24 hours. Fixation and MAP2 immunocytochemistry were performed to determine the effect of KYNA on QUIN-induced reductions in neurite outgrowth by Sholl analysis.

Results of this study showed that treatment with QUIN reduced the number of **neuritic branches** [$T_{(132)} = 4.896$, $P < 0.001$] compared to control NBM (Student's T test). One-way ANOVA showed an effect of KYNA on reductions induced by QUIN [$F_{(3, 236)} = 5.584$, $P = 0.001$]. *Post hoc* analysis revealed an increase in the number of neuritic branches following co-treatment with KYNA (0.3 µM compared to QUIN alone ($P < 0.01$) [*Figure 6.13 (A)*]. Treatment with QUIN reduced the **neuritic length** [$T_{(131)} = 6.885$, $P < 0.001$] compared to control NBM (Student's T test). One-way ANOVA showed an effect of KYNA on reductions induced by QUIN [$F_{(3, 234)} = 14.78$, $P < 0.001$]. *Post hoc* analysis revealed an increase in neuritic length following co-treatment with KYNA (0.1 µM) compared to QUIN ($P < 0.01$) and following co-treatment with KYNA (0.3 µM) compared to QUIN alone ($P < 0.001$) [*Figure 6.13 (B)*]. Treatment with QUIN reduced the **number of primary neurites** [$T_{(133)} = 2.057$, $P = 0.04$] compared to control NBM (Student's T test). One-way ANOVA showed no effect of KYNA on reductions induced by QUIN [$F_{(3, 236)} = 0.866$, $P = 0.46$] [*Figure 6.13 (C)*]. Two-way repeated measures ANOVA of the **number of neuritic branches at specific distances from the neuronal cell soma** showed an effect of distance [$F_{(19, 5548)} = 515.3$, $P < 0.001$], an effect of treatment [$F_{(4, 292)} = 12.21$, $P < 0.001$] and an interaction effect [$F_{(76, 5548)} = 1.670$, $P < 0.001$]. *Post hoc* analysis revealed a significant decrease in the Sholl profile at all distances between 40 and 150 µm following treatment with QUIN compared to control NBM. *Post hoc* analysis also revealed an increase in the Sholl profile at all distances between 50 and 120 µm following treatment with KYNA 0.3 µM compared to QUIN alone [*Figure 6.13 (D)*].

6.3.14 Effect of kynurenic acid on reductions in synaptic protein co-localisation in mature primary cortical neurons induced by QUIN

To investigate the effect of KYNA on QUIN-induced reductions in the co-localisation of synaptic proteins, mature (DIV 21) primary cortical neurons were co-treated with KYNA (0.03, 0.1, 1, 10 µM) and QUIN (0.1 µM) for 24 hours. Fixation and immunocytochemistry were performed to determine the effect of KYNA on QUIN-induced reductions in the co-localisation of synaptic proteins.

Results of this study showed that treatment with QUIN reduced the number of **synaptophysin puncta** [$T_{(155)} = 4.761, P < 0.001$] compared to control NBM (Student's T test). One-way ANOVA showed an effect of KYNA on reductions induced by QUIN [$F_{(3, 357)} = 10.98, P < 0.001$]. *Post hoc* analysis revealed an increase in the number of synaptophysin puncta following co-treatment with KYNA (0.1 and 0.3 µM) compared to QUIN alone ($P < 0.001$) [*Figure 6.14 (A)*]. Treatment with QUIN reduced the number of **PSD-95 puncta** [$T_{(170)} = 4.369, P < 0.001$] compared to control NBM (Student's T test). One-way ANOVA showed an effect of KYNA on reductions induced by QUIN [$F_{(3, 379)} = 28.78, P < 0.001$]. *Post hoc* analysis revealed an increase in the number of PSD-95 puncta following co-treatment with KYNA (0.3 µM) compared to QUIN alone ($P < 0.001$) [*Figure 6.14 (B)*]. Treatment with QUIN reduced the number of **co-localised puncta** [$T_{(155)} = 4.411, P < 0.001$] compared to control NBM (Student's T test). One-way ANOVA showed an effect of KYNA on reductions induced by QUIN [$F_{(3, 364)} = 17.20, P < 0.001$]. *Post hoc* analysis revealed an increase in the number of co-localised puncta following co-treatment with KYNA (0.3 µM) compared to QUIN alone ($P < 0.001$) [*Figure 6.14 (C)*].

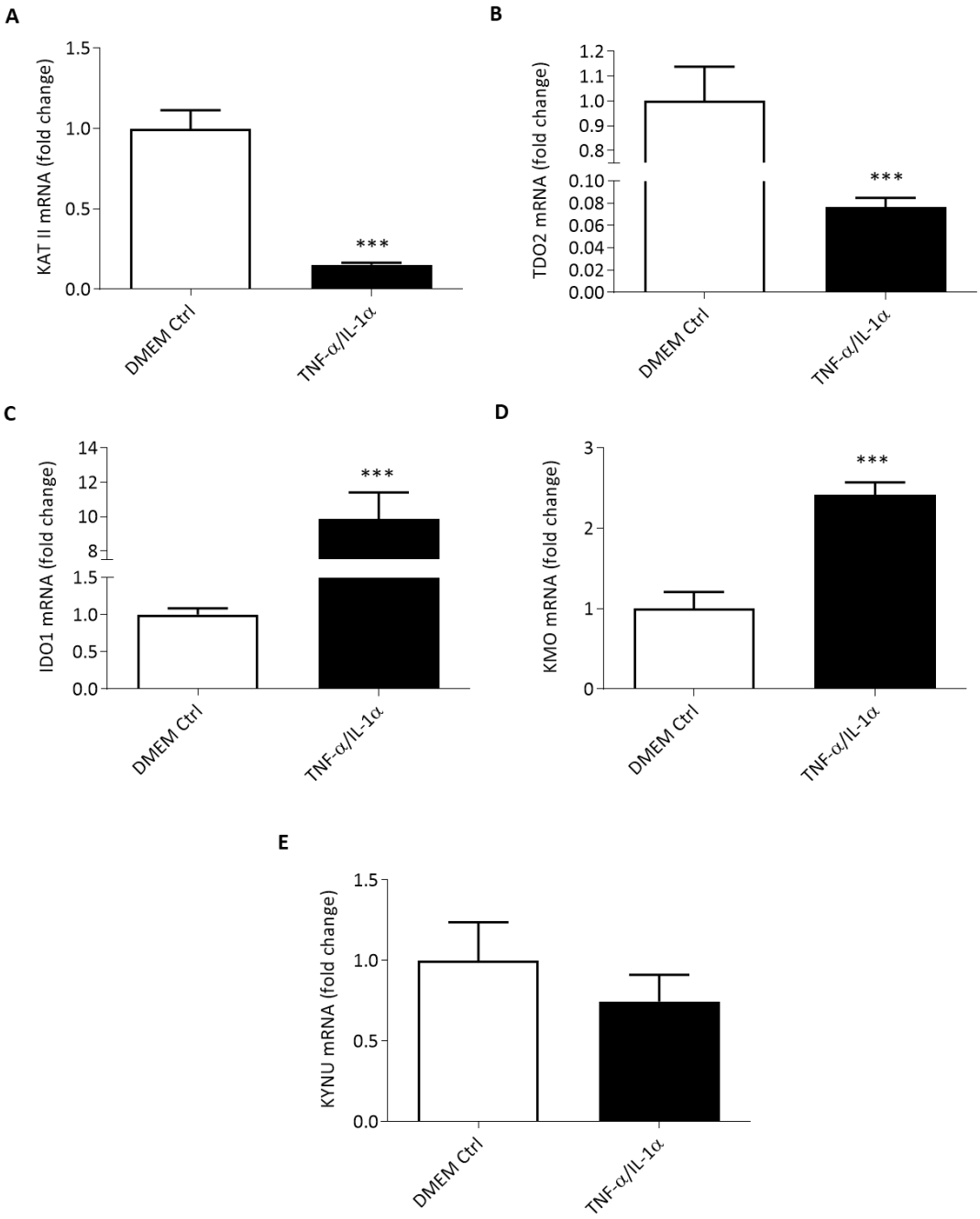

Figure 6.1 TNF-α and IL-1α induces the mRNA expression of kynurenine pathway enzymes in enriched primary cortical astrocytes.

Primary astrocytes (DIV 14) were treated with TNF-α (30 ng/mL) and IL-1α (3 ng/mL) for 24 hours. Cells were harvested for RNA extraction followed by RT-PCR to analyse the expression of the KP enzymes; KAT II (A), TDO2 (B), IDO1 (C), KMO (D) and KYNU (E). Data are expressed as mean ± SEM, n=8 wells per treatment group from 3 independent experiments. ***P<0.001 vs. control DMEM (Newman-Keuls *post hoc* test).

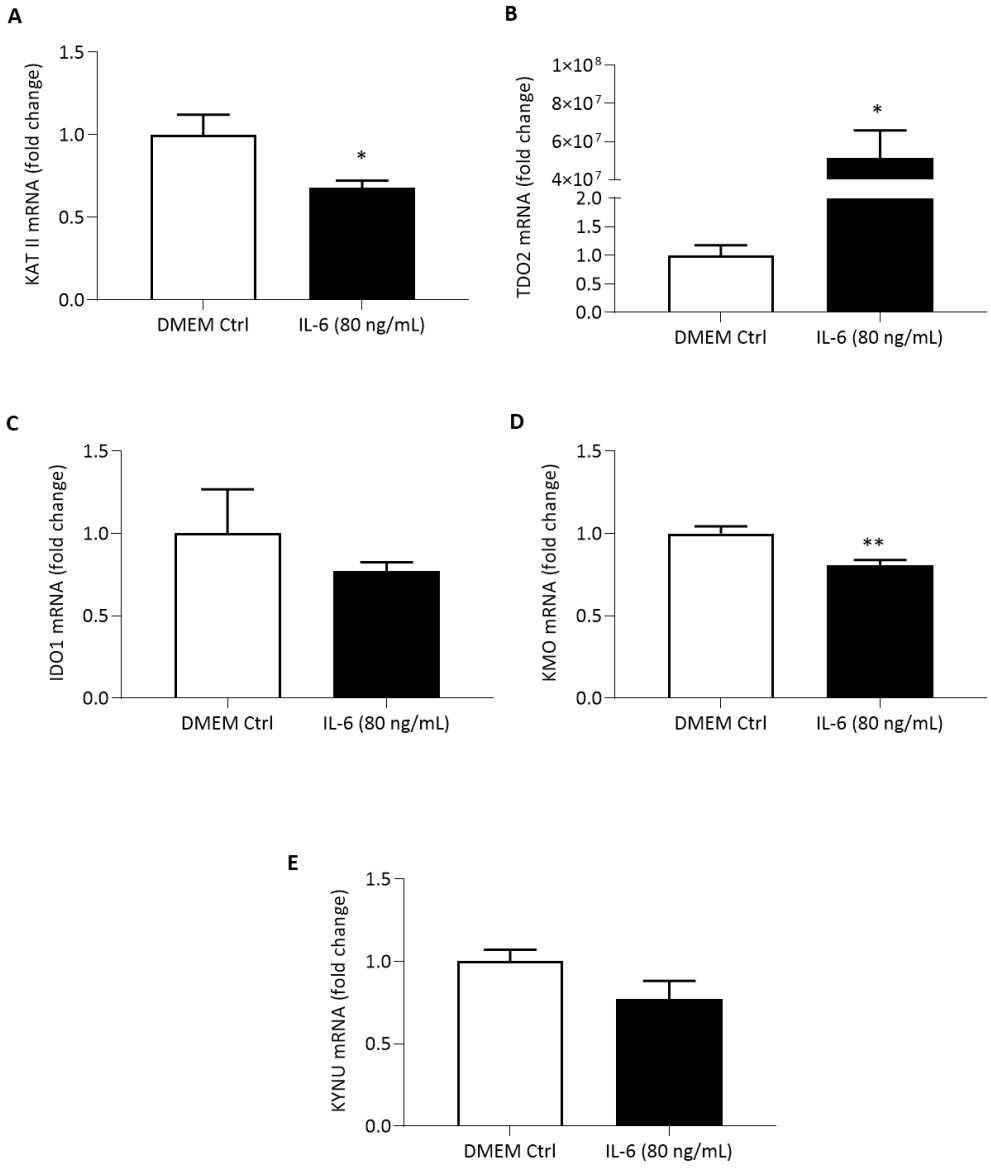

Figure 6.2 IL-6 induces the mRNA expression of kynurenine pathway enzymes in enriched primary cortical microglia.

Primary microglia (DIV 14) were treated with IL-6 (80 ng/mL) for 24 hours. Cells were harvested for RNA extraction followed by RT-PCR to analyse the expression of the KP enzymes; KAT II (A), TDO2 (B), IDO1 (C), KMO (D) and KYNU (E). Data are expressed as mean ± SEM, n=8 wells per treatment group from 3 independent experiments. **P<0.01, *P<0.05 vs. control DMEM (Newman-Keuls *post hoc* test).

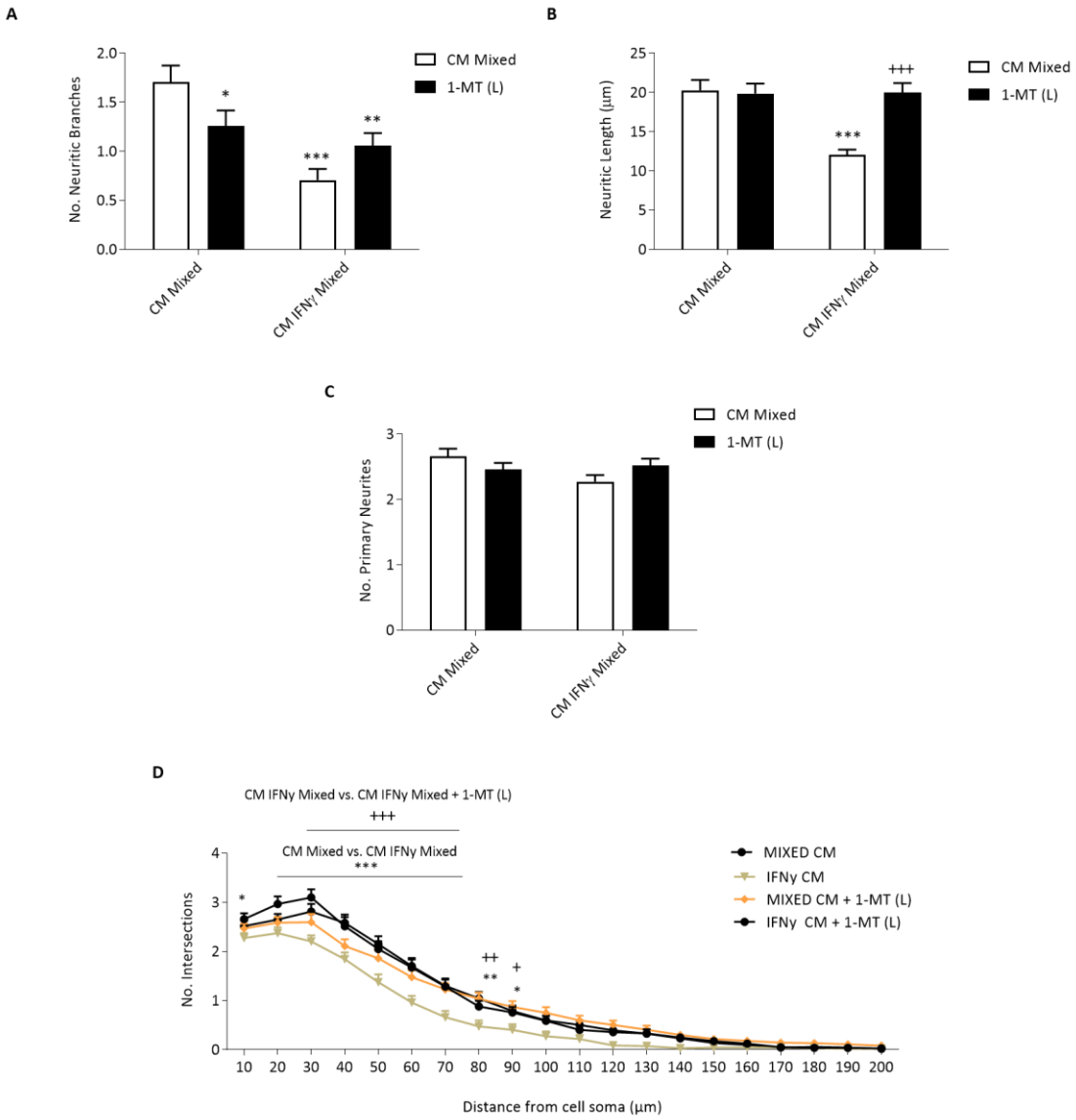

Figure 6.3 1-MT (L) protects against reductions in the complexity of mature primary cortical neurons induced by conditioned media from IFNγ treated mixed glia.
Primary mixed glial cultures (DIV 14) were co-treated with IFNγ (10 ng/mL) and 1-MT (L) (0.5 mM) for 24 hours. The resulting conditioned media was collected and applied to mature neurons (DIV 21) for 24 hours before fixation and MAP2 immunocytochemistry. Sholl analysis was performed to analyse the number of neuritic branches (A), the neuritic length (B), the number of primary neurites (C), and the Sholl profile (D). Data are expressed as mean ± SEM, n=6 coverslips per treatment group from 4 independent experiments. ***P<0.001, **P<0.01, *P<0.05 vs. control DMEM, $^{+++}$P<0.001, $^{++}$P<0.01, $^{+}$P<0.05 vs. CM IFNγ Mixed (Newman-Keuls *post hoc* test).

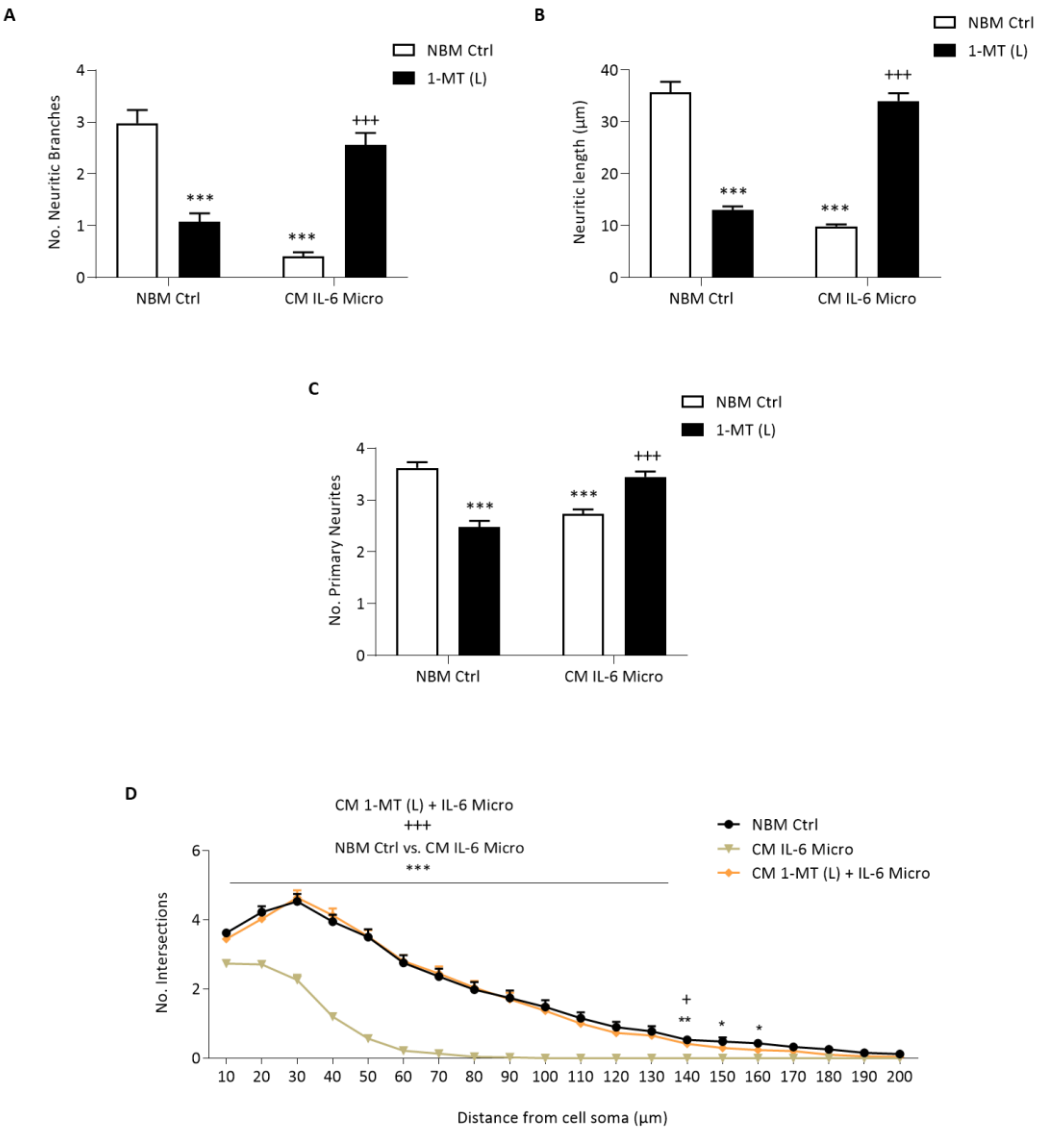

Figure 6.4 1-MT (L) protects against reductions in the complexity of mature primary cortical neurons induced by conditioned media from IL-6 treated microglia.
Primary microglial cultures (DIV 15) were co-treated with IL-6 (80 ng/mL) and 1-MT (L) (0.5 mM) for 24 hours. The resulting conditioned media was collected and applied to mature neurons (DIV 21) for 24 hours before fixation and MAP2 immunocytochemistry. Sholl analysis was performed to analyse the number of neuritic branches (A), the neuritic length (B), the number of primary neurites (C), and the Sholl profile (D). Data are expressed as mean ± SEM, n=6 coverslips per treatment group from 4 independent experiments. ***P<0.001, **P<0.01, *P<0.05 vs. control DMEM, $^{+++}$P<0.001, $^{+}$P<0.05 vs. CM from IL-6 treated microglia (Newman-Keuls *post hoc* test).

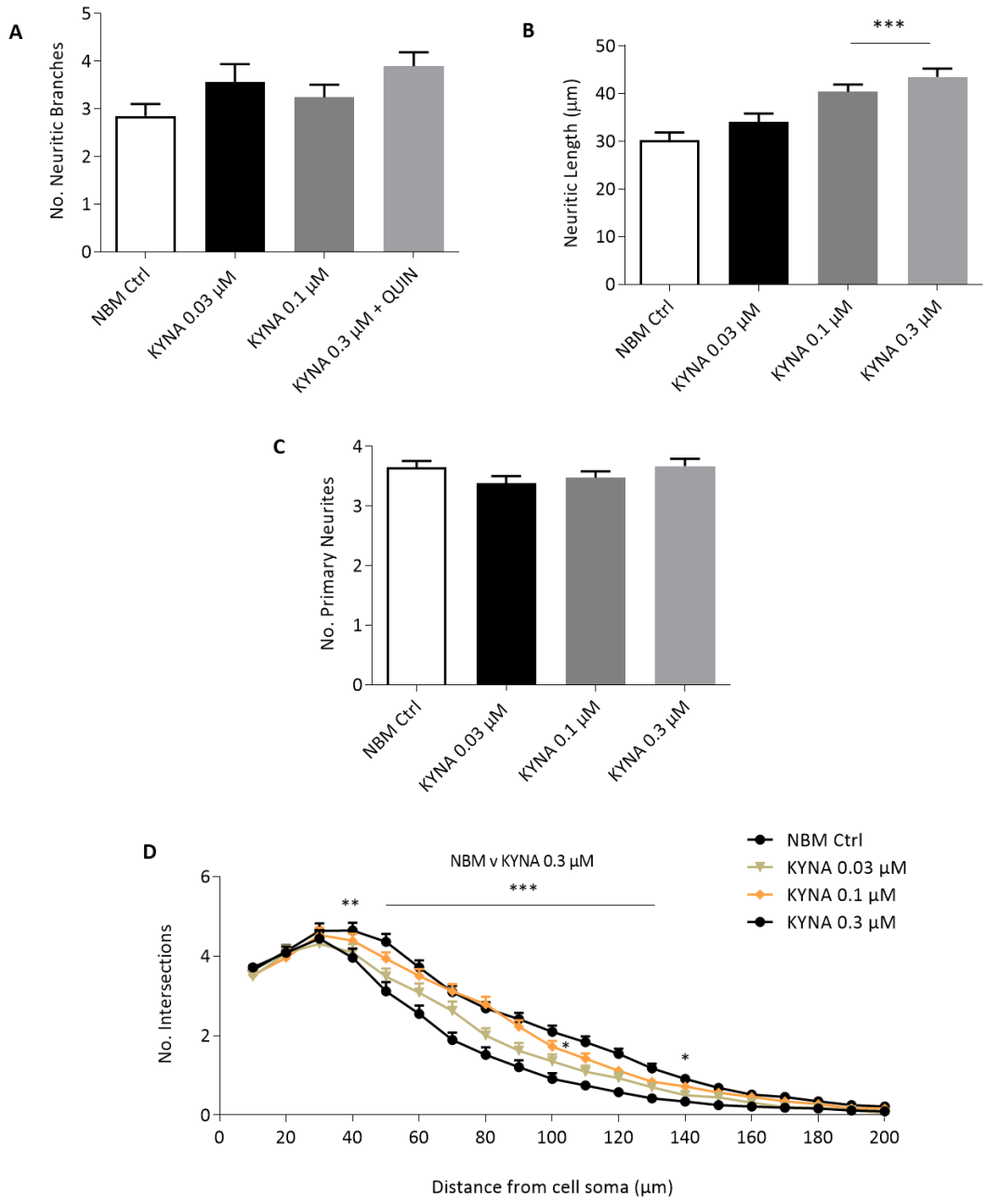

Figure 6.5 Kynurenic acid increases the complexity of mature primary cortical neurons.

Primary cortical mature neurons (DIV 21) were treated with KYNA (0.03, 0.1 and 0.3 µM) for 24 hours before fixation and MAP2 immunocytochemistry. Sholl analysis was performed to analyse the number of neuritic branches (A), the neuritic length (B), the number of primary neurites (C), and the Sholl profile (D). Data are expressed as mean ± SEM, n=6 coverslips per treatment group from 3 independent experiments. ***P<0.001 vs. control NBM (Newman-Keuls *post hoc* test).

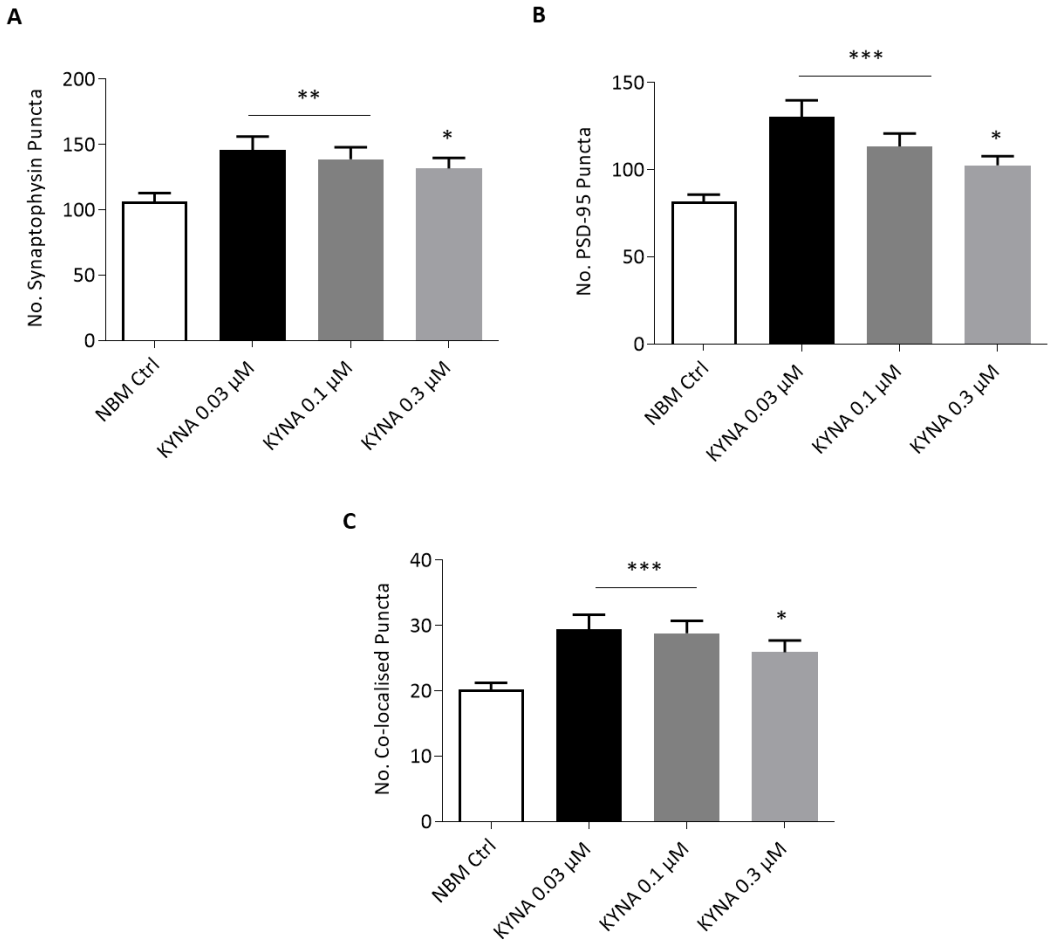

Figure 6.6 Kynurenic acid increases the co-localisation of synaptic proteins in mature primary cortical neurons.

Primary cortical mature neurons (DIV 21) were treated with KYNA (0.03, 0.1 and 0.3 µM) for 24 hours before fixation and immunocytochemistry to quantify the number of synaptophysin puncta (A), PSD-95 puncta (B), and co-localised synaptic puncta (C). Data are expressed as mean ± SEM, n=6 coverslips per treatment group from 3 independent experiments. ***P<0.001, **P<0.01, *P<0.01 vs. control NBM (Newman-Keuls *post hoc* test).

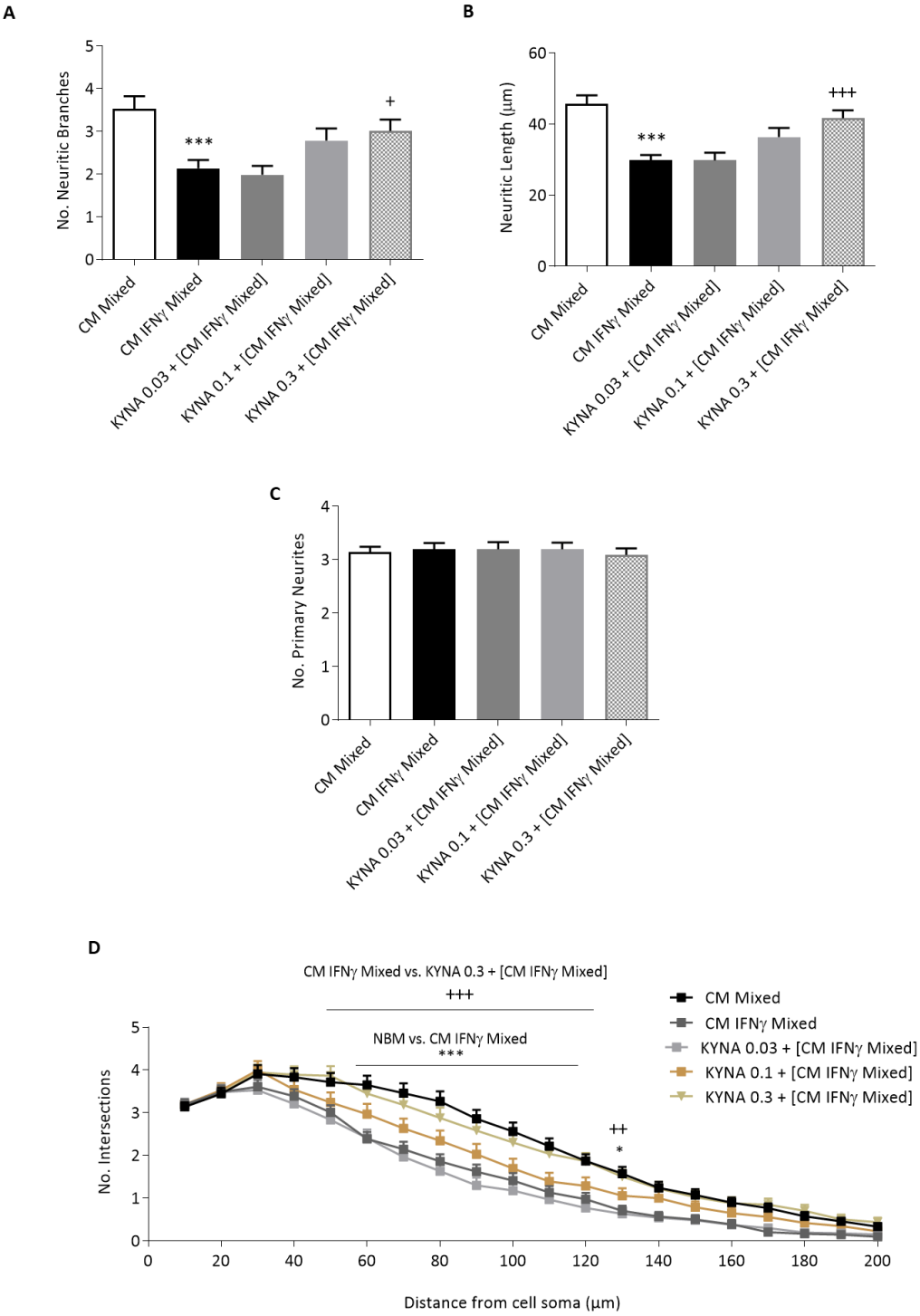

Figure 6.7 Kynurenic acid protects against reductions in the complexity of mature primary cortical neurons induced by conditioned media from IFNγ treated mixed glia. Primary mixed glial cultures (DIV 14) were treated with IFNγ (10 ng/mL) for 24 hours. The resulting conditioned media was collected and applied to mature neurons (DIV 21) with increasing concentrations of KYNA (0.03, 0.1, 0.1 µM) for 24 hours before fixation and MAP2 immunocytochemistry. Sholl analysis was performed to analyse the number of neuritic branches (A), the neuritic length (B), the number of primary neurites (C), and the Sholl profile (D). Data are expressed as mean ± SEM, n=4-5 coverslips per treatment group from 4 independent experiments. ***P<0.001, *P<0.05 vs. CM from untreated mixed glia. $^{+++}$P<0.001, $^{++}$P<0.01, $^{+}$P<0.05 vs. CM from IFNγ treated mixed glia (Newman-Keuls *post hoc* test).

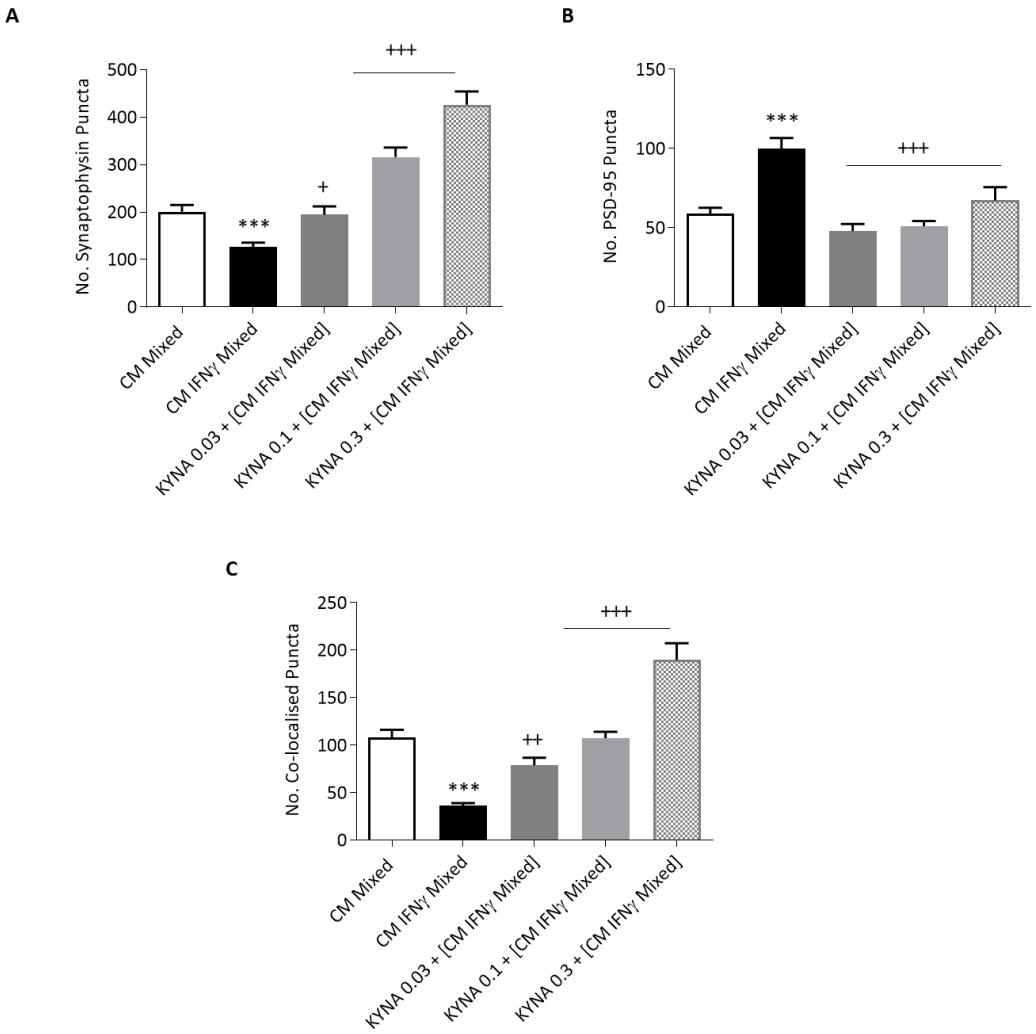

Figure 6.8 Kynurenic acid protects against reductions in synaptic protein co-localisation in mature primary cortical neurons induced by conditioned media from IFNγ treated mixed glia.

Primary mixed glial cultures (DIV 14) were treated with IFNγ (10 ng/mL) for 24 hours. The resulting conditioned media was collected and applied to mature neurons (DIV 21) with increasing concentrations of KYNA (0.03, 0.1, 0.1 µM) for 24 hours before fixation and immunocytochemistry to quantify the number of synaptophysin puncta (A), PSD-95 puncta (B), and co-localised synaptic puncta (C). Data are expressed as mean ± SEM, n=4-5 coverslips per treatment group from 4 independent experiments. ***P<0.001 vs. CM from untreated mixed glia. $^{+++}$P<0.001, $^{++}$P<0.01, $^{+}$P<0.05 vs. CM from IFNγ treated mixed glia (Newman-Keuls *post hoc* test).

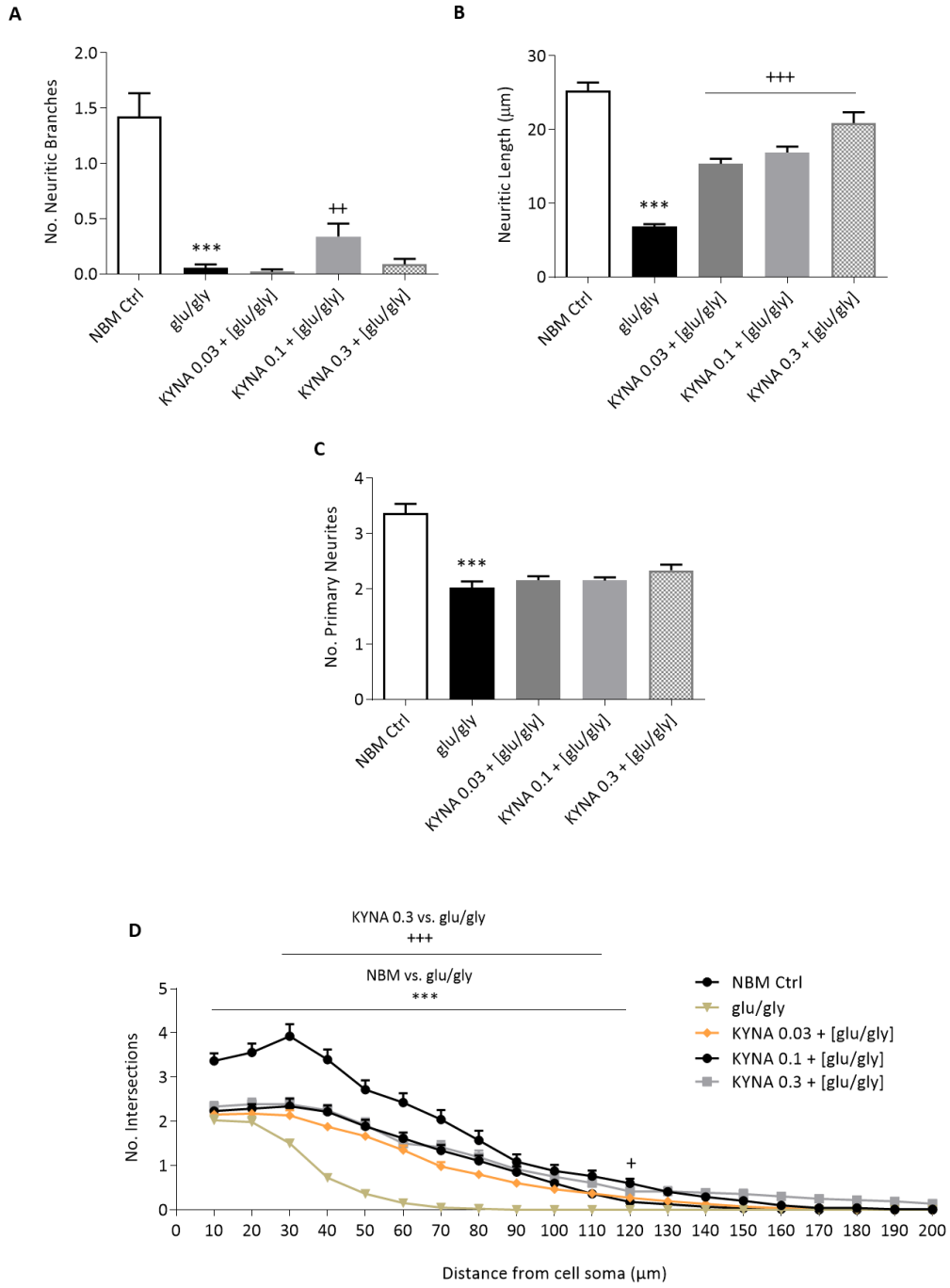

Figure 6.9 Kynurenic acid partially protects against reductions in the complexity of mature primary cortical neurons induced by glutamate and glycine.

Primary cortical mature neurons (DIV 21) were co-treated with [glutamate (50 µM)/glycine (1 µM)] and KYNA (0.03, 0.1 and 0.3 µM) for 24 hours before fixation and MAP2 immunocytochemistry. Sholl analysis was performed to analyse the number of neuritic branches (A), the neuritic length (B), the number of primary neurites (C), and the Sholl profile (D). Data are expressed as mean ± SEM, n=4-5 coverslips per treatment group from 4 independent experiments. ***P<0.001 vs. control NBM, $^{+++}$P<0.001, $^{++}$P<0.01 vs. glutamate and glycine (Newman-Keuls *post hoc* test).

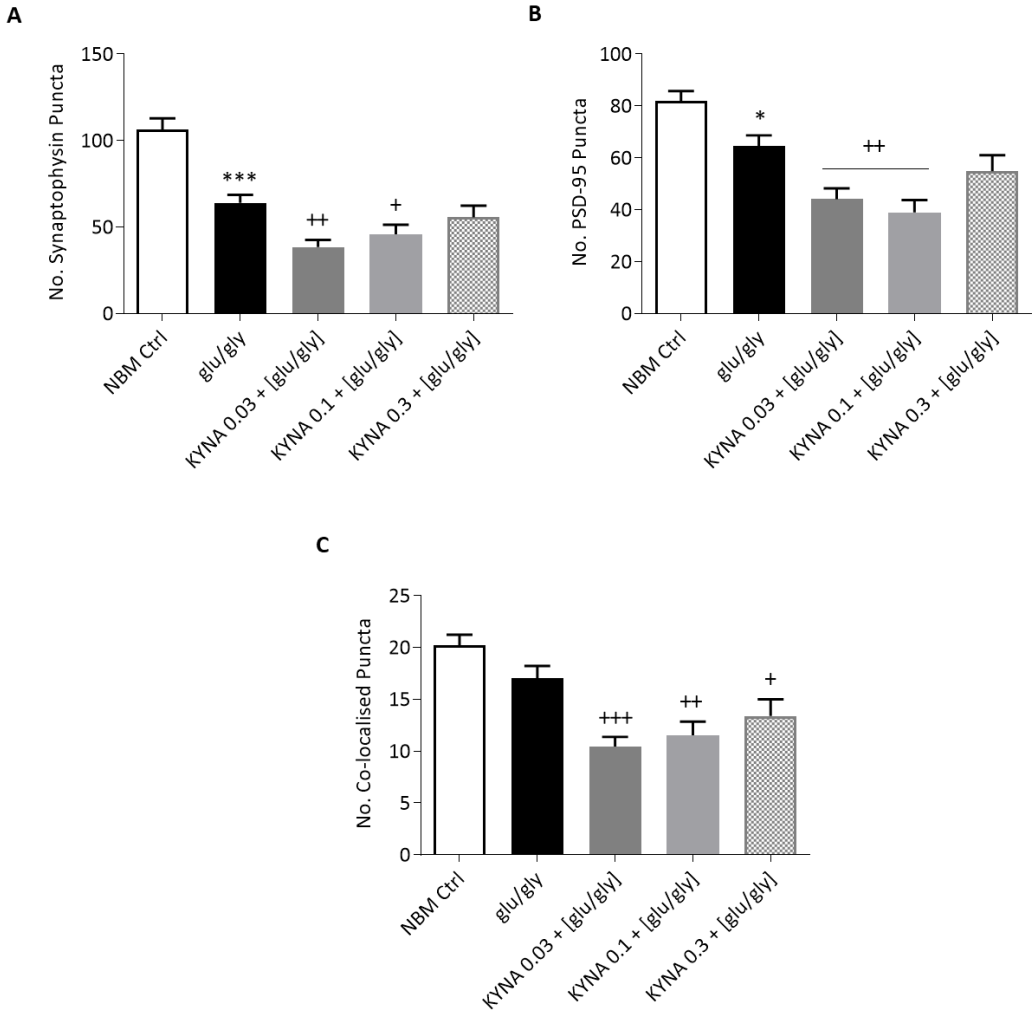

Figure 6.10 Kynurenic acid partially protects against reductions in synaptic proteins co-localisation in mature primary cortical neurons induced by glutamate and glycine.
Primary cortical mature neurons (DIV 21) were co-treated with [glutamate (50 µM)/glycine (1 µM)] and KYNA (0.03, 0.1 and 0.3 µM) for 24 hours before fixation and immunocytochemistry to quantify the number of synaptophysin puncta (A), PSD-95 puncta (B), and co-localised synaptic puncta (C). Data are expressed as mean ± SEM, n=4-5 coverslips per treatment group from 4 independent experiments. ***P<0.001, *P<0.05 vs. control NBM, $^{+++}$P<0.001, $^{++}$P<0.01 vs. glutamate and glycine (Newman-Keuls *post hoc* test).

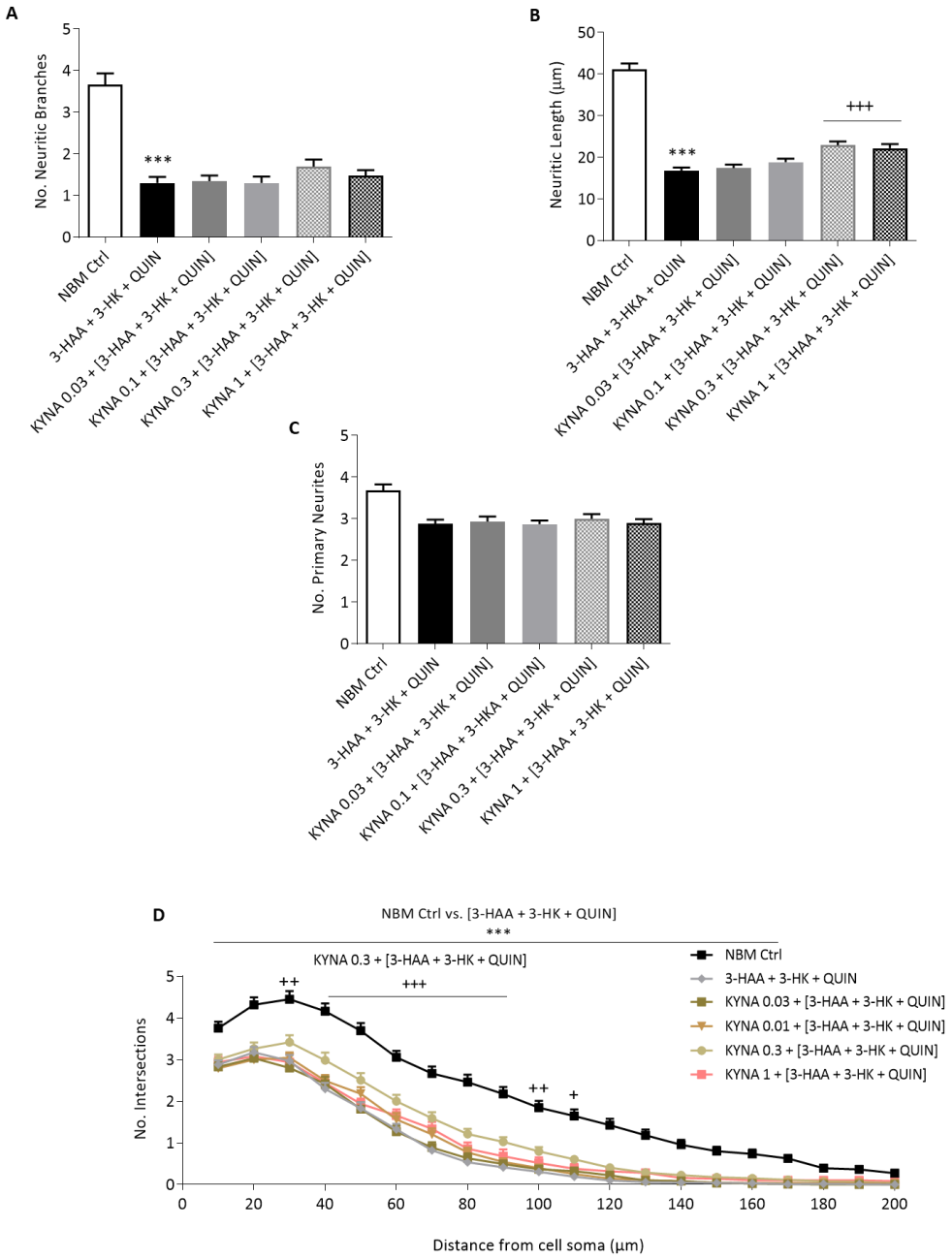

Figure 6.11 Kynurenic acid confers little or no protection against reductions in the complexity of mature primary cortical neurons induced by [3-HAA + 3-HK + QUIN].
Primary cortical mature neurons (DIV 21) were co-treated with [3-HAA (0.03 µM) + 3-HK (0.03 µM) + QUIN (0.1 µM)] and KYNA (0.03, 0.1 and 0.3 µM) for 24 hours before fixation and MAP2 immunocytochemistry. Sholl analysis was performed to analyse the number of neuritic branches (A), the neuritic length (B), the number of primary neurites (C), and the Sholl profile (D). Data are expressed as mean ± SEM, n=4 coverslips per treatment group from 5 independent experiments. ***P<0.001 vs. control NBM, $^{+++}$P<0.001, $^{++}$P<0.01, $^{+}$P<0.05 vs. [3-HAA + 3-HK + QUIN] (Newman-Keuls *post hoc* test).

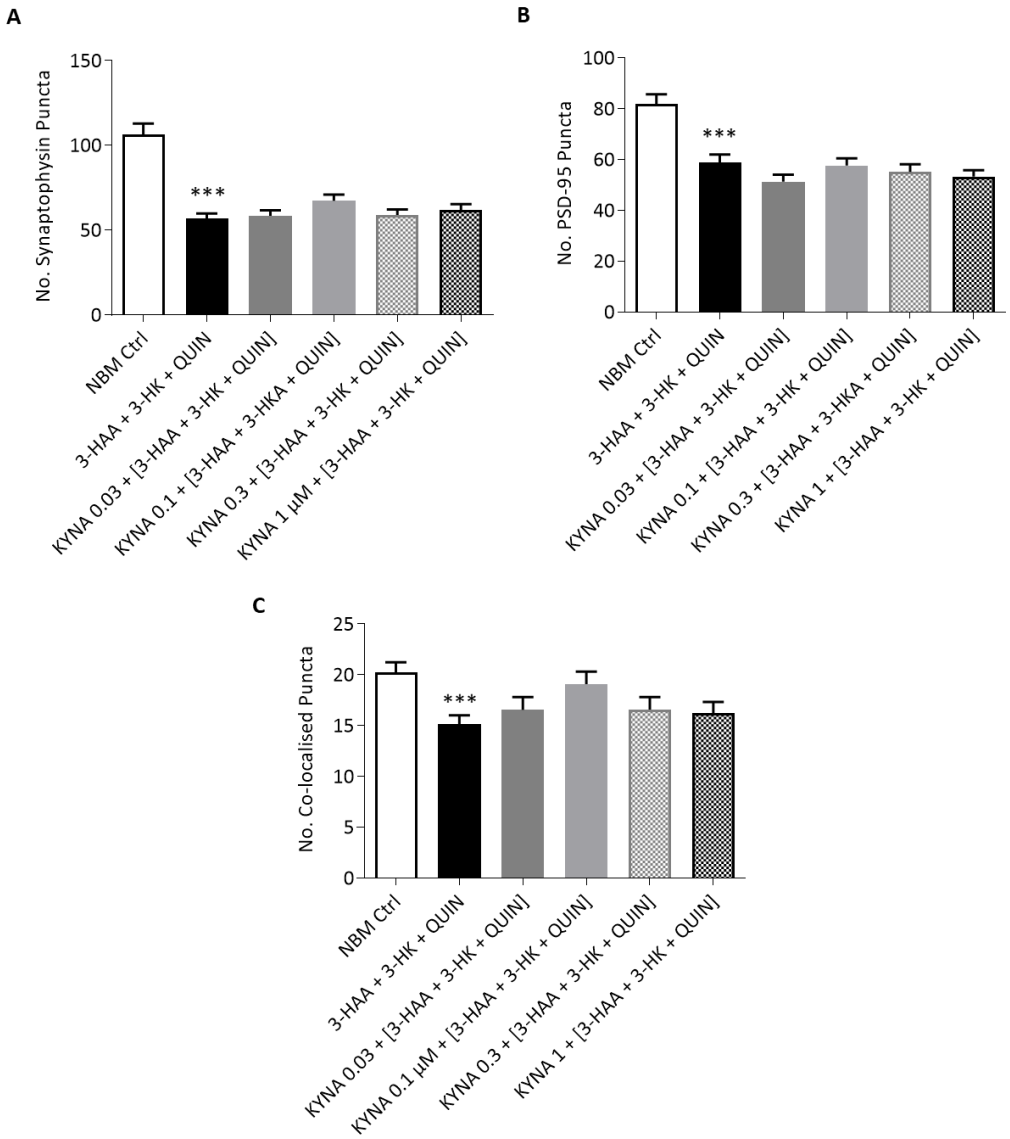

Figure 6.12 Kynurenic acid confers little or no protection against reductions in the co-localisation of synaptic proteins in mature primary cortical neurons induced by [3-HAA + 3-HK + QUIN].

Primary cortical mature neurons (DIV 21) were co-treated with [HAA (0.03 µM) + HK (0.03 µM) + QUIN (0.1 µM)] and KYNA (0.03, 0.1 and 0.3 µM) for 24 hours before fixation and immunocytochemistry to quantify the number of synaptophysin puncta (A), PSD-95 puncta (B), and co-localised synaptic puncta (C). Data are expressed as mean ± SEM, n=5 coverslips per treatment group from 4 independent experiments. ***P<0.001 vs. control NBM (Newman-Keuls *post hoc* test).

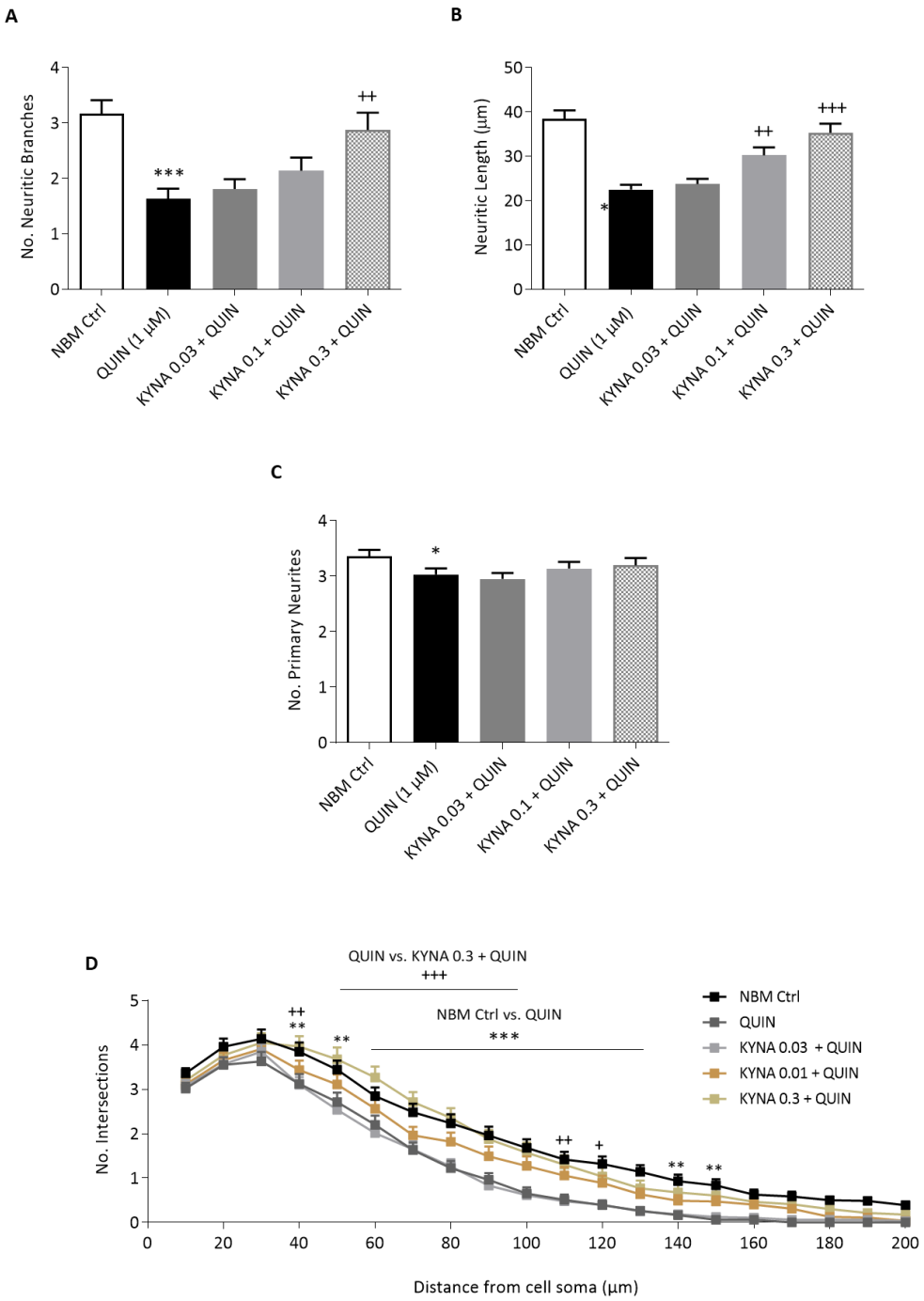

Figure 6.13 Kynurenic acid protects against reductions in the complexity of mature primary cortical neurons induced by quinolinic acid.

Primary cortical mature neurons (DIV 21) were co-treated with QUIN (0.1 µM) and KYNA (0.03, 0.1 and 0.3 µM) for 24 hours before fixation and MAP2 immunocytochemistry. Sholl analysis was performed to analyse the number of neuritic branches (A), the neuritic length (B), the number of primary neurites (C) and the Sholl profile (D). Data are expressed as mean ± SEM, n=4-5 coverslips per treatment group from 4 independent experiments. ***P<0.001, **P<0.01, *P<0.05 vs. control NBM, $^{+++}$P<0.001, $^{++}$P<0.01, $^{+}$P<0.05 vs. QUIN (Newman-Keuls *post hoc* test).

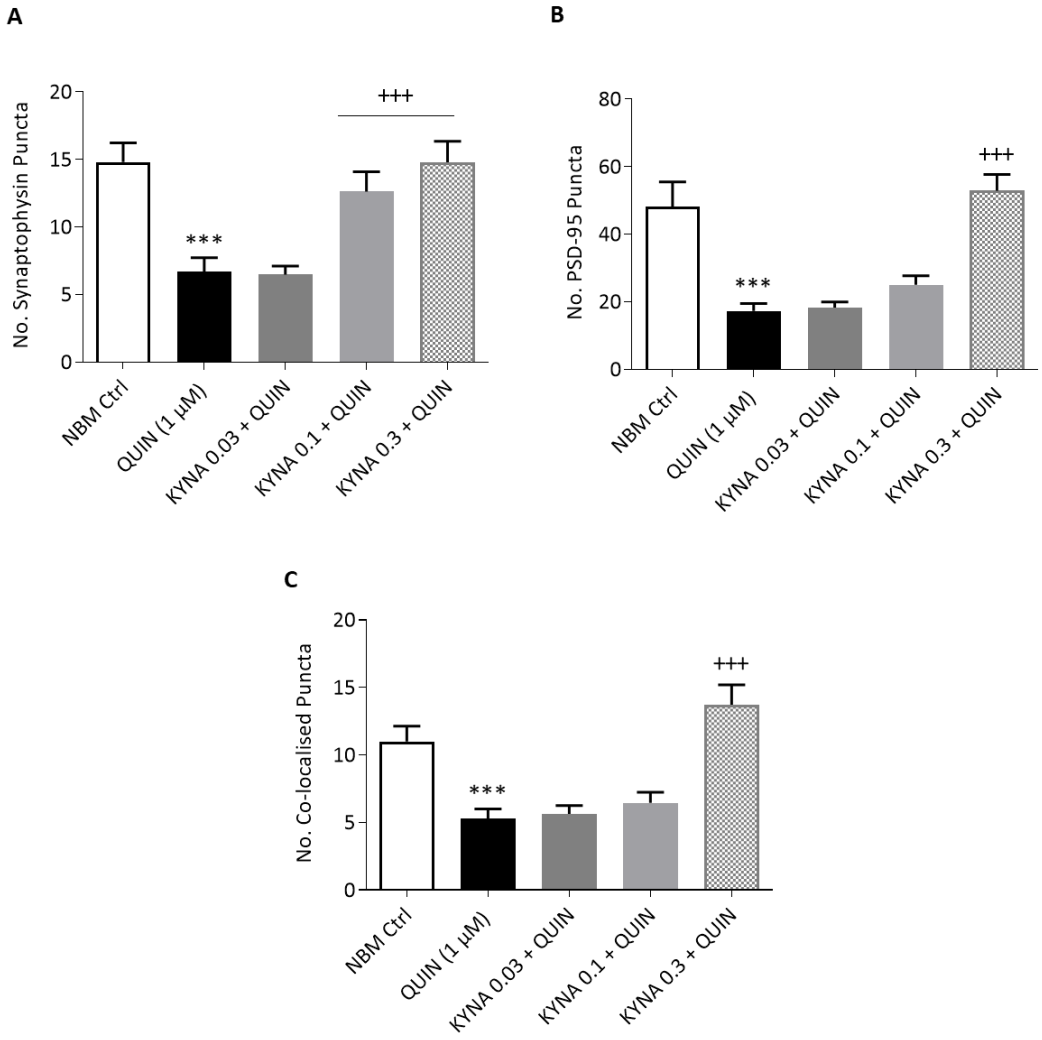

Figure 6.14 Kynurenic acid protects against reductions in the co-localisation of synaptic proteins in mature primary cortical neurons induced by quinolinic acid.
Primary cortical mature neurons (DIV 21) were co-treated with QUIN (0.1 µM) and KYNA (0.03, 0.1 and 0.3 µM) for 24 hours before fixation and immunocytochemistry to quantify the number of synaptophysin puncta (A), PSD-95 puncta (B), and co-localised synaptic puncta (C). Data are expressed as mean ± SEM, n=4-5 coverslips per treatment group from 4 independent experiments. ***P<0.001 vs. control NBM, $^{+++}$P<0.001 vs. QUIN (Newman-Keuls *post hoc* test).

6.4 Discussion

Results from this investigation establish a role for KP activation under inflammatory conditions, in particular following IFNγ-mediated activation of glial cells. They demonstrate that TNF-α and IL-1α increase the expression of KP enzymes indicative of KP induction in enriched astrocytic cultures. Similarly, IL-6 increased the expression of KP enzymes indicative of KP induction in enriched microglial cultures. IDO inhibition using 1-MT provided some protection against reductions in neuronal complexity induced by conditioned media from IFNγ-activated glia, indicating that KP activation plays a role in inflammatory driven changes in neuronal integrity.

The results also demonstrate the importance of maintaining a balance of the production of neuroactive KP metabolites. KYNA protected against reductions in neuronal complexity and synapse formation induced by conditioned media from IFNγ treated mixed glia. KYNA partially protected against reductions in neuronal complexity and synapse formation induced by glutamate and glycine. While KYNA failed to protect against reductions in neuronal complexity induced by the triple metabolite combination 3-HA, 3-HK and QUIN it did confer some protection against reductions in the number of co-localised synaptic puncta. KYNA completely protected against reductions in neuronal complexity and co-localised synaptic puncta induced by QUIN, highlighting its potential in the modulation of inflammatory driven KP activation and corollary disruptions in neuronal plasticity.

6.4.1 TNF-α and IL-1α increase the mRNA expression of kynurenine pathway enzymes in primary cortical astrocytes

Treatment of enriched primary cortical astrocytes with TNF-α and IL-1α increased the mRNA expression of KMO and IDO1, reduced the mRNA expression of KAT II and TDO2 and had no effect on the mRNA expression of KYNU. These results are similar to previous work investigating the effect of IFNγ-induced gene expression in astrocytes. Previous work in the lab has shown that IFNγ-induces gene expression IDO and KMO, reduces the expression of TDO and KYNU, and has no effect on the expression of KAT II in primary astrocytes (O'Farrell, 2016b).

In both cases treatment of enriched primary cortical astrocytic cultures with IFNγ or TNF-α and IL-1α increased the mRNA expression of KMO and IDO1 and reduced the expression of TDO. These results are in line with previous findings describing increased expression of the neurotoxic enzymes KMO and IDO1 in response to inflammatory stimuli both *in vivo* and *in vitro* (Connor et al, 2008). They are also similar to reports in the literature of IFNγ-induced expression of IDO in human foetal astrocytes (Guillemin et al, 2001; Guillemin et al, 2005; O'Farrell, 2016a).

TNF-α and IL-1α reduced the mRNA expression of KAT II in enriched primary cortical astrocytic cultures. This result differs from previous studies demonstrating that IFNγ had no effect on the expression of KAT II (O'Farrell, 2016a). A reduction in KAT II expression suggests the KP shifts in favour of the production of neurotoxic metabolites under TNF-α and IL-1α-induced inflammatory conditions.

TNF-α and IL-1α also reduced the mRNA expression of TDO2. This is in line with previous work demonstrating that IFNγ has no effect on the mRNA expression of TDO2 in BV-2 microglia, primary cortical microglia or mixed glia but reduced its expression enriched primary cortical astrocytic cultures (O'Farrell, 2016a). The reduction in TDO observed in this study is thus not surprising given that TDO2 induction is not traditionally associated with inflammatory stimuli. Expression patterns of TDO have become a matter of intensive research and the potential implications of the reduction in TDO expression observed in this model are manifold. TDO-deficiency or inhibition is neuroprotective in Drosophila and C. elegans (Breda et al, 2016; Campesan et al, 2011). Furthermore, inhibition of TDO is reported to decrease the levels of 3-HK favouring a shift towards neuroprotection via synthesis of the neuroprotective metabolite KYNA (Tan et al, 2012b). In this case a reduction in TDO may act as a protective mechanism from inflammatory driven increase in neurotoxic metabolites. Fluctuations in the expression of TDO mRNA suggest it is important in the regulation of the development of specific brain regions including the hippocampus and cerebellum (Kanai et al, 2010) and reductions in TDO expression have been linked with

perturbations in neurogenesis (Kanai et al, 2009) and anxiety-related behaviours (Funakoshi et al, 2011). It would be of interest to examine the effect of TNF-α and IL-1α on TDO expression *in vivo*. As TDO is primarily regulated by stress induction of the HPA axis and glucocorticoid receptor activation (O'Farrell & Harkin, 2015; Walker et al, 2013) it is possible that an *in vivo* model may yield different results based on integration of inflammatory stimuli such as TNF-α and IL-1α with the stress response.

TNF-α and IL-1α increased the mRNA expression of IDO1 in enriched primary cortical astrocytes. This result is in line with previous work demonstrating that the inflammatory stimulus IFNγ increases the mRNA expression of IDO in primary cortical astrocytes (O'Farrell, 2016a). A role for IDO-related activation of the KP in the pathophysiology of neurological disease and psychiatric disorders has been extensively reviewed (Maes et al, 2011; Myint & Kim, 2014; Schwarcz et al, 2012b). IDO is induced by the stress response via activation of the sympathoadrenal medullary (SAM) system, however it is also induced by inflammatory stimuli including IFNγ and LPS (Wang et al, 2010). These results are in line with the literature describing an induction of IDO by immunological stimuli (Mándi & Vécsei, 2012). While it is one of the first studies investigating the effect of TNF-α on IDO expression in enriched astrocytic cultures these results concur with previous *in vivo* findings demonstrating TNF-α-induced up-regulation of IDO in the cortex of mice following a four week unpredictable chronic mild stress paradigm (Liu et al, 2015). They are also in line with results from *in vivo* work demonstrating that LPS induction of IDO in the lung and brain is significantly suppressed in TNF-α- knock-out mice compared to wild type mice and *in vitro* work demonstrating a reduction in IDO mRNA in LPS-stimulated THP-1 cells co-treated with anti-h-TNF-α antibody (Fujigaki et al, 2001). Taken together, these results highlight TNF-α as a key and dominant inducer of IDO.

TNF-α and IL-1α increased the mRNA expression of KMO in astrocytes. This result is in line with previous work *in vitro* demonstrating that IFNγ increases the mRNA expression of KMO in primary cortical astrocytes (O'Farrell, 2016a) and previous *in vivo* work demonstrating induction of KMO in the rat brain following IFNγ-

induced systemic inflammatory challenge (Connor et al, 2008). They also support previous reports that IFNγ increases the expression of IDO and KMO resulting in increased concentration of KYN and 3-HK, a shift favoring the neurotoxic microglial arm (Lim et al, 2013).

TNF-α and IL-1α had no effect on the mRNA expression of KYNU. This is somewhat surprising as it differs from previous studies demonstrating IFNγ-induced reductions in the expression of KYNU in primary cortical enriched astrocyte cultures after 6 hours (O'Farrell, 2016a). However, it is possible that treatment duration played a role in these discrepancies. We cannot rule out an increased expression of KYNU after 6 hours in this study, given that both studies were carried out under the same conditions otherwise.

6.4.2 IL-6 increases the mRNA expression of kynurenine pathway enzymes in primary cortical microglia

Direct application of IL-6 to microglia increased the expression of TDO and reduced the expression of KMO and KAT II. In line with our expectations increased expression of TDO indicates pathway activation. However, a reduction in KAT II expression suggests the KP shifts in favour of the production of neurotoxic metabolites following activation of IL-6 signalling and induction of TDO expression in microglia. A reduction in KMO is somewhat surprising as it is putatively increased following inflammatory induction of the KP, as described above (Connor et al, 2008).

This is one of the first studies examining the direct effect of IL-6 on KP enzyme expression in microglia. These results are particularly interesting as they suggest a role for IL-6 in stress mediated activation of the KP. As TDO is primarily regulated by stress induction of the HPA axis and glucocorticoid receptor activation (O'Farrell & Harkin, 2015; Walker et al, 2013) these results reveal a novel link between stress activation of the pathway and IL-6 signalling *in vitro*.

6.4.3 1-MT (L) partially protects against reductions in the complexity of mature primary cortical neurons induced by conditioned media from IFNγ treated mixed glia

Conditioned media from IFNγ treated mixed glia reduced neuronal complexity and co-treatment with 1-MT (L) attenuated these reductions. These results are not surprising given that IFNγ is a potent inducer of IDO and previous *in vitro* studies have also previously shown that IFNγ induces IDO expression in cultured murine (Burudi et al, 2002) and human microglia (Guillemin et al, 2005). Furthermore, these results concur with the above findings that the pro-inflammatory cytokine IFNγ activates glial cells causing a release of IL-1α and TNF-α and subsequent induction of KP enzymes, indicative of pathway activation.

Attenuation of these reductions with the well-established IDO inhibitor 1-MT (L) confirms a role of KP activation in mediating effects of IFNγ activated glia on neuronal atrophy. These findings are foremostly in agreement with previous findings in the lab demonstrating that conditioned media from IFNγ stimulated BV-2 microglia suppresses measures of neurite outgrowth and complexity in immature primary cortical neurons (O'Farrell et al, 2017).

Nevertheless, as the IFNγ receptor is expressed by many CNS cell types (Hashioka et al, 2009; John et al, 2003; Lively & Schlichter, 2018; Papageorgiou et al, 2016) and known to stimulate a broad immune response and various signalling cascades in microglia and astrocytes, it is not surprising that 1-MT did not confer complete protection. While this study confirms a contributory role for the KP in driving neuronal atrophy associated with IFNγ activation of mixed glia it also suggests that there are other atrophic, inflammatory pathways at play that are independent of the KP (Stark & Darnell, 2012; Taniguchi et al, 2001).

6.4.4 1-MT (L) protects against reductions in neuronal complexity induced by conditioned media from IL-6 treated microglia

Conditioned media from IL-6 treated microglia reduced all measures of neuronal complexity compared to control NBM. Addition of the IDO inhibitor 1-MT protected against these reductions and reversed all measures back to control

levels. These results confirm that neuronal atrophy driven by IL-6 activation of microglia is mediated by activation of the KP.

Previous studies have shown that IDO induction in primary microglia is accompanied by an increase in IL-6, indicating a link between IL-6 signalling and inflammatory-driven KP activation in murine primary microglia (Wang et al, 2010). These results extend these findings demonstrating a link between IL-6 signalling in microglia, IDO activation and neuronal atrophy.

6.4.5 Kynurenic acid increases the complexity and co-localisation of synaptic proteins in mature primary cortical neurons

KYNA had no effect on the number of neuritic branches but higher concentrations of KYNA (0.1, 0.3 µM) increased neuritic length and increased the Sholl profile. KYNA had no effect on the number of primary neurites. Conversely, all concentrations of KYNA increased the number of synaptophysin puncta, PSD-95 puncta and the number of co-localised synaptic puncta compared to control NBM. These results are not surprising based on our knowledge that KYNA is neuroprotective and activation of the neuroprotective arm would be expected to promote synapse formation and recovery. Increased cortical levels of KYNA are associated with protection against oxidative stress and excitotoxic insult (García-Lara et al, 2015). However, despite extensive literature describing a role for KYNA as a neuroprotectant this is one of the first studies investigating the neurotrophic capacity of KYNA.

Neuroprotective properties of KYNA are thought to be primarily due to its antagonistic action at the glycine recognition site of NMDA receptors and on cholinergic α7 nicotine receptors, both of which are thought to occur at physiologically relevant concentrations (Majláth et al, 2016; Moroni et al, 2012; Prescott et al, 2006; Sas et al, 2007; Szalardy et al, 2012). Antagonism at the AMPAR or at the NMDA and glutamate binding sites of the NMDAR occur at much higher concentrations. While KYNA has the capacity to block all ionotropic glutamate receptors it has highest affinity for the NMDAR given that they are most permeable to Ca^{2+} (Lipton, 2004; Swartz et al, 1990). In addition, KYNA acts at other targets including the G protein-coupled receptor 35 (GPR35) (Ohshiro et

al, 2008; Wang et al, 2006) and the Aryl hydrocarbon Receptor (AhR) (Denison & Nagy, 2003) a transcription factor which induces downstream transcription of inflammatory cytokines such as IL-6 (DiNatale et al, 2010; Nguyen et al, 2010). It is possible that any of these mechanisms contributed to the neurotrophic effects observed in this study.

The lower concentration of KYNA (0.03 μM), was the most neurotrophic in comparison to other concentrations tested as it increased all three parameters (branches, length, primary neurites). These findings are consistent with the hypothesis that nanomolar concentrations of KYNA are neuroprotective while micromolar concentrations may be neurotoxic (Rozsa et al, 2008). Similarly, it is plausible that KYNA exerts its greatest neurotrophic properties at lower concentrations and that excess antagonism of the NMDAR at higher concentrations of KYNA trend towards toxicity. The NMDAR plays a critical role in brain development including cell proliferation, cell migration, neurogenesis, dendrite outgrowth, spine formation and synaptogenesis (Kwon & Sabatini, 2011). Blockade of the NMDAR, especially in the absence of another inflammatory stimulus may disrupt important physiological glutamatergic signaling producing a negative impact on neuronal development. This may explain why higher concentrations of KYNA trend towards toxicity.

The difference in the expression of synaptic markers at varying concentrations of KYNA may be explained by the interaction of KYNA at the presynaptic α7 nicotinic acetylcholine receptors (α7nAChRs) and the G-protein-coupled receptor GPR35 (Albuquerque & Schwarcz, 2013; Wang et al, 2006). At lower concentrations KYNA inhibits presynaptic glutamate release, thereby contributing to its neuroprotective effect (Carpenedo et al, 2001). It may also be explained by the fact that KYNA affects glutamate receptor subtypes to various extents or that it exerts a dose-dependent, dual effect on AMPARs. Higher concentrations of KYNA inhibit them, whereas lower concentrations of KYNA facilitate activation (Majláth et al, 2016; Szalardy et al, 2012).

6.4.6 Kynurenic acid protects against reductions in complexity and co-localisation of synaptic proteins in mature primary cortical neurons induced by conditioned media from IFNγ treated mixed glia

In addition to demonstrating neurotrophism, KYNA protected against reductions in neuronal complexity induced by conditioned media from IFNγ treated mixed glia in a concentration-related manner. In fact, higher concentrations of KYNA completely reversed these reductions bringing the number of branches and neuritic length measurements back to the levels of control.

Similar results were observed for the effect of KYNA on conditioned media from IFNγ treated mixed glial-induced reductions in synaptic puncta. Conditioned media from IFNγ treated mixed glia decreased the number of synaptophysin puncta and KYNA protected against these reductions in a concentration-related manner. Conversely, conditioned media from IFNγ treated mixed glia increased the number of PSD-95 puncta, however KYNA reduced this back to control levels. Additionally, conditioned media from IFNγ treated mixed glia decreased the number of co-localised synaptic puncta and KYNA attenuated these reductions.

In accordance with the role of KYNA as an NMDAR antagonist, previous studies also demonstrate that NMDAR inhibition with MK-801 attenuates reductions in complexity induced by conditioned media from IFNγ stimulated BV-2 microglia (O'Farrell, 2016b). Taken together these results provide evidence for a role of glutamatergic signalling and NMDAR activation in mediating inflammatory-driven, glial associated neuronal atrophy.

6.4.7 Kynurenic acid confers minimal protection against glutamate and glycine-induced reductions in the complexity and co-localisation of synaptic proteins in mature primary cortical neurons

Results of this study demonstrate that glutamate and glycine decrease the number of neuritic branches and number of primary neurites and KYNA fails to protect against these reductions. However, the higher concentration of KYNA (0.3 μM) provided some protection against glutamate and glycine-induced reductions in neuritic length. These results are somewhat surprising given that KYNA acts an NMDAR antagonist and previous work in the lab has confirmed that

the neurotoxic effects of glutamate and glycine are abrogated by NMDAR antagonism, for example with MK-801 (Doucet et al, 2015).

Treatment with glutamate and glycine reduced the number of synaptophysin puncta, PSD-95 puncta and the number of co-localised puncta. Surprisingly, co-treatment with KYNA failed to protect against these reductions. These results are in line with previous work demonstrating a reduction in synaptophysin, PSD-95 and co-localised synaptic puncta in mature neurons following treatment with glutamate (O'Farrell, 2016b). It is somewhat surprising that KYNA did not protect against glutamate and glycine induced-reductions in synaptic markers given that it acts as an endogenous antagonist at the NMDAR. These results suggest that there may be a synergistic effect between low concentrations of KYNA and glutamate/glycine as the lower concentrations of KYNA (0.03 μM) reduced the number of synaptophysin, PSD-95 and co-localised puncta compared to glutamate and glycine alone. It is possible that lower concentrations of KYNA activate other synaptic receptors such as the α7nAchRs engendering a synergistic reduction in the expression of synaptic markers (Albuquerque & Schwarcz, 2013). However, further studies are required to clarify these mechanisms.

These results do suggest that higher concentrations of KYNA may help recover glutamate and glycine-induced reductions in neuronal complexity and synaptic puncta as a concentration-related increase in neuritic length and the number of co-localised puncta is evident. Thus, while high concentrations of KYNA are potentially deleterious when applied to naïve healthy neurons, KYNA may be protective under inflammatory, excitotoxic states where extracellular glutamate is more abundant.

6.4.8 Kynurenic acid confers little or no protection against reductions in the complexity and co-localisation of synaptic proteins in mature primary cortical neurons induced by [3-HAA + 3-HK + QUIN]

Direct treatment of neurons with 3-HAA, 3-HK and QUIN reduced all measures of neuronal complexity including the number of neuritic branches, neuritic length and number of primary neurites. These results are not surprising given the

putative nature of 3-HAA, 3-HK and QUIN as neurotoxic metabolites of the KP and the large body of evidence demonstrating a role for them as endogenous neurotoxins and producers of free radicals with pro-oxidant activity (González Esquivel et al, 2017b). 3-HAA, 3-HK and QUIN are known to produce high levels of ROS which cause disruption of cytoskeletal dynamics, dendritic architecture and axonal transport systems (Reyes-Ocampo et al, 2015b; Wilson & González-Billault, 2015). Given that many cytoskeletal proteins are highly susceptible to oxidative damage it is likely that these mechanisms contribute, at least in part to the reduction in neuronal complexity observed in this study. 3-HAA, 3-HK and QUIN are also reported to cause mitochondrial damage that can lead to perturbations in cellular energy levels (Reyes-Ocampo et al., 2015; González Esquivel et al., 2017). Disruptions in cellular energy mechanisms have also been linked with increased activity of the enzyme KMO, indicative of a shift in KP metabolism towards the neurotoxic KMO branch and production of 3-HK, 3-HAA and QUIN as well as ROS.

KYNA failed to protect against 3-HAA, 3-HK and QUIN-induced reductions in neuronal complexity. These results are surprising given that KYNA is a known antioxidant with free radical scavenging properties, and would thus have been expected to confer some protection against the pro-oxidant 3-HK, and 3-HAA (Vecsei et al, 2013). Similarly, its role as an NMDAR antagonist would be expected to protect against the reductions induced by the NMDA agonist QUIN. Failure of KYNA to reverse the effects of the triple metabolite combination suggests that 3-HAA, 3-HK and QUIN produce synergistic effects when applied to neurons in combination producing a reduction in complexity that cannot be alleviated by KYNA at the concentrations tested.

In addition to effects on complexity, application of the triple metabolite combination to mature neurons reduced the expression of co-localised synaptic puncta. 3-HAA, 3-HK and QUIN decreased the number of synaptophysin, PSD-95 and co-localised synaptic puncta. These results concur with previous findings demonstrating that activation of the neurotoxic arm of the KP (direct application of 3-HAA or 3-HK or the triple metabolite combination [3-HAA + 3-HK + QUIN] to

neurons) impairs synapse formation *in vitro* (O'Farrell, 2016a). Chronic inhibition of KMO *in vivo* has also been shown to reduce synaptic loss as measured by synaptophysin in the hippocampus and frontal cortex of a transgenic mouse model of Alzheimer's disease (Zwilling et al, 2011). Furthermore, mitochondria present in the synaptic terminal are a critical ATP supply for neuronal transmission. As mitochondrial dysfunction induced by 3-HAA, 3-HK and QUIN can deplete this supply resulting in perturbations in synaptic activity (Guo et al, 2017) it is possible that 3-HAA, 3-HK and QUIN-induced mitochondrial dysfunction may also account for the reductions in synaptic puncta observed in this study. In contrast to its effect on neuronal complexity, KYNA did protect against reductions in the number of co-localised synaptic markers induced by the triple metabolite combination indicating a protective effect for KYNA in the context of synapse formation.

It must be noted that there is some evidence supporting a role for 3-HAA and 3-HK as antioxidants when present in lower micromolar concentrations and in the absence of QUIN (Colín-González et al, 2013; Krause et al, 2011). This suggests that these metabolites may be initially protective but become toxic, or contribute to toxicity when in the presence of QUIN (Ramírez-Ortega et al, 2017), indicating that whether these metabolites confer protection or toxicity may be context-dependent. As such it was of interest to investigate the effect of KYNA on reductions in neuronal complexity and synapse formation induced by QUIN alone.

6.4.9 Kynurenic acid protects against reductions in the complexity and co-localisation of synaptic proteins in mature primary cortical neurons induced by quinolinic acid

Results of this study confirm the neurotoxic effects of QUIN, as QUIN induced a significant decrease in all measures of neuronal complexity (number of primary neurites, number of neuritic branches and neuritic length). These results are not surprising given that QUIN has been recognised as a neurotoxic metabolite which has pro-oxidative functions and generates ROS which are known to disrupt the cytoskeleton (Pérez-De La Cruz et al, 2012; Stroissnigg et al, 2007; Wilson & González-Billault, 2015). In particular, QUIN has been shown to disrupt

cytoskeletal dynamics possibly via oxidation of critical cytoskeletal elements culminating in disrupted dendritic architecture, destabilisation of microtubules and impaired axonal trafficking of vesicles which can manifest as suppression of neuronal growth and complexity (Pérez-De La Cruz et al, 2012; Wilson & González-Billault, 2015). In addition to its role as a pro-oxidant, evidence suggests that QUIN primarily elicits its excitotoxic effects via activation of the NMADR in mature neurons (Lugo-Huitrón et al, 2011) causing disruption of the cytoskeleton (Rahman et al, 2009; Simões et al, 2018).

Results of this study also confirm the protective ability of KYNA as there was a significant attenuation of QUIN-induced reductions in the number of primary neurites, neurite length and branches when neurons were co-treated with KYNA. These results are not surprising given that QUIN is a competitive agonist of the NMDAR and KYNA is an endogenous, competitive antagonist of the NMDAR (Schwarcz et al, 2012b; Vecsei et al, 2013). They are also in line with previous work demonstrating protective potential of KYNA against QUIN-induced toxicity in rat striatal slices (Ferreira et al, 2018). Previous *in vivo* studies have shown that quinolinic acid increases phosphorylation of the low molecular weight neurofilament subunit in neurons and the NMDAR antagonist MK-801 prevents this hyperphosphorylation (Pierozan et al, 2010). In addition to its effect on complexity, QUIN decreased the number of synaptophysin, PSD-95 and co-localised synaptic puncta. These results support recent *in vivo* data demonstrating that intraventricular infusion of QUIN produces a decrease in synaptic proteins including PSD-95 (Rahman et al, 2018). Analogous to its effect on complexity, KYNA protected against QUIN-induced reductions in the number of synaptophysin, PSD-95 and co-localised synaptic puncta.

Overall, these findings illustrate the NMDAR as a promising target in disease circumstances where neurotoxic KP metabolites or excitotoxicity are implicated. The ability of KYNA to attenuate inflammatory-induced excitotoxicity illustrates the potential for manipulating the neuroprotective arm of the KP as a strategy for the treatment of brain disorders associated with neuronal atrophy. Given that the NMDAR is an important target for QUIN and KYNA acts as an NMDAR

antagonist, these results also confirm the primary mechanism of QUIN-induced toxicity in primary cortical neurons is mediated via NMDAR activation (Pérez-De La Cruz et al, 2012). Furthermore, the protective effects of KYNA in this study appear to be concentration-related, with lower concentrations showing little effect on QUIN-induced reductions in complexity and the higher concentrations conferring greater protection. These observations may be explained by concentration-related binding of KYNA to the NMDAR; at lower concentrations KYNA binds the glycine site of the NMDAR but at higher concentrations it can also bind the glutamate site (Schwarcz et al, 1992; Zhuravlev et al, 2007) which may offer greater protection via competition with QUIN for binding.

6.5 Conclusion

Results from these studies demonstrate a role for inflammatory-driven KP activation in driving changes in neuronal complexity and synapse loss *in vitro*. While previous work has demonstrated the impact of the KP on neuronal viability and the complexity of immature neurons, this study extends these findings to demonstrate the negative impact of inflammatory driven activation of the KP on the complexity of mature neurons. The implication of investigating the KP in mature neurons means that data is more applicable to diseases of the aged and adult brain.

Results of this study confirm that the inflammatory stimulus IFNγ and the soluble cytokine IL-6 drives KP activation producing reductions in neuronal complexity and synapse formation which may be attenuated by inhibition of the rate-limiting enzyme IDO. They also demonstrate that KYNA, the putative neuroprotective metabolite may act more as a neuromodulator which exhibits differential effects on complexity and synapse formation under homeostatic and inflammatory conditions. These findings also highlight the context-dependent and concentration-related effects of KYNA, with higher concentrations potentially contributing to neurotoxicity. Resultantly, restoring the balance between the astrocytic and microglial arms of the KP may be the most appropriate approach and aim of future research.

7 General discussion

7.1 Summary of main findings

The results presented in this thesis provide insight into the mechanisms underlying inflammatory-driven, reactive glia-induced neuronal atrophy and synapse loss. These studies align with literature evaluating the role of glial cells in a range of neurodegenerative and neuropsychiatric disorders (Almad & Maragakis, 2012; Elsayed & Magistretti, 2015; Liddelow et al, 2017; Mayegowda & Thomas, 2019; Verkhratsky et al, 2014a; Zuchero & Barres, 2015). Greater understanding of these mechanisms may allow identification of specific targets involved in neuroinflammation and the development of treatments for inflammatory CNS conditions.

7.1.1 L-AAA-induced astrocyte impairment induces atrophy and loss of synaptic markers in mature primary cortical neurons *in vitro*

L-AAA has received attention in recent years as an effective method of inducing astrocyte impairment *in vivo* and *in vitro* (David et al, 2018; Lee et al, 2013b; Lima et al, 2014; O'Neill et al, 2019). Previous research has shown that conditioned media derived from healthy astrocytes is neurotrophic and neuroprotective (Song et al, 2019; Takemoto et al, 2015; Yan et al, 2013). By contrast, results of this study demonstrate that conditioned media from L-AAA treated astrocytes is atrophic and provokes a reduction in the co-localisation of synaptic markers, indicative of a decrease in synapse number.

L-AAA reduced GFAP immunoreactivity, AQP4 immunoreactivity, astrocytic cell volume and mitochondrial respiration. These alterations may reflect impaired astrocytic function accounting for the reductions in neuronal outgrowth and synapse formation induced by conditioned media from L-AAA treated astrocytes. As astrocytic mitochondrial respiration is important for the brain's energy balance and for the production of antioxidants (Anderson & Swanson, 2000; Belanger et al, 2011; Dugan & Kim-Han, 2004), it is probable that mitochondrial dysfunction negatively impacts astrocytic neuroprotective function. The lack of effect of L-AAA on the uptake of [^{3}H] aspartate is in accordance with its role as an inhibitor of the intracellular enzymes glutamine synthetase and γ-glutamylcysteine synthetase (Brown & Kretzschmar, 1998; McBean, 1994; Voss

et al, 2016) and indicates that it does not provoke a sustained effect on astrocytic uptake of glutamate.

Conditioned media from healthy astrocytes is trophic (Day et al, 2014; Fang et al, 2019) and is reported to contain soluble factors with neurotrophic and synaptotrophic properties (Chung et al, 2015; Duarte et al, 2012; Farhy-Tselnicker & Allen, 2018; Oksanen et al, 2019; Park & Poo, 2013; Wiese et al, 2012). Taken together, these results suggest that L-AAA negatively impacts astrocytic production of these factors resulting in diminution of astrocytic support. BDNF is one example of an astrocytic factor associated with neuronal support and trophism (Day et al, 2014; Fulmer et al, 2014; Song et al, 2019; Takemoto et al, 2015) and reductions in BDNF or blocking BDNF signalling induces atrophy in hippocampal rodent neuronal cultures (Liu et al, 2017c).

Some of the potential mechanisms underlying the atrophic effects of conditioned media derived from L-AAA treated astrocytes are outlined in *Figure 7.1.*

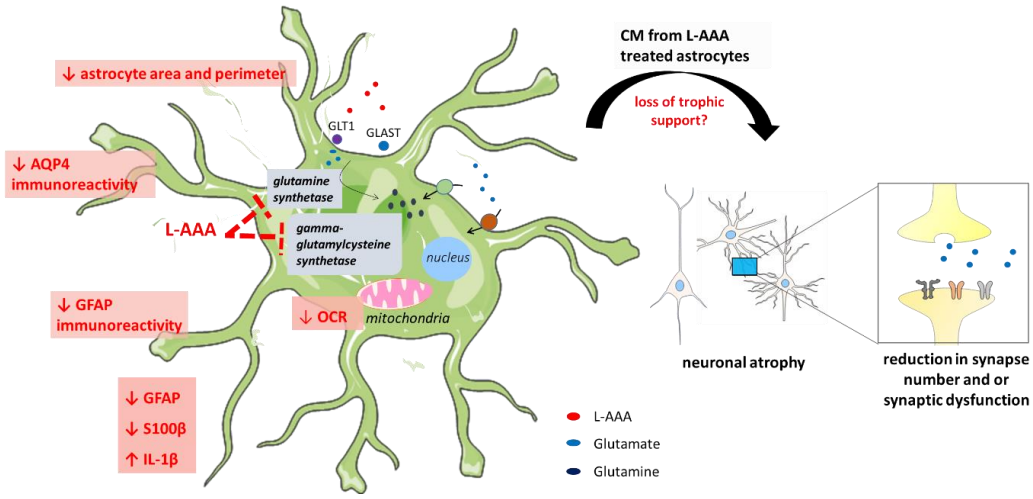

Figure 7.1 Summary of the characteristics of L-AAA-induced astrocyte impairment *in vitro*

Results of this study demonstrate that L-AAA-induced astrocyte impairment *in vitro* is characterised by a reduction in the immunoreactivity of GFAP and AQP4, a reduction in astrocyte mean cell area and perimeter, a reduction in the mRNA expression of GFAP, S100β, and IL-1β, and a reduction in mitochondrial respiration. Transfer of conditioned media from L-AAA treated astrocytes to mature neurons reduces neuronal complexity and the expression of synaptic markers inferring that L-AAA induces an astrocytic phenotype which negatively impacts neuronal growth, possibly via diminished release of trophic factors.

Translation of these *in vitro* findings into an animal model yielded disparate findings as L-AAA increased spine density in the PLC of mice compared to vehicle treated controls. While these results contrast with those obtained from the complexity work carried out *in vitro* they add to the current literature investigating the critical role astrocytes play in the formation and maintenance of neural circuitry *in vivo* (Papouin et al, 2017; Withers et al, 2017; Zuchero & Barres, 2015).

7.1.2 A role for IL-6 in reactive astroglial associated reductions in the complexity of primary cortical neurons

Astroglial associated mechanisms driving neuronal atrophy and synapse loss under inflammatory conditions were also assessed. Direct treatment of microglia with IFNγ produced reductions in cell morphology and Iba1 immunoreactivity typical of inflammatory-mediated microglial activation (Colton & Wilcock, 2010; Luo & Chen, 2012). By contrast, IFNγ induced opposing effects on astrocytes causing an increase in cellular volume and GFAP immunoreactivity characteristic of cellular hypertrophy (Pekny & Pekna, 2014). Conditioned media from IFNγ treated glia (microglia, astrocytes and mixed glia) decreased neuronal complexity. However, conditioned media from IFNγ treated microglia-induced the greatest reduction inferring that microglia may be the first responders and primary contributors to inflammatory driven neuronal atrophy (Bilbo & Stevens, 2017; Cătălin et al, 2013; Norden et al, 2015; Perry & Holmes, 2014). Conditioned media from IFNγ treated mixed glia also reduced the co-localised expression of synaptic markers. These results are in line with reports that activation of IFNγ signalling in glial cells *in vitro* (Hashioka et al, 2010) produces a range of pro-inflammatory responses which drive alterations in neuronal integrity (Loane & Byrnes, 2010a; Sundal, 2014; Yan et al, 2018).

IFNγ increased the expression of TNF-α, IL-1α, and IL-6 in mixed glia and microglia, all of which are reportedly up-regulated following microglial activation (Czeh et al, 2011; Liddelow et al, 2017; Norden et al, 2016; Wang et al, 2015) and known to contribute to neuroinflammation (Jensen et al, 2013; Kohler et al, 2016; O'Neill et al, 2019; Smith et al, 2012). IFNγ also increased the production and release of TNF-α and IL-1α protein from both mixed glia and microglia.

Considering that microglia are a primary source of TNF-α (Welser-Alves & Milner, 2013) and microglial responses are considered rapid by contrast to astrocytes, these results suggest that astrocyte activation likely occurs secondary to microglial.

TNF-α and IL-1α produced paradoxical effects on astrocyte morphology compared to those observed with IFNγ. As with IFNγ, TNF-α and IL-1α also increased GFAP, S100β, IL-1β and IL-6 suggesting that these cytokines are primarily responsible for the downstream effects of IFNγ. Conditioned media from TNF-α and IL-1α treated astrocytes reduced neuronal complexity and the co-localised expression of synaptic markers.

IFNγ treatment of mixed glia, and TNF-α and IL-1α treatment of astrocytes both increased the release of IL-6. As astrocytes are the primary source of IL-6 during neuroinflammation (Jensen et al, 2013) these results suggest that reactive astrocytes sustain microglial activation via an IL-6 dependent mechanism. While there is evidence to suggest that IL-6 signals back, stimulating microglia and astrocytes to release pro-inflammatory cytokines and acute-phase proteins, such as C-reactive protein (Querfurth & LaFerla, 2010), this study demonstrates that it can also directly compromise neuronal integrity provoking a reduction in complexity and synapse formation.

Immunoneutralisation of IL-6 in conditioned media derived from TNF-α and IL-1α treated astrocytes protected against associated neuronal atrophy and synapse loss. This study confirms a role for IL-6 in maintaining microglial activation, highlighting IL-6 as a potential target for the development of anti-inflammatory strategies in inflammatory and degenerative CNS disorders. Some of the mechanisms and mediators underlying inflammatory-induced neuronal atrophy and synapse loss are outlined in *Figure 7.2*.

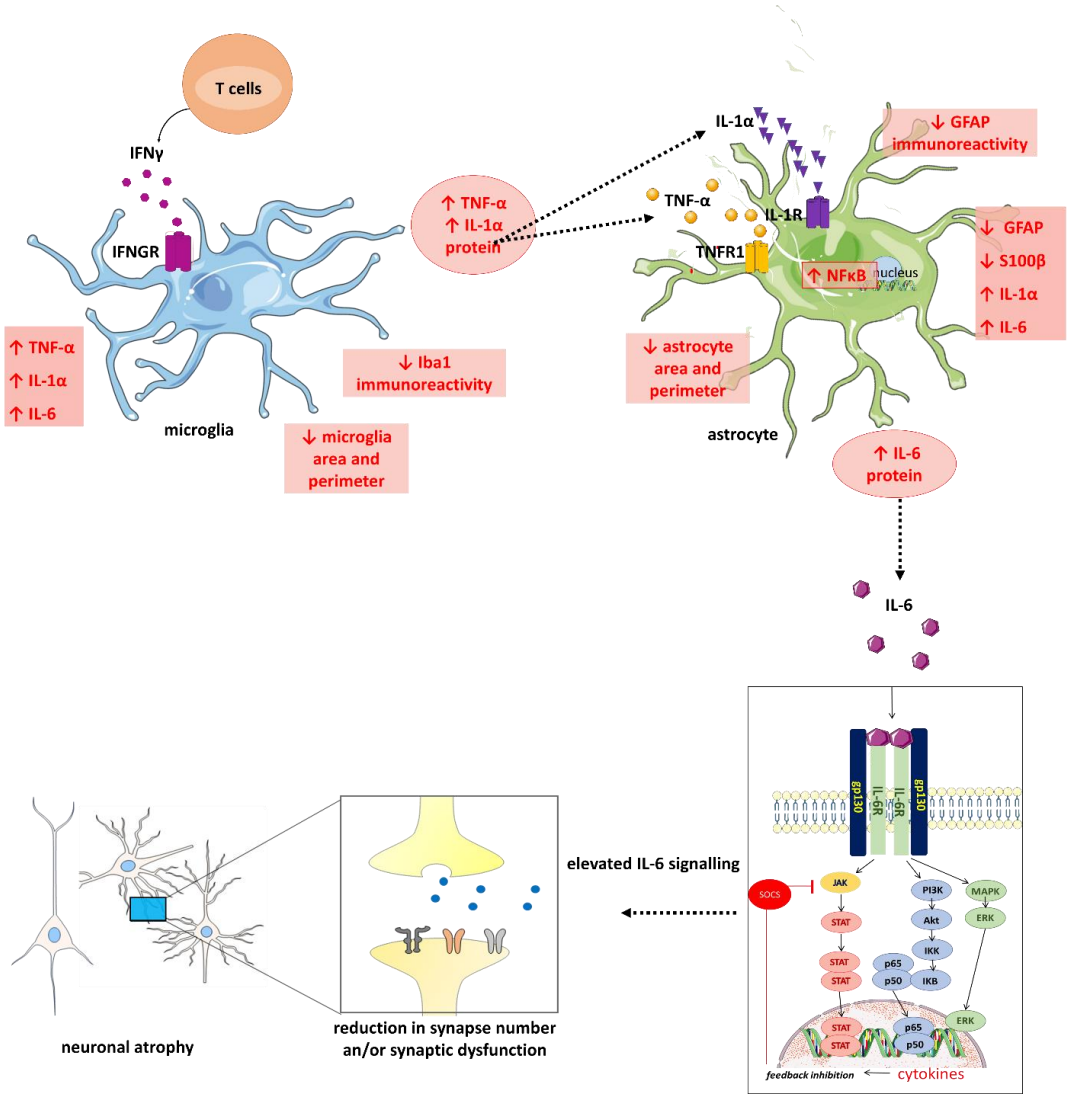

Figure 7.2 Summary of the potential mediators of IFNγ-induced neuronal atrophy
Results of this study demonstrate that IFNγ induces changes in primary cortical microglial cells including a reduction in the cell size, a reduction in Iba1 immunoreactivity, an increase in the mRNA expression of TNF-α, IL-1α, and IL-6, and an increase in the release of TNF-α, and IL-1α protein. Subsequent activation of astrocytes with TNF-α, and IL-1α induces an astrocytic phenotype characterised by a reduction in cell size, a reduction in GFAP immunoreactivity and the expression of GFAP and S100β, an increase in the mRNA expression of IL-1α and IL-6 and an increase in the release of IL-6 protein. Elevated levels of IL-6 directly affect mature neurons causing atrophy and synapse loss while immunoneutralisation of IL-6 in the conditioned media of TNF-α, and IL-1α treated astrocytes attenuates these reductions.

7.1.3 L-AAA attenuates reactive astrocyte-induced neuronal atrophy and synapse loss under inflammatory conditions

L-AAA attenuates LPS-induced neuronal loss in a neuroinflammatory rodent model of Parkinson's disease (O'Neill et al, 2019) suggesting that astrocytes have varying effects on neuronal integrity in the presence and absence of

inflammatory stimuli. This study extends previous findings by exploring the effects of L-AAA-induced astrocyte impairment on reactive glial associated neuronal atrophy and synapse loss.

L-AAA partially protected against reductions in the complexity of immature neurons, but not mature neurons induced by conditioned media from IFNγ treated mixed glial cells. These results suggest that IFNγ mediated activation of mixed glia continues to drive neuronal atrophy and synapse loss despite L-AAA-induced astrocyte impairment. By contrast, L-AAA attenuated reductions in the co-localised expression of synaptic proteins induced by conditioned media from IFNγ treated mixed glial suggesting that reactive astrocytes contribute to synapse loss induced by IFNγ activation of mixed glia.

In line with microglia being a primary source of TNF-α (Welser-Alves & Milner, 2013) L-AAA had no effect on IFNγ-induced TNF-α expression in mixed glia or microglial cultures. However, it did attenuate the increase in IL-1α and IL-6 release indicating that reactive astrocytes contribute to their release under inflammatory conditions. L-AAA failed to protect against IFNγ-induced inflammatory driven neuronal atrophy suggesting that activated microglia are primarily responsible for mediating these effects. This suggests that conditioned media from IFNγ treated mixed glia contains a plethora of pro-inflammatory cytokines, chemokines, and reactive oxidative species (Lehnardt, 2010) in addition to TNF-α and IL-1α culminating in a broad inflammatory response that cannot be solely attributed to reactive astrocytes.

L-AAA attenuated TNF-α and IL-1α-induced changes in astrocyte morphology, GFAP immunoreactivity and IL-6 release which may account for the protective effects of L-AAA in conditioned media collected from L-AAA, TNF-α and IL-1α treated astrocytes. This study adds to the growing body of literature describing a role for reactive astrocytes in expediting alterations in neuronal integrity (Ben Haim et al, 2015; Liddelow & Barres, 2017; Pekny & Pekna, 2014; Pekny et al, 2014).

7.1.4 A role for the kynurenine pathway in regulating inflammatory-induced changes in neuronal atrophy and synapse loss

TNF-α and IL-1α increased the mRNA expression of KMO and IDO1 and reduced the mRNA expression of KAT II and TDO2 in astrocytes indicating induction of the kynurenine pathway. 1-MT (L) attenuated reductions in neuronal complexity induced by conditioned media from IFNγ treated mixed glia confirming that induction of the kynurenine pathway plays a role in inflammatory driven neuronal atrophy. These results concur with previous reports that IFNγ induces expression of IDO and KMO (Lim et al, 2013) and conditioned from IFNγ-stimulated BV-2 microglia suppresses outgrowth in immature primary cortical neurons (O'Farrell et al, 2017). However, as 1-MT does not provide complete protection these results indicate that additional pro-inflammatory mechanisms in IFNγ-induced neuronal atrophy are likely at play. As IFNγ receptors are expressed on all glial cells (Hashioka et al, 2009; John et al, 2003; Lively & Schlichter, 2018; Papageorgiou et al, 2016) it is likely that other cell death pathways such as MAPK-driven pathways and gene regulatory pathways mediated by transcription factors such as interferon regulatory factor 1 (IRF1) and IRF8 (Stark & Darnell, 2012; Taniguchi et al, 2001) are activated in addition to the kynurenine pathway. As reactive glia are also known to produce NO which inhibits cellular respiration and results in rapid glutamate release and excitotoxicity (Bal-Price et al, 2002) we cannot exclude the possibility that NO may have also contributed to the observed reductions in neuronal complexity.

IL-6 induced KP activation in microglia providing a novel link between TDO induction, IL-6 signalling and neuronal atrophy. 1-MT protected against neuronal atrophy induced by conditioned media from IL-6 treated microglia confirming a role for KP induction in microglial cells. Previous studies have provided evidence linking stress-induced changes in dendrite arborisation and reductions in the number and structure of synapses with the pathophysiology of depression (Duman, 2004; Patrício et al, 2015). However, this is one of the first studies illustrating a potential role for IL-6 in stress activation of the pathway via TDO induction, which is typically associated with HPA axis activation.

By virtue of its ability to inhibit the NMDAR and the α7nAChR (Anderson & Maes, 2017; Badawy, 2014; García-Lara et al, 2015) most of the literature to date focuses on the neuroprotective capacity of KYNA. This is one of the first studies demonstrating its neurotrophic capacity which adds to the growing body of literature examining the effect of KP metabolites on neuronal integrity. In accordance with its neuroprotective role, KYNA attenuated reductions in neuronal complexity and the co-localised expression of synaptic markers induced by conditioned media from IFNγ treated mixed glia. KYNA partially attenuated glutamate and glycine-induced reductions in neuronal complexity and the co-localised expression of synaptic markers. KYNA failed to protect against reductions in neuronal complexity and the co-localised expression of synaptic proteins induced by 3-HKA, 3-HA and QUIN, but provided complete protection against reductions in neuronal complexity and the co-localised expression of synaptic markers induced by QUIN alone.

An increase in the neurotoxic metabolites QUIN and 3-HK have been reported in numerous CNS disorders (Schwarcz et al, 2012b) and previous work in the lab has shown that 3-HAA, 3-HK and QUIN reduces the complexity of immature primary cortical neurons *in vitro* (O'Farrell, 2016b). This study extends these findings by demonstrating QUIN-induced atrophy in mature primary cortical neurons. They also infer that synergistic signalling with the triple metabolite combination involves signalling pathways other than glutamatergic ones as KYNA failed to protect against associated reductions in complexity and the co-localised expression of synaptic markers. While the precise mechanisms of these interactions were not explored, it is likely that these metabolites disrupt cytoskeletal dynamics via oxidation of cytoskeletal elements, destabilisation of microtubules or impaired axonal trafficking of vesicles (Pérez-De La Cruz et al, 2012; Wilson & González-Billault, 2015). Microtubules and actin microfilaments are particularly vulnerable to oxidation due to the presence of cysteine residues and oxidation of cysteine residues can cause perturbations in cytoskeleton architecture. Altered neuronal trafficking may be of significance in the case of synaptic dysfunction. Mitochondria and other essential synaptic proteins are delivered to the synaptic terminal via axonal transport which is dependent on

the organisation of neuronal microtubules (Sheng and Cai, 2012). QUIN specifically has been shown to alter phosphorylation of intermediate filaments (Pierozan et al., 2014), and disrupt protein and mitochondrial delivery to synaptic terminals which likely accounts for its negative effect on neuronal integrity (Verstraelen et al., 2017).

These results provide evidence of a role for KP neurotoxic metabolites in mediating inflammatory-glial associated neuronal atrophy and synapse loss in primary cortical neurons. The potential mechanisms of KP induction in glial cells and associated alterations in neuronal integrity are summarised in *Figure 7.3.*

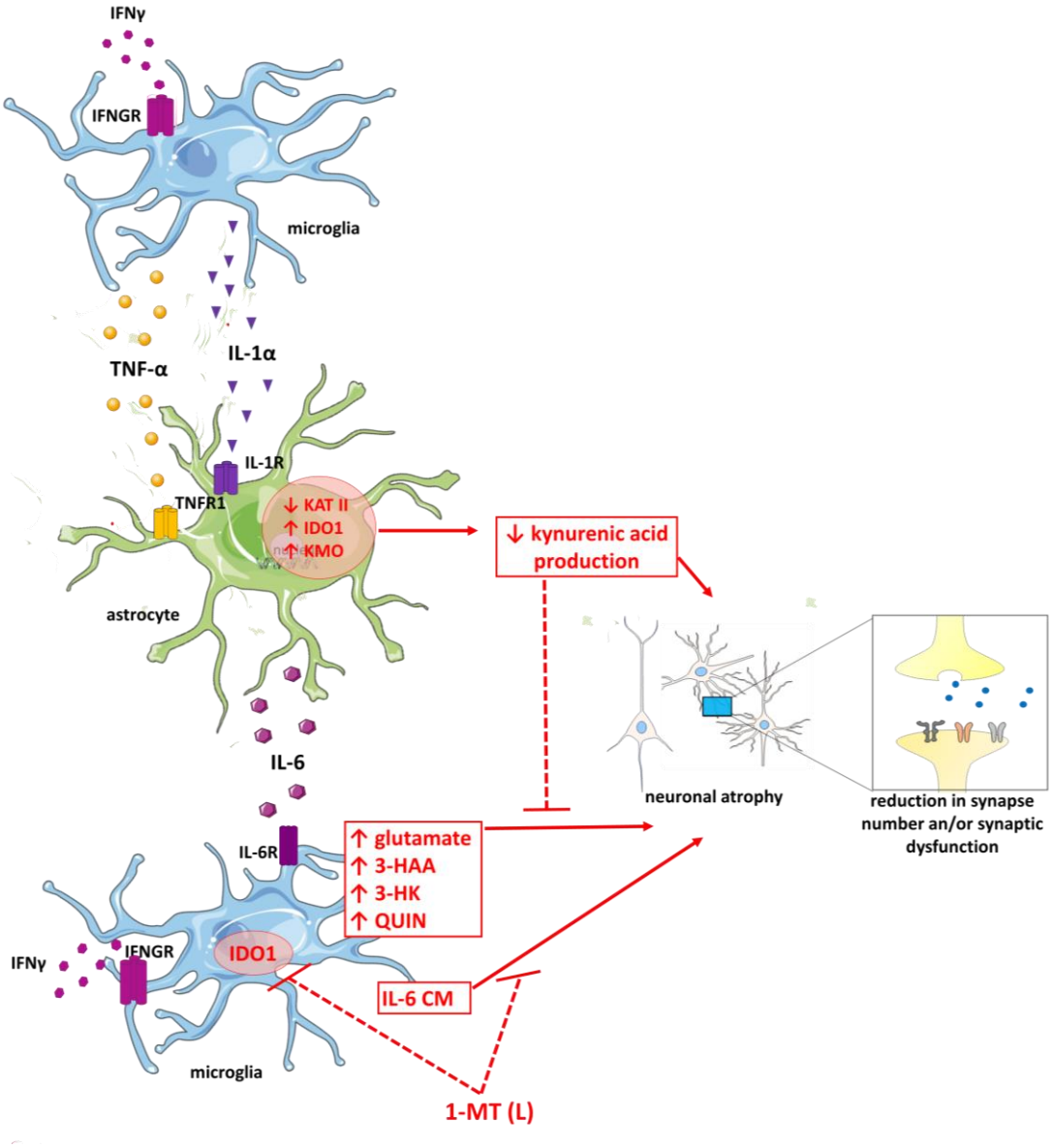

Figure 7.3 Mechanisms of inflammatory driven activation of the kynurenine pathway in glial cells and associated neuronal atrophy

Results of this study demonstrate that IFNγ, TNF-α, IL-1α and IL-6 activate the KP in glia producing a conditioned media that causes neuronal atrophy and synapse loss. Co-treatment of mature neurons with the IDO inhibitor 1-MT (L) protects against reductions in neuronal complexity produced by conditioned media from IFNγ treated mixed glia and IL-6 treated microglia indicating a role for KP activation in inflammatory driven neuronal atrophy. Astrocytic derived kynurenic acid attenuates alterations in neuronal integrity driven by neurotoxic metabolites released from reactive microglia. TNF-α and IL-1α-induced reduction in the expression of KAT II indicates a compromise in this protective pathway branch under inflammatory conditions and pre-eminence of the neurotoxic (microglial) branch of the pathway.

7.2 Translational and clinical relevance

Deficits in information processing is regarded as the core commonality of dysfunction among a range of CNS disorders (Uhlhaas & Singer, 2012; Yizhar et al, 2011). As alterations in the architecture of neural circuits are likely determinants of such deficits (Miller & Hen, 2015) quantifying changes in neuronal complexity, synaptogenesis and dendritic spines may prove useful in investigating the pathophysiology of CNS diseases characterised by aberrant information processing.

Combining analysis of human symptomatology and findings from animal models suggests that synaptic plasticity plays a fundamental regulatory role in the transmission of information through neuronal circuitry. By contrast, synaptic impairment contributes to the pathogenesis of numerous neuropsychiatric disorders (Arguello & Gogos, 2012) and neurodegenerative disorders (Bellucci et al, 2016; Fogarty, 2018; Sepers & Raymond, 2014) where it manifests as cognitive impairments (Duman & Aghajanian, 2012; Duman et al, 2016).

Results of this thesis demonstrate that L-AAA-induced astrocyte impairment, inflammatory-driven activation of glial cells and induction of the neurotoxic branch of KP causes atrophy and reductions in the co-localisation of synaptic markers in mature primary cortical neurons *in vitro*. The significance of these results lies in the fact that neuronal morphology influences signal integration and connectivity between brain regions (Ferrante et al, 2013). These findings are in accordance with numerous clinical studies describing reductions in neural cell size, brain region volumes (Haijma et al, 2013; MacQueen & Frodl, 2011) and the number of synapses in the prefrontal cortex of post mortem brains of patients with major depressive disorder (Kang et al, 2012; Price & Drevets, 2010). Previous brain imaging studies similarly report reduced volumes in the hippocampus and subgenual and anterior cingulate cortices of patients with depression (Evans et al, 2018; MacQueen & Frodl, 2011; Savitz & Drevets, 2009).

Activation of astroglia and inflammatory driven neuronal atrophy were also explored in this thesis. Neuroinflammation has become a well-established hallmark of numerous neurodegenerative (Bronzuoli et al, 2016; Guzman-Martinez et al, 2019; Möller, 2010) and neuropsychiatric disorders (Bauer &

Teixeira, 2019; Kohler et al, 2016; Müller, 2019; Radtke et al, 2017; Réus et al, 2015a; Sethi et al, 2019). Reactive astrocytes are also well accepted contributors to the pathological progression of CNS disorders including epilepsy, schizophrenia and Alzheimer's disease (Verkhratsky et al, 2014b). This study identifies TNF-α, IL-1α and IL-6 as primary factors mediating IFNγ driven neuronal atrophy and synapse loss *in vitro*. There is clinical evidence to show that blood levels of TNF-α, and IL-6 are elevated in patients with major depressive disorder (Janelidze et al, 2011; Liu et al, 2012). High serum levels of TNF-α, and IL-6 have also been reported in patients with schizophrenia (Martínez-Gras et al, 2012) and elevated plasma levels of IL-6 have been reported in patients with bipolar disorder (Munkholm et al, 2015). Two recent meta analyses indicate that IL-6 is the most consistently elevated cytokine in the blood of patients with major depressive disorder (Dowlati et al, 2010; Haapakoski et al, 2015). Consistent with these findings are currently available treatments for neuropsychiatric disorders such as SSRIs, which demonstrate a specific effect on lowering serum levels of IL-6 and TNF-α (Hannestad et al, 2011).

Most of the literature to date focuses on the neuroprotective functions of IL-6 including modulation of cell apoptosis and cytokine secretion, advocating its potential use in the clinic (Feng et al, 2015). Intracerebroventricular injection of IL-6 into mice has previously been shown to have a neuroprotective effect in models of ischemic brain injury (Jung et al, 2011). While the exact mechanism of IL-6-induced neuronal atrophy in this study has not been identified, previous research has shown that pathological levels of IL-6 (10 ng/mL) suppress voltage-gated Na^+ channels of cultured rat cortical neurons reducing neuronal energy consumption and inhibiting the amplitude of action potentials in a dose- and time-dependent manner (Xia et al, 2015).

Of these three targets TNF-α blockade has made some of the best progress towards clinical application. TNF-α blockers currently available include infliximab, etanercept, adalimumab, golimumab, and certolizumab and are authorised to treat inflammatory diseases, including rheumatoid arthritis, ankylosing spondylitis, psoriasis and Crohn's disease (Monaco et al, 2015). While none of these are currently licensed for CNS disorders with a psychiatric component,

TNF-α inhibitors have proven effective in reducing depression and anxiety-like symptoms in rodent models (Krügel et al, 2013). Recent clinical data also suggests efficacy of TNF-α blockers in patients with depression and anxiety (Abbott et al, 2015; Brymer et al, 2019). TNF-α blockade as a therapeutic option has its limitations and long-term neutralisation increases susceptibility to infections and skin cancer (Brown et al, 2017; Burmester et al, 2013). Blockade of the downstream mediator IL-6 may be a more appropriate.

Anakinra, a recombinant form of the naturally occurring IL-1 receptor antagonist (IL-1Ra) is indicated for the treatment of rheumatoid arthritis and currently dominates the field of IL-1 therapeutics owing to its excellent safety record, short half-life and multiple routes of administration. IL-1α neutralisation and orally active small-molecule inhibitors of IL-1 production are among other strategies in early clinical trials (Cohen et al, 2011; Dinarello et al, 2012). The humanised anti-IL-6 receptor antibody tocilizumab (Tanaka et al, 2016) and the human anti-IL-6 monoclonal antibody sirukumab are approved for the treatment of rheumatoid arthritis (Williams, 2013). Sirukumab has recently demonstrated efficacy in reducing depressive symptoms in patients with rheumatoid arthritis (Smolen et al, 2014) and the IL-6 receptor antibody MR16-1 is reported to produce rapid-onset and long-lasting antidepressant effects (Zhang et al, 2017a), highlighting the potential clinical efficacy of IL-6 blockade.

Taken together, these findings highlight that potential treatment strategies are in fact already available but require re-evaluation in psychiatric disorders. This is a major consideration given that re-defining indications to pre-existing treatments would eliminate huge investments in *de novo* research and development. The pathogenesis of most diseases for which anti-cytokine treatment is currently licensed is still far from being completely understood and greater understanding of the underlying mechanisms is fundamental to advancing findings towards the clinic.

The KP has also been acknowledged for the potential role it plays in linking peripheral inflammation with CNS alterations via the regulation of tryptophan availability, production of reactive metabolites and oxidative free radicals in CNS disorders (Hochstrasser et al, 2011; O'Farrell et al, 2017). IL-6 increases the

activity of the KP rate limiting enzyme IDO which is negatively correlated with blood serotonin concentration and causes downstream activation of QUIN (Kim et al, 2012; Zoga et al, 2014). Elevated levels of QUIN and IL-6 have been positively correlated with suicide attempts in patients with major depression (Erhardt et al, 2013). Given the putative role of IDO in the pathophysiology of depression (Kim et al, 2012) these findings infer an important link between inflammatory driven glial activation of the KP, peripheral cytokines and behavioural symptoms of depression (Quak et al, 2014).

Experiments in rodents have shown that 1-MT mediated inhibition of IDO abolishes inflammatory driven depressive-like behaviours as measured by immobility time in the forced swim and tail suspension tests (Lawson et al, 2013; O'Connor et al, 2009). KMO inhibition with the small molecule JM6 has also been shown to reduce extracellular glutamate, increase levels of KYNA in the brain and serum and reduce anxiety-like behaviour in rodents (Zwilling et al, 2011). To this end, the need for a BBB permeable KP enzyme inhibitor for clinical use has not been met but appears a promising target in the clinical translation of KP research.

7.3 Limitations and future directions

7.3.1 *In vitro* cell cultures; strengths and limitations

In vitro primary cell culture systems are suitable for neuronal growth studies *in situ,* as they permit isolation of distinct CNS cell types. However, the complexity of inter-cellular communication and interactions in the human brain are challenging to model using these systems. Inter-culture variability can be problematic as neurite outgrowth is sensitive to small differences in experimental conditions (Blackmore et al, 2010) and we cannot definitively exclude contribution from contaminating cells when analysing results in enriched glial cell cultures (Saura, 2007). Furthermore, the expression of receptors can differ *in vitro* and *in vivo* making it difficult to extrapolate some findings to clinical scenarios. For example, microglia expression levels of IFNγ receptors are reported to be much lower than the expression levels in astrocytes in the human

CNS *in vivo*. However, both glial cell types constitutively express IFNγ receptors when cultured *in vitro* (Hashioka et al, 2010).

Quantitative analysis of neuronal complexity and the expression of synaptic markers require neurons growing in isolation when in reality, both neurons and glia are arranged in highly organised networks. Neurite outgrowth as measured using an updated Sholl analysis technique (Gutierrez & Davies, 2007; SHOLL, 1953) does not accurately reflect the arrangement of neurons *in vivo*. Future studies could aim to examine neurite outgrowth responses in a network using techniques such as live cell Ca^{2+} imaging (Verstraelen et al, 2014b).

The assay used to quantify the co-localised expression of pre and post- synaptic markers is traditionally used to examine changes in synaptic connectivity (Ippolito & Eroglu, 2010), however it only analyses synaptic co-localisations at excitatory synapses and does not always indicate formation of a stable, functional synapse. Future experiments may employ techniques such as electron microscopy which would permit high-resolution analysis of individual synapses, synaptic vesicles and the post synaptic densities. Electrophysiological techniques such as whole-cell patch clamping would also allow measurement of functional changes in synaptic connectivity by quantifying the frequency and amplitude of excitatory and inhibitory activity in neurons (Kelsch et al, 2010). Combining pre and post – synaptic markers with a mature neuronal marker such as MAP2 would also permit quantification of the synapse density and expression of the number of synaptic contacts per dendrite length (Verstraelen et al, 2018).

Despite the shortfalls of *in vitro* investigations there are several specific experiments that are of interest for future studies. Firstly, it would be of interest to examine the composition of the secretome of IFNγ treated mixed glia, TNF-α and IL-1α treated astrocyte cultures and IL-6 treated microglia for other factors i.e. neurotrophic factors and nitric oxide that are also known to alter neuronal outgrowth (Calabrese et al, 2007; Xiao & Le, 2016). In order to clarify the precise source of TNF-α following IFNγ stimulation of glial cells it would be of interest to quantify TNF-α in the media of IFNγ treated astrocytes by ELISA. Despite extensive efforts to image dendritic spines *in vitro* it would be worth pursuing this as an additional measure of neuronal complexity and as a comparator for *in*

vivo findings. Specifically, it would be of interest to investigate the effect of direct application of L-AAA, IFNγ, TNF-α, IL-1α, IL-6 and KP metabolites on dendritic spines *in vitro*.

Evidently, greater *in vivo* work is required in order to push this research towards drug development. Techniques such as magnetic resonance spectroscopy would permit *in vivo* study of the biochemical environment of the brain using a non-invasive approach (Yuksel & Ongur, 2010), while genetic manipulation of pharmacological pathways would help to fully characterise the role of glial interactions in driving neuronal atrophy in IFNγ or KP signalling. Nevertheless, it must be noted that forward translation from *in vitro* systems to animals can be particularly challenging. L-AAA for example, is a useful toxin for researching astrocyte mechanisms *in vitro* but cannot readily cross the mammalian BBB, and would require invasive intracerebral injections. While animal models have been valuable in elucidating disease mechanisms and in providing insights into the function of specific genes, they also have a poor track record when it comes to forward translating findings into humans (Dragunow, 2008). Forward translation from an *in vivo* animal model to humans can be challenging due to hormonal and gender differences confounding physiological characteristics and behavioral differences. For example, levels of sIL-6R, TNF-α and IL-4 cytokines are elevated in healthy women during various stages of the menstrual cycle (O'Brien et al, 2007). Similarly, changes in TNF-α and IL-6 following LPS administration are positively correlated with increased feelings of social isolation in women but not in men (Moieni et al, 2015). While post-mortem tissue can provide insight into alterations in brain structure at a cellular and molecular level, deriving causal inferences from pathological studies of diseases is also associated with many challenges.

Induced pluripotent stem cell (iPSC) models may be the most appropriate means of balancing limitations of forward and backward translation. An iPSC model permits study of discrete cellular and molecular responses in human cells carrying specific genetic information or disease (Bahmad et al, 2017; Dolmetsch & Geschwind, 2011). Reprogramming iPSCs from patients into neuronal cell types has been successfully employed to elucidate phenotypes related to

neuropsychiatric and neurodegenerative pathologies. The approach is particularly useful for neurodevelopmental diseases for which major genes are considered responsible and where culturing primary cells prooves challenging.

7.3.2 Mechanisms of L-AAA-induced astrocyte impairment remain unclear

Despite the collective findings of this study, the mechanism of toxicity of L-AAA remains controversial and deserves further study. It would be of interest to confirm the effect of L-AAA on astrocytic enzymes glutamine synthetase or γ-glutamylcysteine synthetase by measuring L-glutamine release from astrocytes and/or glutamate concentrations in the media. This could be carried out using a colorimetric or bioluminescent assay coupling glutamate oxidation and NADH production with an NADH detection system.

7.3.3 Characteristics and markers of glial activation remain dubious

“Reactive astrocytes” putatively refers to astrocytes that respond to any pathological condition in the CNS. Traditionally, astrocytes are considered reactive when they become hypertrophic and overexpress the intermediate filament GFAP (Pekny & Pekna, 2014; Pekny et al, 2019). However, given the limitations associated with using GFAP as a sole prototypical maker for astrocytes the concept of astrocyte reactivity, as a whole, has become increasingly nebulous (Zhang et al, 2019).

Future studies may employ a panel of astrocytic markers in addition to GFAP, to gather more information about how inflammatory stimuli affects specific astrocytic functions and/or characteristics. Some additional astrocytic markers may include CXCL10, Pentraxin-3 (PTX3), intercellular adhesion molecule 1 (ICAM-1) and Vimentin. CXCL10 is a chemokine that belongs to the CXC chemokine family and is a ligand of the CXCR3 receptor that is up-regulated during gliosis. It is secreted in response to IFNγ by various cell types, including astrocytes (Metzemaekers et al, 2017) and has important functions in mediating leukocyte entry into the inflamed CNS (Zamanian et al., 2012). PTX3 is an acute-phase protein released during inflammation which aids phagocytic clearance of pathogens and its expression has been positively correlated with astrocyte

reactivity (Shindo et al, 2016). Reactive astrocytes are also known to present cell adhesion molecules such as ICAM-1 and vascular cell adhesion protein 1 (VCAM-1), which are important for migration of T cells (Figley & Stroman, 2011). ICAM-1 is up-regulated by several pro-inflammatory cytokines including TNF-α, IL-1 and IFN-γ both *in vitro* and *in vivo* (Fotis et al, 2012) and its expression has been positively correlated with astrocyte reactivity (Lutton et al, 2017). Vimentin is an intermediate filament protein that has also been used as a marker of astrocyte reactivity (Liu et al, 2014). However it is supposedly expressed to a greater extent in immature astrocytes (Hol & Pekny, 2015; Leduc & Etienne-Manneville, 2017). Future experiments may thus seek to profile the precise changes in such markers following inflammatory activation of astrocytes which may be used as a paradigm to quantify reactivity.

In addition to GFAP, Iba1 expression as a measure of microglial activation should be interpreted with caution. Recent evidence demonstrates that Iba1 labels both resting and activated microglia resulting in a heterogeneity of results across various studies. While densitometry can provide a useful indicator of microglial activation, we cannot exclude the fact that inflammatory-induced morphological changes may occur without significantly affecting the optical density. Future studies may employ alternative or additional measures to characterise morphological changes (Karperien et al, 2013) such as the extent of ramification, or the length of the dendritic processes (Franciosi et al, 2012; Morrison & Filosa, 2013), both of which are associated with inflammatory driven microglial activation (Hovens et al, 2015). Determining the activation stage of individual microglia is another approach that could be considered when quantifying reactivity.

In addition to Iba1, CD11b, CD40 and the transmembrane protein 119 (TMEM119) are among the other microglial markers which could be employed to profile a reactive microglia paradigm or prototype. CD11b is a β-integrin marker whose expression reportedly coincides with morphological changes in microglia (Rock et al, 2004). CD40 is a membrane glycoprotein that is also regarded as a marker of activated microglia (Aarts et al, 2017). TMEM119 is a transmembrane protein and microglia-specific marker in both mouse and human (Bennett et al,

2016). It is known to drive an inflammatory and neurotoxic environment in the brain and is essential for mediating various immune responses (Zrzavy et al, 2019).

7.3.4 *In vivo* analysis of dendritic spine density; limitations of Golgi-Cox staining

One of the major limitations in the study of dendritic spines is the arbitrary classification of spines into four categories; thin, stubby, mushroom and cup-shaped. This classification system underestimates the heterogeneity of spine morphology, which may exist along the length of one single dendrite (Spacek & Harris, 1997).

Secondly, the investigation provides for analysis of spines at just one point in time. This produces a static image of spines, which are in fact undergoing continual morphological transition. Future studies may consider live imaging or time lapse two photon imaging in order to capture the dynamicity of spines over timescales of seconds to minutes and of hours to days (Parnass et al, 2000)

Publications

David, J., O'Toole, E., O'Reilly, K., Thuery, G., Assmann, N., Finlay, D. & Harkin, A. (2018) Inhibitors of the NMDA-Nitric Oxide Signalling Pathway Protect Against Neuronal Atrophy and Synapse Loss Provoked by l-alpha Aminoadipic Acid-treated Astrocytes. *Neuroscience.*

In Preparation

A role for IL-6 in mediating reactive glial associated changes in the complexity of primary cortical neurons. *Neuroscience*

L-alpha-aminoadipic acid provokes a loss of complexity of primary cortical neurons and attenuates reactive glial associated neuronal atrophy. *Journal of Neuroscience Research.*

Kynurenic acid protects against reactive glial-associated reductions in the complexity of primary cortical neurons. *European Journal of Pharmacology*

Poster Presentations

O'Reilly, K., David, J., O'Toole, E., Harkin A. Astrocytic ablation by L-alpha aminoadipic acid (L-AAA) induces neuronal atrophy; rescue by NMDA-R antagonists and inhibitors of the PSD-95/nNOS interaction. Poster presentation at the All-Ireland Schools of Pharmacy Conference, April 2017

O'Reilly, K., David, J., Thuery, G., Harkin A. ZL006 has antidepressant effects and attenuates changes in dendritic spines associated with astrocytic impairment in mice. Poster presentation at the European College of Neuropsychopharmacology (ECNP) Workshop, March 2018.

O'Reilly, K., David, J., Thuery, G., Kebede, V., Harkin A. Alterations in dendritic spines following stress and L-α-aminoadipic-acid induced astrocytic impairment are rescued by ZL006 inhibition of the PSD-95/NOS. Poster presentation at the European College of Neuropsychopharmacology (ECNP) Congress, September 2018.

8 Appendix to chapter 3: Developing a protocol for the visualisation of dendritic spines in primary cortical neurons *in vitro*

Following on from the development of a protocol to stain mature neurons for complexity using MAP2, it was of interest to establish a protocol for imaging the morphology of dendritic spines *in vitro*. The following section details the troubleshooting stages of setting up a protocol for the visualisation of dendritic spines *in vitro*.

8.1 Preparation of mature primary cortical neuronal cultures

Primary cortical neuronal cultures were prepared from Wistar rat pups postnatal day 1 -2, as described above (Day et al, 2014). Cells were counted using the trypan blue method as previously described. Neurons were plated at the following densities to determine optimal plating density: 3.75 x 10^4, 5 x 10^4, 7.5 x 10^4 and 1.5 x 10^5 cells/mL. 1.5 x 10^5 cells/mL was initially identified as the optimal plating based on visual inspection of cells and viability. Neurons were matured until DIV 18-21 and fixed for immunocytochemistry.

8.2 β-III tubulin staining

Microtubules play a major role in the determination of neural morphology and differentiation (Howard & Hyman, 2003). Tubulin, the subunit protein of microtubules, exists as an α/β heterodimer, with both α and β-tubulin existing as multiple isotypes. Seven β-tubulin isotypes have been identified in mammals do date and are referred to as βI, βII, βIII, βIVa, βIVb, βV, and βVI (Ludueña, 1998). βIII tubulin is considered to be one of the earliest neuron-associated cytoskeletal proteins to be expressed during development and has been identified as a useful marker to study early phases of neuronal differentiation (Easter et al, 1993; Lee et al, 1990a; Lee et al, 1990b). β-III tubulin is abundant in the central and peripheral nervous systems where it is prominently expressed during fetal and postnatal development (Katsetos et al, 2003a; Katsetos et al, 2003b). In adult tissues, the β-III tubulin isotype exhibits a distinctive neuronal specificity.

However, β-III tubulin is not detectable in the developing or mature Xenopus nervous system. Accordingly, antibodies raised against the neuron-specific class III beta-tubulin (β-III) (Lee et al, 1990b) have been traditionally employed to study the distribution, differentiation and morphology of immature neurons *in vitro*.

For β-III tubulin staining, mature neurons were fixed in 400 µL of 3.7% paraformaldehyde (PFA) (diluted in PBS) which was added to each well and left at room temperature for 20 minutes. PFA was then removed and the coverslips were washed gently 3 times with PBS. After 3 washes, non-specific interactions were blocked by adding 300 µL blocking buffer (4% NGS in PBS) to each well and the plate was left on a rocker at room temperature for 2 hours. The blocking buffer was discarded and primary antibody (200 µL) targeting β-III tubulin (1:1000, mouse) diluted in PBS was added to each well and left overnight at 4°C. The primary antibody was removed, and the cells were washed 3 times in PBS. Secondary antibody (200 µL) containing Alexa Fluor 488 (1:500, goat anti-mouse) diluted in PBS was added to each well. Secondary antibody was removed, and cells were washed 3 times with PBS, before adding dH_2O to each well. Coverslips were mounted using Vectashield fluorescent mounting media with DAPI and slides were allowed to dry before imaging.

On imaging inspection, it was observed that β-III tubulin did not sufficiently and uniformly stain dendrites. In fact, it seemed to stain the neurites closest to the soma but not throughout the entire length meaning that Sholl analysis and quantification of branch length was not possible. Expression of β-III tubulin correlates with the earliest phases of neuronal differentiation (Memberg & Hall, 1995) thus staining for β-III tubulin may not be appropriate for visualising complexity of mature neurons in culture.

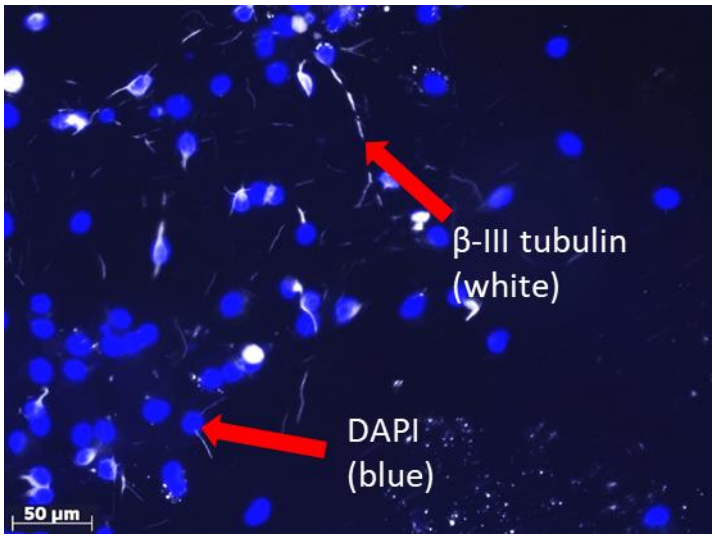

Figure 8.1 Mature cortical neurons stained for β-III tubulin
Representative image of mature cortical neurons (DIV 21) stained for β-III tubulin (1:1000) and the nuclear stain DAPI (blue) followed by fluorescent microscopy (20X magnification).

8.3 Drebrin A staining for visualising dendritic spines

The actin filament (F-actin) is one of the major structural elements of dendrites (Fifková & Delay, 1982; Matus et al, 1982). Drebrin A is the adult isoform of Drebrin and the most abundant neuron-specific F-actin-binding protein regulating the actin cytoskeleton in dendritic spines (Sekino et al, 2007). It is particularly concentrated in dendritic spines receiving excitatory inputs and reported to play a role in cluster formation of actin-cytoskeletal components during spine morphogenesis (Takahashi et al, 2003). It is also known to play an important role in synaptic transmission (Ivanov et al, 2009) and several studies correlate a loss of Drebrin with synaptic dysfunction. A reduction in Drebrin A is thought to underly cognitive impairment associated with normal aging and neurological disorders (Counts et al, 2006; Kojima & Shirao, 2007) including Alzheimer disease and Down's syndrome (Shim & Lubec, 2002).

For drebrin A staining, mature neurons were fixed with 3.7% PFA for 20 minutes as described above. PFA was then removed and the coverslips were washed gently 3 times with PBS. Neurons were co-stained for MAP2 to permit visualisation of dendrites. Non-specific interactions were blocked by adding 300 µL blocking buffer (2% NGS and 2% BSA in PBS-T) to each well and the plate was left on a rocker at room temperature for 2 hours. The blocking buffer was

discarded and primary antibody (200 µL) targeting MAP2 (1:500, mouse) and drebrin A (1:150 or 1:200, rabbit) was diluted in blocking buffer, added to each well and left overnight at 4°C. The primary antibodies were removed, and the cells were washed 3 times with PBS. Secondary antibodies Alexa Fluor 546 (1:500, Goat anti-rabbit) and Alexa Fluor 488 (1:500, Goat anti-mouse) were diluted in blocking buffer and 200 µL of this was added to each well. The plates were left on a rocker at room temperature in a light-protected environment provided by wrapping in tinfoil for 2 hours. Secondary antibodies were removed, and cells were washed 3 times with PBS, before adding dH_2O to each well. Coverslips were mounted using Vectashield fluorescent mounting media with DAPI and slides were allowed to dry before confocal imaging.

On inspection, it was observed that targeting Drebrin did not sufficiently and uniformly stain neuronal dendrites. In fact, it appeared to more strongly stain glial fibres. Resultantly, Sholl analysis and quantification of neuritic branch length was not possible. While F-actin is one of the major structural elements of dendritic spines recent studies have identified Drebrin signals which are not localised along dendrites (Hanamura et al, 2019). It is possible that these signals come from glia or axons, highlighting that Drebrin may not be specific for neuronal cells.

Further review of the literature found that F-actin is in fact, also expressed in astrocytes (Butkevich et al, 2004), but at a much lesser amount than in neurons (Sekino et al, 2006) and is therefore thought to have little impact on neuronal staining. F-actin has been observed particularly in reactive astrocytes where upregulation of F-actin has been documented (Abd-El-Basset & Fedoroff, 1997; Fedoroff et al, 1987; Takahashi et al, 2003). Dampening down astrocyte reactivity may thus result in more selective staining of neurons. Analogously, the addition of Cytosine-D-arabinofuranoside to inhibit glial proliferation may be an option to further optimise this protocol (Takahashi et al, 2003). Inhibiting glial proliferation may however reduce neuronal support resulting in fewer connections, synapses and spines.

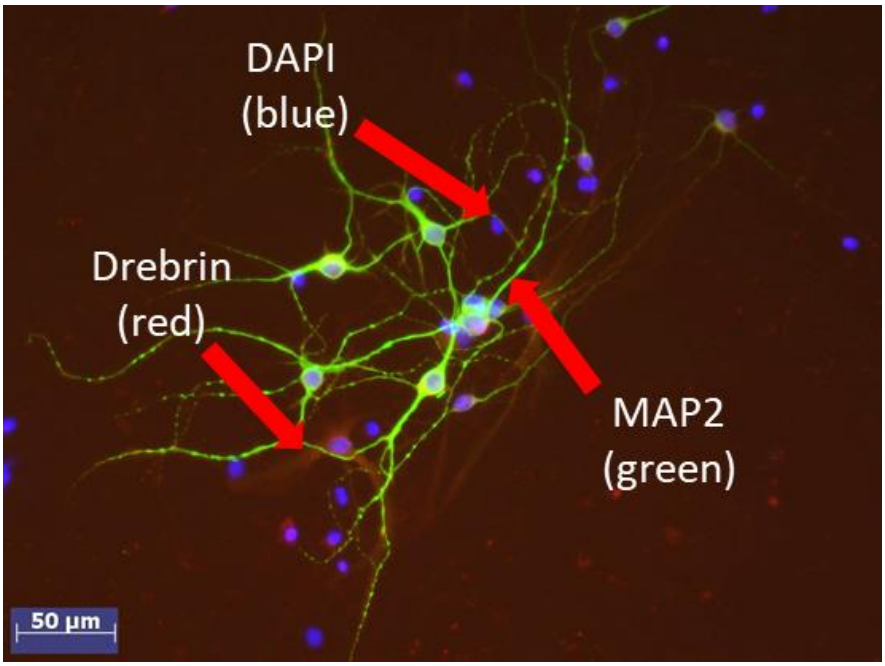

Figure 8.2 Mature cortical neurons stained for MAP2
Representative image of mature cortical neurons (DIV 21) stained with anti-MAP2 (1:500, green), Drebrin (1:150, red) and the nuclear stain DAPI (blue) followed by fluorescent microscopy (20X magnification).

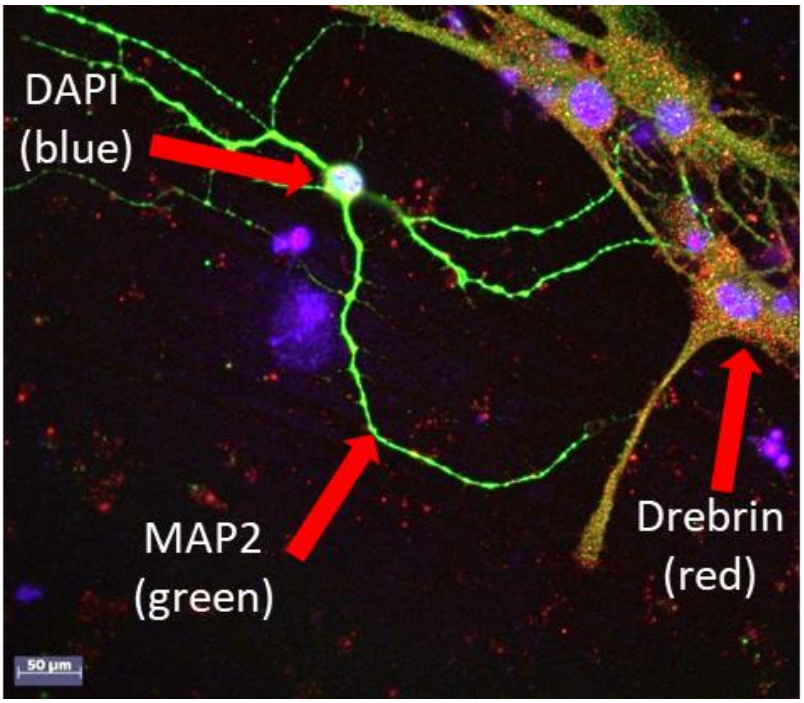

Figure 8.3 Mature cortical neurons stained for MAP2 and drebrin
Representative compressed Z stack images of mature cortical neurons (DIV 21) stained with anti-MAP2 (1:500, green), Drebrin (1:150, red) and the nuclear stain DAPI (blue) followed by confocal microscopy (20X magnification)

8.4 Phalloidin staining for visualising dendritic spines

Phalloidin is a bicyclic peptide isolated from the deadly poisonous *Amanita phalloides* "death cap" mushroom which can also be used to selectively stain for F-actin (Estes et al, 1981; Miyamoto et al, 1986; Wieland & Faulstich, 1978). Phalloidin binds polymeric F actin, resulting in highly stabilised actin filaments (Dancker et al, 1975). Once bound to F-actin, phalloidin inhibits ATP-hydrolysis and stabilises actin filaments by preventing subunit dissociation. The amino acid 7 (γ-δ-dihydroxyleucine) side chain is accessible to modifications, through which fluorescently labelled phalloidin compounds can be generated and this approach has been employed to target the actin cytoskeleton (Belin et al, 2014). Phalloidin is typically conjugated to a fluorescent dye, such as FITC, Rhodamine, TRITC or similar dyes, such as Alexa Fluor® 488 or iFluor 488 (Wehland & Weber, 1981; Wulf et al, 1979).

Fluorescently labelled phalloidin has several advantages over antibodies for actin labelling, including identical interspecies binding properties and low non-specific binding. It has been used successfully to estimate spine volume, surface area, and shape in coronal brain slices from mice (Kirkwood et al, 2013). The capacity for phalloidin to bind more tightly to actin filaments over monomers reduces non-specific staining and background noise resulting in high contrast between stained and unstained areas giving it potential advantage over Drebrin staining. In comparison to antibody staining, phalloidin derivatives' are small (<2 kDa) which permits denser F-actin labelling and allowing greater detail in higher resolution images (Wulf et al, 1979). Nevertheless, Phalloidin is largely restricted to labelling fixed cells, as it has a low permeability for cell membranes. Thus, staining must be carried out following cell fixation and permeabilisation. This may result in loss of important three-dimensional structural information required for studying spines. Under some conditions binding of phalloidin to actin filaments may also perturb normal cellular dynamics (Belin et al, 2014).

For phalloidin staining mature neurons were fixed in 3.7% PFA for 20 minutes as described above. Cells were fixed with paraformaldehyde as methanol fixation methods can destroy the native F-actin conformation resulting in the labelling of

artificial structures and rendering them unsuitable staining with phalloidin (Kellogg et al, 1988). PFA was removed and coverslips were washed gently 3 times with PBS. Neurons were co-stained with MAP2 to permit visualisation of dendrites. After 3 washes, non-specific interactions were blocked by adding 300 µL blocking buffer (2% NGS, and 2% BSA in PBS-T) to each well and the plate was left on a rocker at room temperature for 2 hours. The blocking buffer was discarded and primary antibody (200 µL) targeting MAP2 (1:500, or 1:1000 mouse) diluted in blocking buffer was added to each well and left overnight at 4°C. The primary antibody was then removed and cells were washed 3 times with PBS. Secondary antibody containing Alexa Fluor 546 (1:500, Goat anti-mouse) and phalloidin Alexa 488 (25 µL phalloidin per mL) diluted in 1% BSA and PBS-T was added and left for 2 hours on a rocker at room temperature in a light-protected environment. The secondary antibody was removed and cells were washed 3 times with PBS, before adding dH_2O to each well. Coverslips were mounted using Vectashield fluorescent mounting media with DAPI and slides were allowed to dry prior to imaging.

On inspection it was observed that phalloidin did not sufficiently and uniformly stain spines. In fact, no spines were evident in the images taken. It was possible to see some spines looking at the MAP2 staining (red). However, it was not possible to morphological classify them as thin, stubby or mushroom. Resultantly, Sholl analysis and quantification of spines was not possible using this staining technique. There was a lot of background staining with what appeared to be contaminating glia fibres. As previously discussed F-actin has been observed particularly in glial cells and many protocols include a treatment with Cytosine-β-d-arabinoside to eliminate proliferating glial cells (Nwabuisi-Heath et al, 2012). However, we have also considered that excluding all astrocytic support may be detrimental to the formation of healthy connections, synapses and spines in neurons. Increasing the plating density of neurons from 30,000 to 100,000 cells per well may help encourage the formation of more synaptic connections and spines if including cytosine-β-d-arabinoside treatment.

One other important consideration is that while F-actin is one major structural element of dendritic spines it is not the sole component. Dendritic spines have two major structural elements: postsynaptic densities (PSDs) and actin cytoskeletons. The actin cytoskeleton predominates in spines (Matus et al, 1982) and regulates their morphological plasticity (Fischer et al, 1998). Image analysis suggests that while the actin cytoskeleton establishes fundamental postsynaptic structures, the PSD components play an important role in modifying established postsynaptic structures (Takahashi et al, 2003). In particular, PSD-95 has been used in conjunction with phalloidin and as part of an antibody cocktail mix to stain PSD components of the spine specialisation.

Spine development and maturation involves enrichment of the NMDAR and AMPAR in spines. Densities of the spine-associated NMDAR subunit (NR1) and AMPAR subunit (GluR2) clusters have been shown to increase significantly during spine formation remaining stable during the maintenance phase (DIV 18-21) (Nwabuisi-Heath et al, 2012). Triple fluorescence staining of neurons with phalloidin, synapsin I antibody (presynaptic marker), and the axonal marker SMI312 has been successfully used to identify actin-rich dendritic spines and synapsin I-rich puncta on axons (Efimova et al, 2017). Using a specific combination targeted at individual components of the spine may thus be a better approach to ensure complete labelling of spines during formation and maturation.

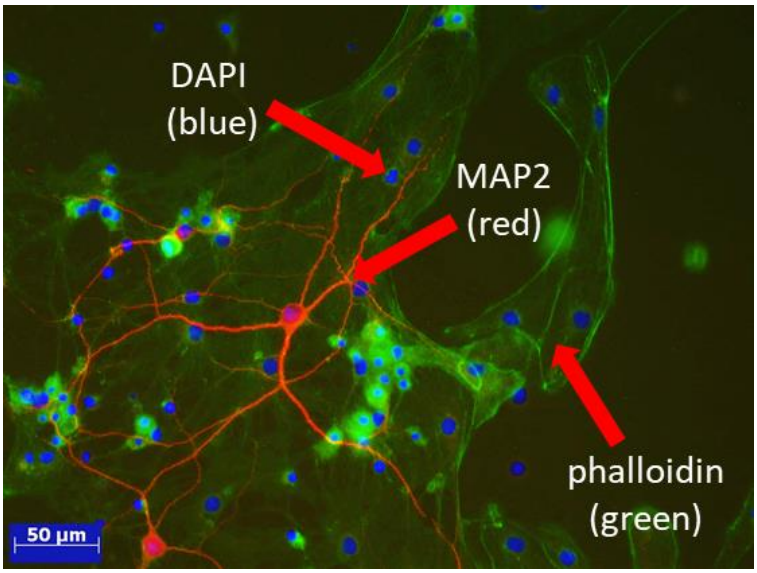

Figure 8.4 Mature cortical neurons stained for MAP2 and phalloidin
Representative image of mature cortical neurons (DIV 20) stained with anti-MAP2 (1:500, red), phalloidin (1:40) and the nuclear stain DAPI (blue) followed by fluorescent microscopy (20X magnification)

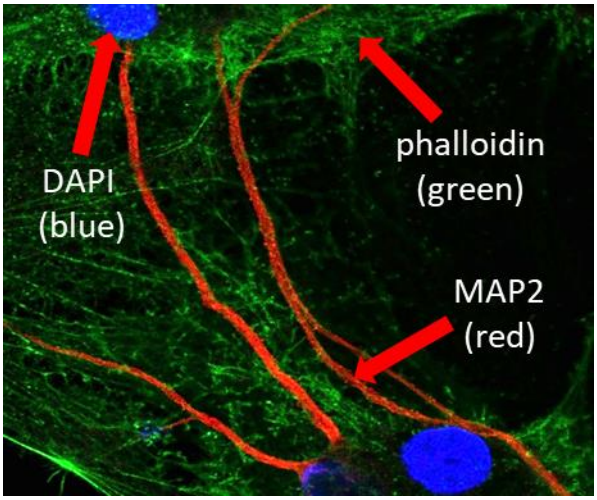

Figure 8.5 Mature cortical neurons stained for MAP2 and phalloidin
Representative compressed Z stack images of mature cortical neurons (DIV 20) stained with anti-MAP2 (1:500, red), phalloidin (1:40) and the nuclear stain DAPI (blue) followed by confocal microscopy (20X magnification).

8.5 Fluorescein staining for viable cell imaging

Fluorescein is a xanthene dye which is used as a labelling agent in biology and as an anionic fluorophore for live cell imaging. Fluorescein analogs such as fluorescein sodium salt are available for viable cell staining. They pass through cell membranes and covalently conjugate with cell proteins. Their high water solubility and small molecular radius makes them particularly useful tracers for studying permeability and perfusion in rodent models (Montermini et al, 2002).

For fluorescein staining, neurons were plated at concentrations of 3.75 x 10^4, and 7.5 x 10^4 cells/mL to determine the optimal plating density for visualising mature neurons in isolation by live cell imaging in an 8 well µ-slide dish. The µ-slide 8-well dish enables high-resolution live cell imaging using different bright field and fluorescence techniques and has been used successfully for live cell imaging studies including F-actin visualisation in living cells using LifeAct-TagGFP2 protein. At DIV 21 neurons were stained with fluorescein salt (1 µL) of 1 mg/mL stock solution which was added directly to the cells for live cell imaging. Using this technique, the soma was clearly visible, but neurites and dendrites were not. One possible explanation for the poor staining observed here was that the cells may not have remained viable after taking up fluorescein.

For successful live imaging of cellular processes several features must be optimised in order to ensure cells are kept in an environment that does not induce stress. Some of the key factors to consider include the type of culture medium and its contents, the temperature of the sample, the pH of the sample, evaporation of the medium and changes in osmolarity. It is possible that any of these factors may have influenced the poor-quality staining of the cultures. However, optimising live cell imaging with fluorescein staining did not seem to demonstrate any potential for quantification and classification of dendritic spines. While it was evident that the stain worked over a short time, we did not get the fine structural detail required. Furthermore, the prospective time required to image sufficient cells for a study would likely result in photo bleaching and would have to be completed by the researcher in one sitting.

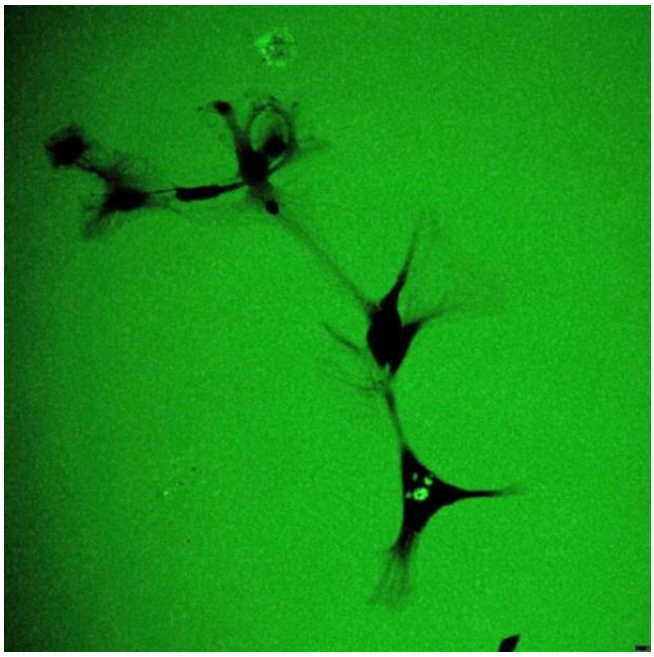

Figure 8.6 Live staining of mature neurons
Representative compressed Z stack images of mature cortical neurons (DIV 21) following live staining and confocal microscopy (20X magnification)

8.6 eGFP transfection

Transfection is the process of introducing nucleic acids into cells (Marwick & Hardingham, 2017). Transfection of primary cortical and hippocampal neurons has proven particularly challenging (Karra & Dahm, 2010; Zeitelhofer et al, 2009). Numerous methods of transfection have been developed and optimised including electroporation, nucleofection, calcium phosphate co-precipitation, and lipofection. Lipofection is the most popular transfection method for gene delivery and is the method of choice which will be focused on from here onwards.

Lipofection involves the formation of unilamellar liposomes from cationic lipid molecules which form aggregates with negatively charged DNA (Felgner et al, 1987; Wiesenhofer & Humpel, 2000). Genetic material is delivered into cells by fusion of this aggregate with the negatively charged plasma membrane. The main advantages of Lipofection as a transfection reagent is that it can be used for cultured primary neurons, it is a relatively quick and simple procedure and has high reproducible transfection efficiencies. The main disadvantages include the need for optimisation for higher transfection efficiencies and the toxicity observed with some reagents (Sariyer, 2013).

For this study primary cortical neurons were transfected with an enhanced green fluorescent protein (eGFP)-Lifeact–expressing plasmid (pEGFP-C1, Lifeact-EGFP) to label dendritic protrusions. The pEGFP-C1 plasmid expresses a cytoplasmic actin filament reporter, the peptide Lifeact, on a CMV promoter (Addgene plasmid # 58470; http://n2t.net/addgene:58470 ; RRID:Addgene_58470). Lifeact is a 17-amino-acid peptide, derived from the nonessential *Saccharomyces cerevisiae* actin-binding protein ABP140 that has been identified for use as a C-terminal GFP fusion (Lifeact-GFP) protein (Asakura et al, 1998). Fused to green fluorescent protein (GFP), Lifeact is reported to permit live-cell imaging of actin without interfering with cellular functions. Lifeact has been used to successfully stain F-actin structures in eukaryotic cells and tissues. It has shown to bind with such a low affinity that it does not interfere with F-actin dynamics or biomechanical activities (Riedl et al, 2008). This is a significant advantage of LifeAct-GFP over actin-GFP which has been reported to affect the biomechanical properties of cells (Belin et al, 2014; Sliogeryte et al, 2016).

Green fluorescent protein (GFP) from the jellyfish *Aequorea victoria* has become an important marker of gene expression. However, the sensitivity of wild-type GFP is below that of standard reporter proteins. Enhanced GFP (eGFP) is a unique GFP variant containing chromophore mutations that make the protein 35 times brighter than wild-type GFP and gives rise to bright and readily detectable fluorescence following a 16-24 hour transfection period (Zhang et al, 1996). As eGFP allows sensitive and convenient detection of gene transfer it is as an ideal molecule for quantitative studies of intra and intercellular tagged-protein dynamics (Cinelli et al, 2000). Thus, the Lifeact-eGFP construct was selected to maximise the transfection processes and will be referred to as eGFP from here onwards.

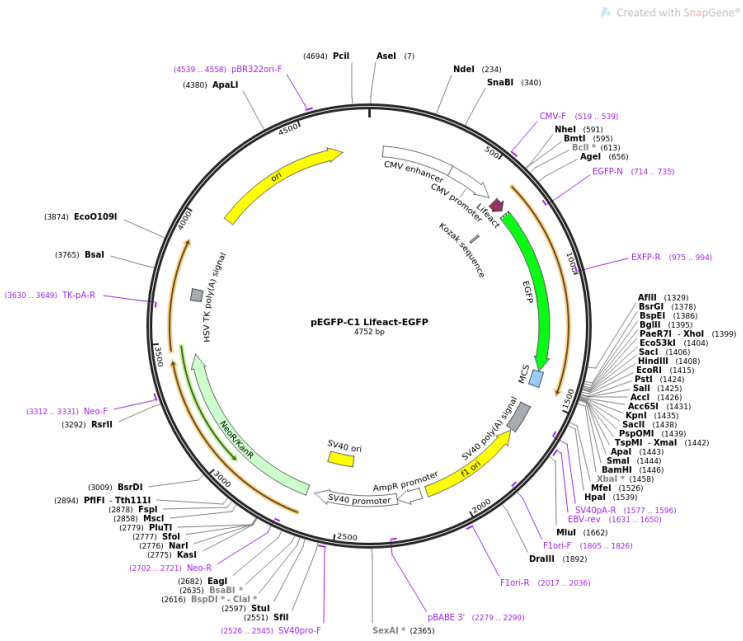

Figure 8.7 Details of the pEGFP-C1 Lifeact-EGFP plasmid construct
The pEGFP-C1 Lifeact-EGFP plasmid is an (eGFP)-Lifeact–expressing plasmid that expresses a cytoplasmic actin filament reporter, the peptide Lifeact, on a CMV promoter (Addgene plasmid # 58470).

8.6.1 Amplification of pEGFP-C1 Lifeact-EGFP (Addgene) plasmid

A bacterial stab containing the pEGFP-C1 Lifeact-EGFP (Addgene) plasmid was streaked out on a kanamycin (30 µg/mL) agar plate and incubated overnight at 37°C as per manufacturer's instructions. A single colony was aseptically selected to inoculate a test tube containing Lysogeny broth (LB) broth (4 mL) supplemented with kanamycin (30 µg/mL) and incubated for 24 hours at 37°C with vigorous shaking. 250 µL of this culture was used to inoculate a baffled conical flask containing LB broth (25 mL) supplemented with kanamycin (30 µg/mL) for 24 hr at 37°C with vigorous shaking. A stock culture was created by aliquoting 500 µL of the overnight culture with 500 µL of 50% glycerol in a 2 mL screw top tube. This was gently mixed and snap frozen in liquid nitrogen for final storage at -80^{o}C. The remaining culture was aliquoted into 1 mL tubes in preparation for plasmid extraction.

8.6.2 Isolation and purification of DNA

Plasmids were isolated from live bacterial cultures using the Qiagen miniprep kit (Qiagen) according to the manufacturer's instructions (Birnboim & Doly, 1979). Briefly, 1 mL of fresh overnight cultures were chemically lysed. The chromosomal

DNA was pelleted by centrifugation and the supernatant containing the plasmid of interest was captured by passing it through a QIAprep spin column. The plasmid was washed with QIAprep Buffer before being eluted using 50 µL of nuclease free water. A Nano-DropTM (Thermo Scientific) was used to measure the concentration and purity of the plasmid at an absorbance range of A260/A280.

The plasmid's structural integrity was examined by resolving it using agar gel electrophoresis. A reaction solution was created (1 µL of purified plasmid, 1 unit of EcoRI restriction enzyme (New England Biolabs) and 8 µL of NEBuffer™ EcoRI (New England Biolabs)) and placed in a thermocycler for 10 minutes at 37^{o}C. The restriction enzyme was inactivated by heating the reaction solution to 65^{o}C for 20 minutes. 1 µL loading buffer (0.25% (w/v) bromophenol blue, 0.25% (w/v) xylene cyanol FF, 30% (v/v) glycerol, 10 mM EDTA) was added to the sample. A 0.5% (w/v) agarose gel was prepared in TAE buffer (40 mM Tris-HCl pH 8.3, 2 mM EDTA, 1 mM acetic acid). Samples were resolved by electrophoresis using a Horizon 58 Agarose Gel Electrophoresis device at 100 volts in the direction of the cathode until desired migration was achieved (based on visual inspection – approximately 1 hour). The running buffer used during the electrophoresis was TAE buffer. Gels were stained in ethidium bromide (1 µg/mL) for 15 – 30 minutes, rinsed in deionised H_2O and the DNA was visualised and photographed by exposing the gel to 300 nm ultraviolet light from a transilluminator (Alpha Imager 2200 gel imaging system, Alpha Innotech Corporation, San Leandro, California, USA). The plasmid integrity was determined by visualisation and its size estimated by comparison to the standard ladder. 25 µL aliquots of the plasmid were transferred into 1 mL tubes and stored at -20^{o}C until required for further use.

8.6.3 Transfection of neurons with eGFP-expressing plasmid

For eGFP transfection, neurons (DIV 13) were transfected with the above pre-prepared plasmid driving expression of eGFP (Srivastava et al, 2011). Primary cortical neuronal cultures were prepared from Wistar rat pups postnatal day 1-2, as described above (Day et al, 2014). Cells were counted using the trypan blue

method and plated at a density of 3 x 10^5 cells/mL as previously described with the aim to study cells in isolation. Based on review of the literature this density was deemed low for transfection where densities of up to 1 × 10^6 cells/mL have reportedly been used. The plating density was then increased to 6 × 10^5 to help support outgrowth and connectivity where reduced serum media is used, and astrocytic support is withdrawn.

Cells were cultured in Opti-MEM® Reduced Serum Medium (Gibco) which is specifically recommended for use with cationic lipid transfection reagents, such as Lipofectamine™. This is because the positive charge on the surfaces of cationic DNA-lipid complexes results in a non-specific adsorption of negatively charged plasma proteins in serum and a loss of transfection efficiency (Felgner & Ringold, 1989). Supplementation of the medium with the neuronal specific supplement mixture, B-27 (Gibco/Invitrogen) was used to support neuronal growth throughout the first 13 days in culture. Immature neurons (DIV 3) were treated with 2.5 µM cytosine β-d-arabinofuranoside (AraC) to control glial division and minimise astrocytic growth (Roqué et al, 2014).

Plasmid transfection was performed using Lipofectamine™ 2000 Transfection Reagent according to the manufactures instructions (Biosciences) (Dalby et al, 2004). Four amounts (2, 3, 4, 5 µL) of Lipofectamine reagent (equivalent to 1:100, 1:67, 1:50, 1:40 dilutions) were prepared in Opti-MEM media (50 µL) to test the optimal amount of Lipofectamine™ 2000 required per well. Purified plasmid DNA (5 µg) was diluted in Opti-MEM media (50 µL). The diluted DNA was added to the diluted Lipofectamine in the ratio of 1:1. The mixture was left to incubate for 5 minutes at room temperature. 100 µL of the DNA-lipid complex was then added to 100 µL of cell media and transferred back into the incubator for 48 hours at 37^{o}C before imaging analysis. Cells were left for 48 hours as eGFP expression is reported to typically start around 6 hours post-transfection, and peak between 48–72 hours (Sariyer, 2013).

8.6.4 Staining eGFP-transfected cells with anti-GFP and MAP2

Neurons were co-stained with MAP2 to permit visualisations of the dendrites. For anti-GFP and MAP2 staining, neurons were fixed in 4% PFA and 4% saccharose diluted in PBS and left for 20 minutes at room temperature. Cells were washed 3 times with PBS, before blocking non-specific interactions by applying 300 µL of blocking buffer (2% NGS and 0.2% Triton-x in PBS) to each well. The plate was left on a rocker at room temperature for 2 hours. The blocking buffer was discarded and primary antibody (200 µL) containing anti-MAP2 (1:1000 mouse) and anti-GFP (1:1000 or 1:500) diluted in blocking buffer was added to each well and left overnight at 4°C. The following day the primary antibody was removed and the cells were washed 3 times with PBS. Secondary antibody containing Alexa Fluor 546 (1:500, Goat anti-mouse) and Alexa Fluor 488 (1:500, Goat anti-chicken) diluted in PBS was added to each well and left for 2 hours on a rocker at room temperature in a light-protected environment. Secondary antibody was removed, and cells were washed gently 3 times with PBS, before adding dH_2O to each well. Coverslips were mounted using Vectashield fluorescent mounting media with DAPI. Slides were allowed to dry before examination under the confocal microscope.

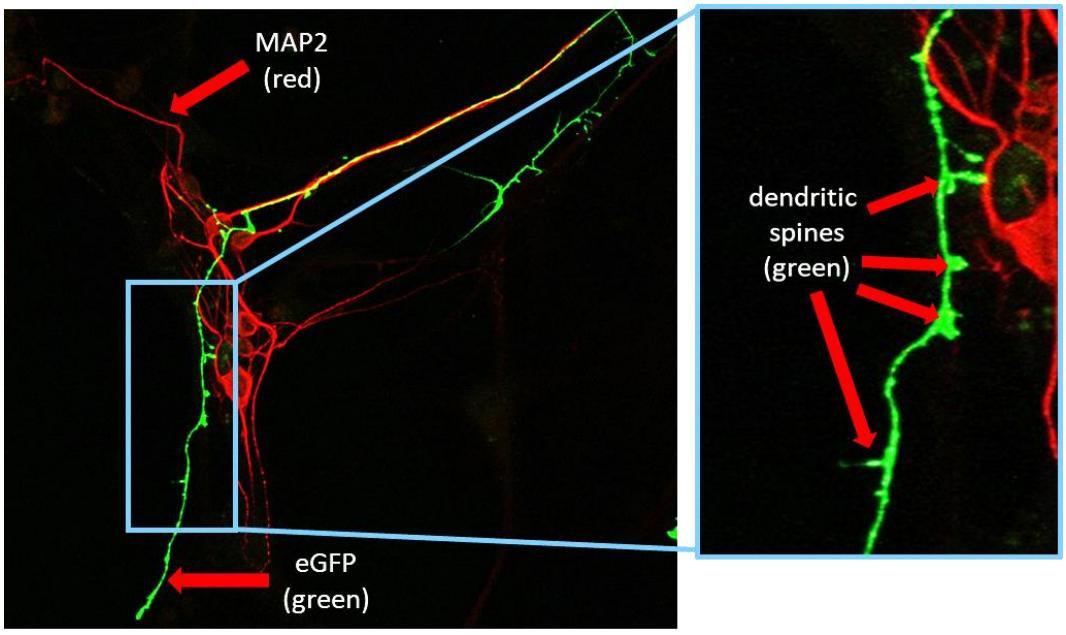

Figure 8.8 eGFP transfection of mature neurons
Representative Z-stack image of anti-MAP2 (1:1000) and anti-eGFP (1:500) stained primary cortical neurons (DIV 15) following eGFP transfection.

On inspection it was observed that eGFP transfection with Lipofectamine was successful in that it sufficiently and uniformly stained dendrites. In addition to permitting quantification, the fine detail anti-GFP staining (green) attained with this method also permitted morphological classification of spines as thin, stubby or mushroom. Resultantly, this image would be suitable for complexity and dendritic spine analysis.

Nevertheless, a limited number of cells were transfected to this standard and quality suggesting that further steps would need to be taken to optimise the transfection efficiency. Further steps taken to optimise the staining included: live cell imaging to avoid cell fixation, increasing the plating density and maintaining astrocytic support by omitting AraC treatment. It is possible that fixation or immunological staining may have affected the quality of eGFP labelling. It has been previously noted that fixation of cells with cold methanol, 4% PFA or ethanol may weaken GFP labelling (Li et al, 2008b). It is also possible that withdrawal of astrocytic support may affect the growth and quality of the cultures. Increasing the plating density may help compensate for this, however contact inhibition may also affect the uptake of DNA.

In accordance with advancing our study of dendritic spines *in vitro*, it is important to consider the most recent developments in the field including measurement of actin dynamics and quantification of the motility of GFP within spines (Hollos et al, 2020). Given that spines exist in a transient state, a snap shot image of one time point is a limitation of the current protocol and future studies might aim to incorporate simultaneous investigation of motility and dynamics in line with most recent advancements.

References

Aarts, S. A. B. M., Seijkens, T. T. P., van Dorst, K. J. F., Dijkstra, C. D., Kooij, G. & Lutgens, E. (2017) The CD40-CD40L Dyad in Experimental Autoimmune Encephalomyelitis and Multiple Sclerosis. *Front Immunol*, 8, 1791.

Abbott, R., Whear, R., Nikolaou, V., Bethel, A., Coon, J. T., Stein, K. & Dickens, C. (2015) Tumour necrosis factor-α inhibitor therapy in chronic physical illness: A systematic review and meta-analysis of the effect on depression and anxiety. *J Psychosom Res*, 79(3), 175-84.

Abd-El-Basset, E. M. & Fedoroff, S. (1997) Upregulation of F-actin and alpha-actinin in reactive astrocytes. *J Neurosci Res*, 49(5), 608-16.

Acaz-Fonseca, E., Ortiz-Rodriguez, A., Azcoitia, I., Garcia-Segura, L. M. & Arevalo, M. A. (2019) Notch signaling in astrocytes mediates their morphological response to an inflammatory challenge. *Cell Death Discov*, 5, 85.

Adlard, P. A. & Vickers, J. C. (2002) Morphologically distinct plaque types differentially affect dendritic structure and organisation in the early and late stages of Alzheimer's disease. *Acta Neuropathol*, 103(4), 377-83.

Agudelo, L. Z., Femenia, T., Orhan, F., Porsmyr-Palmertz, M., Goiny, M., Martinez-Redondo, V., Correia, J. C., Izadi, M., Bhat, M., Schuppe-Koistinen, I., Pettersson, A. T., Ferreira, D. M., Krook, A., Barres, R., Zierath, J. R., Erhardt, S., Lindskog, M. & Ruas, J. L. (2014) Skeletal muscle PGC-1alpha1 modulates kynurenine metabolism and mediates resilience to stress-induced depression. *Cell*, 159(1), 33-45.

Ahmed, R. M., Devenney, E. M., Irish, M., Ittner, A., Naismith, S., Ittner, L. M., Rohrer, J. D., Halliday, G. M., Eisen, A., Hodges, J. R. & Kiernan, M. C. (2016) Neuronal network disintegration: common pathways linking neurodegenerative diseases. *J Neurol Neurosurg Psychiatry*, 87(11), 1234-1241.

Albuquerque, E. X. & Schwarcz, R. (2013) Kynurenic acid as an antagonist of α7 nicotinic acetylcholine receptors in the brain: facts and challenges. *Biochem Pharmacol*, 85(8), 1027-32.

Alexander, W. S. & Hilton, D. J. (2004) The role of suppressors of cytokine signaling (SOCS) proteins in regulation of the immune response. *Annu Rev Immunol*, 22, 503-29.

Alexander, W. S., Starr, R., Fenner, J. E., Scott, C. L., Handman, E., Sprigg, N. S., Corbin, J. E., Cornish, A. L., Darwiche, R., Owczarek, C. M., Kay, T. W., Nicola, N. A., Hertzog, P. J., Metcalf, D. & Hilton, D. J. (1999) SOCS1 is a critical inhibitor of interferon gamma signaling and prevents the potentially fatal neonatal actions of this cytokine. *Cell*, 98(5), 597-608.

Allen, N. J., Bennett, M. L., Foo, L. C., Wang, G. X., Chakraborty, C., Smith, S. J. & Barres, B. A. (2012) Astrocyte glypicans 4 and 6 promote formation of excitatory synapses via GluA1 AMPA receptors. *Nature*, 486(7403), 410-4.

Almad, A. A. & Maragakis, N. J. (2012) Glia: an emerging target for neurological disease therapy. *Stem Cell Res Ther*, 3(5), 37.

Alvestad, S., Hammer, J., Hoddevik, E. H., Skare, Ø., Sonnewald, U., Amiry-Moghaddam, M. & Ottersen, O. P. (2013) Mislocalization of AQP4 precedes chronic seizures in the kainate model of temporal lobe epilepsy. *Epilepsy Res*, 105(1-2), 30-41.

Anderson, C. M. & Swanson, R. A. (2000) Astrocyte glutamate transport: review of properties, regulation, and physiological functions. *Glia*, 32(1), 1-14.

Anderson, G. & Maes, M. (2017) Interactions of Tryptophan and Its Catabolites With Melatonin and the Alpha 7 Nicotinic Receptor in Central Nervous System and Psychiatric Disorders: Role of the Aryl Hydrocarbon Receptor and Direct Mitochondria Regulation. *Int J Tryptophan Res*, 10, 1178646917691738.

Anderson, M. A., Ao, Y. & Sofroniew, M. V. (2014) Heterogeneity of reactive astrocytes. *Neurosci Lett*, 565, 23-9.

Anlauf, E. & Derouiche, A. (2013) Glutamine synthetase as an astrocytic marker: its cell type and vesicle localization. *Front Endocrinol (Lausanne)*, 4, 144.
Araque, A., Carmignoto, G., Haydon, P. G., Oliet, S. H., Robitaille, R. & Volterra, A. (2014) Gliotransmitters travel in time and space. *Neuron*, 81(4), 728-39.
Araújo, M. R., Kyrylenko, S., Spejo, A. B., Castro, M. V., Ferreira Junior, R. S., Barraviera, B. & Oliveira, A. L. R. (2017) Transgenic human embryonic stem cells overexpressing FGF2 stimulate neuroprotection following spinal cord ventral root avulsion. *Exp Neurol*, 294, 45-57.
Arcuri, C., Mecca, C., Bianchi, R., Giambanco, I. & Donato, R. (2017) The Pathophysiological Role of Microglia in Dynamic Surveillance, Phagocytosis and Structural Remodeling of the Developing CNS. *Front Mol Neurosci*, 10, 191.
Arguello, P. A. & Gogos, J. A. (2012) Genetic and cognitive windows into circuit mechanisms of psychiatric disease. *Trends Neurosci*, 35(1), 3-13.
Arikkath, J. (2012) Molecular mechanisms of dendrite morphogenesis. *Front Cell Neurosci*, 6, 61.
Asakura, T., Sasaki, T., Nagano, F., Satoh, A., Obaishi, H., Nishioka, H., Imamura, H., Hotta, K., Tanaka, K., Nakanishi, H. & Takai, Y. (1998) Isolation and characterization of a novel actin filament-binding protein from Saccharomyces cerevisiae. *Oncogene*, 16(1), 121-30.
Askvig, J. M. & Watt, J. A. (2015) The MAPK and PI3K pathways mediate CNTF-induced neuronal survival and process outgrowth in hypothalamic organotypic cultures. *J Cell Commun Signal*, 9(3), 217-31.
Attwell, D., Buchan, A. M., Charpak, S., Lauritzen, M., Macvicar, B. A. & Newman, E. A. (2010) Glial and neuronal control of brain blood flow. *Nature*, 468(7321), 232-43.
Au-Yeung, N., Mandhana, R. & Horvath, C. M. (2013) Transcriptional regulation by STAT1 and STAT2 in the interferon JAK-STAT pathway. *JAKSTAT*, 2(3), e23931.
Azevedo, E. P., Ledo, J. H., Barbosa, G., Sobrinho, M., Diniz, L., Fonseca, A. C., Gomes, F., Romão, L., Lima, F. R., Palhano, F. L., Ferreira, S. T. & Foguel, D. (2013) Activated microglia mediate synapse loss and short-term memory deficits in a mouse model of transthyretin-related oculoleptomeningeal amyloidosis. *Cell Death Dis*, 4, e789.
Bach, E. A., Aguet, M. & Schreiber, R. D. (1997) The IFN gamma receptor: a paradigm for cytokine receptor signaling. *Annu Rev Immunol*, 15, 563-91.
Bachiller, S., Jiménez-Ferrer, I., Paulus, A., Yang, Y., Swanberg, M., Deierborg, T. & Boza-Serrano, A. (2018) Microglia in Neurological Diseases: A Road Map to Brain-Disease Dependent-Inflammatory Response. *Front Cell Neurosci*, 12, 488.
Bachstetter, A. D., Rowe, R. K., Kaneko, M., Goulding, D., Lifshitz, J. & Van Eldik, L. J. (2013) The p38α MAPK regulates microglial responsiveness to diffuse traumatic brain injury. *J Neurosci*, 33(14), 6143-53.
Badaut, J., Fukuda, A. M., Jullienne, A. & Petry, K. G. (2014) Aquaporin and brain diseases. *Biochim Biophys Acta*, 1840(5), 1554-65.
Badawy, A. A. (2014) The tryptophan utilization concept in pregnancy. *Obstet Gynecol Sci*, 57(4), 249-59.
Bahmad, H., Hadadeh, O., Chamaa, F., Cheaito, K., Darwish, B., Makkawi, A. K. & Abou-Kheir, W. (2017) Modeling Human Neurological and Neurodegenerative Diseases: From Induced Pluripotent Stem Cells to Neuronal Differentiation and Its Applications in Neurotrauma. *Front Mol Neurosci*, 10, 50.
Bailey, C. H., Kandel, E. R. & Harris, K. M. (2015) Structural Components of Synaptic Plasticity and Memory Consolidation. *Cold Spring Harb Perspect Biol*, 7(7), a021758.
Bal-Price, A., Moneer, Z. & Brown, G. C. (2002) Nitric oxide induces rapid, calcium-dependent release of vesicular glutamate and ATP from cultured rat astrocytes. *Glia*, 40(3), 312-23.
Baldwin, K. T. & Eroglu, C. (2017) Molecular mechanisms of astrocyte-induced synaptogenesis. *Curr Opin Neurobiol*, 45, 113-120.

Balu, D. T. & Coyle, J. T. (2011) Neuroplasticity signaling pathways linked to the pathophysiology of schizophrenia. *Neuroscience & Biobehavioral Reviews*, 35(3), 848-870.
Bambrick, L., Kristian, T. & Fiskum, G. (2004) Astrocyte mitochondrial mechanisms of ischemic brain injury and neuroprotection. *Neurochem Res*, 29(3), 601-8.
Banasr, M. & Duman, R. S. (2008) Glial loss in the prefrontal cortex is sufficient to induce depressive-like behaviors. *Biol Psychiatry*, 64(10), 863-70.
Banasr, M., Dwyer, J. M. & Duman, R. S. (2011) Cell atrophy and loss in depression: reversal by antidepressant treatment. *Curr Opin Cell Biol*, 23(6), 730-7.
Baran, P., Hansen, S., Waetzig, G. H., Akbarzadeh, M., Lamertz, L., Huber, H. J., Ahmadian, M. R., Moll, J. M. & Scheller, J. (2018) The balance of interleukin (IL)-6, IL-6·soluble IL-6 receptor (sIL-6R), and IL-6·sIL-6R·sgp130 complexes allows simultaneous classic and trans-signaling. *J Biol Chem*, 293(18), 6762-6775.
Barcia, C., Ros, C. M., Annese, V., Gómez, A., Ros-Bernal, F., Aguado-Yera, D., Martínez-Pagán, M. E., de Pablos, V., Fernandez-Villalba, E. & Herrero, M. T. (2011) IFN-γ signaling, with the synergistic contribution of TNF-α, mediates cell specific microglial and astroglial activation in experimental models of Parkinson's disease. *Cell Death Dis*, 2, e142.
Barros, L. F., San Martín, A., Sotelo-Hitschfeld, T., Lerchundi, R., Fernández-Moncada, I., Ruminot, I., Gutiérrez, R., Valdebenito, R., Ceballo, S., Alegría, K., Baeza-Lehnert, F. & Espinoza, D. (2013) Small is fast: astrocytic glucose and lactate metabolism at cellular resolution. *Front Cell Neurosci*, 7, 27.
Basso, M. & Bonetto, V. (2016) Extracellular Vesicles and a Novel Form of Communication in the Brain. *Front Neurosci*, 10, 127.
Batista, C. R. A., Gomes, G. F., Candelario-Jalil, E., Fiebich, B. L. & de Oliveira, A. C. P. (2019) Lipopolysaccharide-Induced Neuroinflammation as a Bridge to Understand Neurodegeneration. *Int J Mol Sci*, 20(9).
Bauer, M. E. & Teixeira, A. L. (2019) Inflammation in psychiatric disorders: what comes first? *Ann N Y Acad Sci*, 1437(1), 57-67.
Beauquis, J., Pavía, P., Pomilio, C., Vinuesa, A., Podlutskaya, N., Galvan, V. & Saravia, F. (2013) Environmental enrichment prevents astroglial pathological changes in the hippocampus of APP transgenic mice, model of Alzheimer's disease. *Exp Neurol*, 239, 28-37.
Belanger, M., Allaman, I. & Magistretti, P. J. (2011) Brain energy metabolism: focus on astrocyte-neuron metabolic cooperation. *Cell Metab*, 14(6), 724-38.
Belin, B. J., Goins, L. M. & Mullins, R. D. (2014) Comparative analysis of tools for live cell imaging of actin network architecture. *Bioarchitecture*, 4(6), 189-202.
Bellucci, A., Antonini, A., Pizzi, M. & Spano, P. (2017) The End Is the Beginning: Parkinson's Disease in the Light of Brain Imaging. *Front Aging Neurosci*, 9, 330.
Bellucci, A., Mercuri, N. B., Venneri, A., Faustini, G., Longhena, F., Pizzi, M., Missale, C. & Spano, P. (2016) Review: Parkinson's disease: from synaptic loss to connectome dysfunction. *Neuropathol Appl Neurobiol*, 42(1), 77-94.
Ben Haim, L., Carrillo-de Sauvage, M. A., Ceyzériat, K. & Escartin, C. (2015) Elusive roles for reactive astrocytes in neurodegenerative diseases. *Front Cell Neurosci*, 9, 278.
Benediktsson, A. M., Marrs, G. S., Tu, J. C., Worley, P. F., Rothstein, J. D., Bergles, D. E. & Dailey, M. E. (2012) Neuronal activity regulates glutamate transporter dynamics in developing astrocytes. *Glia*, 60(2), 175-88.
Bennett, M. L., Bennett, F. C., Liddelow, S. A., Ajami, B., Zamanian, J. L., Fernhoff, N. B., Mulinyawe, S. B., Bohlen, C. J., Adil, A., Tucker, A., Weissman, I. L., Chang, E. F., Li, G., Grant, G. A., Hayden Gephart, M. G. & Barres, B. A. (2016) New tools for studying microglia in the mouse and human CNS. *Proc Natl Acad Sci U S A*, 113(12), E1738-46.
Bennett, M. R. & Lagopoulos, J. (2014) Stress and trauma: BDNF control of dendritic-spine formation and regression. *Prog Neurobiol*, 112, 80-99.

Benveniste, E. N., Sparacio, S. M., Norris, J. G., Grenett, H. E. & Fuller, G. M. (1990) Induction and regulation of interleukin-6 gene expression in rat astrocytes. *J Neuroimmunol*, 30(2-3), 201-12.
Bergmans, R. S., Kelly, K. M. & Mezuk, B. (2019) Inflammation as a unique marker of suicide ideation distinct from depression syndrome among U.S. adults. *J Affect Disord*, 245, 1052-1060.
Bian, W. J., Miao, W. Y., He, S. J., Qiu, Z. & Yu, X. (2015) Coordinated Spine Pruning and Maturation Mediated by Inter-Spine Competition for Cadherin/Catenin Complexes. *Cell*, 162(4), 808-22.
Biederer, T., Kaeser, P. S. & Blanpied, T. A. (2017) Transcellular Nanoalignment of Synaptic Function. *Neuron*, 96(3), 680-696.
Bilbo, S. & Stevens, B. (2017) Microglia: The Brain's First Responders. *Cerebrum*, 2017.
Binder, D. K., Nagelhus, E. A. & Ottersen, O. P. (2012) Aquaporin-4 and epilepsy. *Glia*, 60(8), 1203-14.
Birnboim, H. C. & Doly, J. (1979) A rapid alkaline extraction procedure for screening recombinant plasmid DNA. *Nucleic Acids Res*, 7(6), 1513-23.
Blackmore, M. G., Moore, D. L., Smith, R. P., Goldberg, J. L., Bixby, J. L. & Lemmon, V. P. (2010) High content screening of cortical neurons identifies novel regulators of axon growth. *Mol Cell Neurosci*, 44(1), 43-54.
Boato, F., Hechler, D., Rosenberger, K., Lüdecke, D., Peters, E. M., Nitsch, R. & Hendrix, S. (2011) Interleukin-1 beta and neurotrophin-3 synergistically promote neurite growth in vitro. *J Neuroinflammation*, 8, 183.
Bocchini, V., Mazzolla, R., Barluzzi, R., Blasi, E., Sick, P. & Kettenmann, H. (1992) An immortalized cell line expresses properties of activated microglial cells. *J Neurosci Res*, 31(4), 616-21.
Boche, D., Perry, V. H. & Nicoll, J. A. (2013) Review: activation patterns of microglia and their identification in the human brain. *Neuropathol Appl Neurobiol*, 39(1), 3-18.
Bodakuntla, S., Jijumon, A. S., Villablanca, C., Gonzalez-Billault, C. & Janke, C. (2019) Microtubule-Associated Proteins: Structuring the Cytoskeleton. *Trends Cell Biol*, 29(10), 804-819.
Boesmans, W., Rocha, N. P., Reis, H. J., Holt, M. & Vanden Berghe, P. (2014) The astrocyte marker Aldh1L1 does not reliably label enteric glial cells. *Neurosci Lett*, 566, 102-5.
Bohar, Z., Toldi, J., Fulop, F. & Vecsei, L. (2015) Changing the face of kynurenines and neurotoxicity: therapeutic considerations. *Int J Mol Sci*, 16(5), 9772-93.
Bohár, Z., Toldi, J., Fülöp, F. & Vécsei, L. (2015) Changing the face of kynurenines and neurotoxicity: therapeutic considerations. *Int J Mol Sci*, 16(5), 9772-93.
Bolaños, J. P. & Heales, S. J. (2010) Persistent mitochondrial damage by nitric oxide and its derivatives: neuropathological implications. *Front Neuroenergetics*, 2, 1.
Bongarzone, S., Savickas, V., Luzi, F. & Gee, A. D. (2017) Targeting the Receptor for Advanced Glycation Endproducts (RAGE): A Medicinal Chemistry Perspective. *J Med Chem*, 60(17), 7213-7232.
Bono, J., Wilmes, K. A. & Clopath, C. (2017) Modelling plasticity in dendrites: from single cells to networks. *Curr Opin Neurobiol*, 46, 136-141.
Boomkamp, S. D., Riehle, M. O., Wood, J., Olson, M. F. & Barnett, S. C. (2012) The development of a rat in vitro model of spinal cord injury demonstrating the additive effects of Rho and ROCK inhibitors on neurite outgrowth and myelination. *Glia*, 60(3), 441-56.
Braidy, N. & Grant, R. (2017) Kynurenine pathway metabolism and neuroinflammatory disease. *Neural Regen Res*, 12(1), 39-42.
Braidy, N., Grant, R., Brew, B. J., Adams, S., Jayasena, T. & Guillemin, G. J. (2009) Effects of Kynurenine Pathway Metabolites on Intracellular NAD Synthesis and Cell Death in Human Primary Astrocytes and Neurons. *Int J Tryptophan Res*, 2, 61-9.

Braun, M., Vaibhav, K., Saad, N. M., Fatima, S., Vender, J. R., Baban, B., Hoda, M. N. & Dhandapani, K. M. (2017) White matter damage after traumatic brain injury: A role for damage associated molecular patterns. *Biochim Biophys Acta Mol Basis Dis*, 1863(10 Pt B), 2614-2626.
Breda, C., Sathyasaikumar, K. V., Sograte Idrissi, S., Notarangelo, F. M., Estranero, J. G., Moore, G. G., Green, E. W., Kyriacou, C. P., Schwarcz, R. & Giorgini, F. (2016) Tryptophan-2,3-dioxygenase (TDO) inhibition ameliorates neurodegeneration by modulation of kynurenine pathway metabolites. *Proc Natl Acad Sci U S A*, 113(19), 5435-40.
Brockett, A. T., Kane, G. A., Monari, P. K., Briones, B. A., Vigneron, P. A., Barber, G. A., Bermudez, A., Dieffenbach, U., Kloth, A. D., Buschman, T. J. & Gould, E. (2018) Evidence supporting a role for astrocytes in the regulation of cognitive flexibility and neuronal oscillations through the Ca2+ binding protein S100β. *PLoS One*, 13(4), e0195726.
Bronzuoli, M. R., Iacomino, A., Steardo, L. & Scuderi, C. (2016) Targeting neuroinflammation in Alzheimer's disease. *J Inflamm Res*, 9, 199-208.
Brown, D. R. & Kretzschmar, H. A. (1998) The glio-toxic mechanism of alpha-aminoadipic acid on cultured astrocytes. *J Neurocytol*, 27(2), 109-18.
Brown, G., Wang, E., Leon, A., Huynh, M., Wehner, M., Matro, R., Linos, E., Liao, W. & Haemel, A. (2017) Tumor necrosis factor-α inhibitor-induced psoriasis: Systematic review of clinical features, histopathological findings, and management experience. *J Am Acad Dermatol*, 76(2), 334-341.
Browne, T. C., McQuillan, K., McManus, R. M., O'Reilly, J. A., Mills, K. H. & Lynch, M. A. (2013) IFN-γ Production by amyloid β-specific Th1 cells promotes microglial activation and increases plaque burden in a mouse model of Alzheimer's disease. *J Immunol*, 190(5), 2241-51.
Brozzi, F., Arcuri, C., Giambanco, I. & Donato, R. (2009) S100B Protein Regulates Astrocyte Shape and Migration via Interaction with Src Kinase: Implications for Astrocyte development, activation and tumor growth. *J Biol Chem*, 284(13), 8797-811.
Brymer, K. J., Romay-Tallon, R., Allen, J., Caruncho, H. J. & Kalynchuk, L. E. (2019) Exploring the Potential Antidepressant Mechanisms of TNFα Antagonists. *Front Neurosci*, 13, 98.
Bukalo, O. & Dityatev, A. (2012) Synaptic cell adhesion molecules. *Adv Exp Med Biol*, 970, 97-128.
Burmester, G. R., Panaccione, R., Gordon, K. B., McIlraith, M. J. & Lacerda, A. P. (2013) Adalimumab: long-term safety in 23 458 patients from global clinical trials in rheumatoid arthritis, juvenile idiopathic arthritis, ankylosing spondylitis, psoriatic arthritis, psoriasis and Crohn's disease. *Ann Rheum Dis*, 72(4), 517-24.
Burudi, E. M., Marcondes, M. C., Watry, D. D., Zandonatti, M., Taffe, M. A. & Fox, H. S. (2002) Regulation of indoleamine 2,3-dioxygenase expression in simian immunodeficiency virus-infected monkey brains. *J Virol*, 76(23), 12233-41.
Butkevich, E., Hülsmann, S., Wenzel, D., Shirao, T., Duden, R. & Majoul, I. (2004) Drebrin is a novel connexin-43 binding partner that links gap junctions to the submembrane cytoskeleton. *Curr Biol*, 14(8), 650-8.
Butovsky, O., Jedrychowski, M. P., Moore, C. S., Cialic, R., Lanser, A. J., Gabriely, G., Koeglsperger, T., Dake, B., Wu, P. M., Doykan, C. E., Fanek, Z., Liu, L., Chen, Z., Rothstein, J. D., Ransohoff, R. M., Gygi, S. P., Antel, J. P. & Weiner, H. L. (2014) Identification of a unique TGF-[beta]-dependent molecular and functional signature in microglia. *Nat Neurosci*, 17(1), 131-143.
Butt, A. M. (2011) ATP: a ubiquitous gliotransmitter integrating neuron-glial networks. *Semin Cell Dev Biol*, 22(2), 205-13.
Bylicky, M. A., Mueller, G. P. & Day, R. M. (2018) Mechanisms of Endogenous Neuroprotective Effects of Astrocytes in Brain Injury. *Oxid Med Cell Longev*, 2018, 6501031.

Calabrese, V., Mancuso, C., Calvani, M., Rizzarelli, E., Butterfield, D. A. & Stella, A. M. (2007) Nitric oxide in the central nervous system: neuroprotection versus neurotoxicity. *Nat Rev Neurosci*, 8(10), 766-75.
Cambron, M., D'Haeseleer, M., Laureys, G., Clinckers, R., Debruyne, J. & De Keyser, J. (2012) White-matter astrocytes, axonal energy metabolism, and axonal degeneration in multiple sclerosis. *J Cereb Blood Flow Metab*, 32(3), 413-24.
Campbell, I. L., Erta, M., Lim, S. L., Frausto, R., May, U., Rose-John, S., Scheller, J. & Hidalgo, J. (2014) Trans-signaling is a dominant mechanism for the pathogenic actions of interleukin-6 in the brain. *J Neurosci*, 34(7), 2503-13.
Campesan, S., Green, E. W., Breda, C., Sathyasaikumar, K. V., Muchowski, P. J., Schwarcz, R., Kyriacou, C. P. & Giorgini, F. (2011) The kynurenine pathway modulates neurodegeneration in a Drosophila model of Huntington's disease. *Curr Biol*, 21(11), 961-6.
Caraci, F., Battaglia, G., Sortino, M. A., Spampinato, S., Molinaro, G., Copani, A., Nicoletti, F. & Bruno, V. (2012) Metabotropic glutamate receptors in neurodegeneration/neuroprotection: still a hot topic? *Neurochem Int*, 61(4), 559-65.
Carniglia, L., Ramírez, D., Durand, D., Saba, J., Turati, J., Caruso, C., Scimonelli, T. N. & Lasaga, M. (2017) Neuropeptides and Microglial Activation in Inflammation, Pain, and Neurodegenerative Diseases. *Mediators Inflamm*, 2017, 5048616.
Carpenedo, R., Pittaluga, A., Cozzi, A., Attucci, S., Galli, A., Raiteri, M. & Moroni, F. (2001) Presynaptic kynurenate-sensitive receptors inhibit glutamate release. *Eur J Neurosci*, 13(11), 2141-7.
Cassimeris, L. & Spittle, C. (2001) Regulation of microtubule-associated proteins. *Int Rev Cytol*, 210, 163-226.
Castellano-Gonzalez, G., Jacobs, K. R., Don, E., Cole, N. J., Adams, S., Lim, C. K., Lovejoy, D. B. & Guillemin, G. J. (2019) Kynurenine 3-Monooxygenase Activity in Human Primary Neurons and Effect on Cellular Bioenergetics Identifies New Neurotoxic Mechanisms. *Neurotox Res*, 35(3), 530-541.
Censor, N., Dimyan, M. A. & Cohen, L. G. (2010) Modification of existing human motor memories is enabled by primary cortical processing during memory reactivation. *Curr Biol*, 20(17), 1545-9.
Chaves, M. L., Camozzato, A. L., Ferreira, E. D., Piazenski, I., Kochhann, R., Dall'Igna, O., Mazzini, G. S., Souza, D. O. & Portela, L. V. (2010) Serum levels of S100B and NSE proteins in Alzheimer's disease patients. *J Neuroinflammation*, 7, 6.
Chen, G. Y. & Nuñez, G. (2010) Sterile inflammation: sensing and reacting to damage. *Nat Rev Immunol*, 10(12), 826-37.
Chen, H., Lin, W., Zhang, Y., Lin, L., Chen, J., Zeng, Y., Zheng, M., Zhuang, Z., Du, H., Chen, R. & Liu, N. (2016a) IL-10 Promotes Neurite Outgrowth and Synapse Formation in Cultured Cortical Neurons after the Oxygen-Glucose Deprivation via JAK1/STAT3 Pathway. *Sci Rep*, 6, 30459.
Chen, K., Liu, J. & Cao, X. (2017) Regulation of type I interferon signaling in immunity and inflammation: A comprehensive review. *J Autoimmun*, 83, 1-11.
Chen, L., Mo, M., Li, G., Cen, L., Wei, L., Xiao, Y., Chen, X., Li, S., Yang, X., Qu, S. & Xu, P. (2016b) The biomarkers of immune dysregulation and inflammation response in Parkinson disease. *Transl Neurodegener*, 5(1), 16.
Chen, X., Hu, Y., Cao, Z., Liu, Q. & Cheng, Y. (2018) Cerebrospinal Fluid Inflammatory Cytokine Aberrations in Alzheimer's Disease, Parkinson's Disease and Amyotrophic Lateral Sclerosis: A Systematic Review and Meta-Analysis. *Front Immunol*, 9, 2122.
Chen, X., Levy, J. M., Hou, A., Winters, C., Azzam, R., Sousa, A. A., Leapman, R. D., Nicoll, R. A. & Reese, T. S. (2015) PSD-95 family MAGUKs are essential for anchoring AMPA and NMDA receptor complexes at the postsynaptic density. *Proc Natl Acad Sci U S A*, 112(50), E6983-92.

Chen, Y., Fu, A. K. Y. & Ip, N. Y. (2019) Synaptic dysfunction in Alzheimer's disease: Mechanisms and therapeutic strategies. *Pharmacol Ther*, 195, 186-198.
Chen, Y., Garcia, G. E., Huang, W. & Constantini, S. (2014) The involvement of secondary neuronal damage in the development of neuropsychiatric disorders following brain insults. *Front Neurol*, 5, 22.
Cheng, C., Lau, S. K. & Doering, L. C. (2016) Astrocyte-secreted thrombospondin-1 modulates synapse and spine defects in the fragile X mouse model. *Mol Brain*, 9(1), 74.
Cherry, J. D., Olschowka, J. A. & O'Banion, M. K. (2014) Neuroinflammation and M2 microglia: the good, the bad, and the inflamed. *J Neuroinflammation*, 11, 98.
Chiarugi, A., Meli, E. & Moroni, F. (2001) Similarities and differences in the neuronal death processes activated by 3OH-kynurenine and quinolinic acid. *J Neurochem*, 77(5), 1310-8.
Chucair-Elliott, A. J., Conrady, C., Zheng, M., Kroll, C. M., Lane, T. E. & Carr, D. J. (2014) Microglia-induced IL-6 protects against neuronal loss following HSV-1 infection of neural progenitor cells. *Glia*, 62(9), 1418-34.
Chung, C. Y., Koprich, J. B., Siddiqi, H. & Isacson, O. (2009) Dynamic changes in presynaptic and axonal transport proteins combined with striatal neuroinflammation precede dopaminergic neuronal loss in a rat model of AAV alpha-synucleinopathy. *J Neurosci*, 29(11), 3365-73.
Chung, W. S., Allen, N. J. & Eroglu, C. (2015) Astrocytes Control Synapse Formation, Function, and Elimination. *Cold Spring Harb Perspect Biol*, 7(9), a020370.
Chung, W. S., Clarke, L. E., Wang, G. X., Stafford, B. K., Sher, A., Chakraborty, C., Joung, J., Foo, L. C., Thompson, A., Chen, C., Smith, S. J. & Barres, B. A. (2013) Astrocytes mediate synapse elimination through MEGF10 and MERTK pathways. *Nature*, 504(7480), 394-400.
Cinelli, R. A., Ferrari, A., Pellegrini, V., Tyagi, M., Giacca, M. & Beltram, F. (2000) The enhanced green fluorescent protein as a tool for the analysis of protein dynamics and localization: local fluorescence study at the single-molecule level. *Photochem Photobiol*, 71(6), 771-6.
Clarke, L. E. & Barres, B. A. (2013) Emerging roles of astrocytes in neural circuit development. *Nat Rev Neurosci*, 14(5), 311-21.
Cline, H. T. (2001) Dendritic arbor development and synaptogenesis. *Curr Opin Neurobiol*, 11(1), 118-26.
Cobb, J. A., O'Neill, K., Milner, J., Mahajan, G. J., Lawrence, T. J., May, W. L., Miguel-Hidalgo, J., Rajkowska, G. & Stockmeier, C. A. (2016) Density of GFAP-immunoreactive astrocytes is decreased in left hippocampi in major depressive disorder. *Neuroscience*, 316, 209-20.
Cohen, S. B., Proudman, S., Kivitz, A. J., Burch, F. X., Donohue, J. P., Burstein, D., Sun, Y. N., Banfield, C., Vincent, M. S., Ni, L. & Zack, D. J. (2011) A randomized, double-blind study of AMG 108 (a fully human monoclonal antibody to IL-1R1) in patients with osteoarthritis of the knee. *Arthritis Res Ther*, 13(4), R125.
Colton, C. & Wilcock, D. M. (2010) Assessing activation states in microglia. *CNS Neurol Disord Drug Targets*, 9(2), 174-91.
Colín-González, A. L., Maldonado, P. D. & Santamaría, A. (2013) 3-Hydroxykynurenine: an intriguing molecule exerting dual actions in the central nervous system. *Neurotoxicology*, 34, 189-204.
Connor, T. J., Starr, N., O'Sullivan, J. B. & Harkin, A. (2008) Induction of indolamine 2,3-dioxygenase and kynurenine 3-monooxygenase in rat brain following a systemic inflammatory challenge: a role for IFN-gamma? *Neurosci Lett*, 441(1), 29-34.
Counts, S. E., Nadeem, M., Lad, S. P., Wuu, J. & Mufson, E. J. (2006) Differential expression of synaptic proteins in the frontal and temporal cortex of elderly subjects with mild cognitive impairment. *J Neuropathol Exp Neurol*, 65(6), 592-601.

Coyle, J. T., Basu, A., Benneyworth, M., Balu, D. & Konopaske, G. (2012) Glutamatergic synaptic dysregulation in schizophrenia: therapeutic implications. *Handb Exp Pharmacol*(213), 267-95.
Cuartero, M. I., Ballesteros, I., de la Parra, J., Harkin, A. L., Abautret-Daly, A., Sherwin, E., Fernandez-Salguero, P., Corbi, A. L., Lizasoain, I. & Moro, M. A. (2014) L-kynurenine/aryl hydrocarbon receptor pathway mediates brain damage after experimental stroke. *Circulation*, 130(23), 2040-51.
Czeh, M., Gressens, P. & Kaindl, A. M. (2011) The yin and yang of microglia. *Dev Neurosci*, 33(3-4), 199-209.
Czéh, B. & Nagy, S. A. (2018) Clinical Findings Documenting Cellular and Molecular Abnormalities of Glia in Depressive Disorders. *Front Mol Neurosci*, 11, 56.
Cătălin, B., Cupido, A., Iancău, M., Albu, C. V. & Kirchhoff, F. (2013) Microglia: first responders in the central nervous system. *Rom J Morphol Embryol*, 54(3), 467-72.
Dalby, B., Cates, S., Harris, A., Ohki, E. C., Tilkins, M. L., Price, P. J. & Ciccarone, V. C. (2004) Advanced transfection with Lipofectamine 2000 reagent: primary neurons, siRNA, and high-throughput applications. *Methods*, 33(2), 95-103.
Dancker, P., Löw, I., Hasselbach, W. & Wieland, T. (1975) Interaction of actin with phalloidin: polymerization and stabilization of F-actin. *Biochim Biophys Acta*, 400(2), 407-14.
Dantzer, R. (2017) Role of the Kynurenine Metabolism Pathway in Inflammation-Induced Depression: Preclinical Approaches. *Curr Top Behav Neurosci*, 31, 117-138.
Dantzer, R. & Walker, A. K. (2014) Is there a role for glutamate-mediated excitotoxicity in inflammation-induced depression? *J Neural Transm (Vienna)*, 121(8), 925-32.
Davalos, D., Grutzendler, J., Yang, G., Kim, J. V., Zuo, Y., Jung, S., Littman, D. R., Dustin, M. L. & Gan, W. B. (2005) ATP mediates rapid microglial response to local brain injury in vivo. *Nat Neurosci*, 8(6), 752-8.
David, J., O'Toole, E., O'Reilly, K., Thuery, G., Assmann, N., Finlay, D. & Harkin, A. (2018) Inhibitors of the NMDA-Nitric Oxide Signaling Pathway Protect Against Neuronal Atrophy and Synapse Loss Provoked by l-alpha Aminoadipic Acid-treated Astrocytes. *Neuroscience*, 392, 38-56.
Day, J. S., O'Neill, E., Cawley, C., Aretz, N. K., Kilroy, D., Gibney, S. M., Harkin, A. & Connor, T. J. (2014) Noradrenaline acting on astrocytic beta(2)-adrenoceptors induces neurite outgrowth in primary cortical neurons. *Neuropharmacology*, 77, 234-48.
de Bartolomeis, A., Latte, G., Tomasetti, C. & Iasevoli, F. (2014) Glutamatergic postsynaptic density protein dysfunctions in synaptic plasticity and dendritic spines morphology: relevance to schizophrenia and other behavioral disorders pathophysiology, and implications for novel therapeutic approaches. *Mol Neurobiol*, 49(1), 484-511.
de Pins, B., Cifuentes-Diaz, C., Farah, A. T., Lopez-Molina, L., Montalban, E., Sancho-Balsells, A., Lopez, A., Gines, S., Delgado-Garcia, J. M., Alberch, J., Gruart, A., Girault, J. A. & Giralt, A. (2019) Conditional BDNF Delivery from Astrocytes Rescues Memory Deficits, Spine Density, and Synaptic Properties in the 5xFAD Mouse Model of Alzheimer Disease. *J Neurosci*, 39(13), 2441-2458.
de Weerd, N. A. & Nguyen, T. (2012) The interferons and their receptors--distribution and regulation. *Immunol Cell Biol*, 90(5), 483-91.
Dehmelt, L. & Halpain, S. (2005) The MAP2/Tau family of microtubule-associated proteins. *Genome Biol*, 6(1), 204.
Deng, G. C., Lu, M., Zhao, Y. Y., Yuan, Y. & Chen, G. (2019) Activated spinal astrocytes contribute to the later phase of carrageenan-induced prostatitis pain. *J Neuroinflammation*, 16(1), 189.
Denison, M. S. & Nagy, S. R. (2003) Activation of the aryl hydrocarbon receptor by structurally diverse exogenous and endogenous chemicals. *Annu Rev Pharmacol Toxicol*, 43, 309-34.

Dent, E. W., Gupton, S. L. & Gertler, F. B. (2011) The growth cone cytoskeleton in axon outgrowth and guidance. *Cold Spring Harb Perspect Biol*, 3(3).
Di Stefano, G., Casoli, T., Fattoretti, P., Gracciotti, N., Solazzi, M. & Bertoni-Freddari, C. (2001) Distribution of map2 in hippocampus and cerebellum of young and old rats by quantitative immunohistochemistry. *J Histochem Cytochem*, 49(8), 1065-6.
Dickens, A. M., Tovar-Y-Romo, L. B., Yoo, S. W., Trout, A. L., Bae, M., Kanmogne, M., Megra, B., Williams, D. W., Witwer, K. W., Gacias, M., Tabatadze, N., Cole, R. N., Casaccia, P., Berman, J. W., Anthony, D. C. & Haughey, N. J. (2017) Astrocyte-shed extracellular vesicles regulate the peripheral leukocyte response to inflammatory brain lesions. *Sci Signal*, 10(473).
Dinarello, C. A., Simon, A. & van der Meer, J. W. (2012) Treating inflammation by blocking interleukin-1 in a broad spectrum of diseases. *Nat Rev Drug Discov*, 11(8), 633-52.
DiNatale, B. C., Murray, I. A., Schroeder, J. C., Flaveny, C. A., Lahoti, T. S., Laurenzana, E. M., Omiecinski, C. J. & Perdew, G. H. (2010) Kynurenic acid is a potent endogenous aryl hydrocarbon receptor ligand that synergistically induces interleukin-6 in the presence of inflammatory signaling. *Toxicol Sci*, 115(1), 89-97.
Diniz, L. P., Almeida, J. C., Tortelli, V., Vargas Lopes, C., Setti-Perdigao, P., Stipursky, J., Kahn, S. A., Romao, L. F., de Miranda, J., Alves-Leon, S. V., de Souza, J. M., Castro, N. G., Panizzutti, R. & Gomes, F. C. (2012a) Astrocyte-induced synaptogenesis is mediated by transforming growth factor beta signaling through modulation of D-serine levels in cerebral cortex neurons. *J Biol Chem*, 287(49), 41432-45.
Diniz, L. P., Almeida, J. C., Tortelli, V., Vargas Lopes, C., Setti-Perdigão, P., Stipursky, J., Kahn, S. A., Romão, L. F., de Miranda, J., Alves-Leon, S. V., de Souza, J. M., Castro, N. G., Panizzutti, R. & Gomes, F. C. (2012b) Astrocyte-induced synaptogenesis is mediated by transforming growth factor β signaling through modulation of D-serine levels in cerebral cortex neurons. *J Biol Chem*, 287(49), 41432-45.
Diniz, L. P., Tortelli, V., Matias, I., Morgado, J., Bergamo Araujo, A. P., Melo, H. M., Seixas da Silva, G. S., Alves-Leon, S. V., de Souza, J. M., Ferreira, S. T., De Felice, F. G. & Gomes, F. C. A. (2017) Astrocyte Transforming Growth Factor Beta 1 Protects Synapses against Abeta Oligomers in Alzheimer's Disease Model. *J Neurosci*, 37(28), 6797-6809.
DiSabato, D. J., Quan, N. & Godbout, J. P. (2016) Neuroinflammation: the devil is in the details. *J Neurochem*, 139 Suppl 2, 136-153.
Dokalis, N. & Prinz, M. (2018) Astrocytic NF-κB brings the best and worst out of microglia. *EMBO J*, 37(16).
Dolmetsch, R. & Geschwind, D. H. (2011) The human brain in a dish: the promise of iPSC-derived neurons. *Cell*, 145(6), 831-4.
Donato, R., Cannon, B. R., Sorci, G., Riuzzi, F., Hsu, K., Weber, D. J. & Geczy, C. L. (2013) Functions of S100 proteins. *Curr Mol Med*, 13(1), 24-57.
Dostal, C. R., Carson Sulzer, M., Kelley, K. W., Freund, G. G. & McCusker, R. H. (2017) Glial and tissue-specific regulation of Kynurenine Pathway dioxygenases by acute stress of mice. *Neurobiol Stress*, 7, 1-15.
Dotti, C. G. & Banker, G. A. (1987) Experimentally induced alteration in the polarity of developing neurons. *Nature*, 330(6145), 254-6.
Doucet, M. V., O'Toole, E., Connor, T. & Harkin, A. (2015) Small-molecule inhibitors at the PSD-95/nNOS interface protect against glutamate-induced neuronal atrophy in primary cortical neurons. *Neuroscience*, 301, 421-38.
Dowlati, Y., Herrmann, N., Swardfager, W., Liu, H., Sham, L., Reim, E. K. & Lanctôt, K. L. (2010) A meta-analysis of cytokines in major depression. *Biol Psychiatry*, 67(5), 446-57.
Dragunow, M. (2008) The adult human brain in preclinical drug development. *Nat Rev Drug Discov*, 7(8), 659-66.
Duarte, E. P., Curcio, M., Canzoniero, L. M. & Duarte, C. B. (2012) Neuroprotection by GDNF in the ischemic brain. *Growth Factors*, 30(4), 242-57.

Dugan, L. L. & Kim-Han, J. S. (2004) Astrocyte mitochondria in in vitro models of ischemia. *J Bioenerg Biomembr*, 36(4), 317-21.
Duman, R. S. (2004) Neural plasticity: consequences of stress and actions of antidepressant treatment. *Dialogues Clin Neurosci*, 6(2), 157-69.
Duman, R. S. (2014) Pathophysiology of depression and innovative treatments: remodeling glutamatergic synaptic connections. *Dialogues Clin Neurosci*, 16(1), 11-27.
Duman, R. S. & Aghajanian, G. K. (2012) Synaptic dysfunction in depression: potential therapeutic targets. *Science*, 338(6103), 68-72.
Duman, R. S., Aghajanian, G. K., Sanacora, G. & Krystal, J. H. (2016) Synaptic plasticity and depression: new insights from stress and rapid-acting antidepressants. *Nat Med*, 22(3), 238-49.
Duman, R. S., Li, N., Liu, R. J., Duric, V. & Aghajanian, G. (2012) Signaling pathways underlying the rapid antidepressant actions of ketamine. *Neuropharmacology*, 62(1), 35-41.
Dumont, A. O., Goursaud, S., Desmet, N. & Hermans, E. (2014) Differential regulation of glutamate transporter subtypes by pro-inflammatory cytokine TNF-alpha in cortical astrocytes from a rat model of amyotrophic lateral sclerosis. *PLoS One*, 9(5), e97649.
Dungan, L. S., McGuinness, N. C., Boon, L., Lynch, M. A. & Mills, K. H. (2014) Innate IFN-γ promotes development of experimental autoimmune encephalomyelitis: a role for NK cells and M1 macrophages. *Eur J Immunol*, 44(10), 2903-17.
Dursun, E., Gezen-Ak, D., Hanagasi, H., Bilgic, B., Lohmann, E., Ertan, S., Atasoy, I. L., Alaylioglu, M., Araz, O. S., Onal, B., Gunduz, A., Apaydin, H., Kiziltan, G., Ulutin, T., Gurvit, H. & Yilmazer, S. (2015) The interleukin 1 alpha, interleukin 1 beta, interleukin 6 and alpha-2-macroglobulin serum levels in patients with early or late onset Alzheimer's disease, mild cognitive impairment or Parkinson's disease. *J Neuroimmunol*, 283, 50-7.
Dutta, D. J., Woo, D. H., Lee, P. R., Pajevic, S., Bukalo, O., Huffman, W. C., Wake, H., Basser, P. J., SheikhBahaei, S., Lazarevic, V., Smith, J. C. & Fields, R. D. (2018) Regulation of myelin structure and conduction velocity by perinodal astrocytes. *Proc Natl Acad Sci U S A*, 115(46), 11832-11837.
Easter, S. S., Ross, L. S. & Frankfurter, A. (1993) Initial tract formation in the mouse brain. *J Neurosci*, 13(1), 285-99.
Efimova, N., Korobova, F., Stankewich, M. C., Moberly, A. H., Stolz, D. B., Wang, J., Kashina, A., Ma, M. & Svitkina, T. (2017) betaIII Spectrin Is Necessary for Formation of the Constricted Neck of Dendritic Spines and Regulation of Synaptic Activity in Neurons. *J Neurosci*, 37(27), 6442-6459.
Efremova, L., Chovancova, P., Adam, M., Gutbier, S., Schildknecht, S. & Leist, M. (2017) Switching from astrocytic neuroprotection to neurodegeneration by cytokine stimulation. *Arch Toxicol*, 91(1), 231-246.
Elmore, M. R., Najafi, A. R., Koike, M. A., Dagher, N. N., Spangenberg, E. E., Rice, R. A., Kitazawa, M., Matusow, B., Nguyen, H., West, B. L. & Green, K. N. (2014) Colony-stimulating factor 1 receptor signaling is necessary for microglia viability, unmasking a microglia progenitor cell in the adult brain. *Neuron*, 82(2), 380-97.
Elsayed, M. & Magistretti, P. J. (2015) A New Outlook on Mental Illnesses: Glial Involvement Beyond the Glue. *Front Cell Neurosci*, 9, 468.
Emoto, K. (2012) Signaling mechanisms that coordinate the development and maintenance of dendritic fields. *Curr Opin Neurobiol*, 22(5), 805-11.
Erhardt, S., Lim, C. K., Linderholm, K. R., Janelidze, S., Lindqvist, D., Samuelsson, M., Lundberg, K., Postolache, T. T., Traskman-Bendz, L., Guillemin, G. J. & Brundin, L. (2013) Connecting inflammation with glutamate agonism in suicidality. *Neuropsychopharmacology*, 38(5), 743-52.
Eroglu, C. & Barres, B. A. (2010) Regulation of synaptic connectivity by glia. *Nature*, 468(7321), 223-31.

Erta, M., Quintana, A. & Hidalgo, J. (2012) Interleukin-6, a major cytokine in the central nervous system. *Int J Biol Sci*, 8(9), 1254-66.
Estes, J. E., Selden, L. A. & Gershman, L. C. (1981) Mechanism of action of phalloidin on the polymerization of muscle actin. *Biochemistry*, 20(4), 708-12.
Evans, J. W., Szczepanik, J., Brutsché, N., Park, L. T., Nugent, A. C. & Zarate, C. A. (2018) Default Mode Connectivity in Major Depressive Disorder Measured Up to 10 Days After Ketamine Administration. *Biol Psychiatry*, 84(8), 582-590.
Ewald, R. C., Van Keuren-Jensen, K. R., Aizenman, C. D. & Cline, H. T. (2008) Roles of NR2A and NR2B in the development of dendritic arbor morphology in vivo. *J Neurosci*, 28(4), 850-61.
Fang, A., Li, D., Hao, Z., Wang, L., Pan, B., Gao, L., Qu, X. & He, J. (2019) Effects of astrocyte on neuronal outgrowth in a layered 3D structure. *Biomed Eng Online*, 18(1), 74.
Farhy-Tselnicker, I. & Allen, N. J. (2018) Astrocytes, neurons, synapses: a tripartite view on cortical circuit development. *Neural Dev*, 13(1), 7.
Farhy-Tselnicker, I., van Casteren, A. C. M., Lee, A., Chang, V. T., Aricescu, A. R. & Allen, N. J. (2017) Astrocyte-Secreted Glypican 4 Regulates Release of Neuronal Pentraxin 1 from Axons to Induce Functional Synapse Formation. *Neuron*, 96(2), 428-445.e13.
Farrukh, A., Zhao, S. & del Campo, A. (2018) Microenvironments Designed to Support Growth and Function of Neuronal Cells.
Fedder, K. N. & Sabo, S. L. (2015) On the Role of Glutamate in Presynaptic Development: Possible Contributions of Presynaptic NMDA Receptors. *Biomolecules*, 5(4), 3448-66.
Fedoroff, S., Ahmed, I., Opas, M. & Kalnins, V. I. (1987) Organization of microfilaments in astrocytes that form in the presence of dibutyryl cyclic AMP in cultures, and which are similar to reactive astrocytes in vivo. *Neuroscience*, 22(1), 255-66.
Felgner, P. L., Gadek, T. R., Holm, M., Roman, R., Chan, H. W., Wenz, M., Northrop, J. P., Ringold, G. M. & Danielsen, M. (1987) Lipofection: a highly efficient, lipid-mediated DNA-transfection procedure. *Proc Natl Acad Sci U S A*, 84(21), 7413-7.
Felgner, P. L. & Ringold, G. M. (1989) Cationic liposome-mediated transfection. *Nature*, 337(6205), 387-8.
Feng, Q., Wang, Y. I. & Yang, Y. (2015) Neuroprotective effect of interleukin-6 in a rat model of cerebral ischemia. *Exp Ther Med*, 9(5), 1695-1701.
Fernández-Arjona, M. D. M., Grondona, J. M., Granados-Durán, P., Fernández-Llebrez, P. & López-Ávalos, M. D. (2017) Microglia Morphological Categorization in a Rat Model of Neuroinflammation by Hierarchical Cluster and Principal Components Analysis. *Front Cell Neurosci*, 11, 235.
Ferrante, M., Migliore, M. & Ascoli, G. A. (2013) Functional impact of dendritic branch-point morphology. *J Neurosci*, 33(5), 2156-65.
Ferreira, F. S., Biasibetti-Brendler, H., Pierozan, P., Schmitz, F., Bertó, C. G., Prezzi, C. A., Manfredini, V. & Wyse, A. T. S. (2018) Kynurenic Acid Restores Nrf2 Levels and Prevents Quinolinic Acid-Induced Toxicity in Rat Striatal Slices. *Mol Neurobiol*, 55(11), 8538-8549.
Ferrer-Ferrer, M. & Dityatev, A. (2018) Shaping Synapses by the Neural Extracellular Matrix. *Front Neuroanat*, 12, 40.
Ferrini, F. & De Koninck, Y. (2013) Microglia control neuronal network excitability via BDNF signalling. *Neural Plast*, 2013, 429815.
Fifková, E. & Delay, R. J. (1982) Cytoplasmic actin in neuronal processes as a possible mediator of synaptic plasticity. *J Cell Biol*, 95(1), 345-50.
Figley, C. R. & Stroman, P. W. (2011) The role(s) of astrocytes and astrocyte activity in neurometabolism, neurovascular coupling, and the production of functional neuroimaging signals. *Eur J Neurosci*, 33(4), 577-88.
Filiou, M. D., Bisle, B., Reckow, S., Teplytska, L., Maccarrone, G. & Turck, C. W. (2010) Profiling of mouse synaptosome proteome and phosphoproteome by IEF. *Electrophoresis*, 31(8), 1294-301.

Fischer, M., Kaech, S., Knutti, D. & Matus, A. (1998) Rapid actin-based plasticity in dendritic spines. *Neuron*, 20(5), 847-54.
Fogarty, M. J. (2018) Driven to decay: Excitability and synaptic abnormalities in amyotrophic lateral sclerosis. *Brain Res Bull*, 140, 318-333.
Fontaine, V., Mohand-Said, S., Hanoteau, N., Fuchs, C., Pfizenmaier, K. & Eisel, U. (2002) Neurodegenerative and neuroprotective effects of tumor Necrosis factor (TNF) in retinal ischemia: opposite roles of TNF receptor 1 and TNF receptor 2. *J Neurosci*, 22(7), RC216.
Foo, L. C. & Dougherty, J. D. (2013) Aldh1L1 is expressed by postnatal neural stem cells in vivo. *Glia*, 61(9), 1533-41.
Fotis, L., Agrogiannis, G., Vlachos, I. S., Pantopoulou, A., Margoni, A., Kostaki, M., Verikokos, C., Tzivras, D., Mikhailidis, D. P. & Perrea, D. (2012) Intercellular adhesion molecule (ICAM)-1 and vascular cell adhesion molecule (VCAM)-1 at the early stages of atherosclerosis in a rat model. *In Vivo*, 26(2), 243-50.
Franciosi, S., Ryu, J. K., Shim, Y., Hill, A., Connolly, C., Hayden, M. R., McLarnon, J. G. & Leavitt, B. R. (2012) Age-dependent neurovascular abnormalities and altered microglial morphology in the YAC128 mouse model of Huntington disease. *Neurobiol Dis*, 45(1), 438-49.
Franco, R. & Fernández-Suárez, D. (2015) Alternatively activated microglia and macrophages in the central nervous system. *Prog Neurobiol*, 131, 65-86.
Fricker, M., Vilalta, A., Tolkovsky, A. M. & Brown, G. C. (2013) Caspase inhibitors protect neurons by enabling selective necroptosis of inflamed microglia. *J Biol Chem*, 288(13), 9145-52.
Frischknecht, R., Chang, K. J., Rasband, M. N. & Seidenbecher, C. I. (2014) Neural ECM molecules in axonal and synaptic homeostatic plasticity. *Prog Brain Res*, 214, 81-100.
Frost, G. R. & Li, Y. M. (2017) The role of astrocytes in amyloid production and Alzheimer's disease. *Open Biol*, 7(12).
Frost, J. L. & Schafer, D. P. (2016) Microglia: Architects of the Developing Nervous System. *Trends Cell Biol*, 26(8), 587-597.
Fujibayashi, T., Kurauchi, Y., Hisatsune, A., Seki, T., Shudo, K. & Katsuki, H. (2015) Mitogen-activated protein kinases regulate expression of neuronal nitric oxide synthase and neurite outgrowth via non-classical retinoic acid receptor signaling in human neuroblastoma SH-SY5Y cells. *J Pharmacol Sci*, 129(2), 119-26.
Fujigaki, H., Yamamoto, Y. & Saito, K. (2017) L-Tryptophan-kynurenine pathway enzymes are therapeutic target for neuropsychiatric diseases: Focus on cell type differences. *Neuropharmacology*, 112, 264-274.
Fujigaki, S., Saito, K., Sekikawa, K., Tone, S., Takikawa, O., Fujii, H., Wada, H., Noma, A. & Seishima, M. (2001) Lipopolysaccharide induction of indoleamine 2,3-dioxygenase is mediated dominantly by an IFN-gamma-independent mechanism. *Eur J Immunol*, 31(8), 2313-8.
Fukazawa, Y., Saitoh, Y., Ozawa, F., Ohta, Y., Mizuno, K. & Inokuchi, K. (2003) Hippocampal LTP is accompanied by enhanced F-actin content within the dendritic spine that is essential for late LTP maintenance in vivo. *Neuron*, 38(3), 447-60.
Fulmer, C. G., VonDran, M. W., Stillman, A. A., Huang, Y., Hempstead, B. L. & Dreyfus, C. F. (2014) Astrocyte-derived BDNF supports myelin protein synthesis after cuprizone-induced demyelination. *J Neurosci*, 34(24), 8186-96.
Funakoshi, Masaaki, K. & Toshikazu, N. (2011) Modulation of Tryptophan Metabolism, Promotion of Neurogenesis and Alteration of Anxiety-Related Behavior in Tryptophan 2,3-Dioxygenase-Deficient Mice. *International Journal of Tryptophan Research*, 7.
Gallo, V. & Deneen, B. (2014) Glial development: the crossroads of regeneration and repair in the CNS. *Neuron*, 83(2), 283-308.
Gananca, L., Oquendo, M. A., Tyrka, A. R., Cisneros-Trujillo, S., Mann, J. J. & Sublette, M. E. (2016) The role of cytokines in the pathophysiology of suicidal behavior. *Psychoneuroendocrinology*, 63, 296-310.

Garcia-Oscos, F., Salgado, H., Hall, S., Thomas, F., Farmer, G. E., Bermeo, J., Galindo, L. C., Ramirez, R. D., D'Mello, S., Rose-John, S. & Atzori, M. (2012) The stress-induced cytokine interleukin-6 decreases the inhibition/excitation ratio in the rat temporal cortex via trans-signaling. *Biol Psychiatry*, 71(7), 574-82.
García-Lara, L., Pérez-Severiano, F., González-Esquivel, D., Elizondo, G. & Segovia, J. (2015) Absence of aryl hydrocarbon receptors increases endogenous kynurenic acid levels and protects mouse brain against excitotoxic insult and oxidative stress. *J Neurosci Res*, 93(9), 1423-33.
García-López, P., García-Marín, V. & Freire, M. (2010) Dendritic spines and development: towards a unifying model of spinogenesis--a present day review of Cajal's histological slides and drawings. *Neural Plast*, 2010, 769207.
Garrison, A. M., Parrott, J. M., Tuñon, A., Delgado, J., Redus, L. & O'Connor, J. C. (2018a) Kynurenine pathway metabolic balance influences microglia activity: Targeting kynurenine monooxygenase to dampen neuroinflammation. *Psychoneuroendocrinology*, 94, 1-10.
Garrison, A. M., Parrott, J. M., Tuñon, A., Delgado, J., Redus, L. & O'Connor, J. C. (2018b) Kynurenine pathway metabolic balance influences microglia activity: Targeting kynurenine monooxygenase to dampen neuroinflammation. *Psychoneuroendocrinology*, 94, 1-10.
Gautier, E. L., Shay, T., Miller, J., Greter, M., Jakubzick, C., Ivanov, S., Helft, J., Chow, A., Elpek, K. G., Gordonov, S., Mazloom, A. R., Ma'ayan, A., Chua, W. J., Hansen, T. H., Turley, S. J., Merad, M., Randolph, G. J. & Consortium, I. G. (2012) Gene-expression profiles and transcriptional regulatory pathways that underlie the identity and diversity of mouse tissue macrophages. *Nat Immunol*, 13(11), 1118-28.
Gazzolo, D. & Michetti, F. (2010) Perinatal S100B Protein Assessment in Human Unconventional Biological Fluids: A Minireview and New Perspectives. *Cardiovasc Psychiatry Neurol*, 2010, 703563.
Geraldo, S. & Gordon-Weeks, P. R. (2009) Cytoskeletal dynamics in growth-cone steering. *J Cell Sci*, 122(Pt 20), 3595-604.
Germann, W. a. S. (2005) *Principles of human physiology*. San Francisco: Pearson Benjamin Cummings.
Ghézali, G., Calvo, C. F., Pillet, L. E., Llense, F., Ezan, P., Pannasch, U., Bemelmans, A. P., Etienne Manneville, S. & Rouach, N. (2018) Connexin 30 controls astroglial polarization during postnatal brain development. *Development*, 145(4).
Gigante, A. D., Young, L. T., Yatham, L. N., Andreazza, A. C., Nery, F. G., Grinberg, L. T., Heinsen, H. & Lafer, B. (2011) Morphometric post-mortem studies in bipolar disorder: possible association with oxidative stress and apoptosis. *Int J Neuropsychopharmacol*, 14(8), 1075-89.
Giménez-Llort, L., Maté, I., Manassra, R., Vida, C. & De la Fuente, M. (2012) Peripheral immune system and neuroimmune communication impairment in a mouse model of Alzheimer's disease. *Ann N Y Acad Sci*, 1262, 74-84.
Ginhoux, F., Lim, S., Hoeffel, G., Low, D. & Huber, T. (2013) Origin and differentiation of microglia. *Front Cell Neurosci*, 7, 45.
Gittins, R. A. & Harrison, P. J. (2011) A morphometric study of glia and neurons in the anterior cingulate cortex in mood disorder. *J Affect Disord*, 133(1-2), 328-32.
Glantz, L. A., Gilmore, J. H., Hamer, R. M., Lieberman, J. A. & Jarskog, L. F. (2007) Synaptophysin and postsynaptic density protein 95 in the human prefrontal cortex from mid-gestation into early adulthood. *Neuroscience*, 149(3), 582-91.
Glass, C. K., Saijo, K., Winner, B., Marchetto, M. C. & Gage, F. H. (2010a) Mechanisms underlying inflammation in neurodegeneration. *Cell*, 140(6), 918-34.
Glass, C. K., Saijo, K., Winner, B., Marchetto, M. C. & Gage, F. H. (2010b) Mechanisms Underlying Inflammation in Neurodegeneration. *Cell*, 140(6), 918-934.

Goldstein, L. E., Leopold, M. C., Huang, X., Atwood, C. S., Saunders, A. J., Hartshorn, M., Lim, J. T., Faget, K. Y., Muffat, J. A., Scarpa, R. C., Chylack, L. T., Bowden, E. F., Tanzi, R. E. & Bush, A. I. (2000) 3-Hydroxykynurenine and 3-hydroxyanthranilic acid generate hydrogen peroxide and promote alpha-crystallin cross-linking by metal ion reduction. *Biochemistry*, 39(24), 7266-75.
González Esquivel, D., Ramírez-Ortega, D., Pineda, B., Castro, N., Ríos, C. & Pérez de la Cruz, V. (2017a) Kynurenine pathway metabolites and enzymes involved in redox reactions. *Neuropharmacology*, 112, 331-345.
González Esquivel, D., Ramírez-Ortega, D., Pineda, B., Castro, N., Ríos, C. & Pérez de la Cruz, V. (2017b) Kynurenine pathway metabolites and enzymes involved in redox reactions. *Neuropharmacology*, 112(Pt B), 331-345.
Gordon, G. R., Howarth, C. & MacVicar, B. A. (2011) Bidirectional control of arteriole diameter by astrocytes. *Exp Physiol*, 96(4), 393-9.
Gras, G., Samah, B., Hubert, A., Leone, C., Porcheray, F. & Rimaniol, A. C. (2012a) EAAT expression by macrophages and microglia: still more questions than answers. *Amino Acids*, 42(1), 221-9.
Gras, G., Samah, B., Hubert, A., Léone, C., Porcheray, F. & Rimaniol, A. C. (2012b) EAAT expression by macrophages and microglia: still more questions than answers. *Amino Acids*, 42(1), 221-9.
Grau, V., Herbst, B., van der Meide, P. H. & Steiniger, B. (1997) Activation of microglial and endothelial cells in the rat brain after treatment with interferon-gamma in vivo. *Glia*, 19(3), 181-9.
Green, D. S., Young, H. A. & Valencia, J. C. (2017) Current prospects of type II interferon γ signaling and autoimmunity. *J Biol Chem*, 292(34), 13925-13933.
Gruol, D. L. (2015) IL-6 regulation of synaptic function in the CNS. *Neuropharmacology*, 96(Pt A), 42-54.
Guerra, M. C., Tortorelli, L. S., Galland, F., Da Ré, C., Negri, E., Engelke, D. S., Rodrigues, L., Leite, M. C. & Gonçalves, C. A. (2011) Lipopolysaccharide modulates astrocytic S100B secretion: a study in cerebrospinal fluid and astrocyte cultures from rats. *J Neuroinflammation*, 8, 128.
Guillemin, G. J. (2012) Quinolinic acid, the inescapable neurotoxin. *FEBS J*, 279(8), 1356-65.
Guillemin, G. J., Cullen, K. M., Lim, C. K., Smythe, G. A., Garner, B., Kapoor, V., Takikawa, O. & Brew, B. J. (2007) Characterization of the kynurenine pathway in human neurons. *J Neurosci*, 27(47), 12884-92.
Guillemin, G. J., Kerr, S. J., Smythe, G. A., Smith, D. G., Kapoor, V., Armati, P. J., Croitoru, J. & Brew, B. J. (2001) Kynurenine pathway metabolism in human astrocytes: a paradox for neuronal protection. *J Neurochem*, 78(4), 842-53.
Guillemin, G. J., Smythe, G., Takikawa, O. & Brew, B. J. (2005) Expression of indoleamine 2,3-dioxygenase and production of quinolinic acid by human microglia, astrocytes, and neurons. *Glia*, 49(1), 15-23.
Gulledge, A. T., Carnevale, N. T. & Stuart, G. J. (2012) Electrical advantages of dendritic spines. *PLoS One*, 7(4), e36007.
Gumy, L. F., Katrukha, E. A., Grigoriev, I., Jaarsma, D., Kapitein, L. C., Akhmanova, A. & Hoogenraad, C. C. (2017) MAP2 Defines a Pre-axonal Filtering Zone to Regulate KIF1- versus KIF5-Dependent Cargo Transport in Sensory Neurons. *Neuron*, 94(2), 347-362.e7.
Guo, H., Callaway, J. B. & Ting, J. P. (2015) Inflammasomes: mechanism of action, role in disease, and therapeutics. *Nat Med*, 21(7), 677-87.
Guo, L., Tian, J. & Du, H. (2017) Mitochondrial Dysfunction and Synaptic Transmission Failure in Alzheimer's Disease. *J Alzheimers Dis*, 57(4), 1071-1086.
Gutierrez, H. & Davies, A. M. (2007) A fast and accurate procedure for deriving the Sholl profile in quantitative studies of neuronal morphology. *J Neurosci Methods*, 163(1), 24-30.

Guttenplan, K. A. & Liddelow, S. A. (2019) Astrocytes and microglia: Models and tools. *J Exp Med*, 216(1), 71-83.
Guzman-Martinez, L., Maccioni, R. B., Andrade, V., Navarrete, L. P., Pastor, M. G. & Ramos-Escobar, N. (2019) Neuroinflammation as a Common Feature of Neurodegenerative Disorders. *Front Pharmacol*, 10, 1008.
Gyengesi, E., Rangel, A., Ullah, F., Liang, H., Niedermayer, G., Asgarov, R., Venigalla, M., Gunawardena, D., Karl, T. & Münch, G. (2019) Chronic Microglial Activation in the GFAP-IL6 Mouse Contributes to Age-Dependent Cerebellar Volume Loss and Impairment in Motor Function. *Front Neurosci*, 13, 303.
Haapakoski, R., Mathieu, J., Ebmeier, K. P., Alenius, H. & Kivimäki, M. (2015) Cumulative meta-analysis of interleukins 6 and 1β, tumour necrosis factor α and C-reactive protein in patients with major depressive disorder. *Brain Behav Immun*, 49, 206-15.
Haijma, S. V., Van Haren, N., Cahn, W., Koolschijn, P. C., Hulshoff Pol, H. E. & Kahn, R. S. (2013) Brain volumes in schizophrenia: a meta-analysis in over 18 000 subjects. *Schizophr Bull*, 39(5), 1129-38.
Haj-Yasein, N. N., Jensen, V., Østby, I., Omholt, S. W., Voipio, J., Kaila, K., Ottersen, O. P., Hvalby, Ø. & Nagelhus, E. A. (2012) Aquaporin-4 regulates extracellular space volume dynamics during high-frequency synaptic stimulation: a gene deletion study in mouse hippocampus. *Glia*, 60(6), 867-74.
Hajduková, L., Sobek, O., Prchalová, D., Bílková, Z., Koudelková, M., Lukášková, J. & Matuchová, I. (2015) Biomarkers of Brain Damage: S100B and NSE Concentrations in Cerebrospinal Fluid--A Normative Study. *Biomed Res Int*, 2015, 379071.
Hallen, A., Jamie, J. F. & Cooper, A. J. (2013) Lysine metabolism in mammalian brain: an update on the importance of recent discoveries. *Amino Acids*, 45(6), 1249-72.
Halliday, G. M., Holton, J. L., Revesz, T. & Dickson, D. W. (2011) Neuropathology underlying clinical variability in patients with synucleinopathies. *Acta Neuropathol*, 122(2), 187-204.
Hanamura, K., Koganezawa, N., Kamiyama, K., Tanaka, N., Oka, T., Yamamura, M., Sekino, Y. & Shirao, T. (2019) High-content imaging analysis for detecting the loss of drebrin clusters along dendrites in cultured hippocampal neurons. *J Pharmacol Toxicol Methods*, 106607.
Hannestad, J., DellaGioia, N. & Bloch, M. (2011) The effect of antidepressant medication treatment on serum levels of inflammatory cytokines: a meta-analysis. *Neuropsychopharmacology*, 36(12), 2452-9.
Hansson, E., Werner, T., Björklund, U. & Skiöldebrand, E. (2016) Therapeutic innovation: Inflammatory-reactive astrocytes as targets of inflammation. *IBRO Rep*, 1, 1-9.
Harada, A., Teng, J., Takei, Y., Oguchi, K. & Hirokawa, N. (2002) MAP2 is required for dendrite elongation, PKA anchoring in dendrites, and proper PKA signal transduction. *J Cell Biol*, 158(3), 541-9.
Harnett, M. T., Makara, J. K., Spruston, N., Kath, W. L. & Magee, J. C. (2012) Synaptic amplification by dendritic spines enhances input cooperativity. *Nature*, 491(7425), 599-602.
Haroon, E., Raison, C. L. & Miller, A. H. (2012) Psychoneuroimmunology meets neuropsychopharmacology: translational implications of the impact of inflammation on behavior. *Neuropsychopharmacology*, 37(1), 137-62.
Hashioka, S., Klegeris, A., Schwab, C. & McGeer, P. L. (2009) Interferon-gamma-dependent cytotoxic activation of human astrocytes and astrocytoma cells. *Neurobiol Aging*, 30(12), 1924-35.
Hashioka, S., Klegeris, A., Schwab, C., Yu, S. & McGeer, P. L. (2010) Differential expression of interferon-gamma receptor on human glial cells in vivo and in vitro. *J Neuroimmunol*, 225(1-2), 91-9.

Hayakawa, K., Pham, L. D., Arai, K. & Lo, E. H. (2014) Reactive astrocytes promote adhesive interactions between brain endothelium and endothelial progenitor cells via HMGB1 and beta-2 integrin signaling. *Stem Cell Res*, 12(2), 531-8.
Hayden, M. S. & Ghosh, S. (2014) Regulation of NF-κB by TNF family cytokines. *Semin Immunol*, 26(3), 253-66.
He, P., Liu, Q., Wu, J. & Shen, Y. (2012) Genetic deletion of TNF receptor suppresses excitatory synaptic transmission via reducing AMPA receptor synaptic localization in cortical neurons. *FASEB J*, 26(1), 334-45.
Headland, S. E. & Norling, L. V. (2015) The resolution of inflammation: Principles and challenges. *Semin Immunol*, 27(3), 149-60.
Heinrich, P. C., Behrmann, I., Haan, S., Hermanns, H. M., Müller-Newen, G. & Schaper, F. (2003) Principles of interleukin (IL)-6-type cytokine signalling and its regulation. *Biochem J*, 374(Pt 1), 1-20.
Heneka, M. T., Golenbock, D. T. & Latz, E. (2015) Innate immunity in Alzheimer's disease. *Nat Immunol*, 16(3), 229-36.
Henn, A., Lund, S., Hedtjarn, M., Schrattenholz, A., Porzgen, P. & Leist, M. (2009) The suitability of BV2 cells as alternative model system for primary microglia cultures or for animal experiments examining brain inflammation. *Altex*, 26(2), 83-94.
Herculano-Houzel, S. (2014) The glia/neuron ratio: how it varies uniformly across brain structures and species and what that means for brain physiology and evolution. *Glia*, 62(9), 1377-91.
Hering, H. & Sheng, M. (2001) Dendritic spines: structure, dynamics and regulation. *Nat Rev Neurosci*, 2(12), 880-8.
Hillen, A. E. J., Burbach, J. P. H. & Hol, E. M. (2018) Cell adhesion and matricellular support by astrocytes of the tripartite synapse. *Prog Neurobiol*, 165-167, 66-86.
Hindinger, C., Bergmann, C. C., Hinton, D. R., Phares, T. W., Parra, G. I., Hussain, S., Savarin, C., Atkinson, R. D. & Stohlman, S. A. (2012) IFN-γ signaling to astrocytes protects from autoimmune mediated neurological disability. *PLoS One*, 7(7), e42088.
Hochstrasser, T., Ullrich, C., Sperner-Unterweger, B. & Humpel, C. (2011) Inflammatory stimuli reduce survival of serotonergic neurons and induce neuronal expression of indoleamine 2,3-dioxygenase in rat dorsal raphe nucleus organotypic brain slices. *Neuroscience*, 184, 128-38.
Hodes, G. E., Ménard, C. & Russo, S. J. (2016) Integrating Interleukin-6 into depression diagnosis and treatment. *Neurobiol Stress*, 4, 15-22.
Hoge, J., Yan, I., Jänner, N., Schumacher, V., Chalaris, A., Steinmetz, O. M., Engel, D. R., Scheller, J., Rose-John, S. & Mittrücker, H. W. (2013) IL-6 controls the innate immune response against Listeria monocytogenes via classical IL-6 signaling. *J Immunol*, 190(2), 703-11.
Hol, E. M. & Pekny, M. (2015) Glial fibrillary acidic protein (GFAP) and the astrocyte intermediate filament system in diseases of the central nervous system. *Curr Opin Cell Biol*, 32, 121-30.
Hollos, P., John, J. M., Lehtonen, J. V. & Coffey, E. T. (2020) Optogenetic control of spine-head JNK reveals a role in dendritic spine regression. *eNeuro*.
Hong, S., Beja-Glasser, V. F., Nfonoyim, B. M., Frouin, A., Li, S., Ramakrishnan, S., Merry, K. M., Shi, Q., Rosenthal, A., Barres, B. A., Lemere, C. A., Selkoe, D. J. & Stevens, B. (2016) Complement and microglia mediate early synapse loss in Alzheimer mouse models. *Science*, 352(6286), 712-716.
Hopperton, K. E., Mohammad, D., Trépanier, M. O., Giuliano, V. & Bazinet, R. P. (2018) Markers of microglia in post-mortem brain samples from patients with Alzheimer's disease: a systematic review. *Mol Psychiatry*, 23(2), 177-198.
Horvath, R. J., Nutile-McMenemy, N., Alkaitis, M. S. & De Leo, J. A. (2008) Differential migration, LPS-induced cytokine, chemokine and NO expression in immortalized BV-2

and HAPI cell lines and primary microglial cultures. *Journal of neurochemistry*, 107(2), 557-569.
Hovens, I. B., van Leeuwen, B. L., Nyakas, C., Heineman, E., van der Zee, E. A. & Schoemaker, R. G. (2015) Postoperative cognitive dysfunction and microglial activation in associated brain regions in old rats. *Neurobiol Learn Mem*, 118, 74-9.
Howard, J. & Hyman, A. A. (2003) Dynamics and mechanics of the microtubule plus end. *Nature*, 422(6933), 753-8.
Hu, X., Chakravarty, S. D. & Ivashkiv, L. B. (2008) Regulation of interferon and Toll-like receptor signaling during macrophage activation by opposing feedforward and feedback inhibition mechanisms. *Immunol Rev*, 226, 41-56.
Hu, X. & Ivashkiv, L. B. (2009) Cross-regulation of signaling pathways by interferon-gamma: implications for immune responses and autoimmune diseases. *Immunity*, 31(4), 539-50.
Huang, Y. S., Jung, M. Y., Sarkissian, M. & Richter, J. D. (2002) N-methyl-D-aspartate receptor signaling results in Aurora kinase-catalyzed CPEB phosphorylation and alpha CaMKII mRNA polyadenylation at synapses. *Embo j*, 21(9), 2139-48.
Hubbard, J. A., Szu, J. I. & Binder, D. K. (2018) The role of aquaporin-4 in synaptic plasticity, memory and disease. *Brain Res Bull*, 136, 118-129.
Huganir, R. L. & Nicoll, R. A. (2013) AMPARs and synaptic plasticity: the last 25 years. *Neuron*, 80(3), 704-17.
Hughes, E. G., Elmariah, S. B. & Balice-Gordon, R. J. (2010) Astrocyte secreted proteins selectively increase hippocampal GABAergic axon length, branching, and synaptogenesis. *Mol Cell Neurosci*, 43(1), 136-45.
Hummel, F. C., Heise, K., Celnik, P., Floel, A., Gerloff, C. & Cohen, L. G. (2010) Facilitating skilled right hand motor function in older subjects by anodal polarization over the left primary motor cortex. *Neurobiol Aging*, 31(12), 2160-8.
Hutchinson, J. P., Rowland, P., Taylor, M. R. D., Christodoulou, E. M., Haslam, C., Hobbs, C. I., Holmes, D. S., Homes, P., Liddle, J., Mole, D. J., Uings, I., Walker, A. L., Webster, S. P., Mowat, C. G. & Chung, C. W. (2017) Structural and mechanistic basis of differentiated inhibitors of the acute pancreatitis target kynurenine-3-monooxygenase. *Nat Commun*, 8, 15827.
Höglund, E., Øverli, Ø. & Winberg, S. (2019) Tryptophan Metabolic Pathways and Brain Serotonergic Activity: A Comparative Review. *Front Endocrinol (Lausanne)*, 10, 158.
Ikeshima-Kataoka, H. (2016) Neuroimmunological Implications of AQP4 in Astrocytes. *Int J Mol Sci*, 17(8).
Ippolito, D. M. & Eroglu, C. (2010) Quantifying synapses: an immunocytochemistry-based assay to quantify synapse number. *J Vis Exp*(45).
Ishibashi, M., Egawa, K. & Fukuda, A. (2019) Diverse Actions of Astrocytes in GABAergic Signaling. *Int J Mol Sci*, 20(12).
Ishiyama, M., Miyazono, Y., Sasamoto, K., Ohkura, Y. & Ueno, K. (1997) A highly water-soluble disulfonated tetrazolium salt as a chromogenic indicator for NADH as well as cell viability. *Talanta*, 44(7), 1299-305.
Ishiyama, M., Tominaga, H., Shiga, M., Sasamoto, K., Ohkura, Y. & Ueno, K. (1996) A combined assay of cell viability and in vitro cytotoxicity with a highly water-soluble tetrazolium salt, neutral red and crystal violet. *Biol Pharm Bull*, 19(11), 1518-20.
Ivanov, A., Esclapez, M., Pellegrino, C., Shirao, T. & Ferhat, L. (2009) Drebrin A regulates dendritic spine plasticity and synaptic function in mature cultured hippocampal neurons. *J Cell Sci*, 122(Pt 4), 524-34.
Jan, Y. N. & Jan, L. Y. (2010) Branching out: mechanisms of dendritic arborization. *Nat Rev Neurosci*, 11(5), 316-28.
Janelidze, S., Mattei, D., Westrin, Å., Träskman-Bendz, L. & Brundin, L. (2011) Cytokine levels in the blood may distinguish suicide attempters from depressed patients. *Brain Behav Immun*, 25(2), 335-9.

Jensen, C. J., Massie, A. & De Keyser, J. (2013) Immune players in the CNS: the astrocyte. *J Neuroimmune Pharmacol*, 8(4), 824-39.
Jha, M. K. & Morrison, B. M. (2018) Glia-neuron energy metabolism in health and diseases: New insights into the role of nervous system metabolic transporters. *Exp Neurol*, 309, 23-31.
Jha, S. K., Jha, N. K., Kar, R., Ambasta, R. K. & Kumar, P. (2015) p38 MAPK and PI3K/AKT Signalling Cascades inParkinson's Disease. *Int J Mol Cell Med*, 4(2), 67-86.
Jiang, M., Ash, R. T., Baker, S. A., Suter, B., Ferguson, A., Park, J., Rudy, J., Torsky, S. P., Chao, H. T., Zoghbi, H. Y. & Smirnakis, S. M. (2013) Dendritic arborization and spine dynamics are abnormal in the mouse model of MECP2 duplication syndrome. *J Neurosci*, 33(50), 19518-33.
Jo, H. Y., Kim, Y., Park, H. W., Moon, H. E., Bae, S., Kim, J., Kim, D. G. & Paek, S. H. (2015) The Unreliability of MTT Assay in the Cytotoxic Test of Primary Cultured Glioblastoma Cells. *Exp Neurobiol*, 24(3), 235-45.
John, G. R., Lee, S. C. & Brosnan, C. F. (2003) Cytokines: powerful regulators of glial cell activation. *Neuroscientist*, 9(1), 10-22.
Jones, S. A., Richards, P. J., Scheller, J. & Rose-John, S. (2005) IL-6 transsignaling: the in vivo consequences. *J Interferon Cytokine Res*, 25(5), 241-53.
Jones, S. P., Franco, N. F., Varney, B., Sundaram, G., Brown, D. A., de Bie, J., Lim, C. K., Guillemin, G. J. & Brew, B. J. (2015) Expression of the Kynurenine Pathway in Human Peripheral Blood Mononuclear Cells: Implications for Inflammatory and Neurodegenerative Disease. *PLoS One*, 10(6), e0131389.
Jones, V. C., Atkinson-Dell, R., Verkhratsky, A. & Mohamet, L. (2017) Aberrant iPSC-derived human astrocytes in Alzheimer's disease. *Cell Death Dis*, 8(3), e2696.
Jung, J. E., Kim, G. S. & Chan, P. H. (2011) Neuroprotection by interleukin-6 is mediated by signal transducer and activator of transcription 3 and antioxidative signaling in ischemic stroke. *Stroke*, 42(12), 3574-9.
Kahn, O. I. & Baas, P. W. (2016) Microtubules and Growth Cones: Motors Drive the Turn. *Trends Neurosci*, 39(7), 433-440.
Kajitani, N., Hisaoka-Nakashima, K., Morioka, N., Okada-Tsuchioka, M., Kaneko, M., Kasai, M., Shibasaki, C., Nakata, Y. & Takebayashi, M. (2012) Antidepressant acts on astrocytes leading to an increase in the expression of neurotrophic/growth factors: differential regulation of FGF-2 by noradrenaline. *PLoS One*, 7(12), e51197.
Kalliolias, G. D. & Ivashkiv, L. B. (2016) TNF biology, pathogenic mechanisms and emerging therapeutic strategies. *Nat Rev Rheumatol*, 12(1), 49-62.
Kanai, M., Funakoshi, H. & Nakamura, T. (2010) Implication of Tryptophan 2,3-Dioxygenase and its Novel Variants in the Hippocampus and Cerebellum During the Developing and Adult Brain. *International Journal of Tryptophan Research : IJTR*, 3, 141-149.
Kanai, M., Funakoshi, H., Takahashi, H., Hayakawa, T., Mizuno, S., Matsumoto, K. & Nakamura, T. (2009) Tryptophan 2,3-dioxygenase is a key modulator of physiological neurogenesis and anxiety-related behavior in mice. *Mol Brain*, 2, 8.
Kandel (2012) *Principles of Neural Science*, Fifth edition. New York: McGraw-Hill Education / Medical;.
Kandel & Eric (2012) *Principles of Neural Science*, Fifth edition. New York: McGraw-Hill Education / Medical;.
Kang, H. J., Voleti, B., Hajszan, T., Rajkowska, G., Stockmeier, C. A., Licznerski, P., Lepack, A., Majik, M. S., Jeong, L. S., Banasr, M., Son, H. & Duman, R. S. (2012) Decreased expression of synapse-related genes and loss of synapses in major depressive disorder. *Nat Med*, 18(9), 1413-7.
Kanjhan, R., Noakes, P. G. & Bellingham, M. C. (2016) Emerging Roles of Filopodia and Dendritic Spines in Motoneuron Plasticity during Development and Disease. *Neural Plast*, 2016, 3423267.

Kannampalli, P., Pochiraju, S., Bruckert, M., Shaker, R., Banerjee, B. & Sengupta, J. N. (2014) Analgesic effect of minocycline in rat model of inflammation-induced visceral pain. *Eur J Pharmacol*, 727, 87-98.
Kanski, R., van Strien, M. E., van Tijn, P. & Hol, E. M. (2014) A star is born: new insights into the mechanism of astrogenesis. *Cell Mol Life Sci*, 71(3), 433-47.
Kapitein, L. C. & Hoogenraad, C. C. (2011) Which way to go? Cytoskeletal organization and polarized transport in neurons. *Mol Cell Neurosci*, 46(1), 9-20.
Kapitein, L. C. & Hoogenraad, C. C. (2015) Building the Neuronal Microtubule Cytoskeleton. *Neuron*, 87(3), 492-506.
Karakuła-Juchnowicz, H., Flis, M., Szymona, K., Kuczyńska, M., Stelmach, E. & Kowal-Popczak, A. (2014) [New prospects for antipsychotic treatment - the role of the kynurenine pathway]. *Psychiatr Pol*, 48(6), 1167-77.
Karakuła-juchnowicz, H., Flis, M., Szymona, K., Kuczyńska, M., Stelmach, E. & Kowal-popczak, A. (2015) New prospects for antipsychotic treatment – the role of the kynurenine pathway. *Psychiatry Pol.*, 48(6), 1167-1177.
Karperien, A., Ahammer, H. & Jelinek, H. F. (2013) Quantitating the subtleties of microglial morphology with fractal analysis. *Front Cell Neurosci*, 7, 3.
Karra, D. & Dahm, R. (2010) Transfection techniques for neuronal cells. *J Neurosci*, 30(18), 6171-7.
Kasai, H., Fukuda, M., Watanabe, S., Hayashi-Takagi, A. & Noguchi, J. (2010) Structural dynamics of dendritic spines in memory and cognition. *Trends Neurosci*, 33(3), 121-9.
Katsetos, C. D., Herman, M. M. & Mörk, S. J. (2003a) Class III beta-tubulin in human development and cancer. *Cell Motil Cytoskeleton*, 55(2), 77-96.
Katsetos, C. D., Legido, A., Perentes, E. & Mörk, S. J. (2003b) Class III beta-tubulin isotype: a key cytoskeletal protein at the crossroads of developmental neurobiology and tumor neuropathology. *J Child Neurol*, 18(12), 851-66; discussion 867.
Katsuno, M., Sahashi, K., Iguchi, Y. & Hashizume, A.
Katsuno, M., Sahashi, K., Iguchi, Y. & Hashizume, A. (2018) Preclinical progression of neurodegenerative diseases. *Nagoya J Med Sci*, 80(3), 289-298.
Kellogg, D. R., Mitchison, T. J. & Alberts, B. M. (1988) Behaviour of microtubules and actin filaments in living Drosophila embryos. *Development*, 103(4), 675-86.
Kelsch, W., Sim, S. & Lois, C. (2010) Watching synaptogenesis in the adult brain. *Annu Rev Neurosci*, 33, 131-49.
Khurgel, M., Koo, A. C. & Ivy, G. O. (1996) Selective ablation of astrocytes by intracerebral injections of alpha-aminoadipate. *Glia*, 16(4), 351-8.
Kiank, C., Zeden, J. P., Drude, S., Domanska, G., Fusch, G., Otten, W. & Schuett, C. (2010) Psychological stress-induced, IDO1-dependent tryptophan catabolism: implications on immunosuppression in mice and humans. *PLoS One*, 5(7), e11825.
Kierdorf, K. & Prinz, M. (2013) Factors regulating microglia activation. *Front Cell Neurosci*, 7, 44.
Kim, H., Chen, L., Lim, G., Sung, B., Wang, S., McCabe, M. F., Rusanescu, G., Yang, L., Tian, Y. & Mao, J. (2012) Brain indoleamine 2,3-dioxygenase contributes to the comorbidity of pain and depression. *J Clin Invest*, 122(8), 2940-54.
Kim, H. S., Kim, D. C., Kim, H. M., Kwon, H. J., Kwon, S. J., Kang, S. J., Kim, S. C. & Choi, G. E. (2015) STAT1 deficiency redirects IFN signalling toward suppression of TLR response through a feedback activation of STAT3. *Sci Rep*, 5, 13414.
Kim, J., Hong, H., Heo, A. & Park, W. (2013) Indole toxicity involves the inhibition of adenosine triphosphate production and protein folding in Pseudomonas putida. *FEMS Microbiol Lett*, 343(1), 89-99.
Kim, Y. K. & Jeon, S. W. (2018) Neuroinflammation and the Immune-Kynurenine Pathway in Anxiety Disorders. *Curr Neuropharmacol*, 16(5), 574-582.
Kindler, J., Lim, C. K., Weickert, C. S., Boerrigter, D., Galletly, C., Liu, D., Jacobs, K. R., Balzan, R., Bruggemann, J., O'Donnell, M., Lenroot, R., Guillemin, G. J. & Weickert, T. W.

(2019) Dysregulation of kynurenine metabolism is related to proinflammatory cytokines, attention, and prefrontal cortex volume in schizophrenia. *Mol Psychiatry*.
Kirkwood, C. M., Ciuchta, J., Ikonomovic, M. D., Fish, K. N., Abrahamson, E. E., Murray, P. S., Klunk, W. E. & Sweet, R. A. (2013) Dendritic spine density, morphology, and fibrillar actin content surrounding amyloid-β plaques in a mouse model of amyloid-β deposition. *J Neuropathol Exp Neurol*, 72(8), 791-800.
Kitayama, M., Ueno, M., Itakura, T. & Yamashita, T. (2011) Activated microglia inhibit axonal growth through RGMa. *PLoS One*, 6(9), e25234.
Koffie, R. M., Hyman, B. T. & Spires-Jones, T. L. (2011) Alzheimer's disease: synapses gone cold. *Mol Neurodegener*, 6(1), 63.
Koh, W., Park, Y. M., Lee, S. E. & Lee, C. J. (2017) AAV-Mediated Astrocyte-Specific Gene Expression under Human ALDH1L1 Promoter in Mouse Thalamus. *Exp Neurobiol*, 26(6), 350-361.
Kohler, O., Krogh, J., Mors, O. & Benros, M. E. (2016) Inflammation in Depression and the Potential for Anti-Inflammatory Treatment. *Curr Neuropharmacol*, 14(7), 732-42.
Kojima, N. & Shirao, T. (2007) Synaptic dysfunction and disruption of postsynaptic drebrin-actin complex: a study of neurological disorders accompanied by cognitive deficits. *Neurosci Res*, 58(1), 1-5.
Kolb, B., Harker, A. & Gibb, R. (2017) Principles of plasticity in the developing brain. *Dev Med Child Neurol*, 59(12), 1218-1223.
Kong, G. Y., Kristensson, K. & Bentivoglio, M. (2002) Reaction of mouse brain oligodendrocytes and their precursors, astrocytes and microglia, to proinflammatory mediators circulating in the cerebrospinal fluid. *Glia*, 37(3), 191-205.
Kowiański, P., Lietzau, G., Czuba, E., Waśkow, M., Steliga, A. & Moryś, J. (2018) BDNF: A Key Factor with Multipotent Impact on Brain Signaling and Synaptic Plasticity. *Cell Mol Neurobiol*, 38(3), 579-593.
Kozlowski, C. & Weimer, R. M. (2012) An automated method to quantify microglia morphology and application to monitor activation state longitudinally in vivo. *PLoS One*, 7(2), e31814.
Krashia, P., Nobili, A. & D'Amelio, M. (2019) Unifying Hypothesis of Dopamine Neuron Loss in Neurodegenerative Diseases: Focusing on Alzheimer's Disease. *Front Mol Neurosci*, 12, 123.
Krause, D., Suh, H. S., Tarassishin, L., Cui, Q. L., Durafourt, B. A., Choi, N., Bauman, A., Cosenza-Nashat, M., Antel, J. P., Zhao, M. L. & Lee, S. C. (2011) The tryptophan metabolite 3-hydroxyanthranilic acid plays anti-inflammatory and neuroprotective roles during inflammation: role of hemeoxygenase-1. *Am J Pathol*, 179(3), 1360-72.
Krstic, D. & Knuesel, I. (2013) Deciphering the mechanism underlying late-onset Alzheimer disease. *Nat Rev Neurol*, 9(1), 25-34.
Krügel, U., Fischer, J., Radicke, S., Sack, U. & Himmerich, H. (2013) Antidepressant effects of TNF-α blockade in an animal model of depression. *J Psychiatr Res*, 47(5), 611-6.
Kucukdereli, H., Allen, N. J., Lee, A. T., Feng, A., Ozlu, M. I., Conatser, L. M., Chakraborty, C., Workman, G., Weaver, M., Sage, E. H., Barres, B. A. & Eroglu, C. (2011) Control of excitatory CNS synaptogenesis by astrocyte-secreted proteins Hevin and SPARC. *Proc Natl Acad Sci U S A*, 108(32), E440-9.
Kuijpers, M. & Hoogenraad, C. C. (2011) Centrosomes, microtubules and neuronal development. *Mol Cell Neurosci*, 48(4), 349-58.
Kulkarni, V. A. & Firestein, B. L. (2012) The dendritic tree and brain disorders. *Mol Cell Neurosci*, 50(1), 10-20.
Kumar, A., Chen, S. H., Kadiiska, M. B., Hong, J. S., Zielonka, J., Kalyanaraman, B. & Mason, R. P. (2014) Inducible nitric oxide synthase is key to peroxynitrite-mediated, LPS-induced protein radical formation in murine microglial BV2 cells. *Free Radic Biol Med*, 73, 51-9.

Kumar, M., Verma, S. & Nerurkar, V. R. (2010) Pro-inflammatory cytokines derived from West Nile virus (WNV)-infected SK-N-SH cells mediate neuroinflammatory markers and neuronal death. *J Neuroinflammation*, 7, 73.
Kwon, H. B. & Sabatini, B. L. (2011) Glutamate induces de novo growth of functional spines in developing cortex. *Nature*, 474(7349), 100-4.
Lachenal, G., Pernet-Gallay, K., Chivet, M., Hemming, F. J., Belly, A., Bodon, G., Blot, B., Haase, G., Goldberg, Y. & Sadoul, R. (2011) Release of exosomes from differentiated neurons and its regulation by synaptic glutamatergic activity. *Mol Cell Neurosci*, 46(2), 409-18.
Lam, D., Enright, H. A., Cadena, J., Peters, S. K. G., Sales, A. P., Osburn, J. J., Soscia, D. A., Kulp, K. S., Wheeler, E. K. & Fischer, N. O. (2019) Tissue-specific extracellular matrix accelerates the formation of neural networks and communities in a neuron-glia co-culture on a multi-electrode array. *Sci Rep*, 9(1), 4159.
Lamkanfi, M. & Dixit, V. M. (2012) Inflammasomes and their roles in health and disease. *Annu Rev Cell Dev Biol*, 28, 137-61.
Larkin, J., Ahmed, C. M., Wilson, T. D. & Johnson, H. M. (2013) Regulation of interferon gamma signaling by suppressors of cytokine signaling and regulatory T cells. *Front Immunol*, 4, 469.
Lasič, E., Galland, F., Vardjan, N., Šribar, J., Križaj, I., Leite, M. C., Zorec, R. & Stenovec, M. (2016) Time-dependent uptake and trafficking of vesicles capturing extracellular S100B in cultured rat astrocytes. *J Neurochem*, 139(2), 309-323.
Lasser, M., Tiber, J. & Lowery, L. A. (2018) The Role of the Microtubule Cytoskeleton in Neurodevelopmental Disorders. *Front Cell Neurosci*, 12, 165.
Lawn, S., Krishna, N., Pisklakova, A., Qu, X., Fenstermacher, D. A., Fournier, M., Vrionis, F. D., Tran, N., Chan, J. A., Kenchappa, R. S. & Forsyth, P. A. (2015) Neurotrophin signaling via TrkB and TrkC receptors promotes the growth of brain tumor-initiating cells. *J Biol Chem*, 290(6), 3814-24.
Lawson, M. A., Parrott, J. M., McCusker, R. H., Dantzer, R., Kelley, K. W. & O'Connor, J. C. (2013) Intracerebroventricular administration of lipopolysaccharide induces indoleamine-2,3-dioxygenase-dependent depression-like behaviors. *J Neuroinflammation*, 10, 87.
Leduc, C. & Etienne-Manneville, S. (2017) Intermediate filaments join the action. *Cell Cycle*, 16(15), 1389-1390.
Lee, E. & Chung, W. S. (2019) Glial Control of Synapse Number in Healthy and Diseased Brain. *Front Cell Neurosci*, 13, 42.
Lee, H. U., Yamazaki, Y., Tanaka, K. F., Furuya, K., Sokabe, M., Hida, H., Takao, K., Miyakawa, T., Fujii, S. & Ikenaka, K. (2013a) Increased astrocytic ATP release results in enhanced excitability of the hippocampus. *Glia*, 61(2), 210-24.
Lee, M. K., Rebhun, L. I. & Frankfurter, A. (1990a) Posttranslational modification of class III beta-tubulin. *Proc Natl Acad Sci U S A*, 87(18), 7195-9.
Lee, M. K., Tuttle, J. B., Rebhun, L. I., Cleveland, D. W. & Frankfurter, A. (1990b) The expression and posttranslational modification of a neuron-specific beta-tubulin isotype during chick embryogenesis. *Cell Motil Cytoskeleton*, 17(2), 118-32.
Lee, Y., Son, H., Kim, G., Kim, S., Lee, D. H., Roh, G. S., Kang, S. S., Cho, G. J., Choi, W. S. & Kim, H. J. (2013b) Glutamine deficiency in the prefrontal cortex increases depressive-like behaviours in male mice. *J Psychiatry Neurosci*, 38(3), 183-91.
Lehnardt, S. (2010) Innate immunity and neuroinflammation in the CNS: the role of microglia in Toll-like receptor-mediated neuronal injury. *Glia*, 58(3), 253-63.
Leibinger, M., Müller, A., Gobrecht, P., Diekmann, H., Andreadaki, A. & Fischer, D. (2013) Interleukin-6 contributes to CNS axon regeneration upon inflammatory stimulation. *Cell Death Dis*, 4, e609.
Lenz, K. M. & Nelson, L. H. (2018) Microglia and Beyond: Innate Immune Cells As Regulators of Brain Development and Behavioral Function. *Front Immunol*, 9, 698.

Lestanova, Z., Bacova, Z. & Bakos, J. (2016) Mechanisms involved in the regulation of neuropeptide-mediated neurite outgrowth: a minireview. *Endocr Regul*, 50(2), 72-82.
Levi-Montalcini, R. (1987) The nerve growth factor 35 years later. *Science*, 237(4819), 1154-62.
Lewis, D. A. & Lieberman, J. A. (2000) Catching up on schizophrenia: natural history and neurobiology. *Neuron*, 28(2), 325-34.
Lewitus, G. M., Pribiag, H., Duseja, R., St-Hilaire, M. & Stellwagen, D. (2014) An adaptive role of TNFα in the regulation of striatal synapses. *J Neurosci*, 34(18), 6146-55.
Li, B., Yamamori, H., Tatebayashi, Y., Shafit-Zagardo, B., Tanimukai, H., Chen, S., Iqbal, K. & Grundke-Iqbal, I. (2008a) Failure of neuronal maturation in Alzheimer disease dentate gyrus. *J Neuropathol Exp Neurol*, 67(1), 78-84.
Li, J., Yin, Q. & Wu, H. (2013) Structural basis of signal transduction in the TNF receptor superfamily. *Adv Immunol*, 119, 135-53.
Li, L., Zhang, H., Varrin-Doyer, M., Zamvil, S. S. & Verkman, A. S. (2011) Proinflammatory role of aquaporin-4 in autoimmune neuroinflammation. *FASEB J*, 25(5), 1556-66.
Li, X., Penes, M., Odermatt, B., Willecke, K. & Nagy, J. I. (2008b) Ablation of Cx47 in transgenic mice leads to the loss of MUPP1, ZONAB and multiple connexins at oligodendrocyte-astrocyte gap junctions. *Eur J Neurosci*, 28(8), 1503-17.
Lian, H., Yang, L., Cole, A., Sun, L., Chiang, A. C., Fowler, S. W., Shim, D. J., Rodriguez-Rivera, J., Taglialatela, G., Jankowsky, J. L., Lu, H. C. & Zheng, H. (2015) NFκB-activated astroglial release of complement C3 compromises neuronal morphology and function associated with Alzheimer's disease. *Neuron*, 85(1), 101-115.
Liang, F., Luo, C., Xu, G., Su, F., He, X., Long, S., Ren, H., Liu, Y., Feng, Y. & Pei, Z. (2015) Deletion of aquaporin-4 is neuroprotective during the acute stage of micro traumatic brain injury in mice. *Neurosci Lett*, 598, 29-35.
Liddelow, S. A. & Barres, B. A. (2017) Reactive Astrocytes: Production, Function, and Therapeutic Potential. *Immunity*, 46(6), 957-967.
Liddelow, S. A., Guttenplan, K. A., Clarke, L. E., Bennett, F. C., Bohlen, C. J., Schirmer, L., Bennett, M. L., Münch, A. E., Chung, W. S., Peterson, T. C., Wilton, D. K., Frouin, A., Napier, B. A., Panicker, N., Kumar, M., Buckwalter, M. S., Rowitch, D. H., Dawson, V. L., Dawson, T. M., Stevens, B. & Barres, B. A. (2017) Neurotoxic reactive astrocytes are induced by activated microglia. *Nature*, 541(7638), 481-487.
Lieberman, J. A., Girgis, R. R., Brucato, G., Moore, H., Provenzano, F., Kegeles, L., Javitt, D., Kantrowitz, J., Wall, M. M., Corcoran, C. M., Schobel, S. A. & Small, S. A. (2018) Hippocampal dysfunction in the pathophysiology of schizophrenia: a selective review and hypothesis for early detection and intervention. *Mol Psychiatry*, 23(8), 1764-1772.
Lim, C. K., Brew, B. J., Sundaram, G. & Guillemin, G. J. (2010) Understanding the roles of the kynurenine pathway in multiple sclerosis progression. *Int J Tryptophan Res*, 3, 157-67.
Lim, C. K., Yap, M. M., Kent, S. J., Gras, G., Samah, B., Batten, J. C., De Rose, R., Heng, B., Brew, B. J. & Guillemin, G. J. (2013) Characterization of the kynurenine pathway and quinolinic Acid production in macaque macrophages. *Int J Tryptophan Res*, 6, 7-19.
Lima, A., Sardinha, V. M., Oliveira, A. F., Reis, M., Mota, C., Silva, M. A., Marques, F., Cerqueira, J. J., Pinto, L., Sousa, N. & Oliveira, J. F. (2014) Astrocyte pathology in the prefrontal cortex impairs the cognitive function of rats. *Mol Psychiatry*, 19(7), 834-41.
Lipton, S. A. (2004) Failures and successes of NMDA receptor antagonists: molecular basis for the use of open-channel blockers like memantine in the treatment of acute and chronic neurologic insults. *NeuroRx*, 1(1), 101-10.
Liu, T., Zhang, L., Joo, D. & Sun, S. C. (2017a) NF-κB signaling in inflammation. *Signal Transduct Target Ther*, 2.
Liu, W., Ge, T., Leng, Y., Pan, Z., Fan, J., Yang, W. & Cui, R. (2017b) The Role of Neural Plasticity in Depression: From Hippocampus to Prefrontal Cortex. *Neural Plast*, 2017, 6871089.

Liu, Y., Ho, R. C. & Mak, A. (2012) Interleukin (IL)-6, tumour necrosis factor alpha (TNF-α) and soluble interleukin-2 receptors (sIL-2R) are elevated in patients with major depressive disorder: a meta-analysis and meta-regression. *J Affect Disord*, 139(3), 230-9.
Liu, Y., Yan, Y., Inagaki, Y., Logan, S., Bosnjak, Z. J. & Bai, X. (2017c) Insufficient Astrocyte-Derived Brain-Derived Neurotrophic Factor Contributes to Propofol-Induced Neuron Death Through Akt/Glycogen Synthase Kinase 3β/Mitochondrial Fission Pathway. *Anesth Analg*, 125(1), 241-254.
Liu, Y. N., Peng, Y. L., Liu, L., Wu, T. Y., Zhang, Y., Lian, Y. J., Yang, Y. Y., Kelley, K. W., Jiang, C. L. & Wang, Y. X. (2015) TNFalpha mediates stress-induced depression by upregulating indoleamine 2,3-dioxygenase in a mouse model of unpredictable chronic mild stress. *Eur Cytokine Netw*, 26(1), 15-25.
Liu, Z., Li, Y., Cui, Y., Roberts, C., Lu, M., Wilhelmsson, U., Pekny, M. & Chopp, M. (2014) Beneficial effects of gfap/vimentin reactive astrocytes for axonal remodeling and motor behavioral recovery in mice after stroke. *Glia*, 62(12), 2022-33.
Lively, S. & Schlichter, L. C. Microglia Responses to Pro-inflammatory Stimuli (LPS, IFNγ+TNFα) and Reprogramming by Resolving Cytokines (IL-4, IL-10).
Lively, S. & Schlichter, L. C. (2018) Microglia Responses to Pro-inflammatory Stimuli (LPS, IFNγ+TNFα) and Reprogramming by Resolving Cytokines (IL-4, IL-10). *Front Cell Neurosci*, 12, 215.
Lladó, J., Tolosa, L. & Olmos, G. (2013) Cellular and molecular mechanisms involved in the neuroprotective effects of VEGF on motoneurons. *Front Cell Neurosci*, 7, 181.
Loane, D. J. & Byrnes, K. R. (2010a) Role of microglia in neurotrauma. *Neurotherapeutics*, 7(4), 366-77.
Loane, D. J. & Byrnes, K. R. (2010b) Role of Microglia in Neurotrauma. *Neurotherapeutics : the journal of the American Society for Experimental NeuroTherapeutics*, 7(4), 366-377.
Lopez-Castejon, G. & Brough, D. (2011) Understanding the mechanism of IL-1beta secretion. *Cytokine Growth Factor Rev*, 22(4), 189-95.
Lovelace, M. D., Varney, B., Sundaram, G., Franco, N. F., Ng, M. L., Pai, S., Lim, C. K., Guillemin, G. J. & Brew, B. J. (2016) Current Evidence for a Role of the Kynurenine Pathway of Tryptophan Metabolism in Multiple Sclerosis. *Front Immunol*, 7, 246.
Lowery, L. A. & Van Vactor, D. (2009) The trip of the tip: understanding the growth cone machinery. *Nat Rev Mol Cell Biol*, 10(5), 332-43.
Lu, X., Al-Aref, R., Zhao, D., Shen, J., Yan, Y. & Gao, Y. (2015) Astrocyte-conditioned medium attenuates glutamate-induced apoptotic cell death in primary cultured spinal cord neurons of rats. *Neurol Res*, 37(9), 803-8.
Ludueña, R. F. (1998) Multiple forms of tubulin: different gene products and covalent modifications. *Int Rev Cytol*, 178, 207-75.
Lugo-Huitron, R., Blanco-Ayala T Fau - Ugalde-Muniz, P., Ugalde-Muniz P Fau - Carrillo-Mora, P., Carrillo-Mora P Fau - Pedraza-Chaverri, J., Pedraza-Chaverri J Fau - Silva-Adaya, D., Silva-Adaya D Fau - Maldonado, P. D., Maldonado Pd Fau - Torres, I., Torres I Fau - Pinzon, E., Pinzon E Fau - Ortiz-Islas, E., Ortiz-Islas E Fau - Lopez, T., Lopez T Fau - Garcia, E., Garcia E Fau - Pineda, B., Pineda B Fau - Torres-Ramos, M., Torres-Ramos M Fau - Santamaria, A., Santamaria A Fau - La Cruz, V. P.-D. & La Cruz, V. P. (2011) On the antioxidant properties of kynurenic acid: free radical scavenging activity and inhibition of oxidative stress. *Neurotoxicology and Tetratology*, 33(5), 538-547.
Lugo-Huitron, R., Ugalde Muniz, P., Pineda, B., Pedraza-Chaverri, J., Rios, C. & Perez-de la Cruz, V. (2013) Quinolinic acid: an endogenous neurotoxin with multiple targets. *Oxid Med Cell Longev*, 2013, 104024.
Lugo-Huitrón, R., Blanco-Ayala, T., Ugalde-Muñiz, P., Carrillo-Mora, P., Pedraza-Chaverrí, J., Silva-Adaya, D., Maldonado, P. D., Torres, I., Pinzón, E., Ortiz-Islas, E., López, T., García, E., Pineda, B., Torres-Ramos, M., Santamaría, A. & La Cruz, V. P. (2011) On the antioxidant properties of kynurenic acid: free radical scavenging activity and inhibition of oxidative stress. *Neurotoxicol Teratol*, 33(5), 538-47.

Lugo-Huitrón, R., Ugalde Muñiz, P., Pineda, B., Pedraza-Chaverrí, J., Ríos, C. & Pérez-de la Cruz, V. (2013) Quinolinic acid: an endogenous neurotoxin with multiple targets. *Oxid Med Cell Longev*, 2013, 104024.
Lui, N. P., Chen, L. W., Yung, W. H., Chan, Y. S. & Yung, K. K. (2012) Endogenous repair by the activation of cell survival signalling cascades during the early stages of rat Parkinsonism. *PLoS One*, 7(12), e51294.
Lukens, J. R., Gross, J. M. & Kanneganti, T. D. (2012) IL-1 family cytokines trigger sterile inflammatory disease. *Front Immunol*, 3, 315.
Lundgaard, I., Osório, M. J., Kress, B. T., Sanggaard, S. & Nedergaard, M. (2014) White matter astrocytes in health and disease. *Neuroscience*, 276, 161-73.
Luo, L. (2002) Actin cytoskeleton regulation in neuronal morphogenesis and structural plasticity. *Annu Rev Cell Dev Biol*, 18, 601-35.
Luo, X. G. & Chen, S. D. (2012) The changing phenotype of microglia from homeostasis to disease. *Transl Neurodegener*, 1(1), 9.
Lutton, E. M., Razmpour, R., Andrews, A. M., Cannella, L. A., Son, Y. J., Shuvaev, V. V., Muzykantov, V. R. & Ramirez, S. H. (2017) Acute administration of catalase targeted to ICAM-1 attenuates neuropathology in experimental traumatic brain injury. *Sci Rep*, 7(1), 3846.
Lynch, A. M., Murphy, K. J., Deighan, B. F., O'Reilly, J.-A., Gun'ko, Y. K., Cowley, T. R., Gonzalez-Reyes, R. E. & Lynch, M. A. (2010) The Impact of Glial Activation in the Aging Brain. *Aging and Disease*, 1(3), 262-278.
López-Doménech, G., Higgs, N. F., Vaccaro, V., Roš, H., Arancibia-Cárcamo, I. L., MacAskill, A. F. & Kittler, J. T. (2016) Loss of Dendritic Complexity Precedes Neurodegeneration in a Mouse Model with Disrupted Mitochondrial Distribution in Mature Dendrites. *Cell Rep*, 17(2), 317-327.
MacQueen, G. & Frodl, T. (2011) The hippocampus in major depression: evidence for the convergence of the bench and bedside in psychiatric research? *Mol Psychiatry*, 16(3), 252-64.
Maddison, D. C. & Giorgini, F. (2015) The kynurenine pathway and neurodegenerative disease. *Semin Cell Dev Biol*, 40, 134-141.
Maes, M. (2011) Depression is an inflammatory disease, but cell-mediated immune activation is the key component of depression. *Prog Neuropsychopharmacol Biol Psychiatry*, 35(3), 664-75.
Maes, M., Leonard, B. E., Myint, A. M., Kubera, M. & Verkerk, R. (2011) The new '5-HT' hypothesis of depression: cell-mediated immune activation induces indoleamine 2,3-dioxygenase, which leads to lower plasma tryptophan and an increased synthesis of detrimental tryptophan catabolites (TRYCATs), both of which contribute to the onset of depression. *Prog Neuropsychopharmacol Biol Psychiatry*, 35(3), 702-21.
Magistretti, P. J. & Allaman, I. (2018) Lactate in the brain: from metabolic end-product to signalling molecule. *Nat Rev Neurosci*, 19(4), 235-249.
Mahmoud, S., Gharagozloo, M., Simard, C. & Gris, D. (2019) Astrocytes Maintain Glutamate Homeostasis in the CNS by Controlling the Balance between Glutamate Uptake and Release. *Cells*, 8(2).
Majláth, Z., Török, N., Toldi, J. & Vécsei, L. (2016) Memantine and Kynurenic Acid: Current Neuropharmacological Aspects. *Curr Neuropharmacol*, 14(2), 200-9.
Majoros, A., Platanitis, E., Kernbauer-Hölzl, E., Rosebrock, F., Müller, M. & Decker, T. (2017) Canonical and Non-Canonical Aspects of JAK-STAT Signaling: Lessons from Interferons for Cytokine Responses. *Front Immunol*, 8, 29.
Malhi, G. S. & Mann, J. J. (2018) Depression. *Lancet*, 392(10161), 2299-2312.
Mangano, E. N., Litteljohn, D., So, R., Nelson, E., Peters, S., Bethune, C., Bobyn, J. & Hayley, S. (2012) Interferon-γ plays a role in paraquat-induced neurodegeneration involving oxidative and proinflammatory pathways. *Neurobiol Aging*, 33(7), 1411-26.

Martin, J. L., Magistretti, P. J. & Allaman, I. (2013) Regulation of neurotrophic factors and energy metabolism by antidepressants in astrocytes. *Curr Drug Targets*, 14(11), 1308-21.
Martínez-Gras, I., García-Sánchez, F., Guaza, C., Rodríguez-Jiménez, R., Andrés-Esteban, E., Palomo, T., Rubio, G. & Borrell, J. (2012) Altered immune function in unaffected first-degree biological relatives of schizophrenia patients. *Psychiatry Res*, 200(2-3), 1022-5.
Maruoka, H., Sasaya, H., Sugihara, K., Shimoke, K. & Ikeuchi, T. (2011) Low-molecular-weight compounds having neurotrophic activity in cultured PC12 cells and neurons. *J Biochem*, 150(5), 473-5.
Marwick, K. F. M. & Hardingham, G. E. (2017) Transfection in Primary Cultured Neuronal Cells. *Methods Mol Biol*, 1677, 137-144.
Maslanik, T., Mahaffey, L., Tannura, K., Beninson, L., Greenwood, B. N. & Fleshner, M. (2013) The inflammasome and danger associated molecular patterns (DAMPs) are implicated in cytokine and chemokine responses following stressor exposure. *Brain Behav Immun*, 28, 54-62.
Matias, I., Morgado, J. & Gomes, F. C. A. (2019) Astrocyte Heterogeneity: Impact to Brain Aging and Disease. *Front Aging Neurosci*, 11, 59.
Mattson, M. P. (2008) Glutamate and neurotrophic factors in neuronal plasticity and disease. *Ann N Y Acad Sci*, 1144, 97-112.
Matus, A., Ackermann, M., Pehling, G., Byers, H. R. & Fujiwara, K. (1982) High actin concentrations in brain dendritic spines and postsynaptic densities. *Proc Natl Acad Sci U S A*, 79(23), 7590-4.
Mayegowda, S. B. & Thomas, C. (2019) Glial pathology in neuropsychiatric disorders: a brief review. *J Basic Clin Physiol Pharmacol*, 30(4).
McAllister, A. K., Lo, D. C. & Katz, L. C. (1995) Neurotrophins regulate dendritic growth in developing visual cortex. *Neuron*, 15(4), 791-803.
McBean, G. J. (1994) Inhibition of the glutamate transporter and glial enzymes in rat striatum by the gliotoxin, alpha aminoadipate. *Br J Pharmacol*, 113(2), 536-40.
McDougall, S., Vargas Riad, W., Silva-Gotay, A., Tavares, E. R., Harpalani, D., Li, G. L. & Richardson, H. N. (2018) Myelination of Axons Corresponds with Faster Transmission Speed in the Prefrontal Cortex of Developing Male Rats. *eNeuro*, 5(4).
McNamee, E. N., Griffin, E. W., Ryan, K. M., Ryan, K. J., Heffernan, S., Harkin, A. & Connor, T. J. (2010a) Noradrenaline acting at beta-adrenoceptors induces expression of IL-1beta and its negative regulators IL-1ra and IL-1RII, and drives an overall anti-inflammatory phenotype in rat cortex. *Neuropharmacology*, 59(1-2), 37-48.
McNamee, E. N., Ryan, K. M., Kilroy, D. & Connor, T. J. (2010b) Noradrenaline induces IL-1ra and IL-1 type II receptor expression in primary glial cells and protects against IL-1beta-induced neurotoxicity. *Eur J Pharmacol*, 626(2-3), 219-28.
Medler, J. & Wajant, H. (2019) Tumor necrosis factor receptor-2 (TNFR2): an overview of an emerging drug target. *Expert Opin Ther Targets*, 23(4), 295-307.
Meissl, K., Macho-Maschler, S., Müller, M. & Strobl, B. (2017) The good and the bad faces of STAT1 in solid tumours. *Cytokine*, 89, 12-20.
Memberg, S. P. & Hall, A. K. (1995) Dividing neuron precursors express neuron-specific tubulin. *J Neurobiol*, 27(1), 26-43.
Menon, S. & Gupton, S. L. (2016) Building Blocks of Functioning Brain: Cytoskeletal Dynamics in Neuronal Development. *Int Rev Cell Mol Biol*, 322, 183-245.
Menéndez-González, M. (2014) Biomarkers in neurodegenerative disorders: translating research into clinical practice. *Front Aging Neurosci*, 6, 281.
Metzemaekers, M., Vanheule, V., Janssens, R., Struyf, S. & Proost, P. (2017) Overview of the Mechanisms that May Contribute to the Non-Redundant Activities of Interferon-Inducible CXC Chemokine Receptor 3 Ligands. *Front Immunol*, 8, 1970.
Micheva, K. D., Busse, B., Weiler, N. C., O'Rourke, N. & Smith, S. J. (2010) Single-synapse analysis of a diverse synapse population: proteomic imaging methods and markers. *Neuron*, 68(4), 639-53.

Miller, A. H. & Raison, C. L. (2016) The role of inflammation in depression: from evolutionary imperative to modern treatment target. *Nat Rev Immunol*, 16(1), 22-34.
Miller, B. R. & Hen, R. (2015) The current state of the neurogenic theory of depression and anxiety. *Curr Opin Neurobiol*, 30, 51-8.
Milnerwood, A. J., Gladding, C. M., Pouladi, M. A., Kaufman, A. M., Hines, R. M., Boyd, J. D., Ko, R. W., Vasuta, O. C., Graham, R. K., Hayden, M. R., Murphy, T. H. & Raymond, L. A. (2010) Early increase in extrasynaptic NMDA receptor signaling and expression contributes to phenotype onset in Huntington's disease mice. *Neuron*, 65(2), 178-90.
Minett, T., Classey, J., Matthews, F. E., Fahrenhold, M., Taga, M., Brayne, C., Ince, P. G., Nicoll, J. A., Boche, D. & CFAS, M. (2016) Microglial immunophenotype in dementia with Alzheimer's pathology. *J Neuroinflammation*, 13(1), 135.
Minogue, A. M., Barrett, J. P. & Lynch, M. A. (2012) LPS-induced release of IL-6 from glia modulates production of IL-1beta in a JAK2-dependent manner. *J Neuroinflammation*, 9, 126.
Miyamoto, N., Maki, T., Shindo, A., Liang, A. C., Maeda, M., Egawa, N., Itoh, K., Lo, E. K., Lok, J., Ihara, M. & Arai, K. (2015) Astrocytes Promote Oligodendrogenesis after White Matter Damage via Brain-Derived Neurotrophic Factor. *J Neurosci*, 35(41), 14002-8.
Miyamoto, Y., Kuroda, M., Munekata, E. & Masaki, T. (1986) Stoichiometry of actin and phalloidin binding: one molecule of the toxin dominates two actin subunits. *J Biochem*, 100(6), 1677-80.
Moeton, M., Stassen, O. M., Sluijs, J. A., van der Meer, V. W., Kluivers, L. J., van Hoorn, H., Schmidt, T., Reits, E. A., van Strien, M. E. & Hol, E. M. (2016) GFAP isoforms control intermediate filament network dynamics, cell morphology, and focal adhesions. *Cell Mol Life Sci*, 73(21), 4101-20.
Moieni, M., Irwin, M. R., Jevtic, I., Olmstead, R., Breen, E. C. & Eisenberger, N. I. (2015) Sex differences in depressive and socioemotional responses to an inflammatory challenge: implications for sex differences in depression. *Neuropsychopharmacology*, 40(7), 1709-16.
Molofsky, A. V., Glasgow, S. M., Chaboub, L. S., Tsai, H. H., Murnen, A. T., Kelley, K. W., Fancy, S. P., Yuen, T. J., Madireddy, L., Baranzini, S., Deneen, B., Rowitch, D. H. & Oldham, M. C. (2013) Expression profiling of Aldh1l1-precursors in the developing spinal cord reveals glial lineage-specific genes and direct Sox9-Nfe2l1 interactions. *Glia*, 61(9), 1518-32.
Molofsky, A. V., Krencik, R., Krenick, R., Ullian, E. M., Ullian, E., Tsai, H. H., Deneen, B., Richardson, W. D., Barres, B. A. & Rowitch, D. H. (2012) Astrocytes and disease: a neurodevelopmental perspective. *Genes Dev*, 26(9), 891-907.
Monaco, C., Nanchahal, J., Taylor, P. & Feldmann, M. (2015) Anti-TNF therapy: past, present and future. *Int Immunol*, 27(1), 55-62.
Montermini, D., Winlove, C. P. & Michel, C. (2002) Effects of perfusion rate on permeability of frog and rat mesenteric microvessels to sodium fluorescein. *J Physiol*, 543(Pt 3), 959-75.
Montgomery, S. L. & Bowers, W. J. (2012) Tumor necrosis factor-alpha and the roles it plays in homeostatic and degenerative processes within the central nervous system. *J Neuroimmune Pharmacol*, 7(1), 42-59.
Morel, L., Chiang, M. S. R., Higashimori, H., Shoneye, T., Iyer, L. K., Yelick, J., Tai, A. & Yang, Y. (2017) Molecular and Functional Properties of Regional Astrocytes in the Adult Brain. *J Neurosci*, 37(36), 8706-8717.
Mori, T., Koyama, N., Arendash, G. W., Horikoshi-Sakuraba, Y., Tan, J. & Town, T. (2010) Overexpression of human S100B exacerbates cerebral amyloidosis and gliosis in the Tg2576 mouse model of Alzheimer's disease. *Glia*, 58(3), 300-14.
Morita, M., Ikeshima-Kataoka, H., Kreft, M., Vardjan, N., Zorec, R. & Noda, M. (2019) Metabolic Plasticity of Astrocytes and Aging of the Brain. *Int J Mol Sci*, 20(4).

Moroni, F., Cozzi, A., Sili, M. & Mannaioni, G. (2012) Kynurenic acid: a metabolite with multiple actions and multiple targets in brain and periphery. *J Neural Transm (Vienna)*, 119(2), 133-9.
Morrison, H. W. & Filosa, J. A. (2013) A quantitative spatiotemporal analysis of microglia morphology during ischemic stroke and reperfusion. *J Neuroinflammation*, 10, 4.
Mowla, S. J., Farhadi, H. F., Pareek, S., Atwal, J. K., Morris, S. J., Seidah, N. G. & Murphy, R. A. (2001) Biosynthesis and post-translational processing of the precursor to brain-derived neurotrophic factor. *J Biol Chem*, 276(16), 12660-6.
Moynagh, P. N. (2005) The interleukin-1 signalling pathway in astrocytes: a key contributor to inflammation in the brain. *J Anat*, 207(3), 265-9.
Muller, N. (2013) The role of anti-inflammatory treatment in psychiatric disorders. *Psychiatr Danub*, 25(3), 292-8.
Munkholm, K., Weikop, P., Kessing, L. V. & Vinberg, M. (2015) Elevated levels of IL-6 and IL-18 in manic and hypomanic states in rapid cycling bipolar disorder patients. *Brain Behav Immun*, 43, 205-13.
Myers, J. P., Santiago-Medina, M. & Gomez, T. M. (2011) Regulation of axonal outgrowth and pathfinding by integrin-ECM interactions. *Dev Neurobiol*, 71(11), 901-23.
Myint, A. M. & Kim, Y. K. (2014) Network beyond IDO in psychiatric disorders: revisiting neurodegeneration hypothesis. *Prog Neuropsychopharmacol Biol Psychiatry*, 48, 304-13.
Mándi, Y. & Vécsei, L. (2012) The kynurenine system and immunoregulation. *J Neural Transm (Vienna)*, 119(2), 197-209.
Möller, T. (2010) Neuroinflammation in Huntington's disease. *J Neural Transm (Vienna)*, 117(8), 1001-8.
Müller, N. (2019) COX-2 Inhibitors, Aspirin, and Other Potential Anti-Inflammatory Treatments for Psychiatric Disorders. *Front Psychiatry*, 10, 375.
Nagelhus, E. A. & Ottersen, O. P. (2013) Physiological roles of aquaporin-4 in brain. *Physiol Rev*, 93(4), 1543-62.
Nagy, C., Suderman, M., Yang, J., Szyf, M., Mechawar, N., Ernst, C. & Turecki, G. (2015) Astrocytic abnormalities and global DNA methylation patterns in depression and suicide. *Mol Psychiatry*, 20(3), 320-8.
Nakagami, Y., Saito, H. & Katsuki, H. (1996) 3-Hydroxykynurenine toxicity on the rat striatum in vivo. *Jpn J Pharmacol*, 71(2), 183-6.
Namba, T., Funahashi, Y., Nakamuta, S., Xu, C., Takano, T. & Kaibuchi, K. (2015) Extracellular and Intracellular Signaling for Neuronal Polarity. *Physiol Rev*, 95(3), 995-1024.
Nateghi Rostami, M., Douraghi, M., Miramin Mohammadi, A. & Nikmanesh, B. (2012) Altered serum pro-inflammatory cytokines in children with Down's syndrome. *Eur Cytokine Netw*, 23(2), 64-7.
Newman, L. A., Korol, D. L. & Gold, P. E. (2011) Lactate produced by glycogenolysis in astrocytes regulates memory processing. *PLoS One*, 6(12), e28427.
Nguyen, N. T., Kimura, A., Nakahama, T., Chinen, I., Masuda, K., Nohara, K., Fujii-Kuriyama, Y. & Kishimoto, T. (2010) Aryl hydrocarbon receptor negatively regulates dendritic cell immunogenicity via a kynurenine-dependent mechanism. *Proc Natl Acad Sci U S A*, 107(46), 19961-6.
Nikolic, L., Shen, W., Nobili, P., Virenque, A., Ulmann, L. & Audinat, E. (2018) Blocking TNFalpha-driven astrocyte purinergic signaling restores normal synaptic activity during epileptogenesis. *Glia*, 66(12), 2673-2683.
Nishimura, R. N., Santos, D., Fu, S. T. & Dwyer, B. E. (2000) Induction of cell death by L-alpha-aminoadipic acid exposure in cultured rat astrocytes: relationship to protein synthesis. *Neurotoxicology*, 21(3), 313-20.
Noda, M., Takii, K., Parajuli, B., Kawanokuchi, J., Sonobe, Y., Takeuchi, H., Mizuno, T. & Suzumura, A. (2014) FGF-2 released from degenerating neurons exerts microglial-induced neuroprotection via FGFR3-ERK signaling pathway. *J Neuroinflammation*, 11, 76.

Norden, D. M., Muccigrosso, M. M. & Godbout, J. P. (2015) Microglial priming and enhanced reactivity to secondary insult in aging, and traumatic CNS injury, and neurodegenerative disease. *Neuropharmacology*, 96(Pt A), 29-41.
Norden, D. M., Trojanowski, P. J., Villanueva, E., Navarro, E. & Godbout, J. P. (2016) Sequential activation of microglia and astrocyte cytokine expression precedes increased Iba-1 or GFAP immunoreactivity following systemic immune challenge. *Glia*, 64(2), 300-16.
Nowacka, M. M. & Obuchowicz, E. (2012) Vascular endothelial growth factor (VEGF) and its role in the central nervous system: a new element in the neurotrophic hypothesis of antidepressant drug action. *Neuropeptides*, 46(1), 1-10.
Nwabuisi-Heath, E., LaDu, M. J. & Yu, C. (2012) Simultaneous analysis of dendritic spine density, morphology and excitatory glutamate receptors during neuron maturation in vitro by quantitative immunocytochemistry. *J Neurosci Methods*, 207(2), 137-47.
O'Brien, S. M., Fitzgerald, P., Scully, P., Landers, A., Scott, L. V. & Dinan, T. G. (2007) Impact of gender and menstrual cycle phase on plasma cytokine concentrations. *Neuroimmunomodulation*, 14(2), 84-90.
O'Connor, J. C., Lawson, M. A., Andre, C., Moreau, M., Lestage, J., Castanon, N., Kelley, K. W. & Dantzer, R. (2009) Lipopolysaccharide-induced depressive-like behavior is mediated by indoleamine 2,3-dioxygenase activation in mice. *Mol Psychiatry*, 14(5), 511-22.
O'Donovan, S. M., Sullivan, C. R. & McCullumsmith, R. E. (2017) The role of glutamate transporters in the pathophysiology of neuropsychiatric disorders. *NPJ Schizophr*, 3(1), 32.
O'Farrell, K. (2016a) *The impact of pharmacological modulation of the kynurenine pathway*
on neuronal integrity in vitro. PhD Trinity College Dublin.
O'Farrell, K. (2016b) *The impact of pharmacological modulation of the kynurenine pathway on neuronal integrity in vitro*. Doctor of Philosophy Trinity College Dublin, University of Dublin.
O'Farrell, K., Fagan, E., Connor, T. J. & Harkin, A. (2017) Inhibition of the kynurenine pathway protects against reactive microglial-associated reductions in the complexity of primary cortical neurons. *Eur J Pharmacol*, 810, 163-173.
O'Farrell, K. & Harkin, A. (2015) Stress-related regulation of the kynurenine pathway: Relevance to neuropsychiatric and degenerative disorders. *Neuropharmacology*.
O'Farrell, K. & Harkin, A. (2017) Stress-related regulation of the kynurenine pathway: Relevance to neuropsychiatric and degenerative disorders. *Neuropharmacology*, 112, 307-323.
O'Neill, E. (2015) Protective effects of noradrenergic and neurotrophic signalling on neuronal complexity in vitro. Trinity College Dublin.
O'Neill, E., Chiara Goisis, R., Haverty, R. & Harkin, A. (2019) L-alpha-aminoadipic acid restricts dopaminergic neurodegeneration and motor deficits in an inflammatory model of Parkinson's disease in male rats. *J Neurosci Res*, 97(7), 804-816.
O'Toole, E. (2015) The impact of pharmacological modulation of the NMDA-R/NO signalling pathway on neuronal complexity in vitro. Trinity College Dublin.
Ohshiro, H., Tonai-Kachi, H. & Ichikawa, K. (2008) GPR35 is a functional receptor in rat dorsal root ganglion neurons. *Biochem Biophys Res Commun*, 365(2), 344-8.
Oksanen, M., Lehtonen, S., Jaronen, M., Goldsteins, G., Hämäläinen, R. H. & Koistinaho, J. (2019) Astrocyte alterations in neurodegenerative pathologies and their modeling in human induced pluripotent stem cell platforms. *Cell Mol Life Sci*, 76(14), 2739-2760.
Okuda, S., Nishiyama, N., Saito, H. & Katsuki, H. (1998) 3-Hydroxykynurenine, an endogenous oxidative stress generator, causes neuronal cell death with apoptotic features and region selectivity. *J Neurochem*, 70(1), 299-307.

Olmos, G. & Lladó, J. (2014) Tumor necrosis factor alpha: a link between neuroinflammation and excitotoxicity. *Mediators Inflamm*, 2014, 861231.
Olney, J. W., de Gubareff, T. & Collins, J. F. (1980) Stereospecificity of the gliotoxic and anti-neurotoxic actions of alpha-aminoadipate. *Neurosci Lett*, 19(3), 277-82.
Olney, J. W., Ho, O. L. & Rhee, V. (1971) Cytotoxic effects of acidic and sulphur containing amino acids on the infant mouse central nervous system. *Exp Brain Res*, 14(1), 61-76.
Orihuela, R., McPherson, C. A. & Harry, G. J. (2016) Microglial M1/M2 polarization and metabolic states. *Br J Pharmacol*, 173(4), 649-65.
Ormel, L., Stensrud, M. J., Bergersen, L. H. & Gundersen, V. (2012) VGLUT1 is localized in astrocytic processes in several brain regions. *Glia*, 60(2), 229-38.
Ottum, P. A., Arellano, G., Reyes, L. I., Iruretagoyena, M. & Naves, R. (2015) Opposing Roles of Interferon-Gamma on Cells of the Central Nervous System in Autoimmune Neuroinflammation. *Front Immunol*, 6, 539.
Ouali Alami, N., Schurr, C., Olde Heuvel, F., Tang, L., Li, Q., Tasdogan, A., Kimbara, A., Nettekoven, M., Ottaviani, G., Raposo, C., Röver, S., Rogers-Evans, M., Rothenhäusler, B., Ullmer, C., Fingerle, J., Grether, U., Knuesel, I., Boeckers, T. M., Ludolph, A., Wirth, T., Roselli, F. & Baumann, B. (2018) NF-κB activation in astrocytes drives a stage-specific beneficial neuroimmunological response in ALS. *EMBO J*, 37(16).
Ozcan, A. S. (2017) Filopodia: A Rapid Structural Plasticity Substrate for Fast Learning. *Front Synaptic Neurosci*, 9, 12.
O'Neill, E. (2015) Protective effects of noradrenergic and neurotrophic signalling on neuronal complexity *in vitro*.
Pallmer, K. & Oxenius, A. (2016) Recognition and Regulation of T Cells by NK Cells. *Front Immunol*, 7, 251.
Pallotta, M. T., Orabona, C., Volpi, C., Vacca, C., Belladonna, M. L., Bianchi, R., Servillo, G., Brunacci, C., Calvitti, M., Bicciato, S., Mazza, E. M., Boon, L., Grassi, F., Fioretti, M. C., Fallarino, F., Puccetti, P. & Grohmann, U. (2011) Indoleamine 2,3-dioxygenase is a signaling protein in long-term tolerance by dendritic cells. *Nat Immunol*, 12(9), 870-8.
Pannasch, U., Freche, D., Dallérac, G., Ghézali, G., Escartin, C., Ezan, P., Cohen-Salmon, M., Benchenane, K., Abudara, V., Dufour, A., Lübke, J. H., Déglon, N., Knott, G., Holcman, D. & Rouach, N. (2014) Connexin 30 sets synaptic strength by controlling astroglial synapse invasion. *Nat Neurosci*, 17(4), 549-58.
Pannasch, U. & Rouach, N. (2013) Emerging role for astroglial networks in information processing: from synapse to behavior. *Trends Neurosci*, 36(7), 405-17.
Papadopoulos, M. C. & Verkman, A. S. (2012) Aquaporin 4 and neuromyelitis optica. *Lancet Neurol*, 11(6), 535-44.
Papageorgiou, I. E., Lewen, A., Galow, L. V., Cesetti, T., Scheffel, J., Regen, T., Hanisch, U. K. & Kann, O. (2016) TLR4-activated microglia require IFN-gamma to induce severe neuronal dysfunction and death in situ. *Proc Natl Acad Sci U S A*, 113(1), 212-7.
Papouin, T., Dunphy, J., Tolman, M., Foley, J. C. & Haydon, P. G. (2017) Astrocytic control of synaptic function. *Philos Trans R Soc Lond B Biol Sci*, 372(1715).
Park, H. & Poo, M. M. (2013) Neurotrophin regulation of neural circuit development and function. *Nat Rev Neurosci*, 14(1), 7-23.
Parkhurst, C. N., Yang, G., Ninan, I., Savas, J. N., Yates, J. R., Lafaille, J. J., Hempstead, B. L., Littman, D. R. & Gan, W. B. (2013) Microglia promote learning-dependent synapse formation through brain-derived neurotrophic factor. *Cell*, 155(7), 1596-609.
Parnass, Z., Tashiro, A. & Yuste, R. (2000) Analysis of spine morphological plasticity in developing hippocampal pyramidal neurons. *Hippocampus*, 10(5), 561-8.
Parpura, V. & Verkhratsky, A. (2012) Neuroglia at the crossroads of homoeostasis, metabolism and signalling: evolution of the concept. *ASN Neuro*, 4(4), 201-5.
Parrott, J. M. & O'Connor, J. C. (2015) Kynurenine 3-Monooxygenase: An Influential Mediator of Neuropathology. *Front Psychiatry*, 6, 116.

Parrott, J. M., Redus, L., Santana-Coelho, D., Morales, J., Gao, X. & O'Connor, J. C. (2016) Neurotoxic kynurenine metabolism is increased in the dorsal hippocampus and drives distinct depressive behaviors during inflammation. *Transl Psychiatry*, 6(10), e918.
Patrício, P., Mateus-Pinheiro, A., Irmler, M., Alves, N. D., Machado-Santos, A. R., Morais, M., Correia, J. S., Korostynski, M., Piechota, M., Stoffel, R., Beckers, J., Bessa, J. M., Almeida, O. F., Sousa, N. & Pinto, L. (2015) Differential and converging molecular mechanisms of antidepressants' action in the hippocampal dentate gyrus. *Neuropsychopharmacology*, 40(2), 338-49.
Pekny, M. & Pekna, M. (2014) Astrocyte reactivity and reactive astrogliosis: costs and benefits. *Physiol Rev*, 94(4), 1077-98.
Pekny, M., Wilhelmsson, U. & Pekna, M. (2014) The dual role of astrocyte activation and reactive gliosis. *Neurosci Lett*, 565, 30-8.
Pekny, M., Wilhelmsson, U., Tatlisumak, T. & Pekna, M. (2019) Astrocyte activation and reactive gliosis-A new target in stroke? *Neurosci Lett*, 689, 45-55.
Pena, I. A., Marques, L. A., Laranjeira, Â., Yunes, J. A., Eberlin, M. N., MacKenzie, A. & Arruda, P. (2017) Mouse lysine catabolism to aminoadipate occurs primarily through the saccharopine pathway; implications for pyridoxine dependent epilepsy (PDE). *Biochim Biophys Acta Mol Basis Dis*, 1863(1), 121-128.
Pena-Ortega, F. (2017) Pharmacological Tools to Activate Microglia and their Possible use to Study Neural Network Patho-physiology. *Curr Neuropharmacol*, 15(4), 595-619.
Penzes, P., Cahill, M. E., Jones, K. A., VanLeeuwen, J. E. & Woolfrey, K. M. (2011) Dendritic spine pathology in neuropsychiatric disorders. *Nat Neurosci*, 14(3), 285-93.
Perry, V. H. & Holmes, C. (2014) Microglial priming in neurodegenerative disease. *Nat Rev Neurol*, 10(4), 217-24.
Petanjek, Z., Judaš, M., Šimic, G., Rasin, M. R., Uylings, H. B., Rakic, P. & Kostovic, I. (2011) Extraordinary neoteny of synaptic spines in the human prefrontal cortex. *Proc Natl Acad Sci U S A*, 108(32), 13281-6.
Pfrieger, F. W. & Barres, B. A. (1997) Synaptic efficacy enhanced by glial cells in vitro. *Science*, 277(5332), 1684-7.
Pierozan, P., Ferreira, F., de Lima, B. O. & Pessoa-Pureur, R. (2015) Quinolinic acid induces disrupts cytoskeletal homeostasis in striatal neurons. Protective role of astrocyte-neuron interaction. *J Neurosci Res*, 93(2), 268-84.
Pierozan, P., Zamoner, A., Soska, A. K., Silvestrin, R. B., Loureiro, S. O., Heimfarth, L., Mello e Souza, T., Wajner, M. & Pessoa-Pureur, R. (2010) Acute intrastriatal administration of quinolinic acid provokes hyperphosphorylation of cytoskeletal intermediate filament proteins in astrocytes and neurons of rats. *Exp Neurol*, 224(1), 188-96.
Pierozan, P., Zamoner, A., Soska, Â., de Lima, B. O., Reis, K. P., Zamboni, F., Wajner, M. & Pessoa-Pureur, R. (2012) Signaling mechanisms downstream of quinolinic acid targeting the cytoskeleton of rat striatal neurons and astrocytes. *Exp Neurol*, 233(1), 391-9.
Ponath, G., Park, C. & Pitt, D. (2018) The Role of Astrocytes in Multiple Sclerosis. *Front Immunol*, 9, 217.
Pont-Lezica, L., Bechade, C., Belarif-Cantaut, Y., Pascual, O. & Bessis, A. (2011) Physiological roles of microglia during development. *J Neurochem*, 119(5), 901-8.
Posfai, B., Cserep, C., Orsolits, B. & Denes, A. (2019) New Insights into Microglia-Neuron Interactions: A Neuron's Perspective. *Neuroscience*, 405, 103-117.
Prajeeth, C. K., Lohr, K., Floess, S., Zimmermann, J., Ulrich, R., Gudi, V., Beineke, A., Baumgartner, W., Muller, M., Huehn, J. & Stangel, M. (2014) Effector molecules released by Th1 but not Th17 cells drive an M1 response in microglia. *Brain Behav Immun*, 37, 248-59.
Prendergast, G. C., Chang, M. Y., Mandik-Nayak, L., Metz, R. & Muller, A. J. (2011) Indoleamine 2,3-dioxygenase as a modifier of pathogenic inflammation in cancer and other inflammation-associated diseases. *Curr Med Chem*, 18(15), 2257-62.

Prescott, C., Weeks, A. M., Staley, K. J. & Partin, K. M. (2006) Kynurenic acid has a dual action on AMPA receptor responses. *Neurosci Lett*, 402(1-2), 108-12.
Previtera, M. L., Langhammer, C. G., Langrana, N. A. & Firestein, B. L. (2010) Regulation of dendrite arborization by substrate stiffness is mediated by glutamate receptors. *Ann Biomed Eng*, 38(12), 3733-43.
Price, J. L. & Drevets, W. C. (2010) Neurocircuitry of mood disorders. *Neuropsychopharmacology*, 35(1), 192-216.
Probert, L. (2015) TNF and its receptors in the CNS: The essential, the desirable and the deleterious effects. *Neuroscience*, 302, 2-22.
Puppo, F., George, V. & Silva, G. A. (2018) An Optimized Structure-Function Design Principle Underlies Efficient Signaling Dynamics in Neurons. *Sci Rep*, 8(1), 10460.
Puram, S. V. & Bonni, A. (2013) Cell-intrinsic drivers of dendrite morphogenesis. *Development*, 140(23), 4657-71.
Pérez-De La Cruz, V., Carrillo-Mora, P. & Santamaría, A. (2012) Quinolinic Acid, an endogenous molecule combining excitotoxicity, oxidative stress and other toxic mechanisms. *Int J Tryptophan Res*, 5, 1-8.
Quak, J., Doornbos, B., Roest, A. M., Duivis, H. E., Vogelzangs, N., Nolen, W. A., Penninx, B. W., Kema, I. P. & de Jonge, P. (2014) Does tryptophan degradation along the kynurenine pathway mediate the association between pro-inflammatory immune activity and depressive symptoms? *Psychoneuroendocrinology*, 45, 202-10.
Querfurth, H. W. & LaFerla, F. M. (2010) Alzheimer's disease. *N Engl J Med*, 362(4), 329-44.
Radtke, F. A., Chapman, G., Hall, J. & Syed, Y. A. (2017) Modulating Neuroinflammation to Treat Neuropsychiatric Disorders. *Biomed Res Int*, 2017, 5071786.
Rahman, A., Rao, M. S. & Khan, K. M. (2018) Intraventricular infusion of quinolinic acid impairs spatial learning and memory in young rats: a novel mechanism of lead-induced neurotoxicity. *J Neuroinflammation*, 15(1), 263.
Rahman, A., Ting, K., Cullen, K. M., Braidy, N., Brew, B. J. & Guillemin, G. J. (2009) The excitotoxin quinolinic acid induces tau phosphorylation in human neurons. *PLoS One*, 4(7), e6344.
Raison, C. L., Dantzer, R., Kelley, K. W., Lawson, M. A., Woolwine, B. J., Vogt, G., Spivey, J. R., Saito, K. & Miller, A. H. (2010) CSF concentrations of brain tryptophan and kynurenines during immune stimulation with IFN-alpha: relationship to CNS immune responses and depression. *Mol Psychiatry*, 15(4), 393-403.
Rajkowska, G. & Stockmeier, C. A. (2013) Astrocyte pathology in major depressive disorder: insights from human postmortem brain tissue. *Curr Drug Targets*, 14(11), 1225-36.
Rama Rao, K. V. & Kielian, T. (2015) Neuron-astrocyte interactions in neurodegenerative diseases: Role of neuroinflammation. *Clin Exp Neuroimmunol*, 6(3), 245-263.
Ramos, H. J., Lanteri, M. C., Blahnik, G., Negash, A., Suthar, M. S., Brassil, M. M., Sodhi, K., Treuting, P. M., Busch, M. P., Norris, P. J. & Gale, M., Jr. (2012) IL-1beta signaling promotes CNS-intrinsic immune control of West Nile virus infection. *PLoS Pathog*, 8(11), e1003039.
Ramos-Chávez, L. A., Lugo Huitrón, R., González Esquivel, D., Pineda, B., Ríos, C., Silva-Adaya, D., Sánchez-Chapul, L., Roldán-Roldán, G. & Pérez de la Cruz, V. (2018) Relevance of Alternative Routes of Kynurenic Acid Production in the Brain. *Oxid Med Cell Longev*, 2018, 5272741.
Ramírez-Ortega, D., Ramiro-Salazar, A., González-Esquivel, D., Ríos, C., Pineda, B. & Pérez de la Cruz, V. (2017) 3-Hydroxykynurenine and 3-Hydroxyanthranilic Acid Enhance the Toxicity Induced by Copper in Rat Astrocyte Culture. *Oxid Med Cell Longev*, 2017, 2371895.
Reemst, K., Noctor, S. C., Lucassen, P. J. & Hol, E. M. (2016) The Indispensable Roles of Microglia and Astrocytes during Brain Development. *Front Hum Neurosci*, 10, 566.

Reus, G. Z., Jansen, K., Titus, S., Carvalho, A. F., Gabbay, V. & Quevedo, J. (2015) Kynurenine pathway dysfunction in the pathophysiology and treatment of depression: Evidences from animal and human studies. *J Psychiatr Res*.
Reyes-Ocampo, J., Ramirez-Ortega, D., Cervantes, G. I., Pineda, B., Balderas, P. M., Gonzalez-Esquivel, D., Sanchez-Chapul, L., Lugo-Huitron, R., Silva-Adaya, D., Rios, C., Jimenez-Anguiano, A. & Perez-de la Cruz, V. (2015a) Mitochondrial dysfunction related to cell damage induced by 3-hydroxykynurenine and 3-hydroxyanthranilic acid: Non-dependent-effect of early reactive oxygen species production. *Neurotoxicology*, 50, 81-91.
Reyes-Ocampo, J., Ramírez-Ortega, D., Cervantes, G. I., Pineda, B., Balderas, P. M., González-Esquivel, D., Sánchez-Chapul, L., Lugo-Huitrón, R., Silva-Adaya, D., Ríos, C., Jiménez-Anguiano, A. & Pérez-de la Cruz, V. (2015b) Mitochondrial dysfunction related to cell damage induced by 3-hydroxykynurenine and 3-hydroxyanthranilic acid: Non-dependent-effect of early reactive oxygen species production. *Neurotoxicology*, 50, 81-91.
Rice, R. A., Spangenberg, E. E., Yamate-Morgan, H., Lee, R. J., Arora, R. P., Hernandez, M. X., Tenner, A. J., West, B. L. & Green, K. N. (2015) Elimination of Microglia Improves Functional Outcomes Following Extensive Neuronal Loss in the Hippocampus. *J Neurosci*, 35(27), 9977-89.
Rider, P., Kaplanov, I., Romzova, M., Bernardis, L., Braiman, A., Voronov, E. & Apte, R. N. (2012) The transcription of the alarmin cytokine interleukin-1 alpha is controlled by hypoxia inducible factors 1 and 2 alpha in hypoxic cells. *Front Immunol*, 3, 290.
Riedl, J., Crevenna, A. H., Kessenbrock, K., Yu, J. H., Neukirchen, D., Bista, M., Bradke, F., Jenne, D., Holak, T. A., Werb, Z., Sixt, M. & Wedlich-Soldner, R. (2008) Lifeact: a versatile marker to visualize F-actin. *Nat Methods*, 5(7), 605-7.
Rochefort, N. L. & Konnerth, A. (2012) Dendritic spines: from structure to in vivo function. *EMBO Rep*, 13(8), 699-708.
Rock, R. B., Gekker, G., Hu, S., Sheng, W. S., Cheeran, M., Lokensgard, J. R. & Peterson, P. K. (2004) Role of microglia in central nervous system infections. *Clin Microbiol Rev*, 17(4), 942-64, table of contents.
Roelfsema, P. R. & Holtmaat, A. (2018) Control of synaptic plasticity in deep cortical networks. *Nat Rev Neurosci*, 19(3), 166-180.
Roqué, P. J., Guizzetti, M. & Costa, L. G. (2014) Synaptic structure quantification in cultured neurons. *Curr Protoc Toxicol*, 60, 12.22.1-32.
Rose, C. F., Verkhratsky, A. & Parpura, V. (2013) Astrocyte glutamine synthetase: pivotal in health and disease. *Biochem Soc Trans*, 41(6), 1518-24.
Rose, C. R., Felix, L., Zeug, A., Dietrich, D., Reiner, A. & Henneberger, C. (2017) Astroglial Glutamate Signaling and Uptake in the Hippocampus. *Front Mol Neurosci*, 10, 451.
Rose, C. R., Ziemens, D., Untiet, V. & Fahlke, C. (2018) Molecular and cellular physiology of sodium-dependent glutamate transporters. *Brain Res Bull*, 136, 3-16.
Rose-John, S. (2012) IL-6 trans-signaling via the soluble IL-6 receptor: importance for the pro-inflammatory activities of IL-6. *Int J Biol Sci*, 8(9), 1237-47.
Rose-John, S. (2017) The Soluble Interleukin 6 Receptor: Advanced Therapeutic Options in Inflammation. *Clin Pharmacol Ther*, 102(4), 591-598.
Rossi, F., Miggiano, R., Ferraris, D. M. & Rizzi, M. (2019) The Synthesis of Kynurenic Acid in Mammals: An Updated Kynurenine Aminotransferase Structural KATalogue. *Front Mol Biosci*, 6, 7.
Rothaug, M., Becker-Pauly, C. & Rose-John, S. (2016) The role of interleukin-6 signaling in nervous tissue. *Biochim Biophys Acta*, 1863(6 Pt A), 1218-27.
Rozsa, E., Robotka, H., Vecsei, L. & Toldi, J. (2008) The Janus-face kynurenic acid. *J Neural Transm (Vienna)*, 115(8), 1087-91.

Rubio-Casillas, A. & Fernández-Guasti, A. (2016) The dose makes the poison: from glutamate-mediated neurogenesis to neuronal atrophy and depression. *Rev Neurosci*, 27(6), 599-622.
Réus, G. Z., Fries, G. R., Stertz, L., Badawy, M., Passos, I. C., Barichello, T., Kapczinski, F. & Quevedo, J. (2015a) The role of inflammation and microglial activation in the pathophysiology of psychiatric disorders. *Neuroscience*, 300, 141-54.
Réus, G. Z., Jansen, K., Titus, S., Carvalho, A. F., Gabbay, V. & Quevedo, J. (2015b) Kynurenine pathway dysfunction in the pathophysiology and treatment of depression: Evidences from animal and human studies. *J Psychiatr Res*, 68, 316-28.
Sabio, G. & Davis, R. J. (2014) TNF and MAP kinase signalling pathways. *Semin Immunol*, 26(3), 237-45.
Sainath, R. & Gallo, G. (2015) Cytoskeletal and signaling mechanisms of neurite formation. *Cell Tissue Res*, 359(1), 267-78.
Sanacora, G. & Banasr, M. (2013) From pathophysiology to novel antidepressant drugs: glial contributions to the pathology and treatment of mood disorders. *Biol Psychiatry*, 73(12), 1172-9.
Sanchez, C., Diaz-Nido, J. & Avila, J. (2000) Phosphorylation of microtubule-associated protein 2 (MAP2) and its relevance for the regulation of the neuronal cytoskeleton function. *Prog Neurobiol*, 61(2), 133-68.
Santello, M., Calì, C. & Bezzi, P. (2012) Gliotransmission and the tripartite synapse. *Adv Exp Med Biol*, 970, 307-31.
Santello, M. & Volterra, A. (2012) TNFα in synaptic function: switching gears. *Trends Neurosci*, 35(10), 638-47.
Sariyer, I. K. (2013) Transfection of neuronal cultures. *Methods Mol Biol*, 1078, 133-9.
Sas, K., Robotka, H., Toldi, J. & Vécsei, L. (2007) Mitochondria, metabolic disturbances, oxidative stress and the kynurenine system, with focus on neurodegenerative disorders. *J Neurol Sci*, 257(1-2), 221-39.
Sato, K. (2015) Effects of Microglia on Neurogenesis. *Glia*, 63(8), 1394-405.
Saura, J. (2007) Microglial cells in astroglial cultures: a cautionary note. *J Neuroinflammation*, 4, 26.
Savitz, J. & Drevets, W. C. (2009) Bipolar and major depressive disorder: neuroimaging the developmental-degenerative divide. *Neurosci Biobehav Rev*, 33(5), 699-771.
Schafer, D. P., Lehrman, E. K., Kautzman, A. G., Koyama, R., Mardinly, A. R., Yamasaki, R., Ransohoff, R. M., Greenberg, M. E., Barres, B. A. & Stevens, B. (2012) Microglia sculpt postnatal neural circuits in an activity and complement-dependent manner. *Neuron*, 74(4), 691-705.
Scharfman, H. E. & Binder, D. K. (2013) Aquaporin-4 water channels and synaptic plasticity in the hippocampus. *Neurochem Int*, 63(7), 702-11.
Scheller, J., Garbers, C. & Rose-John, S. (2014) Interleukin-6: from basic biology to selective blockade of pro-inflammatory activities. *Semin Immunol*, 26(1), 2-12.
Schiweck, J., Eickholt, B. J. & Murk, K. (2018) Important Shapeshifter: Mechanisms Allowing Astrocytes to Respond to the Changing Nervous System During Development, Injury and Disease. *Front Cell Neurosci*, 12, 261.
Schoenborn, J. R. & Wilson, C. B. (2007) Regulation of interferon-gamma during innate and adaptive immune responses. *Adv Immunol*, 96, 41-101.
Schousboe, A., Scafidi, S., Bak, L. K., Waagepetersen, H. S. & McKenna, M. C. (2014) Glutamate metabolism in the brain focusing on astrocytes. *Adv Neurobiol*, 11, 13-30.
Schroder, K., Hertzog, P. J., Ravasi, T. & Hume, D. A. (2004) Interferon-gamma: an overview of signals, mechanisms and functions. *J Leukoc Biol*, 75(2), 163-89.
Schroder, K. & Tschopp, J. (2010) The inflammasomes. *Cell*, 140(6), 821-32.
Schroeter, M. L., Sacher, J., Steiner, J., Schoenknecht, P. & Mueller, K. (2013) Serum S100B represents a new biomarker for mood disorders. *Curr Drug Targets*, 14(11), 1237-48.

Schuck, P. F., Tonin, A., da Costa Ferreira, G., Viegas, C. M., Latini, A., Duval Wannmacher, C. M., de Souza Wyse, A. T., Dutra-Filho, C. S. & Wajner, M. (2007) Kynurenines impair energy metabolism in rat cerebral cortex. *Cell Mol Neurobiol*, 27(1), 147-60.
Schwarcz, R., Bruno Jp Fau - Muchowski, P. J., Muchowski Pj Fau - Wu, H.-Q. & Wu, H. Q. (2012a) Kynurenines in the mammalian brain: when physiology meets pathology. *Nature Reviews. Neuroscience*, 13(7), 465-77.
Schwarcz, R., Bruno, J. P., Muchowski, P. J. & Wu, H. Q. (2012b) Kynurenines in the mammalian brain: when physiology meets pathology. *Nat Rev Neurosci*, 13(7), 465-77.
Schwarcz, R., Du, F., Schmidt, W., Turski, W. A., Gramsbergen, J. B., Okuno, E. & Roberts, R. C. (1992) Kynurenic acid: a potential pathogen in brain disorders. *Ann N Y Acad Sci*, 648, 140-53.
Schwieler, L., Larsson, M. K., Skogh, E., Kegel, M. E., Orhan, F., Abdelmoaty, S., Finn, A., Bhat, M., Samuelsson, M., Lundberg, K., Dahl, M. L., Sellgren, C., Schuppe-Koistinen, I., Svensson, C., Erhardt, S. & Engberg, G. (2015) Increased levels of IL-6 in the cerebrospinal fluid of patients with chronic schizophrenia--significance for activation of the kynurenine pathway. *J Psychiatry Neurosci*, 40(2), 126-33.
Segal, B. M. & Giger, R. J. (2016) Stable biomarker for plastic microglia. *Proc Natl Acad Sci U S A*, 113(12), 3130-2.
Seif, F., Khoshmirsafa, M., Aazami, H., Mohsenzadegan, M., Sedighi, G. & Bahar, M. (2017) The role of JAK-STAT signaling pathway and its regulators in the fate of T helper cells. *Cell Commun Signal*, 15(1), 23.
Seifert, H. A., Collier, L. A., Chapman, C. B., Benkovic, S. A., Willing, A. E. & Pennypacker, K. R. (2014) Pro-inflammatory interferon gamma signaling is directly associated with stroke induced neurodegeneration. *J Neuroimmune Pharmacol*, 9(5), 679-89.
Sekino, Y., Kojima, N. & Shirao, T. (2007) Role of actin cytoskeleton in dendritic spine morphogenesis. *Neurochem Int*, 51(2-4), 92-104.
Sekino, Y., Tanaka, S., Hanamura, K., Yamazaki, H., Sasagawa, Y., Xue, Y., Hayashi, K. & Shirao, T. (2006) Activation of N-methyl-D-aspartate receptor induces a shift of drebrin distribution: disappearance from dendritic spines and appearance in dendritic shafts. *Mol Cell Neurosci*, 31(3), 493-504.
Sepers, M. D. & Raymond, L. A. (2014) Mechanisms of synaptic dysfunction and excitotoxicity in Huntington's disease. *Drug Discov Today*, 19(7), 990-6.
Sethi, R., Gómez-Coronado, N., Walker, A. J., Robertson, O. D., Agustini, B., Berk, M. & Dodd, S. (2019) Neurobiology and Therapeutic Potential of Cyclooxygenase-2 (COX-2) Inhibitors for Inflammation in Neuropsychiatric Disorders. *Front Psychiatry*, 10, 605.
Shen, K. & Cowan, C. W. (2010) Guidance molecules in synapse formation and plasticity. *Cold Spring Harb Perspect Biol*, 2(4), a001842.
Shen, Y., Qin, H., Chen, J., Mou, L., He, Y., Yan, Y., Zhou, H., Lv, Y., Chen, Z., Wang, J. & Zhou, Y. D. (2016) Postnatal activation of TLR4 in astrocytes promotes excitatory synaptogenesis in hippocampal neurons. *J Cell Biol*, 215(5), 719-734.
Sheppard, O., Coleman, M. P. & Durrant, C. S. (2019) Lipopolysaccharide-induced neuroinflammation induces presynaptic disruption through a direct action on brain tissue involving microglia-derived interleukin 1 beta. *J Neuroinflammation*, 16(1), 106.
Shih, R. H., Wang, C. Y. & Yang, C. M. (2015) NF-kappaB Signaling Pathways in Neurological Inflammation: A Mini Review. *Front Mol Neurosci*, 8, 77.
Shim, K. S. & Lubec, G. (2002) Drebrin, a dendritic spine protein, is manifold decreased in brains of patients with Alzheimer's disease and Down syndrome. *Neurosci Lett*, 324(3), 209-12.
Shimamoto, S., Tsuchiya, M., Yamaguchi, F., Kubota, Y., Tokumitsu, H. & Kobayashi, R. (2014) Ca2+/S100 proteins inhibit the interaction of FKBP38 with Bcl-2 and Hsp90. *Biochem J*, 458(1), 141-52.

Shindo, A., Maki, T., Mandeville, E. T., Liang, A. C., Egawa, N., Itoh, K., Itoh, N., Borlongan, M., Holder, J. C., Chuang, T. T., McNeish, J. D., Tomimoto, H., Lok, J., Lo, E. H. & Arai, K. (2016) Astrocyte-Derived Pentraxin 3 Supports Blood-Brain Barrier Integrity Under Acute Phase of Stroke. *Stroke*, 47(4), 1094-100.
Shirey, K. A., Jung, J. Y., Maeder, G. S. & Carlin, J. M. (2006) Upregulation of IFN-gamma receptor expression by proinflammatory cytokines influences IDO activation in epithelial cells. *J Interferon Cytokine Res*, 26(1), 53-62.
SHOLL, D. A. (1953) Dendritic organization in the neurons of the visual and motor cortices of the cat. *J Anat*, 87(4), 387-406.
Shors, T. J. (2002) Opposite effects of stressful experience on memory formation in males versus females. *Dialogues Clin Neurosci*, 4(2), 139-47.
Shors, T. J., Chua, C. & Falduto, J. (2001) Sex differences and opposite effects of stress on dendritic spine density in the male versus female hippocampus. *J Neurosci*, 21(16), 6292-7.
Shors, T. J., Falduto, J. & Leuner, B. (2004) The opposite effects of stress on dendritic spines in male vs. female rats are NMDA receptor-dependent. *Eur J Neurosci*, 19(1), 145-50.
Simões, A. P., Silva, C. G., Marques, J. M., Pochmann, D., Porciúncula, L. O., Ferreira, S., Oses, J. P., Beleza, R. O., Real, J. I., Köfalvi, A., Bahr, B. A., Lerma, J., Cunha, R. A. & Rodrigues, R. J. (2018) Glutamate-induced and NMDA receptor-mediated neurodegeneration entails P2Y1 receptor activation. *Cell Death Dis*, 9(3), 297.
Skaper, S. D., Facci, L., Zusso, M. & Giusti, P. (2018) An Inflammation-Centric View of Neurological Disease: Beyond the Neuron. *Front Cell Neurosci*, 12, 72.
Skucas, V. A., Mathews, I. B., Yang, J., Cheng, Q., Treister, A., Duffy, A. M., Verkman, A. S., Hempstead, B. L., Wood, M. A., Binder, D. K. & Scharfman, H. E. (2011) Impairment of select forms of spatial memory and neurotrophin-dependent synaptic plasticity by deletion of glial aquaporin-4. *J Neurosci*, 31(17), 6392-7.
Sliogeryte, K., Thorpe, S. D., Wang, Z., Thompson, C. L., Gavara, N. & Knight, M. M. (2016) Differential effects of LifeAct-GFP and actin-GFP on cell mechanics assessed using micropipette aspiration. *J Biomech*, 49(2), 310-7.
Smiałowska, M., Szewczyk, B., Woźniak, M., Wawrzak-Wleciał, A. & Domin, H. (2013) Glial degeneration as a model of depression. *Pharmacol Rep*, 65(6), 1572-9.
Smith, J. A., Das, A., Ray, S. K. & Banik, N. L. (2012) Role of pro-inflammatory cytokines released from microglia in neurodegenerative diseases. *Brain Res Bull*, 87(1), 10-20.
Smolen, J. S., Weinblatt, M. E., Sheng, S., Zhuang, Y. & Hsu, B. (2014) Sirukumab, a human anti-interleukin-6 monoclonal antibody: a randomised, 2-part (proof-of-concept and dose-finding), phase II study in patients with active rheumatoid arthritis despite methotrexate therapy. *Ann Rheum Dis*, 73(9), 1616-25.
Sofroniew, M. V. (2009) Molecular dissection of reactive astrogliosis and glial scar formation. *Trends Neurosci*, 32(12), 638-47.
Sofroniew, M. V. (2014) Multiple roles for astrocytes as effectors of cytokines and inflammatory mediators. *Neuroscientist*, 20(2), 160-72.
Sofroniew, M. V. & Vinters, H. V. (2010a) Astrocytes: biology and pathology. *Acta Neuropathol*, 119(1), 7-35.
Sofroniew, M. V. & Vinters, H. V. (2010b) Astrocytes: biology and pathology. *Acta Neuropathologica*, 119(1), 7-35.
Soltani, M. H., Pichardo, R., Song, Z., Sangha, N., Camacho, F., Satyamoorthy, K., Sangueza, O. P. & Setaluri, V. (2005) Microtubule-associated protein 2, a marker of neuronal differentiation, induces mitotic defects, inhibits growth of melanoma cells, and predicts metastatic potential of cutaneous melanoma. *Am J Pathol*, 166(6), 1841-50.
Soltoggio, A., Stanley, K. O. & Risi, S. (2018) Born to learn: The inspiration, progress, and future of evolved plastic artificial neural networks. *Neural Netw*, 108, 48-67.

Song, C., Wu, Y. S., Yang, Z. Y., Kalueff, A. V., Tsao, Y. Y., Dong, Y. & Su, K. P. (2019) Astrocyte-Conditioned Medium Protects Prefrontal Cortical Neurons from Glutamate-Induced Cell Death by Inhibiting TNF-α Expression. *Neuroimmunomodulation*, 26(1), 33-42.
Sorci, G., Bianchi, R., Riuzzi, F., Tubaro, C., Arcuri, C., Giambanco, I. & Donato, R. (2010) S100B Protein, A Damage-Associated Molecular Pattern Protein in the Brain and Heart, and Beyond. *Cardiovasc Psychiatry Neurol*, 2010.
Sorci, G., Riuzzi, F., Arcuri, C., Tubaro, C., Bianchi, R., Giambanco, I. & Donato, R. (2013) S100B protein in tissue development, repair and regeneration. *World J Biol Chem*, 4(1), 1-12.
Spacek, J. & Harris, K. M. (1997) Three-dimensional organization of smooth endoplasmic reticulum in hippocampal CA1 dendrites and dendritic spines of the immature and mature rat. *J Neurosci*, 17(1), 190-203.
Spruston, N. (2008) Pyramidal neurons: dendritic structure and synaptic integration. *Nat Rev Neurosci*, 9(3), 206-21.
Srivastava, D. P., Woolfrey, K. M. & Penzes, P. (2011) Analysis of dendritic spine morphology in cultured CNS neurons. *J Vis Exp*(53), e2794.
Stark, G. R. & Darnell, J. E. (2012) The JAK-STAT pathway at twenty. *Immunity*, 36(4), 503-14.
Stavale, L. M., Soares, E. S., Mendonça, M. C., Irazusta, S. P. & da Cruz Höfling, M. A. (2013) Temporal relationship between aquaporin-4 and glial fibrillary acidic protein in cerebellum of neonate and adult rats administered a BBB disrupting spider venom. *Toxicon*, 66, 37-46.
Steiner, J., Bernstein, H. G., Bogerts, B., Gos, T., Richter-Landsberg, C., Wunderlich, M. T. & Keilhoff, G. (2008) S100B is expressed in, and released from, OLN-93 oligodendrocytes: Influence of serum and glucose deprivation. *Neuroscience*, 154(2), 496-503.
Stephenson, J., Nutma, E., van der Valk, P. & Amor, S. (2018) Inflammation in CNS neurodegenerative diseases. *Immunology*, 154(2), 204-219.
Stobart, J. L. & Anderson, C. M. (2013) Multifunctional role of astrocytes as gatekeepers of neuronal energy supply. *Front Cell Neurosci*, 7, 38.
Stogsdill, J. A., Ramirez, J., Liu, D., Kim, Y. H., Baldwin, K. T., Enustun, E., Ejikeme, T., Ji, R. R. & Eroglu, C. (2017) Astrocytic neuroligins control astrocyte morphogenesis and synaptogenesis. *Nature*, 551(7679), 192-197.
Stone, T. W. & Darlington, L. G. (2002) Endogenous kynurenines as targets for drug discovery and development. *Nat Rev Drug Discov*, 1(8), 609-20.
Stork, T., Sheehan, A., Tasdemir-Yilmaz, O. E. & Freeman, M. R. (2014) Neuron-glia interactions through the Heartless FGF receptor signaling pathway mediate morphogenesis of Drosophila astrocytes. *Neuron*, 83(2), 388-403.
Stroissnigg, H., Trancíková, A., Descovich, L., Fuhrmann, J., Kutschera, W., Kostan, J., Meixner, A., Nothias, F. & Propst, F. (2007) S-nitrosylation of microtubule-associated protein 1B mediates nitric-oxide-induced axon retraction. *Nat Cell Biol*, 9(9), 1035-45.
Stuss, D. P., Boyd, J. D., Levin, D. B. & Delaney, K. R. (2012) MeCP2 mutation results in compartment-specific reductions in dendritic branching and spine density in layer 5 motor cortical neurons of YFP-H mice. *PLoS One*, 7(3), e31896.
Sublette, M. E., Galfalvy, H. C., Fuchs, D., Lapidus, M., Grunebaum, M. F., Oquendo, M. A., Mann, J. J. & Postolache, T. T. (2011) Plasma kynurenine levels are elevated in suicide attempters with major depressive disorder. *Brain Behav Immun*, 25(6), 1272-8.
Sukhorukova, E. G., Kruzhevskiĭ, D. & Alekseeva, O. S. (2015) [Glial fibrillary acidic protein: the component of intermediate filaments in the vertebrate brain astrocytes]. *Zh Evol Biokhim Fiziol*, 51(1), 3-10.
Sullivan, S. M. (2014) GFAP variants in health and disease: stars of the brain... and gut. *J Neurochem*, 130(6), 729-32.

Sun, D. & Jakobs, T. C. (2012) Structural remodeling of astrocytes in the injured CNS. *Neuroscientist*, 18(6), 567-88.
Sun, H., Liang, R., Yang, B., Zhou, Y., Liu, M., Fang, F., Ding, J., Fan, Y. & Hu, G. (2016) Aquaporin-4 mediates communication between astrocyte and microglia: Implications of neuroinflammation in experimental Parkinson's disease. *Neuroscience*, 317, 65-75.
Sun, L., Shen, R., Agnihotri, S. K., Chen, Y., Huang, Z. & Büeler, H. (2018) Lack of PINK1 alters glia innate immune responses and enhances inflammation-induced, nitric oxide-mediated neuron death. *Sci Rep*, 8(1), 383.
Sun, W., Cornwell, A., Li, J., Peng, S., Osorio, M. J., Aalling, N., Wang, S., Benraiss, A., Lou, N., Goldman, S. A. & Nedergaard, M. (2017) SOX9 Is an Astrocyte-Specific Nuclear Marker in the Adult Brain Outside the Neurogenic Regions. *J Neurosci*, 37(17), 4493-4507.
Sundal, C. (2014) Microglia: multiple roles in surveillance, circuit shaping, and response to injury. *Neurology*, 82(20), 1846.
Suthaus, J., Stuhlmann-Laeisz, C., Tompkins, V. S., Rosean, T. R., Klapper, W., Tosato, G., Janz, S., Scheller, J. & Rose-John, S. (2012) HHV-8-encoded viral IL-6 collaborates with mouse IL-6 in the development of multicentric Castleman disease in mice. *Blood*, 119(22), 5173-81.
Suzuki, H., Ohgidani, M., Kuwano, N., Chrétien, F., Lorin de la Grandmaison, G., Onaya, M., Tominaga, I., Setoyama, D., Kang, D., Mimura, M., Kanba, S. & Kato, T. A. (2019) Suicide and Microglia: Recent Findings and Future Perspectives Based on Human Studies. *Front Cell Neurosci*, 13, 31.
Swanger, S. A., Yao, X., Gross, C. & Bassell, G. J. (2011) Automated 4D analysis of dendritic spine morphology: applications to stimulus-induced spine remodeling and pharmacological rescue in a disease model. *Mol Brain*, 4, 38.
Swartz, K. J., During, M. J., Freese, A. & Beal, M. F. (1990) Cerebral synthesis and release of kynurenic acid: an endogenous antagonist of excitatory amino acid receptors. *J Neurosci*, 10(9), 2965-73.
Szalardy, L., Zadori, D., Toldi, J., Fulop, F., Klivenyi, P. & Vecsei, L. (2012) Manipulating kynurenic acid levels in the brain - on the edge between neuroprotection and cognitive dysfunction. *Curr Top Med Chem*, 12(16), 1797-806.
Szepesi, Z., Manouchehrian, O., Bachiller, S. & Deierborg, T. (2018) Bidirectional Microglia-Neuron Communication in Health and Disease. *Front Cell Neurosci*, 12, 323.
Szu, J. I. & Binder, D. K. (2016) The Role of Astrocytic Aquaporin-4 in Synaptic Plasticity and Learning and Memory. *Front Integr Neurosci*, 10, 8.
Ta, T. T., Dikmen, H. O., Schilling, S., Chausse, B., Lewen, A., Hollnagel, J. O. & Kann, O. (2019) Priming of microglia with IFN-gamma slows neuronal gamma oscillations in situ. *Proc Natl Acad Sci U S A*, 116(10), 4637-4642.
Tabata, H. (2015) Diverse subtypes of astrocytes and their development during corticogenesis. *Front Neurosci*, 9, 114.
Tada, T. & Sheng, M. (2006) Molecular mechanisms of dendritic spine morphogenesis. *Curr Opin Neurobiol*, 16(1), 95-101.
Takada, M. & Hattori, T. (1986) Fine structural changes in the rat brain after local injections of gliotoxin, alpha-aminoadipic acid. *Histol Histopathol*, 1(3), 271-5.
Takahashi, H., Sekino, Y., Tanaka, S., Mizui, T., Kishi, S. & Shirao, T. (2003) Drebrin-dependent actin clustering in dendritic filopodia governs synaptic targeting of postsynaptic density-95 and dendritic spine morphogenesis. *J Neurosci*, 23(16), 6586-95.
Takaki, J., Fujimori, K., Miura, M., Suzuki, T., Sekino, Y. & Sato, K. (2012) L-glutamate released from activated microglia downregulates astrocytic L-glutamate transporter expression in neuroinflammation: the 'collusion' hypothesis for increased extracellular L-glutamate concentration in neuroinflammation. *J Neuroinflammation*, 9, 275.

Takemoto, T., Ishihara, Y., Ishida, A. & Yamazaki, T. (2015) Neuroprotection elicited by nerve growth factor and brain-derived neurotrophic factor released from astrocytes in response to methylmercury. *Environ Toxicol Pharmacol*, 40(1), 199-205.
Takesian, A. E. & Hensch, T. K. (2013) Balancing plasticity/stability across brain development. *Prog Brain Res*, 207, 3-34.
Tan, L., Yu, J.-T. & Tan, L. (2012a) The kynurenine pathway in neurodegenerative diseases: Mechanistic and therapeutic considerations. *Journal of the Neurological Sciences*, 323(1), 1-8.
Tan, L., Yu, J. T. & Tan, L. (2012b) The kynurenine pathway in neurodegenerative diseases: mechanistic and therapeutic considerations. *J Neurol Sci*, 323(1-2), 1-8.
Tanaka, T., Narazaki, M. & Kishimoto, T. (2016) Immunotherapeutic implications of IL-6 blockade for cytokine storm. *Immunotherapy*, 8(8), 959-70.
Tang, F., Guo, S., Liao, H., Yu, P., Wang, L., Song, X., Chen, J. & Yang, Q. (2017) Resveratrol Enhances Neurite Outgrowth and Synaptogenesis Via Sonic Hedgehog Signaling Following Oxygen-Glucose Deprivation/Reoxygenation Injury. *Cell Physiol Biochem*, 43(2), 852-869.
Taniguchi, T., Ogasawara, K., Takaoka, A. & Tanaka, N. (2001) IRF family of transcription factors as regulators of host defense. *Annu Rev Immunol*, 19, 623-55.
Tashiro, A., Minden, A. & Yuste, R. (2000) Regulation of dendritic spine morphology by the rho family of small GTPases: antagonistic roles of Rac and Rho. *Cereb Cortex*, 10(10), 927-38.
Tenenbaum, L. & Humbert-Claude, M. (2017) Glial Cell Line-Derived Neurotrophic Factor Gene Delivery in Parkinson's Disease: A Delicate Balance between Neuroprotection, Trophic Effects, and Unwanted Compensatory Mechanisms. *Front Neuroanat*, 11, 29.
Thenral, S. T. & Vanisree, A. J. (2012) Peripheral assessment of the genes AQP4, PBP and TH in patients with Parkinson's disease. *Neurochem Res*, 37(3), 512-5.
Thornton, P., Pinteaux, E., Gibson, R. M., Allan, S. M. & Rothwell, N. J. (2006) Interleukin-1-induced neurotoxicity is mediated by glia and requires caspase activation and free radical release. *J Neurochem*, 98(1), 258-66.
Tian, L., Ma, L., Kaarela, T. & Li, Z. (2012) Neuroimmune crosstalk in the central nervous system and its significance for neurological diseases. *J Neuroinflammation*, 9, 155.
Tien, A. C., Tsai, H. H., Molofsky, A. V., McMahon, M., Foo, L. C., Kaul, A., Dougherty, J. D., Heintz, N., Gutmann, D. H., Barres, B. A. & Rowitch, D. H. (2012) Regulated temporal-spatial astrocyte precursor cell proliferation involves BRAF signalling in mammalian spinal cord. *Development*, 139(14), 2477-87.
Timmerman, R., Burm, S. M. & Bajramovic, J. J. (2018) An Overview of in vitro Methods to Study Microglia. *Front Cell Neurosci*, 12, 242.
Torres-Platas, S. G., Comeau, S., Rachalski, A., Bo, G. D., Cruceanu, C., Turecki, G., Giros, B. & Mechawar, N. (2014) Morphometric characterization of microglial phenotypes in human cerebral cortex. *J Neuroinflammation*, 11, 12.
Torres-Platas, S. G., Nagy, C., Wakid, M., Turecki, G. & Mechawar, N. (2016) Glial fibrillary acidic protein is differentially expressed across cortical and subcortical regions in healthy brains and downregulated in the thalamus and caudate nucleus of depressed suicides. *Mol Psychiatry*, 21(4), 509-15.
Toy, D. & Namgung, U. (2013) Role of glial cells in axonal regeneration. *Exp Neurobiol*, 22(2), 68-76.
Tremblay, M., Lowery, R. L. & Majewska, A. K. (2010) Microglial interactions with synapses are modulated by visual experience. *PLoS Biol*, 8(11), e1000527.
Tremblay, M. E. & Majewska, A. K. (2011) A role for microglia in synaptic plasticity? *Commun Integr Biol*, 4(2), 220-2.
Tremblay, M. E., Stevens, B., Sierra, A., Wake, H., Bessis, A. & Nimmerjahn, A. (2011) The role of microglia in the healthy brain. *J Neurosci*, 31(45), 16064-9.

Turner, M. D., Nedjai, B., Hurst, T. & Pennington, D. J. (2014) Cytokines and chemokines: At the crossroads of cell signalling and inflammatory disease. *Biochim Biophys Acta*, 1843(11), 2563-2582.
Turski, M. P., Turska, M., Paluszkiewicz, P., Parada-Turska, J. & Oxenkrug, G. F. (2013) Kynurenic Acid in the digestive system-new facts, new challenges. *Int J Tryptophan Res*, 6, 47-55.
Tynan, R. J., Naicker, S., Hinwood, M., Nalivaiko, E., Buller, K. M., Pow, D. V., Day, T. A. & Walker, F. R. (2010) Chronic stress alters the density and morphology of microglia in a subset of stress-responsive brain regions. *Brain Behav Immun*, 24(7), 1058-68.
Tynan, R. J., Weidenhofer, J., Hinwood, M., Cairns, M. J., Day, T. A. & Walker, F. R. (2012) A comparative examination of the anti-inflammatory effects of SSRI and SNRI antidepressants on LPS stimulated microglia. *Brain Behav Immun*, 26(3), 469-79.
Tønnesen, J., Katona, G., Rózsa, B. & Nägerl, U. V. (2014) Spine neck plasticity regulates compartmentalization of synapses. *Nat Neurosci*, 17(5), 678-85.
Tønnesen, J. & Nägerl, U. V. (2016) Dendritic Spines as Tunable Regulators of Synaptic Signals. *Front Psychiatry*, 7, 101.
Ueno, M., Fujita, Y., Tanaka, T., Nakamura, Y., Kikuta, J., Ishii, M. & Yamashita, T. (2013) Layer V cortical neurons require microglial support for survival during postnatal development. *Nat Neurosci*, 16(5), 543-51.
Uhlhaas, P. J. & Singer, W. (2012) Neuronal dynamics and neuropsychiatric disorders: toward a translational paradigm for dysfunctional large-scale networks. *Neuron*, 75(6), 963-80.
Unver, N. & McAllister, F. (2018) IL-6 family cytokines: Key inflammatory mediators as biomarkers and potential therapeutic targets. *Cytokine Growth Factor Rev*, 41, 10-17.
Uren, R. T. & Turnley, A. M. (2014) Regulation of neurotrophin receptor (Trk) signaling: suppressor of cytokine signaling 2 (SOCS2) is a new player. *Front Mol Neurosci*, 7, 39.
Vandresen-Filho, S., Severino, P. C., Constantino, L. C., Martins, W. C., Molz, S., Dal-Cim, T., Bertoldo, D. B., Silva, F. R. & Tasca, C. I. (2015) N-methyl-D-aspartate preconditioning prevents quinolinic acid-induced deregulation of glutamate and calcium homeostasis in mice hippocampus. *Neurotox Res*, 27(2), 118-28.
Vecsei, L., Szalardy, L., Fulop, F. & Toldi, J. (2013) Kynurenines in the CNS: recent advances and new questions. *Nat Rev Drug Discov*, 12(1), 64-82.
Veijola, J., Guo, J. Y., Moilanen, J. S., Jääskeläinen, E., Miettunen, J., Kyllönen, M., Haapea, M., Huhtaniska, S., Alaräisänen, A., Mäki, P., Kiviniemi, V., Nikkinen, J., Starck, T., Remes, J. J., Tanskanen, P., Tervonen, O., Wink, A. M., Kehagia, A., Suckling, J., Kobayashi, H., Barnett, J. H., Barnes, A., Koponen, H. J., Jones, P. B., Isohanni, M. & Murray, G. K. (2014) Longitudinal changes in total brain volume in schizophrenia: relation to symptom severity, cognition and antipsychotic medication. *PLoS One*, 9(7), e101689.
Vergara, D., Nigro, A., Romano, A., De Domenico, S., Damato, M., Franck, J., Coricciati, C., Wistorski, M., Cardon, T., Fournier, I., Quattrini, A., Salzet, M., Furlan, R. & Maffia, M. (2019) Distinct Protein Expression Networks are Activated in Microglia Cells after Stimulation with IFN-γ and IL-4. *Cells*, 8(6).
Verkhratsky, A., Olabarria, M., Noristani, H. N., Yeh, C. Y. & Rodriguez, J. J. (2010) Astrocytes in Alzheimer's disease. *Neurotherapeutics*, 7(4), 399-412.
Verkhratsky, A., Parpura, V., Pekna, M., Pekny, M. & Sofroniew, M. (2014a) Glia in the pathogenesis of neurodegenerative diseases. *Biochem Soc Trans*, 42(5), 1291-301.
Verkhratsky, A., Rodríguez, J. J. & Steardo, L. (2014b) Astrogliopathology: a central element of neuropsychiatric diseases? *Neuroscientist*, 20(6), 576-88.
Verstraelen, P., Pintelon, I., Nuydens, R., Cornelissen, F., Meert, T. & Timmermans, J.-P. (2014a) Pharmacological Characterization of Cultivated Neuronal Networks: Relevance to Synaptogenesis and Synaptic Connectivity. *Cellular and Molecular Neurobiology*, 34(5), 757-776.

Verstraelen, P., Pintelon, I., Nuydens, R., Cornelissen, F., Meert, T. & Timmermans, J. P. (2014b) Pharmacological characterization of cultivated neuronal networks: relevance to synaptogenesis and synaptic connectivity. *Cell Mol Neurobiol*, 34(5), 757-76.
Verstraelen, P., Van Dyck, M., Verschuuren, M., Kashikar, N. D., Nuydens, R., Timmermans, J. P. & De Vos, W. H. (2018) Image-Based Profiling of Synaptic Connectivity in Primary Neuronal Cell Culture. *Front Neurosci*, 12, 389.
Vinet, J., Weering, H. R., Heinrich, A., Kälin, R. E., Wegner, A., Brouwer, N., Heppner, F. L., Rooijen, N., Boddeke, H. W. & Biber, K. (2012) Neuroprotective function for ramified microglia in hippocampal excitotoxicity. *J Neuroinflammation*, 9, 27.
von Bernhardi, R., Bernhardi, L. E. & Eugenin, J. (2017) What Is Neural Plasticity? *Adv Exp Med Biol*, 1015, 1-15.
Voss, L. J., Harvey, M. G. & Sleigh, J. W. (2016) Inhibition of astrocyte metabolism is not the primary mechanism for anaesthetic hypnosis. *Springerplus*, 5(1), 1041.
Vécsei, L., Szalárdy, L., Fülöp, F. & Toldi, J. (2012) Kynurenines in the CNS: recent advances and new questions. *Nature Reviews Drug Discovery*, 12, 64.
Wadhwa, M., Prabhakar, A., Ray, K., Roy, K., Kumari, P., Jha, P. K., Kishore, K., Kumar, S. & Panjwani, U. (2017) Inhibiting the microglia activation improves the spatial memory and adult neurogenesis in rat hippocampus during 48 h of sleep deprivation. *J Neuroinflammation*, 14(1), 222.
Walker, A. K., Budac, D. P., Bisulco, S., Lee, A. W., Smith, R. A., Beenders, B., Kelley, K. W. & Dantzer, R. (2013) NMDA receptor blockade by ketamine abrogates lipopolysaccharide-induced depressive-like behavior in C57BL/6J mice. *Neuropsychopharmacology*, 38(9), 1609-16.
Walker, D. G. & Lue, L. F. (2015) Immune phenotypes of microglia in human neurodegenerative disease: challenges to detecting microglial polarization in human brains. *Alzheimers Res Ther*, 7(1), 56.
Walsh, J. G., Muruve, D. A. & Power, C. (2014a) Inflammasomes in the CNS. *Nat Rev Neurosci*, 15(2), 84-97.
Walsh, K. P., Minamide, L. S., Kane, S. J., Shaw, A. E., Brown, D. R., Pulford, B., Zabel, M. D., Lambeth, J. D., Kuhn, T. B. & Bamburg, J. R. (2014b) Amyloid-β and proinflammatory cytokines utilize a prion protein-dependent pathway to activate NADPH oxidase and induce cofilin-actin rods in hippocampal neurons. *PLoS One*, 9(4), e95995.
Wang, J., Simonavicius, N., Wu, X., Swaminath, G., Reagan, J., Tian, H. & Ling, L. (2006) Kynurenic acid as a ligand for orphan G protein-coupled receptor GPR35. *J Biol Chem*, 281(31), 22021-8.
Wang, W. Y., Tan, M. S., Yu, J. T. & Tan, L. (2015) Role of pro-inflammatory cytokines released from microglia in Alzheimer's disease. *Ann Transl Med*, 3(10), 136.
Wang, X., Huang, S., Jiang, Y., Liu, Y., Song, T., Li, D. & Yang, L. (2018) Reactive astrocytes increase the expression of Pgp and Mrp1 via TNFalpha and NFkappaB signaling. *Mol Med Rep*, 17(1), 1198-1204.
Wang, Y., Lawson, M. A., Dantzer, R. & Kelley, K. W. (2010) LPS-induced indoleamine 2,3-dioxygenase is regulated in an interferon-gamma-independent manner by a JNK signaling pathway in primary murine microglia. *Brain Behav Immun*, 24(2), 201-9.
Wang, Y. F. & Hatton, G. I. (2009) Astrocytic plasticity and patterned oxytocin neuronal activity: dynamic interactions. *J Neurosci*, 29(6), 1743-54.
Weber, A., Wasiliew, P. & Kracht, M. (2010) Interleukin-1 (IL-1) pathway. *Sci Signal*, 3(105), cm1.
Wehland, J. & Weber, K. (1981) Actin rearrangement in living cells revealed by microinjection of a fluorescent phalloidin derivative. *Eur J Cell Biol*, 24(2), 176-83.
Wei, H., Zou, H., Sheikh, A. M., Malik, M., Dobkin, C., Brown, W. T. & Li, X. (2011) IL-6 is increased in the cerebellum of autistic brain and alters neural cell adhesion, migration and synaptic formation. *J Neuroinflammation*, 8, 52.

Wei, Y. P., Kita, M., Shinmura, K., Yan, X. Q., Fukuyama, R., Fushiki, S. & Imanishi, J. (2000) Expression of IFN-gamma in cerebrovascular endothelial cells from aged mice. *J Interferon Cytokine Res*, 20(4), 403-9.
Weishaupt, N., Mason, A. L., Hurd, C., May, Z., Zmyslowski, D. C., Galleguillos, D., Sipione, S. & Fouad, K. (2014) Vector-induced NT-3 expression in rats promotes collateral growth of injured corticospinal tract axons far rostral to a spinal cord injury. *Neuroscience*, 272, 65-75.
Welser-Alves, J. V. & Milner, R. (2013) Microglia are the major source of TNF-α and TGF-β1 in postnatal glial cultures; regulation by cytokines, lipopolysaccharide, and vitronectin. *Neurochem Int*, 63(1), 47-53.
Wieland, T. & Faulstich, H. (1978) Amatoxins, phallotoxins, phallolysin, and antamanide: the biologically active components of poisonous Amanita mushrooms. *CRC Crit Rev Biochem*, 5(3), 185-260.
Wiese, S., Karus, M. & Faissner, A. (2012) Astrocytes as a source for extracellular matrix molecules and cytokines. *Front Pharmacol*, 3, 120.
Wiesenhofer, B. & Humpel, C. (2000) Lipid-mediated gene transfer into primary neurons using FuGene: comparison to C6 glioma cells and primary glia. *Exp Neurol*, 164(1), 38-44.
Williams, S. C. (2013) First IL-6-blocking drug nears approval for rare blood disorder. *Nat Med*, 19(10), 1193.
Wilson, C. & González-Billault, C. (2015) Regulation of cytoskeletal dynamics by redox signaling and oxidative stress: implications for neuronal development and trafficking. *Front Cell Neurosci*, 9, 381.
Winchenbach, J., Düking, T., Berghoff, S. A., Stumpf, S. K., Hülsmann, S., Nave, K. A. & Saher, G. (2016) Inducible targeting of CNS astrocytes in Aldh1l1-CreERT2 BAC transgenic mice. *F1000Res*, 5, 2934.
Winding, M., Kelliher, M. T., Lu, W., Wildonger, J. & Gelfand, V. I. (2016) Role of kinesin-1-based microtubule sliding in Drosophila nervous system development. *Proc Natl Acad Sci U S A*, 113(34), E4985-94.
Wirthgen, E., Hoeflich, A., Rebl, A. & Günther, J. (2017) Kynurenic Acid: The Janus-Faced Role of an Immunomodulatory Tryptophan Metabolite and Its Link to Pathological Conditions. *Front Immunol*, 8, 1957.
Withers, G. S., Farley, J. R., Sterritt, J. R., Crane, A. B. & Wallace, C. S. (2017) Interactions with Astroglia Influence the Shape of the Developing Dendritic Arbor and Restrict Dendrite Growth Independent of Promoting Synaptic Contacts. *PLoS One*, 12(1), e0169792.
Wolf, J., Rose-John, S. & Garbers, C. (2014) Interleukin-6 and its receptors: a highly regulated and dynamic system. *Cytokine*, 70(1), 11-20.
Wu, W., Nicolazzo, J. A., Wen, L., Chung, R., Stankovic, R., Bao, S. S., Lim, C. K., Brew, B. J., Cullen, K. M. & Guillemin, G. J. (2013) Expression of tryptophan 2,3-dioxygenase and production of kynurenine pathway metabolites in triple transgenic mice and human Alzheimer's disease brain. *PLoS One*, 8(4), e59749.
Wulf, E., Deboben, A., Bautz, F. A., Faulstich, H. & Wieland, T. (1979) Fluorescent phallotoxin, a tool for the visualization of cellular actin. *Proc Natl Acad Sci U S A*, 76(9), 4498-502.
Xia, W., Peng, G. Y., Sheng, J. T., Zhu, F. F., Guo, J. F. & Chen, W. Q. (2015) Neuroprotective effect of interleukin-6 regulation of voltage-gated Na(+) channels of cortical neurons is time- and dose-dependent. *Neural Regen Res*, 10(4), 610-7.
Xiao, N. & Le, Q. T. (2016) Neurotrophic Factors and Their Potential Applications in Tissue Regeneration. *Arch Immunol Ther Exp (Warsz)*, 64(2), 89-99.
Xu, S. L., Bi, C. W., Choi, R. C., Zhu, K. Y., Miernisha, A., Dong, T. T. & Tsim, K. W. (2013) Flavonoids induce the synthesis and secretion of neurotrophic factors in cultured rat astrocytes: a signaling response mediated by estrogen receptor. *Evid Based Complement Alternat Med*, 2013, 127075.

Xu, Z., Xiao, N., Chen, Y., Huang, H., Marshall, C., Gao, J., Cai, Z., Wu, T., Hu, G. & Xiao, M. (2015) Deletion of aquaporin-4 in APP/PS1 mice exacerbates brain Aβ accumulation and memory deficits. *Mol Neurodegener*, 10, 58.
Yamaguchi, S., Fujii-Taira, I., Murakami, A., Hirose, N., Aoki, N., Izawa, E., Fujimoto, Y., Takano, T., Matsushima, T. & Homma, K. J. (2008) Up-regulation of microtubule-associated protein 2 accompanying the filial imprinting of domestic chicks (Gallus gallus domesticus). *Brain Res Bull*, 76(3), 282-8.
Yamamoto, M., Takeya, M., Ikeshima-Kataoka, H., Yasui, M., Kawasaki, Y., Shiraishi, M., Majima, E., Shiraishi, S., Uezono, Y., Sasaki, M. & Eto, K. (2012) Increased expression of aquaporin-4 with methylmercury exposure in the brain of the common marmoset. *J Toxicol Sci*, 37(4), 749-63.
Yan, J. W., Tan, T. Y. & Huang, Q. L. (2013) Protective effect of astrocyte-conditioned medium on neurons following hypoxia and mechanical injury. *Chin J Traumatol*, 16(1), 3-9.
Yan, X., Shi, Z. F., Xu, L. X., Li, J. X., Wu, M., Wang, X. X., Jia, M., Dong, L. P., Yang, S. H. & Yuan, F. (2017) Glutamate Impairs Mitochondria Aerobic Respiration Capacity and Enhances Glycolysis in Cultured Rat Astrocytes. *Biomed Environ Sci*, 30(1), 44-51.
Yan, Z., Gibson, S. A., Buckley, J. A., Qin, H. & Benveniste, E. N. (2018) Role of the JAK/STAT signaling pathway in regulation of innate immunity in neuroinflammatory diseases. *Clin Immunol*, 189, 4-13.
Yang, P., Wen, H., Ou, S., Cui, J. & Fan, D. (2012) IL-6 promotes regeneration and functional recovery after cortical spinal tract injury by reactivating intrinsic growth program of neurons and enhancing synapse formation. *Exp Neurol*, 236(1), 19-27.
Yang, Y., Boza-Serrano, A., Dunning, C. J. R., Clausen, B. H., Lambertsen, K. L. & Deierborg, T. (2018) Inflammation leads to distinct populations of extracellular vesicles from microglia. *J Neuroinflammation*, 15(1), 168.
Yang, Y., Vidensky, S., Jin, L., Jie, C., Lorenzini, I., Frankl, M. & Rothstein, J. D. (2011) Molecular comparison of GLT1+ and ALDH1L1+ astrocytes in vivo in astroglial reporter mice. *Glia*, 59(2), 200-7.
Yasuda, R. (2017) Biophysics of Biochemical Signaling in Dendritic Spines: Implications in Synaptic Plasticity. *Biophys J*, 113(10), 2152-2159.
Yates, D. (2015) Neurodegenerative disease: Factoring in astrocytes. *Nat Rev Neurosci*, 16(2), 67.
Yates, D. (2017) Glia: A toxic reaction. *Nat Rev Neurosci*, 18(3), 130.
Ye, L., Huang, Y., Zhao, L., Li, Y., Sun, L., Zhou, Y., Qian, G. & Zheng, J. C. (2013) IL-1β and TNF-α induce neurotoxicity through glutamate production: a potential role for neuronal glutaminase. *J Neurochem*, 125(6), 897-908.
Yeh, C. Y., Vadhwana, B., Verkhratsky, A. & Rodríguez, J. J. (2011) Early astrocytic atrophy in the entorhinal cortex of a triple transgenic animal model of Alzheimer's disease. *ASN Neuro*, 3(5), 271-9.
Yin, H. Z., Hsu, C. I., Yu, S., Rao, S. D., Sorkin, L. S. & Weiss, J. H. (2012) TNF-α triggers rapid membrane insertion of Ca(2+) permeable AMPA receptors into adult motor neurons and enhances their susceptibility to slow excitotoxic injury. *Exp Neurol*, 238(2), 93-102.
Yizhar, O., Fenno, L. E., Prigge, M., Schneider, F., Davidson, T. J., O'Shea, D. J., Sohal, V. S., Goshen, I., Finkelstein, J., Paz, J. T., Stehfest, K., Fudim, R., Ramakrishnan, C., Huguenard, J. R., Hegemann, P. & Deisseroth, K. (2011) Neocortical excitation/inhibition balance in information processing and social dysfunction. *Nature*, 477(7363), 171-8.
Yogev, S. & Shen, K. (2017) Establishing Neuronal Polarity with Environmental and Intrinsic Mechanisms. *Neuron*, 96(3), 638-650.
Yoshihara, Y., De Roo, M. & Muller, D. (2009) Dendritic spine formation and stabilization. *Curr Opin Neurobiol*, 19(2), 146-53.

Yoshimura, A., Suzuki, M., Sakaguchi, R., Hanada, T. & Yasukawa, H. (2012) SOCS, Inflammation, and Autoimmunity. *Front Immunol*, 3, 20.
Yuan, J., Ge, H., Liu, W., Zhu, H., Chen, Y., Zhang, X., Yang, Y., Yin, Y., Chen, W., Wu, W. & Lin, J. (2017) M2 microglia promotes neurogenesis and oligodendrogenesis from neural stem/progenitor cells via the PPARγ signaling pathway. *Oncotarget*, 8(12), 19855-19865.
Yuksel, C. & Ongur, D. (2010) Magnetic resonance spectroscopy studies of glutamate-related abnormalities in mood disorders. *Biol Psychiatry*, 68(9), 785-94.
Yuste, R. (2013) Electrical compartmentalization in dendritic spines. *Annu Rev Neurosci*, 36, 429-49.
Zamanian, J. L., Xu, L., Foo, L. C., Nouri, N., Zhou, L., Giffard, R. G. & Barres, B. A. (2012) Genomic analysis of reactive astrogliosis. *J Neurosci*, 32(18), 6391-410.
Zeitelhofer, M., Vessey, J. P., Thomas, S., Kiebler, M. & Dahm, R. (2009) Transfection of cultured primary neurons via nucleofection. *Curr Protoc Neurosci*, Chapter 4, Unit4.32.
Zeng, G., Huang, X., Jiang, T. & Yu, S. (2019) Short-term synaptic plasticity expands the operational range of long-term synaptic changes in neural networks. *Neural Netw*, 118, 140-147.
Zeug, A., Müller, F. E., Anders, S., Herde, M. K., Minge, D., Ponimaskin, E. & Henneberger, C. (2018) Control of astrocyte morphology by Rho GTPases. *Brain Res Bull*, 136, 44-53.
Zhang, G., Gurtu, V. & Kain, S. R. (1996) An enhanced green fluorescent protein allows sensitive detection of gene transfer in mammalian cells. *Biochem Biophys Res Commun*, 227(3), 707-11.
Zhang, J. & Dong, X. P. (2012) Dysfunction of microtubule-associated proteins of MAP2/tau family in Prion disease. *Prion*, 6(4), 334-8.
Zhang, J., Yang, B., Sun, H., Zhou, Y., Liu, M., Ding, J., Fang, F., Fan, Y. & Hu, G. (2016) Aquaporin-4 deficiency diminishes the differential degeneration of midbrain dopaminergic neurons in experimental Parkinson's disease. *Neurosci Lett*, 614, 7-15.
Zhang, J. & Zhang, Q. (2019) Using Seahorse Machine to Measure OCR and ECAR in Cancer Cells. *Methods Mol Biol*, 1928, 353-363.
Zhang, J. C., Yao, W., Dong, C., Yang, C., Ren, Q., Ma, M. & Hashimoto, K. (2017a) Blockade of interleukin-6 receptor in the periphery promotes rapid and sustained antidepressant actions: a possible role of gut-microbiota-brain axis. *Transl Psychiatry*, 7(5), e1138.
Zhang, Q., Lenardo, M. J. & Baltimore, D. (2017b) 30 Years of NF-kappaB: A Blossoming of Relevance to Human Pathobiology. *Cell*, 168(1-2), 37-57.
Zhang, W., Smith, C., Howlett, C. & Stanimirovic, D. (2000) Inflammatory activation of human brain endothelial cells by hypoxic astrocytes in vitro is mediated by IL-1beta. *J Cereb Blood Flow Metab*, 20(6), 967-78.
Zhang, Z., Ma, Z., Zou, W., Guo, H., Liu, M., Ma, Y. & Zhang, L. (2019) The Appropriate Marker for Astrocytes: Comparing the Distribution and Expression of Three Astrocytic Markers in Different Mouse Cerebral Regions. *Biomed Res Int*, 2019, 9605265.
Zhao, Y. & Rempe, D. A. (2010) Targeting astrocytes for stroke therapy. *Neurotherapeutics*, 7(4), 439-51.
Zheng, C., Zhou, X. W. & Wang, J. Z. (2016) The dual roles of cytokines in Alzheimer's disease: update on interleukins, TNF-alpha, TGF-beta and IFN-gamma. *Transl Neurodegener*, 5, 7.
Zhou, B., Zuo, Y. X. & Jiang, R. T. (2019) Astrocyte morphology: Diversity, plasticity, and role in neurological diseases. *CNS Neurosci Ther*, 25(6), 665-673.
Zhou, T., Huang, Z., Sun, X., Zhu, X., Zhou, L., Li, M., Cheng, B., Liu, X. & He, C. (2017) Microglia Polarization with M1/M2 Phenotype Changes in rd1 Mouse Model of Retinal Degeneration. *Front Neuroanat*, 11, 77.

Zhou, X., Xiao, H. & Wang, H. (2011) Developmental changes of TrkB signaling in response to exogenous brain-derived neurotrophic factor in primary cortical neurons. *J Neurochem*, 119(6), 1205-16.
Zhou, Y. & Danbolt, N. C. (2014) Glutamate as a neurotransmitter in the healthy brain. *J Neural Transm (Vienna)*, 121(8), 799-817.
Zhu, L., Okano, S., Takahara, M., Chiba, T., Tu, Y., Oda, Y. & Furue, M. (2013) Expression of S100 protein family members in normal skin and sweat gland tumors. *J Dermatol Sci*, 70(3), 211-9.
Zhu, Y. B., Gao, W., Zhang, Y., Jia, F., Zhang, H. L., Liu, Y. Z., Sun, X. F., Yin, Y. & Yin, D. M. (2016) Astrocyte-derived phosphatidic acid promotes dendritic branching. *Sci Rep*, 6, 21096.
Zhu, Z. H., Yang, R., Fu, X., Wang, Y. Q. & Wu, G. C. (2006) Astrocyte-conditioned medium protecting hippocampal neurons in primary cultures against corticosterone-induced damages via PI3-K/Akt signal pathway. *Brain Res*, 1114(1), 1-10.
Zhuravlev, A. V., Shchegolev, B. F., Savvateeva-Popova, E. V. & Popov, A. V. (2007) [Stacking-interactions in the control-gear binding of kynurenic acid with NR2A- and GluR2-subunits of glutamate ionotropic receptors]. *Ross Fiziol Zh Im I M Sechenova*, 93(6), 609-24.
Zinger, A., Barcia, C., Herrero, M. T. & Guillemin, G. J. (2011) The involvement of neuroinflammation and kynurenine pathway in Parkinson's disease. *Parkinsons Dis*, 2011, 716859.
Zoga, M., Oulis, P., Chatzipanagiotou, S., Masdrakis, V. G., Pliatsika, P., Boufidou, F., Foteli, S., Soldatos, C. R., Nikolaou, C. & Papageorgiou, C. (2014) Indoleamine 2,3-dioxygenase and immune changes under antidepressive treatment in major depression in females. *In Vivo*, 28(4), 633-8.
Zrzavy, T., Höftberger, R., Berger, T., Rauschka, H., Butovsky, O., Weiner, H. & Lassmann, H. (2019) Pro-inflammatory activation of microglia in the brain of patients with sepsis. *Neuropathol Appl Neurobiol*, 45(3), 278-290.
Zuchero, J. B. & Barres, B. A. (2015) Glia in mammalian development and disease. *Development*, 142(22), 3805-9.
Zunszain, P. A., Anacker, C., Cattaneo, A., Choudhury, S., Musaelyan, K., Myint, A. M., Thuret, S., Price, J. & Pariante, C. M. (2012) Interleukin-1β: a new regulator of the kynurenine pathway affecting human hippocampal neurogenesis. *Neuropsychopharmacology*, 37(4), 939-49.
Zwilling, D., Huang, S. Y., Sathyasaikumar, K. V., Notarangelo, F. M., Guidetti, P., Wu, H. Q., Lee, J., Truong, J., Andrews-Zwilling, Y., Hsieh, E. W., Louie, J. Y., Wu, T., Scearce-Levie, K., Patrick, C., Adame, A., Giorgini, F., Moussaoui, S., Laue, G., Rassoulpour, A., Flik, G., Huang, Y., Muchowski, J. M., Masliah, E., Schwarcz, R. & Muchowski, P. J. (2011) Kynurenine 3-monooxygenase inhibition in blood ameliorates neurodegeneration. *Cell*, 145(6), 863-74.
Şovrea, A. S. & Boşca, A. B. (2013) Astrocytes reassessment - an evolving concept part one: embryology, biology, morphology and reactivity. *J Mol Psychiatry*, 1, 18.